VISIT…

CRC Press
Taylor & Francis Group

# Handbook of Lapping and Polishing

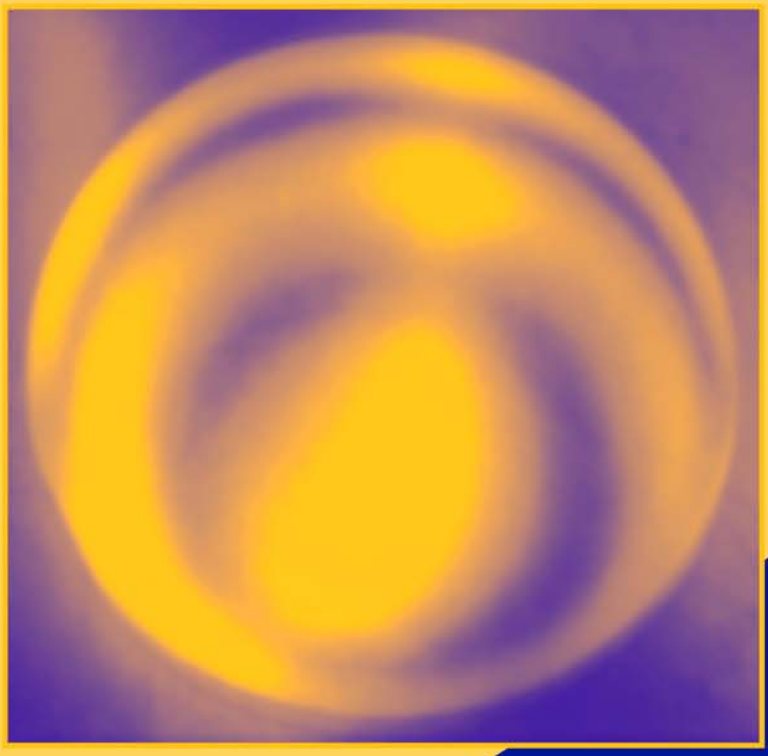

edited by
Ioan D. Marinescu
Eckart Uhlmann
Toshiro K. Doi

# Handbook of Lapping and Polishing

**MANUFACTURING ENGINEERING**
**AND MATERIALS PROCESSING**
A Series of Reference Books and Textbooks

SERIES EDITOR

**Geoffrey Boothroyd**
*Boothroyd Dewhurst, Inc.*
*Wakefield, Rhode Island*

1. Computers in Manufacturing, *U. Rembold, M. Seth, and J. S. Weinstein*
2. Cold Rolling of Steel, *William L. Roberts*
3. Strengthening of Ceramics: Treatments, Tests, and Design Applications, *Harry P. Kirchner*
4. Metal Forming: The Application of Limit Analysis, *Betzalel Avitzur*
5. Improving Productivity by Classification, Coding, and Data Base Standardization: The Key to Maximizing CAD/CAM and Group Technology, *William F. Hyde*
6. Automatic Assembly, *Geoffrey Boothroyd, Corrado Poli, and Laurence E. Murch*
7. Manufacturing Engineering Processes, *Leo Alting*
8. Modern Ceramic Engineering: Properties, Processing, and Use in Design, *David W. Richerson*
9. Interface Technology for Computer-Controlled Manufacturing Processes, *Ulrich Rembold, Karl Armbruster, and Wolfgang Ülzmann*
10. Hot Rolling of Steel, *William L. Roberts*
11. Adhesives in Manufacturing, *edited by Gerald L. Schneberger*
12. Understanding the Manufacturing Process: Key to Successful CAD/CAM Implementation, *Joseph Harrington, Jr.*
13. Industrial Materials Science and Engineering, *edited by Lawrence E. Murr*
14. Lubricants and Lubrication in Metalworking Operations, *Elliot S. Nachtman and Serope Kalpakjian*

15. Manufacturing Engineering: An Introduction to the Basic Functions, *John P. Tanner*
16. Computer-Integrated Manufacturing Technology and Systems, *Ulrich Rembold, Christian Blume, and Ruediger Dillman*
17. Connections in Electronic Assemblies, *Anthony J. Bilotta*
18. Automation for Press Feed Operations: Applications and Economics, *Edward Walker*
19. Nontraditional Manufacturing Processes, *Gary F. Benedict*
20. Programmable Controllers for Factory Automation, *David G. Johnson*
21. Printed Circuit Assembly Manufacturing, *Fred W. Kear*
22. Manufacturing High Technology Handbook, *edited by Donatas Tijunelis and Keith E. McKee*
23. Factory Information Systems: Design and Implementation for CIM Management and Control, *John Gaylord*
24. Flat Processing of Steel, *William L. Roberts*
25. Soldering for Electronic Assemblies, *Leo P. Lambert*
26. Flexible Manufacturing Systems in Practice: Applications, Design, and Simulation, *Joseph Talavage and Roger G. Hannam*
27. Flexible Manufacturing Systems: Benefits for the Low Inventory Factory, *John E. Lenz*
28. Fundamentals of Machining and Machine Tools: Second Edition, *Geoffrey Boothroyd and Winston A. Knight*
29. Computer-Automated Process Planning for World-Class Manufacturing, *James Nolen*
30. Steel-Rolling Technology: Theory and Practice, *Vladimir B. Ginzburg*
31. Computer Integrated Electronics Manufacturing and Testing, *Jack Arabian*
32. In-Process Measurement and Control, *Stephan D. Murphy*
33. Assembly Line Design: Methodology and Applications, *We-Min Chow*
34. Robot Technology and Applications, *edited by Ulrich Rembold*
35. Mechanical Deburring and Surface Finishing Technology, *Alfred F. Scheider*

36. Manufacturing Engineering: An Introduction to the Basic Functions, Second Edition, Revised and Expanded, *John P. Tanner*
37. Assembly Automation and Product Design, *Geoffrey Boothroyd*
38. Hybrid Assemblies and Multichip Modules, *Fred W. Kear*
39. High-Quality Steel Rolling: Theory and Practice, *Vladimir B. Ginzburg*
40. Manufacturing Engineering Processes: Second Edition, Revised and Expanded, *Leo Alting*
41. Metalworking Fluids, *edited by Jerry P. Byers*
42. Coordinate Measuring Machines and Systems, *edited by John A. Bosch*
43. Arc Welding Automation, *Howard B. Cary*
44. Facilities Planning and Materials Handling: Methods and Requirements, *Vijay S. Sheth*
45. Continuous Flow Manufacturing: Quality in Design and Processes, *Pierre C. Guerindon*
46. Laser Materials Processing, *edited by Leonard Migliore*
47. Re-Engineering the Manufacturing System: Applying the Theory of Constraints, *Robert E. Stein*
48. Handbook of Manufacturing Engineering, *edited by Jack M. Walker*
49. Metal Cutting Theory and Practice, *David A. Stephenson and John S. Agapiou*
50. Manufacturing Process Design and Optimization, *Robert F. Rhyder*
51. Statistical Process Control in Manufacturing Practice, *Fred W. Kear*
52. Measurement of Geometric Tolerances in Manufacturing, *James D. Meadows*
53. Machining of Ceramics and Composites, *edited by Said Jahanmir, M. Ramulu, and Philip Koshy*
54. Introduction to Manufacturing Processes and Materials, *Robert C. Creese*
55. Computer-Aided Fixture Design, *Yiming (Kevin) Rong and Yaoxiang (Stephens) Zhu*
56. Understanding and Applying Machine Vision: Second Edition, Revised and Expanded, *Nello Zuech*
57. Flat Rolling Fundamentals, *Vladimir B. Ginzburg and Robert Ballas*

58. Product Design for Manufacture and Assembly: Second Edition, Revised and Expanded, *Geoffrey Boothroyd, Peter Dewhurst, and Winston A. Knight*
59. Process Modeling in Composites Manufacturing, *edited by Suresh G. Advani and E. Murat Sozer*
60. Integrated Product Design and Manufacturing Using Geometric Dimensioning and Tolerancing, *Robert Campbell*
61. Handbook of Induction Heating, *edited by Valery I. Rudnev, Don Loveless, Raymond Cook and Micah Black*
62. Re-Engineering the Manufacturing System: Applying the Theory of Constraints, Second Edition, *Robert Stein*
63. Manufacturing: Design, Production, Automation, and Integration, *Beno Benhabib*
64. Rod and Bar Rolling: Theory and Applications, *Youngseog Lee*
65. Metallurgical Design of Flat Rolled Steels, *Vladimir B. Ginzburg*
66. Assembly Automation and Product Design: Second Edition, *Geoffrey Boothroyd*
67. Roll Forming Handbook, *edited by George T. Halmos*
68. Metal Cutting Theory and Practice: Second Edition, *David A. Stephenson and John S. Agapiou*
69. Fundamentals of Machining and Machine Tools: Third Edition, *Geoffrey Boothroyd and Winston A. Knight*
70. Manufacturing Optimization Through Intelligent Techniques, *R. Saravanan*
71. Metalworking Fluids: Second Edition, *Jerry P. Byers*
72. Handbook of Machining with Grinding Wheels, *Ioan D. Marinescu, Mike Hitchiner, Eckart Uhlmann, W. Brian Rowe, and Ichiro Inasaki*
73. Handbook of Lapping and Polishing, *edited by Ioan D. Marinescu, Eckart Uhlmann, and Toshiro K. Doi*

# Handbook of Lapping and Polishing

edited by
Ioan D. Marinescu
Eckart Uhlmann
Toshiro K. Doi

CRC Press
Taylor & Francis Group
Boca Raton London New York

CRC Press is an imprint of the
Taylor & Francis Group, an informa business

CRC Press
Taylor & Francis Group
6000 Broken Sound Parkway NW, Suite 300
Boca Raton, FL 33487-2742

© 2007 by Taylor & Francis Group, LLC
CRC Press is an imprint of Taylor & Francis Group, an Informa business

No claim to original U.S. Government works
Printed in the United States of America on acid-free paper
10 9 8 7 6 5 4 3 2 1

International Standard Book Number-10: 1-57444-670-3 (Hardcover)
International Standard Book Number-13: 978-1-57444-670-8 (Hardcover)

This book contains information obtained from authentic and highly regarded sources. Reprinted material is quoted with permission, and sources are indicated. A wide variety of references are listed. Reasonable efforts have been made to publish reliable data and information, but the author and the publisher cannot assume responsibility for the validity of all materials or for the consequences of their use.

No part of this book may be reprinted, reproduced, transmitted, or utilized in any form by any electronic, mechanical, or other means, now known or hereafter invented, including photocopying, microfilming, and recording, or in any information storage or retrieval system, without written permission from the publishers.

For permission to photocopy or use material electronically from this work, please access www.copyright.com (http://www.copyright.com/) or contact the Copyright Clearance Center, Inc. (CCC) 222 Rosewood Drive, Danvers, MA 01923, 978-750-8400. CCC is a not-for-profit organization that provides licenses and registration for a variety of users. For organizations that have been granted a photocopy license by the CCC, a separate system of payment has been arranged.

**Trademark Notice:** Product or corporate names may be trademarks or registered trademarks, and are used only for identification and explanation without intent to infringe.

**Library of Congress Cataloging-in-Publication Data**

Handbook of lapping and polishing / editors, Ioan D. Marinescu, Eckart Uhlmann, and Toshiro Doi.
p. cm.
Includes bibliographical references and index.
ISBN-13: 978-1-57444-670-8 (alk. paper)
ISBN-10: 1-57444-670-3 (alk. paper)
1. Grinding and polishing--Handbooks, manuals, etc. I. Marinescu, Ioan D. II. Uhlmann, Eckart. III. Doi, Toshiro.

TJ1280.H424 2006
671.3'5--dc22 2006017436

**Visit the Taylor & Francis Web site at**
**http://www.taylorandfrancis.com**

**and the CRC Press Web site at**
**http://www.crcpress.com**

# Preface

Lapping and polishing are the most precise processes used to finish the surfaces of mechanical and electronic or semiconductor components. *The Handbook of Lapping and Polishing* is the first book written in English to thoroughly cover these processes. Even though these processes are very precise, there has been very little scientific research undertaken into the study and application of these processes. These processes may be characterized as "more an art than a science." The aim of this book is to review all the developments of recent years so that a foundation may be laid to enable the transformation of these operations into more deterministic processes by the involvement of some mechanical and tribological science.

The "Fundamentals of Lapping" (Chapter 2) will give an overview of the lapping process starting with the basics. The stock removal mechanisms of lapping and polishing are very different from any other processes, and because both lapping and polishing are free abrasive processes, most of their mechanisms are under a probability percentage. All abrasive processes have an overlap of rubbing, plowing, and scratching mechanisms that are functions of a large number of parameters of the process, of the abrasive, and of the work piece. All these make any prediction of outcomes of these processes very difficult.

Most of the applications of these processes are kept as confidential as possible (proprietary information), and specific details are not seen in professional or technical journals and magazines. This is the reason for not having a book until now that emphasizes these processes.

The editors of this book have put together the latest knowledge concerning these processes in three leading industrial countries: United States, Japan, and Germany. The contributors are from academia as well as from industry, and they all possess extensive experience in both the theoretical and application domains.

Due to the high pace of development of the electronics and semiconductors industry, many of the presented processes and applications come from these industries, which are also the engines of the developments of these processes. Few people using a computer realize how much lapping, polishing, and chemomechanical polishing (CMP) are involved in the computer's components. The most critical components of the disk drive are finished with special superlapping and nanopolishing techniques not to mention the CMP of the chips, which has already become a standard technology.

Developments in the abrasive industry in recent years, mainly of the superabrasives, have generated more challenges for industries that utilize these processes. The reality that day-by-day we get finer diamond and cubic

boron nitride (CBN) grits is changing these industries. It is not unusual today to talk about nanogrit, mainly in the case of diamonds. Relatively new technology such as obtaining diamonds by explosion has allowed the development of products with grits as small as 5 nm. To use these grits, avoiding the formation of clusters is a challenge, which has only been partially solved.

Most of the knowledge used in the study of lapping and polishing has been borrowed from tribology, the science of wear, friction, and lubrication. A book I wrote in 2004 (*Tribology of Abrasive Processes*) was exclusively dedicated to the application of tribology to abrasive processes, but had more emphasis on the grinding process, which is largely used in industry. Not many researchers from the tribology field are dealing with manufacturing processes, even though this marriage is a win–win solution. Lately more people, mainly from academia, have been taking this approach, and the results are great.

The audience for this book is very large. The book can be useful for a large category of professionals starting with technicians and engineers and extending to researchers and academics. The book can be used also as a complementary textbook for undergraduate and graduate studies.

Finally, I would like to sincerely thank all the contributors to this book, including their companies and universities for allowing them to spend the time required for writing the chapters of this book.

**Ioan D. Marinescu**
Toledo, Ohio

# Editors

**Dr. Ioan D. Marinescu** is a professor of mechanical, industrial, and manufacturing engineering at the University of Toledo. He is also the director of the Precision Micro-Machining Center of the College of Engineering of the same university.

Professor Marinescu is the author of more than 15 books and over 300 technical and scientific papers. He has given lectures and workshops in more than 40 countries around the world.

**Dr. Eckart Uhlmann** is a professor of production engineering at the Technical University of Berlin. He is also the director of the Institute for Machine Tools and Management, a Fraunhofer Institute.

Professor Uhlmann is well known in Germany and internationally through his studies in abrasive processes, especially in coated abrasive processes, lapping, polishing, and grinding with lapping kinematics.

**Dr. Toshiro K. Doi** is a professor of mechanical engineering at the School of Education of Saitama University. He is also the director of the Precision Engineering Laboratory at Saitama University.

Professor Doi is a world expert in chemomechanical polishing, the field in which he published several books and over 100 papers in Japan and abroad. He is the author or coauthor of more than 170 patents.

# Contributors

**Thomas Ardelt**
Technische Universitat Berlin
Berlin, Germany

**Ion Benea**
Engis Corporation
Wheeling, Illinois

**Toshiro K. Doi**
Saitamata University
Saitama, Japan

**Masanobu Hanazono**
SONAC, Inc.
Nara, Japan

**Uwe Heisel**
Universitat Stuttgart
Stuttgart, Germany

**Daizo Ichikawa**
Fujikoshi Machinery Corp.
Nagano, Japan

**Junichi Ikeno**
Saitama University
Saitama, Japan

**Ken-ich Isahikawa**
Kanazawa Institute of Technology
Ishikawa, Japan

**Toshio Kasai**
Tokyo Denki University
Tokyo, Japan

**Masaharu Kinoshita**
Nitta Haas, Inc.
Tokyo, Japan

**Ioan Marinescu**
University of Toledo
Toledo, Ohio

**Hitoshi Ohmori**
Institute for Physical and Chemical Research of Japan (RIKEN)
Saitama, Japan

**Mariana Pruteanu**
Insaco Inc.
Quakertown, Pennsylvania

**Naga Jyothi Sanku**
University of Toledo
Toledo, Ohio

**Hitoshi Suwabe**
Kanazawa Institute of Technology
Ishikawa, Japan

**Keisuke Suzuki**
SONAC, Inc.
Nara, Japan

**Eckart Uhlmann**
Technical University of Berlin,
Institute for Machine Tools and Management
Berlin, Germany

**Hitomi Yamaguchi**
Utsunomiya University
Tochigi, Japan

# Table of Contents

**Chapter 1**
Introduction ..... 1
*Ioan Marinescu*

**Chapter 2**
Fundamentals of Lapping ..... 7
*Eckart Uhlmann*

**Chapter 3**
Lapping of Ductile Materials ..... 93
*Ioan Marinescu, Ion Benea, and Naga Jyothi Sanku*

**Chapter 4**
Lapping of Brittle Materials ..... 123
*Ioan Marinescu, Ion Benea, and Mariana Pruteanu*

**Chapter 5**
Lapping and Lapping Machines ..... 265
*Toshiro K. Doi and Daizo Ichikawa*

**Chapter 6**
Polishing Technology ..... 281
*Toshiro K. Doi*

**Chapter 7**
Chemical Mechanical Polishing and Its Applications
in ULSI Process ..... 341
*Toshiro K. Doi*

**Index** ..... 479

# 1 Introduction

*Ioan Marinescu*

## CONTENTS

1.1 From Craft to Science ..... 1
1.2 Importance of the Abrasive ..... 3
1.3 Problem Solving ..... 4
References ..... 5

## 1.1 FROM CRAFT TO SCIENCE

Abrasive processes have been employed in manufacturing for more than a 100 years although the earliest practice can be traced back to Neolithic times (Woodbury, 1959). The lack of machine tool technology meant that primitive operations were mostly limited to simple handheld operations. An early device for dressing a sandstone-grinding wheel was patented by Altzschner in 1860 (Woodbury, 1959).

The twentieth century saw the burgeoning of grinding, lapping, and polishing as modern processes. Seminal publications by Alden and Guest started the process of bringing the art of grinding and polishing onto a scientific basis (Alden, 1914; Guest, 1915).

Lapping and polishing are very similar processes. Very fine surface finishes, high dimensional accuracy and flatness, and minimal subsurface damage are common with both the methods. These techniques have been used for many years and, in a crude form, since the origin of humans. Many different industries achieve high precision surfaces with these techniques. For example, lapping and polishing are very critical processes in semiconductor manufacturing, read or write heads, and hard disk preparation. Lapping has become a very important finishing technique in ceramic seal industry.

The above-mentioned micromachining processes are all used for a common purpose: to remove material and obtain the desired part form and finish on brittle and ductile materials by randomly oriented abrasive and superabrasive particles. As previously mentioned, lapping and polishing are free abrasive processes that are categorically different from other micromachining processes such as honing, fine grinding, and superfinishing (CIRP, 2005; Czichos, 1978).

The mechanics of lapping and polishing processes are identical and are performed to produce flat surfaces. Parts are placed in contact with a rotating

plate and rotated mechanically or frictionally in numerous motions. Abrasives suspended in paste or liquid carrier are applied initially to the plate or supplied during the process (continuously or at specific intervals) or embedded into the plate, or all the three. Abrasive sizes are similar for both processes. Lapping and polishing machines are very similar. Many machines available can perform both lapping and polishing. The difference lies in the material removal mechanism (Marinescu et al., 2004; Rowe et al., 1994).

With both processes, material removal is by rolling abrasive, sliding abrasive, or microcutting embedded abrasive. The action of sliding abrasive and rolling abrasive are implied. They are mechanically similar in their cutting action except that sliding abrasives are more platelike and behave like tiny scrapers. Microcutting abrasives are abrasives that have embedded into the lapping plate and act like small cutting tools (Rowe et al., 1999).

Polishing involves only one or two of the abrasive mechanisms aforementioned. This widely used ceramic finishing process is one in which parts are finished on a plate covered with an abrasive pad. The polishing pad comes in a variety of thicknesses and hardnesses. Abrasive is often supplied in a paste suspension, but can be continuously fed suspended in a liquid carrier. Only two material mechanisms occur with this form of polishing—rolling and sliding. Abrasive is not embedded into the pad, therefore the microcutting mechanism is not active. Other types of mechanical polishing use different mechanisms for material removal. One type uses abrasive embed into the plate or a pad, but no additional abrasive is applied to the polishing surface. With this type, material removal is only through the microcutting abrasive mechanism. For all types of polishing, only two abrasive mechanisms are involved.

Lapping on the other hand, incorporates all three abrasive mechanisms: rolling abrasive, sliding abrasive, and microcutting abrasive. The plate is not covered with a pad and therefore contributes in the material removal process. With typical lapping operations, abrasive is forced into the lap plate, called charging, and the parts are lapped with continuously supplied abrasive suspended in a liquid medium.

It is a general perception that smoother surfaces can be obtained with polishing. Polishing is a surface smoothing operation that removes or smoothes grinding lines, scratches, and other defects to improve surface finish. It is often applied to previously lapped or ground surfaces to reduce damage to surface caused by previous machining, to provide a reflective wear surface, or to obtain a clear finish for transparent glass optic materials.

Lapping is also perceived to be a process used mainly for removing materials and reducing the dimensions, while decreasing the surface roughness. It is thought of as a greater material removal process that is able to obtain flatter surfaces albeit with greater surface damage. Lapping is a process followed by polishing steps to clean up the surface. However, the science of lapping as it pertains to ceramic materials has progressed to such a point that the surface of finished parts rivals that of polished parts. In addition, parts have a greater

flatness and take less time to reach the desired dimensions and surface finish. Greater flatness is achieved because the pad is not an intermediate between the hard solid lap plate and the part. Because of the flexibility in the pad used in polishing, the flatness usually deteriorates with longer polishing times; nonflat surfaces are not improved because the soft pad follows the out-of-flat surface, and the edges have a tendency to round off. With lapping, the lack of intermediate material (pad) allows larger material-removal rates to be achieved due to additional abrasive wear active. Greater amounts of surface damage are still witnessed with lapping. However, the disparity of the damage produced between processes is shrinking. In addition, damage in the form of compressive residual stress can be beneficial in some cases.

Lapping is a process that can easily generate good surface finishes, but is very difficult to obtain excellent surface finishes; whereas polishing is a simple process that can easily result in excellent surfaces.

Advances in productivity have relied on increasing sophistication in the application of abrasives. The range of abrasives employed in lapping and polishing has increased with the introduction of new ceramic abrasives based on sol gel technology, the development of superabrasive cubic boron nitride and diamond abrasives based on natural and synthetic diamond.

Lapping and polishing processes are not without their share of problems. A correct understanding of the interplay of factors in lapping and polishing helps in overcoming these problems quickly and efficiently. Commonly encountered problems are analyzed in succeeding chapters to show how parameters can be optimized and how the quality of lapping and polishing can be improved.

## 1.2 IMPORTANCE OF THE ABRASIVE

The importance of the abrasive cannot be overemphasized. The enormous differences in typical hardness values of abrasive grains are illustrated in Table 1.1. A value for a typical M2 tool steel is given for comparison. The values given are approximate as variations can arise due to the particular form, composition, and directionality of the abrasive.

In lapping and polishing, it is essential that the abrasive grain is harder than the workpiece at the point of interaction. This means that the grain must be harder than the workpiece at the temperature of the interaction. As these local temperatures of short duration can be relatively high, the abrasive grains must retain hot hardness. This is true in all abrasive processes, without exception, because if the workpiece is harder than the grain, it is the grain that suffers most wear.

The hardness of the abrasive is substantially reduced at typical contact temperatures between a grain and a workpiece. At 1000°C, the hardness of most abrasives is approximately halved. Cubic boron nitride (CBN) retains its hardness better than most abrasives, which makes CBN a wear-resistant material. Fortunately, the hardness of the workpiece is also reduced. As can

**TABLE 1.1**
**Typical Hardness of Abrasive Grain Materials at Ambient Temperatures in GPa**

| | |
|---|---|
| Diamond | 56–102 |
| Cubic boron nitride (CBN) | 42–46 |
| Silicon carbide | ~24 |
| Aluminium oxide | ~21 |

*Source*: DeBeer, Internal Document.

be seen from Table 1.1, the abrasive grains are at least one order of magnitude harder than hardened steel.

The behavior of an abrasive depends not only on hardness but also on wear mode. Depending on whether wear progresses by attritions wear, microfracture, or macrofracture, will determine whether the process remains stable or whether problems will progressively develop through wheel blunting or wheel breakdown. This range of alternatives means that productivity is improved when lapping and polishing slurries are best suited for the particular lapping and polishing purpose.

## 1.3 PROBLEM SOLVING

Few readers have time and fortitude to read a handbook from the beginning to end. Although much could be learned from such an approach, readers are encouraged to cherry-pick their way through the most appropriate chapters. Most readers are busy people who want to solve a problem. The handbook is therefore structured to allow individual areas of interest to be pursued without necessarily reading chapters consecutively.

Chapter 2 is a general presentation on fundamentals of lapping, which includes process mechanism and subsurface damage, removal system, tool specification, lapping with planetary kinematics, and lapping models and simulation. Chapter 3 provides a general view of lapping of ductile materials and the objective of Chapter 4 is lapping of brittle materials with an extensive case study. Chapter 5 deals with the hardware of the lapping process, mainly the lapping machines.

Chapter 6 is dedicated to polishing technologies including polishing principles, polishing accuracy, and polishing machines together with various polishing methods. Chapter 7 presents the relatively new chemical mechanical polishing (CMP) method and its application in semiconductors manufacturing technology.

The authors draw on industrial and research experience, giving numerous references to scientific publications and trade brochures wherever appropriate. Readers will find the references to the various manufacturers of machine

tools, auxiliary equipment, and abrasives a useful starting point for sourcing suppliers. The references to scientific publications provide an indication of the wide scope of research and development in this field around the world.

## REFERENCES

Alden, G.I., Operation of grinding wheels in machine grinding, *Trans. ASME*, 1914, 36, 451–460.

CIRP, *Dictionary of Production Engineering II—Material Removal Processes*, Springer, Heidelberg, 2005.

Czichos, H., *Tribology—A Systems Approach to the Science and Technology of Friction, Lubrication and Wear*, Elsevier, Amsterdam, 1978.

Guest, J.J., *Grinding Machinery*, Edward Arnold, London, 1915.

HMSO, Lubrication (Tribology) Education and Research (Jost Report), Department of Education and Science, London, 1966.

Marinescu, I.D., Rowe, W.B., Dimitrov, B., and Inasaki, I., *Tribology of Abrasive Machining Processes*, William Andrew Publishing, Norwich, NY, 2004.

Rowe, W.B., Li, Y., Inasaki, I., and Malkin, S., Applications of artificial intelligence in grinding, *Ann. CIRP, Keynote Paper*, 1994, 43(2), 521–532.

Rowe, W.B., Statham, C., Liverton, J., and Moruzzi, J., An open CNC interface for grinding machines, *Int. J. Manuf. Sci. Technol.*, 1999, 1(1), 17–23.

Woodbury, R.S., *History of the Grinding Machine*, MIT Press, Cambridge, MA, 1959.

# 2 Fundamentals of Lapping

*Eckart Uhlmann*

## CONTENTS

2.1 General Considerations ..... 9
2.2 Historical Development of Lapping ..... 9
2.3 Definition of Lapping and Classification of Lapping Processes ..... 12
2.4 Process Mechanisms and Subsurface Damage in Lapping ..... 15
2.4.1 Material Removal and Grain Engagement Mechanisms in Case of Ductile Materials ..... 16
2.4.2 Material Removal and Grain Engagement Mechanisms in Case of Brittle-Hard Materials ..... 17
2.4.3 Influence of the Specification of the Lapping Abrasive on the Grain Engagement and on the Material Removal ..... 21
2.4.4 Subsurface Damage ..... 22
2.5 Lapping Process as a Removal System ..... 24
2.5.1 Removal System ..... 24
2.5.2 Subsurface Stress ..... 25
2.5.3 Surface Formation ..... 25
2.5.4 Subsurface Damage ..... 25
2.5.5 Parameters of the Removal System ..... 26
2.5.6 Subsurface-Related Work Result ..... 27
2.5.7 Process Parameters of Lapping ..... 27
2.5.8 Formation of the Removal System ..... 27
2.5.9 Working Gap ..... 29
2.6 Tool Specification ..... 29
2.6.1 Lapping Tools ..... 29
2.6.2 Lapping Wheels ..... 31
2.6.3 Slurry ..... 31
2.6.4 Lapping Medium ..... 32
2.6.5 Lapping Abrasives ..... 32
2.6.6 Process Grain Size Distribution ..... 33
2.7 Machine Settings ..... 34
2.7.1 Engagement Pressure ..... 34
2.7.2 Process Kinematics ..... 34
2.8 Fundamentals of Planetary Kinematics ..... 35
*Thomas Ardelt*

2.8.1 Definition ..... 35
2.8.1.1 Macrokinematics ..... 36
2.8.1.2 Path Curve ..... 36
2.8.1.3 Path Movement ..... 37
2.8.1.4 Cycle and Part Cycle ..... 37
2.8.1.5 Microkinematics ..... 37
2.8.2 Geometrical and Kinematical Parameters of the Relative Movement ..... 37
2.8.3 Calculation of Path Curves and Movements ..... 39
2.8.3.1 Path Curve ..... 40
2.8.3.2 Path Velocity ..... 40
2.8.3.3 Path Acceleration and Scalar Acceleration ..... 41
2.8.3.4 Path Curvature ..... 41
2.8.4 Description of the Movement Pattern by Means of the Rotational Speed Ratio ..... 41
2.8.4.1 Definition of the Rotational Speed Ratio ..... 41
2.8.4.2 Kinematical Parameters ..... 42
2.8.4.3 Possible Path Movements ..... 44
2.8.4.4 Determination of the Path Pattern of a Workpiece Point ..... 46
2.8.4.5 Progression of the Path Velocity ..... 48
2.8.5 Calculation of the Path Length Distribution over the Lapping Wheel Radius ..... 49
2.8.5.1 Profile and Grain Wear during Machining ..... 49
2.8.5.2 Description of Workpiece Geometry by the Geometric Function ..... 50
2.8.5.3 Path Length Distribution ..... 51
2.8.6 Cutting Conditions in the Case of One-Sided and Two-Sided Machining ..... 54
2.9 Process Models and Simulation ..... 57
2.9.1 Process Model According to Imanaka ..... 58
2.9.2 Process Model According to Chauhan et al. ..... 59
2.9.3 Process Model According to Buijs and Korpel-van Houten ..... 61
2.9.4 Summarizing Assessment of Process Models According to Imanaka, Chauhan et al., and Buijs and Korpel-van Houten ..... 62
2.9.5 Process Model According to Engel ..... 63
2.9.5.1 Model Boundary Conditions and Validity Limits ..... 63
2.9.5.2 Tool Formation ..... 64
2.9.5.3 Tool Engagement ..... 67
2.9.5.4 Model Verification ..... 70
2.9.6 Process Model According to Evans ..... 72
*Uwe Heisel*
2.9.7 Process Model According to Heisel ..... 73
*Uwe Heisel*

Symbols and Abbreviations ..... 81
References ..... 85

## 2.1 GENERAL CONSIDERATIONS

Lapping is the finest machining method that allows very high surface qualities, form accuracies, and very close dimensional tolerances. Lapped surfaces are flat-lustrous and are characterized by isotropic properties. The specific surface structure of lapped surfaces offers an especially good basis for polishing [1–3].

Nearly all materials can be lapped, which are not subject to plastic deformation due to their own weight or to mechanical load by machining: metals, nonferrous metals, insulating materials, glass, natural materials such as marble, granite, basalt, gemstones of all kinds, plastics, semiconductors such as silicon, germanium, and materials like carbon and graphite. A uniform material removal is also guaranteed in the case of machining compound materials.

The spectrum of parts comprises small fragile parts of a thickness of 0.1 mm up to big machine parts of 800 mm circumference diameter and 500 kg workpiece mass.

The following characteristics of lapping are to be emphasized [1,4]:

- There are hardly any restrictions with respect to the material and workpiece size.
- Machined surfaces have no directional machining marks. Lapped surfaces have characteristics, which are independent of direction.
- Workpieces are carried without stress. Therefore, the costs of the devices are very low. Changeover times are very short.
- During lapping, the machining temperatures and forces are low. Thus, there is no heat or stress distortion in the case of lapped surfaces.
- Only simple geometries can be lapped.
- There is high grain consumption during lapping.

The parts must be cleaned due to the strong dirt development through the slurry. The slurry has to be disposed of as hazardous waste.

- Removal rates during lapping are relatively small compared with those of machining with bound grain.

## 2.2 HISTORICAL DEVELOPMENT OF LAPPING

Lapping is one of the oldest machining processes. As early as in the Stone Age, workpieces and equipment were lapped: holes were worked into them by twisting a stick sprinkling sand in between. Excavations and research lead to the draft of such a lapping machine, shown in Figure 2.1 (Deutsches Museum in Munich, Germany) [4].

The principle of lapping can be understood on the basis of the draft. The lapping process is a result of the interaction of rotational friction, velocity, load,

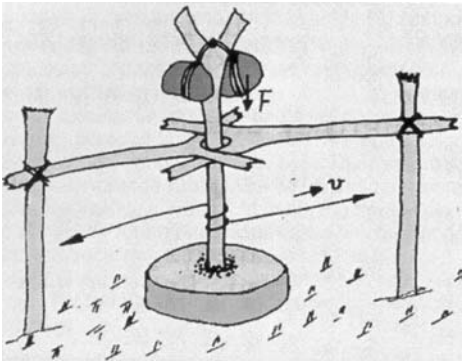


**FIGURE 2.1** Principle of the lapping process (draft from the Deutsches Museum in Munich, Germany). (From Stähli, A.W., *Die Läpp-Technik*. Firmendruckschrift der A.W. Stähli AG, Pieterlen, Schweiz, 2001.)

addition of abrasive grains, and liquid. Already in that time, the material removal could be influenced by the material of the tool, the grain (hardness and shape), the velocity of the tool (friction velocity), the fluid added (e.g., water), and the selectable load (stone weights) of the tool or the workpiece (surface pressure).

The draft of a face lapping machine in Figure 2.2 was made by Leonardo da Vinci [5]. This kinematical concept from the year 1493 was only recognized as applicable in the 1950s and is still being used in face lapping machines [6].

Often, extreme quality requirements as in the case of gauge blocks can only be met by lapping. Figure 2.3 shows a sewing machine converted into a single-wheel lapping machine with vertical wheel arrangement. The Swede C.E. Johannsson (1864–1943) produced the first parallel gauge blocks on this

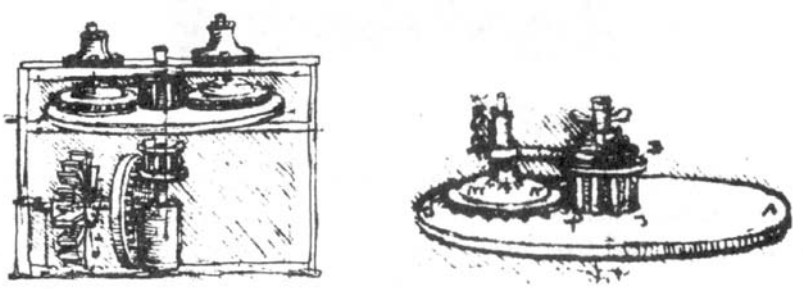

**FIGURE 2.2** Concept by Leonardo da Vinci around 1493 of a face lapping machine with externally geared operator-controlled workpiece holders. (From Da Vinci, L., *Codices Madrid I. Tratado de Estatica y Mechanica en Italiano*. Faksimile-Ausgabe, S. Fischer Verlag, Schweiz, 1974.)

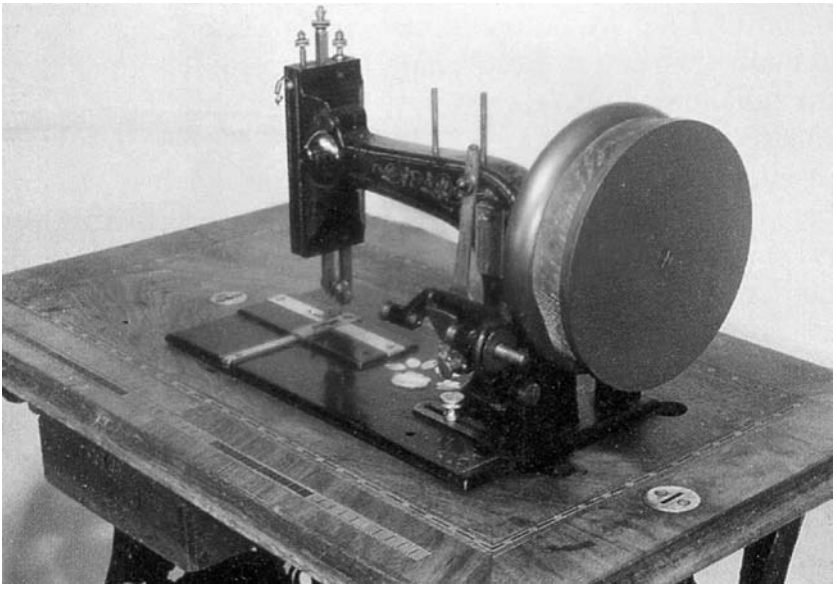

**FIGURE 2.3** Single-plate vertical lapping machine with spindle and drive from a sewing machine. (From Häuser, K., *Werkstatt und Betrieb*, 121(8), 677, 1988.)

machine manually, which could be adhesively wrung. The tolerance of the manufacturing result was 0.1 μm [7].

The machining with loose grain has been often replaced by machining with bound grain since the 1990s. This particularly applies to plane-parallel machining on double-wheel machines. The use of grinding wheels of the finest grains on double-wheel machines was mentioned as early as 1932 [8]. First reports on the embedding of abrasive grains in metallic wheels originate from the 1930s. The main advantages of grinding in contrast to lapping are the achievement of higher time-related workpiece height reductions and the use of cooling lubricants instead of the slurry. The achievable work results in terms of surface quality and evenness are similar to those of lapping. The formed surfaces, however, have clear grinding marks in different directions. A substitution is only reasonable, if the surface structures achieved by lapping are no target criterion for the machining. Higher relative velocities and the use of higher machining pressures require stiff machines with high-capacity drives. Temperatures higher than during lapping require the cooling of the grinding wheels and the tempering of the cooling lubricant.

New, difficult-to-cut materials place high demands on the manufacturing technology. Thus, lapping is still used if no economical machining is possible with other manufacturing methods. Examples are the machining of ceramics, glass, monocrystals, or reinforced materials [3].

## 2.3 DEFINITION OF LAPPING AND CLASSIFICATION OF LAPPING PROCESSES

Like grinding with rotating tool, abrasive belt grinding, grinding by linear cutting, honing, blasting, and free abrasive cutting, lapping belongs to the group of cutting with geometrically undefined cutting edges according to DIN 8589 (Figure 2.4). In contrast to grinding and honing, the cutting edges in lapping are formed by loose abrasive grains. The group of cutting with geometrically undefined cutting edges belongs to the main group cutting [9].

According to DIN 8589 part 15, lapping is defined as a cutting process with loose abrasive grains dispersed in a paste, which is guided on the lapping tool with nondirectional paths [10]. Basically, all lapping processes can be divided into the two main groups lapping with and lapping without shape-transferring counterpart. Lapping without shape-transferring counterpart is used if only the surface is to be improved without considering the form and geometrical accuracy [3].

During lapping with a shape-transferring counterpart, workpiece and counterpart glide on each other with continuous change of direction and with loose grain dispersed in a liquid between them. The single lapping grains engage temporarily and stochastically due to the lapping pressure transmitted by the counterpart leading to material removal.

According to the classification surface to be generated, type of surface, kinematics of the cutting process, and tool shape (profile), the following process variants can be distinguished [10].

Figure 2.5 shows the face lapping processes. Surface lapping is the lapping of an even surface of single and mass parts for the generation of high-quality surfaces in terms of evenness and surface roughness. Mainly

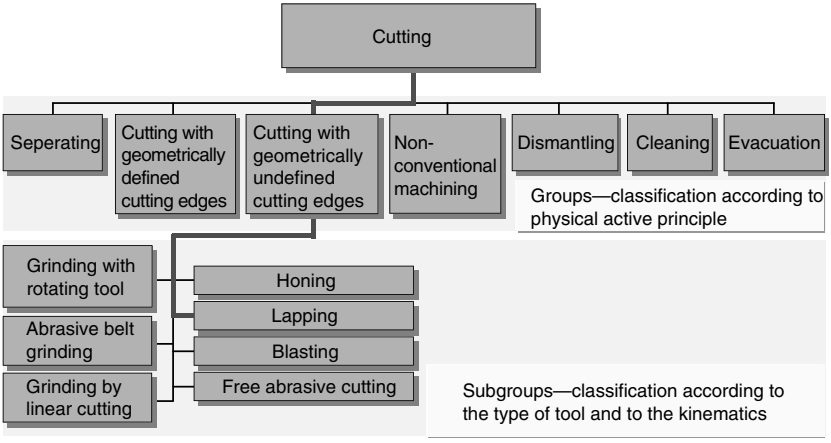


**FIGURE 2.4** Placement of lapping in DIN 8589 part 15.

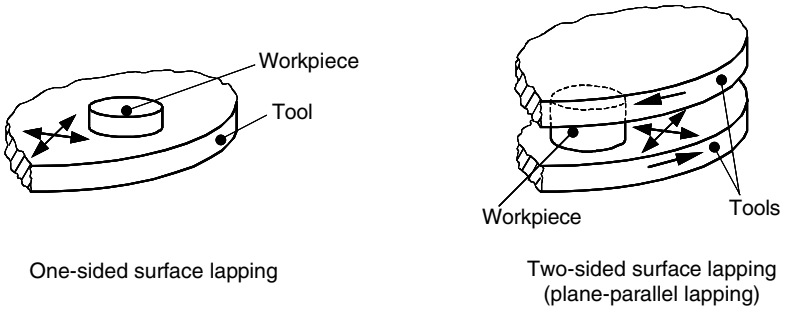


**FIGURE 2.5** Surface lapping according to DIN 8589 part 15.

single-wheel lapping machines are used for this purpose. Workpieces vary from small sealing washers to cylinder head faces in combustion engines. In plane-parallel lapping, two parallel even surfaces are simultaneously lapped. Very good evenness and high-plane parallelities can be achieved. The dimensional variability within one batch (up to 100 parts can be machined at the same time) and dimensional tolerances from batch to batch are very small. Among different lapping processes, plane-parallel lapping is the most widespread lapping process.

Cylindrical lapping is lapping with the aim to generate or improve cylindrical surfaces. Figure 2.6 shows the process variants. External peripheral cylindrical lapping is the lapping of an external cylindrical contour by means of a sleeve enclosing the workpiece. In external cylindrical face lapping, the workpieces are guided radially in a workpiece holder on a double-wheel lapping machine. The workpieces roll between the two lapping wheels with an eccentric movement. This process is used for the production of accurate cylindrical shapes and high surface qualities. Valve pins for injection pumps, high-precision carbide tools, and hydraulic pistons can be named as few examples. Internal cylindrical peripheral lapping is the lapping of internal

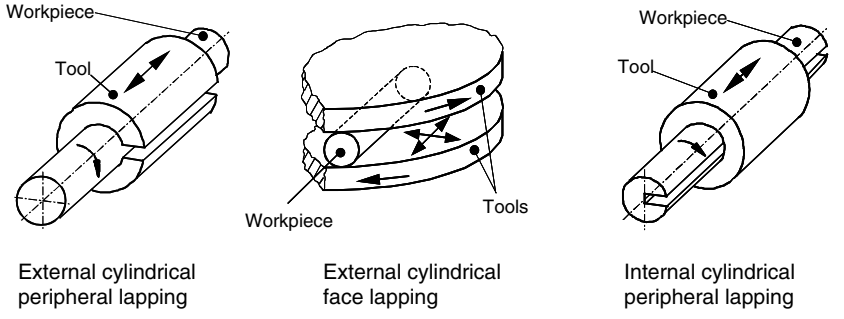


**FIGURE 2.6** Cylindrical lapping processes according to DIN 8589 part 15.

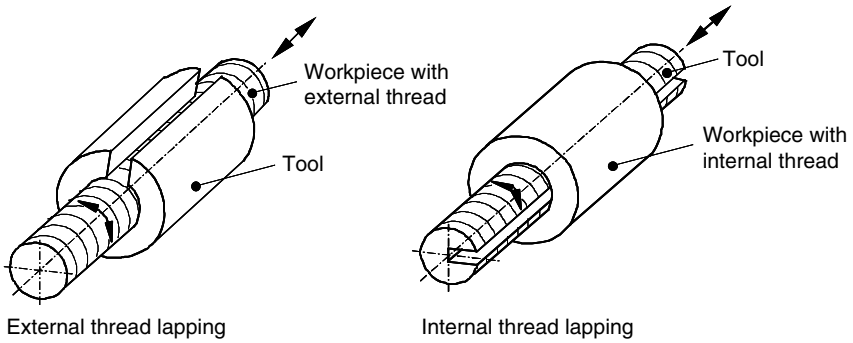


**FIGURE 2.7** Thread lapping processes according to DIN 8589 part 15.

cylindrical surfaces by means of a cylindrical lapping tool carrying out a combined rotational and traverse motion. The workpieces have to be prehoned or preground. Typical examples for this machining are cylinders for injection pumps, hydraulic cylinders, and high-precision machine components with precision turned or reamed surfaces.

Thread lapping (Figure 2.7) is the lapping for the improvement of thread surfaces. External thread lapping is the lapping of external threads, the shape-transferring counterpart (tool) being shaped like a screw nut. In contrast, the shape-transferring counterpart in internal screw lapping is shaped like a screw.

Lapping for the improvement of pitch surfaces by a rolling process is called roll lapping. Figure 2.8 shows the example of lapping of gear teeth.

In profile lapping, a lapping tool is used, which is profiled according to a target shape. Figure 2.9 shows spherical lapping and conical lapping as examples. Spheres can also be lapped on double-wheel lapping machines. The upper lapping wheel is even, and on the lower wheel, there is a semicircular groove. Through the permanently changing direction of movement, the shape of the sphere as well as of the groove are improved [3,4].

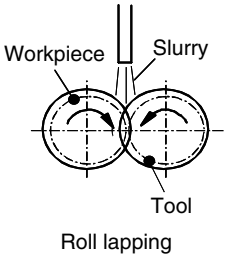


**FIGURE 2.8** Roll lapping at the example of lapping of gear teeth according to DIN 8589 part 15.

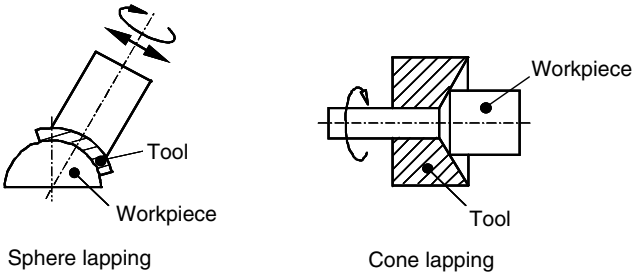


**FIGURE 2.9** Sphere and cone lapping as examples of profile lapping according to DIN 8589 part 15.

Additionally to the above-mentioned lapping processes, the following special processes are to be mentioned [3,10].

Ultrasonic-assisted lapping is suitable for three-dimensional forming of brittle-hard materials such as ceramics and carbides. The shape-transferring counterpart oscillates with ultrasonic frequency, and induces the impulsive engagement of the abrasive grains in the working gap.

Pairwise lapping of workpieces for the adjustment of form and geometrical diversions of assigned workpiece surfaces is called lapping-in. In this case, the workpieces serve as shape-transferring tools. The lapping-in of gear pairs or the lapping-in of bearing pins and bearing shells or the lapping-in of valve seats in automobile engines are common examples of this process.

Lapping with a grain guided by a liquid jet for the improvement of surface properties is called vapor lapping. The lapping slurry is blasted with high speed onto the workpiece. There are uniform machining marks on the surface, whose structures depend on the blasting abrasive used. No shape improvement can be achieved by this process [11].

Dip lapping aims exclusively at surface improvement. On the machined surfaces, there are nonuniform, straight, or crossed groves. Workpieces of any shape are dipped into a flowing slurry [12].

## 2.4 PROCESS MECHANISMS AND SUBSURFACE DAMAGE IN LAPPING

During lapping, material removal takes place by lapping grains dispersed in a watery or oily liquid. The shape to be generated is transferred to the workpiece by shape-transferring counterparts. Hereby, different kinds of material removal can be distinguished. Material removal by cutting, microfusion processes, and material removal by microdeformation or by the induction of microcracks are to be underlined. The effective principles during material removal and grain engagement mechanisms are partially contradictory.

### 2.4.1 Material Removal and Grain Engagement Mechanisms in Case of Ductile Materials

As early as the 1920s, deliberations were made on the removal mechanisms during the machining of metals. The theory of Beilby [13], an English metallographer, describes material that melts partially for a short time, flows into the grooves on the surface and solidifies amorphously. This theory was considered undisputable for metallic surfaces. Lichtenberger [14] later restricted the formation of Beilby layers to the lapping of metallic materials with the use of lapping abrasives of small grain size (graining > F 1000) and grain strength.

In the 1940s, Bornemann [15] postulated a rolling and a crushing movement behavior of lapping grains. In contrast, it was assumed in the 1950s and 1960s that the lapping grains are temporarily fixed in the surface of the active partners if under load. This results in an abrasive effect on the tool and a cutting effect on the workpiece [16–24]. Lichtenberger [14] derived from this possibility of a permanent reengagement of the lapping grains in altered position and orientation that polydirectional cutting edge wear must occur. The lapping grains blunt with increasing lapping time and break into small sharp-edged lapping grains capable of cutting as a result of the lapping pressure or of the increase of the shear force linked to it. The lapping pressure is distributed to a higher number of lapping grains so that the depth of indentation of the lapping grains decreases. This leads to improved surfaces on the workpiece.

According to Bödrich and Enger [16], the roughness of the lapping wheel, the effective grain height, and the roughness of the workpiece have to be set in relation with each other for the engagement of a grain. Grain engagement takes place if the sum of the three values exceeds a certain quantity.

Among others, Fischer [25–27] describes that there can be a rolling motion alongside the Beilby-layer formation and the temporary anchoring of lapping grains in the workpiece surface. According to this idea, the tips of the grains indent the surface in a wedge-shaped way and blast off microchippings. Thus, all the three removal mechanisms occur parallel to each other.

Due to the small indentation depth of the lapping grains in the workpiece, a chip-forming removal mechanism is being disputed by some scientists [28–31]. Martin [29,30] was able to experimentally prove a rolling grain movement during lapping on the basis of model lapping tests on polished metal surfaces. Based on scanning electron microscopy (SEM) images, he proved that lapped surfaces have no directional marks. This led him to the hypothesis of a pure rolling movement of the lapping grains between the effective surfaces. The grains are pushed with their tips into the material and leave crater-shaped plastic marks. The great number of lapping grains causes a deformation of the material on its surface, which, according to the Hall–Petch relation, provokes surface strengthening [32]. If the deformation resistance

(increasing with the strengthening) exceeds the cohesive resistance of the material, small, slab-shaped material particles break off of the surface [25,26,33,34]. Later, the basis of this theory was approved through investigations by Özhan [35]. It was proved that for stretched, schist-shaped grains the grain tips are able to carve small particles out of the material during further rolling.

According to Kling [36,37], a cutting effect of the lapping grains is supported by the following factors:

- High loads per lapping grain
- Soft lapping wheel material
- Grain shape of small compactness
- Small concentration of lapping abrasive
- Low viscosity of the slurry

Opposite boundary conditions, however, benefit the rolling of the lapping grains.

Deviant from the three above-mentioned material removal theories, Grünwald and Jaksch [38] transfer the fundamentals of wear research to the lapping process [23,39,40]. In analogy to the five basic types of surface destruction through frictional connections [41], they interpret the material removal process in terms of a material abrasion provoked by elastic and plastic deformations, cutting processes, and cold welding in special cases. On the basis of a grooving deformation of the material, there is a smearing of plastic groove edge material through superposition of lapping grooves. The cracks developing in the subsurface overlap with fatigue cracks in the base material. Further cracks under the surface developing through inner friction lead finally to its destruction.

### 2.4.2 Material Removal and Grain Engagement Mechanisms in Case of Brittle-Hard Materials

The material removal during the lapping of brittle-hard materials such as ceramics, glass, as well as monocrystal materials like silicon is different from that of ductile materials. In the case of these materials, the removal is based on the generation, propagation, and networking of microcracks, which accrue due to the stress fields induced in the material. The superposition of the crack systems generated below the grain cutting edges as a result of the engagement of a number of grains in the lapping process effects the measurable material removal through material break off and finally leads to the typically dim, isotropic appearance of the lapped surface [42–60].

The type, size, and shape of the developing crack system depend on the induced contact stress field. It is basically determined by the geometry of the indenter and by the material properties like Young's modulus, hardness,

and fracture toughness [61]. In the case of monocrystal materials, further important aspects are their anisotropy and the position of the gliding system in relation to the surface. The generation of microcrack systems was investigated on the basis of indentation tests on a number of brittle-hard materials.

The stressing of brittle-hard materials with blunt indenters leads to a purely elastic contact case, inducing a Hertzian stress field below the contact area [47,51,61–63]. Due to the tensile stresses, a stable ring crack is generated next to the contact zone. With continuous stress, it grows to a conical crack along the tensile stress field, which quickly decreases deeper below, in an angle of 68° to the direction of stress. From a critical load on, the conical crack grows in an unstable way, forming the Hertzian cone crack, which closes after unload [47,61]. The typical load case is the load of an even, elastic sample with a hard spherical indenter [61].

The stressing of brittle-hard materials with sharp indenters leads to an elastic–plastic contact case. There is a superposition of an expanding plastic cavity (as a result of the hydrostatic stress condition below the indenter) with a Boussinesquian stress (as a result of the stress of an elastic half-space by a punctual load) [47,48,61,63–65]. Lawn et al. and Marshall et al. provided a fundamental description of the procedure of crack formation on the basis of their investigations with soda-lime glass [64,65]. From a critical load on, incipient cracks become unstable in the boundary of the plastic zone and grow to circular axial cracks below the surface along the axial tensile stress levels. The axial cracks grow with increasing stress. Their propagation is provoked by the tensile stress field developing upon the elastic stress of the surface. In case of unload, they spread up to the surface; in case of complete unload, they appear as half-penny-cracks. Radial cracks occur during unloading along incipient cracks at the boundary of the plastic zone. They diffuse due to the residual stress field, which arises from accommodation of the impression volume by expansion of the deformation zone against the constraining elastic matrix. The lateral cracks below the plastic zone also arise during the unload cycle. They diffuse with progressing unload [47,61].

The above-described sequence of crack formation is not considered universal any more [47,61]. It is undisputed that half-penny-cracks develop after unload. It is often obscure whether they develop through the progression of the axial cracks to the surface or through the progression of the radial cracks into the depth, or through the combination of both crack types. Lateral cracks can develop below the plastic zone (deep lateral cracks) or at the edges of the indentation (shallow lateral cracks). Then, they diffuse nearly parallel to the surface. Also, it could be observed that radial and lateral cracks develop during the stress phase [47]. The crack types and sequence of cracks depend on the material, the environmental conditions, the indenter, and the height of the load [47].

On the basis of short-time lapping tests on polished glass surfaces, Phillips et al. [56] proved a conformance of the indentation morphologies, which had been caused by the single grains of the lapping abrasive or by Vickers indentation tests. Meanwhile, it is generally accepted especially in recent publications that the grains of the lapping abrasive are in elastic–plastic contact to the material surface during the lapping of brittle-hard materials, thus inducing an axial–radial–lateral crack system [44–48,50,52–54,56].

The elementary process of chip formation is the diffusion of lateral cracks to the surface of the workpiece [45,47,48,56,66]. While it is assumed that deep lateral cracks develop in this process, Cook and Pharr show on the basis of indentation tests on glass and ceramics that the formation and propagation of shallow lateral cracks must be considered a basic material removal mechanism [47]. In contrast, Engel [49] concluded from the results of his indentation tests on silicon that the surface formation leading to material removal takes place through the formation and propagation of shallow as well as deep lateral cracks. Material particles are removed through the propagation of lateral cracks to the surface.

Alongside the material removal mechanisms, also the grain movements were analyzed and the parameters of the grain engagement during the lapping of brittle-hard and monocrystal materials were investigated.

As early as 1966, Imanaka [51] described that the relation of the force input remains always the same compared to the size of the shell-like chippings, independently of the fact whether the grains involved are rolling or scratching. Experiments with single grains showed that the contact surface of the workpiece is always circular independent of the grain shape (pyramid, conical, or spherical). There is purely an elastic contact.

According to Wiese and Wagner [67], the lapping grain rolls over the surface of the workpiece provoking a local stress at a contact point between the grain and the workpiece. It is assumed that the lapping grain only provokes material removal if it gets caught in the lapping wheel and then contacts the workpiece. For the statistical evaluation of the grain engagements, a model was developed, in which material break off only takes place if there is an adjacent crack. If this condition is met, a correlation can be realized between the force acting on the grain and the amount of the material break off.

Among others, Phillips [56] carried out a detailed investigation on the grain engagement during the lapping of glass. Based on the experimentally determined relation between indentation frequency and material removal rate as well as measurements of the friction coefficient during lapping, they formulated a rotational–indentation model of the abrasion. The grains of the lapping abrasive first get caught in a certain angle between the rough patches of the workpiece and the lapping wheel, are stressed, and rotate due to the relative movement between the lapping wheel and the workpiece around a

certain value. During the rotational cycle, the normal force transmitted to the grain grows to a maximum (until the grain is in an upright position) and decreases during further rotation of the grain until its unload. Thus, this model contradicts the principles of rolling grain movement. After its unload, the grain is not moved any more by the workpiece and the lapping wheel.

In their experiments on lapping of glass, Buijs and Korpel-van Houten [45,46] also stated a rolling grain movement. At the same time, however, they observed grains being caught in the lapping wheel. The evaluation of their graphical material resulted in a small ratio of scratches and plastic deformations on the surface. They explained the grain engagement as follows: during the rolling motion, the grain tips are pushed into the material, thus forming a plastic zone underneath the indentation. Based on this zone, lateral cracks develop, which provoke shell-like particle break offs. There is always a constant number of grains engaged in the working gap.

Chauhan et al. [48] concluded from investigations on lapping of ceramics that the lapping grains between the lapping wheel and the workpiece do not roll permanently but indent the workpiece due to anchoring in the lapping wheel. After lapping, the surfaces have mainly slab-like break offs and plastic scratches. After the break offs, however, surface cracks much more; they interpreted the processes as quasistatistical: the grain gets caught first in the lapping wheel, then indents the surface of the workpiece, leads there to material break off, and leaves the lapping gap.

When lapping monocrystal materials like silicon, it is especially important that the temporary anchoring of grains in the lapping wheel and the resulting scratching grain engagement are avoided [57,58,68]. Scratching grain engagement leads to scratches and other faults on the wafer surface and the subsurface below it.

In lapping model tests on silicon, however, Engel [49] could exclude a purely rolling movement of the grain. He describes the grain engagement mechanism as follows: the grains are transported by flow conditions in the lapping gap, which result from the relative movement and the superimposed normal force. Due to this and other principles, the grains hit the protuberances of the lapping wheel (and/or of the workpiece) and get caught in them. Thus, a force acting mainly tangentially to the surface is transmitted to the grain, as a result of which the grains scratch the surface of the workpiece material. Simultaneously to an increase of the depth of scratch of the radial scratches, the resistance of the material to plastic deformation increases, leading to an erection of the grain above its maximum grain diameter. From a certain depth of scratch on, the material is not capable of plastic deformation any more. With a growing normal grain force component, there is brittle crack formation with subsequent break off. All observed break offs are to be assigned to the half-penny-lateral-crack system for the pressing of solid bodies into brittle materials on the basis of the Boussinesquian stress states below the surface.

### 2.4.3 Influence of the Specification of the Lapping Abrasive on the Grain Engagement and on the Material Removal

The specification of the lapping abrasive has essential influence on the parameters of the grain engagement and the mechanisms of material removal. The lapping abrasive is basically characterized by grain type, grain shape, grain size distribution, and its wear behavior [1,2,59,69,70].

The danger of scratches through scratching grain engagement grows with the use of harder and sharp-edged lapping abrasives. The reason is the lighter temporary anchoring of the hard, sharp edged, mostly needle-shaped grains in the lapping wheel [57,68,71–74]. During investigations on lapping and lapping–polishing with diamond grainings, it was shown that blocky grainings with a tight grain size distribution are best suited for the avoidance of scratches [71,74,75].

The special significance of the parameters of the grain size distribution of the lapping abrasive on the grain engagement parameters and the work result of lapping is emphasized in several experimental works [16,45,46,48,51,74,76]. The number of the active grains is determined by the average grain size and the standard deviation of the grain size distribution of the lapping abrasive. This leads to the single grain normal force of the individual lapping grain. This is the force the grain acts on the material in the moment of engagement. Thus, together with the material removal mechanisms effective in lapping, the achievable surface roughness and material removal rate are defined.

During the lapping process, the lapping abrasive is being worn due to grain splintering and grain breakage. As a result of the high wear of large single grains, grain breakage leads to a decrease of the average grain diameter and the spread of the grain size distribution of the lapping abrasive, and thus to reduced single grain normal forces until there is a stationary condition in the working gap [76–78]. Due to grain breakage, the number of active grains grows. This leads to reduced damaging of the surface without causing a lower material removal rate. The experimental results show a decrease of roughness at simultaneously growing material removal rates with increasing lapping pressure [76].

The behavior of grain breakage is significantly influenced by the type, size, and shape of the grains [24,59,71,79,80]. The description of the wear behavior of the graining in the lapping process merely by material parameters like hardness or the elasticity module is insufficient. Therefore, test methods were developed for the verification of the suitability for lapping, in which the lapping process is imitated under standard conditions [24,80].

Stotko [24] and Pahlitzsch [80] hereby determined a reduction of the active grain size depending on the grain specification, the test method, and the settings. Stotko developed the quality parameter of the effective grain size for standardized control conditions. Not only infeed force and test length, which depend on the graining, are defined as control conditions, but also the

grain size distribution of the lapping abrasive and the involved grain number. Thus, the application behavior of the graining can be determined depending on its mechanical properties and the grain size distribution as well as on the engagement conditions such as the number of active grains and lapping pressure per grain. Another possibility of verifying the suitability of the lapping abrasive under consideration of the wear of the lapping abrasive is the determination of the material removal rates in machining [79].

The control of the lapping abrasives is standardized especially for the requirements of the optical industry [81]. For the determination of the suitability for lapping and of the wear behavior of the lapping abrasive, a machining test is compulsory, which determines the so-called lapping performance, the class of cleanness (absence of scratches on the surface), and the decrease of the lapping performance through grain wear.

### 2.4.4 Subsurface Damage

The locally acting high forces and temperatures occurring during cutting processes affect the properties of the subsurface of a workpiece. The subsurface can be characterized by its structure, hardness, and state of stress. The investigations on the determination of residual stress states and hardness measurements on lapped metallic materials are partially contradictory. Based on residual stress progress in deeper material subsurface areas, conclusions can be drawn on the cutting behavior [35,82–88].

After the machining of manganese steel with $Al_2O_3$-lapping abrasive of a graining of F 800 with very low pressures of 0.05 and 0.45 $N/cm^2$, Letner and Snyder [86] prove isotropic residual compressive stress of an average of 700 $N/mm^2$. Already in a medium depth of approximately 5 μm, these were completely decayed. They traced the reduced marginal values and the increased deep effects of the residual stresses at higher loads back to a cutting material removal effect of the lapping grains.

Sridhar et al. [89] reported on a pressure increasing with the residual compressive stress and a parallel increased wear resistance of lapped high-speed steel surfaces. According to Matalin [90], the residual compressive stress in lapped carbon steel grows with increasing grain wear. In contrast, König [1] describes the advantages of lapping in residual-stress-poor machining.

While Kedrow [91] was able to completely remove by lapping the microhardness increase measured after the grinding of tempered steels, Özhan [35] stated a clear increase of microhardness through lapping of soft magnetic materials. The depth of the affected subsurface and the boundary hardness value depend on the size of the lapping grains as well as on the pressure. Rystsova et al. [87] detected an increase of microhardness with decreasing pressure stress in the case of steels of a hardness of 40 HRC. From this, they concluded an especially hardening effect of lapping grains loose at low pressure. In contrast, the lapping grains temporarily embedded in the tool

surface at high pressure have a cutting effect and are thus less hardening for the workpiece surface. Miller's [39] proposal contradicts this theory. He suggests reducing the pressure especially for the machining with smaller grainings (3 to 6 μm) in order to reduce the plastic deformation ratio.

Chandrasekar et al. [82,92] defined the residual stresses with brittle Ni–Zn–ferrite after lapping with diamond grainings of 3 μm. The residual compressive stresses determined at the surface were considerably higher than those achieved by grinding under equal conditions. At a depth of approximately 4 μm, the compressive residual stresses transcended into tensile residual stresses and decayed at a depth of approximately 15 μm.

The subsurface damage during the machining of monocrystal materials such as silicon deserves special attention. All mechanically induced deviations of the crystalline structure of the monocrystal subsurface from the ideal crystal structure are considered subsurface damage. These are for instance microcracks, dislocations, as well as residual stresses [55]. These subsurface damages are caused by the development of depth effecting stress fields as a result of the surface stress through grain engagement [50,59,93–95].

In the past, a number of investigations were carried out on the structure and the depth of subsurface damage of lapped silicon [26,50,57,58,60,94–98]. As early as in the 1960s, models were developed on the structure of subsurface damages [94,98], which are summarized in the damaged subsurface model by Mohr [50] and are still considered valid. However, detailed specifications on the technological dependencies of the depth of subsurface damage on the machining parameters are only rudimentary and mainly refer to the specification of the depth of subsurface damage of single machining parameters. Stickler and Booker [94] carried out detailed investigations of the subsurface damage during lapping with diamond grains (kerosene as lapping medium). According to their SEM and transmission electron microscopy (TEM) investigations, the damaged subsurface consists of single dislocation lines closely below the surface and dislocation and crack networks reaching deep below it. The dislocation and scratch networks are similar in the electron microscope and are therefore called dislocation cracks according to the terminology of Allen [99]. They develop due to very high short-time stresses as a result of the grain engagement. Thereby, cracks are induced, which recombine immediately after unload leaving behind atomic shifts, which finally cause dislocation networks. Some of the cracks do not cure completely leaving cracks near the surface, which decay in dislocation networks farther below.

By means of the traverse grinding method and subsequent structure etching, Pugh and Samuels [98] analyzed the structure of damaged subsurfaces of silicon samples machined in different ways. They found microcrack networks in the upper subsurface, which deeper below run out in dislocation networks. The microcracks are always bent and mostly to be found along the {111}-cleavage planes.

According to Mohr [50], the damaged subsurface is basically characterized by four layers: the polycrystalline zone, the crack zone, the transition zone, and the elastic strain zone. Structural faults like single dislocations are probable in all areas. Depending on the concrete machining conditions, the layer order of the damaged subsurface and the zone expansions may change.

Buck and Meek [96] presented the depth of damaged subsurface specifications of different authors available at that time. Their specifications refer to the fact that the depth of damaged subsurface values of lapping with equal grain sizes depend on the type of lapping abrasive, crystal orientation, and lapping medium, and are different for differing measuring methods.

According to Fischer [26], the depth of damaged subsurface resulting from lapping corresponds to the grain size of the lapping abrasive. The measurements of the depth of damaged subsurface with SIRD by Lundt et al. [97] showed a direct dependence of the depth of damaged subsurface on the grain size of the lapping abrasive.

Engel [49] carried out detailed investigations on grain engagement and subsurface damage on the basis of model lapping tests. The measuring results show that the depth of damaged subsurface increases due to the superposition of the single grain engagements. Thus, the superposition of the crack systems below the grain cutting edges leads to a superposition of the accompanying stress fields. A characteristic pattern of the depth of damaged subsurface was observed with increasing machining time for all lapping abrasives of a grain size above 5 μm. The grain shape or the mechanical properties of the investigated lapping abrasives had no influence on it.

## 2.5 LAPPING PROCESS AS A REMOVAL SYSTEM

In order to comprehend the lapping process, the knowledge of the interactions between the stress of the subsurface of the workpiece by tool engagement and the resulting surface formation and subsurface damage are indispensable. The removal system is defined for the accurate description of the relations and their basic mechanisms. It serves the description of the real procedures during the engagement of the tool in the workpiece and is explained with the following example of plane-parallel lapping as the most widespread lapping process.

### 2.5.1 Removal System

There are complex abrasive interactions between the tool and the subsurface of the workpiece in the real lapping process. These lead to surface formation through material removal and damage of the subsurface. As the processes of these interactions are similar to those in tribological systems, Engel [49] defined the lapping process as a forced material removal system. It was defined in analogy to the definition of the tribological system according to Pursche [100]. Due to the interactions of two system elements (tool, workpiece), the

removal system induces intended material loss (material removal) and unintended subsurface damage on the workpiece as well as unintended material loss (wear) on the tool.

With the help of the methodology of system analysis, the entirety of the parameters describing the abrasive interactions of the removal system can be classified [101]. According to this system, the subsurface damages of the workpiece and the tool wear are loss parameters. Material removal is a useful parameter. The function of the removal system is realized through the transformation over loss parameters into useful parameters. The removal system can be completely described through the following parameters [101]:

- Function (machining of the material)
- Abrasive stress (stress collective, duration and path)
- Structure (matching of active partners)
- Interaction of the active partners (contact conditions)
- Manifestation of material removal (surface formation and subsurface damage)
- Parameters of material removal (subsurface-related work results and material removal rate)

The mechanisms of surface formation and subsurface damage, which are induced by the tool–workpiece interactions, are thus defined system characteristics (Figure 2.10).

### 2.5.2 Subsurface Stress

In lapping, stress is induced to the subsurfaces of the workpiece through the engagement of the abrasive grains of the tool in the surface as a result of the simultaneous effect of the engagement pressure and the relative velocity of the tool and the workpiece. Grain engagement is the force driven indentation of a cutting edge in the subsurface of the workpiece material.

### 2.5.3 Surface Formation

The surface formation takes place through the material removal, i.e., chip formation on the basis of the overcoming of the chemical bonds in the material under the formation and propagation of microcracks.

### 2.5.4 Subsurface Damage

Subsurface damage is the formation of defect structures in the surface-near area of the workpiece due to the subsurface stress. With respect to the abrasive material removal, microcracks and dislocations are relevant types of defects.

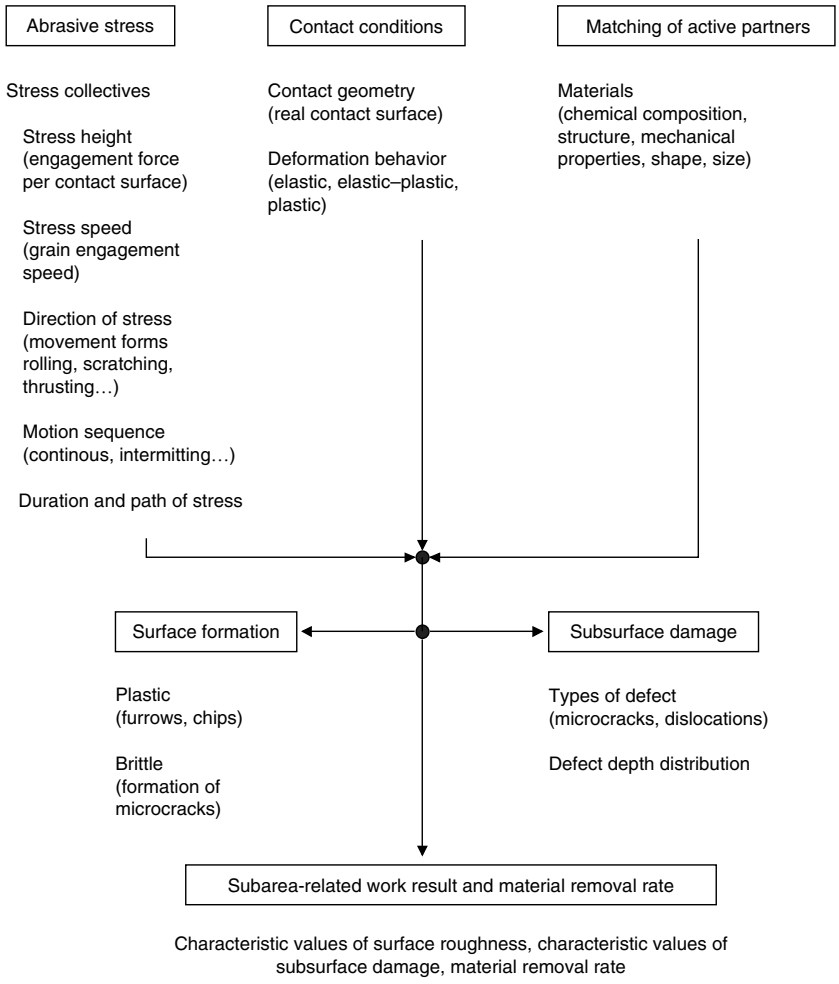
Abrasive stress
Contact conditions
Matching of active partners
Stress collectives
Stress height (engagement force per contact surface)
Stress speed (grain engagement speed)
Direction of stress (movement forms rolling, scratching, thrusting…)
Motion sequence (continous, intermitting…)
Duration and path of stress
Contact geometry (real contact surface)
Deformation behavior (elastic, elastic–plastic, plastic)
Materials (chemical composition, structure, mechanical properties, shape, size)
Surface formation
Subsurface damage
Plastic (furrows, chips)
Brittle (formation of microcracks)
Types of defect (microcracks, dislocations)
Defect depth distribution
Subarea-related work result and material removal rate
Characteristic values of surface roughness, characteristic values of subsurface damage, material removal rate

**FIGURE 2.10** Surface formation and subsurface damage as system characteristics. (From Pursche, G., *Oberflächenschutz vor Verschleiß,* Verlag Technik, Berlin, 1990.)

### 2.5.5 Parameters of the Removal System

Surface formation and subsurface damage are dynamic processes and are consequences of the abrasive stress of the subsurface through the cutting edges of the tool under certain contact conditions. In this sense, the parameters of the surface formation and subsurface damage are system parameters.

In lapping, the cutting edges and the workpiece surface are relevant active partners for the surface formation and subsurface damage. Both are defined by their chemical composition, structure, mechanical properties, as well as by shape and size.

The abrasive stress takes place according to the stress collective. It induces the engagement of the grain cutting edges in the workpiece subsurface with a certain stress duration or path. During lapping, the stress collective consists of stress level, stress speed, and stress direction as a result of the form of movement of the cutting edges and the type of the movement process. The constitution has a direct effect on the effective conditions of the active partners such as contact geometry or real contact surface of their deformation behavior. Thus, the stress level results from the engagement force of the grain cutting edges and the real contact surface. The engagement force consists of tangential and normal fractions. The proportion of the two partial engagement forces defines the direction of stress.

### 2.5.6 Subsurface-Related Work Result

In the lapping process as a removal system, the material removal is induced by the simultaneous stochastic engagement of a number of geometrically undefined grain cutting edges. The parameters of the surface formation and subsurface damage as well as the material removal rate are results of the superposition of the single engagements of the grain cutting edges. The surface roughness and the depth of the subsurface damage are caused by subsurface stress with certain contact conditions and matching of active partners. Therefore, they are called subsurface-related work result.

### 2.5.7 Process Parameters of Lapping

The lapping process is realized through the joint effect of the setting parameters as well as the tool and workpiece parameters under the formation of the removal system (Figure 2.11). The parameters of economic efficiency and the influencing of the tool and workpiece parameters directly affect the formation of the removal system.

Process parameters of lapping, which have only a direct effect on the formation of the removal system, are the parameters of lapping kinematics with the resulting form deviation of the lapping wheels and the shape and dimensional accuracy of the wafers. These parameters are marked with an asterisk (*) in Figure 2.11.

### 2.5.8 Formation of the Removal System

The removal system in the lapping process is formed by the interaction of the setting, tool, and workpiece parameters. The parameters of the removal system are influenced by the tool and workpiece-related result parameters, which, at the same time, are process parameters (Figure 2.11).

The removal system is influenced by the following parameters:

- Tool wear (especially the wear of the lapping abrasive)
- Surface quality (especially surface topography)

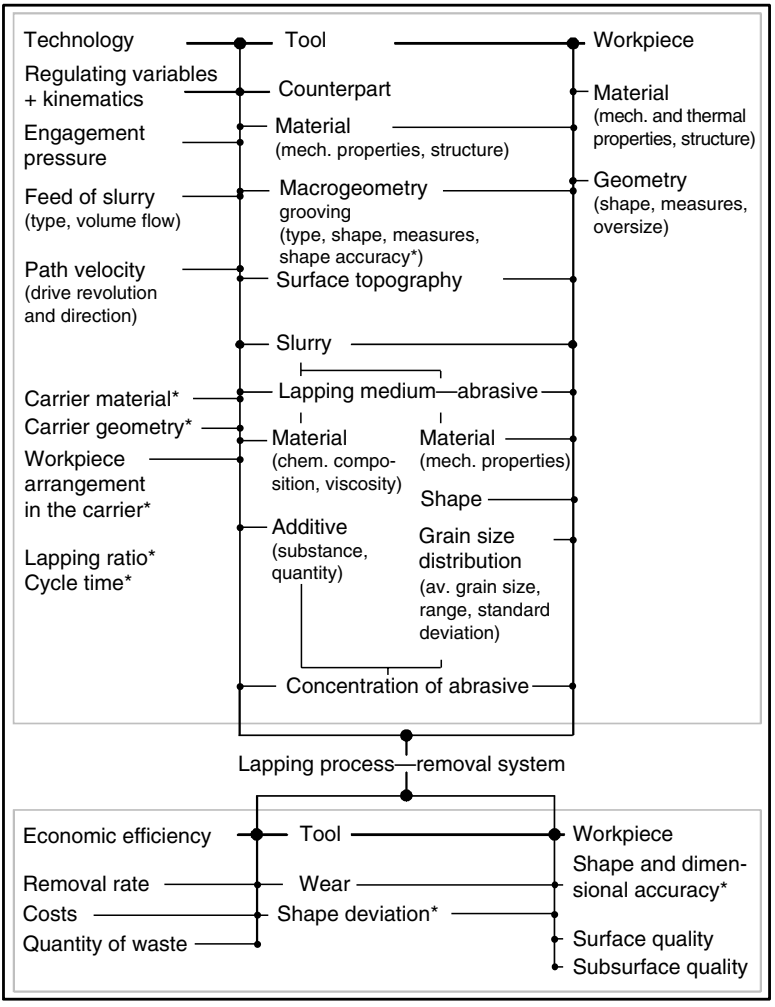


**FIGURE 2.11** Process parameters of lapping.

- Subsurface quality (especially the type and depth distribution of the damages)

Wear of the lapping abrasive and surface topography have a retro effect on the contact conditions, the stress collective, and the matching of the active partners (shape, size). The type and the depth distribution of the induced subsurface damages influence the system parameters, surface formation, and subsurface damage. Existing damages and the stress fields surrounding them are in permanent interaction with the damages and stress fields continuously generated through subsurface stress.

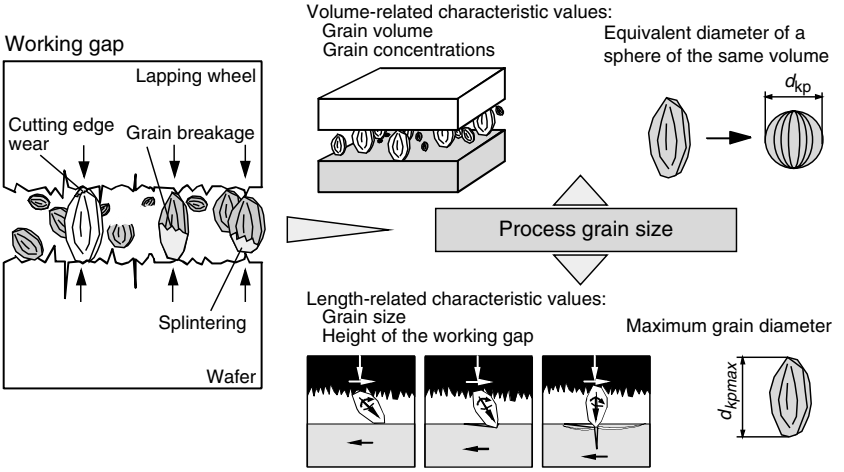


**FIGURE 2.12** Schematic representation of the working gap, the grain wear, and the grain parameters.

### 2.5.9 Working Gap

The removal system is formed in the working gap. The working gap is the space, which is opened up by the slurry between the surfaces of the lapping wheels and the workpieces (Figure 2.12).

## 2.6 TOOL SPECIFICATION

According to DIN 8580, tools are means of manufacture, which affect the generation or change of the shape and the position and sometimes the material properties of a workpiece through relative motion to it under energy transfer [102].

### 2.6.1 Lapping Tools

The lapping tool is formed during the process by the shape-transferring counterpart and the slurry (Table 2.1). In surface, plane-parallel, external cylindrical, and sphere lapping, and the lapping wheels constitute the counterparts. They carry the slurry, the workpieces, and in the case of surface lapping the dressing rings. In the following, the lapping tool and its components will be specified by the example of plane-parallel lapping as the most common lapping process.

The change of the shape, position, and the material properties (subsurface structure) of the workpieces are caused by the shape-transferring counterpart (the lapping wheels) and the slurry. The relative motion between tool and workpiece is generated by the restricted guidance of the workpieces in the

**TABLE 2.1**
**Tool Components and Their Characteristics in Plane-Parallel Lapping**

| Counterpart | | Slurry | | | |
|---|---|---|---|---|---|
| **Lapping Wheel** | | **Lapping Medium** | | **Lapping Abrasive** | |
| *Material*: mechanical properties, structure | *Macrogeometry*: grooving (type, geometry) | *Material*: chem. composition, viscosity | *Additivity*: chemical composition | *Material*: mechanical properties (cleavage, fracture toughness . . .) | *Grain size distribution*: average and maximum grain diameter, standard deviation |
| *Microgeometry*: characteristic values of the Abott-curve | | *Mixing ratio*: viscosity<br>*Volumetric mixing ratio*: grain concentration | | *Grain shape*: length–width ratio, cutting-edge shape | |

*Source*: From Spur, G. and Engel, H. In: *Jahrbuch Schleifen, Honen, Läppen und Polieren*, Bd. 58. Hrsg.: H.K. Tönshoff, Vulkan, Essen, 1996.

carriers driven between inner and outer pin circle, and the lapping wheel rotation. The energy transfer takes place through the simultaneous effect of the relative speed and the engagement pressure.

The lapping tool is formed during the process. Therefore, it is specific for a certain removal system. Changes of the parameters of the removal system cause changes in the specification of the lapping tool.

The specification of the lapping tool decisively influences the subsurface-related work result as well as the material removal rate. Therefore, the derivation of the relevant tool parameters is an indispensable prerequisite for the elaboration of technological functions for the process description.

### 2.6.2 Lapping Wheels

The lapping wheels are characterized by their macrogeometry, surface topography as well as by material, its mechanical properties, and its structure. The macrogeometry of the lapping wheel affects the distribution of the slurry in the working gap and thus the formation of the lapping wheel topography. The mechanical properties and the structure of the lapping wheel material determine the resistance of the lapping wheel to the force of the grains, thus influencing the formed surface topography.

The lapping wheels usually consist of fine-grain cast pearlite. A homogeneous structure and uniform hardness are very important. In the ideal case, the lapping grain rolls in the process. The formed surface is dim; the surface structure consists of craters due to the rolling grain. There is no directional structure on the surface [4].

The hardness of the lapping wheels influences the kind of movement of the lapping grain. Soft lapping wheels keep the grain firmly in its position. As a result, the grains scratch the workpieces. A surface of very low roughness is formed. The machining marks consist of fine ridges. If very hard wheels are used, the lapping grain is pushed deeply into the material to be machined. Gliding marks are generated on the lapping wheel. Multimetal lapping wheels consist of two to three materials, which are combined in spiral inlays, mosaic, or annular shape. These lapping wheels are much more expensive than conventional ones; they are, however, best suited for the use of diamond media. The dressing rings have to be adjusted to these lapping wheels.

Lapping wheels can be grooved in order to avoid slurry stasis and to improve the chip removal. This is particularly advantageous in the case of machining workpieces of large surfaces.

### 2.6.3 Slurry

The other component of the lapping tool is the slurry. It consists of the lapping abrasive (grain) and the lapping medium (fluid or paste). There is always a certain volumetric concentration, which is often called grain concentration, of

the lapping abrasive in the slurry. Usually, volumetric mixing ratios of 1:2 to 1:6 are used [4].

The optimum amount of slurry depends on the machine size and the surface of the workpiece. It should be determined experimentally, as the slurry consumption is an important cost factor. If slurry supply is too high, the parts may float (aquaplaning effect). A too thick lapping film leads to a reduction of the material removal rate. A break off of the lapping film may lead to cold welding through the direct contact of the lapping wheel and the workpiece. The limits of the lapping film thickness, which vary in the case of different materials, are reached if no typical lapping pattern can be seen on the surface of the workpiece. The surface then resembles the grinding pattern with directional machining marks.

### 2.6.4 Lapping Medium

The grains are dispersed in the medium. During the process the slurry is supplied in a way that a lapping film develops between the tool and the workpiece. The task of the lapping fluid is to transport the grains to the lapping gap and to make new grains engage in the lapping process. Desired characteristics are the carrying capacity with respect to the lapping abrasive, corrosion protection, and chemical resistance. The type of the lapping fluid and the mixing ratio of lapping abrasive and fluid influence the material removal and surface quality.

The lapping fluid is mostly water with added corrosion inhibitors, agents for the enhancement of viscosity as well as lubricants and moistening abrasives. Besides, mixtures of oil, petroleum paraffin, vaseline, and other additives are used.

### 2.6.5 Lapping Abrasives

The lapping abrasive is defined by its material characteristics, the shape of the grains, and its grain size distribution, which are in close connection to each other. The shape of the grains is crucially influenced not only by the material properties such as cleavability and fracture toughness, but also by the manufacturing process. Even with equal average grain size parameters, every type of lapping abrasive has a characteristic grain size distribution also determined by the grain shape.

The actual material removal is realized by the grains of the lapping abrasive. The grain engagement is described in detail in Section 2.4 “Process Mechanisms and Subsurface Damage in Lapping.” Basically, the lapping abrasive (lapping grain) has to be harder than the material to be machined. With rough graining, the possible material removal rates are higher (rough lapping). In order to achieve high surface qualities, often a second work cycle with fine grain and respectively reduced material removal rate is required. Basic quality properties of lapping powders are even grain size distribution, hardness,

as well as type and number of the grain cutting edges. Grain sizes between 0.1 and 150 μm are used; in general, grain size ranges from 5 to 40 μm [4].

Silicon carbide is the most common lapping powder. It can be used for almost all the materials. Corundum (aluminum oxide) is used for softer materials. A further case of application is the realization of a polishing effect due to rounded cutting edges under a strong decrease of the material removal rate. Boron carbide is much harder than aluminum oxide and silicon carbide. Due to its price, however, it is not used for the machining of softer materials. The diamond grain is harder and its cutting edge is sharper than the lapping abrasives mentioned so far. Even inhomogeneous materials such as carbide or ceramics can be cut evenly, so as to the formed surface remains coherently even. Despite its high price, the use of diamond is economically efficient in many cases because of the reduced machining times in contrast to softer lapping abrasives.

In general, the grain size of lapping abrasives is characterized by the specification of the average equivalent diameter of the sphere, called average grain diameter or equivalent diameter, and its standard deviation. These parameters can be used for the description of the grain volume and the grain concentration in the slurry.

As the grains usually have an ellipsoid projection surface, the relevant parameters of grain engagement defined in Section 2.4 are the average maximum diameter of the grain projection surface, called maximum grain diameter, and its standard deviation [59].

The grain size parameters of the lapping abrasive are always random values with a characteristic distribution function. For grain collectives, this is usually the normal distribution function. During lapping, only a part of the grains in the working gap is able to close the contact chain and to engage in the material. This grain fraction, which is always at the upper limit of the distributive function, is the amount of active grains.

### 2.6.6 Process Grain Size Distribution

A crucial process parameter affecting the work result and the material removal is the grain size distribution of the lapping abrasive. Due to the mechanical stress through the effect of the engagement pressure and the path velocity, the active lapping grains are subject to typical signs of wear (Figure 2.12). These grain wear mechanisms lead to an in-process change of the size distribution of the grain size parameters of the lapping abrasive. The following grain damaging and grain wear mechanisms can be named: cutting edge wear, grain splintering, and grain breakage. The occurrence of these wear mechanisms is a stochastic process. Influencing parameters are the mechanical properties of the grains, their shape and cleavability, as well as the actual action of force and its direction in the working gap. The grain size distribution occurring in a defined removal system in the lapping process is called process grain size distribution.

With a continuous slurry supply during machining, a stationary condition arises after a certain lapping time, which is characterized by a constant surface topography of the lapping wheels and of the workpieces as well as a constant grain size distribution of the lapping abrasive. This process grain size distribution of the lapping abrasive, which is characteristic for the removal system, diverges by a certain extent from the grain size distribution of the unused slurry. The parameters of the process grain size distribution are the average equivalent process grain diameter, the average maximum process grain size diameter, and their standard deviations (Figure 2.12).

## 2.7 MACHINE SETTINGS

The machine settings are explained by the example of plane-parallel lapping, which is the most common lapping process. The engagement pressure and process kinematics are to be mentioned here.

### 2.7.1 Engagement Pressure

In plane-parallel lapping, the engagement pressure $p_e$ is a quotient resulting from the normal force $F_N$ applied over the upper lapping wheel and the workpiece surface $A_{Wges}$ contacted by the lapping wheels:

$$p_e = \frac{F_N}{A_{Wges}} \tag{2.1}$$

The actual material removal force is applied through the acting engagement pressure in combination with the relative movement between the workpiece and the lapping grain. It leads to a local abolition of the material cohesion. Due to the easy overrun of the workpieces beyond the edges of the lapping wheels, the effective engagement pressure is slightly higher than that calculated with the theoretical complete workpiece surface and the workpiece surface engaged slightly differs from the total workpiece surface [103–106]. It must be considered that much higher pressures occur locally than the nominal pressure because the contact areas between lapping grain and workpiece are much smaller than the workpiece surfaces.

### 2.7.2 Process Kinematics

In plane-parallel lapping, the rotational speeds and directions of the lapping wheels can be set independently of each other. These wheels, combined with the variations of the pin circles, result in a number of different forms of movement of any workpiece point on the lapping wheel. Therefore, the term lapping velocity is inappropriate. In many citations, it specifies the

rotational speed of the lapping wheels. In plane-parallel lapping, a workpiece point covers epicycloids and hypocycloid path curves, in special cases even circular paths relatively to the lapping wheel. The velocity between the workpiece and the tool constantly changes. The rotational speed of the lapping wheel therefore does not describe the real path velocity of the single workpieces.

The process kinematics has great influence on the process behavior and work result of lapping. Thus, it is described and analyzed in detail for plane-parallel lapping in Section 2.8.

## 2.8 FUNDAMENTALS OF PLANETARY KINEMATICS

*THOMAS ARDELT*

During lapping and face grinding on lapping machines, several workpieces are moved simultaneously between two horizontally positioned lapping or grinding wheels. The parts are fixed in holders that are led between two pin circles. This way, the characteristic cycloidal path curves are generated between parts and wheels. Corresponding to these path curves, characteristic wear profiles emerge in the process, which make wheel conditioning necessary in regular intervals. To increase process economy and part quality, it is necessary to minimize the inhomogeneous wear of the wheels and to maximize the time intervals between two of the profiling processes. This article describes the mathematical relations to calculate the relative movement between the workpieces and the wheels as a basis for better process control and wheel profile wear minimization [107–109].

### 2.8.1 Definition

The relative movement between the workpieces and a lapping wheel is generated by the interference of two rotational movements: the rotation of the lapping wheel and the rolling of the workpiece holder between the two pin circles. The movement of the workpiece holders corresponds to one of the planet wheel in a planetary gear. The workpieces move relatively to the lapping wheels on the so-called cycloids (Figure 2.13). Depending on the distance of the observed point from the rotation center, stretched, common, and interlaced cycloids can be distinguished. Common cycloids punctually touch the pitch circle. Interlaced cycloids have loops and stretched cycloids are characterized by rounded tips [110].

Rotationally symmetrical workpieces can rotate in their carriers. In this case, the workpiece rotation interferes with the two above-mentioned movements as an additional component, which leads to the so-called modulated cycloidal movements. The rotation of the workpieces is therefore exempt from all following considerations.

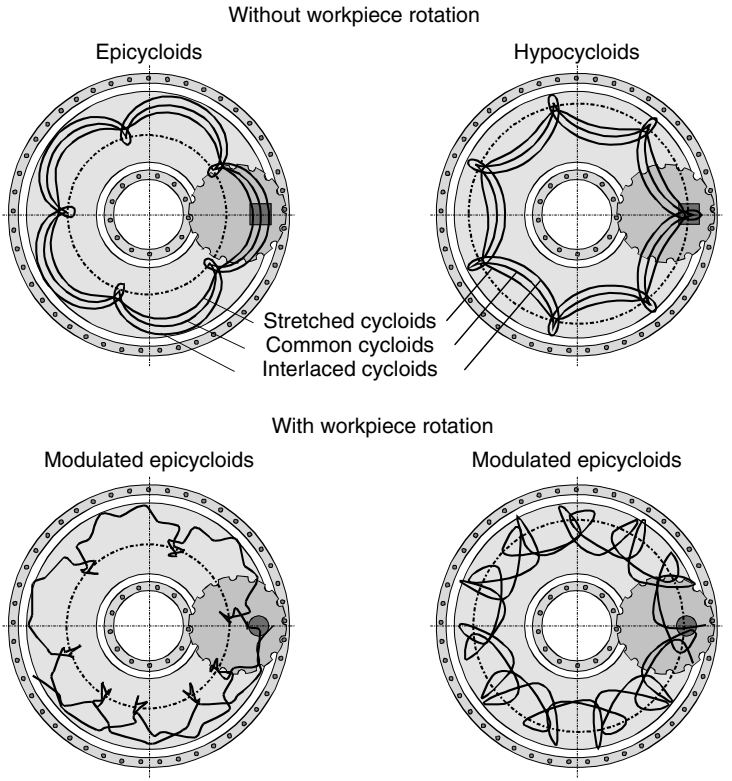


**FIGURE 2.13** Possible movements of the workpieces relative to the lapping wheel. (From Ardelt, Th., Einfluss der Relativbewegung auf den Prozess und das Arbeitsergebnis beim Planschleifen mit Planetenkinematik. Dissertation, TU Berlin, 2000; zugl. Reihe Berichte aus dem Produktionstechnischen Zentrum Berlin, 2001.)

### 2.8.1.1 Macrokinematics

Macrokinematics is the movement of the workpieces relative to the lapping wheels. In the scope of macrokinematical considerations, all active partners are assumed in their ideal geometry. The terms lapping or planetary kinematics are used as synonyms for macrokinematics. In this chapter, macrokinematical parameters are identified with the index L.

In the presented investigations, only movements between the workpieces and the lower lapping wheel are considered. For double-sided lapping, the kinematical conditions relative to the upper lapping wheel are to be determined analogously.

### 2.8.1.2 Path Curve

The path curve is the line a workpiece point describes relatively to the lapping wheel. The term path curve comprises only the geometrical properties of the

described path, i.e., its coordinates and the derived parameters such as path length and curvature [111].

#### 2.8.1.3 Path Movement

Alongside the geometry of a path curve, the term path movement comprises the movement of a workpiece point along this path. This path movement is characterized by the time-dependent parameters path velocity and path acceleration [111].

#### 2.8.1.4 Cycle and Part Cycle

Neglecting the workpiece rotation, the path curves are composed of uniform, cyclically recurrent geometrical elements (see Figure 2.13). These path curve elements are called part cycles. The starting point of a path movement is chosen where the observed workpiece point has its maximum distance from the lapping wheel center. As soon as it reaches this distance for a second time, a part cycle is finished. A cycle is covered when, after several finished part cycles, the observed point is at its initial point again and the path curve is closed [106].

#### 2.8.1.5 Microkinematics

Microkinematics describe the engagement conditions in the contact zone between the workpiece and the tool. The material removal mechanisms by the movement of loose abrasive grains in a fluid between the three-dimensional surface structures of tool and the lapping wheel are the object of discussion in other chapters of this book.

### 2.8.2 Geometrical and Kinematical Parameters of the Relative Movement

The equations describing the relative movements are formulated in a coordinate system, which is fixed relative to the lapping wheel. The *Z*-axis of this cartesian coordinate system corresponds to the rotational axis of the lower lapping wheel. The *X*- and *Y*-axes define the working area relative to the lower lapping wheel and are firmly fixed in it. For an observer standing next to the lapping machine, this coordinate system rotates with the lower lapping wheel. A point can have two translatory degrees of freedom, and a solid body has two translatory and one rotational degrees of freedom in this plain. The description of the movement conditions is based on the geometrical and kinematical parameters (Figure 2.14). Geometrical parameters are the geometries of the individual machine elements and workpieces as well as the arrangement of the workpieces in the holder. The kinematical parameters include the rotary speeds of pin circles, lapping wheel, workpiece holder, and workpiece [70,106].

The angular velocity $\omega_H$ identifies the rotation of the holder around H, its own center, whereas $\omega_Z$ identifies the translatory movement of the holder around Z,

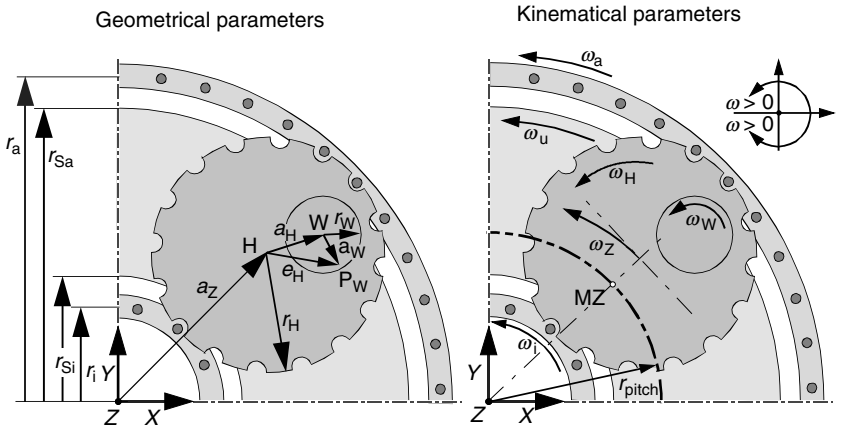


**FIGURE 2.14** Geometrical and kinematical parameters of planetary kinematics. (From Funck, A., Planschleifen mit Läppkinematik. Dissertation, TU Berlin, 1994; Simpfendörfer, D., Entwicklung und Verifizierung eines Prozeßmodelles beim Planläppen mit Zwangsführung. Dissertation, TU Berlin, 1988; Spur, G. and Eichhorn, H., *Vortragsband Seminar Poznan—Berlin* "*Dokladna Obrabotka Elementov maszyn*," Poznan, 1995.)

the rotational axis of the wheel. Figure 2.15 shows the vectorial velocities at the workpiece holder for the calculation of these angular velocities. If the illustrated velocity vectors are substituted by the scalar parameters of the angular velocities and the radii, the following equation can be defined for point A:

$$|\vec{\mathbf{v}}_Z| + |\vec{\mathbf{v}}_H| = |\vec{\mathbf{v}}_a|$$
$$\omega_Z a_Z + \omega_H r_H = 2\pi n_u r_a \tag{2.2}$$

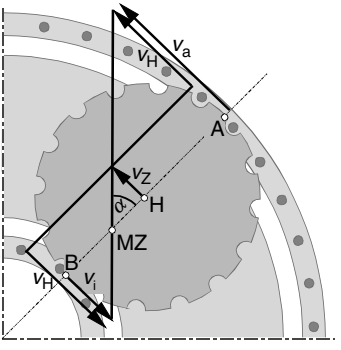


**FIGURE 2.15** Velocities at the workpiece holder in the lapping wheel coordinate system. (From Simpfendörfer, D., Entwicklung und Verifizierung eines Prozeßmodelles beim Planläppen mit Zwangsführung. Dissertation, TU Berlin, 1988.)

For point B, the adequate derivation leads to

$$|\vec{\mathbf{v}}_Z| - |\vec{\mathbf{v}}_H| = |\vec{\mathbf{v}}_i|$$
$$\omega_Z a_Z - \omega_H r_H = 2\pi(n_i - n_u) r_i \tag{2.3}$$

A positive algebraic sign corresponds to a counterclockwise rotation. The substitution of the geometrical relations $r_H = (r_a - r_i)/2$ and $a_Z = r_i + r_H$ in these equations leads to the matrix equation

$$\begin{bmatrix} \omega_H \\ \omega_Z \end{bmatrix} = 2\pi \begin{bmatrix} -\dfrac{r_i}{r_a - r_i} & \dfrac{r_a}{r_a - r_i} & -1 \\ \dfrac{r_i}{r_a + r_i} & \dfrac{r_a}{r_a + r_i} & -1 \end{bmatrix} \cdot \begin{bmatrix} n_i \\ n_a \\ n_u \end{bmatrix} \tag{2.4}$$

as a relation between the angular velocities and the settings of the machine [106].

### 2.8.3 Calculation of Path Curves and Movements

In this section, equations for path velocities and path movements will be derived. As an overview, Table 2.2 shows the used geometrical and kinematical

**TABLE 2.2**
**Parameters for the Description of Path Curves and Path Movements**

| | Path Movement | |
|---|---|---|
| **Path Curve Geometry** | **Velocities** | **Accelerations** |
| $\vec{\mathbf{r}}(t)$ path curve, position vector | $\vec{\mathbf{v}}(t)$ path velocity | $\vec{\mathbf{a}}(t)$ path acceleration |
| $r(t)$ absolute value of the position vector | $v(t)$ absolute value of the path velocity<br>$v_m$ average path velocity | $a(t)$ absolute value of the path acceleration<br>$a_m$ average path acceleration<br>$a_s(t) = \dot{v}(t)$ scalar acceleration in the direction of the path movement |

*Source*: From Ardelt, Th., Einfluss der Relativbewegung auf den Prozess und das Arbeitsergebnis beim Planschleifen mit Planetenkinematik. Dissertation, TU Berlin, 2000; zugl. Reihe Berichte aus dem Produktionstechnischen Zentrum Berlin, 2001.

parameters. The derivation presented here is based on the work of Spur and Eichhorn [105,106].

#### 2.8.3.1 Path Curve

Any given workpiece point $P_W$ with the distance $e_H$ from the holder center moves along the path curve $\vec{\mathbf{r}}(t)$ in the $X,Y$-plane. If its coordinates are $x = a_Z + e_H$ and $y = 0$ at the time $t_0 = 0$, then it has the position

$$\vec{\mathbf{r}}(t) = \begin{pmatrix} x(t) \\ y(t) \end{pmatrix} = \begin{pmatrix} a_Z \cos(\omega_Z t) + e_H \cos(\omega_H t) \\ a_Z \sin(\omega_Z t) + e_H \sin(\omega_H t) \end{pmatrix} \tag{2.5}$$

at the time $t$ on its path curve $\vec{\mathbf{r}}(t)$. The distance to the wheel center corresponds to the absolute value of the positional vector and is

$$r(t) = |\vec{\mathbf{r}}(t)| = \sqrt{a_Z^2 + e_H^2 + 2a_Z e_H \cos((\omega_Z - \omega_H)t)\vec{\mathbf{v}}} \tag{2.6}$$

As all the workpieces are between the two pin circles, the range of the absolute values of all positional vectors is limited by the interval $r_i < r(t) < r_a$ [106].

#### 2.8.3.2 Path Velocity

The path velocity $\vec{\mathbf{v}}(t)$ is defined as the first derivation of the path velocity $\vec{\mathbf{r}}(t)$ in relation of time:

$$\vec{\mathbf{v}}(t) = \begin{pmatrix} \dot{x}(t) \\ \dot{y}(t) \end{pmatrix} = \begin{pmatrix} -a_Z\omega_Z \sin(\omega_Z t) - e_H\omega_H \sin(\omega_H t) \\ a_Z\omega_Z \cos(\omega_Z t) + e_H\omega_H \cos(\omega_H t) \end{pmatrix} \tag{2.7}$$

The generation of the absolute value leads to the term

$$v(t) = |\vec{\mathbf{v}}(t)| = \sqrt{a_Z^2\omega_Z^2 + e_H^2\omega_H^2 + 2a_Z e_H \omega_H \omega_Z \cos((\omega_Z - \omega_H)t)} \tag{2.8}$$

for the scalar path velocity $v(t)$ [106]. The arithmetic mean value of the minimum and the maximum path velocity does not correspond to the average path velocity $v_m$ of a workpiece point. According to the equation

$$v_m = \frac{1}{t_{\Delta Zykl}} \int_0^{t_{\Delta Zykl}} v(t)\,\mathrm{d}t \tag{2.9}$$

the complete part cycle must be considered for the calculation of $v_m$.

#### 2.8.3.3 Path Acceleration and Scalar Acceleration

According to Spur and Eichhorn [106], the path acceleration follows from the second derivation of Equation 2.4 in relation of time and is as follows:

$$\vec{\mathbf{a}}(t) = \begin{pmatrix} \ddot{x}(t) \\ \ddot{y}(t) \end{pmatrix} = \begin{pmatrix} -a_Z\omega_Z^2\cos(\omega_Z t) - e_H\omega_H^2\cos(\omega_H t) \\ -a_Z\omega_Z^2\sin(\omega_Z t) - e_H\omega_H^2\sin(\omega_H t) \end{pmatrix} \tag{2.10}$$

The equation of the absolute values of the path velocity results in

$$a(t) = |\vec{\mathbf{a}}(t)| = \sqrt{e_H^2\omega_H^4 + a_Z^2\omega_Z^4 + 2a_Z e_H\omega_H^2\omega_Z^2\cos((\omega_Z - \omega_H)t)} \tag{2.11}$$

#### 2.8.3.4 Path Curvature

The curvature $k$ of a path curve at the time $t$ can be calculated from the parameterized equations for path velocity and path acceleration according to the formula

$$\begin{aligned} k(t) &= \frac{\dot{x}\ddot{y} - \ddot{x}\dot{y}}{\sqrt{(\dot{x}^2 + \dot{y}^2)^3}} \\ &= \frac{e_H^2\omega_H^3 + a_Z^2\omega_Z^3 + a_Z e_H\omega_Z\omega_H(\omega_H + \omega_Z)\cos((\omega_Z - \omega_H)t)}{\sqrt{[e_H^2\omega_H^2 + a_Z^2\omega_Z^2 + 2a_Z e_H\omega_Z\omega_H\cos((\omega_Z - \omega_H)t)]^3}} \end{aligned} \tag{2.12}$$

[105]. The unit of the path curve is $m^{-1}$. A change of the algebraic sign indicates an inflection point of the respective curve.

### 2.8.4 Description of the Movement Pattern by Means of the Rotational Speed Ratio

#### 2.8.4.1 Definition of the Rotational Speed Ratio

In the case of most conventional lapping machines, the outer pin circle cannot rotate in the machine base. The condition

$$n_a = 0 \tag{2.13}$$

reduces the selectable kinematical parameters to the rotational speed numbers of the inner pin circle $n_i$ and the lapping wheel $n_u$. Hence, all movement patterns between the workpieces and the lower lapping wheel are explicitly defined by $n_i$ and $n_u$. On this basis, the rotational speed ratio $N_L$

$$N_L = \frac{n_i}{n_u} \tag{2.14}$$

is defined as the quotient of the two rotational speeds for the description of the machining kinematics between the workpiece and the lower lapping wheel.

Beyond these two rotational speeds, only the radii of the two pin circles $r_i$ and $r_a$ are used for the description of all kinematic relations.

The rotational speed ratio $N_L$ explicitly assigns a movement pattern to each set of kinematical machine parameters, which depends on the geometry of the machine used. This means that equal rotational speed conditions on different machines might lead to differing path curves.

### 2.8.4.2 Kinematical Parameters

In the following, parameters for the description of kinematical conditions will be defined [70,105,106].

#### *2.8.4.2.1 Cycle Time and Part-Cycle Time*

The cycle time $t_{cycl}$ is the time required for the coverage of a complete cycle. The time required for an individual path element is called part-cycle time $t_{\Delta cycl}$ and depends on the cycle time according to

$$t_{\Delta cycl} = \frac{t_{cycl}}{p} \tag{2.15}$$

A part cycle is completed when any observed workpiece point reaches its maximum distance from the wheel center a second time [106]. The distance between workpiece point and wheel center is not influenced by the rotational speed of the lapping wheel. It only depends on the rotational speed of the pin circles. For $n_a = 0$, the part-cycle time can be traced back to a geometrical factor and the rotational speed of the pin circle $n_i$ according to

$$t_{\Delta cycl} = \frac{r_a^2 - r_i^2}{2 r_a r_i} \frac{1}{|n_i|} \tag{2.16}$$

#### *2.8.4.2.2 Pitch Circle Radius*

In mechanical terms, an epicycloid is formed when a circle unrolls externally on a pitch circle. A hypocycloid is formed if the rolling movement takes place on the internal part of a pitch circle (Figure 2.13) [110]. The pitch circle as well as the unrolling circle do not result from the machine design, but from the rotational speeds. The relative velocity in the contact point of both the circles is zero. This contact point is called the momentary center MZ of the movement. Its path curve is equal to the pitch circle. In the momentary center, the effective holder velocity relative to the lapping wheel is zero. The trigonometrical relation

$$\tan \alpha = \frac{v_i}{r_i - r_{pitch}} = \frac{v_a}{r_a - r_{pitch}} \tag{2.17}$$

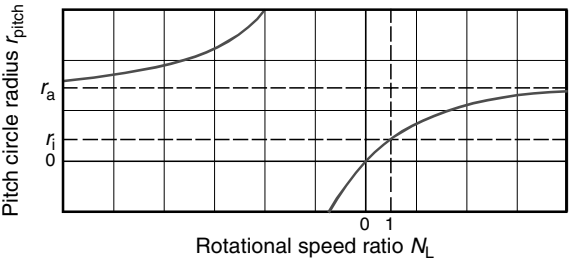


**FIGURE 2.16** Relation between pitch circle radius and rotational speed ratio.

applies to the angle $\alpha$ in Figure 2.15. If the velocities $v_i$ and $v_a$ are equalized in this equation according to Equation 2.2 and Equation 2.3, the result is

$$r_{pitch} = \frac{N_L r_i r_a}{N_L r_i + r_a - r_i} \tag{2.18}$$

for the pitch circle radius $r_{pitch}$. This term describes a function with an infinity point with the change of the algebraic sign.

Figure 2.16 shows the pitch circle radius $r_{pitch}$ as a function of the rotational speed ratio $N_L$. For $|n_i| \gg |n_u|$, the pitch circle radius asymptotically approaches the radius of the outer pin circle $r_a$. The rotational speed of the lapping wheel is not significant compared to the rotational speed of the pin circle, and the relative movement is determined by the unrolling of the workpiece holder on the outer pin circle. For $N_L = 0$, $r_{pitch}$ is zero too. In the case of $N_L = 1$, the lapping wheel and the pin circle rotate with the same rotational speed. Then, relatively to the lapping wheel, the workpiece holders unroll on the inner pin circle, and the pitch circle radius is $r_i$.

#### *2.8.4.2.3 Cycle Angle and Part-Cycle Angle*

A part-cycle angle $\beta_{\Delta cycl}$ is the angle the observed workpiece point $P_W$ covers relative to the center of the lapping wheel $Z$ within one part cycle. The part-cycle angle corresponds to the angle the center of the workpiece holder H covers within the part-cycle time and can be calculated by the equation

$$\beta_{\Delta cycl} = \omega_Z \cdot t_{\Delta cycl} \tag{2.19}$$

By substituting these two values, the part-cycle angle is

$$\beta_{\Delta cycl} = \pi \left( \frac{r_a - r_i}{r_a} - \frac{r_a^2 - r_i^2}{r_a r_i} \frac{1}{N_L} \right) \tag{2.20}$$

A whole cycle is completed when $P_W$ reaches its starting point on the lapping wheel a second time and the path curve closes. This condition is met if the sum of $p$ covered part-cycle angles

$$p \cdot \beta_{\Delta cycl} = q \cdot 2\pi \tag{2.21}$$

is a whole-numbered multiple of the angle of the full circle $2\pi$. The condition in Equation 2.21 leads to the relation of planetary kinematics. It is defined as the quotient of the factors $p$ and $q$. The factor $p$ as numerator of the fraction represents the number of part cycles covered in each cycle. The denominator of the fraction $q$ represents the number of revolutions around the wheel center the circle requires to close. This relation of planetary kinematics can be traced back to the geometrical parameters and the rotational speed ratio according to the equation

$$\frac{p}{q} = \frac{2}{\dfrac{r_a - r_i}{r_a} - \dfrac{r_a^2 - r_i^2}{r_a r_i}\dfrac{1}{N_L}} \tag{2.22}$$

The decimal number resulting from the calculation of Equation 2.22 is formed to a fraction $p/q$ by prime factor decomposition in a way that $p$ and $q$ are coprime. In the case of $q = 1$, the curve path closes after one revolution around the wheel center. If the conversion of $p$ and $q$ into natural numbers is impossible, the path curve never closes [106].

### 2.8.4.3 Possible Path Movements

On the basis of the mathematical fundamentals defined, the patterns of relative movements during face lapping with planetary kinematics with fixed outer pin circle can be analyzed.

All workpiece points with the same distance $e_H$ from the holder center cover analogous path curves with a time shift. If a workpiece point punctually touches the pitch circle radius on its path, it covers a common epicycloid or hypocycloid relatively to the lapping wheel (see Figure 2.13). If its path intersects the pitch circle radius, interlaced, otherwise stretched cycloids occur. The rotational speed ratio $N_L$ and the distance of the point from the holder center $e_H$ must be known for the determination of the effective path pattern. Table 2.3 shows how the path pattern (stretched, common, or interlaced cycloid) is dependent on $e_H$.

**TABLE 2.3**
**Relation between Part Position in the Holder and Occurring Path Pattern**

| Position of the Point | Respective Path Pattern |
|---|---|
| $e_H > \lvert a_Z - r_{pitch}\rvert$ | Interlaced cycloids |
| $e_H = \lvert a_Z - r_{pitch}\rvert$ | Common cycloids |
| $e_H < \lvert a_Z - r_{pitch}\rvert$ | Stretched cycloids |

*Source*: From Spur, G. and Eichhorn, H., *IDR*, 31(2), 169, 1997.

It can be derived from the conditions, shown in Table 2.2, on which kinematical parameters have to be set on the machine for the formation of common cycloids. If the relation $r_{\text{pitch}} = \mid a_{\text{Z}} - e_{\text{H}} \mid$ is substituted in Equation 2.17, the result is

$$N_{\text{L common cycloids}} = \frac{\pm\dfrac{r_{\text{a}} + r_{\text{i}}}{2e_{\text{H}}} - 1}{\pm\dfrac{r_{\text{i}}}{2e_{\text{H}}} + \dfrac{r_{\text{i}}}{r_{\text{a}} - r_{\text{i}}}} \begin{cases} + & \text{common epicycloid} \\ - & \text{common hypocycloid} \end{cases} \tag{2.23}$$

as a formulation for the respective rotational speed ratio. For certain values of the pitch circle radius $r_{\text{pitch}}$, special movement conditions occur, which are characterized by all workpiece points covering geometrically identical path curves independently of their position in the holder. The following section explains these special cases and calculates the respective rotational speed ratios. Here too, the prerequisite is that a rotation of the workpiece in the holder gaps is not possible.

If the pitch circle radius is $r_{\text{pitch}} = r_{\text{i}} + r_{\text{a}}$, the circumference of the pitch circle is exactly twice the circumference of the unrolling circle. Then, the unrolling circle revolves twice in one cycle. If this condition is substituted in Equation 2.17, the result is

$$N_{\text{L centric ellipse}} = -\frac{r_{\text{a}}^2 - r_{\text{i}}^2}{r_{\text{i}}^2} \tag{2.24}$$

for the respective rotational speed ratio. In the case of this rotational speed ratio, all workpiece points cover centric ellipses on the lapping wheel.

If the pitch circle radius tends to infinite in the positive or the negative range, the angle velocity $\omega_{\text{H}}$ of the holder rotation tends to zero. This is a purely translatory holder movement relative to the lapping wheel, hence the workpieces cover eccentric circular paths around the rotation center of the lapping wheel. If $r_{\text{pitch}}$ $\lim \pm\infty$ is substituted in Equation 2.17, the result is

$$N_{\text{L eccentric circular path}} = -\frac{r_{\text{a}} - r_{\text{i}}}{r_{\text{i}}} \tag{2.25}$$

for the respective rotational speed ratio. In this case, all workpiece points cover eccentric circles of the same geometry on the lapping wheel.

In the case of a pitch circle radius of zero, Equation 2.17 is only solvable for the trivial case of

$$N_{\text{L centrical circular path}} = 0 \tag{2.26}$$

In the case of this rotational speed ratio, the internal pin circle stands still with $n_i = 0$ and only the lapping wheel rotates. Thus, the workpieces move on centric circular paths. Here the kinematical description shows a lack of definition, as the centric circular path cannot be divided into uniform path elements. Accordingly, the formulas have a lack of definition for the part-cycle time and the part-cycle angle. Therefore, no average path velocity can be calculated for a workpiece point. This can be traced back to the fact that the velocity of a point in the case of a stationary inner pin circle does not only depend on its eccentricity in the holder, but also on the angular holder position. This position, however, is not defined in the present description of kinematical conditions.

In the case of $r_{pitch} = a_Z$, the pitch circle crosses the rotational center of the holder. Through the substitution of the condition in Equation 2.18, the rotational speed ratio is

$$N_{L\ \text{circular path around the holder center}} = \frac{r_a + r_i}{r_i} \tag{2.27}$$

In this case the holder center does not move relatively to the wheel. Pure holder rotation occurs, and all workpiece points move on circular path curves around the holder center H.

### 2.8.4.4 Determination of the Path Pattern of a Workpiece Point

Like Figure 2.16, Figure 2.17 shows the pitch circle radius $r_{pitch}$ as a function of the rotational speed ratio $N_L$. In this figure, however, the range between the two pin circles $r_a$ and $r_i$, where workpiece points can be located, is depicted

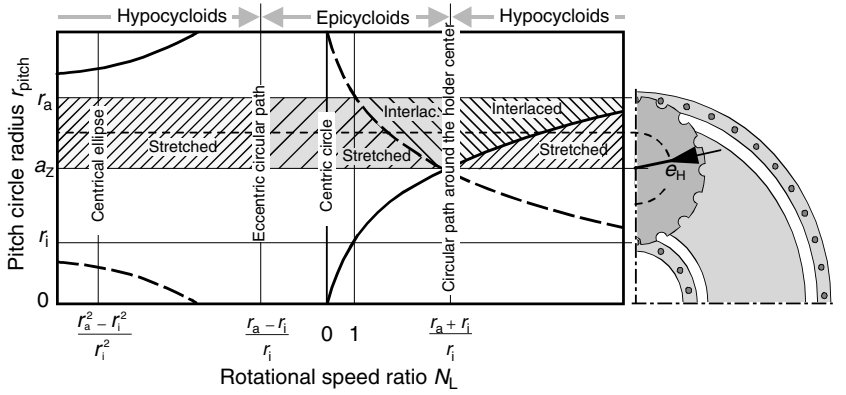


**FIGURE 2.17** Determination of the path of a workpiece point. (From Ardelt, Th., Einfluss der Relativbewegung auf den Prozess und das Arbeitsergebnis beim Planschleifen mit Planetenkinematik. Dissertation, TU Berlin, 2000; zugl. Reihe Berichte aus dem Produktionstechnischen Zentrum Berlin, 2001.)

with a bigger scale. The relation between the diagram and the machine geometry is demonstrated by the drawing on the right margin of the image. According to Table 2.3, the possible locations of workpiece points are divided into fields, which mark the different movement patterns. The dark area in the center of the diagram marks epicycloids, the two light areas at the sides mark hypocycloids. The fields of interlaced and stretched cycloids are marked with different hatchings. The distance $e_H$ of a point $P_W$ on the workpiece surface from the holder center is plotted in the diagram as a horizontal, dashed line. The effective movement pattern of a workpiece point for every rotational speed ratio $N_L$ can be read from this line.

Hypocycloids occur if the pitch circle radius is bigger than the distance $a_Z$ between the rotation center $Z$ and the holder center H. If $r_{pitch}$ is smaller than $a_Z$, epicycloids occur. In the case of rotational speed ratios of $N_L \leq 1$, the pitch circle radius is outside of the pin circles, hence, the path curves of the workpiece points cannot intersect it. Here, the occurring path pattern is defined independently of $e_H$. In the case of rotational speed ratios of $N_L > 1$, the value of the pitch circle radius lies between the pin circles. Thus, interlaced, common, and stretched cycloids can simultaneously occur here.

As a concretion, these considerations are reproduced using the example of a real machine. The basis of the kinematical analyses of this chapter is the design of a Duomat ZL 500 by the Stähli Läpp-Technik Company, Schönaich, Germany. Characteristic geometrical properties are pin circle radii with $r_i = 86$ mm and $r_a = 289.5$ mm. A workpiece point $P_W$ with the distance of $e_H = 0.5 \cdot r_H = 50.86$ mm was chosen for the following considerations. This value corresponds to the example marked with a dashed line in Figure 2.17. Table 2.4 shows the rotational speed ratios, which have to be set for certain path curves on the selected machine.

Figure 2.18 shows path patterns, which occur at different rotational speed ratios between the workpieces and a lapping wheel. The images marked with the numbers 1 to 5 are path pattern classes occurring in certain ranges of the

**TABLE 2.4**
**Special Path Curves on the Duomat ZL 500**

| Path Pattern | Calculation | $N_L$ |
|---|---|---|
| Ellipse around the wheel center | Equation 2.23 | −10.3 |
| Eccentric circular path | Equation 2.24 | −2.4 |
| Common epicycloids | Equation 2.22 | 2.1 |
| Circular path around the holder center | Equation 2.26 | 4.4 |
| Common hypocycloid | Equation 2.22 | 11.1 |

*Source*: From Ardelt, Th., Einfluss der Relativbewegung auf den Prozess und das Arbeitsergebnis beim Planschleifen mit Planetenkinematik. Dissertation, TU Berlin, 2000; zugl. Reihe Berichte aus dem Produktionstechnischen Zentrum Berlin, 2001.

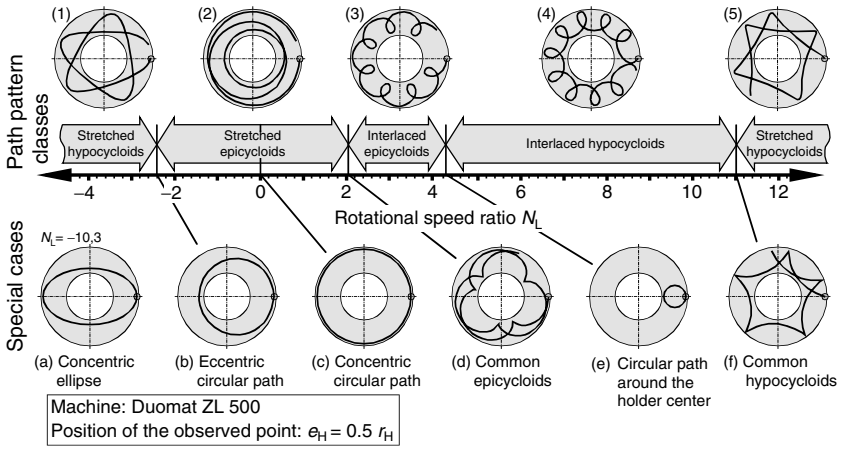


**FIGURE 2.18** Occurring path patterns depending on the rotational speed ratio. (From Uhlmann, E. and Ardelt, Th., *Ann CIRP*, 48/1, 281, 1999.)

rotational speed ratio $N_L$. The curves marked with the letters a to f are special cases, which occur only at a certain rotational speed ratio.

In the case of big negative rotational speed ratios, the observed workpiece point $P_W$ covers stretched hypocycloids (1) on the lapping wheel. These consist of relatively large form elements, which encircle the center of the lapping wheel. As a special case, centric ellipses occur in this range at $N_L = -10.3$ (a). With increasing $N_L$, the form elements keep stretching until they transform into eccentric circular paths at $N_L = -2.4$. This special form is the transition to stretched epicycloids (2). As a special form in the field of epicycloids, circular paths occur around the center of the wheel (c) at $N_L = 0$. At a rotational speed ratio of 2.1, the path curves change into the special case of common epicycloids (d), which are characterized by a vertex near the center of the lapping wheel. In the case of further increasing $N_L$, the paths change into interlaced epicycloids (3), whose form elements are smaller than before and recur on one-half of the wheel. With further increasing $N_L$, the size of the evolving loops grows until they change over into circular paths (e) at $N_L = 4.4$. These paths are centrally running around the holder center. With a further increase of the rotational speed ratio, interlaced hypocycloids are formed (4), which change over into the special case of common hypocycloids (f) at $N_L = 11.1$, which, in turn, have no recurring vertexes. Further on, the path curves change over into stretched hypocycloids (5).

### 2.8.4.5 Progression of the Path Velocity

The geometry of a path curve depends on the rotational speed ratio $N_L$. The velocities of a workpiece point $P_W$ covering this curve are determined by

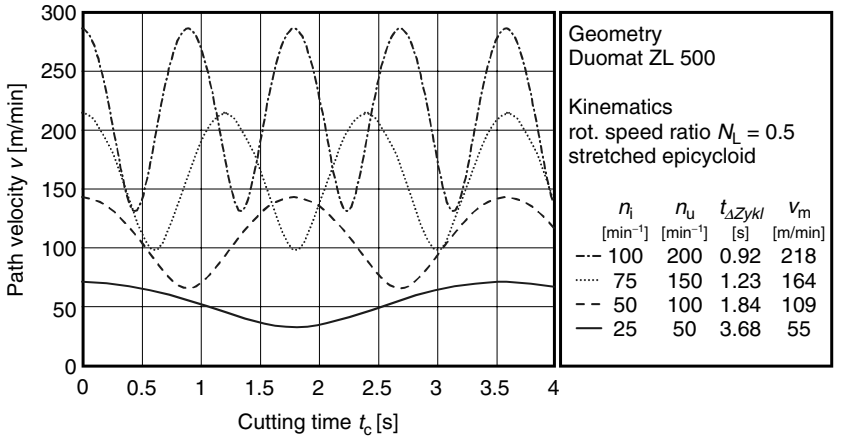


**FIGURE 2.19** Path velocities at constant path curve geometry. (From Ardelt, Th., Einfluss der Relativbewegung auf den Prozess und das Arbeitsergebnis beim Planschleifen mit Planetenkinematik. Dissertation, TU Berlin, 2000; zugl. Reihe Berichte aus dem Produktionstechnischen Zentrum Berlin, 2001.)

the absolute values of the rotational speeds set on a pin circle and a lapping wheel. This fact is demonstrated by Figure 2.19, which contains the path velocities for the rotational speed ratio of $N_L = 0.5$. The four demonstrated velocity progressions from the bottom up are each based on a rotational speed $n_i$ increased by 25 min$^{-1}$, and, accordingly, a rotational speed $n_u$ increased by 50 min$^{-1}$. This makes clear that the part-cycle time $t_{\Delta cycl}$ is halved by a duplication of the two rotational speeds. The absolute values of the path velocity duplicate simultaneously. The relation of maximum and minimum path velocity is constant at fixed $N_L$.

## 2.8.5 Calculation of the Path Length Distribution over the Lapping Wheel Radius

### 2.8.5.1 Profile and Grain Wear during Machining

Like all tools, lapping wheels are subject to wear. Due to the planetary movement patterns, the workpieces spend different amounts of time in the individual radial areas of the wheel covering different distances. This leads to inhomogeneous strains, which cause inhomogeneous wear.

Many methods published so far on the forecast of the wear of lapping wheels are based on the idea that the volume removed from the workpiece as well as worn from the lapping wheel are proportional to the distance they cover relatively to each other. In the case of the workpiece, the covered distance and the length of its path curve are identical. A surface element of the lapping wheel has no constant workpiece contact, it is rather multiply

crossed by individual workpieces. This leads to the wear hypothesis that the wear of a surface element of the lapping wheels is proportional to the path on which workpieces are contacted in the process [70,105,112–115]. The following pages show a way to calculate the distribution of path curve lengths over the wheel radius.

### 2.8.5.2 Description of Workpiece Geometry by the Geometric Function

For the numerical calculation of the path length distribution, information on number, geometry, and position of the workpieces in the workpiece carrier have to be transformed into a manageable form. This is realized by making use of the fact that all workpiece points at the same distance $e_H$ from the holder center carry out the same path movement with a shift in time and location, thus equally stressing the lapping wheel. These points can be discussed as a group.

The geometric function $g_W(e_H)$ is defined for this purpose. It describes the amount of workpiece surface being at a certain distance $e_H$ from the holder center H. For the calculation of the geometric function, concentric circles with a radius of $e_H$ and a circumference of $2\pi e_H$ are laid into the holder starting at the holder center H. Then, the length of all arc segments of all circles lying in the workpiece area is determined (Figure 2.20). The number of equally occupied workpiece holders will be considered in factorial terms further on.

In physical terms, the geometric function $g_W(e_H)$ has the dimension of a length, and the surface below the curve corresponds to the surface of all

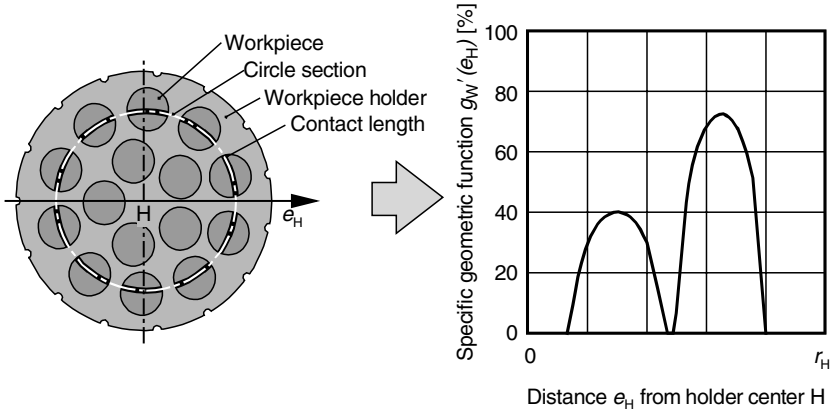


**FIGURE 2.20** Simulation of the holder occupancy as a two-dimensional geometric function. (From Ardelt, Th., Einfluss der Relativbewegung auf den Prozess und das Arbeitsergebnis beim Planschleifen mit Planetenkinematik. Dissertation, TU Berlin, 2000; zugl. Reihe Berichte aus dem Produktionstechnischen Zentrum Berlin, 2001.)

metered workpieces. The best method to compare different holder occupancies is to standardize the biggest possible contact length between an arc and the workpieces, which is theoretically the circumference of the workpiece holder $2\pi r_H$. This results in the specific geometric function

$$g'_w(e_H) = \frac{g_w(e_H)}{2\pi r_H} \tag{2.28}$$

which is not a physical unit, but has the character of a weighting factor. It is indicated in terms of percentage.

### 2.8.5.3 Path Length Distribution

Figure 2.21 shows the subdivision of the working surface in a finite number $i$ of circular classes $K_i$. All lapping wheel classes are grouped centrally around the lapping wheel center $Z$ and have the same width. Each of these lapping wheel classes is limited by its internal and external class radii $r_{iK_i}$ and $r_{aK_i}$, and has the surface area $A_{SK_i}$.

The path length distribution can be calculated on the basis of the lapping wheel classing. It is sufficient to determine each path curve for the half part-cycle time $0 < t < t_{\Delta cycl}/2$, as the progression of the further path curve is adequate to this time period. The path length distribution calculated for half a part-cycle time is subsequently extrapolated to the whole machining time. The length of stay of a workpiece point $P_W$ within a lapping wheel class $K_i$ is determined by the points in time $t_{1i}$ and $t_{2i}$, at which it enters and leaves a

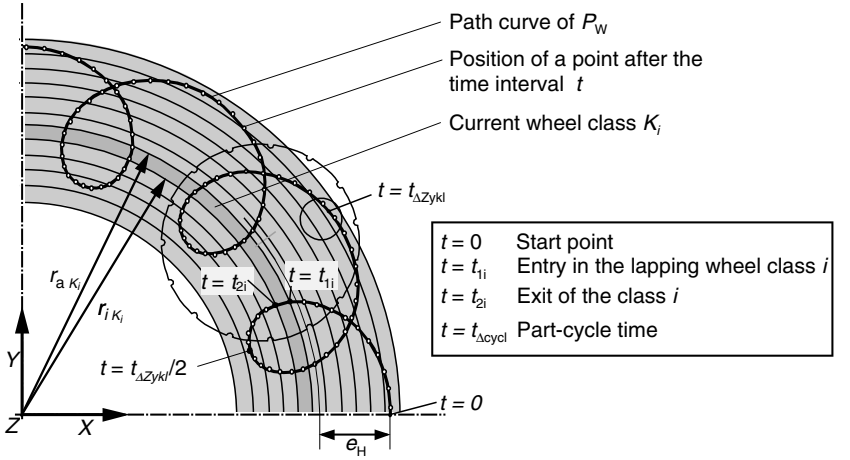


**FIGURE 2.21** Classing of the lapping wheel and determination of the path curve segments in the individual classes. (From Spur, G. and Eichhorn, H., *IDR*, 31 (2), 169, 1997.)

class. The time limits $t_{1i}$ and $t_{2i}$ result from the intersections of the path curve and the margins of the respective class $r_{aK_i}$ and $r_{iK_i}$. According to Spur and Eichhorn [106], if these radii are substituted in Equation 2.6 for the absolute value of the path curve vector, the points in time $t_{1i}$ and $t_{2i}$ result from the equation

$$t_{1i,2i} = \frac{1}{\omega_H - \omega_Z} \arccos\left(\frac{r^2_{1i,2iK_i} - a^2_Z - e^2_H}{2a_Z e_H}\right) \tag{2.29}$$

The path curve segment of the point $P_W$ covered in the lapping wheel class can be calculated by the integral of the path velocity in the calculated time limits

$$s_{P_W K_i} = \int_{t_{1i}}^{t_{2i}} v_{P_W}(t)\,\mathrm{d}t \tag{2.30}$$

To numerically determine the totality of all workpiece surfaces, the path curves of a finite number of workpiece points have to be calculated. For this purpose, the distance from the holder center $e_H$ is varied starting from zero in $n$ increments up to the radius of the holder. Then, the path curve and the length of its path curve segments in the individual lapping wheel classes are calculated for each value of $e_H$. The set of all workpiece points moving along this path curve is weighted by the value of the specific geometric function $g'_w$ ($e_H$). This procedure leads to the term

$$s_{K_i} = \sum_{j=0}^{n} g'_W\left(e_H = j \cdot \frac{r_H}{n}\right) \cdot \int_{t_{1i}}^{t_{2i}} v(t)\,\mathrm{d}t \tag{2.31}$$

for the class path length $s_{K_i}$ covered in a lapping wheel class. In this numerical procedure, the absolute values of $s_{K_i}$ depend on the number of the sampling points and the increment $n$. Accordingly, the class path lengths $s_{K_i}$ represent no quantitative path lengths but qualitatively describe the distribution of all covered distances on the wheel classes. To represent the class path lengths independently of the numerical accuracy of the calculation, the maximum value has to be standardized. Thus, the class path lengths can be represented in terms of percentage and the different machining cases can be compared. The result of the standardization is the specific class path length $s_{K'_i}$. As Figure 2.22 shows, the envelope curve of the specific class path lengths $s_{K'_i}$ to $s_{K'_i}$ can be represented as specific path length distribution $s'(r_s)$ over the lapping wheel radius in case of sufficient numerical accuracy. Particularly if several calculation results are compared, the representation as a curve is much clearer than a bar chart.

The qualitative progression of the path length distribution depends on the machine design and on the movement pattern. Its quantitative height increases linearly with the lapping time and with the average path velocity.

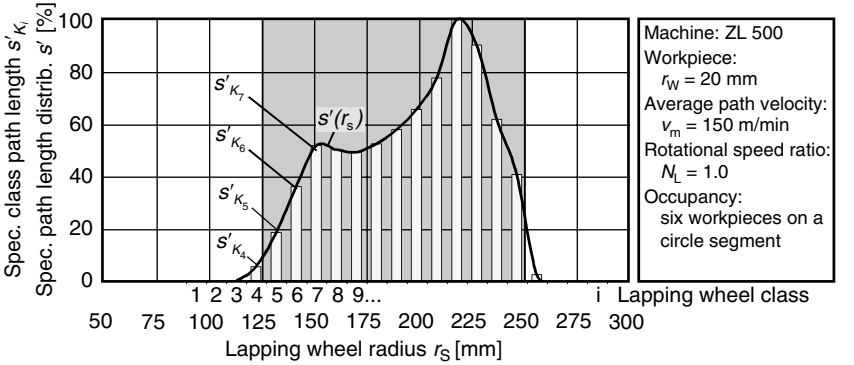


**FIGURE 2.22** Transition from the specific class path lengths to the specific path length distribution. (From Ardelt, Th., Einfluss der Relativbewegung auf den Prozess und das Arbeitsergebnis beim Planschleifen mit Planetenkinematik. Dissertation, TU Berlin, 2000; zugl. Reihe Berichte aus dem Produktionstechnischen Zentrum Berlin, 2001.)

The two diagrams in Figure 2.23 show specific path length distributions $s'(r_s)$ for different rotational speed conditions $N_L$. An even arrangement of six workpieces on a circle with a radius of 54 mm was assumed for the curves depicted in the diagram on the left side. The diagram on the right

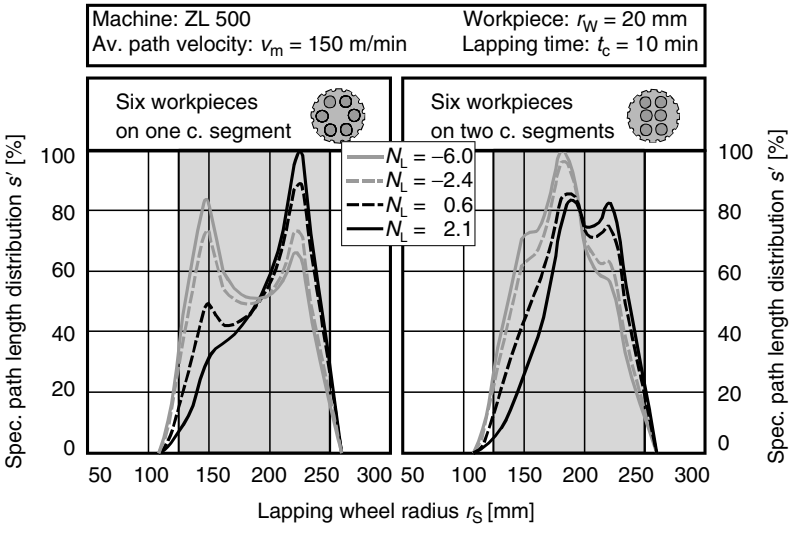


**FIGURE 2.23** Specific path length distribution for different rotational speed ratios and holder occupancies. (From Ardelt, Th., Einfluss der Relativbewegung auf den Prozess und das Arbeitsergebnis beim Planschleifen mit Planetenkinematik. Dissertation, TU Berlin, 2000; zugl. Reihe Berichte aus dem Produktionstechnischen Zentrum Berlin, 2001.)

shows results of the arrangement on two circles with the radii 54 and 23 mm. All specific path length distributions in the left diagram show two local maxima, occurring symmetrically to the center between the inner and outer lapping wheel edges. The radial lengths of these maxima result from the distance of the workpiece centers from the holder center and are independent of the rotational speed ratio. Although the relative heights of the two maxima change relatively to each other through a variation of $N_L$, the progression of the curves remains the same. In the case of hypocycloid path curves, like occurring at a rotational speed ratio $N_L = -6$, (see Figure 2.18), the absolute maximum of the specific path length distribution is at the inner edge of the lapping wheel. At $N_L = -2.4$, all workpieces cover eccentric circular paths around the center of the lapping wheels. In this case, there is a path length distribution, which is symmetrical to the center, with two equal local maxima. At $N_L = 0.6$, the absolute maximum is near the outer edge of the lapping wheel. If the workpiece centers cover common epicycloids on the lapping wheel, the path curve segments on the inner part of the lapping wheel are relatively short, so that no local maximum occurs here.

If the workpieces are arranged on two circle segments, the specific path length distributions have different progressions than in the diagram on the left side. In this case, they cover especially long distances in the middle of the inner and outer lapping wheel edges, whereas the contact frequency to the lapping wheel edges is different according to the chosen rotational speed ratio.

This illustration shows that the influence of the arrangement of the workpieces in the holder on the specific path length distribution is as big as the rotational speeds of the inner pin circle and of the lapping wheel.

### 2.8.6 Cutting Conditions in the Case of One-Sided and Two-Sided Machining

Different authors have reported that the material removal rate during face lapping increases linearly with the average path velocity [69,103,116]. This means that the material removal per lapping path length is independent of the path velocity.

Figure 2.24 shows two workpieces A and B, which move on a stretched epicycloid. In the case of this path pattern, the path velocity increases monotonously with the lapping wheel radius, as the diagram on the right shows. As an average value in every part cycle, both workpieces have the same path velocity and cover the same distances. If a shorter time interval $\Delta t_c < t_{\Delta cycl}$ is considered, significant differences can be observed. The workpiece B, which starts at the inner edge of the lapping wheel at the time $t_0$, covers a shorter path distance in the time interval $\Delta t_c$ than the workpiece A, which starts near the outer edge of the wheel.

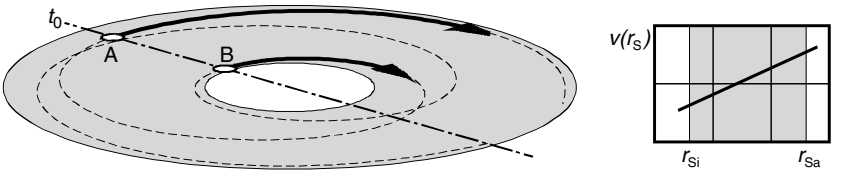


**FIGURE 2.24** Path curve segments of two workpiece points in the time interval $\Delta t_c$. (From Ardelt, Th., Einfluss der Relativbewegung auf den Prozess und das Arbeitsergebnis beim Planschleifen mit Planetenkinematik. Dissertation, TU Berlin, 2000; zugl. Reihe Berichte aus dem Produktionstechnischen Zentrum Berlin, 2001.)

During the time interval $\Delta t_c$, the upper lapping wheel descends onto the lower wheel. Its feed speed results from the workpiece height reduction $\Delta h_W$ and the grinding time $t_c$ to

$$\Delta \dot{h}_W = \frac{\Delta h_W}{t_c} \tag{2.32}$$

and is called time-related workpiece height reduction $\Delta \dot{h}_W$ according to a proposal of Funck [103]. As all workpieces in the working space have the same height at every point in time independently of their radial position, also the time-related workpiece height reduction has to be independent of the radius of the lapping wheel. In the process, it can be subject to temporal fluctuations, it must be, however, locally constant as the lapping wheel cannot descend on certain radii faster than others.

The workpiece height reduction can be determined from the path-related point of view according to

$$\Delta h_W = s(r_S) \cdot \Delta h'_W(r_S) \tag{2.33}$$

as a product of the grinding path $s$ and the path-related height reduction $\Delta h'_W$ [103]. The path a workpiece covers in a time interval can be calculated from its path velocity $v(t, r_S)$, which functionally depends on the time and on the lapping wheel radius. For this reason, the dependence $s(t, r_S)$ also applies to the covered path. According to Equation 2.33, the path-related workpiece height reduction, too, is a function of the lapping wheel radius. The result for the example in Figure 2.24 is that the two workpieces A and B are subject to the same workpiece height reduction $\Delta h_W$ during their movement on different paths $\Delta s_A \neq \Delta s_B$. The transposition of Equation 2.33 leads to the equation

$$\Delta h'_W(t, r_S) = \frac{\Delta h_W(t)}{\Delta s(t, r_S)} = \frac{\Delta \dot{h}_W(t)}{v(t, r_S)} \tag{2.34}$$

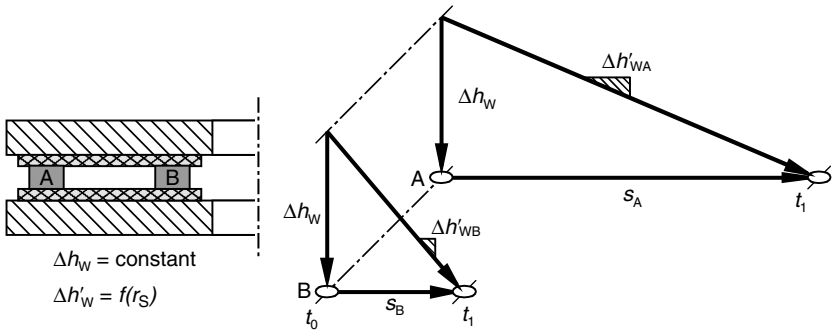


**FIGURE 2.25** Time- and path-related workpiece height reduction during double-sided machining. (From Ardelt, Th., Einfluss der Relativbewegung auf den Prozess und das Arbeitsergebnis beim Planschleifen mit Planetenkinematik. Dissertation, TU Berlin, 2000; zugl. Reihe Berichte aus dem Produktionstechnischen Zentrum Berlin, 2001.)

for the path-related workpiece height reduction, according to which $\Delta h'_W$ is indirectly proportional to the covered distance and the path velocity $v$ of a workpiece. According to this, the highest path-related workpiece height reductions occur where the path velocities are the lowest. Figure 2.25 depicts the time- and path-related workpiece height reduction and the path movement of the two workpieces A and B as vectors.

The draft shows a two-sided machining between two wheels corresponding to face lapping with planetary kinematics. Despite different path lengths $s_A$ and $s_B$, the heights of both workpieces are reduced evenly by the workpiece height reduction $\Delta h_W$. Due to the different grinding paths, different path-related workpiece height reductions $\Delta h'_{WA} \neq \Delta h'_{WB}$ result for the two workpieces. According to Equation 2.34, they correspond to the slopes of the vectors running diagonally downwards.

Figure 2.26 shows vectorially the time- and path-related workpiece height reductions in the case of single-sided machining under individually applied overloads. Here, the two workpieces A and B do not influence each other. As both are loaded with identical forces, the workpiece height removed from the two workpieces corresponds to the covered distances. Thus, the path-related workpiece height reduction $\Delta h'_W$ is constant here, the workpiece heights removed per time unit $\Delta h_{WA} \neq \Delta h_{WB}$, however, are different and depend on the current radial position. Consequently, in the case of this second configuration, the distribution of the path lengths over the lapping wheel radius suggests the load of the lapping wheel. The heights of the individual workpieces differ according to their radial position.

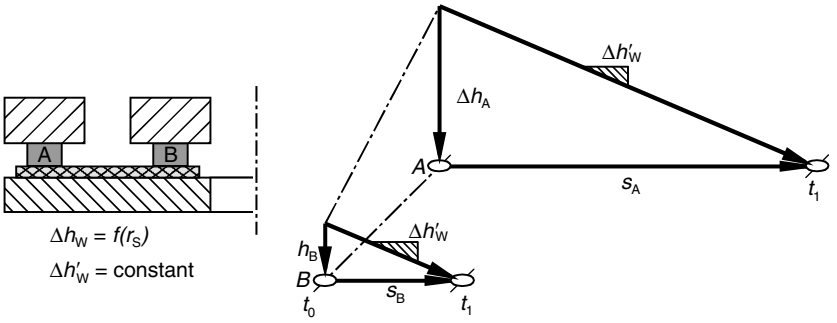


**FIGURE 2.26** Time- and path-related workpiece height reduction in the case of one-sided face machining.

## 2.9 PROCESS MODELS AND SIMULATION

The real process events are depicted by a process model within defined validity limits. The goal of process modeling is to achieve a preferably high concordance between reproduction and the real process events [117]. The extent of technological verifiability characterizes the quality of a process model [104]. The modeling allows the programmable description of the process. The implementation in the computer provides a program, which simulates the real process [118]. Analytical models describe the system processes by equation systems. The results are mathematically exact or approximate (heuristic) solutions [118]. Numerical models describe system processes through programmable algorithms. They are used if no deterministic rules are defined for the time response in the system or certain events cannot be predicted [119,120].

For the use of the process model, the processes have to be simulated in real or imaginary systems with the help of physical and formal models. This procedure is called process simulation [70,118]. Thus, it has no independent calculation or optimization process, but is a kind of virtual experiment with concrete reference to reality [104]. Consequently, the process simulations are an instrument for cost minimizing optimization of processes before realization [104,121].

The description of technological dependencies of the material removal rate and of the work result on the process parameters of lapping by characteristic curves is often insufficient for a cohesive representation of the interaction between process control and target qualities. The cause is that it is only during the lapping process that the effective tool specification is stochastically generated and must be described with statistical principles. Additionally, there are a number of influencing parameters, whose effects on the tool specification, the lapping process, and the work result are strongly interconnected [59]. This leads to the system structure of the interaction between the

tool and the workpiece as explained in Section 2.5. This makes it impossible to give a deterministic description of the machining process.

These relationships prevented the definition of characteristic values of lapping, which make possible the optimization of the lapping process in advance. Due to the incomplete knowledge of the functional dependencies, the quality of the work result in lapping often depends on the internal experience in the enterprise. The process layout is always linked to a concrete material removal system. The alteration of the parameters of the material removal system requires new knowledge from experiments.

There are different model approaches for the description of material removal during lapping. These approaches by Imanaka [51], Chauhan et al. [48], Buijs, and Korpel-van Houten [45,46] are based on the observation of the force relations at the single grain and the resulting stress field in the subsurface of the workpiece, which lead to material removal and surface formation. The goal of these process models is first of all the analytical forecast of the achievable surface quality for different lapping systems.

### 2.9.1 Process Model According to Imanaka

The process model by Imanaka [51] is used for the predetermination of the maximum surface roughness. A lapping system for the lapping of glass is taken as an example. The single lapping grains are supposed to have rounded edges. In case of pressure load, the grains do not penetrate the workpiece, but are subject to elastic deformation depending on the edge radius. This leads to the formation of a circular contact area with the radius $a_c$. A Hertzian stress field is induced in the workpiece. If a critical stress is exceeded, an annular crack develops, which propagates deep into the subsurface along a material-dependent angle to the workpiece surface by the value $h$. The truncated cone typical for the Hertzian load case develops in this process (Figure 2.27). The superposition of adjacent conical cracks leads to the break off of single material particles. The parameters $\theta$, $a_c$, and $h$ of the conical cracks are calculated with the classical Hertzian equations in dependence on the pressure per grain, the Poisson ratio, and Young's modulus of the grain and the workpiece, the cutting edge radius, as well as on the relation of the elasticity limit and the surface stress to the specific surface energy of the workpiece. The latter parameter is generated from indentation tests. The cutting edge radius is assumed to be 1/10 of the grain diameter.

The maximum surface roughness corresponds to the depth extension of the conical crack $h$ vertically to the workpiece surface. This depends on the compressive force the active grains are charged with. The pressure per grain results from the number of grains involved in the lapping process. It can be calculated on the basis of statistical considerations suggesting that the grain size distribution of the lapping abrasive corresponds to the Gaussian normal distribution. The biggest grain determines the height of the lapping gap less

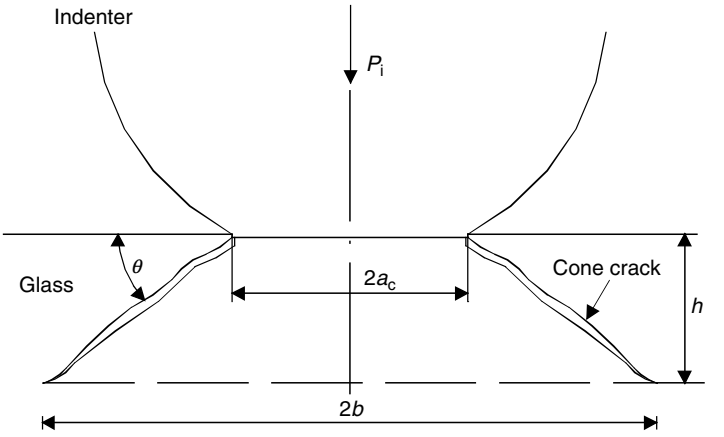


**FIGURE 2.27** Schematic representation of the conical crack behavior. (From Imanaka, O., *Ann CIRP*, 23, 227, 1966.)

the elastic deformation of the active partners. The size of the biggest grain results from the total number of lapping grains in the working gap, the average equivalent diameter of the sphere of equal sinking speed according to Stokes, and its standard deviation. Imanaka specifies the average Stokes diameter with 8/10 of the grain diameter of the sphere of equal projected area.

The total number of the grains in the working gap depends on the height of the lapping gap and the grain concentration in the lapping slurry. The number of active lapping grains involved in the material removal process is calculated with the distribution function of the normal distribution for the probability that the grains of the basic population are bigger than the height of the lapping gap. As the lapping pressure is distributed to the number of active grains, also the elastic deformation of the active partners and thus the height of the lapping gap depend on the number of active grains, leading to a recursive calculation.

This process model is only applicable to other lapping systems, if the material removal takes place through the networking of Hertzian conical cracks. Further problems are the negligence of crack superposition, the calculation of the height of the lapping gap without considering the penetration of the grains into the lapping wheel and when using the Stokes diameter, as well as the fact that the $\theta$ angle can only be estimated and occurs in the equation with the tangent.

### 2.9.2 Process Model According to Chauhan et al.

The approach of Chauhan et al. [48] should make possible the calculation of the resulting surface quality of lapping of ceramics on the basis of the active grain number and the pressure distribution to the grains. According to

Chauhan et al., the material removal takes place through crack formation, which, in contrast to the assumptions of Imanaka, can be traced back to the penetration of pointed, conical bodies. At the moment of penetrating the workpiece material, these provoke a Boussinesquian state of tension. The material removal takes place through the formation and propagation of an axial–lateral crack system. The resulting average roughness height $R_z$ corresponds to the depth of lateral crack formation below the engaging active grains.

The depth of lateral crack formation depends on the depth of penetration of the pointed body and the extension of the plastic zone below the grain (Figure 2.28). The extension of the plastic zone can be calculated with Hill's relation between the average contact pressure (hardness) and the Young's modulus of the workpiece depending on half the aperture angle of the grain tip, on the radius $a$ of the conical indentation at the surface, on the radius $u$ of the plastic zone, and on the Poisson number $v$ of the workpiece [48,122]. The average contact pressure depends on the pressure per active grain.

For the calculation of the active grain number, Chauhan et al. use an approach similar to Imanaka's. Through the use of the Stokes diameter, he obtained a higher number of grains than Chauhan et al., whose calculation was done using the equivalent diameter. In contrast to Imanaka, Chauhan et al. consider the penetration of lapping grains into the workpiece for the calculation of the working gap geometry.

Chauhan et al. also have to make assumptions for the calculations of the crack system below the single-grain cutting edges. The grain aperture angle,

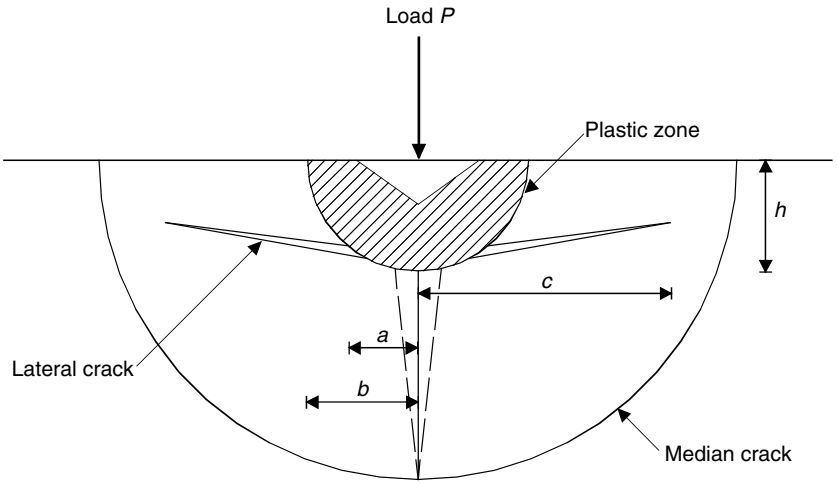


**FIGURE 2.28** Schematic representation of an axial–lateral crack system. (From Chauhan, R., Ahn, Y., Chandrasekar, S., and Farris, T.N., *Wear*, 162–164, 246, 1993.)

which is very difficult to calculate, strongly influences the result of the calculation. The specification of this angle should not be possible, as it is very different in the case of each single lapping grain and thus hardly measurable. In the calculation of the working gap geometry, the penetration of the lapping grains into the lapping wheel is neglected. The use of statistical principles for the calculation of the active grain number from the grain size distribution of the lapping abrasive reflects the stochastic nature of the tool formation. Hereto, Chauhan et al. do not use the maximum, but the equivalent diameter of the grains.

### 2.9.3 Process Model According to Buijs and Korpel-van Houten

Buijs and Korpel-van Houten [45,46] describe a process model for the lapping of glass. They use it as a basis for the derivation of equations for the material removal rate, surface roughness, and axial crack propagation. Hereby, they act on the assumption of rolling lapping grains, whose edges are pressed into the workpiece in a quasistatistical way, provoking an axial–lateral crack. The average depth of roughness corresponds to the depth of lateral crack formation under an engaging grain according to Marshall et al. [65]. They calculate the axial crack propagation with the equations by Lawn et al. [64]. For the calculation of the material removal rate, they use the model by Wiese and Wagner, which is a model of calculating the material removal rate as a product of the frequency of grain engagement and material removal per grain (see Section 2.4) [67]. The frequency of grain engagement depends on the number of cutting edges of the rolling grains and the relative speed of the lapping wheels and the workpiece.

Based on the formulas of Marshall et al., the depth of the formation of lateral cracks $h$, as well as its lateral propagation $c$ can be calculated over the pressure by means of material characteristic values and factors of grain shape [65]. The material volume removed by a single grain engagement results in a volume of a cylinder with the height $h$ and the diameter $2c$.

For the calculation of the number of active grains, it is assumed that the height of the working gap is twice as high as the average grain size. The active grain number results from the Gaussian distribution function of the grain size and the number of grains in the working gap for the probability of the grains being larger than twice the average grain diameter. Buijs and Korpel-van Houten calculate the number of grains in the working gap for a certain working gap height from the single grain volume for sphere geometry and the grain concentration of the slurry.

One of the three target values, material removal rate, axial crack depth, or roughness, must be always known for the calculation of the pressure per grain. Thus determined pressure per grain is then used for the calculation of the two unknown values. In this way, the model approach provides no clear solution for the relations in the removal system.

The fact that the material break off is considered a cylindrical volume with the depth and the extension of the lateral crack leads to considerably higher calculated material removal rates than in reality. Furthermore, the assumption of the height of the lapping gap being twice the average grain diameter leads to a very high number of active grains with an accordingly lower pressure per single grain. According to Lawn et al. and Marshall et al., factors defined for the lapping system and the grain aperture angle have to be considered for the calculations of the crack system geometry [64,65]. The aperture angle, which can only be estimated, occurs in the calculations with the cotangent and is thus a particular source of failure.

Buijs and Korpel-van Houten assume a rolling movement of the lapping grains in the working gap. Using the model approach by Wiese and Wagner, the superimposition of the individual crack systems under the grain cutting edges occur in the calculations of the material removal rate. This does not apply to the roughness and the depth of the axial crack.

### 2.9.4 Summarizing Assessment of Process Models According to Imanaka, Chauhan et al., and Buijs and Korpel-van Houten

The models by Imanaka, Chauhan et al., and Buijs and Korpel-van Houten are based on the fracture mechanical calculation of crack systems below the engaging single grain cutting edges. This requires a very exact knowledge of the geometrical and mechanical properties of the active parameters. Parameters, which are difficult to ascertain, such as the aperture angle or corner radii of the single grains, have a particularly high influence on the measuring result. As the geometrical characteristic values of grain collectives are stochastic, the aperture angles of the grains and other grain parameters have to be ascertained and evaluated by statistical methods.

A number of parameters for the calculations in the model approaches have to be determined in experiments. Thus, the universal validity of the observed removal system is not guaranteed. The basis of the calculations of the active grain number is grain size parameters, which are measured before the process start. The grain size distribution changes during machining as a result of the wear of the abrasive. The consideration of the equivalent diameter as determining parameter partially leads to decisively smaller dimensions of the lapping gap assuming that the penetration by the lapping grain mainly takes place over the maximum grain diameter.

Apart from the calculations of the material removal rate by Buijs and Korpel-van Houten, an interaction of single material break offs is as little considered as the engagement conditions between the grain and the lapping wheel, though they are crucial elements of the total material removal process.

Although the models reflect the material removal systems presented within the scope of modeling, they cannot be transmitted to other removal

systems and no clear description is possible. No parameters of universal validity are developed for the description of the interrelations in the removal system.

### 2.9.5 Process Model According to Engel

Due to the described deficits of the process models represented so far, Engel [49,123] developed a numerical process model for the lapping of monocrystal silicon, which makes it possible to describe the interaction between the tool formation and the tool engagement, as well as between the removal rate and the subsurface-related work result on the basis of technological functions for relevant process parameters. Hereby, focus is not placed on the determination of the work result, but on the simulation of a removal system in order to identify effective possibilities for its specific optimization.

The removal rate is described by the modeling of the tool formation and the tool engagement. The number of lapping grains in the working gap and the ratio of active grains are determined for the description of the tool formation. The frequency and the depth of removal processes are determined for the description of the tool engagement. A qualitative assessment of the process can take place on basis of the engagement frequency and intensity. These specifications are comprised in a parameter. This parameter reflects the effectiveness of the process, which is defined by a low surface and subsurface stress as well as by a high removal rate.

The process model developed by Engel differs from the previous ones in the following three aspects:

- Removal results from the sum of all crack systems generated by the engagement of the active grains. The removal takes place in layers.
- Working gap is considered a space, whose height is determined by the interaction of three distribution functions: the functions of material distribution with increasing depth of the roughness profile of the workpieces and of the lapping wheels (Abott curves) formed as a result of the grain engagement as well as the distribution function of the maximum process grain size developing as a result of the grain wear during the process.
- All parameters of the tool formation and of the tool engagement are derived from measurable parameters with statistical methods for given probabilities.

#### 2.9.5.1 Model Boundary Conditions and Validity Limits

Engel defines that the application of load by engaging lapping grains is mainly normal to the workpiece surface and takes place under the formation of a Boussinesquian state of stress. The removal process of monocrystal silicon takes place through lateral crack formation, propagation, and superposition.

The subsurface damage is caused by the formation, propagation, and superposition of half-penny-cracks. The size parameters of the lapping grains are characterized by normal distribution; the lapping grains engage stochastically. The lapping grains do not continuously roll in the working gap. In case of continuous slurry feed, a stationary state occurs in the process after a certain lapping period characterized by a constant process grain distribution of the abrasive and by constant roughness profiles of the lapping wheels and the workpieces. The lapping grains must be able to move freely in the working gap. There is no polish lapping or polishing through scratching by grains temporarily embedded in the lapping wheel.

### 2.9.5.2 Tool Formation

The lapping tool is formed during the machining by the lapping wheel and the active grains distributed in the lapping fluid. The decisive parameter for tool formation is the process grain size distribution of the maximum grain diameter of the respective abrasive (Figure 2.29).

A working gap volume $V_{AS}$ is formed above the workpiece by the normal lapping grains distributed in the slurry. This volume is determined by the height of the working gap $h_{AS}$ and the workpiece surface $A_W$:

$$V_{AS} = A_W \cdot h_{AS} \tag{2.35}$$

The height of the working gap is crucially determined by the maximum process grain diameter of the biggest lapping grain $d_{kpmax}$ in the working gap. The biggest value appearing in a distribution increases with the total

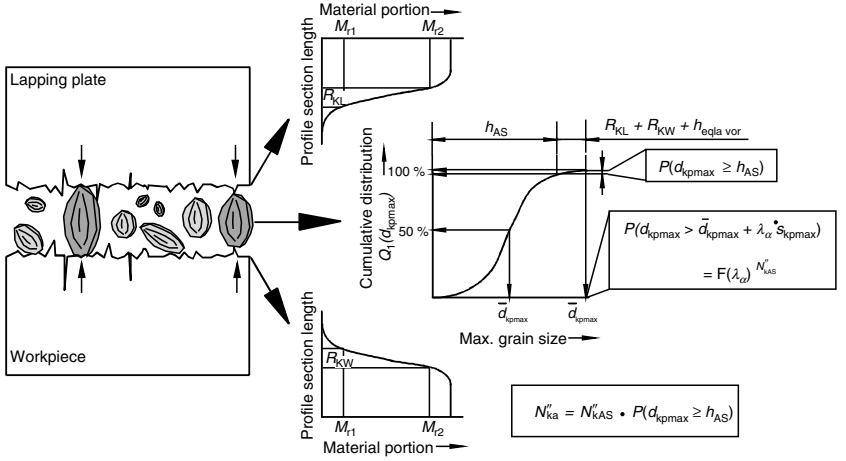


**FIGURE 2.29** Schematic representation of the parameters of tool formation. (From Engel, H., Läppen von einkristallinem Silicium. Dissertation, TU Berlin, 1997.)

number of existing individuals. Therefore, the following equation defining the probability of a biggest maximum process grain size applies to a normal abrasive collective with the average value $\bar{d}_{\mathrm{kpmax}}$ and the standard deviation $s_{\mathrm{kpmax}}$ [124–126]:

$$P(d_{\mathrm{kpmax}} > \bar{d}_{\mathrm{kpmax}} + \lambda_\alpha \cdot s_{\mathrm{kpmax}}) = \Phi(\lambda_\alpha)^{N''_{\mathrm{kAS}}} = \alpha \tag{2.36}$$

with

$$\lambda_\alpha = \frac{d_{\mathrm{kpmax}} - \bar{d}_{\mathrm{kpmax}}}{s_{\mathrm{kp\ max}}} \tag{2.37}$$

After the specification of the significance level $\alpha$, $\lambda_\alpha$ can be determined according to the following equation:

$$\Phi(\lambda_\alpha) = \frac{1}{\sqrt{2\pi}} \int_{-\infty}^{\alpha/N''_{\mathrm{kAS}}} \mathrm{e}^{\frac{-\lambda_\alpha^2}{2}} \mathrm{d}\lambda_\alpha \tag{2.38}$$

The absolute number of the lapping grains in the surface-related working gap volume results from the specific volume of the lapping grains in the working gap and the average grain volume (Equation 2.38). Equation 2.38 can be solved with this indication:

$$N''_{\mathrm{kAS}} = \frac{V''_{\mathrm{kpAS}}}{\bar{\nu}_{\mathrm{kp}}} = \frac{6C_{\mathrm{k}}A_{\mathrm{W}}d_{\mathrm{kpmax\ max}}}{\pi \bar{d}_{\mathrm{kp}}^3 A_{\mathrm{W}}} \tag{2.39}$$

If the workpiece and the lapping wheel had ideal surfaces, only the biggest grain would close the contact chain between the wafer and the lapping wheel. In reality, there are always profile deviations in technical surfaces. Figure 2.29 depicts the decrease of the real working gap height through these profile deviations. Thus, also small lapping grains can engage in the removal process. A removal process takes place if a lapping grain gets caught in a profile unevenness of the lapping wheel and of the workpiece and erects as a result of the relative movement. Therefore, the working gap height must be reduced by the value of the profile depth the lapping grain gets caught in. This value is described by the kernel roughness depth derived from the Abbott curve. The kernel roughness depth of the grain can be measured after the process.

The grain engages in the workpiece at each erection. This fact is taken into account in the value of the kernel roughness depth measured after lapping. The microtopography of the lapping wheel is plastically deformed by engaging grains. The roughness profile after the process represents the respective instantaneous value of the grain engagement depth (for stationary process conditions).

In the case of lapping monocrystal silicon, the engagement of the grain in the workpiece leads to deep lateral cracks. Therefore, the roughness profile of the workpieces after the process does not provide direct information on the grain engagement depth. Engel introduced the concept of removal depth. The removal depth indicates the depth where the crack formation leading to material removal starts below the engaging grain. Thus, for the calculation of the working gap height, it must be additionally reduced by a default value for the removal depth of the lapping grain in the workpiece, as this value cannot be changed subsequently. This leads to a resulting working gap height of

$$h_{\mathrm{AS}} = d_{\mathrm{kpmax}} - R_{\mathrm{KL}} - R_{\mathrm{KW}} - h_{\mathrm{eqla\ vor}} \tag{2.40}$$

For the further description of the tool formation, it is necessary to detect the number of active grains, which actually close the contact chain between the lapping wheel and the workpiece, engage in the material, leading to removal. This applies to all grains in the working gap, whose maximum process grain diameter exceeds the resulting height of the working gap. This is the part of the basic population of the existing grains, which results from the product of the total number of grains in the working gap $N''_{\mathrm{kAS}}$ and the probability of the maximum process grain size exceeding the working gap height:

$$N''_{\mathrm{ka}} = N''_{\mathrm{kAS}} \cdot P(d_{\mathrm{kpmax}} \geq h_{\mathrm{AS}}) \tag{2.41}$$

If the distribution function of the maximum process grain size corresponds to a normal distribution, this probability calculated with the standardized form of the distribution function results in

$$P(d_{\mathrm{kpmax}} \geq h_{\mathrm{AS}}) = 1 - \Phi(z_{h_{\mathrm{AS}}}) = \frac{1}{2\pi} \int_{h_{\mathrm{AS}}}^{\infty} \mathrm{e}^{-\frac{1}{2}(z_{h_{\mathrm{AS}}})^2} \mathrm{d}z_{h_{\mathrm{AS}}} \tag{2.42}$$

with

$$z_{h_{\mathrm{AS}}} = \frac{h_{\mathrm{AS}} - \bar{d}_{\mathrm{kpmax}}}{s_{\mathrm{kpmax}}} \tag{2.43}$$

The number of active grains thus results in

$$N''_{\mathrm{kAS}} = N''_{\mathrm{kAS}}[1 - \Phi(z_{h_{\mathrm{AS}}})] \tag{2.44}$$

This equation describes the lapping tool formed in the removal system. The way this tool leads to the removal on the workpiece is described in Section 2.9.5.3.

### 2.9.5.3 Tool Engagement

This section describes the parameters of tool engagement. This will take place on the basis of the calculation of active grains in the working gap discussed in Section 2.9.5.2. In the working gap, the active grains $N_{ka}$ are homogeneously distributed over the workpiece surface. The average distance $a_{ka}$ between the active grains can therefore be indicated in a simplified way:

$$a_{ka} = \sqrt{\frac{A_W}{N_{ka}}} = \frac{1}{\sqrt{N''_{ka}}} \tag{2.45}$$

Engel found out in the model lapping tests that a sequence of grain engagements does not take place through rolling lapping grains. The distance between two engagements does not depend on the grain geometry, but on the distance between the active grains. The frequency of an engagement is determined by the distance of two active grains and the relative speed of the lapping grains in the working gap. If these relative speeds are equated with the average path velocity $v_m$, the grain engagement frequency $f_e$ is

$$f_e = \frac{v_m}{a_{ka}} = v_m \cdot \sqrt{N''_{ka}} \tag{2.46}$$

It is reasonable to describe the interactions of all single grain engagements for a technological process description. Due to the normally distributed grain geometry parameters, removal can only be determined statistically for the single engagement. Furthermore, the interactions between the material break offs have to be taken into account. Engel considers the removal process by layers. Due to the plane contact between the tool and the material, the material is not removed in locally differing ways, but exclusively in planes from the entire contact surface (Figure 2.30).

One layer material is removed if the working gap volume $V''_{AS}$ (related to the workpiece basic surface $A_W$) has been filled with active grains exactly once. This happens if the maximum number of active grains $N''_{kaAS}$, i.e., the number of grains completely filling the working gap once, has been engaged:

$$V''_{AS} = N''_{kaAS} \cdot \bar{v}_{kpa} \tag{2.47}$$

A material layer is only removed if the active grains have engaged several times, as the number of active grains at any point in time $t$ cannot completely fill the working gap volume. This frequency is described with the help of the volumetric concentration of active grains in the working gap volume:

$$N''_{kaAS} = n_{ka} \cdot N''_{ka} = \frac{N''_{ka}}{C_{ka}} \tag{2.48}$$

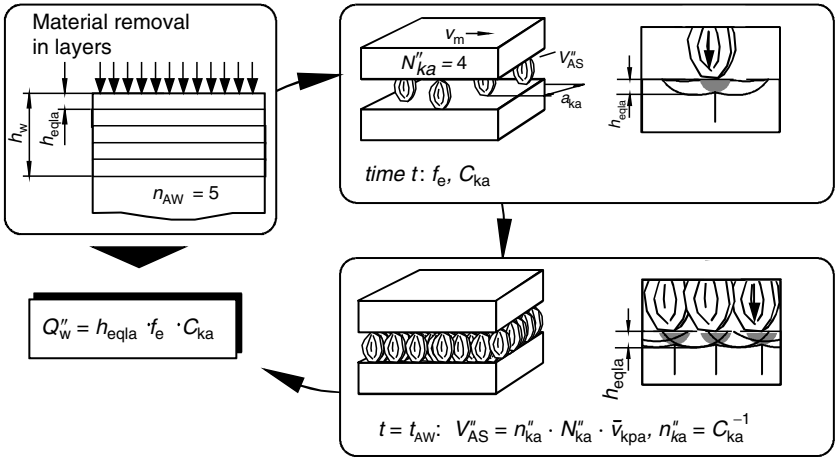


**FIGURE 2.30** Schematic representation of the parameters of the tool engagement. (From Engel, H., Läppen von einkristallinem Silicium. Dissertation, TU Berlin, 1997.)

The volumetric concentration of the active grains (also called active grain concentration) results from the ratio of the volume of the active grains $V''_{kpa}$, of the volume of all grains in the working gap $V''_{kpAS}$, and of the concentration of the lapping grains in the working gap volume:

$$C_{ka} = C_k \cdot \frac{V''_{kpa}}{V''_{kpAS}} \tag{2.49}$$

The single-grain volume is modeled in a simplified way as sphere volume, even if the grains of the abrasive mainly have ellipsoid projected areas. With the help of the average equivalent diameter of the active grains, the volume of the active grains at time $t$ is calculated as follows:

$$V''_{kpa} = N''_{ka} \cdot \bar{v}_{kpa} = N''_{ka} \cdot \frac{\pi}{6} \cdot \bar{d}^3_{kpa} \tag{2.50}$$

The total volume of all lapping grains in the working gap volume results from the average equivalent diameter of the abrasive:

$$V''_{kpAS} = N''_{kAS} \cdot \bar{v}_{kp} = N''_{kAS} \cdot \frac{\pi}{6} \cdot \bar{d}^3_{kp} \tag{2.51}$$

Through the insertion of Equation 2.50 and Equation 2.51 in Equation 2.49, the following term results for the active grain concentration:

$$C_{ka} = C_k \cdot \frac{N''_{ka}}{N''_{kAS}} \cdot \frac{\bar{d}^3_{kpa}}{\bar{d}^3_{kp}} \tag{2.52}$$

During the machining of monocrystal silicon, the thickness of the material layer removed through the engagement of the $N''_{\mathrm{kaAS}}$ grains results from the removal depth appearing upon the engagement of the single grains, and the overlapping of the crack systems. This thickness is defined as equivalent removal depth during lapping $h_{\mathrm{eqla}}$. The time $t_{\mathrm{AW}}$ is required for the removal of this material layer of a thickness of $h_{\mathrm{eqla}}$. This results from the number of necessary engagements of the active grains $n_{\mathrm{ka}}$ and the grain engagement frequency $f_{\mathrm{e}}$:

$$t_{\mathrm{AW}} = \frac{n_{\mathrm{ka}}}{f_{\mathrm{e}}} = \frac{1}{f_{\mathrm{e}} \cdot C_{\mathrm{ka}}} \tag{2.53}$$

The total thickness $h_{\mathrm{W}}$ of the removed wafer material after a lapping time $t_{\mathrm{L}}$ is after a $n_{\mathrm{AW}}$-fold removal of the layer thickness $h_{\mathrm{eqla}}$:

$$h_{\mathrm{W}} = n_{\mathrm{AW}} \cdot h_{\mathrm{eqla}} \tag{2.54}$$

The lapping time $t_{\mathrm{L}}$ needed for the removal of a workpiece thickness of $h_{\mathrm{W}}$ is

$$t_{\mathrm{L}} = n_{\mathrm{AW}} \cdot t_{\mathrm{AW}} = \frac{1}{f_{\mathrm{e}} \cdot C_{\mathrm{ka}}} \cdot \frac{h_{\mathrm{W}}}{h_{\mathrm{eqla}}} \tag{2.55}$$

Under consideration of the removal rate, which is defined as

$$Q''_{\mathrm{W}} = \frac{h_{\mathrm{W}}}{t_{\mathrm{L}}}$$

the equivalent removal depth $h_{\mathrm{eqla}}$ is

$$h_{\mathrm{eqla}} = \frac{Q''_{\mathrm{W}}}{f_{\mathrm{e}} \cdot C_{\mathrm{ka}}} \tag{2.56}$$

The equivalent removal depth is a characteristic value for the subsurface stress in the removal system, which leads to material wear and subsurface damage. It describes the depth and the extent of the lateral crack formation below the single cutting edges and their overlapping. Thus, it is in direct relation to the generated surface topography on the workpiece. Due to the effective stress field, there are direct relations between the lateral crack formation and the formation of half-penny-cracks in the crack system below the engaging cutting edges. Thus, the equivalent removal depth can serve as measure of the material damage generated in the subsurface.

The effectiveness quotient $K_{\mathrm{eff}}$ describes the effectiveness of the machining process. It indicates the relation of the achievable cutting performance and

the resulting subsurface influence. It results from the creation of the quotient of removal rate $Q''_W$ and the equivalent removal depth $h_{eqla}$. $Q''_W$ is used as a measure for the removal performance and $h_{eqla}$ for the subsurface influence:

$$K_{eff} = \frac{Q''_W}{h_{eqla}} = f_e \cdot C_{ka} \tag{2.57}$$

Equation 2.56 describes a removal system during the lapping of silicon. The parameters in the equation take into account the stochastic character and the system structure of the interactions of tool formation, tool engagement, and the development of the surface and the subsurface damage. The equation contains all relevant process parameters. The input parameters required for the calculation are measurable with sufficient statistic certainty. Thus, Engel provided the basis of the simulated description and analysis of different removal systems during the lapping of monocrystal silicon for the specific preparation and optimization of manufacture.

#### 2.9.5.4 Model Verification

The presented process model was verified by Engel through the calculation of the efficiency quotient. The isolated representation of the process parameters' grain engagement frequency $f_e$, active grain concentration $C_{ka}$, and equivalent removal rate $h_{eqla}$ is not acceptable for the verification. The grain engagement frequency and the active grain concentration are directly linked through the active grain number (see Equation 2.46 and Equation 2.47). According to Equation 2.56, the product of grain engagement frequency and active grain concentration is the proportionality factor between equivalent removal depth and the removal rate $Q''_W$ of the removal system. This equation makes clear that any change of an input parameter entails the adequate change of all process parameters including the removal rate. The removal system cannot be described in a deterministic way. The process parameters $f_e$, $C_{ka}$, $Q''_w$, and $h_{eqla}$ thus represent the procedures within a concrete removal system and cannot be used for the comparison of two removal systems. According to Equation 2.57, the effectiveness quotients $K_{eff}$ stand for a removal system. Thus, different removal systems can be compared with each other on the basis of this quotient.

Figure 2.31 shows the course of the characteristic curves from the theoretical and real effectiveness quotient over the engagement pressure for selected removal systems for the machining of monocrystal silicon. Hereby, the theoretical effectiveness quotient is the quotient from removal rate and equivalent removal depth $K_{eff}$. The real effectiveness quotient $K_{eff,\ HD}$ indicates the quotient of removal rate and of subsurface damage depth. In qualitative terms, the characteristic curves of the real and the theoretical effectiveness quotient run nearly equally. The quantitative difference between

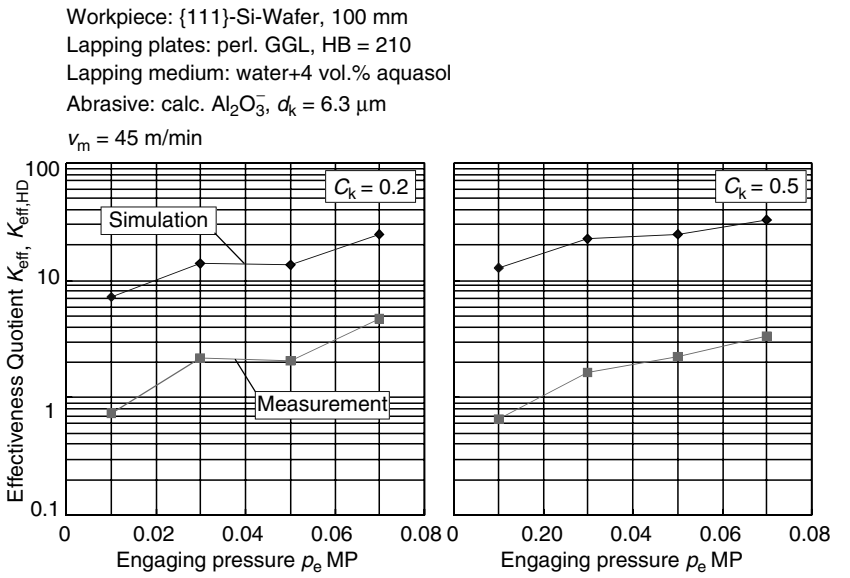


**FIGURE 2.31** Theoretical and real effectiveness quotients for selected process parameters. (From Engel, H., Läppen von einkristallinem Silicium. Dissertation, TU Berlin, 1997.)

the two effectiveness quotients results from the fact that, over the equivalent depth of removal, the theoretical effectiveness quotient includes the direct effect of the active lapping grains on the material removal. Thus, this parameter refers to the surface topography. In contrast, the real effectiveness quotient reflects the effect on the deep crystal structure. The measured depths of subsurface damage are always above the calculated equivalent depths of removal.

The effectiveness quotients $K_{eff}$ and $K_{eff,\,HD}$ sharply increase with growing engagement pressure. The increase of effectiveness results from the nearly linear rise of the removal rates with growing pressure. In contrast, the growing pressure leads to only slight changes in the investigated depths of subsurface damage.

The comparison of the theoretical and real effectiveness quotient of the lapping processes in Figure 2.31 shows that the developed process model reflects the real conditions of lapping. The theoretical parameters of the removal systems summarized in the effectiveness quotient correlates with the real test results. Therewith Engel proved that the effectiveness quotient is an eligible parameter to describe the effects of single process parameters on the structure of a removal system and the removal results by simulation.

An algorithm was described for the application of the process simulation, which can be used for the methodical work preparation and process control. Through the application of the algorithm, the experimental effort for the work

preparation is minimized. Simultaneously, a flexible process layout is guaranteed, which is based on the functional relations in the lapping process. This process layout takes into account the really existing optimum process effectiveness.

### 2.9.6 Process Model According to Evans

***Uwe Heisel***

The approach of Evans et al. [127] describes a simple lapping model, which allows some process result forecasts, i.e., material removal rate and surface roughness. The precondition is that there are no rolling motions of active grains into the working gap. Figure 2.32 schematically illustrates the position and the implication of an active grain.

The penetration of a nonrolling grain into both affecting partners (i.e., lap and workpiece) happens similarly to the static indentation of a two-sided indenter. For this reason the model was named simple pseudostatic indentation model of ductile lapping. The hardness $H$ is defined as the pressure on the projected indentation area with the normal force $F_n$ and the geometrical indentation parameter $s_{ind}$. The parameters $k_i$ are further proportionality coefficients. With the assumption that the grains have a regular polyhedron form it follows that the penetration depths $d_W$ with respect to $d_L$ depend on the hardness parameters $H_W$ with respect to $H_L$. Here the geometrical coefficient $k_2$ depends on the polyhedrons number of edges i.e., on the angle $2\beta$:

$$H = \frac{k_1 \cdot F_n}{s_{ind}^2} \tag{2.58}$$

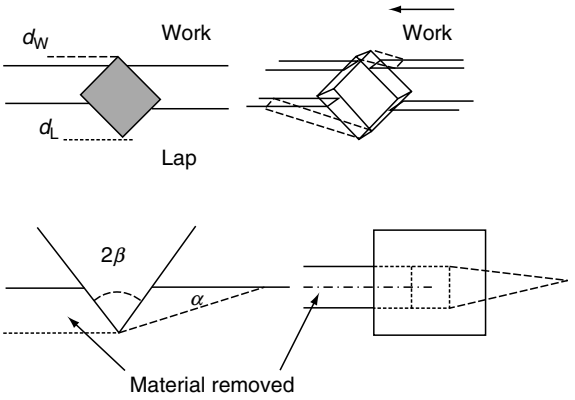


**FIGURE 2.32** Schematic illustration of the position and the implication of an active grain.

$$d_W = \sqrt{\frac{k_2}{H_W}}, \quad d_L = \sqrt{\frac{k_2}{H_L}} \tag{2.59}$$

The cross-sectional area of a grain-caused mark is proportional to $d_W^2$. The removal rate, i.e., surface recession $dh/dt$ will be proportional to $d_W^2$, to the surface speed $v$, and to the number of grains $N$. Hence the surface recession can be calculated with the following equation where $F_j$ is the force per grain:

$$\frac{dh}{dt} = k_3 v N d_W^2 = k_4 v N \frac{F_j}{H_W} \tag{2.60}$$

The number $N$ of grains in contact is inversely proportional to $s^3$. Thus the force per grain is

$$F_j = \frac{F}{N} = k_5 s^3 \tag{2.61}$$

By inserting Equation 2.61 into Equation 2.60 it follows

$$\frac{dh}{dt} = k_6 v \frac{F}{H_W} \tag{2.62}$$

i.e., the removal rate does not depend on the grain size.

Within the bound of the model removal rate is also predicted to be independent of concentration.

Surface finish $\sigma$ should be directly proportional to the penetration of the grain

$$\sigma = k_7 d_W = k_8 \sqrt{\frac{F s^3}{H_W}} \tag{2.63}$$

i.e., finish is predicted to be proportional to $s^{3/2}$.

### 2.9.7 Process Model According to Heisel

***Uwe Heisel***

As with all removal machining, the surface formation and the material removal are influenced in lapping by the geometry and the motion of the tool. To estimate the process parameters the authors of the abovementioned models make some approaches with regard to the movement type of abrasive grains in the working gap. For example, Evans et al. [127] affirmed that there are no rolling grains. Against this Engel excludes sliding grains [49]. The topography of a lapped surface is the evidence of the availability of different simultaneous forms of the grain motion.

The model according to Heisel [128] even deals with the behavior of loose grains in a space between two parallel and relatively moving affecting partners. The possibility to roll a body pressed between two parallel and relatively moving areas apparently depends on the body's form and the tribological properties of the acting partners. But it is not clear what kind of characters determine the possibility to roll. For example, the respectively arising form of grain motion, which means rolling or anchoring with sliding, has been referred to the boundary conditions [37], however without quantitatively defining the parameter of the grain form that determines the way of motion. The obvious prediction that the resistance against rolling increases with the body's circle form deviation cannot always be accepted. For example, it is easier to roll a bar with triangular cross section than to roll a bar with quadratic cross section, though a square is less out of the circle than a triangle. Well-known form coefficients like length–width ratio as well as the ratio between maximum and minimum grain diameter are also ill-suited to determine the grain motion form. In a two-dimensional presentation, the lapping grains are irregular polygons with $m$ slightly rounded corner points. As shown in Figure 2.33 at the motion of a grain, its angle position is determined by the angle $\varphi$.

The angle $\varphi_0$ brings the grain in contact with both affecting partners and friction connections, transferring a certain tangential force $F_\tau$ occurring in the contact points 1 and 2. As long as $F_\tau < F_{\tau\,\max} = \min(f_1, f_2) \cdot F_n$ ($f_i$ represents coefficients of friction within the contact points with the respective affecting partner), the friction connections do not break and the grain moves without sliding in the contact points, which means it rolls. The force relation $F_\tau/F_n$, which means the gradient of the affecting line of the resulting force, is consequently a measure for the rolling resistance of a grain. Due to the fact that the affecting line of the resulting one differs just slightly from the line 1–2, which connects the highest and the lowest point of the grain, tan $\alpha(\varphi)$ (gradient of line 1–2) can serve as a shape-dependent rolling resistance coefficient $K_r(\varphi)$. To enable a grain to roll, it has to apply to the following in each position:

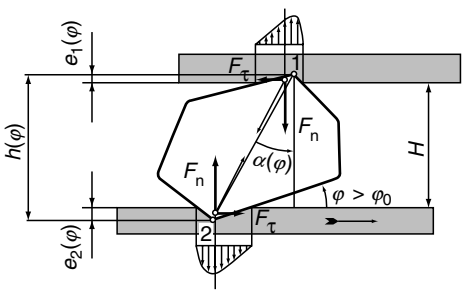


**FIGURE 2.33** Definition of the rolling resistance coefficient.

$$K_r(\varphi) < f_1 \tag{2.64}$$

$$K_r(\varphi) < f_2 \tag{2.65}$$

If just one of the conditions in Equation 2.64 and Equation 2.65 is met, one of the friction connections breaks and the grain slides together with the affecting partner whose coefficient of friction is relatively bigger to the other. In case none of the conditions in Equation 2.64 and Equation 2.65 is met, the grain loses its connection to both affecting partners and its position to them gets relatively indefinite. This behavior is defined as passive. Though the passive lapping grains can represent the majority, in no known lapping process model, their presence was regarded. This leads to a strong over-assessment of the number of active grains as important model parameter. To determine the behavior of a lapping grain by using Equation 2.64 and Equation 2.65, one has to know the friction parameters $f_1$ and $f_2$ as well as the rolling resistance coefficient $K_r$ according to all grain positions $\varphi$, i.e., dependence $K_r(\varphi)$. In investigating lapping grains with the help of a microscope combined with an image processing software, it is possible to measure the characteristic $h(\varphi)$ (height of grain $h$ depending on the angle $\varphi$) of several grains at the same time.

The dependence of $K_r(\varphi)$ can be derived from the relation to $h(\varphi)$:

$$K_r(\varphi) = -\frac{1}{h(\varphi)} \cdot \frac{\mathrm{d}h(\varphi)}{\mathrm{d}\varphi} \tag{2.66}$$

The ordinary coefficient of friction is dependent on the materials of the affecting partners, on the lubrication of the contact surface as well as more or less on the speed of relative motion and only insignificantly on the normal force. This was introduced at the research of the motion resistance of the macrobodies, whose real contact surface presents an entity of elementary contact areas being isolated from each other or more or less evenly distributed on the whole contact surface. For a small body like the lapping grain, whose total contact surface represents one sole contact area, the stochastic conformities with a natural law as mentioned before, are not valid anymore. For the description of the motion resistance of small bodies, the results gained from several theoretical and experimental examinations on the motion of a hard indenter are better suitable. At the examinations carried out with cone-shaped indenter it was found out that the coefficient of friction can be presented as a sum of material and penetrating dependent components [129]:

$$f = \begin{cases} f_0 + \dfrac{2}{\pi}\left(\dfrac{a\sin\varepsilon}{\varepsilon^2} - \sqrt{\dfrac{1}{\varepsilon^2} - 1}\right), & \varepsilon < \sin\varphi \\ f_0 + \dfrac{2\tan\varphi}{\pi}\left(1 - \dfrac{\tan\varphi - \varphi}{\tan\varphi \cdot \varepsilon^2}\right), & \varepsilon \geq \sin\varphi \end{cases} \tag{2.67}$$

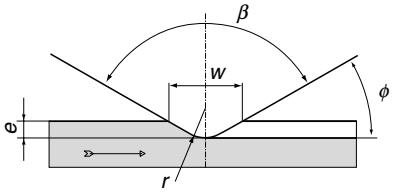


**FIGURE 2.34** Motion of a cone-shaped indenter.

where $f_0$ is the the ordinary material-dependent coefficient of friction, $\varphi = (\pi - \beta)/2$, $\varepsilon = w/2r$. This is shown in Figure 2.34.

Eliminating the parameter $\varphi$ from the dependencies $f(\varphi)$ and $h(\varphi)$ results in the dependence $f(h)$. As mentioned above, in contrary to the machining processes with a geometrically determined tool as well as with a tool with bound grains, in the machining with loose grain, the tool develops just immediately during the machining. The formation of a lapping tool, which means the entity of all lapping grains being in the working gap between the workpiece and the lap plate. With regard to the particular types of grain behavior it could be illustrated as showed in Figure 2.35.

Due to the relative motion of the affecting partner, several grains (such as grain 6 in Figure 2.35) leave the working gap and other grains out of the supplied lapping means enter the working gap. According to their size and shape, only a particular part of all grains is able to enter the working gap whose height $H_{gap}$ is appropriate to the lapping pressure (for example, grain 1 is too big) and only a particular part from it is active, which means it rolls like grain 4 or slides like grain 5. Grain 2 is too small and grain 3 does not stick to the affecting partner and remains passive.

Next to the permanent restoration of the lapping tool due to the regular escape and entry of the grains, phenomena that occur within the working gap lead to changes of the starting structure of the lapping tool. To start with, those grains which are the strongest loaded do break, whereby the developing fragments can take part in further machining depending on their size and shape. Thereby, the structure of the lapping tool changes in such a way that the shares of the bigger grains decrease and the shares of the smaller ones increase. Secondly, as a result of the irregularity of the grain way and speed, some grains collide with each other or with grain particles.

Due to the chaotically moving grains within the working gap, the distances between the grains vary constantly and can therefore be considered as

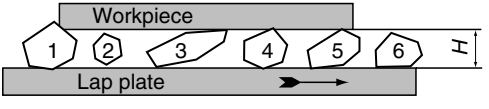


**FIGURE 2.35** Formation of a lapping tool.

random variables. The frequency of collisions is calculated as probability that the distance between the centers of two grains becomes smaller than $\overline{D}_{MIT}$ ($\overline{D}_{MIT}$—the average of the middle grain diameter):

$$p_{col} = 1 - e^{-\pi \cdot N_{1A} \overline{D}_{MIT}^2} \tag{2.68}$$

One can assume hereby that the grains shortly unite to an agglomerate after such a collision. At a later time, this agglomerate can fall apart again. For it, a new one develops, so that a certain part of agglomerates exists in the working gap at every moment. The unique behavior of the agglomerate is determined in the same way as the single grain with respect to its shape and size.

The active grains close the contact chain between the workpiece and the lap plate, they transfer the normal forces, get under their impact into the surface of the affecting partner, and displace a proportionate material volume. A stationary working gap height is reached if the sum of all normal forces transferred by active grains and eventually of the part of load transferred by the lapping oil is equivalent to the set lapping pressure.

For example, with the help of the image processing system ImageC, gross-grained (g - # 400) and fine-grained (f - # 800) lapping powders made of corundum (C) and silicon carbide (S) were examined. The geometrical parameters of the individual grains (Figure 2.36a, darker objects) as well as those of the overlaid grains (Figure 2.36b, darker objects), which can both be considered as grain agglomerates developed after the collision, were recorded out of several measuring fields under a microscope.

With a given volumetric grain concentration, it is possible to calculate the number of grains within a surface unit of the working gap $N_{1A}$ on the basis of the grain size distribution. Considering the occurrence of collisions, one surface unit contains $N_{1A} \cdot (1 - 2p_{col})$ single grains and $N_{1A} \cdot p_{col}$ agglomerates. All of these objects—single grains and agglomerates—are considered in the following as grains. During the examinations carried out on lapping grains, the grain height $h$ was measured in dependence on the angle position $\varphi$ (each 5°) for each grain. For example, the dependence $h(\varphi)$ for the grain marked with a circle in Figure 2.37a is presented in Figure 2.37b.

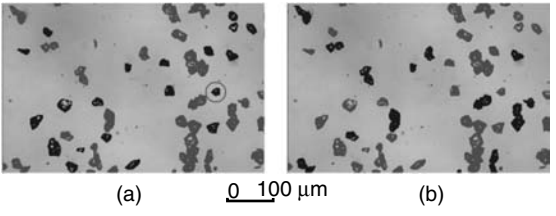


**FIGURE 2.36** Lapping grains made of gross-grained corundum (Cg).

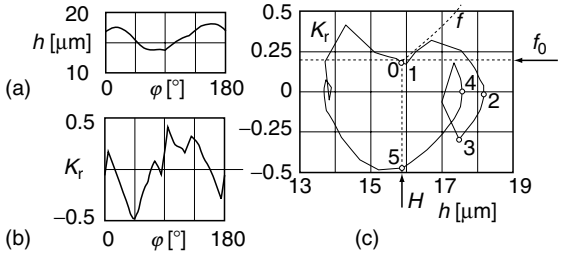


**FIGURE 2.37** Shape-depending parameter of a grain.

The relation $K_r(\varphi)$ for the same grain is presented in Figure 2.37b. Excluding the parameter $\varphi$ from the dependencies $K_r(\varphi)$ and $h(\varphi)$ results in a dependence $K_r(h)$ as presented in Figure 2.37c. The local minima of the rolling resistance coefficient corresponds to the position in which the grain rolls over its edges, and its number is equivalent to the number $m$ of the corner points. The grain in the presented example was identified as a square. In Figure 2.38, the experimentally determined distributions of the grain shape parameter are presented: (a) maximum rolling resistance coefficient and (b) number of corner points.

To calculate the penetrating parameter, the corner points of the grain are regarded approximately as rounded cones with a cone angle $\beta$ being the same as with a regular $m$-corner and a rounding-off radius $r = 1$ µm. This was also assumed by Suh and Sin [129] and corresponds to the estimation of the grain pictures. The sum of the penetrating depths $e_1 + e_2$ results from the difference between grain and gap height to $h-H$ and the relation between the penetrating depths is determined by the relation of hardness.

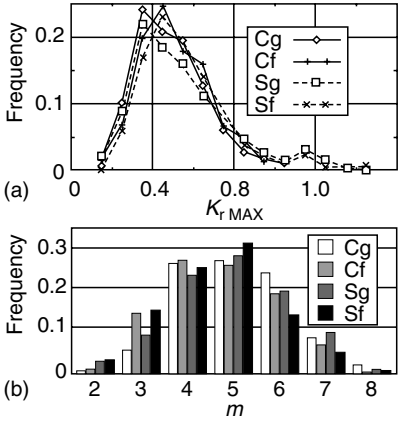


**FIGURE 2.38** Distribution of grain shape parameter.

From it, the penetrating depths are calculated and depending on them, further penetrating parameters such as penetrating width $w$, shape surface $A$, cross-sectional area, and displaced volume $V$ are also calculated. For each position $i$ of each grain $j$, the normal force $F_{\mathrm{n}ji}$ results from the product of shape surface and hardness $V \cdot H$ toward $A_{ji} \cdot V \cdot H$. The tangential force $F_{\tau ji}$ results from the product of normal force $F_{\mathrm{n}ji}$ and rolling resistance coefficient $K_{\mathrm{r}ji}$. For each grain, the effective values of the power components $F_{\mathrm{n}j}$ and $F_{\tau j}$ are calculated, whose sum results in the total surface-related power components $F_{\mathrm{n}}$ and $F_{\tau}$.

Joining the dependencies of $K_{\mathrm{r}}(h)$ and $f(h)$ into a diagram as presented in Figure 2.37c enables one to determine the way of motion of the grain according to Equation 2.60 and Equation 2.61, considering the given gap height. For the grain presented in the example, the rolling resistance coefficient $K_{\mathrm{r}}$ lies beneath the coefficient of friction (calculated from a coefficient of friction $f_0 = 0.2$ and a relation of hardness $V \cdot H_1 : V \cdot H_2 = 2:1$), within the whole penetrating range $h > H = 15.8$ μm (taken a grain position of 0 to 5 in Figure 2.37c), which means the grain rolls at $H = 15.8$ μm.

Due to the breakup of a grain, two or several smaller parts develop and the total number of grains increase. Therefore, the part of bigger grains decrease and accordingly the part of smaller grains increase. In order to calculate the changed grain size distribution, the regularities gained from Ref. [130] were used. An example of the calculated break-dependent changes of the grain size distribution is presented in Figure 2.39.

The particles remain in the working gap and participate according to their size and shape at further machining. Due to the grain examinations, where it was determined that the distribution of grain shapes of the different grain size areas are practically equal, it can be suspected that a particle with a certain size has the same shape as an unbroken grain with the same size.

For the determination of the actual grain size distribution, an algorithm was used, taking into account the the breakup process not as a continuous process but as a discrete order of momentary changes of the formation of the lapping tool.

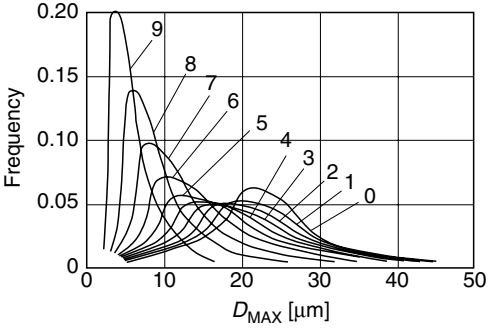


**FIGURE 2.39** Sequence of break-dependent changes of the grain size distribution of Cg.

At the simulation of lapping, the lapping pressure $Q$ serves as entry parameter. The calculations are carried out cyclical at a variable $H$, starting with its maximum value. The grains situated in a surface unit of the working gap transfer the normal force $F_n$. If the normal force is smaller than the lapping pressure, the grains are entering deeper. The calculations are repeated at a slightly smaller gap height. Although the deeper entering grains leave the working gap very fast and the newly entering grains are smaller, the normal force increases. This is due to the fact that the number of active grains increases to a certain value at diminution of the gap height. If $F_n < Q$ remains, the calculations are repeated. As long as the normal force thereby increases and tends to the value $Q$, the calculations are carried out at an invariable grain size distribution. If however a decrease of the gap height $H$ does not lead to an increase of the normal force anymore, the calculations are carried out at a changed grain size distribution. The number of grains increases the normal force again. The calculations are repeated until the normal force reaches the value of the lapping pressure at a current grain size distribution and a gap height $H$. The gap height being up to date at the last cycle is regarded as a stationary working gap height at which the working results (roughness, removal) are estimated.

The effect of rolling and sliding grains is different. While moving, the rolling grains leave chain-formed traces from the prints of their corner points (such as in grain position 2 and 4 in Figure 2.37c) and edges (such as in grain position 1 and 3), while sliding grains produce cracks.

Analogical to the arithmetical average height $R_a$, the arithmetic average of the deviation of the penetration depths according to its average can be calculated. Thereby each print has to be considered with one weight factor dependent on its contribution to the roughness profile, which depends on its probability $l_{ji}/L_j$ and width $w_{ji}$ (Figure 2.40).

The displacement rate results from the sum of all print volumes $V_{ji}$ within a surface unit based on a certain unit of time. The unevenness heights of the worked surfaces with respect to the material removals are not necessarily equal to the penetration depths of the grains with respect to the displaced material volume (this is only valid for pure cutting removal mechanisms

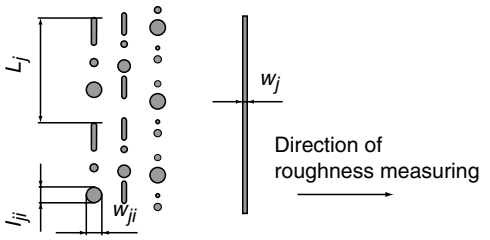


**FIGURE 2.40** Traces of rolling (left) and sliding (right) grains.

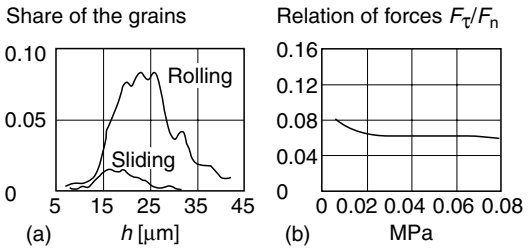


**FIGURE 2.41** Process parameter at lapping with grains Cg.

[131]). Yet a proportionality between these parameters can be supposed, however with different unknown proportionality factors, depending on the material characteristics.

The calculation shows that most of the grains within the working gap remain passive. The share of the active grains with the respective way of motion (calculated for the lapping powder Cg at $f_0 = 0.2$ and $V \cdot H_1 : V \cdot H_2 = 2:1$), depending on the gap height, are excellently presented in Figure 2.41a.

In Figure 2.41b, a dependence of the relation of forces on the lapping pressure is shown at equal conditions. As shown before, the tangential force $F_\tau$ results from the sum of the effective values $F_{\tau j}$ of the elementary forces $F_{\tau ji}$. The latter are not determined by the coefficient of friction $f$, but by the rolling resistance coefficient $K_{\tau ji}$, which changes from 0 to a maximum value (not exceeding $f$). This explains the unexpected low values of the relation of forces at lapping. Experimental tests carried out by Engel [49] have shown that too. In this way it is possible to forecast qualitatively machining results by measuring grain form parameters. This enables an optimized chance of adapted lapping powders.

## Symbols and Abbreviations

| | | |
|---|---|---|
| $\vec{a}$ | | Acceleration of a workpiece point |
| $a_c$ | μm | Radius of the Hertzian contact area |
| $a_H$ | mm | Distance between holder- and workpiece center |
| $a_{ka}$ | μm | Average distance between the active grains |
| $a_m$ | $m/s^2$ | Average acceleration of a workpiece point |
| $a_s$ | $m/s^2$ | Scalar acceleration of a workpiece point |
| $a_w$ | mm | Distance of a workpiece point from the workpiece center |
| $a_Z$ | mm | Distance between wheel and holder center |
| A | | Discrete point |

| | | |
|---|---|---|
| $A_{\mathrm{H}}$ | $\mathrm{mm}^2$ | Surface area of one workpiece holder |
| $A_{\mathrm{S}K_i}$ | $\mathrm{mm}^2$ | Surface area of wheel class $i$ |
| $A_{\mathrm{S}}$ | $\mathrm{mm}^2$ | Wheel surface area |
| $A_{\mathrm{W}K_i}$ | $\mathrm{mm}^2$ | Class surface area fraction of all workpieces |
| $A_{\mathrm{W}}$ | $\mathrm{mm}^2$ | Workpiece area |
| $b$ | µm | Radius of the plastic zone |
| B | | Discrete point |
| $c$ | µm | Length of lateral crack |
| $C_{\mathrm{k}}$ | | Volumetric concentration of the grains in the slurry |
| $C_{\mathrm{ka}}$ | | Volumetric concentration of the active grains in the working gap |
| $\bar{d}_{\mathrm{kp}}$ | µm | Average process equivalent diameter of all grains |
| $\bar{d}_{\mathrm{kpa}}$ | µm | Average equivalent diameter of the active grains |
| $\bar{d}_{\mathrm{kpmax}}$ | µm | Average maximum process diameter of all grains |
| $d_{\mathrm{kpmax\ max}}$ | µm | Biggest maximum process grain diameter |
| $d_{\mathrm{L}}$ | mm | Penetration depth in respect of length |
| $d_{\mathrm{W}}$ | mm | Penetration depth in respect of width |
| $\overline{D}_{\mathrm{MIT}}$ | µm | Average of the middle grain diameter |
| $e_{\mathrm{H}}$ | mm | Distance between a workpiece point and the holder center |
| $f_{\mathrm{e}}$ | 1/s | Grain engagement frequency |
| $f_i$ | | Friction coefficients |
| $F_j$ | N | Force per grain |
| $F_\tau$ | N | Tangential force |
| $F_{\tau\mathrm{max}}$ | N | Maximum tangential force |
| $F_{\mathrm{n}}$ | N | Normal force |
| $g_{\mathrm{W}}$ | mm | Geometric function |
| $g'_{\mathrm{W}}$ | % | Related geometric function |
| $h$ | µm | Depth of the Hertzian cone crack |
| $h_{\mathrm{AS}}$ | µm | Height of the working gap |
| $h_{\mathrm{egla}}$ | µm | Equivalent removal depth during lapping |
| $h_{\mathrm{eqla\ vor}}$ | µm | Default value for the equivalent removal depth |
| $h_{\mathrm{W}}$ | µm | Removal depth |
| $\Delta h$ | mm | Height difference |
| $\Delta h_{\mathrm{W}}$ | mm | Workpiece height reduction |
| $\Delta h'_{\mathrm{W}}$ | µm/m | Path-related workpiece height reduction |
| $\Delta h_{\mathrm{W}}$ | µm/s | Time-related workpiece height reduction |
| H | | Workpiece holder center |
| $H$ | | Hardness |
| $H_{\mathrm{gap}}$ | mm | Height of working gap |
| $H_{\mathrm{L}}$ | | Hardness in respect of length |
| $H_{\mathrm{W}}$ | | Hardness in respect of width |
| $i$ | | Number of wheel classes |

| | | |
|---|---|---|
| $k$ | 1/m | Path curve curvature |
| $k_\mathrm{i}$ | | Proportionality coefficient |
| $K_\mathrm{eff}$ | (μm/min)/μm | Effectiveness quotient |
| $K_{\mathrm{eff,\ HD}}$ | (μm/min)/μm | Effectiveness quotient on the basis of measured values or of the subsurface damage |
| $K_i$ | | Wheel class with index $i$ |
| $K_\mathrm{L}$ | | Lapping ratio |
| $K_\mathrm{r}$ | | Rolling resistance coefficient |
| MZ | | Momentary center of a rotary movement |
| $n_\mathrm{a}$ | $\mathrm{min}^{-1}$ | Outer pin circle rotational velocity |
| $n_\mathrm{AW}$ | | Number of removed material layers |
| $n_\mathrm{i}$ | $\mathrm{min}^{-1}$ | Inner pin circle rotational velocity |
| $n_\mathrm{ka}$ | | Number of engagements per active grain |
| $n_\mathrm{o}$ | $\mathrm{min}^{-1}$ | Upper grinding wheel rotational velocity |
| $n_\mathrm{u}$ | $\mathrm{min}^{-1}$ | Lower grinding wheel rotational velocity |
| $N$ | | Number of grains |
| $N_\mathrm{1A}$ | | Number of grains within a surface unit of the working gap |
| $N_\mathrm{ka}$ | | Number of active grains in the working |
| $N''_\mathrm{ka}$ | $1/\mathrm{mm}^2$ | Area-related number of active grains in the working gap |
| $N''_\mathrm{kaAS}$ | $1/\mathrm{mm}^2$ | Area-related maximum number of active grains |
| $N''_\mathrm{kAS}$ | $1/\mathrm{mm}^2$ | Area-related number of grains in the working gap |
| $N_\mathrm{L}$ | | Rotational speed ratio |
| $p$ | | Number of part cycles in one complete cycle |
| $p_\mathrm{e}$ | MPa | Engagement pressure |
| $p$ | | Probability |
| $P_\mathrm{W}$ | | Point of the workpiece surface |
| $q$ | | Number of rotations around the wheel center within a path cycle |
| $Q''_\mathrm{W}$ | μm/min | Removal rate |
| $\vec{\mathbf{r}}$ | | Position vector, path curve |
| $r$ | mm | Absolute value of the position vector |
| $r_\mathrm{a}$ | mm | Outer pin circle radius |
| $r_{\mathrm{a}K_i}$ | mm | Outer radius of wheel class $i$ |
| $r_\mathrm{H}$ | mm | Workpiece holder radius |
| $r_\mathrm{i}$ | mm | Inner pin circle radius |
| $r_{\mathrm{i}K_i}$ | mm | Inner radius of wheel class $i$ |
| $r_{\mathrm{m}K_i}$ | mm | Medium radius of wheel class $i$ |
| $r_\mathrm{S}$ | mm | Distance from the wheel center |
| $r_\mathrm{Sa}$ | mm | Outer lapping wheel radius |
| $r_\mathrm{Si}$ | mm | Inner lapping wheel radius |
| $r_\mathrm{W}$ | mm | Outer workpiece radius |

| | | |
|---|---|---|
| $r_{\text{pitch}}$ | mm | Pitch circle radius |
| $R_{\text{K}}$ | µm | Kernel roughness depth according to DIN 4776 |
| $R_{\text{KL}}$ | µm | Kernel roughness depth of the lapping wheel according to DIN 4776 |
| $R_{\text{KW}}$ | µm | Kernel roughness depth of the workpiece according to DIN 4776 |
| $R_{\text{z}}$ | µm | Average depth of roughness according to DIN 4768 |
| $s$ | mm | Path length |
| $s'$ | | Related path length distribution |
| $s_{\text{ind}}$ | | Geometrical indentation parameter |
| $s_{K_i}$ | mm | Class path length |
| $s_{K_i}$ | % | Related class path length |
| $s_{\text{kpmax}}$ | µm | Standard deviation of the average maximum process grain diameter |
| $s_{\text{PW}K_i}$ | mm | Path curve segment in a wheel class |
| SEM | | Scanning electron microscope |
| SIRD | | Scanning infrared depolarization |
| $t$ | s | Time |
| $t_0$, $t_1$ | s | Discrete time points |
| $t_{1i}$ | s | Time point of class entry $i$ |
| $t_{2i}$ | s | Time point of class exit $i$ |
| $t_{\text{AW}}$ | s | Lapping time for the removal of one layer |
| $t_{\text{c}}$ | s | Cutting time |
| $t_{\text{cycl}}$ | s | Cycle time |
| $t_{\Delta\text{cycl}}$ | s | Part-cycle time |
| $t_{\text{L}}$ | s | Lapping time |
| TEM | | Transmission electron microscope |
| $\vec{\mathbf{v}}$ | | Path velocity |
| $v$ | m/s | Scalar value of the path velocity |
| $v_{\text{c}}$ | m/min | Cutting velocity |
| $v_{\text{H}}$ | m/min | Rotational speed of the workpiece holder |
| $\bar{v}_{\text{kpa}}$ | $\mu\text{m}^3$ | Average volume of the active grains |
| $\bar{v}_{\text{kp}}$ | $\mu\text{m}^3$ | Average volume of all grains |
| $v_{\text{m}}$ | m/min | Average path velocity |
| $v_{\text{Z}}$ | m/min | Translatory velocity of the workpiece holder |
| $V''_{\text{AS}}$ | $\mu\text{m}^3/\text{mm}^2$ | Area-related volume of the working gap |
| $V''_{\text{kpa}}$ | $\mu\text{m}^3/\text{mm}^2$ | Area-related total volume of the active grains in the working gap |
| $V''_{\text{kpAS}}$ | $\mu\text{m}^3/\text{mm}^2$ | Area-related total volume of all grains in the working gap |
| W | | Workpiece center point |

| | | |
|---|---|---|
| $Z_{h_{AS}}$ | | Quantile of the standard normal distribution of the maximum process grain diameter for the probability that the maximum process grain diameter is bigger than the working gap height |
| $\alpha$ | | Level of significance (probability of error) for the biggest maximum process grain diameter |
| $\beta$ | ° | Edge angle |
| $\beta_{\Delta cycl}$ | ° | Part-cycle angle |
| $\theta$ | ° | Angle of the Hertzian cone crack |
| $\lambda_\alpha$ | | Quantile of the standard normal distribution of the maximum process grain diameter for the level of significance of the biggest maximal process grain diameter |
| $\nu$ | | Poisson ratio |
| $\sigma$ | | Surface finish parameter |
| $\varphi$ | ° | Angle position of grain |
| $\omega_a$ | $2\pi$/min | Angular velocity of the outer pin circle |
| $\omega_H$ | $2\pi$/min | Angular velocity of the workpiece holder around its center H |
| $\omega_i$ | $2\pi$/min | Angular velocity of the inner pin circle |
| $\omega_o$ | $2\pi$/min | Angular velocity of the upper lapping wheel |
| $\omega_u$ | $2\pi$/min | Angular velocity of the lower lapping wheel |
| $\omega_W$ | $2\pi$/min | Angular velocity of the workpiece |
| $\omega_Z$ | $2\pi$/min | Angular velocity of the workpiece holder around the wheel center Z |

## REFERENCES


1. König, W. and Klocke, F., *Fertigungsverfahren*, Band 2. Schleifen, Honen, Läppen. Düsseldorf: VDI-Verlag, 1996.
2. Spur, G. and Stöferle, T., *Handbuch der Fertigungstechnik*. Spanen, Band 3/2. München: Hanser-Verlag, 1980.
3. Eversheim, W. and Schuh, (Hrsg.) G., *Betriebshütte. Produktion und Management*. T. 2. Berlin, Heidelberg, New York: Springer-Verlag, 1996.
4. Stähli, A.W., *Die Läpp-Technik*. Firmendruckschrift der A.W. Stähli AG. Schweiz: Pieterlen, 2001.
5. Da Vinci, L., *Codices Madrid I. Tratado de estatica y mechanica en italiano. Faksimile-Ausgabe*. Schweiz: S. Fischer Verlag, 1974.
6. Reti, L. and Dibner, B., *Leonardo da Vinci. Technologist*. Norwalk, CT: Burndy Library Inc., 1969.
7. Häuser, K., Entstehen der Endmaßsätze und Endmaßfertigung. *Werkstatt und Betrieb* 121(8) (1988) 677–681.
8. Feinstbearbeitung. N. N., *Polieren, Läppen, Honen, Presspolieren, Polierdrehen. Ausschuss für wirtschaftliche Fertigung beim Reichskuratorium für Wirtschaftlichkeit. RKW-Veröffentlichungen 74*. Berlin: Beuth, 1932, S. 48–49.

9. DIN 8589. *Fertigungsverfahren Spanen—Teil 0: Einordnung, Unterteilung, Begriffe*. Berlin: Beuth, 1981.
10. DIN 8589. *Fertigungsverfahren Spanen—Teil 15: Läppen. Einordnung, Unterteilung, Begriffe*. Berlin: Beuth, 1985.
11. DIN 8200. *Strahlverfahrenstechnik. Begriffe, Einordnung der Strahlverfahren*. Berlin: Beuth, 1982.
12. DIN 8589. *Fertigungsverfahren Spanen—Teil 17: Gleitspanen. Einordnung, Unterteilung, Begriffe*. Berlin: Beuth, 1985.
13. Beilby, G., *Aggregation and Flow of Solids*. London: Macmillan, 1921.
14. Lichtenberger, H., Die Spanmengenleistung beim Flachläppen. *Werkstattstechnik und Maschinenbau* 45(4) (1955) 145–153.
15. Bornemann, U., Gleitung und Werkstoffabtrag beim Läppen von Rundteilen. Dr.-Ing.-Diss. TH Berlin, 1942.
16. Böderich, K. and Enger, U., Einflüsse auf die Formgenauigkeit beim Läppen ebener Werkstücke. In: *Vortragsberichtsband XIV*. Int. Wiss. Koll., TH Ilmenau, Vortr. Reihe "Feinbearbeitungstechnik", 1969.
17. Burkart, W. and Schmid, O., Über Läppmittel und ihren Einfluss auf das Läppen. *Fachberichte für Oberflächentechnik* 1(1) (1963) 23–24.
18. Finkelnburg, H.H., *Läppen Werkst und Betr*. 83(1) (1950) 1–8.
19. Lätzig, W., *Läppen*. München: Carl Hanser Verlag, 1950.
20. Lichtenberger, H., Über die Läppwirkung und ihre Arbeitsergebnisse. *Werkstattstechnik und Maschinenbau* 42(8) (1952) 310–314.
21. Lichtenberger, H., Forschungsergebnisse über Läppbearbeitung. *Werkstattstechnik und Maschinenbau* 43(3) (1953) 121–122.
22. Matsunaga, M., Fundamental studies on lapping. Report of the Institute of Industrial Science, University of Tokyo, 16(2) (1966) 101–164.
23. Rabinowicz, E. and Mutis, A., Effect of abrasive particle size on wear. *Wear* 8 (1965) 381–390.
24. Stotko, H., Ein neuer Weg zur Prüfung von losem Schleifkorn. Dr.-Ing.-Diss. TH Braunschweig, 1959.
25. Fischer, E., Zur Art der zyklischen Bewegung und zum eigentlichen Prozeß zwischen Werkstück und Werkzeug bei verschiedenen Präzisionsläppmethoden. *Wiss Z TU Dresden* 13(5) (1964) 1379–1389.
26. Fischer, E., Wechselbeziehungen zwischen dem Schneiden, Läppen und Ätzen von Germanium bzw. Silicium bei der Herstellung von Halbleiterbauelementen. *Wissenschaftliche Zeitung der Technischen Universität Dresden* 13 (1964) 3.
27. Fischer, E., Bewegungszyklen und Richtungsfelder beim Planläppen. *Werkst u Betr* 99(4) (1966) 237–243.
28. Bastian, H.G., Miszler, J., and Pistauer, R., Die Finishbearbeitung von Dichtflächen bei der Armaturenfertigung. *Technische Information Armaturen* 11(1) (1976) 12–14.
29. Martin, K., Läppen. VDI-Z. 113(11) (1971) 912–913.
30. Martin, K., Neue Erkenntnisse über den Werkstoffabtragsvorgang beim Läppen. *Fachberichte für Oberflächentechnik* 10(6) (1972) 197–202.
31. Schienle, H., Das Läppen als eines der ältesten Bearbeitungsverfahren hat gute Zukunftsaussichten. *Ind Anz* 105(9) (1983) 16–18.

32. Grosch, J., Grundlagen des Festigkeitsverhaltens technischer metallischer Werkstoffe. Berlin: TU Berlin, Habilitationsschrift, 1970. Zugl. In: *HTM* 26(4) (1971) 253–297.
33. Sulies, P., Untersuchungen über das Einlaufläppen von breitenballigen Stirn- und Kegelradgetrieben. Aachen: TH Aachen, Dr.-Ing. Diss., 1970.
34. Tsuwa, H., Researches on the lapping of metals. In Technology Reports of the Osaka University, Osaka, 1951.
35. Özhan, F., Feinbearbeitung weichmagnetischer Werkstoffe. *Reihe Produktionstechnik—Berlin, Forschungsberichte für die Praxis*, Bd. 36. Hrsg.: G. Spur. München, Wien: Hanser, 1985.
36. Kling, J., Verschleiß und Abtrag beim Läppen. *Technische Rundschau Bern* 78(11) (1986) 107–111.
37. Kling, J. and Matthias, E., Workpiece material removal and lapping wheel wear in plane- and plane-parallel lapping. *Ann CIRP* 35(1) (1986) 219–222.
38. Grünwald, F. and Jaksch, M., Einfluβ des Läppscheibenwerkstoffs auf die Herstellung von Oberflächen mit geringster Rauheit. *Feingerätetechnik* 25(6) (1976) 272–274.
39. Miller, N.E., Three-body abrasive wear with small size diamond abrasives. *Wear* 58 (1980) 249–259.
40. Mulhearn, T.O. and Samuels, L.E., The abrasion of metals: A model of the process. *Wear* 5 (1962) 478–498.
41. Kragelski, I.W., *Reibung und Verschleiβ*. Berlin: VEB Verlag Technik, 1971.
42. Ajayi, O.O. and Ludema, K.C., Surface damage of structural ceramics: Implications for wear modelling. *Wear* 124 (1988) 237–245.
43. Baehr, R., Zur Realstruktur bearbeiteter Silizium-Einkristallscheiben. *Kristall und Technik* 11(5) (1976) 549–558.
44. Buijs, M. and Martens, L.A.A.G., Effect of indentation interacting on cracking. *J Am Ceram Soc* 75 (1992) 10.
45. Buijs, M. and Korpel-van Houten, K., A model for lapping of glass. *J Mater Sci* 28 (1993) 3014–3020.
46. Buijs, M. and Korpel-van Houten, K., Three-body abrasion of brittle materials as studied by lapping. *Wear* 166 (1993) 237–245.
47. Cook, R.F. and Pharr, G.M., Direct observation and analysis of indentation cracking in glasses and ceramics. *J Am Ceram Soc* 73 (1990) 4.
48. Chauhan, R., Ahn, Y., Chandrasekar, S., and Farris, T.N., Role of indentation fracture in free abrasive machining of ceramics. *Wear* 162–164 (1993) 246–257.
49. Engel, H., Läppen von einkristallinem Silicium. Dissertation, TU Berlin, 1997.
50. Hadamovsky, H.F. (Hrsg.), *Werkstoffe der Halbleitertechnik*. Leipzig: VEB Dt. Verlag für Grundstoffindustrie, 1985.
51. Imanaka, O., Lapping mechanics of glass-especially on roughness of lapped surface. *Ann CIRP* 23 (1966) 227.
52. Izumitani, T. and Suzuki. I., Indentation hardness and lapping hardness of optical glass. *Glass Technol* 14 (1973) 2.
53. Marshall, D.B., Evans, A.G., Khuri Yakub, B.T., Tien, J.W., and Kino, G.S., The nature of machining damage in brittle materials. *Proc R Soc Lond A* (1983) 385.

54. Morita, N., Wu, T.-C., and Yoshida, Y., The effect of interaction of abrasive grains on the deformation and fracture behavior of brittle materials. In: *Proceedings of the ASPE 1992 Annual Meeting*, Grenelefe, FL, 1992.
55. O'Mara, W.C., Herring, R.B., and Hunt, L.P. (Hrsg.), *Handbook of Semiconductor Silicon Technology*. Park Ridge: Noyes Publications, 1990.
56. Phillips, K., Crimes, G.M., and Wilshaw, T.R., On the mechanism of material removal by free abrasive grinding of glass and fused silica. *Wear* 41 (1977) .
57. Spur, G. and Holz, B., Oberflächenqualität und Kristallschädigung beim Läppen und Schleifen von monokristallinen Siliciumscheiben. In: *Jahrbuch Oberflächentechnik*, Bd. 47. Berlin: Metall Verlag, 1991.
58. Spur, G., Holz, B., Sabotka, I., and Uhlmann, E., Oberflächenentstehung bei der spanenden Bearbeitung sprödharter Werkstoffe. In: *Tagungsband zum 8 Internationalen Oberflächenkolloquium*, Bd. 1. Chemnitz, 1992.
59. Spur, G. and Engel, H., Werkzeugeingriff und Oberflächenentstehung beim Läppen spröder Werkstoffe. In: *Jahrbuch Schleifen, Honen, Läppen und Polieren*, Bd. 58. Hrsg.: H.K. Tönshoff, Essen: Vulkan, 1996.
60. Tönshoff, H.K., Schmieden, W.V., Inasaki, I., König, W., and Spur, G., Abrasive machining of silicon. *Ann CIRP* 39(2) (1990) 621–635.
61. Lawn, B., *Fracture of Brittle Solids*, 2nd ed, Cambridge: Cambridge University Press, 1993.
62. Lawn, B.R., Hertzian fracture in single crystals with the diamond structure. *J Appl Phys* 39 (1968) 10.
63. Lawn, B. and Wilshaw, R., Review indentation fracture: Principles and applications. *J Mater Sci* 10 (1975) 1049–1081.
64. Lawn, B.R., Evans, A.G., and Marshall, D.B., Elastic/plastic indentation damage in ceramics: The median/radial crack system. *J Am Ceram Soc* 63 (1980) 9–10.
65. Marshall, D.B., Lawn, B.R., and Evans, A.G., Elastic/plastic indentation damage in ceramics: The lateral crack system. *J Am Ceram Soc* 65 (1982) 11.
66. Lawn, B.R., Marshall, D.B., and Chantikul, P., Mechanics of strength-degrading contact flaws in silicon. *J Mater Sci* 16 (1981) 1769–1775.
67. Wiese, G.E. and Wagner, R.E., Physical model for predicting grinding rates. *Appl Opt* 13 (1974) 11.
68. Dudley, J.A., Abrasive technology for wafer lapping. *Microelectr Manuf Test* 4 (1986) 1–6.
69. Sabotka, I.A.W., Planläppen Technischer Keramiken. Dissertation, TU Berlin, 1991.
70. Simpfendörfer, D., Entwicklung und Verifizierung eines ProzeÔmodelles beim Planläppen mit Zwangsführung. Dissertation, TU Berlin, 1988.
71. Davis, C.E., Untersuchung der EinfluÔgröÔen beim Flachläppen mit Diamant-Mikrokörnungen. *IDR* 7 (1973) 4.
72. Godo, R., Eigenschaften und Anwendung von Läppmitteln und Poliermitteln. Schorndorf: Seminar Feinschleifen, Läppen, Polieren, 1989.
73. Koshiyama, I., Lapping and polishing for modern monolithic micro-circuits. *Microelectr Manuf Test* 10 (1988) 19–20.
74. Rostoker, D., How users can optimize machine performance in production lapping operations. *Microelectr Manuf Test* May (1987) 9–10.
75. Wagemann, A., Wirkzusammenhänge beim Planparallelpolieren von Hochleistungskeramik. Dissertation, RWTH Aachen, 1994.

76. König, W. and Popp, M., Zum Schlichten und Schruppen geeignet. Siliziuminfiltriertes Siliziumkarbid wirtschaftlich läppen. *Industrie-Anzeiger* 97, 1986.
77. König, W., Wagemann, A., Popp, M., and Wemhöner, J., Werkstoffgerecht bearbeiten, Qualitätssicherung an Bauteilen aus Hochleistungskeramik. *Industrie-Anzeiger* 112 (1990).
78. König, W., Verlemann, E., and Wagemann, A., Hoher Abtrag. Gesinterte Keramik schleifen und läppen mit groβem Abtrag und hoher Güte. Maschinenmarkt, Würzburg (1990) 41.
79. Bogenschütz, A.F., George, U., Jentzsch, J., and Mussinger, W., *Die Prüfung von Polier-, Läpp- und Schleifmitteln.* Saulgau: Leuze, 1973.
80. Pahlitzsch, G., Vergleichende Untersuchung von natürlichem und sythetischem Diamantkorn. *Ann CIRP* 10 (1961) 2.
81. DIN 58751. Lose Schleifmittel für die Optik. Teil 1: Anforderungen. Beuth: Berlin, 1970. Teil 2: Prüfung. Berlin: Beuth, 1972.
82. Chandrasekar, S., Shaw, M.C., and Bushan, B., Comparison of grinding and lapping of ferrites and metals. In: *Proceedings of the ASME—Machining of Ceramic Materials Symposium*, Miami Beach, FL, 1985.
83. Degner, W., Bedeutung der Oberflächenbeschaffenheit für die Erhöhung der Qualität und Zuverlässigkeit der Bauteile. *Feingerätetechnik* 25(2) (1976) 85–88.
84. Eigenmann, B. and Scholtes, B., Zerstörungsfreie Eigenspannungsanalyse an ingenieurkeramischen Teilen. *CFI* 66(9) (1989) 364–374.
85. Kloos, K.H. and Macherauch, E., Development of mechanical surface strengthening processes from the beginning until today. In: *Shot Peening; Science, Technology, Application*. Hrsg.: H. Wohlfahrt u. a., Deutsche Gesellschaft für Metallkunde e. V., Oberursel, 1987.
86. Letner, H.R. and Snyder, H.J., Grinding and lapping stresses in manganese oil-hardening tool steel. *Trans ASME* 75 (1953) 873–882.
87. Rystsova, V.S. et al., Improving the wear resistance of lapped surfaces. *Russian Eng J* 53(6) (1973) 52–54.
88. Spur, G. and Simpfendörfer, D., Neue Erkenntnisse und Entwicklungstendenzen beim Planläppen. In: *Tagungsberichtsband des 5. Internationalen Feinbearbeitungskolloquiums*, Braunschweig, 1987. Zugl. In: *Jahrbuch Schleifen, Honen, Läppen und Polieren*. Hrsg.: E. Saljé. Essen: Vulkan, 55. Ausg., S. 459–480, 1988.
89. Sridhar, H.K., Krishnamurthy, R., and Balasubramanian, G., On some aspects of fine finishing. In: *Proceedings of the Eighth AIMTDR Conference*, IIT, Bombay, India, 1978.
90. Matalin, A.A., Restspannungen beim Schleifen. *Werkst u Betr* 103(9) (1970) 639–644.
91. Kedrow, S.M., Neuzeitliche Läppmaschinen. *Maschinenbautechnik* 2(7) (1953) 300–306.
92. Chandrasekar, S., Shaw, M.C., and Bushan, B., Morphology of ground and lapped surfaces of ferrite and metal. In: *Proceedings of the ASME—Machining of Ceramic Materials Symposium*, Miami Beach, FL, 1985.
93. Genzel, Ch. and Genzel, A., Shear stress distribution in crystals induced by mechanical surface load. *Phys Status Solidi A* 117 (1990) 141–154.
94. Stickler, R. and Booker, G.R., Surface damage on abraded silicon specimens. *Philos Mag* 89 (1963) 859–876.

95. Verhey, J., Bismayer, U., Güttler, B., and Lundt, H., The surface of machined silicon wafers: A Raman spectroscopic study. *Semicond Sci Technol* 9 (1994) 404–408.
96. Buck, T.M. and Meek, R.L., Crystallographic damage to silicon by typical slicing, lapping and polishing operations. Silicon Device Processing, NBS Special Publication Nr. 337, Washington, 1970.
97. Lundt, H., Kerstan, M., and Hahn, P.O., Subsurface damage of abraded silicon wafers. In: *Proceedings of the Seventh International Symposium on Silicon Material Science and Technology*, San Francisco, May 1994.
98. Pugh, E.N. and Samuels, L.E., Damaged layers in abraded silicon surfaces. *J Electrochem Soc* 111 (1964) 12.
99. Allen, J.W., On a new mode of deformation in indium antimonide. *Philos Mag* 4 (1959).
100. Pursche, G., *Oberflächenschutz vor Verschleiβ*. Berlin: Verlag Technik, 1990.
101. Gräfen, H. (Hrsg.), *Lexikon Werkstofftechnik*. Düsseldorf: VDI-Verlag, 1993.
102. DIN 8580. *Fertigungsverfahren. Einteilung*. Berlin: Beuth, 1970.
103. Funck, A., Planschleifen mit Läppkinematik. Dissertation, TU Berlin, 1994.
104. Spur, G. and Eichhorn, H., Untersuchungen zum Verschleiβ von Läppscheiben beim Planparallelläppen. In: *Vortragsband Seminar Poznan—Berlin "Dokladna Obrabotka Elementov Maszyn*," Poznan, 1995.
105. Spur, G. and Eichhorn, H., Grundlegende Untersuchungen zur Produktivitätssteigerung des Fertigungsverfahrens Planparallelläppen durch Konditionieren der Läppscheiben. Arbeitsbericht zum DFG-Projekt Sp84/137-2, 1995.
106. Spur, G. and Eichhorn, H., Kinematisches Simulationsmodell des Läppscheibenverschleiβes. *IDR* 31(2) (1997) 169–178.
107. Ardelt, Th., Einfluss der Relativbewegung auf den Prozess und das Arbeitsergebnis beim Planschleifen mit Planetenkinematik. Dissertation, TU Berlin, 2000; zugl. Reihe Berichte aus dem Produktionstechnischen Zentrum Berlin, 2001.
108. Hitchiner, M., Willey, B., and Ardelt, T., Developments in flat grinding with superabrasives. In: *Proceedings of the Precision Grinding and Finishing in the Global Economy—2001*, 1–3 October, 2001, Oak Brook, IL, 2001.
109. Uhlmann, E. and Ardelt, Th., Influence of kinematics on the face grinding process on lapping machines. *Ann CIRP* 48(1) (1999) 281–284.
110. Gellert, W. (Hrsg.), *Kleine Enzyklopädie Mathematik*. Thun und Frankfurt: Verlag Harry Deutsch, 1977.
111. Spur, G., *Die Genauigkeit von Maschinen: Eine Konstruktionslehre*. München, Wien: Hanser, 1996.
112. Ber, A. and Gueva, I., On the wear of the plane lapping plate. *Ann CIRP* XVI (1968) 409–413.
113. Fischer, E., Zur Vorausbestimmung des Abschliffes und der Abnutzung beim Präzisionsläppen. *Wiss Z TU Dresden* 14(1) (1965) 177–181.
114. Fischer, E., Optimale Überdeckungsverhältnisse an zwangsgeführt umlaufenden Plan-Läppmaschinen. *Wiss Z TU Dresden* 14(3) (1965) 719–731.
115. Lichtenberger, H., Die Spanmengenleistung beim Läppen ebener metallischer Werkstücke. Dissertation, TH Hannover, 1954.
116. Uhlmann, E. and Ardelt, Th., Kinematik und ProzeÔverhalten beim Planschleifen mit Läppkinematik. In: *Feinstbearbeitung Technischer Oberflächen*. Tagungsband zum "5. Int. IWF_Kolloquium" der ETH Zürich am 11/12 Mai 2000, S. 93–105, 2000.

117. Eversheim, W., Simulation als Hilfsmittel zur Strategie-, Produkt- und Produktionsplanung. In: *Vorträge des Produktionstechnischen Kolloquiums*, Berlin, 1986.
118. Spur, G. u. a., Simulation zur Auslegungsplanung und Optimierung von Produktionssystemen. *ZwF* 77 (1982) 9.
119. Bouzakis, K. and Mitsi, S., Hochgenaues Läppen. *Mathematische Beschreibung der sich ergebenden Oberflächenform und Rauhigkeit*. VDI-Z 128: 23/24, 1986.
120. König, W. and Steffens, K., A numerical method to describe the kinematics of grinding. *Ann CIRP* 31 (1982) 1.
121. Spur, G., Aufschwung, Krisis und Zukunft der Fabrik. In: *Vorträge des Produktionstechnischen Kolloquiums*, Berlin, 1983.
122. Hill, R., *The Mathematical Theory of Plasticity*. Oxford: Clarendon Press, 1985.
123. Spur, G. and Engel, H., Tool engagement and surface formation in lapping of brittle materials. In: *Proceedings of the International Journal of Japan Society of Precision Engineering* 33(3) (1999) 191–196.
124. Grubbs, F.E., Procedures for detecting outlying observations in samples. *Technometrics* 11 (1969) 1.
125. Smirnov, N.W. and Dunin-Barkowski, I.W., *Mathematische Statistik in der Technik*. Berlin: VEB Dt. Verlag der Wissenschaften, 1973.
126. Tippett, L.H.C., On the extreme individuals and the range of samples taken from a normal population. *Biometrika* 17 (1925) 364–387.
127. Evans, C.J., Parks, R.E., Roderick, D.J., and McGlaufin, M.L., Rapidly renewable lap: Theory and practice. *Ann CIRP* 47(1) (1998) 239–244.
128. Heisel, U. and Avroutine, J., Process analysis for the evaluation of the surface formation and removal rate in lapping. *Ann CIRP* 50 (2001) 229.
129. Suh, N.P. and Sin, H.-C., The genesis of friction. *Wear* 69 (1981) 91–114.
130. Yoshioka, M., Simulation of time dependent distribution of abrasive grain size in lapping. In: *Proceedings of the International Conference on Precision Engineering*, Taipei, 1997, 431–436.
131. Heisel, U., Avroutine, J., and Eggert, U., Simulationsmodell des Läppens für rein spanenden Abtragsmechanismus, Jahrbuch Schleifen, Honen, Läppen und Po-lieren 58 (1997) 506–520.

# 3 Lapping of Ductile Materials

*Ioan Marinescu, Ion Benea, and Naga Jyothi Sanku*

## CONTENTS

3.1 Introduction ..... 93
3.2 Physics of the Process ..... 97
3.2.1 Lap Plate ..... 99
3.2.2 Abrasives ..... 102
3.2.3 Abrasive Slurry ..... 105
3.2.4 Condition Rings ..... 107
3.2.5 Parts Carriers ..... 108
3.2.6 Carrier ..... 108
3.2.7 Auto Stirrer ..... 109
3.2.8 Lapping Methods ..... 109
3.2.8.1 Single-Side Lapping ..... 109
3.2.8.2 Double-Side Lapping ..... 111
3.2.8.3 Cylindrical Lapping ..... 113
3.2.8.4 Lapping with Bonded Abrasives ..... 114
3.2.9 Advantages of Lapping Process ..... 114
3.3 Mechanism of the Process ..... 115
3.3.1 Two-Body and Three-Body Abrasion Mechanisms ..... 118
References ..... 120
Bibliography ..... 121

## 3.1 INTRODUCTION

The high demands required today by manufacturing engineers for machine parts and tools necessitate very precise machining. The finishing processes are an important perspective to be considered today to meet the goals like parallelism, tolerances, flatness, and smooth surface. These processes are high-precision abrasive processes used to generate surfaces of desired characteristics such as geometry, form, tolerances, surface integrity, and roughness characteristics. Abrasive finishing processes are used in a wide range of material applications and industries. Typical examples are finishing of various components used in aerospace, automotive, mechanical seals, fluid handling,

and many other precision engineering industries. The lapping process is a fine finishing process, which has a leading importance in this perspective. The lapping process leads to a surface with low roughness and high precision. The topographical structure resulting from lapping is very advantageous in sliding joints, because of the high ability of lubricant retention, as well as in nonsliding joints because of the high load-carrying ability. The range of lapped materials is very wide. This necessitates the use of natural and artificial abrasive materials and mainly materials such as micrograins of alumina, silicon carbide, boron carbide, and diamond. Both the solid and liquid carriers distribute these grains on the surface of the lapping tool and the chemical action takes place, which the active components aid for the machining to occur intensively.

The lapping process has its roots from the origin of the finishing process. It is considered as one of the oldest processes suggested to meet the requirements of the dimensions and to obtain a relatively good surface finish that is aimed mainly to decrease surface roughness and surface waviness, and to obtain closer tolerances.

The process is also suitable to machine hard materials, brittle materials, etc. Although hardness is one of the greatest attributes of ceramic materials it also sometimes becomes their drawback especially when machining them to tight tolerances. To obtain closer tolerances, ceramic materials demand a very highly sophisticated equipment and skilled labor, which will obviously lead to high manufacturing costs and this is not at all desired. Subsurface damage is one of the problems that is seriously affecting the performance of ceramic components. Hence to obtain all the necessary machining qualities without much investment, design engineers have suggested the lapping process.

Lapping has a wide range of applications. The process is also preferred for finishing of optical glasses, for finishing different materials, and is also used in producing the required finishing for silicon wafers, which is a major component in computer architecture and electronic fields. Lapping can also be used for finishing both metals and ceramic materials.

Lapping processes chiefly have the following characteristics that vary in degree according to the particular system and equipment: (1) the rate of stock removal is low because of the low cutting speeds and shallow penetration of the fine abrasive grains into the work surface; (2) this process is considered a cool process because it is carried out without generating significant heat and hence does not cause thermal damage; (3) relative low force is exerted on the workpiece that is usually held in a supported manner, which supports it to machine fragile and brittle parts; (4) the general shape of the surfaces worked by lapping is mostly limited to basic forms such as flat, cylindrical and spherical, and in exceptional cases it is used for other shapes like screw threads, but the accuracy achieved in lapping is excellent especially for flat surfaces; (5) lapping produces surfaces with very low degree of roughness, in general lapped surfaces are very smooth with regard to both the measurable surface finish and the visually discernible reflectivity. Work material and its

hardness usually affect the reflectivity of the lapped surfaces, so soft materials have low reflectivity and are of matte finish even when lapped to a high degree of physical smoothness; (6) surface characteristics such as a random lay pattern, an adaptability to microscopic examination at very high magnifications, a high ratio of bearing surface to the total surface area, etc., can also be accomplished by lapping; (7) due to the low and constant material removal rate, the particle size can be controlled excellently as the lapping action is consistent and uniform; (8) economically, it is a suggestible process when compared to other processes such as lighting cutting force, which requires simple work retainment only, and dependable control of size reduction without expensive instrumentation, freedom from warpage, etc., can be the determining factors [1,2].

The following are the general points that should be followed in the lapping process to obtain the desired finishing:

- A lap should be softer than the part to be lapped.
- The abrasive in a compound should be as hard as the metal being lapped. Hard abrasives will charge or embed in a softer metal. A non-embedding or noncharging compound should be used for soft metals as garnet abrasives are used for brass or bronze. The softer the metal, the softer the abrasive. The harder the metal, the harder the abrasive.
- High lap speed will increase stock removal. For a rotary lap, a speed of approximately 275 rpm is recommended. If lap pressure is too high it will score the part.
- Increase of pressure of part against the lap will increase the speed of cut.
- Serrated or grooved laps are best for flat surfaces with large areas, and also for flat areas with holes in the surface.
- Laps with no serration or grooves are preferred for cylindrical lapping.
- Abrasives when mixed into an oily paste or greasy vehicle will give better results than just a mixture of fluid oils and abrasives.
- Tungsten carbide is best lapped with diamond compounds. Norbide or boron carbide abrasive will slowly abrade the metal, but the finish is not at all equal to that of the finish obtained by the diamond compounds.
- A gray or frost-like surface may be as smooth and accurate as a bright finish. A bright or polished surface does not indicate that it is smooth, but a smooth surface may be bright or polished.
- A polished surface is harder to produce than a gray matte finish and will show scratches more readily.
- It is more difficult to lap soft metals than hard metals.
- A soft lap will cut faster than a hard lap. It will wear longer and give a brighter surface. A hard lap cuts slowly, wears faster, and gives a dull finish, but its accuracy of lapping is greater.
- Final finishing should be done only with a charged lap lubricated with thin oil, naphtha, gasoline, spindle, etc.
- Thin workpieces can be lapped parallel but not necessarily flat.

- Final finishes are best obtained with no loose abrasive on the plate. Hence, the embedded abrasive granules and a very thin lubricant are used in the surface of the plate to get the final finish.
- When soft metal parts such as brass or bronze running seals are lapped, a nonembedding abrasive should be used.
- Different kinds of abrasives or grit sizes should not be used at the same time on the same plate. It is recommended to use different plates for roughing and finishing operations.
- Diamond compounds should be used for lapping tungsten carbide or other metals when the Rockwell C hardness exceeds 64.
- An abrasive particle will produce a scratch one-half of its size. Thus, a 10 μm sized particle will produce a scratch of 5 μm.
- Brightness does not indicate flatness. A gray or matte finish can be just as smooth and accurate as a bright finish.
- Fine abrasive grit sizes do not mean fine finishes. Abrasives can be very fine. The abrasive should just be coarse enough to abrade or remove the desired amount of stock or metal that causes the abrasive granules to break down into inert sized particles. These fine particles produce the desired finish.
- For measuring flat lapped surfaces a polish is necessary and an optical flat is used. An optical flat is a transparent disc, preferably quartz. With proper reflective surface conditions, the phenomenon of interference bands is created with an optical flat. As seen through the optical flat these bands appear as a pattern of dark strips on the illuminated work surface. Interference bands can be used with great accuracy to determine the flatness of a surface, i.e., the location and amount of concavity or convexity. Straight band indicates a flat surface. Curved or irregular bands show a lack of flatness. Bands that curve toward the line of contact and away from the line of contact indicate a convex surface and concave surface, respectively.
- To obtain a reading with an optical flat on a flat workpiece the surface must have a reflective finish and be flat within $5\times10^{-5}$ in.
- Every abrasive has a different finishing quality as to brightness or reflective ability. Silicon carbide abrasive, no matter how it is used, will only produce a gray, frosted, or matte finish.
- A mixture of just oil and abrasive is not a good lapping medium. The abrasive granules should be held in a film on the plate that resists the movement or rolling of abrasive granules. This resistance causes the cutting edges of the abrasive to abrade or remove the metal.
- The compounds having a pasty base or vehicle create an important film. The crushed abrasive granules in this film create a protective medium between the lap and part.
- For lapping various grades of aluminum metal, garnet and silicon carbide compounds are recommended. Linde powders are used to create a high polish or mirror finish.

- For lapping hardened steels, stainless steels, chrome plate, etc., which have Rockwell C hardness of 55–63, aluminum oxide abrasive compounds are recommended. Aluminum oxide abrasives are also recommended for beryllium and ceramics. It is available in all standard sizes.
- The corundum abrasive is well suited for softer steels.
- Carbon seals should not be lapped with loose abrasive on a plate. The lapping plate should be a bonded abrasive disk using a thin oil lubricant.
- Surface finish is a function of abrasive grit size, part material, and part hardness. Coarse abrasives produce higher rms finishes than finer abrasives. Harder materials exhibit lower rms finishes from a given abrasive than softer materials.

Lapping with diamond abrasives has more benefits than conventional abrasives. With diamond slurries, the lapping and polishing phases can be achieved in one step. The time required for cleaning and processing the waste is less, thereby increasing the overall productivity. The main applications of these abrasives are superior surface finish, aggressive material removal, uniform edge to edge flatness, surface finishes to 0.2 $\mu$ in. Ra, flatness to 1/20th wavelength, superior cleanability, and precise repeatability besides obtaining both lapping and polishing properties in one process.

Lapping is a process, which basically can work on any material or shape. Although its aim is to obtain surface finish, it basically imparts the dimensional tolerances and accurate shape by concentrating more on stock removal than that of surface finish. It is basically described for the flat, round, and square parts but it can also work on intricate parts. If the lap material is chosen in such a way that it is softer than the workpiece material then the lapping process can impart any dimensional shape. Hence, it is finding new applications in different industries. Even the lapping can be done on wafers to obtain smooth surface and planarity. Hence the demand for these finishing processes is growing day by day in electronic industries, industries manufacturing computer hardware parts, and precision micromachine industries. Lapping is the basic process used in obtaining smooth finishes in silicon wafer manufacturing and in finishing some ingredients of chips, etc. Mainly, ceramic industries are depending on this process for finishing. Lapping can be done on any material like copper, iron, alumina pieces, silicon carbide pieces, etc. Figure 3.1 shows some of the shapes that are being lapped in various industries for various applications.

## 3.2 PHYSICS OF THE PROCESS

Lapping is a fine finishing abrasive process aimed at imparting specific characteristics to the workpiece with respect to form, size, and surface conditions. It is a process in which a rotation lap, charged with loose abrasive slurry, removes a very small amount of material from metallic or nonmetallic surfaces. Low speed and low pressure result in fine finished surfaces of

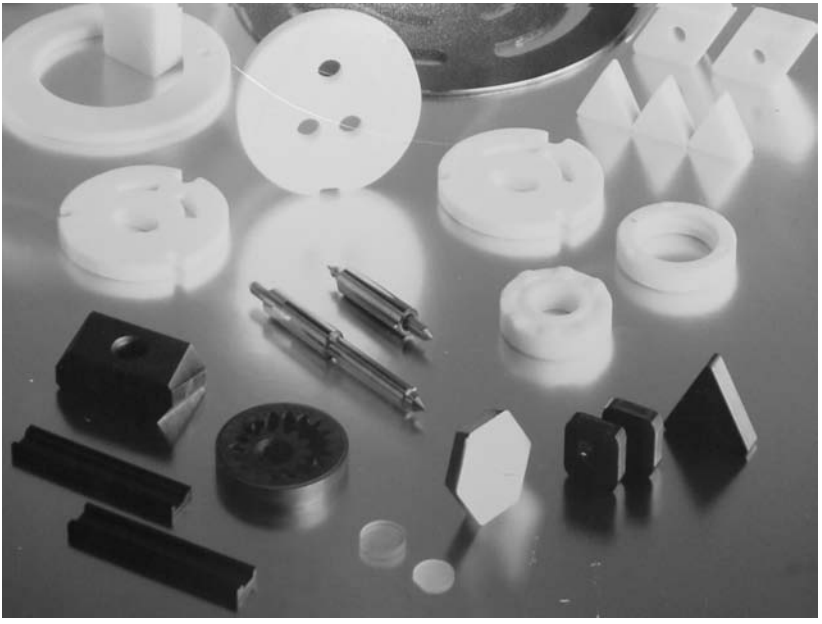

**FIGURE 3.1** Different shapes that are lapped in various industries. (From Indge, J.H., *Tooling and Production*, 55, 116, 1990.)

extreme flatness. It is mainly a three-body abrasion wear in which abrasives are loosely held between workpiece and lap plate, which are mainly responsible for fine finish and a high degree of geometric accuracy. Lapping is generally carried out on a Lapmaster. This lapping machine is the simplest available and is used for a general lapping process. The usage of highly sophisticated and highly mechanized machines is demanded as the demands of surface finish and tolerances are to be closer or finer [3]. Lapping generally can machine more than one part.

Lapping mainly includes lap plate, abrasives, vehicle or carrier, condition rings, and work holders. Laps are usually made of soft cast iron, copper, brass, lead, or ceramic. Abrasives used in ceramic industries are basically the hardest materials. The vehicle or carrier carries the abrasive slurry to the lap plates. Condition rings are made of a material that is compatible with the lap plate hence avoiding any chemical action. Work holders hold the workpieces so that the area of contact with the lap plate is uniform.

The following are the most distinguishable characteristics of the lapping process:

1. Contact points between tool and workpiece are constantly changed through relative motions.
2. Rotation tools store the abrasive particles.

3. It is a low speed and low pressure abrading operation.
4. Results in fine surface finish and extreme flatness.

Generally, for a higher degree of accuracy in the finished product, soft cast iron is the best lap material to use. Usually, a high-density cast iron alloy, radially serrated, precision-machined, highly planar circular plate is used for bulk stock removal. This plate may be removed by an Allen wrench. Samples to be lapped are placed face down, wax-mounted to the diamond stop fixture, which itself will rotate once the wheel rotation is started, and held in place over the lapping plate within a conditioning ring or retainer ring wedged inside a roller yoke. As both the condition and planarity (i.e., concavity or convexity) of the lapping plate's topography will be transferred as a mirror image to the sample that is lapped, it is important to properly check and adjust or correct the planarity of the lapping plate before and during a lapping process. The plate should be heavy enough and properly designed to avoid distortion over use. Its surface may be plain or grooved. Plain plates are best suited for extreme accuracy and for lapping cylindrical work and, grooved laps are used for lapping flat work only [4,5]. To produce a perfectly smooth surface free from scratches, the lap should be well charged with the fine abrasives initially and kept moistened during moderate use; it will cut for a longer time. The pressure upon the work should be just enough to ensure constant contact. The lapping plates are mainly grouped as natural and special composites. Special composite laps are prepared with a unique blend of powdered metal or ceramic, combined in a resin system. These are used instead of pure metal as the special formulations of powders and resins allow composite laps to take a more uniform charge of diamond, as compared to pure metal plates. The result is a more consistent and controlled performance. And also, composite plates are superior in applications where lapping and polishing are combined into one step. Typical applications of composite laps are fuel injector components, magnetic head substrates, bars and sliders, CD molds, stamping dies, valves and pump components, ceramic seals and components, mechanical seal faces, semiconductor substrates, carbide cutting tools and inserts, electro-optical and fiber-optic devices, electronic substrates, and laser rods.

The main factors influencing the lapping characteristics are the type of the lap, the type and size of the abrasive grains, the lapping fluid type, the lapping pressure, and the lapping speed.

### 3.2.1 Lap Plate

The composition of lap plate is of great importance because it can affect the results of the lapping process and hence the type of lapping plate is important as a workpiece can be badly scratched and contaminated with abrasives if the

lap plate is too hard. A hard lapping plate resists being embedded with abrasive particles. Therefore, the grains roll more than they slide so that most of the material removal is by stress inducing micro fracture and also the grains are embedded more in the workpiece. A softer lapping plate allows abrasives to partially embed themselves in the lap, resulting in more sliding motion and material removal by ploughing. The result is a finer surface finish from soft plates but less planarity. A hard plate and very fine abrasives can impart better surface finish with respect to planarity. To obtain a perfectly smooth surface it is important that the lap plates should be charged with a very fine abrasive and should be charged until the lap surface has a gray appearance. One should bear in mind that the lap plates should not be over charged as it may result in inaccuracy because of excessive rolling action between the workpieces and the lapping plate. The rotation of lap plate also may affect the planarity and hence appropriate plates should be selected to achieve the desired purpose.

The most widely used types of lapping plates in the industry are the following:

*Iron lap plate*: The plate has aggressive stock removal rate and it is an excellent primary or roughing lap plate, with a long service life often used as an alternative for cast iron plate. It produces a good surface finish on most materials, especially metals and ceramics and typically used with coarse to medium diamond sizes (Figure 3.2).

*Copper plate*: This is the most widely used and universal composite lap plate, excellent when primary and finishing operations are combined in one

**FIGURE 3.2** Cast iron plate. (From www.engis.com.)

**FIGURE 3.3** Copper plate. (From www.engis.com.)

step. It is suitable for metals, ceramics, glass, carbon, etc. It minimizes fracturing and chipping tendencies when lapping. It is preferred for lapping medium to fine diamond sizes (Figure 3.3).

*Ceramic plate*: This plate is generally used to lap or polish ceramic parts and other stain-sensitive materials and used in applications where metallic-type contamination cannot be tolerated. It is affordable, more machinable, and alternative to natural ceramic plates. These are very flexible and hence can be used with coarse to fine diamond sizes. This plate encourages moderate stock removal (Figure 3.4).

*Tin or lead plate*: It is most widely used as finishing lap plate, often used in place of polishing pads, suitable for metal, ceramic, and other materials. It is typically used with fine to very fine diamonds and it minimizes fracturing and chipping tendencies when lapping crystal components. These plates are aimed at obtaining a fine stock removal (Figure 3.5).

*Tin plate*: It is aiming at having a fine stock removal and is often used where lead-type contamination cannot be tolerated and is suitable for charging extra-fine particulates. It is used with fine to extra fine (micron to nanometer) diamond sizes. Typically used with coarse to medium diamond sizes (Figure 3.6).

Square, spiral, concentric, and radial grooved lap plates are available and these lap plate sizes are in the range of 12–42 in. They can be used according to the demand of the material to be machined.

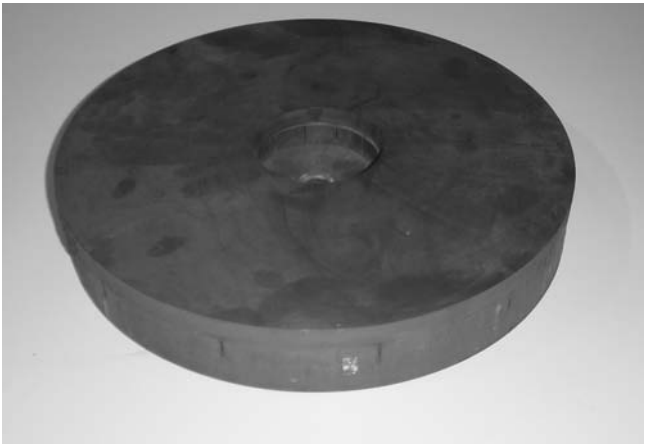

**FIGURE 3.4** Ceramic plate. (From www.engis.com.)

### 3.2.2 Abrasives

The abrasive grains used for lapping have sharp, irregular shapes, with each other backed by a lapping plate. When a relative motion is induced and pressure applied, the sharp edges of the grains are forced into the ceramic material to abrade away microscopic particles. Thus the cutting action takes place continuously over the entire surface of the workpieces. The abrasives come into contact with the abrasive slurry backed by a lapping plate. This

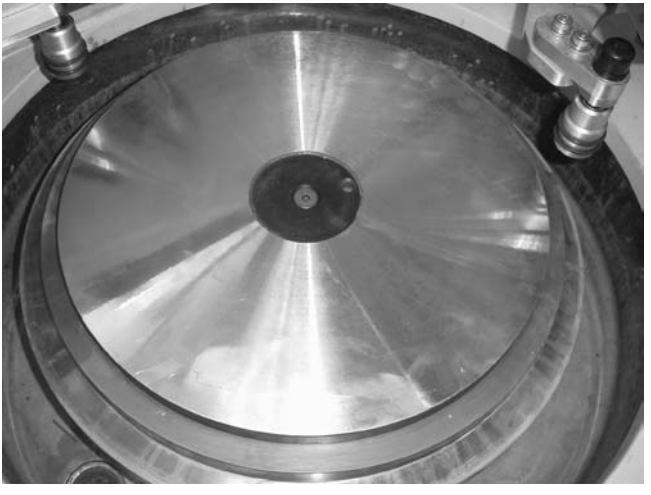

**FIGURE 3.5** Tin or lead plate. (From www.engis.com.)

**FIGURE 3.6** Tin plate. (From www.engis.com.)

type of abrasive machining action is unique when compared with other forms of machining. The abrasives mixed with slurry can be of a variety of shapes and sizes. Three abrasive cutting mechanisms—rolling, sliding, and charged plate mechanisms—simultaneously occur in lapping. Rolling abrasives and sliding abrasives act very similar except that the sliding abrasives are more plate-like and act like tiny scrapers whereas rolling abrasives are more round in shape. Charged plate abrasives are the abrasives that have imbedded into the lapping plate. The size and size distribution of the abrasives are the important factors in the surface obtained by lapping and so the size of the abrasive is directly proportional to the material removal rate and surface roughness [6–8].

Abrasives are either natural or artificial crystalline forms. Natural abrasives are diamond, corundum, garnet, emery, quartz, and other softer materials found in the Earth. Artificial abrasives, such as diamond, borazon TM CBN, silicon carbide, aluminum oxide, boron carbide, and various aluminas that are divided into two groups, fused and unfused, are manufactured.

- Fused abrasives are the result of tremendously high electric furnace temperatures, which produce hard crystals.
- Unfused alumina abrasives are the result of lower temperatures and chemical additives. They do not have the hard crystalline structure of fused abrasives.

The following are the different types of abrasives and their respective applications:

*Diamond*: Both a natural and human-made synthetic abrasive of Mohs 10 and is the hardest and the sharpest abrasive known. It is best suited for

tungsten carbide and other very hard materials. Since it is so hard it should not be used on softer metals where embedding may be a factor. When a plate has been embedded with the diamond abrasive, it cuts faster and produces fine finishes. In recent years, synthetic fine diamond powders have been increasingly used in industrial applications.

*Cubic boron nitride*: Commonly known as borazon TM CBN, cubic boron nitride is a human-made synthetic abrasive that is almost as hard as diamond on the Mohs scale. This abrasive material is well suited to ferrous metals in a lapping operation, as it will not carbonize like diamond when interacting with Fe (iron). Borazon TM CBN is especially well suited for lapping 52100 bearing steel, cast iron, die steel, tool steel, stellite, super alloys, and in some cases ceramic materials.

*Norbide abrasive*: A fused abrasive with high grain strength and of Mohs 9.7 has a hexagonal structure and is not easily friable. It is useful only for unusual or special lapping operations.

*Silicon carbide*: A fused, hard crystalline abrasive of Mohs 9.5 is fast cutting with a good crystal breakdown when used to lap either high or low tensile strength material. It is well suited for rough lapping operations, forged or hardened gears, valves, toolroom work, and general maintenance where polish is not essential. With silicon carbide, all lapped material will have a frosty or gray finish.

*Aluminum oxide*: A fused crystalline abrasive of Mohs 9, which is just under silicon carbide, has very hard crystal structure that is slowly dulled and hard to fracture. It is best suited for use on high tensile strength materials, rough lapping operations, hardened gears, ball bearing grooves, or lapping operations where pressure can be exerted to break down the crystals. It does not lend itself to fine finishes or precision lapping.

*Fused alumina*: With hardness of Mohs 9, another form of fused alumina is the 38 white aluminum oxide abrasive, white in color with friable crystals. The pressure on (friable) crystals, when lapping, causes them to keep breaking down into still smaller particles, which perform the finishing operation, to produce the low rms finishes or polish. 38 white aluminum oxide is valuable for lapping stainless steel, chrome plate, beryllium, and ferrite whose hardness range is below the 62–63 Rockwell C scale.

*Corundum*: A natural abrasive of Mohs 9 is found in the Earth with softer crystalline structure than silicon carbide or aluminum oxide. It breaks down readily and is important for lapping a great variety of medium hard metals (Rockwell C 35–45). It gives a medium polish or reflective finish.

*Garnet*: A natural abrasive of Mohs 8–9, mined from the Earth with a blocky crystalline structure that does not readily embed itself in lapped parts. Its greatest asset is that it may be safely used for lapping cast iron gears, brass or bronze running seals, and instrument gears where such nonembedding qualities are desired. It has a medium polishing quality.

*Unfused alumina (hydrate–calcined)*: Aluminas are produced in a wide variety—γ and α, hydrate and calcined. Hydrate alumina is relatively soft and is used for polishing. Calcined aluminas are produced by heat treatment and the degree of calcination determines the characteristics of the product. The terms soft, medium, and hard relate to them as mild, medium, and high degree of calcination. The calcined types are recommended for the lapping and polishing of harder metals (Rockwell C 45–63). Their shape, unlike the blocky crystals, is composed of flat or platey crystals with their thickness about one-sixth their diameter. Unfused aluminas allow more equal pressure to be distributed over a larger surface area than with fused because of their platey shape.

The disk-shaped particles work with a shaving action rather than the rolling and gouging action of ordinary abrasives and are not apt to scratch the work being lapped [9].

### 3.2.3 Abrasive Slurry

The purpose of any vehicle is to carry the abrasive grains and to position them to work efficiently. The vehicle also lubricates the surfaces and carries away the abraded material removed from the workpieces. The abrasive slurries are mainly divided into three groups as water-soluble slurries, oil-based slurries, and oil–water emulsion slurries. Water-based vehicles are commonly used for lapping although oil vehicles can be and are used. Oil is a good vehicle; however, it is often objectionable because of its tendency to penetrate into the pores of some materials. In addition, oil is expensive to purchase, and its disposal is difficult and expensive because according to industrial regulations, disposal of oil is now considered a hazardous waste. Water-soluble slurries are preferred to avoid health hazards. Oil-based slurries are the products that are formed by the mixture of oil and abrasives. These slurries work well because surface tension of lapping oil is similar to that of the ceramic workpiece. Modern oil-soluble slurries are capable of suspending super abrasives like diamond and CBN without clumping and lubricating and cooling the workpiece, absorbing the swarf, and thereby providing easy cleanup while maintaining viscosity. Similarly, water-based slurries are comprised of water-soluble and water-emulsifiable materials. These slurries are used for soft lap plates like brass, tin, lead, and copper. Water-soluble slurries can achieve fine finish when compared to oil-based slurries. To prevent rusting of the machine components, inhibitors are added to water vehicles. In some cases, depending on the equipment, the vehicle acts as a cooling agent to carry away the heat generated by the lapping process. Suspension agents are occasionally added to prevent settling of the abrasive. These agents do not necessarily improve the actual lapping action. There are a variety of methods that can keep the abrasive in suspension with minimal negative effect at the area where the machining

takes place. Apart from these two groups, oil–water emulsions can also be used for lapping. But it has many disadvantages such as shorter shelf life than oil-soluble emulsions, difficulty in suspending and resuspending super abrasives, and a viscosity that varies on use. In oil–water emulsions, droplets break up during lapping, allowing their oil components to coat the workpiece. The oil-based slurries are cleaner than the water-based slurries and they can be wiped off with the mineral spirits. The concentration of abrasives that is the amount of abrasives per volume of carrier affects the stock removal and surface finish. When the concentration, i.e., the number of grains in contact with the surface of the workpiece material varies, the load distribution varies thus resulting in an uneven surface [3,10]. When once applied on the lap plate, how these different slurries work during the process are shown in Figure 3.7.

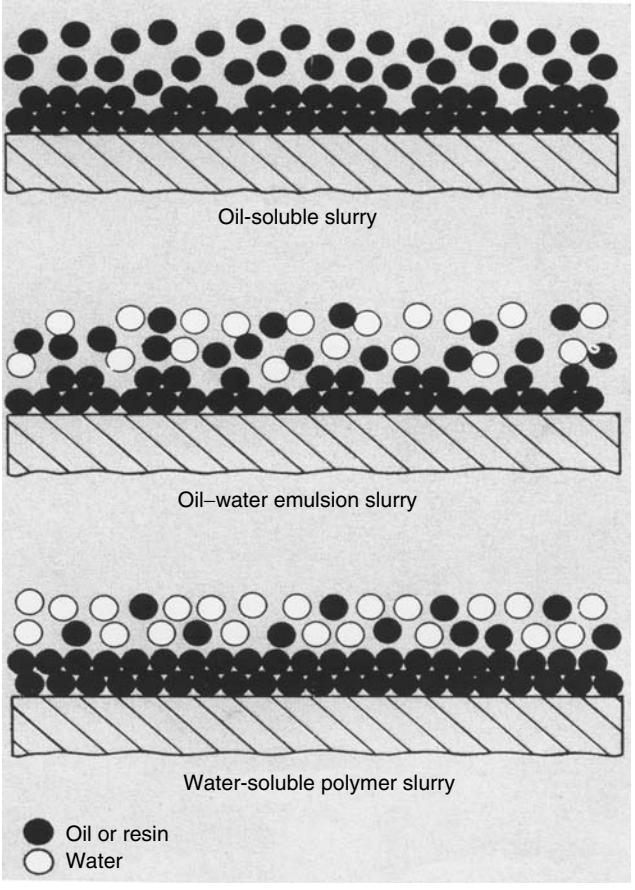


**FIGURE 3.7** The action of abrasives in three different slurries. (From Emond, G.T., *Ceramic Industry*, 30, 1987.)

### 3.2.4 Condition Rings

The condition rings are mainly aimed at consistently regenerating surface textures and flatness of lap plates. Mainly there are solid ceramic conditioning rings, stainless steel rings, diamond-plated rings, and even rubber pads are used (Figure 3.8). Conditioning rings are specially designed to correspond with the various lap plates mentioned previously. These rings serve a dual purpose; they are used primarily for retaining parts during processing and at the same time maintain lap plate flatness. Some examples include

- Cast iron—general engineering
- Hardened steel—for use with hardened steel plates
- Ceramic—polishing applications
- Micarta—polishing applications
- Polycarbonate—polishing applications

*Solid ceramic condition rings*: These are ideal for use in the electronics, automotive, medical, audio and visual, and optical industries. These high-quality alumina ceramic rings provide an unmatched level of control in the final finishing process and 12 serrations per ring. These are available for 12 in. and 15 in. lap plates.

*Stainless-steel-backed ceramic conditioning rings*: These are backed with 304 stainless steel for greater tensile strength, and these rings are highly resistant to corrosion and available for 12, 15, 24, 28, 36, and 42 in. lap plates.

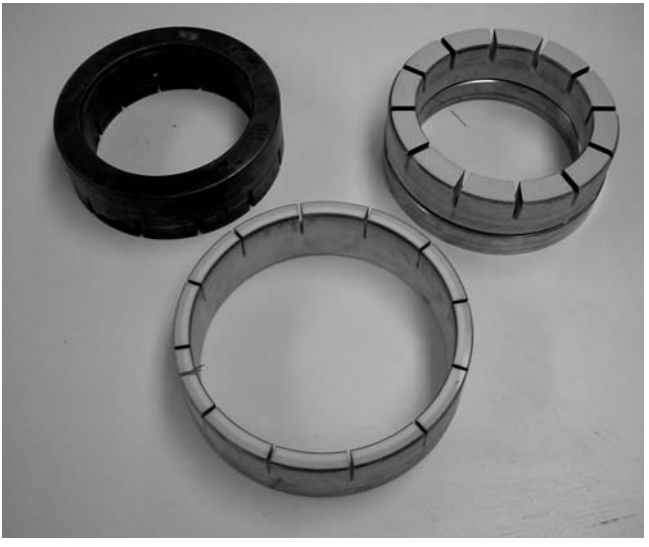

**FIGURE 3.8** Various condition rings used in lapping process. (From www.engis.com.)

*Diamond-plated conditioning rings*: These diamond-plated rings are designed specifically for composite lapping plates. These are engineered to consistently regenerate surface texture and flatness of composite lap plates, and also these rings eliminate varying results usually associated with conventional abrasive reconditioning and are available for lap plates from 12 in. up to 42 in.

### 3.2.5 Parts Carriers

These are mainly designed to increase productivity while attaining precision surface flatness and finish. These are available in fiberglass and conventional phenolic plastic and a range of other materials, in various diameters and thickness.

*Polishing pads*: Polishing pads are available in a wide range of sizes and materials to fit almost any application. The pads come with adhesive backing for mounting to machine plates and can be used for polishing a wide variety of materials including metals, glass, semiconductor materials, and more.

*Rubber pads*: These pads enable greater productivity when lapping parts of varying thickness and are designed to apply even pressure to all parts and are available in 1/2 in. thick soft rubber and 1/8 in. hard rubber.

### 3.2.6 Carrier

The carrier's main purpose is to carry the abrasive grains and position them to work most efficiently. It also lubricates the surfaces and carries away the abraded material removed from the workpieces. Inhibitors are added to avoid rusting and suspension agents are occasionally added to prevent settling of the abrasive. When using imbedded abrasives, the vehicle is made as a paste and is applied initially to the lap to charge them. It can be applied as either paste form or liquid form as the case demands. Water-based carriers are used more than oil-based carriers, but oil slurries are used extensively in diamond lapping.

Carriers can be machined using punch and die tooling, computer numerical control (CNC) machining, electrical discharge machining (EDM), and laser cutting. Work holes can be custom-cut to suit any application and any geometry. Different materials can be used in the production of carriers.

*Steel*: Spring steel is the strongest, most durable carrier material. Closer tolerances of thickness and flatness are obtainable with spring steel material making it ideal for thin work.

*Lamitex*: Lamitex, also known as G-10 and FR-4, is an epoxy-based material reinforced with fiberglass. Lamitex is an excellent alternative to steel offering excellent machining capabilities, high mechanical strength, noncorrosive, and low water-absorbing properties. Lamitex is also an excellent choice for large thick parts.

*PVC*: PVC is a thermoplastic vinyl. Combining chemical inertness, high strength-to-weight ratio and economical cost, PVC is an excellent choice for

corrosion-resistant applications. PVC can be sanded to achieve tight thickness tolerances and is commonly used for lapping thick parts.

*Phenolic*: Phenolic is a resin binder reinforced with cotton fabric. Phenolic is very wear-resistant and stronger than most plastics. It is typically used with oil-based slurries due to its water-absorbing qualities. Phenolic is an excellent choice when steel or fiberglass is not permitted in a process.

*Lexan*: A plastic without fiber reinforcement, this material gives up some of the strength of lamitex but does not cause scratches in polishing applications.

*Vinyl*: Softer and less expensive than lexan, vinyl is an economical choice for short runs on smaller lapping machines.

*Zinc*: This zinc alloy is a soft material that helps protect the edges of fragile parts. This material is only available for use on small machines.

### 3.2.7 Auto Stirrer

This unit stirs and keeps abrasive slurry completely dispersed during usage. To accelerate dispersion, shake bottle thoroughly and then place in the auto stirrer. It will not be necessary to shake bottle again. It is especially helpful when the grain grit size is 15 and coarser. It has the ability to keep an equal dispersion of abrasives, consistent stock removal and finish at all times. Lap Master accomplishes this by providing a unit capable of accommodating both diamond slurry and lubricant. The diamond slurry mixture is kept in suspension by means of a magnet driven by an electric motor [11].

Work parameters that affect the efficiency of the lapping process are the process parameters: speed, pressure, and time; abrasives: types, shape, grit size, distribution, carrier types, and finally material properties of workpiece and lapping plate. Among all the parameters, lap plate is considered to be the major variable because all the other parameters depend on it in one way or the other, as the concerned properties of the mechanism, dimensional accuracy, and surface finish.

### 3.2.8 Lapping Methods

The machining methods used in lapping operations can be classified as

- Single-side flat lapping
- Double-side flat lapping
- Cylindrical lapping between laps
- Lapping with bonded abrasives

#### 3.2.8.1 Single-Side Lapping

It is the best known and most widely used process (Figure 3.9). Many ceramic workpieces require one flat surface. Single-side lapping is the most frequently

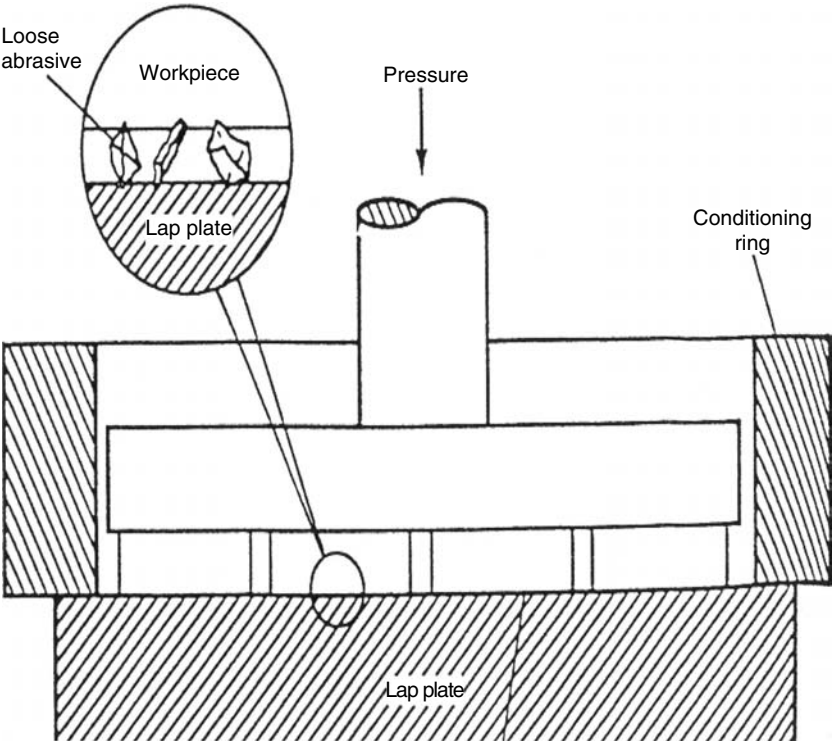


**FIGURE 3.9** Single-side lapping process. (From Corsini, A.M. *Proceedings of Grinding and Machining of Advanced Materials*, Pittsburg, PA, October 11–13, 1995.)

used machining process for producing such flat surfaces. The advantages of this type of lapping is that many pieces can be machined at one time and besides this, work holding is very simple, cut rates are consistent, and close accuracies are inherent with the process. The machines used in this lapping have a rotating annular-shaped lap plate and workpieces are placed on the flat rotating wheel. To keep the wheel flat and also to guide the workpieces numerous devices are employed when pressure is applied on the wheel. In addition, the abrasive slurry is then added, often automatically, to the wheel surface. Designers have strived to overcome some of the problems that are common in this type by keeping the wheel flat, by applying uniform and predictable pressure, and lastly by applying and maintaining a uniform and consistent flow of abrasive. These three variables are to be taken care of well because these are the most influencing factors on the surface finish. The two major causes of wheel out of flatness condition are deflection and uneven wear. Deflection in the lap wheel due to pressure applied on top of the

workpieces must be kept to a minimum by providing heavy and sturdy support of the rotating wheel. Thermal expansion due to heat can cause an out of flatness condition and therefore a temperature-resistant wheel is an essential requirement. However, modern production machines have devices to carry away the heat generated during the process, and ideal systems are designed to keep the hot spots and cold spots to a minimum. Uneven wheel wear is another factor to be considered during this single-side lapping process. The lapping action on the workpiece tends to wear the wheel away where the workpieces contact the wheel, causing the out of flatness condition to develop. In most instances, condition rings are applied to wear away the higher points on the wheel that do not contact the workpieces, thus keeping the wheel face flat. These rings are rotated either by the force of action from the rotating lap wheel face or by some drive device in the center of the wheel. To provide control of lap flatness and uniformity of lapping action, the condition rings should be rigidly supported and always power driven in one direction only. In addition, position means should be provided to correct for either a concave or a convex lap wheel condition. These are corrected by positioning the rings more to the center of the wheel. Generally, this type of machining normally requires uniform pressure on the top of the workpieces and uniform abrasive slurry flow to obtain the desired surface smoothness. The abrasive feeding system should distribute the abrasive slurry evenly over the working area of the wheel utilizing the forces such as gravity, centrifugal force, and rotating action of the wheel and condition rings.

#### 3.2.8.2 Double-Side Lapping

This method is considered as the most accurate one in terms of parallelism and uniformity of size as it machines on both sides of the workpieces simultaneously using batch-mode type processing (Figure 3.10). The concept used in this machining is very similar to that of the single-side machining but here the machining is done on both sides. There is no chance of intrusion of any foreign particles into the process to settle between the workpiece and the device applying the pressure because of the relative motion between the wheels. When the lapping or wheel surfaces are flat, the pressure is applied to the thicker portions of each workpiece, thereby reducing the size at these specific points. The double-sided machine consists of two rotating lap plates, upper and lower laps, which increases lapping efficiency as the machining of two surfaces of the workpieces takes approximately the same time as it takes to machine one surface. Abrasive for lapping is automatically fed into the workpiece through the top lap during the cycle to provide necessary abrasive action on both the sides of the complete load of workpieces. Pressure is applied gradually by the upper lap against the workpiece until an optimum pressure is reached. Hence, there is no separate loading on the workpiece as in single-side machining. The typical process cycle consists of the following

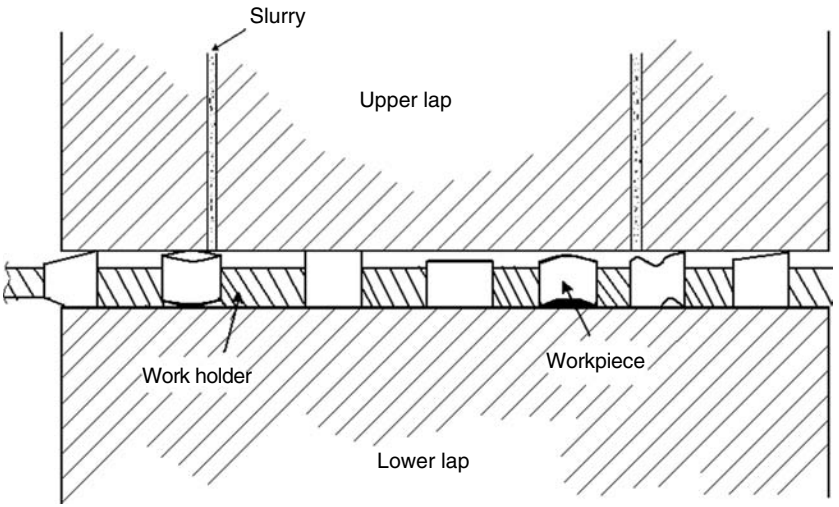


**FIGURE 3.10** Double-side lapping process. (From Indge, J.H., *Tooling and Production*, 55, 116, 1990.)

sequences: (1) loading of the workpieces, in which the top wheel swings from the load position on the left to center over the lower wheel; (2) top wheel is lowered gently to rest lightly on top of the workpieces; (3) rotation of the lower wheel, upper wheel, and carrier drive units starts slowly either automatically, or by operator; (4) abrasive for lapping is automatically fed through the top wheel during the cycle to provide the necessary abrasive action on both sides of the complete load of workpieces; (5) pressure of the top wheel against the workpieces is initially light and as the high points are machined away, the pressure is gradually increased automatically until the optimum pressure best suited for the job is reached; (6) cycle continues until the desired size is obtained at which time the rotation stops, the top wheel lifts and swings to the left for unloading the finished workpieces.

Workpiece is exposed to minimal internal stress and surface damage as abrading takes place from both sides and generates no heat. Cut rate is uniform and repeatable. Hence it is preferred for large stocks. Operational costs by double-side lapping are reduced because condition rings are not wearing away the lap and themselves, more efficient use of the abrasive slurry takes place, and cost of consumables is less per workpiece. The advantages of this type of lapping process is that it has the ability to machine two sides of a workpiece in the same time as required to machine one side; the process produces a large number of workpieces simultaneously; ability to hold nonmagnetic materials; capability of machining any kind of material from plastic to diamond; best available method to obtain close tolerances for

flatness, parallelism, and size; removing stock from both sides of a workpiece helps to relieve internal stress of the workpiece, thus making it easier to achieve flatness; simple work holder design with no need to clamp or rigidly hold the workpiece eliminates stresses in the workpiece thus improving tolerances for flatness, parallelism, and size; accuracy with double face lapping is achieved by using flat lap faces and a free floating top wheel, no critical machine alignment, precision high speed spindle bearing, or accurately machined sliding ways are involved; workpieces exposed to minimal stress and surface damage because it generates no heat; cut rate is uniform and repeatable, no dulling of the abrasive takes place because fresh sharp abrasive particles are gradually fed to the lapping area continuously during the processing cycle; and less handling, higher efficiency, and the feasibility of combining machining operations often result in lower operation costs.

### 3.2.8.3 Cylindrical Lapping

Basically, the cylindrical type of lapping is aimed to lap the outer diameter of cylindrical-shaped parts between flat laps (Figure 3.11). The machine consists of two annular-shaped laps each mounted on a vertical spindle. This is aimed at lapping outer diameter of cylindrical-shaped parts using flat laps. One or both wheels rotate depending on the type of the machine and parts that are placed in work holder are guided against the laps to produce an abrading action. The work holder is generally disk-shaped and thinner than the

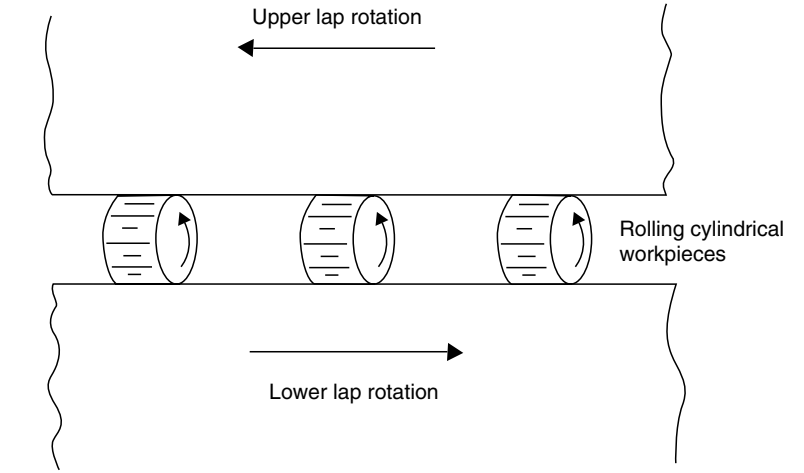


**FIGURE 3.11** Cylindrical lapping process. (From Indge, J.H., *Tooling and Production*, 55, 116, 1990.)

diameter of the workpieces. This is guided in the center by a rotating pin that can be adjusted to move eccentric to the center of the lap. The cylindrical workpieces are placed in the slots, the centerline of which are tangent to a circle in the center of the work holder. The rolling action of the parts causes the work holder to rotate. Controlled lapping occurs as the part slide and slip during rolling, caused by the nonradial position of the work holder slots. Lap flatness and operational procedure are the two major factors that determine the machine capability to lap to extremely close tolerances. Accuracy of size and straightness up to 0.125 μm, surface finish of 0.025 μm, and roundness of the parts up to 0.125 μm can be achieved.

#### 3.2.8.4 Lapping with Bonded Abrasives

This is a lapping method, which contrasts with the conventional lapping process. In conventional lapping method, the main principle characteristic is that it undergoes machining with loose abrasives. The machines that use bonded abrasives for tools closely resemble the grinding machines in their general appearance and function. However, the methods, which such machines serve, differ from grinding in various significant respects, some of which may be considered technological sequences of the divergent primary objectives of grinding and lapping. In particular applications, lapping with bonded abrasives has several potential advantages that warrant the use of this method instead of conventional lapping using loose abrasives. When lapping with bonded abrasive wheels, there is no need for an abrasive distribution system as the abrasive bonded into the wheel structure lasts through the life of the lap. Although the work produced has essentially the same dimensional characteristics and finish as that resulting from processing with cast iron, and consequently, in the work free from embedded abrasives the need for subsequent washing and polishing is eliminated.

### 3.2.9 Advantages of Lapping Process

The following are the main advantages of the lapping process when compared to other finishing processes:

1. Since there is no or very less stress induced, little distortion occurs when compared with conventional machining or grinding on thin parts, parts made of dissimilar material, or stress and heat-sensitive materials like stainless steel. Using lapping techniques, it is possible to remove as little as $2 \times 10^{-6}$ in. or as much as desired. Typical stock removal after grinding is $2 \times 10^{-4}$ to $-5 \times 10^{-4}$ in.
2. Produces highly accurate surface geometry. Components can be produced with flatness, parallelism, or squareness tolerances of 0.5 μm ($2 \times 10^{-6}$ in.) over areas as large as $32 \times 18$ sq. in.

3. Sizes and dimensions can be held to very close tolerances. Overall size can be maintained to within 0.5 μm ($2 \times 10^{-5}$ in.), angularity to within 5 arc seconds. Size tolerance to 0.1 μm can be maintained at a given temperature. These figures can be greatly improved through optical polishing.
4. Very good quality and excellent repeatability of surface finish on all types of materials. Soft nonferrous materials as well as hardened tool steel, carbide ceramics, and even diamond can be lapped to surface roughness below 2 μ in. [7,12,13].

Single-sided high-speed lapping allows a competitive alternative to grinding with better-finished part quality. Some of the applications of this process are first surface reference for subsequent operations; small, thin, or hard-to-hold pieces can be finished; fuel injector components; any sealing face or surface; gear and rotary pumps; slitter knives and spacers; valve plates and bodies, ceramic, carbide, titanium, molybdenum, stainless steel, inconel, and other hard-to-machine materials; hard coat anodized surfaces; extrusion, CNC, and screw machine cutoff sizing.

Double-sided machining is the most desirable choice when processing is required on both sides of a part and exacting requirements for thickness, parallel, or flatness exist. Some of the applications that can be noted here are precision computer components, gauging blocks, precision spacers, slitter knives and spacers, seals, valve components, cutting inserts, precision piston rings, automotive sensing devices, hydraulic gear pump components.

Among all the applications, fine lapping of silicon wafers is a demanding technique in the electronics field.

*Thin parts*—washers, stampings, gaskets, spacers, wafers, clutch disks, rings, seals, thrust washers.

*Screw machine products*—bushings, collars, spacers, jam nuts, bearings, valve and fitting components, air motor components.

*Mechanical seals*—metallic, ceramic, carbon, plastic, sintered materials, chrome pump and compressor seals, rotating unions, valve seats, reconditioning of worn seals.

## 3.3 MECHANISM OF THE PROCESS

Generally, lapping is a finishing process used to obtain dimensional accuracy, surface flatness, and fine finish. The lapping mechanisms are very complex as there are many variables and work parameters that should be considered in the process. The different variables and work parameters that should be considered in the process. The different variables and work parameters that have significant effect on the total lapping process are: (1) abrasives: grit size, type, shape, and distribution; (2) work parameters: speed, normal force, lapping time; (3) materials: workpiece material and lapping plate materials; (4) carrier: oil

based and water based; (5) slurry: concentration of the abrasive and the flow rate of the slurry.

The concerned properties in this mechanism are basically

- Stock removal rate
- Surface roughness
- Surface flatness
- Surface and subsurface damage
- Residual stress

A lapping machine consists of one or more lapping plates on which carriers are placed to hold the workpieces. Condition rings are also arranged on these plates. The workpieces are arranged in the respective work holders and then load is applied by keeping in mind the material of the workpiece, material of the lap plate, and the desired surface finish. The abrasive slurry is applied to the lap at a constant flow rate and an automatic flow controller is set to adjust the constant flow rate of the abrasive slurry. Then the lap plate is given some velocity that should be low enough to do the machining. The lap plates move in the opposite directions in double-side machining and in the case of single-side lapping the load is applied on the workpieces at a constant rate so that the abrasives in between the workpieces and the lap plate penetrate into the workpiece and abrade the workpieces. Three-body abrasion takes place in this process. The condition rings carry away the chips or the waste material, which also helps the abrasive slurry to distribute equally between the lap plate and the workpieces. Loads are applied at a constant rate depending on the stock removal rate and dimensional tolerances. Lapping is a very low-speed process and due to the mechanism of the abrasion, it is considered as a cold process. Hence there will be very little or no thermal distortion. As shown in Figure 3.12 the abrasive grains will first roll, slide, and then the actual chipping action starts. Figure 3.12 depicts the lapping process in a chronological sequence. From this figure it is clearly understood that the abrasives will distribute all along the workpiece, i.e., in between the workpiece and lapping plate with the help of the carriers. First the abrasives roll along the workpiece and then slide and with the application of load, the pressure on the grains constantly rise, leading to chipping action. This is the basic mechanism of the lapping process.

As the lapping process is basically an abrasive process, the motional pattern of the abrasive and its action on the workpieces is a very important factor to be considered.

1. *The real active abrasive percentage*: It is very important to clarify how much percentage abrasive bears the active force. The average normal force per active abrasive can be determined if the percentage and the total normal force are detected. On the action of abrasives we can study

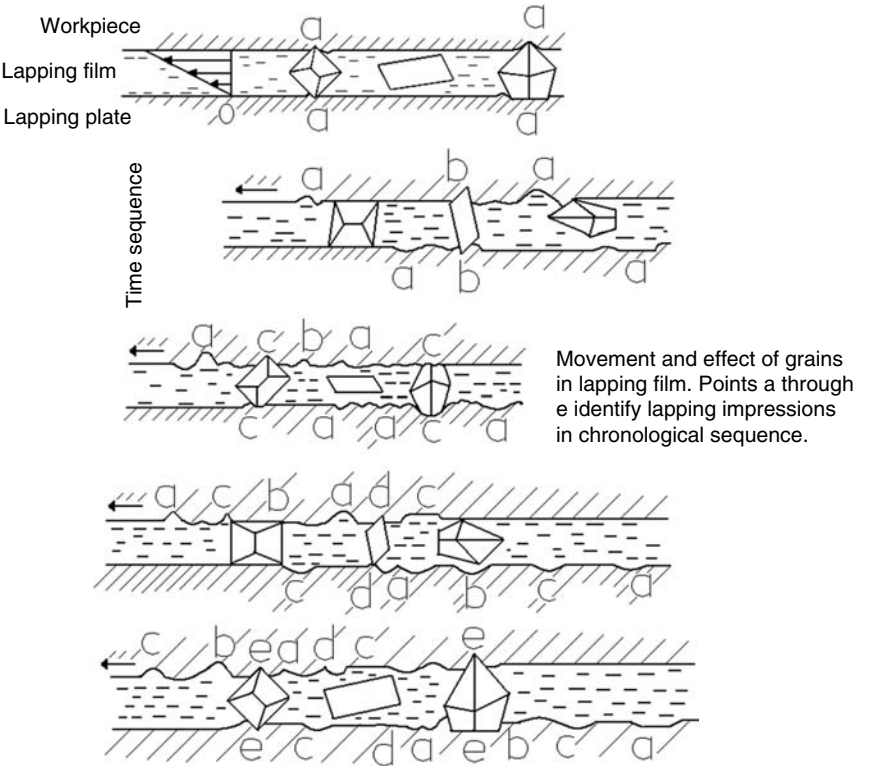
Workpiece
Lapping film
Lapping plate
Time sequence
Movement and effect of grains in lapping film. Points a through e identify lapping impressions in chronological sequence.

**FIGURE 3.12** The rolling and sliding action of abrasives when lapping. (From Indge, J.H., *Tooling and Production*, 55, 116, 1990.)

the happenings on the workpieces. There are two methods to detect the contact percentage. The first method is based on experiment. A polished cast iron pin is placed on the workpiece and the slurry is put between the two surfaces. Here the pressure is very similar to the real lapping situation. The total number of the abrasives per unit area can be counted under microscope. After the loading process, by observing the workpiece under the microscope we can directly count the contact number in the surface of the cast iron. The other method is based on calculation. If the diameter of abrasives and its parameters and the distance between the pin and the workpiece are known then the contact percentage can be calculated very easily.

2. *The motional pattern on the contact abrasive*: In general, the action of the abrasives is of three forms: stationary, rolling, and sliding. The three forms can be determined by the repeated single abrasive particle experiments. If the abrasive is stationary then only one indentation is observed on the cast iron pin, if it slides then there would be grooves on

the pins surfaces, and if it rolls then there would be a set of indentations along a straight line. We can calculate the percentage of motional pattern of the abrasives if we know the total distance the pin moved and the set of indentations.

The indentation models that are observed in a lapping process are

1. *Fracture theory*: This theory proposes that during indentation process, three types of cracks will occur and they are lateral, radial, and medial cracks. Lateral cracks usually take place during the unloading process and play an important role in material removal whereas medial cracks result in workpiece damage.
2. *Shear theory*: This theory states that there is a plastic zone formed between abrasives and the indenter and this zone transmits the pressure in all directions and it can exert normal and tangential forces against surround material and hence the surround materials are sheared off. These phenomena are basically observed when scratching glass and the shear marks show that the nature of scratching is the same as that of indentation.

Lapping mainly produces flat and round surfaces compared to any undefined shape. Although it can lap some irregular shapes, the dimensional sizes may not be to the specified tolerances. Hence it is preferred for regular flat, square, and round surfaces. Lapping produces very accurate dimensions and close tolerances besides producing the desired surface roughness, surface finish, and surface flatness.

Lapping is basically a slow material removal operation, though it tends to decrease the surface roughness, its main purposes are to remove material and modify the shape. It is used less for finishing and more for form accuracy such as flatness in the case of flat objects or spherical shape in the case of balls. Lapping is used for many work materials including glass, ceramic, plastic, metals and their alloys, sintered materials, stellite, ferrite, copper, cast iron, steel, etc. The relative speeds in lapping are much lower than grinding. Consequently, the concentration of the energy in the contact area is much lower. The benefit is that average temperatures tend to be lower than in grinding and may be negligible, and the disadvantage is that specific energy is higher although the volume of material to be removed is small. The main abrasions observed in the lapping processes are two-body abrasion mechanism and three-body abrasion mechanism.

### 3.3.1 Two-Body and Three-Body Abrasion Mechanisms

Wear is the term that represents gradual material removal from a surface due to a mechanical movement or chemical process. Abrasive wear means detachment of material from surfaces in relative motion, caused by protrusions of hard

particles between the opposing surfaces or fixed in one of them. The common classifications of abrasive wear into the categories two-body abrasion and three-body abrasion are widely used by most researchers in the field. The primary meaning of the two-body or three-body concept is to describe whether the abrasive particles are bound (two-body) or free to roll or slide (three-body). So the term three-body abrasion refers to wear caused by free and loose abrasive particles existing as interfacial elements between a solid body and a counter body, whereas two-body abrasive wear is caused by abrasive particles or asperities that are rigidly attached in the second body. Because of that, the abrasive particles in a two-body mechanism are able to cut deeply into the workpiece material whereas in the case of three-body abrasion, the abrasive grains may spend only part of their time cutting into the material. Therefore, the first mechanism is considered to produce wear rates three times bigger than the second mechanism using the same loading condition. Lapping is basically a three-body abrasion process due to the fact that it uses free abrasives that can roll or slide between the workpiece surface and the lapping plate although some grains become embedded in the lap, leading to two-body abrasion. Although the mechanisms are the same, there are some obvious differences between the two methods. In two-body abrasion, the abrasive grains are constrained against the abraded surface and the pressures that can be exercised by them. Another difference is the effect of particle size on wear rate. In three-body abrasion, the distribution of grains in the contact is subject to greater uncertainty. With an ample supply of abrasive, the average pressure on the grains is likely to be lower than in a two-body process. The pressures exerted by an abrasive particle also tend to depend on the grain size. The pressures are likely to be higher with large grain sizes and this affects the scratch depths on the workpiece surface. With low pressure and fine particle sizes, the scratches will be very small. Hence in three-body abrasive system with nonreplenished slurry, the removal rate will decrease with time and increase with increasing load. Figure 3.13 is the schematic diagram of the two-body and three-body abrasion [14–16].

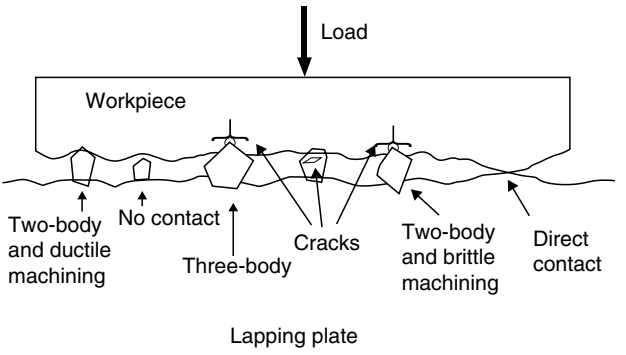


**FIGURE 3.13** Two-body and three-body abrasion. (From *Grinding and Lapping Compounds*, internal publication of United States Products Co, 1995.)

The main outcomes of the lapping process are stock removal rate, roughness, and flatness. These are experimentally calculated against different variables like speed, lapping time, type of abrasive slurry, the grit size of the abrasives in the abrasive slurry, and the pressure applied on the workpieces. As the silicon carbide workpieces were already ground, we expected very few stock removal rates. The roughness however decreased thereby increasing the surface parallelism. The further chapters deal in great detail about the experimental part.

## REFERENCES


1. M. Matsunga, Fundamental Studies of Lapping, Internal Report of the Institute of Industrial Science, University of Tokyo, 1949, 16(2).
2. Anon., What's new in machining systems, *Manufacturing Engineering*, 135, 1990, 34–36.
3. S. Jahanmir, M. Ramulu, and P. Koshy eds., *Machining of Ceramics and Composites,* Marcel Deckker Inc., New York, 1999.
4. I.D. Marinescu et al., Study of the influence on flat lapping, SME, Michigan Mr86-633, 1986.
5. J.H. Indge, Lapping: More of a science, less an art form, Peter Wolters of America, Inc., *Ceramic Industry*, 1990, 135, 26–28.
6. S. Runnels, Feature scale fluid based erosion modeling for chemical mechanical polishing, *Journal of Electrochemical Society*, 1994, 141(7), 1900–1904.
7. J. Simons, Lapping: Grand finale of machining symphony, *Manufacturing Engineering*, 1990, 135, 39–41.
8. G.R. Abrahamson, E.J. Duwell, and W.J. McDonald, Wear and lubrication as observed on a lap table with loose and bonded abrasive grit, *Journal of Tribology*, 1991, 113, 249–254.
9. *Grinding and Lapping Compounds*, internal publication of United States Products Co, 1995.
10. A.M. Corsini, Abrasive micro machining of advanced materials to precision tolerances, *Grinding and Machining of Advanced Materials*, October 11–13, 1995, Pittsburgh, PA.
11. www.engis.com
12. A.W. Barylski, Surface contamination of cast iron after lapping, *Lubrication Engineering*, 1996, 52(1), 63–67.
13. P.C. Metler, Lapping machine boosts quality output, *Tooling and Production*, 1986, 52, 60–61.
14. J.D. Gates, Two body and three body abrasion: A critical discussion, *Wear*, 1998, 214, 139–146.
15. M.A. Verspui and G. de With, Three-body abrasion: Influence of applied load on bed thickness and particle size distribution in abrasive process, *Journal of European Ceramic Society*, 1997, 17, 473–477.
16. J.H. Indge, The nitty gritty machining of ceramic, Peter Wolters of America, Inc., *Tooling and Production*, 1990, 55, 116–119.

## BIBLIOGRAPHY

Anon. Optimizing a lapping process, *American Ceramic Society Bulletin*, 1990, 69, 211.

Bozzi, A.C. and De Mello, J.D.B. Wear resistance and mechanisms of WC–12%Co thermal sprayed coatings in three-body abrasion, *Wear*, 1999, 233–235, 575–587.

Emond, G.T. Water soluble slurry for fine finish lapping, *Ceramic Industry*, 1987, 67, 30–31.

Indge, J.H. Lapping, honing and polishing, Peter Wolters of America Inc., *Engineering Materials Handbook Ceramics and Glasses*, vol. 4, ASM International, Metals Park, OH, 1991, pp. 353–356.

Kim, J.-D. and Choi, M.S. Stochastic approach to experimental analysis of cylindrical lapping process, Research Report 1995, Department of Precision Engineering and Mechatronics, Korea Advanced Institute of Science and Technology, Taejon, Korea.

Marinescu, I.D. High-performance ceramics: Laser assisted grinding of ceramics, *Interceram*, 1998, 47(5), 314–316.

Millar, J. Lapping and polishing technology, *Abrasive Engineering Society*, 1991, 30(4), 9–13.

Narayan, P.B., Brar, A.S., and Sharma, J.P. Lapping and polishing of ceramics: Some concerns and solutions, *Solid State Technology*, 1998, 31, 150–153.

Somiya, S. *Advanced Technical Ceramics*, Academic Press, San Diego, CA, 1984.

Tonshoff, H.K., Karpuschewski, B., and Mandrysch, T. Grinding process achievements and their consequences on machine tools challenges and opportunities, *Annals of CIRP*, 1998, 47(2), 669–688.

Wilfield, K. and Matthias, P. Precision machining of advanced ceramics, *American Ceramic Society Bulletin*, 1989, 68, 550–553.

www.LapMaster.com

www.carbo.com

www.carborundum.com

www.mime.eng.utoledo.edu/people/faculty/imarinescu/imarinescu.html

www.matweb.com

# 4 Lapping of Brittle Materials

*Ioan Marinescu, Ion Benea, and Mariana Pruteanu*

## CONTENTS

4.1 Introduction ..... 125
4.2 Background Information ..... 127
*Mariana Pruteanu*
4.2.1 Ceramic Materials ..... 127
4.2.2 Fundamentals of Lapping Process ..... 129
4.2.2.1 Lapping Plate ..... 129
4.2.2.2 Abrasive ..... 130
4.2.2.3 Lapping Fluid ..... 132
4.2.3 Two-Body and Three-Body Abrasive Mechanisms ..... 133
4.2.4 Tool Formation and Material-Removal Mechanisms in Lapping Process ..... 137
4.2.5 Characteristics of the Lapping Process ..... 141
4.3 Nontraditional Lapping Processes ..... 142
*Hitoshi Suwabe and Ken-ichi Ishikawa*
4.3.1 Vibration Lapping ..... 142
4.3.2 Lapping Using Low-Frequency Vibration ..... 143
4.3.2.1 Principle and Features of Vibration Lapping ..... 143
4.3.2.2 Low-Frequency Vibration Lapping Model and Experimental Technique ..... 146
4.3.2.3 Processing Characteristics and Mechanism ..... 147
4.3.2.4 Processing Surface Roughness ..... 151
4.3.3 Low-Frequency Vibration Correcting of Lapping Plate Using Rectangular Correcting Carrier ..... 152
4.3.3.1 Correcting of Lapping Plate ..... 152
4.3.3.2 Friction Distance Characteristics of Rectangular Correcting Carrier ..... 153
4.3.3.3 Experimental Apparatus and Method ..... 155
4.3.3.4 Correcting Process by Rectangular Correcting Carrier ..... 156
4.3.4 Lapping by Ultrasonic Vibration ..... 158
4.3.4.1 Principle of Ultrasonic Exciter ..... 158
4.3.4.2 Application to Lapping of Ultrasonic Vibration ..... 158

4.4 ELID-Lap Grinding ..... 159
*Hitoshi Ohmori*
4.4.1 Introduction ..... 159
4.4.2 Principle of ELID-Lap Grinding ..... 160
4.4.3 Experimental Systems ..... 162
4.4.4 Experimental Method ..... 163
4.4.5 Characteristics of ELID-Lap Grinding ..... 163
4.4.5.1 Effects of Grain Size on Surface Roughness and Removal Mechanism ..... 163
4.4.5.2 Efficient Mirror Surface Finish by ELID-Lap Grinding ..... 165
4.4.6 Desk-Top ELID-Lap Grinding System ..... 166
4.4.6.1 Background ..... 166
4.4.6.2 Concept of the System ..... 167
4.4.7 Experimental System and Method ..... 168
4.4.7.1 Experimental System ..... 168
4.4.7.2 Experimental Method ..... 168
4.4.8 Experimental Results ..... 168
4.4.8.1 Grinding Characteristics of Cemented Carbide Alloy ..... 168
4.4.8.2 Grinding Characteristics of Nitrided Steel ..... 170
4.4.8.3 Grinding Characteristics of Sapphire ..... 172
4.4.9 Conclusions ..... 174
4.5 Materials, Experimental Setup, and Testing Procedure (Study Case) ..... 174
*Mariana Pruteanu*
4.5.1 Materials ..... 174
4.5.1.1 Workpiece Materials ..... 174
4.5.1.2 Abrasives ..... 177
4.5.2 Experimental Equipment and Lapping Setup ..... 178
4.5.3 Testing Procedure ..... 182
4.5.3.1 Lapping Setup ..... 182
4.5.3.2 Measuring Procedures ..... 184
4.6 Experimental Results and Discussion ..... 188
*Mariana Pruteanu*
4.6.1 Test A ..... 188
4.6.2 Test B ..... 204
4.6.3 Summary of Test A and Test B ..... 211
4.6.4 Test C ..... 212
4.6.4.1 Fractional Factorial Experiment ..... 214
4.6.5 Modeling of Lapping Process ..... 235
4.6.6 Conclusions of the Case Study ..... 242
References ..... 244
Bibliography ..... 246
Appendix A ..... 249
Appendix B ..... 261

## 4.1 INTRODUCTION

Abrasive finishing processes are manufacturing methods used to produce surfaces of desired characteristics with an adequate rate of surface generation. They operate with wear-resistant abrasives in the surface generation process. Often, these processes are described as "finishing methods using random cutting edges" [1].

Lapping and polishing are precision finishing processes, which involve a different mechanical arrangement. Lapping is a slow material-removal operation; though lapping tends to decrease the original surface roughness, its main purpose is to remove material and modify the shape. It is used less for finish and more for form accuracy, such as flatness in the case of flat objects or sphericity in the case of balls. In contrast, the term polishing implies better finish with little attention for form accuracy. Lapping is used for many workmaterials including glass, ceramic, plastic, metals and their alloys, sintered materials, stellite, ferrite, copper, cast iron, steel, etc. Typical examples of the diverse range of processed components are pump parts (seal faces, body castings, rotating valves, impellers), transmission equipments (spacers, gears, shims, clutch plates), cutting tools (tool tips, slitter blades), hydraulic and pneumatics (valves plates, seals, cylinder bodies, castings, slipper plates), aerospace parts (lock plates, gyro components, seals), inspection equipment (test blocks, micrometer anvils, optical flats, surface plates), stamping and forging (spacers, type hammers, bosses, and a variety of other complex shapes).

The relative speeds in lapping are much lower than in grinding. Consequently, the concentration of energy in the contact area is much lower. The benefit is that average temperatures tend to be lower than in grinding and may be negligible. The disadvantage is that specific energy is higher, although the volumes of material to be removed are small, this is not usually important.

Lapping is a loose abrasive machining process that uses abrasive particles combined within an oil or aqueous medium depending on the material being finished. Fine abrasive is applied, continuously or at specific intervals, to a work surface to form an abrasive film between the lapping plate and the parts to be lapped. Each abrasive grain used for lapping has sharp irregular shapes and when a relative motion is induced and pressure applied (by means of load positioned on the top of the workpiece), the sharp edges of the grains are forced into the workpiece material. Each loose abrasive particle that comes into contact with the surface of the part acts as a microscopic cutting tool that either makes an indentation or causes the material to cut away very small particles.

Even though the abrasive grains are irregular in size and shape, they are used in large quantities and thus a cutting action takes place continuously over the entire surface in contact (Figure 4.1). The depth of the marks and scratch grooves will determine the roughness of the surface, which is usually measured with a surface analyzer and described in terms of parameters such as $R$a, $R$t in microns or microinches. The larger and harder the abrasive grains, the rougher will be the finish. Conversely, the finer the abrasive grains, the

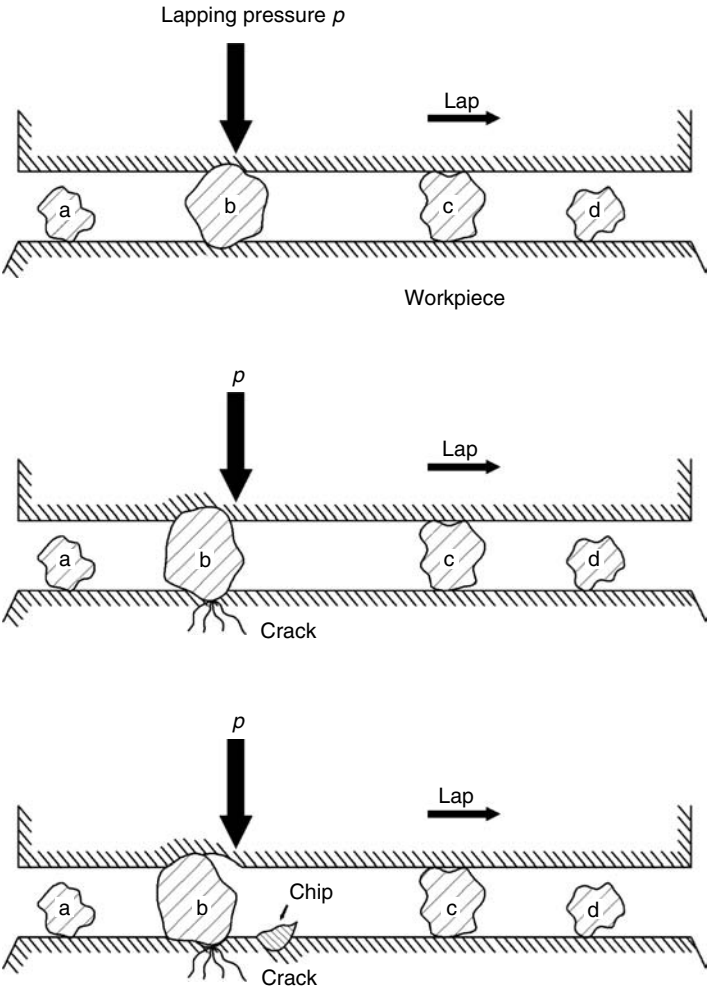


**FIGURE 4.1** Model of the lapping process for hard, brittle materials.

smoother will be the finish. There is often a limit to the smoothness that can be obtained by lapping, even when very fine abrasive grains are used.

Abrasive processes have a large number of parameters that can be varied in order to obtain the desired process output. The lapping process is influenced by load, rotation of the lapping plate, material of the lapping plate, lapping time, type of slurry used (monocrystalline or polycrystalline diamond slurry), grain size of the abrasive, flow rate, slurry concentration, etc. It is almost impossible to vary all the parameters that influence the lapping process; one solution is to limit the number of variables and thus narrow the research field.

The following are the most significant areas the lapping optimization research was focused on:

- Surface quality
- Dimensional and form accuracy of the part (flatness in the case of flat parts and sphericity in the case of round parts)
- Material-removal rate (MRR)
- Behavior of different types of diamond slurries

The main objectives of this research are as follows:

- Study the correlation between the output parameters (surface roughness and MRR)
- Optimization of process parameters (rotation of the lapping plate, load, lapping time, different materials of the lapping plate)

## 4.2 BACKGROUND INFORMATION

*MARIANA PRUTEANU*

### 4.2.1 Ceramic Materials

The engineering materials can be generally classified as metals, polymers, semiconductors, and ceramics. Ceramics are known as solid compounds that are formed by the application of heat, and sometimes heat and pressure, comprising at least one metal and a nonmetallic elemental solid or a nonmetal, a combination of at least two nonmetallic elemental solids, or a combination of at least two nonmetallic elemental solids and a nonmetal [2].

Ceramics were the primary materials of the Stone Age and have remained the most used materials ever since. Ceramic materials have become increasingly important in today's world of materials even though they are difficult and expensive to machine due to their high hardness and brittle nature. The successful application of ceramics depends to a great extent on their special properties (mechanical, chemical, optical, and magnetic) that require their use in almost every production line: health, energy, transportation, agriculture, information/communication, civil construction, automotive industry, and defense [3].

Traditional ceramics refer to bricks and other clay products and traditional glasses include normal window glass, optical glasses, and different glasses used for sealing. Most advanced ceramics are composed of oxides, carbides, nitrides, silicides, and borides of all metals that lead to a vast number of compounds. They are made from fine porous particles that are formed, pressed, and thermally treated under precisely controlled conditions [4]. The

motivating factors for the use of this kind of materials are excellent chemical and corrosion resistance in a wide range of environments and temperatures, superior electromagnetic properties, very high hardness and resistance to wear, special electrical characteristics, and optical transparency over a wide range of wavelengths from the ultraviolet to the infrared.

Ceramics are available as single crystal or in polycrystalline form, consisting of many grains. Grain size has a major influence on the strength and properties of ceramics. The finer the grain size, the higher the strength and toughness of ceramic materials. The properties of ceramics result from a combination of the effect of atomic bonding and microstructure. The atomic bond is reflected in the intrinsic properties: chemical, physical, thermal, electrical, magnetic, and optic. The microstructure has major effect on the mechanical properties.

In accordance with their chemical composition, the technical ceramic materials can be classified into several important groups:

1. Oxide ceramics: the materials in this group consist 90% of single phase and single component metal oxides. These materials are no or low glass-phase. Aluminum oxide ($Al_2O_3$), magnesium oxide (MgO), zirconium oxide (ZrO), aluminum titanate (AT), and piezoelectrical ceramic (PZT) belong to this category. The main oxide materials are alumina (in spark plugs, substrates, and wear applications), zirconia (in oxygen sensors, wear applications, and thermal barrier coatings), titanates, and ferrites.
2. Silicate ceramics: these materials combine the basic electrical, mechanical, and thermal properties of technical ceramics. Amongst this kind of ceramics are technical porcelain, steatite, cordierite, and mullite-ceramic.
3. Nonoxide ceramics: ceramic materials such as compounds of silicon and aluminum with nitrogen or carbon fit in this category. Generally, they have covalent bonding that provides them with very good mechanical properties. Carbide ceramics and nitride ceramics are examples of nonoxide ceramic materials. Carbides (mainly silicon carbide SiC and boron carbide BC) are used in wear applications whereas nitrides (primarily silicon nitride $Si_3N_4$ and Sialon) are used in wear applications and cutting tools.

Research and development have generated new technologies for machining ceramic materials. Because of their hardness and brittle nature, ceramics cannot be successfully machined with the type of cutting tools used for metals; the tools need to have a higher hardness than the ceramic being machined and must be of a configuration that does not cause surface fracture and subsurface damage of the part. Ceramic materials can be detached by mechanical, thermal, or chemical action. Mechanical approaches

are used most frequently and they can be divided into three big categories: mounted-abrasive machining, free-abrasive machining, and impact machining [5]. The first refers to small abrasive particles (e.g., $Al_2O_3$, SiC, $Si_3N_4$, diamond) bonded or immersed in a softer matrix (rubber, organic resin, glass, or a crystalline ceramic composition softer than the abrasive grains). The second category consists of the use of loose abrasives and is typically used for achieving the final surface finish and dimensional accuracy. Impact machining is generally performed by accelerating loose abrasive particles to high velocity such that they cause local impact damage when they hit the part to be machined. Examples of impact abrasive machining include sandblasting, water-jet machining, and ultrasonic machining.

### 4.2.2 Fundamentals of Lapping Process

Lapping is a three-body abrasion process in which grinding is performed with loose abrasive particles [6]. It is preferentially chosen in the case of rigorous requirements as to flatness and dimensional accuracy of the parts being machined. The main factors influencing the lapping characteristics are the type of the lapping plate, the type and size of the abrasive grains, and the type of the lapping fluid [7].

#### 4.2.2.1 Lapping Plate

The material of the lapping plate is important since a workpiece can be badly scratched and contaminated with abrasives if the lapping plate is too hard [8]. The composition of the lapping plate is of great importance because it can affect the results of the lapping process. A hard lapping plate resists being embedded with abrasive particles. Therefore, the grains roll more than slide so that most of the material removal is by stress-induced microfracture. Also, the grains are more likely to become embedded in the workpiece. A softer lapping plate allows abrasives to partially embed themselves in the lapping plate, resulting in more sliding motion and material removal by ploughing. The result is a finer surface finish from soft plates but less planarity. To obtain a better surface quality with respect to planarity, modern lapping often uses a hard plate and very fine grit abrasives.

To produce a plane surface, it is important that the abrasive slurry be distributed uniformly between the workpiece and the lap. There is a tendency for abrasive particles to build up in some areas, increasing the local pressure and hence increasing the removal rate in those areas [9]. Also, the leading edge of the lap will tend to engage the grains more quickly causing a barreled lap shape. Consideration should therefore be given to rotation of the lap and use of the three-lap technique described in workshop technology texts to maintain the planarity of the tools as well as the workpieces [9].

To produce a perfectly smooth surface, free from scratches, the lapping plate should be charged with a very fine abrasive. When the entire surface of

**FIGURE 4.2** Types of lapping plates.

the lap is charged, one should examine the lap for bright spots; if there are any visible bright spots, the charging will continue until the entire surface has a gray appearance (this is done when using cast iron lapping plates). If a lap is once charged it should be used without applying more abrasives until it ceases to cut. If a lap is overcharged and an excessive amount of abrasive is used, there is a rolling action of the abrasive grains between the workpiece and the lapping plate that results in inaccuracy.

A large variety of lapping plates is accessible for almost any application: cast iron (for general engineering purposes), ceramic (for ceramic and other hard materials), glass (for electro-optic materials), aluminum/stainless steel, and many more (Figure 4.2).

Serrated or grooved lapping plates are best for flat surfaces with large areas, also for flat areas with holes in the surface. Laps with no serration or grooves are preferred for cylindrical lapping.

#### 4.2.2.2 Abrasive

There is a variety of abrasives that can be used for lapping: aluminum oxide (for general lapping with low surface roughness), silicon carbide (fast stock removal for hard or soft materials), boron carbide (for use with ceramic, carbide, and other hard materials), calcined alumina (for use with metals, optics, silicon wafers, and other semiconductor materials), diamond slurries and pastes (available in a wide variety of micron sizes and concentrations).

Abrasives are either natural (diamond, corundum, emery, garnet, quartz) or artificial crystalline forms (diamond, silicon carbide, aluminum oxide, cubic boron nitride, boron carbide, etc.). The second category can be divided into two groups:

- Fused abrasives that are the result of very high electric furnace temperatures that produce hard crystals.
- Unfused abrasives that are the result of lower temperatures and chemical additives. Unfused abrasives are not as hard as the fused abrasives.

The most widely used abrasives in industry include the following:

- Diamond is the hardest and sharpest known abrasive. It is both a natural and human-made synthetic abrasive, which measures 10.0 on the Mohs scale of hardness (Table 4.1) and so is the hardest material. Diamond is best suited for tungsten carbide and other very hard materials. When a plate is embedded with the diamond abrasive, it cuts fast and produces fine finishes.
- Cubic boron nitride (CBN) is a synthetic abrasive almost as hard as diamond on the Mohs scale (9.9). It is recommended for lapping ferrous metals and especially for lapping bearing steel, cast iron, tool steel, stellite, super alloys, and in some cases ceramic materials.

**TABLE 4.1**
**Mohs Scale of Hardness**

| Abrasives | Mohs Scale |
|---|---|
| Diamond | 10.0 |
| Cubic boron nitride (Borazon CBN) | 9.9 |
| Silicon carbide | 9.5 |
| Aluminum oxide | 9.0 |
| 38 White aluminum oxide | 9.0 |
| Corundum | 9.0 |
| Chromium oxide | 8.5 |
| Garnet | 8–9.0 |
| Quartz | 7.0 |
| Aluminas (hydrates) | 5–7.0 |
| Observations: | |

*Notes*:
Abrasives though of equal or nearly equal hardness on Mohs scale do not have equal cutting, lapping, or metal abrading power nor do they produce the same lapped finish.
Crystalline shapes, lines of cleavage, friableness, chemical composition, etc. are responsible for lapping variables.
Aluminas have a softer lapping action.

- Silicon carbide (SiC) is a fused, hard crystalline abrasive, 9.5 on Mohs scale. Fast cutting is achieved with good crystal breakdown to maintain abrasive sharpness when used to lap either high or low tensile strength materials. It is well suited for rough lapping operations, valves, tool room work, and general maintenance where polish is not essential.
- Aluminum oxide ($Al_2O_3$) is a fused abrasive with a very hard crystal structure that is hard to fracture. It is utilized for lapping high tensile strength materials, rough lapping operations, ball bearing grooves or lapping operations where pressure can be exerted to break down the crystals.
- Corundum is a natural abrasive found in the earth with a softer crystalline structure than silicon carbide or fused $Al_2O_3$. It is used for lapping a great variety of medium hard metals.
- Unfused alumina (hydrate-calcined) is relatively soft and used for polishing. Calcined aluminas are produced by heat treatment and the degree of calcination determines the characteristics of the product. The terms soft, medium, and hard relate to abrasives resulting from mild, medium, and high degree of calcination. Unfused alumina abrasives are recommended for the lapping and polishing of harder metals. The shape, unlike the blocky crystals, is composed of flat or plated crystals with a thickness of about one-sixth the diameter. Unfused aluminas allow more equal pressure to be distributed over a large surface area than the fused ones because of their plated shape. The disk-shaped particles work with a shaving action rather than the rolling and gouging action of blocky abrasives and are less likely to produce deep scratches on the workpiece.

The size and size distribution of the abrasive are important factors in the surface obtained by lapping (Figure 4.3). The MRR and surface roughness are directly proportional to the size of the abrasive. Larger grain sizes have a higher MRR than smaller abrasive grains but the latter would produce a lower surface roughness than the former.

Another important factor is the concentration of abrasive (the amount of abrasive per unit volume of carrier) that influences the number of grains in contact with the surface of the workpiece material. When the concentration varies, the load distribution changes. This means that with an increase in the number of grains, the effective load per grain decreases because of the larger number of contact points. If the size of the abrasive grains decreases below submicron sizes, the number of grains in contact with the workpiece increases accordingly.

#### 4.2.2.3 Lapping Fluid

Abrasive grains are transported to the lapping zone suspended in an oil or aqueous medium with the aim of achieving a continuous and even distribution

**FIGURE 4.3** Abrasives used in lapping process.

across the lapping plate (Figure 4.4). This liquid carrier is available in various viscosities to cover almost any process requirement.

The carrier function is to lubricate the two surfaces. Lubrication is necessary to reduce friction between the abrasive and the workpiece, help disperse the abrasive product uniformly across the lap plate, and remove the abraded debris from the work zone. Probably the most important characteristic of the carrier is its ability to suspend and uniformly disperse abrasive particles throughout the interface between the workpiece and the lap plate [8]. These days, environmental considerations of waste disposal are pushing lapping processes in the direction of water-based carriers. During operation, the abrasive grains in the slurry suffer a process of rounding and comminution, which reduces the grain size, and the effectiveness of the abrasive as a machining tool. With wear, replacement of the abrasive with fresh slurry is essential to maintain constant cutting conditions. If the fluid is always delivered to the same position on the lap, the increased concentration of slurry in that area can lead to uneven wear rates, a situation that is best to be avoided.

### 4.2.3 Two-Body and Three-Body Abrasive Mechanisms

Wear is the term that represents gradual material removal from a surface due to a mechanical movement and/or chemical process [10]. There are many types of wear: erosion wear, adhesive wear, etc. Among these, one of the most important due to its frequency is abrasive wear, which means detachment of

**FIGURE 4.4** Lapping fluids.

material from surfaces in relative motion, caused by protrusions and/or hard particles between the opposing surfaces or fixed in one of them.

The common classification of abrasive wear into the categories two-body abrasion and three-body abrasion is widely used by most researchers in the field. The primary meaning of the two-body/three-body concept (Figure 4.5)

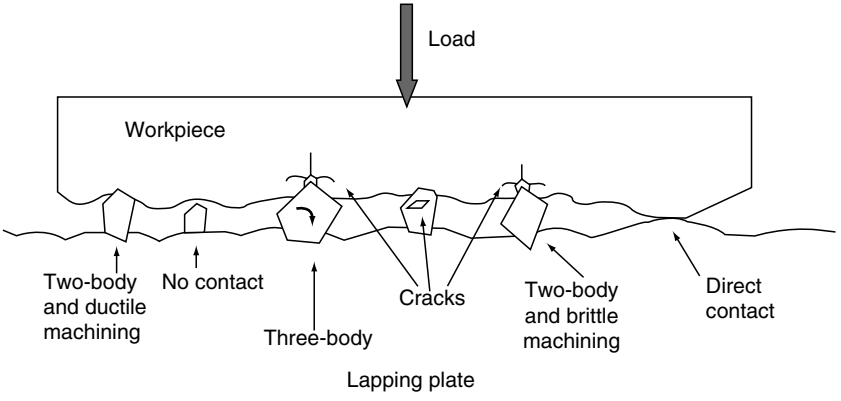


**FIGURE 4.5** Schematic showing two-body and three-body abrasions.

is to describe whether the abrasive particles are bound (two-body) or free to roll or slide (three-body). So, the term "three-body abrasion" refers to wear caused by free and loose abrasive particles existing as interfacial elements [11] between a solid body and a counterbody, whereas two-body abrasive wear is caused by abrasive particles or asperities which are rigidly attached (embedded) in the second body [12]. Because of that, the abrasive particles in a two-body mechanism are able to cut deeply into the workpiece material whereas, in the case of three-body abrasion, the abrasive grains may spend only part of their time cutting into the material.

Therefore, the first mechanism is considered to produce wear rates three times greater than the second mechanism using the same loading condition [13].

In 1998, Gates illustrated that this categorizing of two-body and three-body abrasion is ambiguous because there are situations when these two concepts could create misinterpretations [4]. In his opinion, this classification can be used only when describing if abrasive grains are rigidly held or free to roll. From a tribological point of view, one should take into account the severity of wear behavior: mild, severe, and extreme.

Consideration should be given to the specific situation: gouging abrasion, high-stress (or grinding) abrasion, and low-stress (or scratching) abrasion. The difference between high-stress and low-stress abrasion is whether or not the abrasive grains are broken during abrasion. This is important since fracturing could create sharp cutting edges and give higher wear rates. So, Gates proposes that this new classification (Table 4.2 and Table 4.3) is an improvement (without being considered precise).

Another group of researchers (R.I. Trezona, D.N. Allsopp, and I.M. Hutchings) explained that new terms should be adopted in order to explain

**TABLE 4.2**
**Possible Situation-Based Classification for Abrasive Wear**

| | | Contact Stress | | |
|---|---|---|---|---|
| | | **Low (Particles Do not Fracture)** | **High (Particles Fracture)** | **Extreme (Gross Deformation)** |
| Abrasive particles | Free | Low-stress free-abrasive | High-stress free-abrasive | Extreme-stress fixed-abrasive |
| | Constrained | Low-stress fixed-abrasive | High-stress fixed-abrasive | |

*Source*: Ishikawa, K., Suwabe, H., Ichikawa, K., and Moriya, N. High efficiency correcting process of lapping plate using correcting carrier electro deposited diamond grains. *Proceedings of ABTEC93*, 305, 1993.

**TABLE 4.3**
**Proposed Severity-Based Classification for Abrasive Wear**

| | Abrasive Wear Mode | | |
|---|---|---|---|
| **Typical Situations** | **Mild** | **Severe** | **Extreme** |
| Particle size | Small | Moderate | Large |
| Constraint | Unconstrained | Partially constrained by counterface | Strongly constrained |
| Particle shape | Rounded | Sharp | Sharp |
| Contact stress | Low insufficient to fracture particles | Moderate sufficient to fracture particles | Very high may cause macroscopic deformation or brittle fracture of material being worn |
| Dominant[b] mechanism | Microploughing | Microcutting | Microcutting and/or microfracture |
| Equivalent terms[c] | • Low-stress abrasion<br>• Scratching abrasion[d]<br>• Low-stress three-body[e] | • High-stress abrasion<br>• Grinding abrasion[d]<br>• High-stress three-body[e]<br>• Low-stress two-body[e] | • Gouging abrasion<br>• High-stress two-body[e] |

[a] Not all aspects of the "typical" situation necessarily apply simultaneously.
[b] Debris-removal mechanism is highly material-dependent.
[c] It has already been demonstrated at length that these alternative terminologies are ambiguous, therefore, no fully reliable correspondence with the proposed new terms can be expected.
[d] Term not favored even within the alternative classification scheme.
[e] Dominant sense of two-body/three-body distinction.
*Source*: Ishikawa, K., Suwabe, H., Ichikawa, K., and Moriya, N. High efficiency correcting process of lapping plate using correcting carrier electro deposited diamond grains. *Proceedings of ABTEC93*, 305, 1993.

abrasive particles' behavior. According to them, the expression "two-body abrasion" is better to be replaced by "grooving abrasive wear" and "three-body abrasion" by "rolling abrasive wear" [14]. The term "grooving abrasive wear" describes an abrasive wear process in which the same region of the abrasive grain is in contact with the workpiece surface throughout the process and the grooves are parallel to the direction of sliding. Consequently, rolling abrasive wear is an abrasive wear process in which the region of the abrasive grain in contact with the surface of the part being machined is repeatedly varying. The surfaces produced by this type of mechanism have no directionality and are characterized by a heavily deformed, multiply indented appearance [14].

They concluded that both these mechanisms (grooving abrasive wear and rolling abrasive wear) could be produced in a nominally three-body situation by varying the normal load, abrasive type, and concentration of abrasive in the slurry. Lapping is a three-body abrasion mechanism because the abrasive particles may roll or slide between the lapping plate and the workpiece surface. Sometimes the particles indent only one or both of the surfaces. In a sliding mode, the wear process is basically that of two-body abrasion but usually for a short period of time. In a rolling mode, the wear processes involve plowing damage and wear debris formation from the exposed lips of deformed material adjacent to the grooves. The abrasive particle shape influences the sliding mode and the rolling mode. If the particles are round and of the same size, the probability of rolling is increased. If the particles are rectangular, with larger width than thickness, the probability of sliding is enhanced.

The abrasive wear rate is expected to increase with contact pressure and this means an increased number of contact points per unit area and a deeper penetration of the abrasive grains, leading to deeper groove formation. Also, the contact pressure influences the fracture of the abrasive grains. At lower pressures, particle fracture may not be possible and the potential for wear is low while higher contact pressure causes some particle fracture (new sharp edges are produced on a greater number of particles) and the potential for wear may increase.

### 4.2.4 Tool Formation and Material-Removal Mechanisms in Lapping Process

During the lapping operation, two active movements of the abrasive grains have an important influence on surface formation and removal rate. These are rolling and sliding of the individual abrasive grains within the working gap [15].

The formation of the lapping tool, which means all abrasive grains being in the working gap connecting the workpiece and lapping plate, is illustrated in Figure 4.6. Because of the relative motion between lapping plate and workpiece the abrasive grains act differently during the process: grain 1 is too big, grain 2 is too small and is not actively involved in the cutting process, grains 4 and 5 are actively implicated because one can roll and the other can slide in the working gap whose height $H$ is fitting to the lapping pressure. The structure of the lapping tool changes all the time because the grains that are strongest loaded might break leading to fragments, which will take part in further machining depending on their size and shape. Thus, the percent of the bigger grains decreases while the percent of the smaller grains increases.

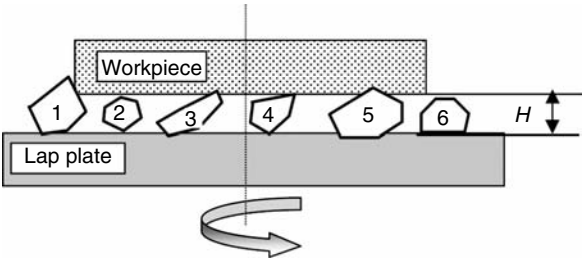


**FIGURE 4.6** Formation of the lapping tool. (From Heisel, U. and Avroutine, J., *Annu. CIRP*, 48(2), 229, 1999.)

The abrasive grains that actively take part in the cutting process seal off the chain between lapping plate and workpiece surface, transmit the normal forces, get into the workpiece and edge out a proportionate material volume.

During the abrasive finishing processes, the interactions between the abrasive grains and the workpiece material can be grouped into cutting (material-removal process), plowing (material displacement process), and sliding (surface modification process). Therefore, each of these finishing methods is an attempt to maintain equilibrium between cutting (surface generation) and plowing/sliding (which controls the modification of the surface and, consequently, its characteristics).

The mechanism of material removal during free-abrasive machining of brittle materials is very different from that of ductile materials (metals) due to the difference in material properties and structure. The nature of atomic bonding determines the hardness and Young's modulus of the material. For ductile metallic-bonded materials the ratio $E/H$ is about 250, whereas for covalent-bonded brittle materials, the ratio is about 20 [4]. Depending on the atomic bond, various material-removal mechanisms can happen. The indentation of ceramics causes vertical cracks during application of the load and lateral cracks during removal of the load. The development of lateral cracks causes chipping, which is the most important mode of material removal. The formation of vertical cracks influences the surface and subsurface damage (Figure 4.7).

While machining ductile materials, substantial plastic deformation occurs prior to material removal. The mechanisms of stock removal are very well described, according to Rabinowicz and Samuels, by microcutting and plastic zone, lateral cracks, median/radial cracks and abrasion.

Observations during lapping of brittle solids confirm the fact that fracture plays an important role in material removal except in ductile regime machining [4]. Ductile regime machining is based on the fact that all materials will deform plastically if the scale of deformation is very small. In fact, material removal takes place by a combination of plasticity and extensive microfracture.

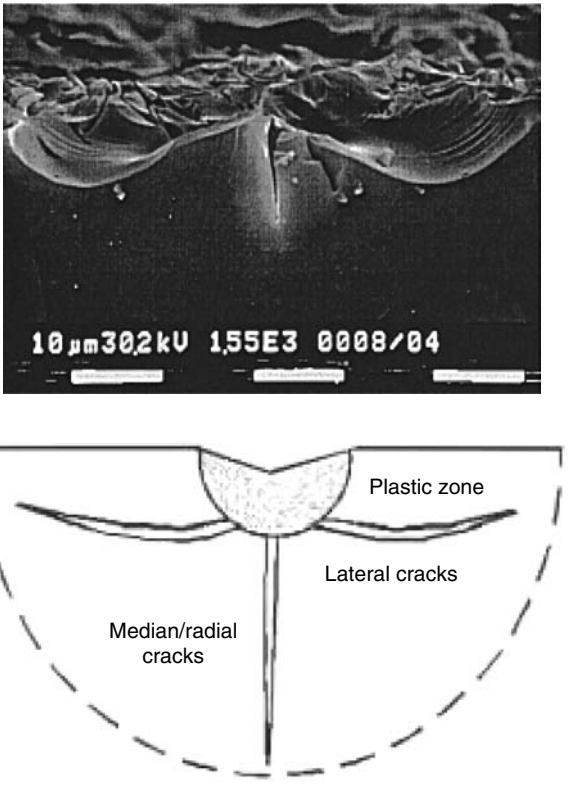


**FIGURE 4.7** Plastic zone, radial, and lateral cracks caused by indentation. (From Sreejith, P.S. and Ngoi, B.K.A., *Int. J. Mach. Tools Manuf.*, 41, 1831, 2001.)

The mechanisms of material removal in glasses and ceramics consist of brittle fracture and plastic deformation. The first one is analogous to indentation on brittle material by a hard indenter causing lateral and median cracks. The second one is comparable to the chip formation process in metal grinding that involves scratching, plowing, and formation of chips. The applied load and the properties of the workpiece material control the extent of brittle fracture. Plastic deformation is favored in the following cases: (1) the load applied on the abrasive particle is small; (2) the abrasive grain is blunt or blunts during machining; and (3) the ratio of fracture toughness to hardness of the material is high [16]. Indentation fracture will occur when: (1) the load on the abrasive particle is high; (2) the abrasive is sharp or remains sharp, because it fractures during contact with the workpiece; and (3) the ratio of fracture toughness to hardness of the material is low.

All materials will undergo a transition from brittle to ductile machining region below a critical depth of cut (according to P.S. Sreejith, ceramics can be machined in a ductile manner if the depth of cut is below 10 nm).

This transition is described in terms of energy balance between strain energy and surface energy [17]. The critical penetration depth $d_c$ for fracture initiation is described by the following equation:

$$d_c = b\left(\frac{K_c}{H}\right)^2\left(\frac{E}{H}\right) \tag{4.1}$$

where $K_c$ is the material fracture toughness, $H$ is the hardness, $E$ is the elastic modulus, and $b$ is a constant depending on tool geometry. Equation 4.1 illustrates that plastic deformation is favored over fracture when the indentation depth is small or when the ratio fracture toughness to hardness is high.

Williams and Hyncica [18] have studied the transition between three-body and two-body abrasion in lubricated contacts. They showed that an abrasive particle between two surfaces undergoes a transition from grooving to rolling at a critical value. It was found that there exists a critical ratio called "critical particle size: film thickness ratio" ($D/h$), which divides the material-removal mechanisms:

$$\left(\frac{D}{h}\right)_{\text{crit}} = \sec\beta \tag{4.2}$$

where $D$ is the longest diagonal of the cross section of the abrasive grain, $h$ is separation of the surfaces, and $\beta$ is the angle that describes the shape of the abrasive grain (Figure 4.8).

The value $h$ is determined by the load applied and by the number of particles within the contact (equivalently, by the load per grain). The model they found to predict wear mechanism is determined by load per particle, length of the major axis of the grain $D$, surface hardness, and a constant $B$, which is a geometry factor dependent on the particle shape.

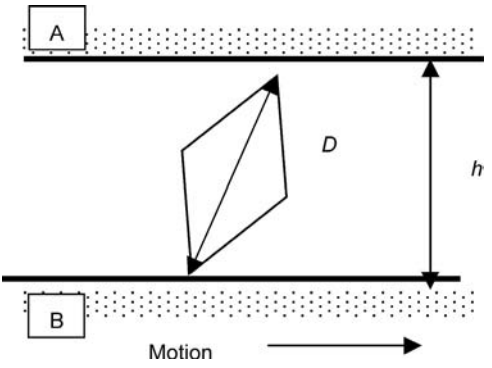


**FIGURE 4.8** Abrasive particle described by parameters $D$ and $\beta$.

When the size ratio is low the recorded wear rate is small and tiny erosion pits similar to indentation marks cover the worn surface. When the ratio is high excessive wear is found to occur.

### 4.2.5 Characteristics of the Lapping Process

In summary, the lapping process has the following characteristics, which vary in degree according to the particular system and equipment:

1. The rate of material removal is low due to the low cutting speeds and low superficial penetration of the abrasive grains into the work surface.
2. The lapping process does not generate significant temperatures; it is considered a cool process, which does not cause thermal damage. Since lapping is a relatively slow motion operation, there is less friction to build up high temperatures.
3. An important advantage is the ease of workholding. For the most parts the fixtures are elementary, inexpensive, and easily constructed.
4. Since there is no or very low stress induced, little distortion occurs compared with conventional machining. Using lapping techniques it is possible to remove as little as 0.00002″. Typical stock removal after grinding is 0.0002″ to 0.0005″.
5. The general shape of the parts worked by lapping is mainly limited to flat, cylindrical, and spherical surfaces. However, irregularly shaped parts can be processed.
6. The accuracy of form produced by lapping can be very good with appropriate techniques, especially for flat surfaces:
   - Flatness to less than one light band (He) 0.0000116″/0.3 μm
   - Roughness of less than 1 μin. $R_a$/0.025 μm $R_a$
   - Size control to less than 0.0001″/2.5 μm
   - Parallelism within 0.00005″/1.3 μm
7. Lapping may be successfully applied to brittle materials and fragile parts because a relative uniform pressure is exerted on the workpiece.
8. Sizes and dimensions can be held to very close tolerances. Overall size can be maintained within 0.5 μm (0.000020″).
9. Very good quality and excellent repeatability of surface finish on all types of materials. Soft nonferrous materials as well as hardened tool steel, carbide ceramics, and even diamond can be lapped to surface roughness below 2 μin.
10. The lapping operation produces a gray mat finish (a nonreflective surface) due to the configuration of the randomized nondirectional pattern left by the rolling abrasive grains.

## 4.3 NONTRADITIONAL LAPPING PROCESSES

*HITOSHI SUWABE AND KEN-ICHI ISHIKAWA*

### 4.3.1 Vibration Lapping

The sound frequency audible to the human ear is about 20 Hz to 20 kHz. Therefore, frequency vibration exceeding 20 kHz is usually classified as ultrasonic vibration. On the other hand, frequency vibration below 100 Hz is called low-frequency vibration. Processing machinery that applies this vibration enables a broad range of processing methods such as slicing of ID-blade saws [19], OD-blade saws [20], multiwire saws [21], dicing [22], cutting [23], drilling [24], and surface finishing [25], etc. In most cases, these machines use ultrasonic vibration within 20 to 60 kHz and low-frequency vibration within a few Hz to 100 Hz.

Vibration applied to the processing will impart vibration energy during processing, allowing high processing efficiency and accuracy. Application of vibration to processing, however, requires special attention to the following points:

1. Low-frequency vibration is regarded as solid vibration that operates the entire tool or workpiece in the same action, while ultrasonic vibration is elastic vibration with vibration characteristics completely different from those of solid vibration (see Table 4.4).
2. As vibration is avoided in ordinary processing machinery, random vibration that includes noise should strictly be avoided as well.

**TABLE 4.4**
**Difference between Ultrasonic Vibration and Low-Frequency Vibration**

| Low-Frequency Vibration | Ultrasonic Vibration |
|---|---|
| Frequency: 0 to 100 Hz | Frequency: 20 to 60 kHz |
| Amplitude: About 0 to 1 mm | Amplitude: About 0 to 20 μm |
| Solid vibration (concentrated constant system) | Elastic vibration (de-concentrated constant system) |
| Vibration is dependent on the frequency of the excitation source | Vibration is inherent in the frequency of the vibration element itself |
| The entire vibration element vibrates with the same amplitude | Amplitude differs according to the position because of the nodes |
| Because the excitation source can be relatively simple, handling is easy | Because excitation is not possible if resonance frequency is misaligned even slightly, handling is difficult |
| Frequency is within the audible range so that excitation sound can be audible | Frequency out of the audible range is used so that excitation sound is not audible |

3. When imparting vibration, an appropriate type of vibration (related to vibrating direction and method, frequency, amplitude, etc.) needs to be selected for each processing method.

To take the above points into account, it goes without saying that reasonable experience and knowledge are essential. Surface finishing in particular needs special attention, as vibration applied in the direction of hitting the processing surface may deteriorate the surface roughness.

Lapping in the mechanical engineering field, in a broad sense of the term, includes all processing methods that use working fluid consisting of oil (or water) and abrasive grains. Therefore, a substantial number of processing methods fall under this category including the previously cited methods using vibration. This section describes low-frequency and ultrasonic vibration lapping methods limited to the surface finishing field only.

### 4.3.2 Lapping Using Low-Frequency Vibration [26]

#### 4.3.2.1 Principle and Features of Vibration Lapping

In lapping, the lapping plate is contacted with the workpiece surface under some lapping pressure, and working fluid (sometimes called slurry) is supplied to both the lapping plate and the workpiece. Lapping is one of the surface finishing methods in which microprojections and waviness on the workpiece surface are removed by moving of abrasive grains in the working fluid. In this lapping, the processing amount depends on the friction distance caused by relative motions based on the working fluid supply status and the rotational motions of the lapping plate and the workpiece. The friction distance, however, may not be increased easily according to the workpiece dimensions and shape. If the friction distance caused by the relative motions is limited, the lapping plate or the workpiece can be excited at higher vibration speed.

Assuming that the working fluid is supplied in a constant status, processing characteristics are in proportion to the friction distance. The following is a calculation of the friction distance when vibration is applied to lapping. Firstly, vibration applied in the lapping plate movement direction is defined as the $X$ direction vibration and vibration applied in the direction perpendicular to the $X$ direction on the same horizontal plane is defined as the $Y$ direction vibration (see Figure 4.9).

When $a$ and $b$ are the amplitudes in respective directions and $\omega$ is the angular frequency, vibration displacement in each direction is as shown below:

$$\begin{aligned} x &= a \sin \omega t \\ y &= b \sin \omega t \end{aligned} \tag{4.3}$$

As harmonic vibration indicated by Equation 4.3 is applied in each direction, the friction distance between the lapping plate and the workpiece increases

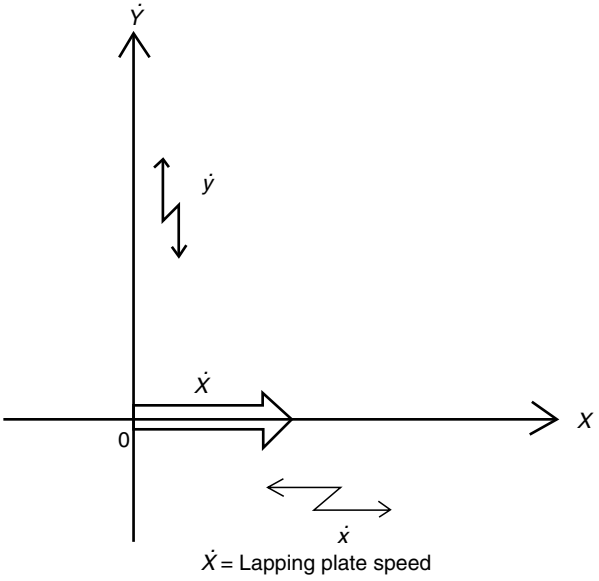


**FIGURE 4.9** Moving direction of lapping plate and vibration directions.

compared to that of nonvibration processing. Therefore, the friction distance while vibration is applied needs to be calculated.

#### *4.3.2.1.1 Friction Distance When the X Direction Vibration Is Applied*

When the $X$ direction vibration is applied, the relative speed $V_x$ between the lapping plate and the workpiece is calculated as below. The lapping plate speed is indicated as $\dot{X}$ at this time:

$$V_x = \dot{x} - \dot{X} = a\omega \cos \omega t - \dot{X} \tag{4.4}$$

Times $\tau_1$ and $\tau_2$ when the relative speed $V_x$ is zero are calculated as below from Equation 4.4:

$$\begin{aligned} \tau_1 &= \cos^{-1} V \\ \tau_2 &= 2\pi - \cos^{-1} V \end{aligned} \tag{4.5}$$

where $V = \dot{X}/a\omega$ (speed ratio).

The friction distance $\Delta L$ for one cycle of vibration can be divided among the following three cases based on the time obtained from the Equation 4.5. When the relative friction distance between the lapping plate and the workpiece is $\Delta L_1$, $\Delta L_2$, and $\Delta L_3$ for each case, the following calculation is available:

$$\begin{aligned}
\Delta L_1 &= a\sin\tau_1 - \dot{X}\frac{\tau_1}{\omega} && (0 < \omega t < \tau_1)\\
\Delta L_2 &= 2a\sin\tau_1 + \dot{X}\frac{\tau_2 - \tau_1}{\omega} && (\tau_1 < \omega t < \tau_2)\\
\Delta L_3 &= a\sin\tau_2 - \dot{X}\frac{\tau_1}{\omega} && (\tau_1 < \omega t < 2\pi)
\end{aligned} \tag{4.6}$$

$\Delta L$ can be calculated as below:

$$\Delta L = \Delta L_1 + \Delta L_2 + \Delta L_3 \tag{4.7}$$

As the friction distance between the lapping plate and the workpiece for each unit time is $\Delta L \cdot f$ from the relation of $f = \omega/2\pi$, the friction distance for arbitrary processing time $T$ is as shown below:

$$L_x = \dot{X}\left\{1 + \frac{2}{\pi}\left(\frac{\sqrt{1-V^2}}{V} - \cos^{-1}V\right)\right\}T \tag{4.8}$$

When $V \geq 1$, the lapping plate movement speed becomes larger than the vibration speed, eliminating the effect of vibration. From this fact, it is important to realize that the vibration has effect or no effect when vibration is applied in the same direction with the movement speed of the lapping plate. Otherwise, the vibration processing machine that has a hard time to make it will just become a insignificant machine with no vibration effect at all.

#### *4.3.2.1.2 Friction Distance When the Y Direction Vibration Is Applied*

When vibration is applied in the perpendicular direction to the lapping plate movement direction on the same horizontal plane, displacement in each direction is as shown below:

$$\begin{aligned}
x &= \dot{X}\cdot t\\
y &= b\sin\omega t
\end{aligned} \tag{4.9}$$

When $\Omega = \omega/\dot{X}$ from the above equation, $y$ becomes as shown below if $t$ is not considered:

$$y = b\sin\Omega x \tag{4.10}$$

When the microlength on the locus of the lapping plate is $ds\ (= \sqrt{(dx)^2 + (dy)^2})$, the friction distance $S$ for one cycle of vibration is calculated as shown below:

$$S = \oint \sqrt{1 + \left(\frac{dy}{dx}\right)^2}\, dx$$
$$= b\sqrt{1 + U^2} \oint \sqrt{1 - k^2 \sin^2 \phi}\, d\phi \tag{4.11}$$

where $\phi = \Omega x$, $U = \dot{X}/b\omega$ (speed ratio), $k^2 = 1/(1 + U^2)$.

The friction distance $L$ between the lapping plate and the workpiece when the arbitrary processing time $T$ is as shown below:

$$L = \frac{\dot{X}}{2\pi} \frac{T}{U} \sqrt{1 + U^2} \oint \sqrt{1 - k^2 \sin^2 \phi}\, d\phi \tag{4.12}$$

From the above equation, the friction distance when the $Y$ direction vibration is applied is as shown below:

$$L_y = \dot{X} \frac{2}{\pi} \frac{\sqrt{1 + U^2}}{U} E\left\{\frac{\pi}{2}, k\right\} T \tag{4.13}$$

where $E\{\pi/2,\ k\}$ is the complete elliptic integral of Grade 2.

#### 4.3.2.2 Low-Frequency Vibration Lapping Model and Experimental Technique

Figure 4.10 shows a model of low-frequency vibration lapping by the pin disk system. The prototype lapping machine is composed of

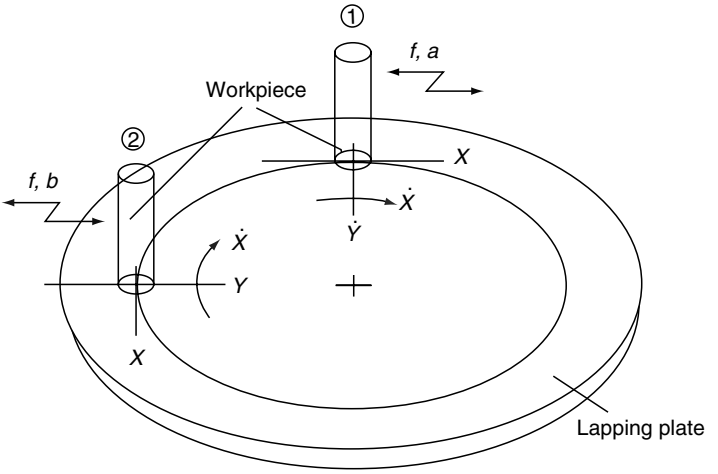


**FIGURE 4.10** Model of low-frequency vibration lapping using pin disk system.

**TABLE 4.5**
**Experimental Conditions of Vibration Lapping**

| | |
|---|---|
| Friction distance | 100 m |
| Lapping pressure | 0.294 MPa |
| Concentration of slurry | 50%wt |
| Frequency | 80 Hz |
| Amplitude | 1 mm |
| Grain | C#180–#1500 |
| Working fluid | Machine oil no. 120 |
| Lapping plate | FC30 |
| Workpiece | S45C |

1. Abrasive grain applying section
2. Exciting section
3. Workpiece support section

Working fluid is stirred in the working fluid tank to prevent abrasive grains from settling, and pumped up to be supplied to the processing section continuously. Working fluid used is machine oil no. 120 or the equivalent and the type of abrasive grain is C#180–#1500. Concentration of working fluid is based on the weight. A series of experiments was performed by exciting pins (FC30) as workpieces with frequency of 80 Hz and amplitude of 0–1 mm. Table 4.5 shows the major conditions of the experiments.

#### 4.3.2.3 Processing Characteristics and Mechanism

Figure 4.11 shows the relationship between the processing time and processing amount in nonvibration lapping and *X*/*Y* direction vibration lapping. In vibration lapping, the friction distance per unit time increases, and the curve indicating the increase of processing amount inclines sharply accordingly, as shown in the result.

Figure 4.12 shows the relationship between the processing pressure and processing efficiency (processing amount per unit friction distance) in nonvibration lapping based on the working fluid concentration as a parameter. In nonvibration lapping, the processing efficiency is significantly affected by the working fluid concentration, and the processing efficiency becomes saturated when the working fluid concentration is about 55%wt or less, and the limit processing pressure is regarded as 0.6 MPa or less. When the working fluid concentration is over 60%wt, the processing pressure does not show any limit value within the range of this experiment. As the working fluid concentration becomes higher, the number of abrasive grains entering between the lapping plate and the workpiece decreases. When the abrasive grain lapping effect cannot be expected any longer even if the processing pressure is increased, such processing pressure is called "limit processing pressure $P_L$."

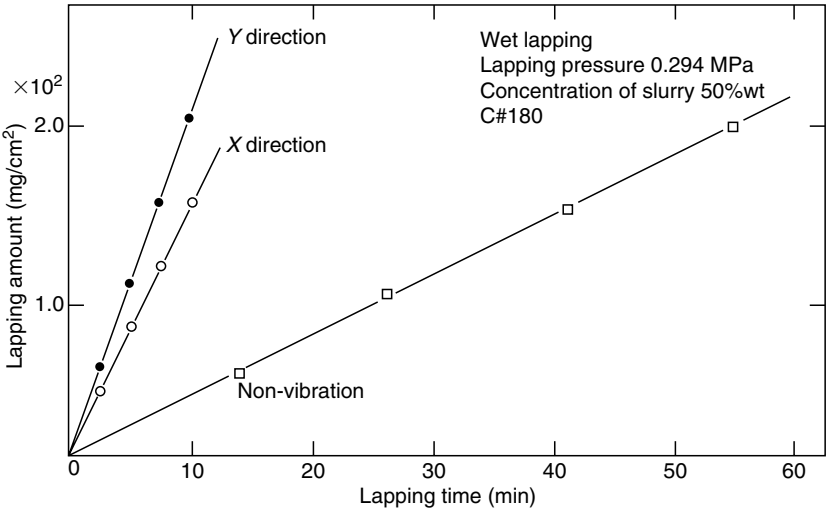


**FIGURE 4.11** Relationship between lapping time and lapping amount.

Figure 4.13 and Figure 4.14 show the relationship between the processing efficiency and processing pressure in vibration lapping. Figure 4.13 shows the case when vibration is applied in the *X* direction, and Figure 4.14 shows the case when vibration is applied in the *Y* direction. According to the direction of vibration, the different effects on the processing efficiency and limit processing pressure are shown. Nonvibration lapping and *X* direction

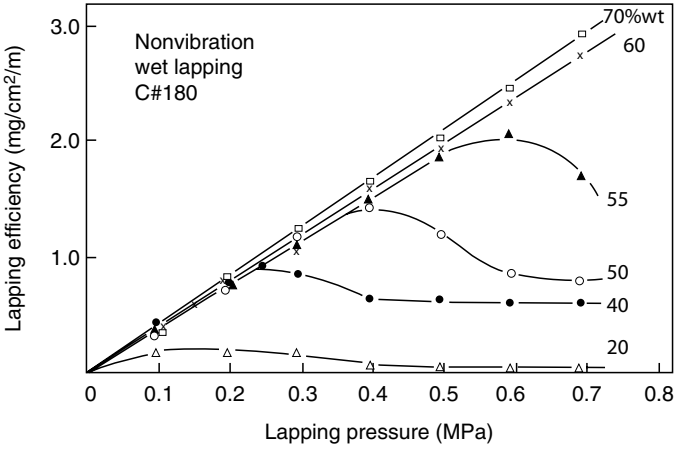


**FIGURE 4.12** Relationship between lapping pressure and lapping efficiency (nonvibration).

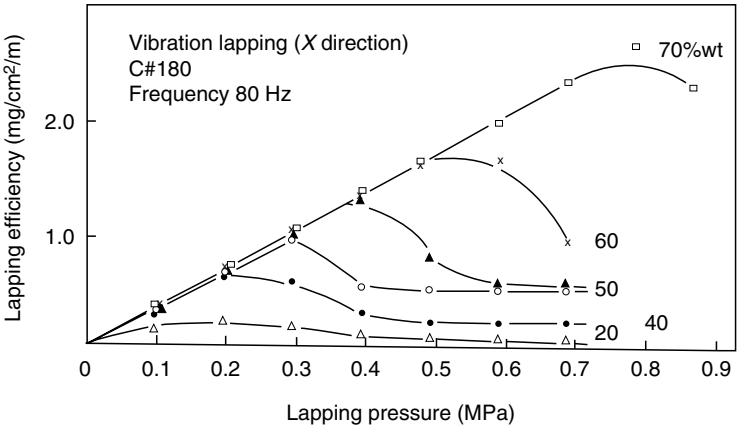


**FIGURE 4.13** Relationship between lapping pressure and lapping efficiency (*X* direction).

vibration lapping, however, show relatively similar tendencies. In the *Y* direction vibration lapping, the limit processing pressure is observed similarly when the working fluid concentration is below 55%wt. However, it is not observed when the working fluid concentration is over 60%wt. The processing efficiency decreases instead.

The effect of vibration on lapping is considered next. Figure 4.15 shows respective processing methods and models of abrasive grain conditions before and after each processing. In nonvibration lapping as shown in Figure 4.15a,

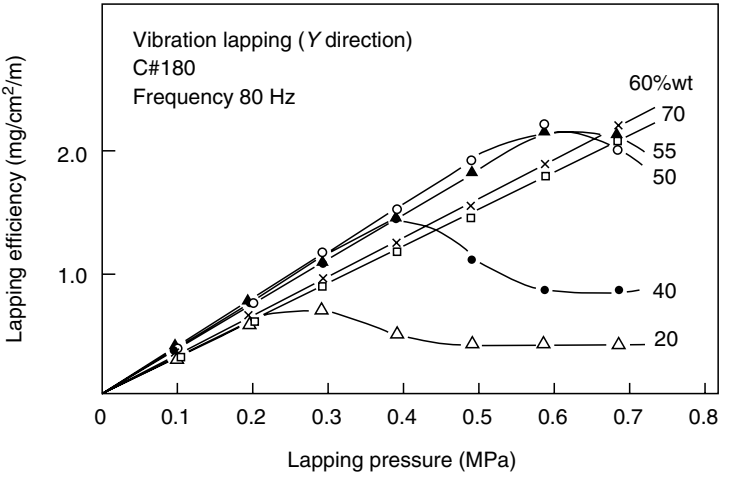


**FIGURE 4.14** Relationship between lapping pressure and lapping efficiency (*Y* direction).

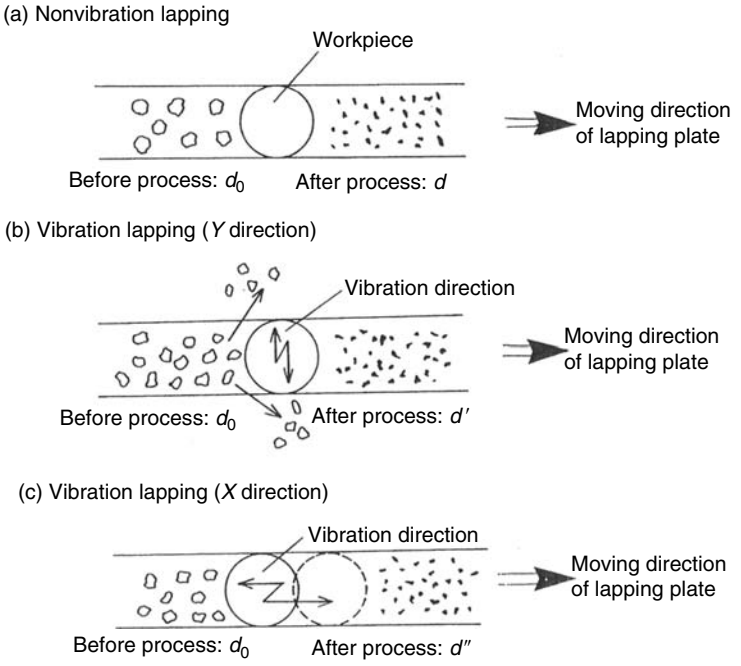


**FIGURE 4.15** Vibration lapping mechanism.

the size of abrasive grains after processing the workpiece becomes $d$ ($d_0 > d$) when the grain size is $d_0$, for example, before processing.

In $Y$ direction vibration lapping as shown in Figure 4.15b, vibration of the workpiece is applied in the direction perpendicular to the lapping plate movement direction. In this case, the size of abrasive grains after processing the workpiece becomes $d'$ ($d_0 > d'$) when the grain size is $d_0$ before processing. The effect of vibration is that the limit processing pressure ($P_{LY} = 0.6$ MPa) that indicates the limit of processing efficiency increases considerably compared to the case of nonvibration ($P_{LO} = 0.4$ MPa) when the working fluid concentration is rather low ($Q \leqq 50\%$wt). From this fact, it is considered that dynamic energy due to vibration is applied to abrasive grains during vibration processing so that abrasive grains easily enter between the workpiece and the lapping plate. As a result, processing efficiency improves compared to that of nonvibration lapping.

Figure 4.15c shows a processing mechanism of vibration lapping in the $X$ direction. As the workpiece vibration direction is identical to the lapping plate movement direction, it does not always indicate that the workpiece is processed only with grains of diameter $d_0$ under the condition of $V < 1$. In one cycle of vibration, processing is done with abrasive grain size of $d_0$ before

process at the time $\tau_0$ and processing is done with abrasive grain size of $d''$ after process at the time of $\tau$. From the relationship of $d_0 > d$, the processing amount is dependent on the abrasive grain size so that the processing efficiency in the $X$ direction decreases compared to that of nonvibration processing or $Y$ direction vibration processing. The limit processing pressure ($P_{LX} = 0.3$ MPa) is thought to decrease as well.

#### 4.3.2.4 Processing Surface Roughness

Figure 4.16 shows one example of limit processing surface roughness (processing surface roughness that cannot be improved even by increasing the friction distance and processing pressure). As shown in this figure, the limit processing surface roughness is reached at the friction distance of 100 m when the initial processing surface roughness is 12 μm, abrasive grain type is C#800, processing pressure is 0.294 MPa, working fluid concentration is 50%wt, and $Y$ direction vibration (amplitude: 1 mm, vibration: 80 Hz) is applied.

Figure 4.17 shows the relationship between the limit processing surface roughness and the limit friction distance in case of $Y$ direction vibration processing. From this figure, it is found that the limit friction distance to achieve the limit processing surface roughness of 1 μm is 220 m when the average abrasive grain diameter is 10 μm, and that the limit processing surface roughness depends on the average abrasive grain size and friction distance. Using this figure, vibration conditions and processing time can be calculated easily.

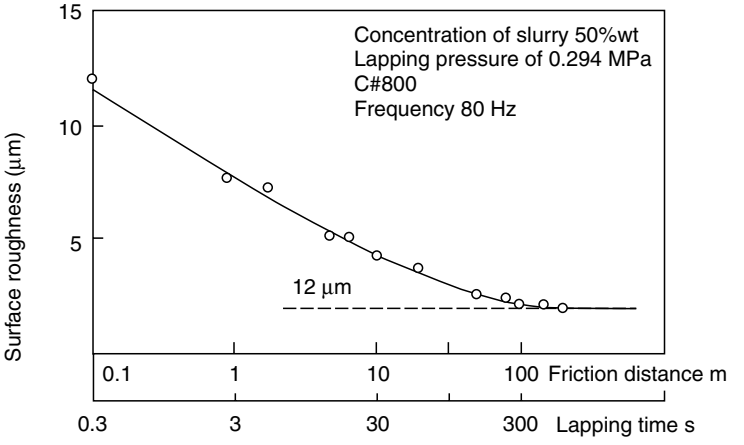


**FIGURE 4.16** Relationship between friction distance (time) and surface roughness ($Y$ direction).

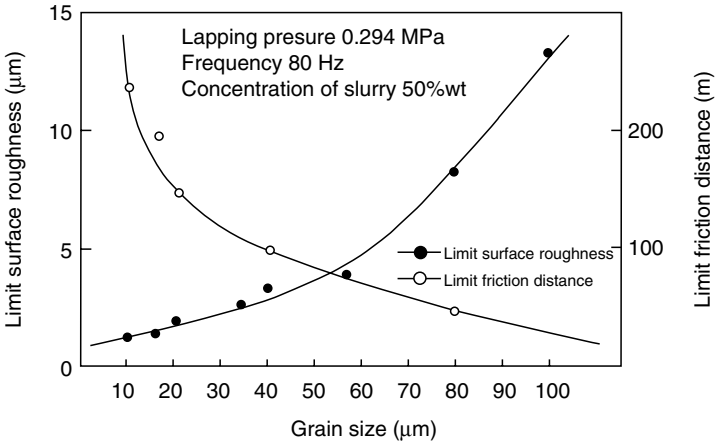


**FIGURE 4.17** Behavior of limit processing surface roughness and limit lapping distance.

### 4.3.3 Low-Frequency Vibration Correcting of Lapping Plate Using Rectangular Correcting Carrier [27]

#### 4.3.3.1 Correcting of Lapping Plate

One of the lapping plate correcting techniques is to use a disk-type or circular-type correcting carrier (ring) with parallel planes and correct the lapping plate by revolving the correcting carrier while rotating. This method has many merits because it does not require any particular device and can easily be applied to lapping plates that are larger in size. To achieve appropriate correcting surface, however, correcting conditions including the shape of the optimum correcting carrier according to the abrasion status of the lapping plate need to be set. It still depends on the workers' long years of experience and intuition, and such know-how remains only in the field of craftsmen's skills in general.

Concerning the lapping plate correcting technique using a correcting carrier, the authors have been investigating theoretically the correcting conditions that are dependant on the workers' experience, so that the conditions can be used easily by anybody. As a result, the lapping plate can be worn in the concave or convex shape by using various kinds of correcting carriers. This abrasion pattern has been demonstrated theoretically and experimentally. One of the processing methods, to ensure efficient correcting using the same shape of correcting carrier regardless of the abrasion pattern on the lapping plate, is vibration processing using a rectangular correcting carrier as introduced below.

#### 4.3.3.2 Friction Distance Characteristics of Rectangular Correcting Carrier

Figure 4.18 shows a part of the lapping plate and a model of the rectangular correcting carrier set on it. As shown in this figure, it is assumed that the middle point of rectangular correcting carrier is set on the $X$ axis of the $X$–$Y$ plane of the lapping plate when the processing time $t = 0$. When the rectangular correcting carrier is used, rotation of the rectangular correcting carrier is absurd at the point in using it. Therefore, it has been so designed that the combined speed of the lapping plate rotation and the correcting carrier vibration only works in correcting operation.

The friction distance using rectangular correcting carrier considers the speed component that works on an arbitrary point $Na(t)$ on the lapping plate, which is separated by the distance $a$ from the center $O$ on the lapping plate. The speeds that work on the point $Na(t')$ in $t'$ seconds after the start of processing are the lapping plate rotation speed and the correcting carrier vibration speed. When the combined speed of the lapping plate

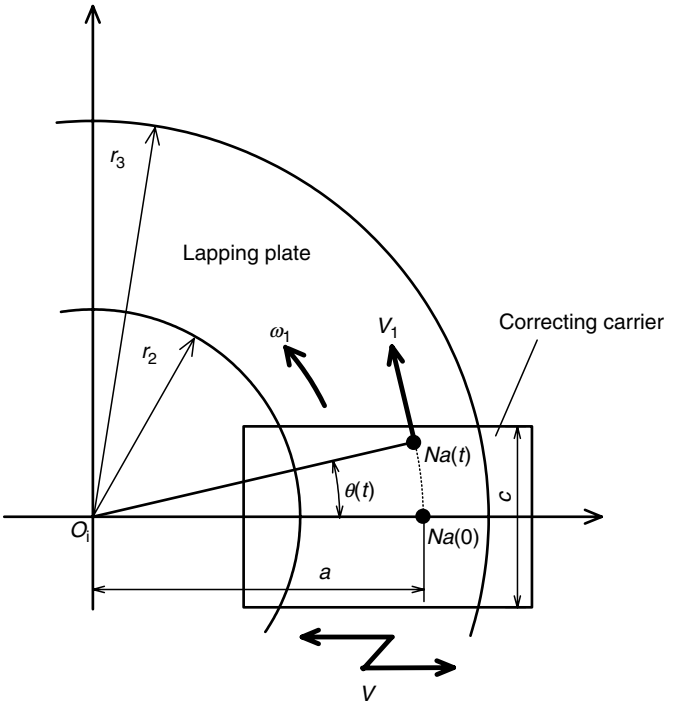


**FIGURE 4.18** Components of velocity at an arbitary point *Na*.

rotation speed $V_1$ and the correcting carrier vibration speed $V$ is $V(a)$ at the arbitrary point $Na(t)$ on the lapping plate, the following equation holds:

$$V(a) = \sqrt{(V_1 \sin\theta(t) - V)^2 + (V_1 \cos\theta(t))^2} \tag{4.14}$$

where $\theta(t)$ is the angle made by the $X$ axis and a straight line $\overline{ONa(t)}$ in time $t$, $V = b \sin \omega t$, where $b$ is the amplitude, $\omega$ the circular vibration, and $V_1 = a\omega_1$, $\omega_1$ is the plate rotation angle speed.

The friction distance $L(a)$ until the arbitrary point $Na(t)$ on the lapping plate passes the rectangular correcting carrier is calculated as shown below:

$$L(a) = \int_{-ta}^{a} V(a)\,\mathrm{d}t \tag{4.15}$$

$ta$ is the time required for the arbitrary point $Na(t)$ on the lapping plate to pass half of the width of the rectangular correcting carrier in the direction of friction, and needs to satisfy the following conditions:

$$\frac{c}{2} = a \sin\theta(t) \tag{4.16}$$

where $c$ in the above equation indicates the width of the rectangular correcting carrier in the direction of friction.

The rectangular correcting carrier is always in contact with the lapping plate during correcting process, so the friction distance $L(a)$ of the rectangular correcting carrier is expressed as shown below:

$$L'(a) = \int_{0}^{t_b} V(a)\,\mathrm{d}t \tag{4.17}$$

where $t_b$ is the time for one rotation of the lapping plate.

Figure 4.19 shows the result of the above calculation. Figure 4.19a and Figure 4.19b show respectively the friction distance characteristics of the lapping plate and the rectangular correcting carrier. The horizontal axis indicates the ratio of the distance $a$ between the lapping plate center and an arbitrary point $Na(t)$ to the lapping plate outer radius $r_3$. The vertical axis indicates the ratio of the friction distance obtained from the calculation result to the plate width $(r_3 - r_2)$. The result of calculation proved that abrasion on the lapping plate becomes flat when the rectangular correcting carrier is used, and that abrasion on the outer periphery of the correcting carrier is larger than that of the inner periphery. This indicates that the rectangular correcting carrier can be an effective method for the deteriorated lapping plate only if abrasion of the carrier can be prevented during correcting process.

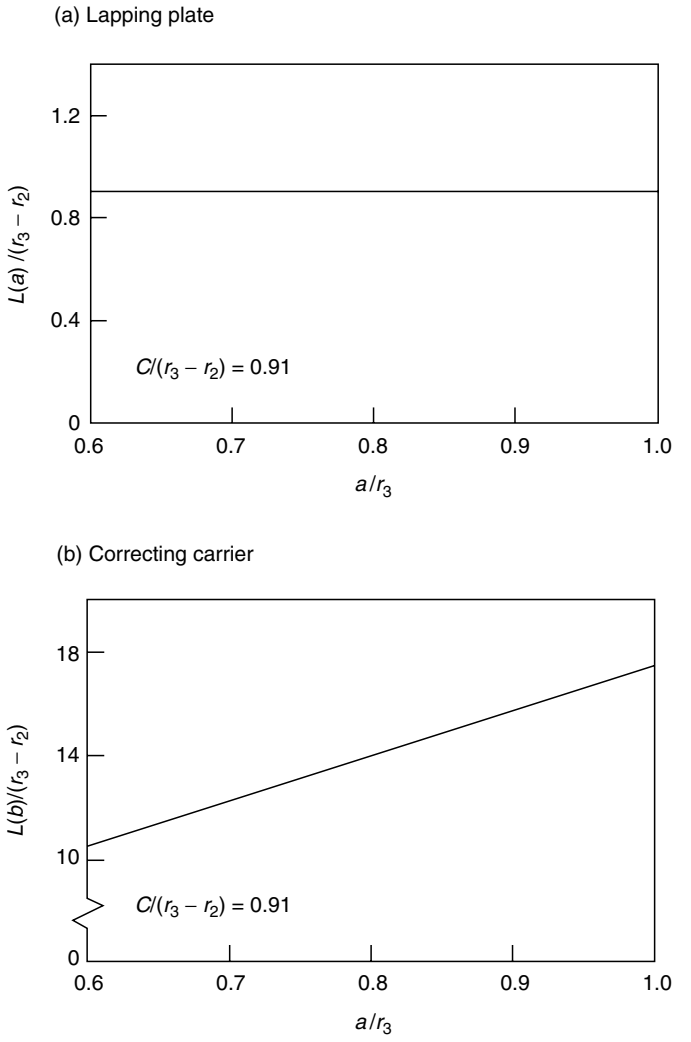


**FIGURE 4.19** Friction distance characteristics.

### 4.3.3.3 Experimental Apparatus and Method

Figure 4.20 shows the outline of the experimental apparatus. In this apparatus, a commercially available lapping machine is equipped with an arm having a carrier holder to support the rectangular correcting carrier. The rectangular correcting carrier is mounted on the carrier holder that is guided by direct-acting bearing in the direction vertical to the contacting surface with the lapping plate, in order to restrict the moment generated from misalignment of the center of gravity of contacting surface and the correcting carrier center

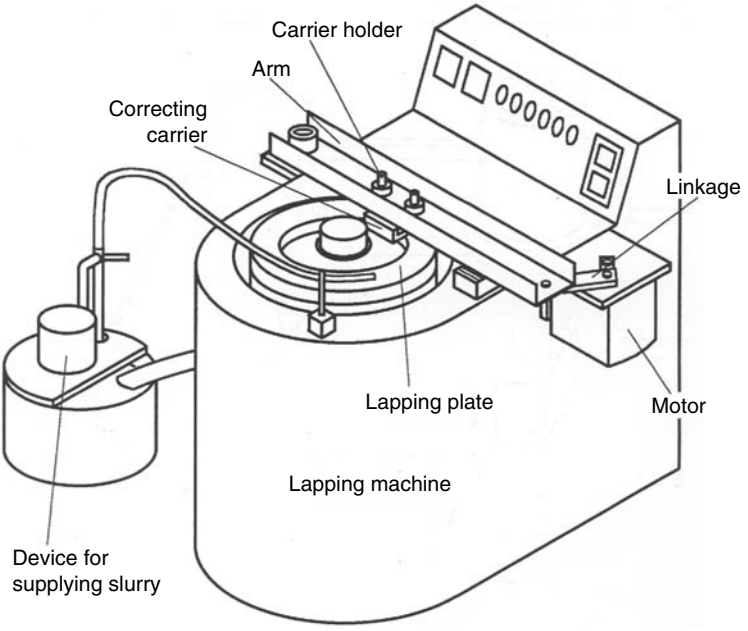


**FIGURE 4.20** Outline of experimental apparatus.

point. And, low-frequency vibration (amplitude, 5 mm; frequency, 0–5 Hz) can be applied to the correcting carrier in the direction vertical to the lapping plate rotation by using the link mechanism.

In the experiment, a ground lapping plate of the initial surface waviness of less than 1 μm is used. Working fluid is continuously supplied to the processing area by the working fluid pump. The main experimental conditions are as shown in Table 4.6.

#### 4.3.3.4 Correcting Process by Rectangular Correcting Carrier

The result of correcting process on the deteriorated lapping plate using a rectangular correcting carrier with electrodeposited diamond grains is as shown in Figure 4.21. This figure shows a profile of the deteriorated lapping plate, a profile of the lapping plate after being corrected for 1 h using the electrodeposited rectangular correcting carrier under conditions of amplitude of 5 mm and frequency of 0.8 Hz, and a profile of the lapping plate after being corrected for an additional 4 h (total 5 h). This figure proves that the profile of the lapping plate after being corrected for 1 h is almost flat. The profile of the lapping plate after being corrected for the additional 4 h (i.e., 5 h from the start of correcting) also shows that the processing amount is increased without deteriorating the flat shape formed in about 1 h after the start of processing.

**TABLE 4.6**
**Experimental Conditions of Low-Frequency Vibration Correcting Process**

| **Lapping Pressure** | | **5.0 kPa** |
|---|---|---|
| Lapping plate | Material | FC300 |
| | Inner radius | 99.0 mm |
| | Outer radius | 154.0 mm |
| | Angular velocity | 4.82 rad/s |
| Correcting carrier | Material | FC300 |
| | Width | 50.0 mm |
| | Amplitude | 5.0 mm |
| | Vibration angular velocity | 5.0 rad/s |
| Slurry | | GC#600 + water |
| Concentration of slurry | | 35%wt |
| Working time | | 0–10 h |

This concludes that the profile of the processing surface ensures accurate profile because of diamond grains electrodeposited on the carrier surface. Correcting the deteriorated lapping plate in the concave shape can be done similarly only in about 1 h.

The above explains that highly efficient and accurate correcting surface is possible by applying low-frequency vibration to the rectangular correcting

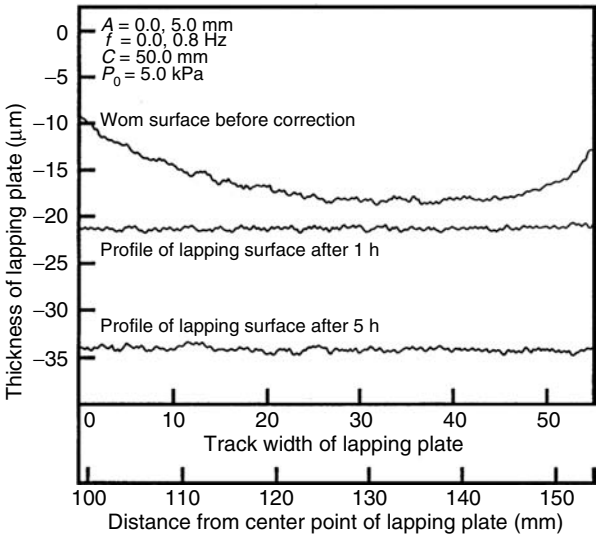


**FIGURE 4.21** Machining characteristics of lapping plate.

carrier with diamond grains or CBN grains irrespective of the deteriorated profile of the lapping plate.

### 4.3.4 Lapping by Ultrasonic Vibration

#### 4.3.4.1 Principle of Ultrasonic Exciter

A model of the ultrasonic exciter we currently use is shown in Figure 4.22 [22]. This exciter generates ultrasonic vibration while rotating the tool, and the spindle shaft for mounting a tool has a vibration element and an ultrasonic cone in it. The ultrasonic cone in the spindle shaft is fixed by supporting the node of cone. When processing, a special tool for ultrasonic processing is mounted on the end of the spindle shaft and used for drilling and cutting. This type of exciter is commercially available for each application within the frequency range of 20–60 kHz and amplitude range of 5–100 μm, and some spindle shafts rotate at more than 10,000 rpm. Recently, the smaller exciters for drilling are developed by Takesho Co. (Fukuoka in Japan), to be used with the automatic tool changer of machining centers.

In ultrasonic vibration processing, commercial power is converted to the designated ultrasonic frequency by ultrasonic generator, and excites the vibration element as shown in Figure 4.22. Vibration generated by this vibration element is transmitted until the end of the spindle shaft as longitudinal wave. The tool is excited in either the longitudinal or torsional direction according to the shape of hone in the tool mounted on the end of the spindle shaft. If the tool resonance frequency deviates from the generator frequency, amplitude generated at the tool becomes smaller. If this deviation is excessive, no vibration will be generated. Pay special attention to the design and fabrication of tools.

#### 4.3.4.2 Application to Lapping of Ultrasonic Vibration [28]

Lapping process using ultrasonic vibration includes drilling, surface finishing, and microstructure processing. This section introduces a lapping method

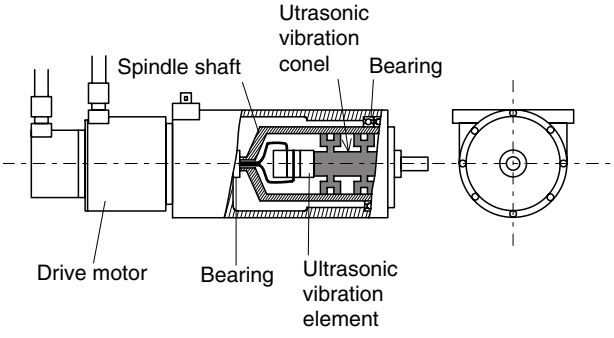


**FIGURE 4.22** Ultrasonic vibration exciter.

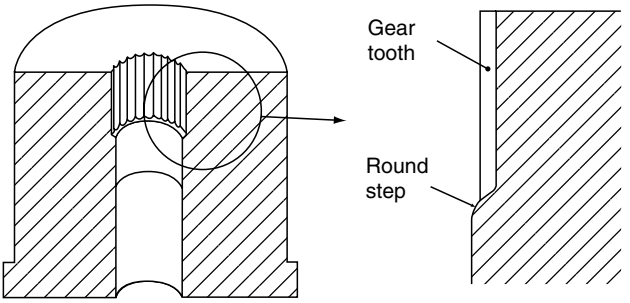


**FIGURE 4.23** Metal mold with complex form. (From Mizuno, M. and Iyama, T. *Adv. Abrasive Technol.*, 3, 359, 2000.)

of die with gear teeth and round steps inside the through hole as shown in Figure 4.23.

Figure 4.24 shows the outline of the system. An aluminum pipe mounted on the end of the hone is used for elliptical vibration by exciting the pipe in both the longitudinal and radial directions at the same time. The tool vibration has frequency of 27 kHz and amplitude of 3 μm, and the workpiece is made of heat-treated SKD11 with hardness of 58–62 HRC. Working fluid is composed of diluted water soluble coolant with tap water and mixed with abrasive grains #400, #800, #1500, or #3000. The amount of working fluid to supply to the processing area is 17 mL/min.

Figure 4.25 shows one example of the experimental result. Within the range of the size of abrasive grains used in the experiment, improvement in surface roughness is observed in ultrasonic vibration lapping compared to that of nonvibration lapping even if processing pressure is changed, under all but some special conditions. Processing using ultrasonic vibration has the problem of air bubbles in the processing section due to cavitation. Therefore, it is important to find and use the optimum conditions of processing.

## 4.4 ELID-LAP GRINDING

*HITOSHI OHMORI*

### 4.4.1 Introduction

Mirrors and lens are usually finished by loose abrasive lapping and polishing, but these methods have such disadvantages as wastewater processing problems, mechanical damage, wear by scattering abrasive, dirty workplace, and difficulty in using different grains on the same machine. For these reasons, alternative grinding methods are required for finishing process applying loose abrasives. Ohmori and Nakagawa have proposed a lap grinding method

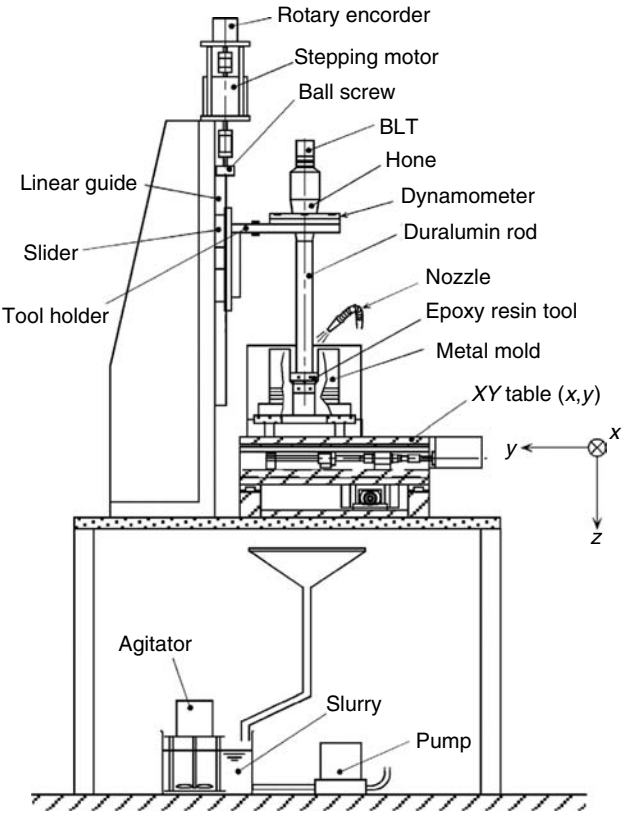


**FIGURE 4.24** Outline of experimental lapping machine. (From Mizuno, M. and Iyama, T. *Adv. Abrasive Technol.*, 3, 359, 2000.)

applying ELID [29], namely "ELID-lap grinding," and carried out experimental studies to pursue efficient and highly accurate finishing [30,31]. In this section, ELID-lap grinding using metallic-bonded wheels with different grain size diamonds (#1200–#3000000 wheels) is demonstrated as a finishing technique realizing nanometer-level smoothness.

### 4.4.2 Principle of ELID-Lap Grinding

Figure 4.26 shows the schematic illustration of ELID-lap grinding. This grinding is a constant pressure grinding technique using rigid metallic bond diamond/CBN wheels with the assistance of special pulse electrolytic in-process dressing. In this process, the wheel functions as the positive pole by means of a brush that smoothly contacts its surface. The negative electrode is fixed at a short distance of about 0.3 mm from the wheel surface. In this small clearance between the fixed electrode and wheel surface, electrolysis

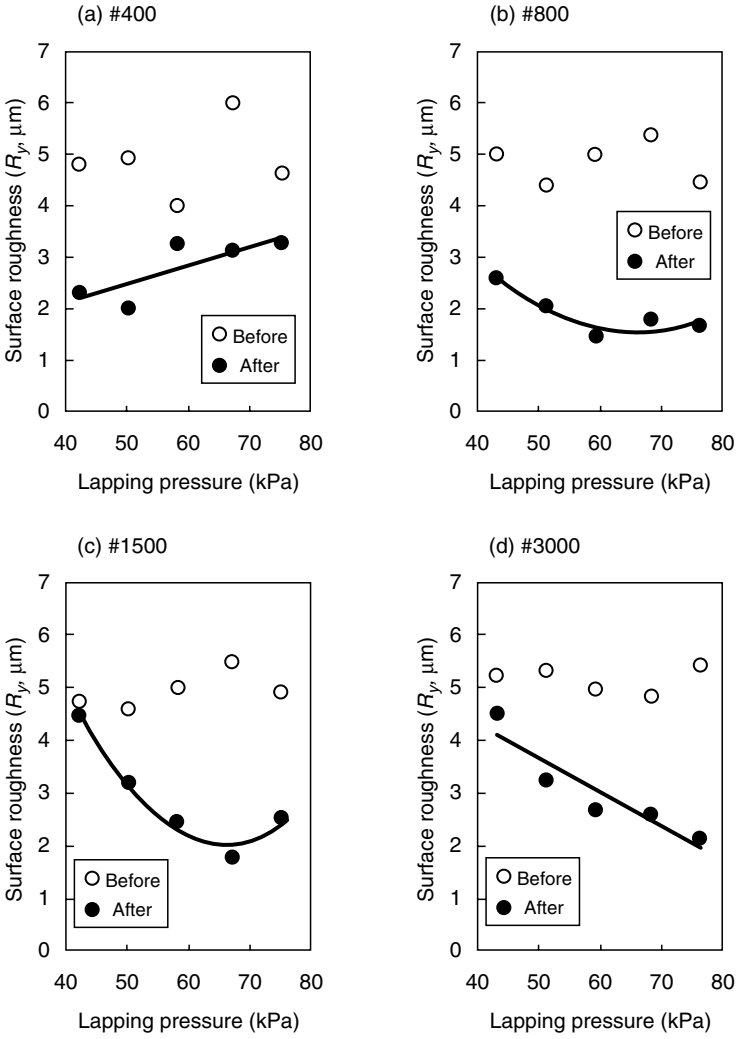


**FIGURE 4.25** Effect of lapping pressure and abrasive grain size on surface roughness. (From Mizuno, M. and Iyama, T. *Adv. Abrasive Technol.*, 3, 359, 2000.)

occurs through the grinding fluid and an electric current. This process stabilizes the protruding grains during grinding. The ELID-lap grinding system is composed of components essential for generating typical electrolyzing phenomena. These are composed of an electric conductive wheel, power supply, grinding fluid, and electrode. Figure 4.27 shows a close-up view of the ELID-lap grinding machine.

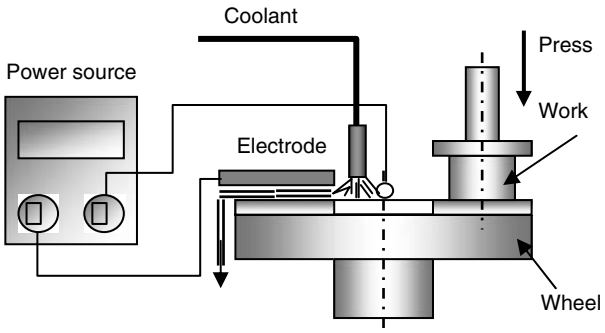


**FIGURE 4.26** Schematic illustration of ELID-lap grinding.

### 4.4.3 Experimental Systems

The specifications of the experimental equipment used for the ELID-lap grinding are as follows:

Grinding machine: A single-sided lapping machine was used in this experiment. The workpiece is mounted onto the main spindle, which rotates the holder. The contact pressure of the workpiece can be regulated by adjusting the air pressure of the main spindle.

Grinding wheel: Metal–resin bonded diamond wheels of different grain sizes from #1200 to #3000000 (#1200 to #3000000MRB-D wheels) were used. This metal–resin bonding system was developed for the purpose of improving the surface qualities in the ELID-lap grinding [32]. These wheels have a diameter of 250 mm and width of 55 mm.

Power source and grinding fluid: An ELID power supply generating high-frequency pulse voltage was used. A chemical solution type grinding fluid was diluted to 2% with water.

Workpiece: The workpiece used was CVD-SiC.

**FIGURE 4.27** External view of ELID-lap grinding machine.

### 4.4.4 Experimental Method

After the usage of truing wheels, the electrical behavior of the pre-dressing of these wheels was measured and grinding characteristics were investigated. The surface roughness and surface properties were studied. Grinding tests were carried out at a wheel speed of 100 rpm, workpiece speed of 100 rpm, and applied pressure of 150 kPa.

### 4.4.5 Characteristics of ELID-Lap Grinding

#### 4.4.5.1 Effects of Grain Size on Surface Roughness and Removal Mechanism

Figure 4.28 shows the difference in the ground surface roughness by different mesh numbers. The surface finish improved as the grain diameter decreased. With this method and use of the #3000000 wheel, the surface could be ground to a very good finish of PV 5.0 nm. Figure 4.29 shows the scanning electron microscopy (SEM) photographs of the ground surface of CVD-SiC. The surface ground by the #1200 wheel shows the typical brittle fracture removal in the SEM observation. On the surface ground by the #4000 wheel, no brittle fracture along the grain paths can be observed. The surfaces ground by the #8000, #120000, and #3000000 wheels are smoother than that by #4000 wheel. In the case of this material, brittle–ductile transition was achieved using wheels over #4000 with ELID-lap grinding. For the purpose of investigating removal mechanism of ELID-lap grinding, the surface ground by the #3000000 wheel was observed by atomic force microscopy (AFM). Figure 4.30 shows the AFM image of the ground surface by the #3000000 wheel. AFM observation shows that the ground surface is very smooth and consists of fine grinding marks that cross each other. Through the analysis of the cross section of parts A-A and B-B as shown in Figure 4.30, the depth of the grinding mark (A-A) is very shallow (approximately 2.8 nm) and the surface irregularities of the smooth part (B-B) were 1.5 nm. The experiment confirmed that ELID-lap grinding using this wheel enables mechanical removal of materials in the order of several nanometers.

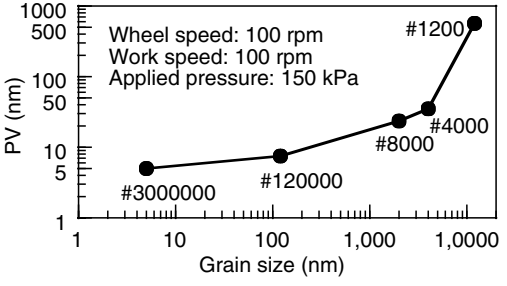


**FIGURE 4.28** Effects of grain size on surface roughness.

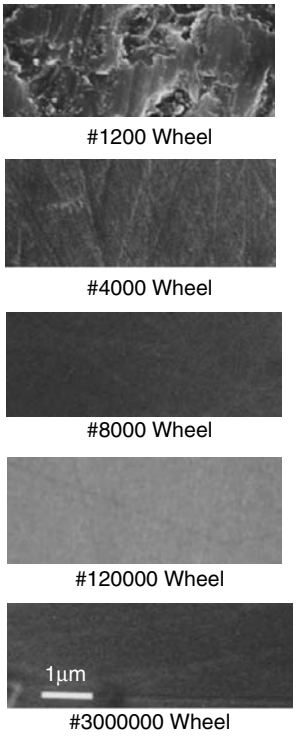


**FIGURE 4.29** SEM photographs of ground surface.

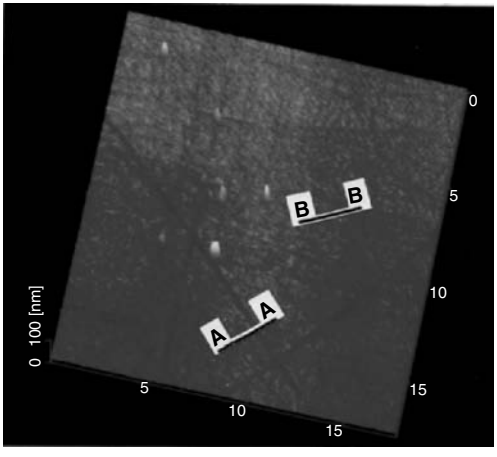


**FIGURE 4.30** AFM image (#3000000 wheel).

### 4.4.5.2 Efficient Mirror Surface Finish by ELID-Lap Grinding

For realizing excellent mirror surface, it is necessary to grind the workpiece in the ductile resume. From the above results, it was clear that ductile mode grinding can be achieved using wheels over #4000 with ELID-lap grinding. The detailed grinding characteristics of CVD-SiC using fine grit diamond wheels (#4000, #8000, and #120000MRB-D wheels) were investigated.

#### *4.4.5.2.1 Stability of Grinding Performance on Fine Grit Diamond Wheels*

Figure 4.31 shows the stability of the grinding performance. For all wheels, the stock removal increased linearly as the grinding time increased, indicating that stable grinding was achieved without clogging. Like the results of stock removal, the surface roughness values were stable during grinding tests. These results show that ELID-lap grinding can realize the stable use of fine grit diamond wheels and is a very useful method for stable mirror surface finish.

#### *4.4.5.2.2 Relation between Grinding Time and Surface Roughness*

For the purpose of realizing efficient mirror surface finishing, the relation between the grinding time and surface roughness was studied. In this experiment, rough grinding was performed using the #1200MRB-D wheel, followed by mirror surface finishing using the #4000, #8000, and #120000MRB-D wheels, and the change in the obtained surface roughness was investigated. Figure 4.32 shows the relation between the grinding time and obtained surface roughness. The workpieces used were ground by the #1200MRB-D wheel to equalize the initial conditions before testing. The obtained surface roughnesses were about 400 nm $R_y$. In the case of #4000MRB-D wheel, when grinding starts, the surface roughness rapidly improved within 1 min of grinding, and then the surface roughness showed constant values. For #8000MRB-D wheel, like the results of the #4000MRB-D wheel, the surface roughness rapidly improved within 2 min of grinding, and then the surface roughness gradually improved and stabilized. After 5 min of grinding, the surface roughness improved from 395 to 25 nm $R_y$. The above results indicate that efficient

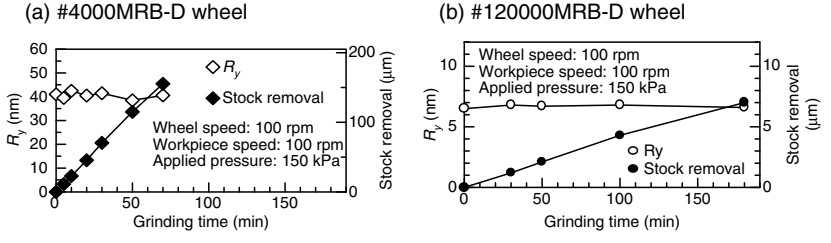


**FIGURE 4.31** Stability of grinding performance.

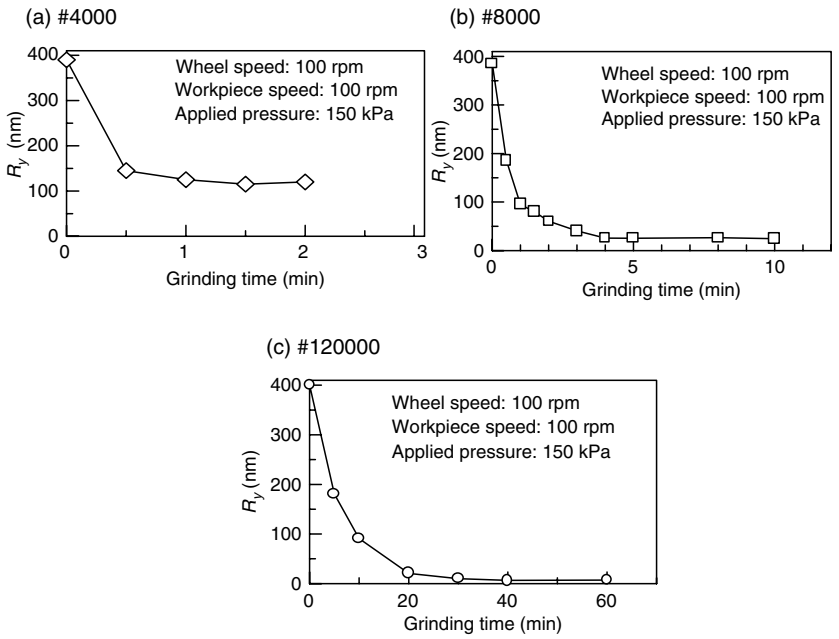


**FIGURE 4.32** Relation between working time and surface.

mirror surface grinding can be realized in this system. On the other hand, for the #120000MRB-D wheel, although the surface roughness improved when grinding started, it took a long time for the surface roughness to show constant values. In this case, efficient mirror surface finishing could not be achieved under these conditions, but it must be realized to perform middle grinding using the #4000 or #8000MRB-D wheel after rough grinding.

### 4.4.6 Desk-Top ELID-Lap Grinding System

#### 4.4.6.1 Background

The increasing emergence of high-tech compact mobile equipments is the strong reason why parts need to be even smaller. The precision grinding of such microparts does not necessarily require conventional large grinding machines. In some cases, a compact grinding machine may prove more efficient by enabling easier handling and saving energy. From this viewpoint, a compact grinding machine applying ELID ultraprecision grinding has been developed, and experimental studies aiming to realize high-quality grinding of microparts have been conducted. The newly developed desk-top ELID-lap grinding system, as well as the results of investigations into the grinding characteristics of cemented carbide alloy, nitrided steel, and sapphire by the system, is introduced.

#### 4.4.6.2 Concept of the System

The desk-top ELID-lap grinding system was developed based on the principle of ELID lap-grinding shown in Figure 4.26. This system is a desk-top type ELID-lap grinding equipment developed to realize precision mirror surface grinding of microcomponents made of various hard and brittle materials simply and easily by applying the principle of ELID lap-grinding. The wheels and work axis of this machine are rotated independently at a speed of 0 to 120 rpm. Up to 200 N, air pressure can be applied during grinding. The wheel used was a $\varphi 150 \times 40$ mm disk wheel. Figure 4.33 shows the external view of the grinding system. The main body dimensions are W390 $\times$ D515 $\times$ H430 mm and its weight is approximately 41 kg. The salient features are as follows:

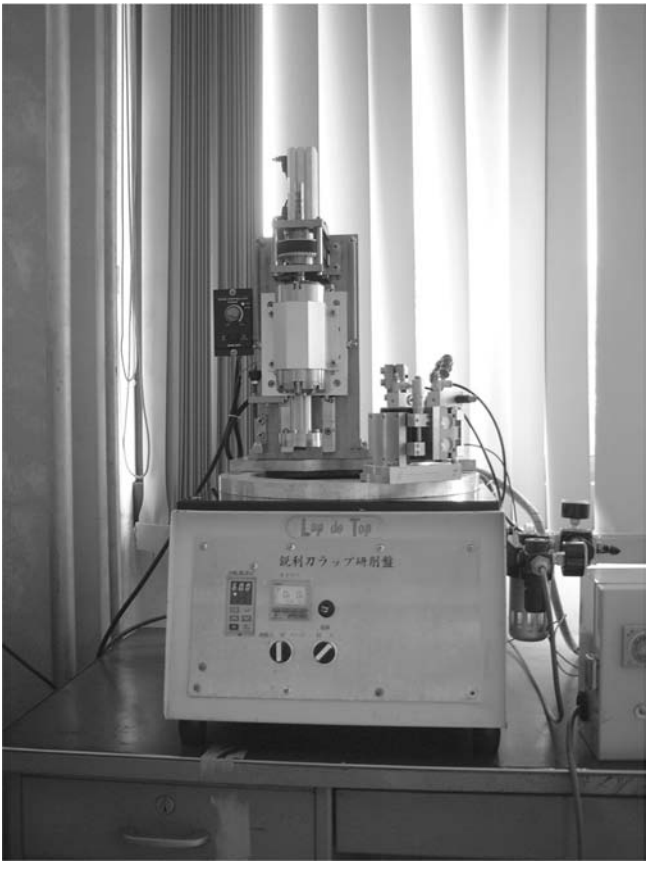


**FIGURE 4.33** External view of grinding machine.

1. It can use a commercial electric power line of 100 V.
2. Use of fixed abrasives (wheel) enables easy maintenance of clean working environment.
3. Use of fixed abrasives (wheel) allows various grinding processes from roughing to mirror surface grinding to be performed on one machine.
4. Compact and lightweight features allow the machine to be moved easily, thus saving energy and space.

### 4.4.7 Experimental System and Method

#### 4.4.7.1 Experimental System

The experimental setup includes the following equipment and test conditions:

Machine: Desk-top ELID-lap grinding system "Lap de Top"(The Nexsys Corp.)
Wheel: #1200 to #20000 metal–resin bonded (copper:resin, 7:3) diamond wheel (NX-GW-KFSI) of size specifications of φ150 × w40, conc. 100 [33]
Electrolytic power supply: High-frequency electrolytic power supply for ELID (NX-ED910)
Grinding fluid: Chemical solution type grinding fluid (CM2) diluted 50 times by tap water
Work: Cemented carbide alloy (equivalent to K10, φ35 × t2 mm), nitrided steel (SKD61, φ10 × t3 mm), sapphire (φ4 × t1 mm)

For some of the grinding experiments, the #325 cast iron bonded diamond wheel was used.

#### 4.4.7.2 Experimental Method

In the experiment, at first the grinding wheels were trued, and initial electrolytic dressing is performed. The grinding experiments are then carried out on the newly developed grinding machine using cemented carbide alloy, nitrided hot die steel, and sapphire as specimens to determine their grinding characteristics. The grinding characteristics included the wheel and work rotational speed of 100 rpm, and the electrolytic dressing conditions were open voltage of 90 V, maximum current of 10 A, and the pulse power supply and stopping time of 2 μs.

### 4.4.8 Experimental Results

#### 4.4.8.1 Grinding Characteristics of Cemented Carbide Alloy

Cemented carbide alloy is used broadly for mechanical seal, cutting tool, cutter, mold, etc., due to its high strength. In recent years, these parts are also becoming smaller and smaller, and as a result, better efficiency and higher quality in the grinding of these parts are being sought. To answer to such

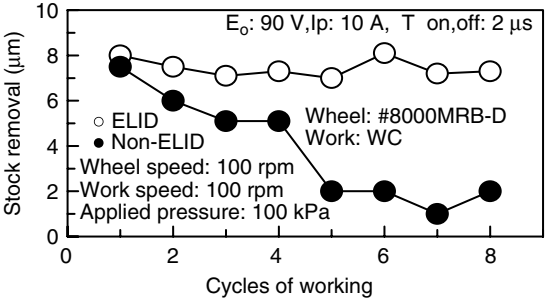


**FIGURE 4.34** Effects of ELID on stock removal.

needs, the basic grinding characteristics of cemented carbide alloy on the grinding machine developed were investigated.

#### *4.4.8.1.1 Effects of Electrolytic Dressing on Grinding Performance and Ground Surface Roughness*

Figure 4.34 shows the change in the number of operation times and stock removal with the application of electrolytic dressing (ELID) and without it in grinding using a #8000 metal resin–bonded wheel. One operation time is 15 min. If electrolytic dressing is not applied, the stock removal gradually decreases with the number of grindings performed, resulting in clogging. On the other hand, when electrolytic dressing is applied, the stock removal does not decrease even after eight cycles of grinding, indicating that grinding is stable. Figure 4.35 shows the relation between the number of cycles of grinding and ground surface roughness. In grinding with electrolytic dressing, stable ground surface roughness was achieved from the start to the end of grinding, confirming that a stable grinding was maintained. If electrolytic dressing is not used, the ground surface roughness gradually decreases.

This is apparently due to the increase in the number of effective abrasives contributing to grinding and reduced protrusion of the tip of the abrasives, caused by the increased wear at the edge of the wheel due to the contact

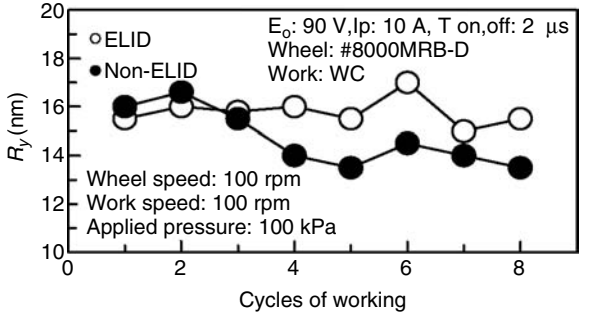


**FIGURE 4.35** Effects of ELID on surface roughness.

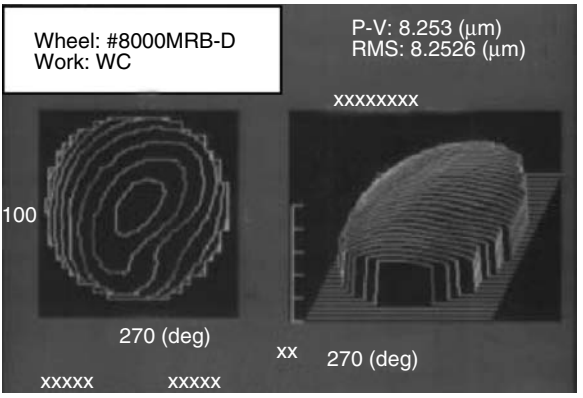


**FIGURE 4.36** Surface flatness of ground surface.

between the abrasives of the grinding wheel and work. The application of electrolytic dressing was confirmed to realize a stable grinding by achieving both good grinding performance and ground surface roughness.

*4.4.8.1.2 Ground Surface Shape and Ground Surface Properties*

Figure 4.36 shows the ground surface shape after eight grinding cycles (when electrolytic dressing is also employed). A flatness of 0.25 μm was achieved. Figure 4.37 shows the SEM image and the workpiece. No brittle fracture can be observed on the ground surface, indicating that ductile mode grinding was achieved.

### 4.4.8.2 Grinding Characteristics of Nitrided Steel

Generally electronic equipment, machine parts, and the products we use in daily life are manufactured by molding. Recent years have seen even higher demands

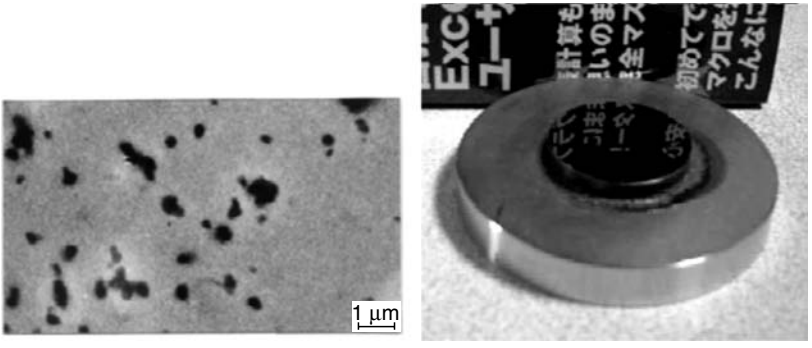


**FIGURE 4.37** SEM image and workpiece.

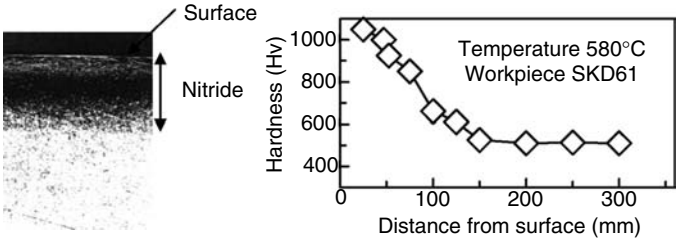


**FIGURE 4.38** Surface structure and surface hardness distribute after nitriding.

for diversification, high precision, and low costs of these products. As a result, while high precision of forming molds is required, improved mold life is also keenly sought. Nitriding is one of the methods used to effectively improve mold life, but it also presents such problems as rough ground surfaces and poor dimensional accuracy. Moreover, as the nitrided surface has a hardness of more than HV1000, re-polishing after nitriding is difficult. For this reason, the application of nitriding is limited to certain cases. Basic grinding experiments were therefore conducted to create high-quality nitrided surfaces.

#### *4.4.8.2.1 Nitriding Method*

The work used in this experiment was made from SKD61 steel quenched (1030°C) and then tempered (550°C) for 3 h at 580°C. Figure 4.38 shows the work surface structure and the surface hardness distribution after nitriding. The total nitrided layer depth by this process was approximately 0.15 mm, whereas the maximum hardness of the surface was 1050 Hv.

#### *4.4.8.2.2 Grinding Experiment Results*

Figure 4.39a shows changes in the ground surface roughness for a nitrided work ground by using a #1200 metal resin–bonded wheel. The surface roughness rapidly improves after grinding starts, then reaches 200 nm $R_y$ after 60 s, and finally stabilizes. Figure 4.39b shows the change in the ground surface roughness when ground for 60 s using a #1200 wheel, followed by a

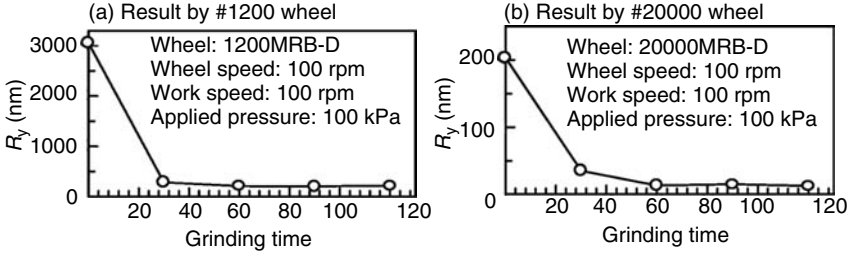


**FIGURE 4.39** Changes in the ground surface roughness for nitrided ground using MRB-wheels.

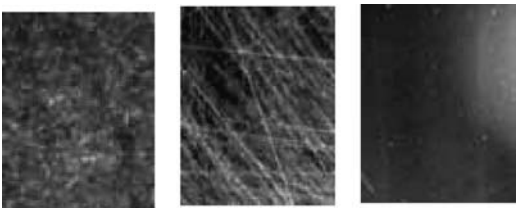

**FIGURE 4.40** Work surface before and after grinding.

#20000 wheel. High-quality surface with a surface roughness of 13 nm $R_y$ was achieved in 60 s of grinding. Figure 4.40 shows the microscopic photo of the ground surface before grinding and after grinding using #1200 and #20000 wheels. These results also confirm that the surface becomes smoother with the finer wheel abrasives. In particular, the surface ground by the #20000 wheel was very smooth with fine grinding marks. Figure 4.41 shows the mirror surface finished sample by the #20000 wheel.

### 4.4.8.3 Grinding Characteristics of Sapphire

Sapphire has excellent electrical insulation qualities, excellent heat conductivity, and stable chemical and thermal features, and is therefore used broadly for semiconductors and optical devices. However, because it has similar hardness as diamond, high-quality grinding cannot be achieved efficiently. We therefore investigated the grinding characteristics of sapphire by ELID-lap grinding using a #325 cast iron bonded wheel, and #8000 metal resin–bonded wheel.

#### *4.4.8.3.1 Relation between Grinding Time and Grinding Characteristics*

Figure 4.42a shows the relation between the grinding time, grinding performance, and ground surface roughness using the #325 wheel. Stable grinding performance and ground surface roughness results were achieved. Figure 4.42b shows the results for the #8000 wheel. Like the results of the #325 wheel, good grinding results were obtained for both grinding performance and ground surface roughness (approximately 17.5 nm $R_y$). Stable grinding was maintained for both wheels with no abnormal electrolytic current values, etc.

**FIGURE 4.41** Example finished by #20000 wheel.

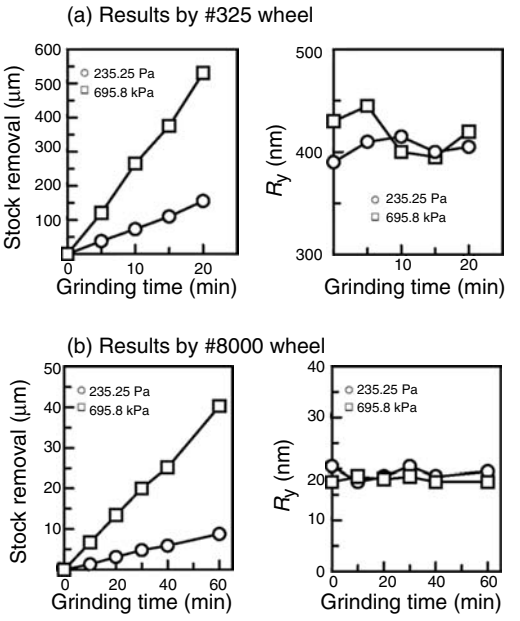


**FIGURE 4.42** Relation between the grinding time, grinding performance, and ground surface roughness.

#### *4.4.8.3.2 Changes in Grinding Time and Ground Surface*

The relation between the grinding time and ground surface state when roughing was performed using the #325 wheel, followed by finishing using #8000 wheel was investigated. Figure 4.43 shows the change in the grinding time and ground surface state under the applied pressure of 695.8 kPa. The ground surface using #325 wheel showed both brittle fracture and ductile removal. When finishing using #8000 wheel was performed in this state, though the brittle fracture and grinding marks of the grain path, which occurred with the #325 wheel were observed after 0.5 min of grinding, the ground surface was more or less smooth. After 2 min of grinding, the overall surface was smooth with no brittle removal marks. The results confirmed that the grinding machine developed enables high-quality ground surfaces to be achieved for sapphire.

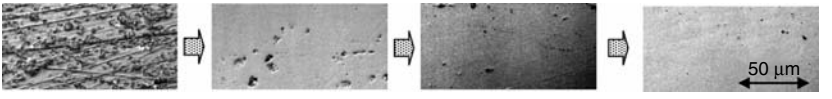


**FIGURE 4.43** Change in the grinding time and ground surface state.

### 4.4.9 Conclusions

For the purpose of realizing efficient grinding of mirror and lens production, grinding characteristics of CVD-SiC in ELID-lap grinding were studied. The surface quality achieved by this system using different sized grain wheels was excellent. The resultant surface roughness was PV 5.0 nm using the #3000000 wheel. SEM observation clarified that brittle–ductile transition was achieved using wheels over #4000 with ELID-lap grinding. The AFM image of the surface ground using the #3000000 wheel showed that ELID-lap grinding using this wheel mechanically eliminates in order of several nanometers.

To realize the ELID-lap grinding in desk-top style, the desk-top ELID-lap grinding system has been developed, and representative experiments were performed on cemented carbide alloy, nitrided steel, and sapphire on the system, and results of investigations of the basic grinding characteristics suggest that grinding is stable for all these materials, and at the same time high-quality surfaces could be achieved by the desk-top grinding system for microcomponents.

## 4.5 MATERIALS, EXPERIMENTAL SETUP, AND TESTING PROCEDURE (STUDY CASE)

*MARIANA PRUTEANU*

### 4.5.1 Materials

#### 4.5.1.1 Workpiece Materials

The properties of the material to be lapped are certainly the deciding factors on how the material will be machined. All the material properties such as: hardness, porosity, wear resistance, chemical inertness, and toughness, are important among others. In the case of ceramic materials, thermal properties are not so significant since during the lapping operation the temperature in the work zone is relatively low.

For the purpose of this project several lapping tests were performed using different materials for the workpieces. The parts utilized were made of aluminum oxide ($Al_2O_3$) and hexoloy-sintered alpha silicon carbide (hexoloy).

The workpieces made of aluminum oxide were rings having 0.5″ ID, 0.8″ OD, and 0.2″ thickness (Figure 4.44). Physical and mechanical properties of $Al_2O_3$ are listed in Table 4.7

Aluminum oxide is one of the hardest materials known. Its high hardness promotes a series of applications in mechanical engineering, such as bearings and seals. It is a good material to use for lapping tests for various reasons. Because of its hardness it can be lapped to produce very good finishes and porosity is pretty low.

Hexoloy SiC is a new sintered alpha silicon carbide material designed specifically for optimum performance in sliding contact applications. It is

**FIGURE 4.44** $Al_2O_3$ workpieces.

produced by pressureless sintering ultrapure submicron powder. This powder is mixed with nonoxide-sintering aids, then formed into the desired shapes by a variety of methods, and consolidated by sintering at temperatures above 2000°C (3632°F). The sintering process results in single-phase, fine-grain SiC

**TABLE 4.7**
**Ceramic Properties of $Al_2O_3$**

| **Material $Al_2O_3$—99.8%** | |
|---|---|
| ***Physical properties*** | |
| Density (g/cc) | 3.96 |
| ***Mechanical properties*** | |
| Tensile strength (MPa) | 310 (at 25°C) |
| | 220 (at 1000°C) |
| Modulus of elasticity (GPa) | 366 |
| Poisson ratio | 0.22 |
| Compressive strength (MPa) | 3790 (at 25°C) |
| | 1.929 GPa (at 1000°C) |

product that is very pure and uniform, with virtually no porosity. Whether used in corrosive environments, subjected to extreme wear and abrasive conditions, or exposed to high temperatures, hexoloy-sintered alpha silicon carbide outperforms other advanced ceramics. This kind of ceramic material is ideal for applications such as chemical and slurry pump seals and bearings, nozzles, pump, and valve trim and more.

Table 4.8 illustrates the outstanding properties of hexoloy silicon carbide. It is an extremely hard material, lightweight, and low in porosity. This material has exceptional corrosion and erosion-resisting properties through the addition of spherical pores.

These pores are discrete, noninterconnecting, and dispersed in a controlled manner throughout the body of the material. The spherical pores act as fluid or lubricant reservoirs helping to promote the interface of sliding component surfaces.

The parts made of hexoloy are pump seals having 0.55″ ID, 1.36″ OD, and 0.38″ thickness (Figure 4.45).

Another material utilized as workpiece material was hardened steel W-1. The chemical composition is presented in Table 4.9. The high content of carbon allows high hardness to be achieved by hardening and also formation of carbide, which gives the high wear resistance. The dimensions for the parts made of W-1 were 0.8″ OD and 0.4″ thickness (as seen in Figure 4.46).

The initial hardness of the steel was about 10–14 HRC.

The parts were heat-treated and, after quenching in oil, the resulting hardness was 44–48 HRC. The steps followed for the heat treatment were:

**TABLE 4.8**
**Properties of Hexoloy SiC**

| Properties | Units | Values |
|---|---|---|
| Density | $g/cm^3$ | 3.04 |
| Hardness (knoop) | $kg/mm^2$ | 2800 |
| Elastic modulus at RT | GPa | 400 |
| Poisson's ratio | | 0.14 |
| Flexural strength | MPa | 240 |
| Weibull modulus | | 19 |
| Fracture toughness at RT | $Mpa/m^{1/2}$ | 4.3 |
| Coefficient of thermal expansion at RT to 700°C | $\times 10^{-6}$ mm/mm·K | 4.2 |
| Mean specific heat at RT | J/gm·K | 0.59 |
| Thermal conductivity at RT | W/m·K | 110 |
| Pore volume fraction | % | 5.0–6.0 |
| Pore size (typical) | μm | 50 |
| Grain size (SiC) | μm | 4–6 |

**FIGURE 4.45** Hexoloy silicon carbide parts.

(1) preheat oven to 1425°F–1500°F; (2) place part in the oven for 0.5 h per inch of thickness; (3) quench the part in oil; and (4) test the hardness.

Hardness was measured with a hardness tester device—ACCUPRO AR-10. The surfaces of the workpieces were ground after heat treatment and prior to lapping for the following reasons: (1) the thickness varied slightly on some parts and this step (grinding) eliminated the variation. Thickness variation is not a critical problem when large normal forces are used but might initiate problems when lapping with small normal forces; (2) the initial surface roughness of the parts averaged approximately 0.8 μm $R_a$. Surface grinding lowered the roughness values of each workpiece and gave them similar starting surfaces (approximate $R_a = 0.65$ μm); (3) as a rule, some machining may be done before lapping. Grinding is an operation that usually takes place before lapping.

#### 4.5.1.2 Abrasives

A large number of abrasives are available to the finishing industry. The type of abrasive is dependent on the properties of the material being machined. For ultrahard materials, such as ceramics and carbides, the choices are restricted to superabrasive powders: diamond and CBN. For the fine finishing of ceramic materials, diamond is the best option to be considered.

**TABLE 4.9**
**Chemical Composition of W-1 Steel**

| %C | %Si | %Mn | %P | %S | %Cr | %V |
|---|---|---|---|---|---|---|
| 0.95–1.5 | 0.1–0.25 | 0.3–0.4 | 0.025 | 0.02 | 0.15 | 0.1 |

**FIGURE 4.46** W-1 parts.

Throughout all lapping experiments, diamond slurries were utilized as abrasives. First set of experiments done in lapping used water-based monocrystalline (K35 SYN) and polycrystalline (K35 SPD) diamond slurries (grain size 0.25 μm) provided and produced by Warren Diamond Powder Company. K35 is a synthetic diamond specifically formulated for free-abrasive lapping. It provides excellent removal rates, imparts improved surface finish, and enhances plate life. It has the capability to replenish the lapping plate with fresh diamond, allowing cut rates and surface finishes remaining consistent for long periods of time. K35 diamond slurry, as well as all the other slurries made by this company, offers a greater number of cutting facets that leads to a smooth, uniform result with less random scratching and subsurface deformation. Also, it presents no environmental or health risks.

The second set of lapping tests was also performed with water-based monocrystalline (K35W—HS) and polycrystalline (K35W—SPD) diamond slurries supplied by Warren Diamond Powder Company. Grain sizes for diamond slurries were 0.75, 1.5, 3, and 6 μm. The slurry used for the third series of experiments was monocrystalline Hyprez diamond slurry delivered by Engis Corporation in water-based (S4889)STD–MA formulation and oil-based (S1313–T4)STD–MA formulation. This is a synthetic diamond produced in controlled high-temperature and high-pressure process. It is a manufactured metal-bond monocrystalline diamond having blocky crystals, regularly shaped, and less friable (tougher) than resin-bond diamond.

### 4.5.2 Experimental Equipment and Lapping Setup

The experimental equipment that was used in this research is listed below:

- Lapmaster lapping machine, model 12C, variable speed 90 VDC, 7.5 A motor (0–60 rpm) with 12″ grooved cast iron plate, 5″ cast iron conditioning rings, and a magnetic stirrer
- Cole-Parmer peristaltic pump, 7021–24 pump head and Masterflex Tygon

Other instruments which were utilized:

- Roughness meter Hommel Tester LV 15 and ProfileView 3.44 software for processing the surface roughness and profile data
- Optical flat and monochromatic light source P-5012
- Precision electronic scale HR-120 (minimum unit weighing—0.1 mg)
- Dial indicator (0.0001″)
- Hardness tester ACCUPRO AR-10

The experimental equipment used during the lapping tests is shown in Figure 4.47. All the experiments were done on Lapmaster International lapping machine, model 12C. The model 12C uses a 12″ lapping plate and Lapmaster lapping machine variable-speed DC motor as in Figure 4.47.

It is equipped with a magnetic stirrer and a carrier delivery system. The 90 VDC, 7.5 A motor can vary plate revolutions over a range of 0–60 rpm.

The Lapmaster machine is delivered with radially grooved cast iron lapping plate and conditioning rings. The machine comes with a carrier delivery system that could not give a consistent flow rate. The diamond slurry is supplied in a mist so the quantity of slurry is not exact every time and it is difficult to measure the slurry dispensed at specific intervals. Due to the difficulties associated with this system, an alternative arrangement, a Cole-Parmer peristaltic pump (model 7521–40) was used. This variable-speed peristaltic pump allows adjustable delivery of the diamond slurry; flow rate can be continually monitored through the peristaltic pump to assure that exact slurry delivery requirements are attained (Figure 4.48).

**FIGURE 4.47** Lapmaster lapping machine.

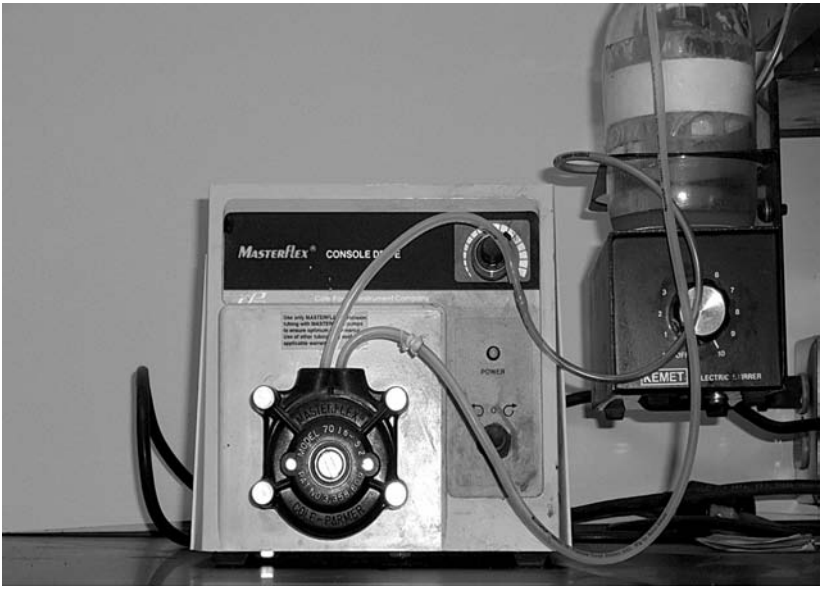


**FIGURE 4.48** Cole-Parmer peristaltic pump.

The peristaltic pump comes with Masterflex Tygon silicon tubing having 0.061″ ID and 0.181″ OD. It is a high-performance precision tubing that has a thick wall that improves pressure generation suction lift and the capability to pump viscous fluids.

The flatness of the plate is one of the most crucial factors that can affect the performance of the lap because the flatness of the lapping plate is transferred to the workpieces during the process. Consequently, if the lapping plate is concave, the workpiece will become convex and vice versa. Lapping plates tend to run out of true as either spherically concave (the most common condition) or spherically convex surfaces. The lap can be brought back to true flatness by simple movement of the conditioning rings to the outboard or inboard positions, as can be seen in Figure 4.49.

The flatness of the lapping plate determines the degree of flatness, parallelism, size uniformity, and surface finish of the parts being lapped

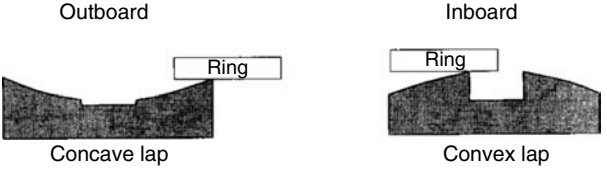


**FIGURE 4.49** Outboard and inboard positions for conditioning rings.

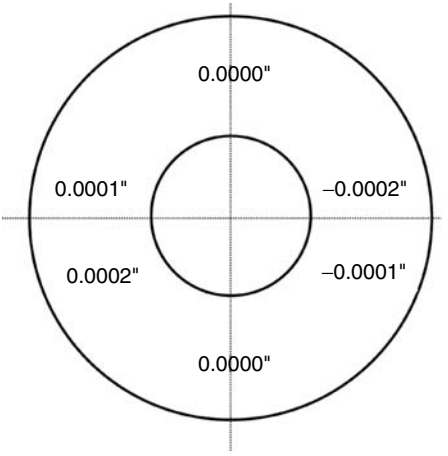


**FIGURE 4.50** Flatness of the lapping plate after facing.

more than any other variable in the lapping process. As a general rule, a 12″. lapping plate should not vary in flatness more than plus or minus one thousandth of an inch.

Prior to lapping, the plate flatness was measured using a profilometer device. This was done to assure that deviation from flat was kept to a minimum. Figure 4.50 depicts the value of the flatness measured over the entire surface of the lapping plate.

A specific lapping plate, conditioning rings, and slurry delivery tube were used for each diamond abrasive size. Taking into consideration that many abrasives were used throughout lapping tests, this was done in order to avoid the contamination of the lapping plates and, for this reason, the possibility of imprecise results.

The plates go through two steps throughout the preparation period. The first step is to machine the plate flat. The cast iron lapping plates were initially faced using a Blanchard rotary surface grinding machine (Figure 4.51). Because the surface finish of the lapping plate did not meet the expectations, the next step was to improve the flatness and the surface roughness of the plate using a surface grinder machine (Figure 4.52). After this operation was performed, the plate flatness was according to standard recommendations (see Figure 4.50).

As for the next step, the lapping plate must be charged before efficient lapping can occur. Usually, during charging the diamond slurry flows over the plate while the conditioning ring loaded against the plate forces the particles into the surface. Observations of the plate surface during charging (according to A. Barylski) showed that the diamond micrograins are compressed, first of all, into the graphite and, to a lesser degree, into the cast iron metallic matrix. The smaller micrograins are implanted in the plate graphite and larger ones are embedded in the nodular graphite inclusions [34].

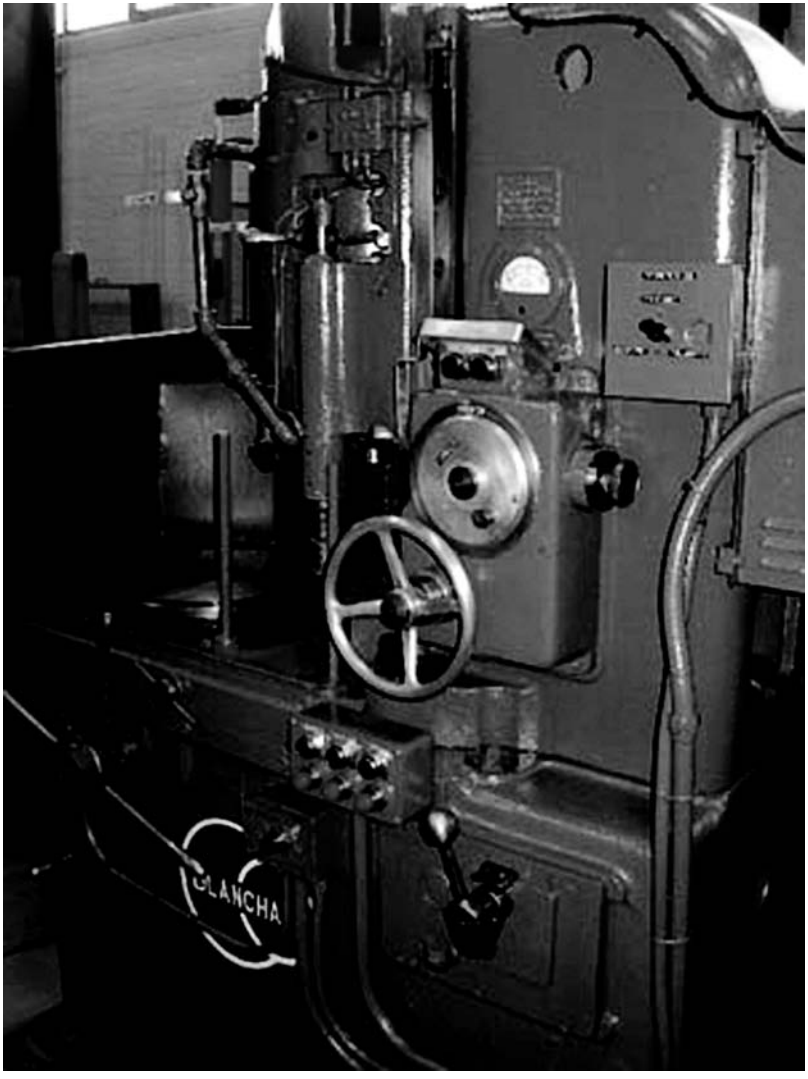


**FIGURE 4.51** Blanchard rotary surface grinding machine.

### 4.5.3 Testing Procedure

#### 4.5.3.1 Lapping Setup

Figure 4.53 illustrates the lapping setup. Two conditioning rings were used: one to hold the workpieces and the other to distribute the slurry evenly on the entire surface of the plate. Conditioning rings are not only for retaining the parts during machining but also for maintaining the lapping plate flatness.

**FIGURE 4.52** Surface grinder machine.

Diamond abrasive was suspended in a water-based or oil-based carrier and supplied by the peristaltic pump. This device was used in order to keep a consistent and measurable flow rate throughout all lapping experiments. Three workpieces were lapped simultaneously being fixed at the bottom of a weight with a holder. The part holder has a diameter of 4.17″. (105.92 mm), slightly smaller than the inner diameter of the conditioning ring. Parts are positioned 120° equidistant on a circle having the diameter 2.067″. (52.5 mm) from the edge of the part holder. The slurry was based on either monocrystalline or polycrystalline diamond grains with identical particle size distribution.

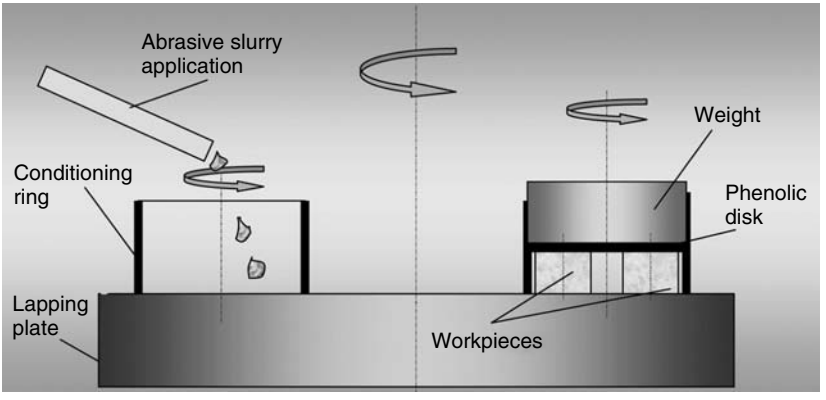


**FIGURE 4.53** Lapping setup.

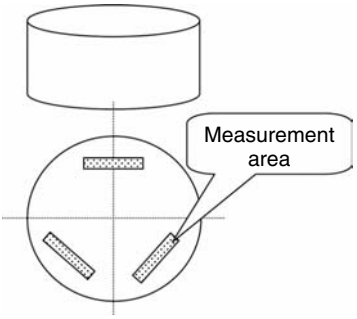


**FIGURE 4.54** Schematic representation of measurement areas.

For all the workpieces the following characteristics were measured before and after each experiment: thickness, mass, and surface roughness (measured in three areas, as it can be seen from Figure 4.54).

The lapping machine was set to warm up for at least 60 min, and diamond slurry and the conditioning rings are set on the lap plate 10 min before lapping the workpieces; this was done in order to stabilize the system.

### 4.5.3.2 Measuring Procedures

Surface analysis for all the tests performed was done using a Hommel tester T1000 E roughness meter, a stylus type profilometer with a stylus tip radius of $0.0002''$. It has a tracing length $l_t = 4.8$ mm and a cut-off length $l_c = 0.8$ mm. The measuring principle is inductive, the tracing speed is 0.5 mm/s, and the reverse speed is 2 mm/s. It allows surface roughness measurements in the range of $\pm 40$ μm (Figure 4.55) with 0.1 μm accuracy.

Roughness, waviness, and form are three parameters when characterizing surface finish. Roughness is short (fine) wavelength or microirregularities on a surface. Roughness is of significant interest in manufacturing because it is the roughness of a surface (given reasonable waviness and form error) that determines its friction in contact with another surface. The roughness of a surface defines how that surfaces feels, how it looks, how it behaves in a contact with another surface, and how it behaves for coating or sealing. For moving parts, the roughness determines how the surface will wear, how well it will retain lubricant, and how well it will hold a load. Waviness is long wavelength or macroirregularities of a surface from its nominal shape. It can be used as a measure of flatness. Waviness errors are intermediate in wavelength between roughness and form error. Form is the deviation in the surface profile from the nominal, other than roughness or waviness (e.g., form refers to roundness or straightness). Form is not a major issue in micromachining processes such as lapping since material removal is small and therefore the form is not altered. Waviness and, more importantly,

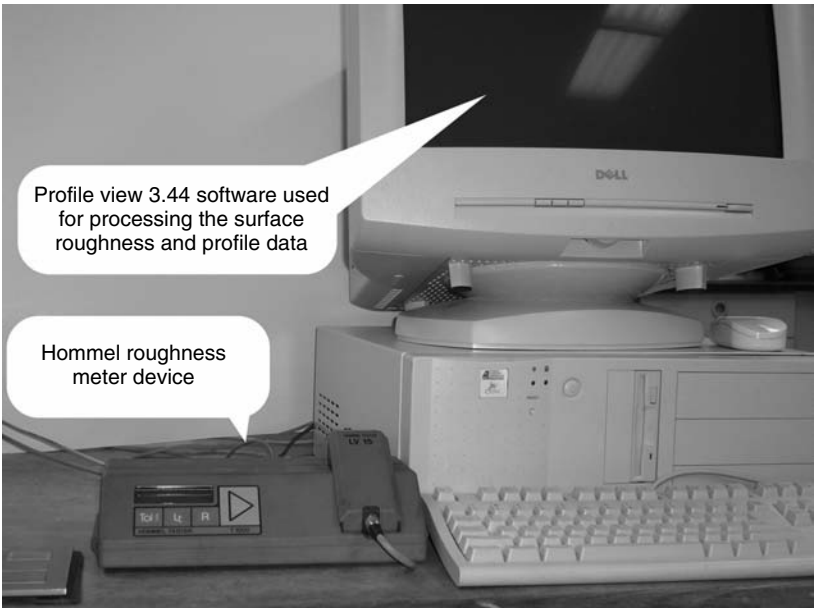


**FIGURE 4.55** Hommel tester T1000 E.

roughness are the significant characteristics to the effectiveness of the process.

The roughness average parameter (Figure 4.56) is the area between the roughness profile and its mean line, or the integral of the absolute value of the roughness profile height over the evaluation length. RMS is the root-mean-square roughness; it is the standard deviation of the arithmetic mean

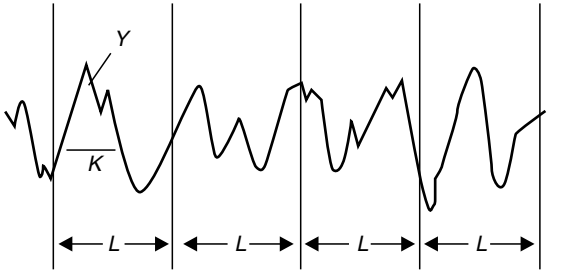


$$R_a = \frac{1}{L}\int_0^L \left| Y(X) \right| dx \qquad \text{RMS} = \sqrt{\frac{1}{L}\int_0^L Y^2(X)\, dx}$$

**FIGURE 4.56** Roughness average parameter $R_a$.

value $R_a$. In the above formula, $L$ is the sampling length and $Y$ is the ordinate of the profile curve. The average roughness is by far the most commonly used parameter in surface finish measurement and it is accepted as a good parameter to describe a surface. The disadvantages of this parameter are: (1) peaks and valleys are not differentiated and (2) defects in the surface do not change the result greatly.

Material removal was measured by thickness change and weight loss. The thickness change was determined using a Mitutoyo micrometer, 0–1″ (resolution 0.0001″ or 0.001 mm). Measurements were taken before and after each lapping time as shown in Figure 4.54; a template was used to make sure that the same location was measured each time. The weight loss was checked every time using a precision electronic balance HR – 120 having a weighing capacity of 120 g.

The formulas used in order to calculate the MRR were as follows:

$$\text{MRR} = (\text{area/lapping time})/(\text{average thickness change}) \ [\text{mm}^3/\text{min}]$$
$$\text{MRR} = (\text{average weight change})/(\text{lapping time}) \ [\text{mg/min}]$$

All the workpieces were ultrasonically cleaned and dried with compressed air before each measurement took place.

Three sets of experiments were performed in order to have firm conclusions on the behavior of monocrystalline and polycrystalline diamond slurries.

#### *4.5.3.2.1 Test A*

Test A consisted of lapping aluminum oxide rings with water-based monocrystalline and polycrystalline diamond slurries using cast iron lapping plates. During the experiments, the following parameters were kept constant:

- Flow rate—0.75 ml/min
- Carrier type—water-based slurry
- Slurry concentration—1.4 g/500 ml (7 ct/500 ml)
- Grain size—0.25 μm

The variable parameters during lapping were:

- Diamond type—mono and polycrystalline diamond slurry
- Rotation of the lapping plate—3, 6, and 9 rpm
- Loads—380, 750, and 1200 g
- Lapping time—5, 15, 30, and 60 min

As mentioned before, workpiece characteristics were measured (surface roughness, thickness, and weight) before lapping and after each lapping time. The average initial surface roughness was $R_a = 0.716$ μm.

#### 4.5.3.2.2 Test B

Test B was done on W-1 parts (62–64 HRC) using several grain sizes for diamond abrasive grains. The conditioning rings and lapping plates used for the experiment were made of cast iron. The initial average roughness of the W-1 workpieces was 0.65 μm.
The constant parameters were:

- Flow rate—1.5 ml/min
- Slurry concentration—1.4 g/500 ml (7 ct/500 ml)
- Rotation of the lapping plate—56 rpm
- Carrier type—water-based diamond slurry

The variable parameters considered for this test were:

- Diamond type—monocrystalline and polycrystalline
- Diamond grain size—0.75, 1.5, 3, and 6 μm
- Lapping time—5, 15, and 30 min
- Loads—91, 364, 1455, and 5820 g

#### 4.5.3.2.3 Test C

This experiment was carried out in different conditions than the previous tests. The aim was not only to determine the behavior of diamond slurry but also to establish the influence of lapping plate material on lapping performance.

Two types of lapping plates were utilized, composite copper and composite iron. The composite plates are made with a blend of powdered metal or ceramic, combined in a resin system. They are used in industrial applications because the special formulation of powders and resins allows composite plate to take a more uniform charge of diamond, compared to pure metal plates. The composite material efficiently and rapidly removes stock, while producing high-quality surface finish and flatness with diamond superabrasives.

The diamond slurry, grain sizes 1, 3, and 15 μm, was monocrystalline in water-based formulation and oil-based formulation. The average initial roughness for hexoloy silicon carbide parts was $R_a = 0.057$ μm and for hardened steel W-1 parts $R_a = 0.65$ μm.
Constant parameters for this set of experiments were:

- Flow rate—0.7 ml/min
- Diamond type—monocrystalline

Parameters varied during the tests were:

- Carrier type—water-based and oil-based slurry
- Grain size—1, 3, and 15 μm
- Lapping plate material—composite copper and composite iron
- Rotation of the lapping plate—30 and 60 rpm
- Load—3 and 5 psi
  - 3 psi (4941 g for hexoloy parts and 2130 g for W-1 parts)
  - 5 psi (8239 g for hexoloy parts and 3551 g for W-1 parts)
- Lapping time—1, 3, 6, 11, 21, 36, and 66 min

## 4.6 EXPERIMENTAL RESULTS AND DISCUSSION

*MARIANA PRUTEANU*

This section is separated into three sections presenting the results for tests A, B, and C.

### 4.6.1 Test A

A significant component of these lapping experiments is the evaluation of the performance of monocrystalline versus polycrystalline diamond slurry. The test was also planned to determine the effect of the machining time, load and rotation of the plate on the surface roughness, and MRR.

The results for surface finish and material removal are presented in Table 4.10 and Table 4.11. Each value for $R_a$ and MRR is the average of three measurements taken on each of the three parts lapped at a time. Figure 4.57 and Figure 4.58 illustrate the effect of load and time on surface roughness for different rotations of the lapping plate for both types of diamond.

Figure 4.59 and Figure 4.60 illustrate the influence of time and rotation of the plate and Figure 4.61 and Figure 4.62 exemplify the effect of load and rotation of the plate on surface roughness. The roughness average values represented on the graphs were recorded in micrometers. The variables considered—time, load, and rotation of the lapping plate (lapping speed)—were displayed in minutes, grams, and rotations per minute, respectively.

Results for both types of diamond used show that surface finish improves with time for all rotations of the lapping plate considered. As it can be seen in the above figures, the surface roughness is decreasing more rapidly with the time at the beginning of machining. Within the first 30 min the surface finish was brought down from about 0.716 μm to about 0.2 μm. After approximately 30 min, the surface roughness does not decrease significantly; continuing the lapping process after this period of time will not notably improve the surface finish. Concluding, a 30-min lapping cycle is long enough to obtain the best surface finish with the tested grit size (0.25 μm diamond grain size). Also, the surface roughness decreases faster in time when higher loads are applied for both monocrystalline and polycrystalline diamond slurries.

**TABLE 4.10**
**Results for Monocrystalline Diamond (Test A)**

| Load (g) | Lap Speed (rpm) | Elapsed Time (min) | Roughness ($R_a$) (μm) | MRR ($mm^3$/min) |
|---|---|---|---|---|
| 380 | 3 | 5 | 0.629 | 0.0677 |
| | | 15 | 0.553 | 0.0474 |
| | | 30 | 0.523 | 0.0135 |
| | | 60 | 0.449 | 0.0089 |
| | 6 | 5 | 0.625 | 0.0677 |
| | | 15 | 0.627 | 0.0613 |
| | | 30 | 0.559 | 0.0361 |
| | | 60 | 0.478 | 0.0248 |
| | 9 | 5 | 0.448 | 0.0677 |
| | | 15 | 0.402 | 0.0270 |
| | | 30 | 0.395 | 0.0180 |
| | | 60 | 0.362 | 0.0089 |
| 750 | 3 | 5 | 0.523 | 0.0541 |
| | | 15 | 0.422 | 0.0406 |
| | | 30 | 0.388 | 0.0225 |
| | | 60 | 0.320 | 0.0135 |
| | 6 | 5 | 0.552 | 0.0670 |
| | | 15 | 0.415 | 0.0270 |
| | | 30 | 0.354 | 0.0361 |
| | | 60 | 0.320 | 0.0135 |
| | 9 | 5 | 0.496 | 0.1084 |
| | | 15 | 0.434 | 0.0406 |
| | | 30 | 0.374 | 0.0180 |
| | | 60 | 0.328 | 0.0135 |
| 1200 | 3 | 5 | 0.530 | 0.0813 |
| | | 15 | 0.424 | 0.0406 |
| | | 30 | 0.326 | 0.0185 |
| | | 60 | 0.270 | 0.0203 |
| | 6 | 5 | 0.505 | 0.1220 |
| | | 15 | 0.358 | 0.0406 |
| | | 30 | 0.316 | 0.0361 |
| | | 60 | 0.278 | 0.0225 |
| | 9 | 5 | 1.142 | 0.1491 |
| | | 15 | 0.807 | 0.0406 |
| | | 30 | 0.663 | 0.0225 |
| | | 60 | 0.755 | 0.0112 |

Regarding the influence of load and lapping speed on surface finish, one can say that roughness improves at higher speeds and lower loads when monocrystalline slurry is employed and it improves at both higher speeds and loads when polycrystalline slurry is utilized.

**TABLE 4.11**
**Results for Polycrystalline Diamond (Test A)**

| Load (g) | Lap Speed (rpm) | Elapsed Time (min) | Roughness ($R_a$) (μm) | MRR ($mm^3$/min) |
|---|---|---|---|---|
| 380 | 3 | 5 | 0.570 | 0.0813 |
| | | 15 | 0.528 | 0.0406 |
| | | 30 | 0.463 | 0.0146 |
| | | 60 | 0.371 | 0.0068 |
| | 6 | 5 | 0.505 | 0.0670 |
| | | 15 | 0.453 | 0.0338 |
| | | 30 | 0.445 | 0.0135 |
| | | 60 | 0.422 | 0.0067 |
| | 9 | 5 | 0.496 | 0.0677 |
| | | 15 | 0.422 | 0.0338 |
| | | 30 | 0.382 | 0.0180 |
| | | 60 | 0.371 | 0.0067 |
| 750 | 3 | 5 | 0.537 | 0.0813 |
| | | 15 | 0.447 | 0.0203 |
| | | 30 | 0.386 | 0.0316 |
| | | 60 | 0.710 | 0.0089 |
| | 6 | 5 | 0.513 | 0.1220 |
| | | 15 | 0.418 | 0.0270 |
| | | 30 | 0.344 | 0.0180 |
| | | 60 | 0.311 | 0.0112 |
| | 9 | 5 | 0.526 | 0.0813 |
| | | 15 | 0.464 | 0.0338 |
| | | 30 | 0.369 | 0.0225 |
| | | 60 | 0.329 | 0.0135 |
| 1200 | 3 | 5 | 0.540 | 0.0813 |
| | | 15 | 0.463 | 0.0406 |
| | | 30 | 0.332 | 0.0270 |
| | | 60 | 0.286 | 0.0157 |
| | 6 | 5 | 0.505 | 0.0677 |
| | | 15 | 0.395 | 0.0338 |
| | | 30 | 0.361 | 0.0225 |
| | | 60 | 0.313 | 0.0225 |
| | 9 | 5 | 0.464 | 0.1220 |
| | | 15 | 0.370 | 0.0474 |
| | | 30 | 0.341 | 0.0225 |
| | | 60 | 0.305 | 0.0157 |

According to the data represented in the above graphs, load is the parameter that plays one of the most important roles in obtaining the final surface finish. The graphs show that at lower load (380 g) the polycrystalline diamond produces a slightly better surface finish than the monocrystalline diamond

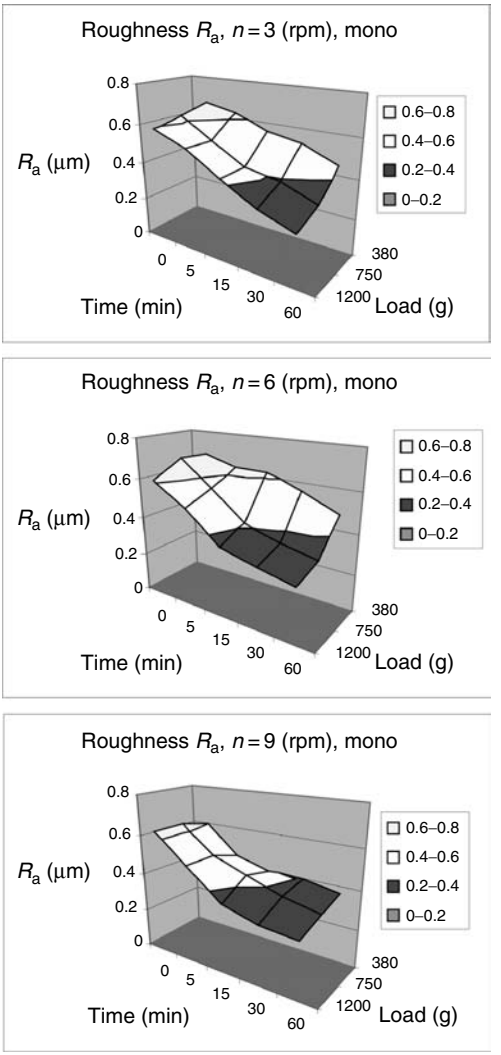


**FIGURE 4.57** Influence of load and time on surface roughness $R_a$ for monocrystalline diamond slurry.

(an average of 0.37 μm for polycrystalline as compared to 0.45 μm for monocrystalline diamond) whereas at higher load (1200 g) the latter behaves a little bit better from the roughness point of view (0.27 μm as compared to 0.31 μm). The rotation of the lapping plate, in the range considered for this test—3, 6, and 9 rpm—has no substantial influence on the surface roughness.

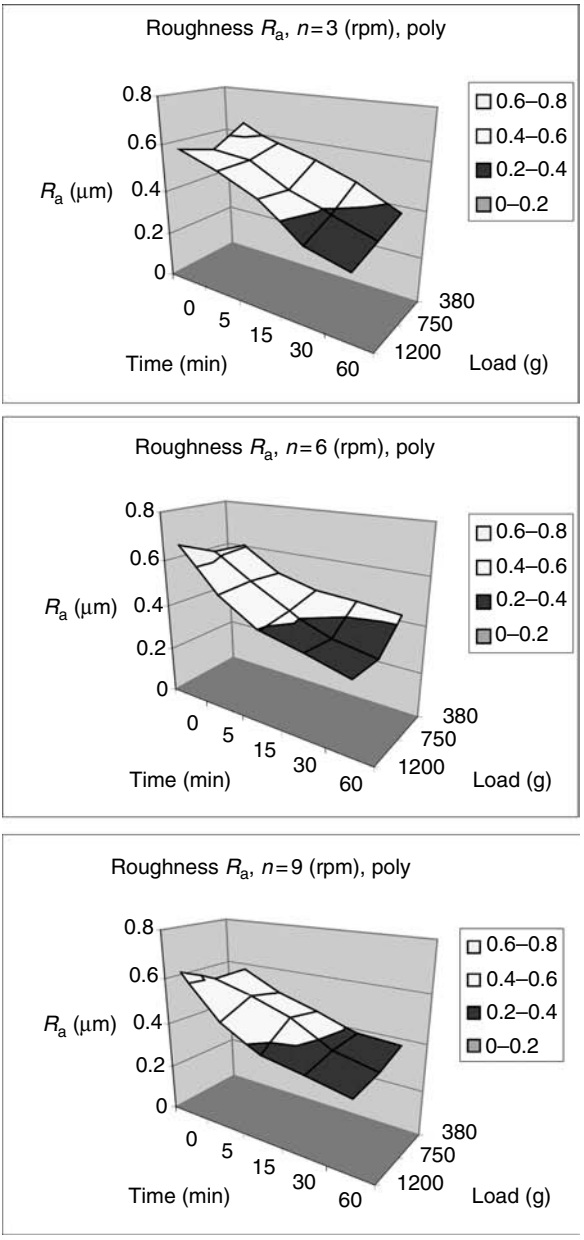


**FIGURE 4.58** Influence of load and time on surface roughness $R_a$ for polycrystalline diamond slurry.

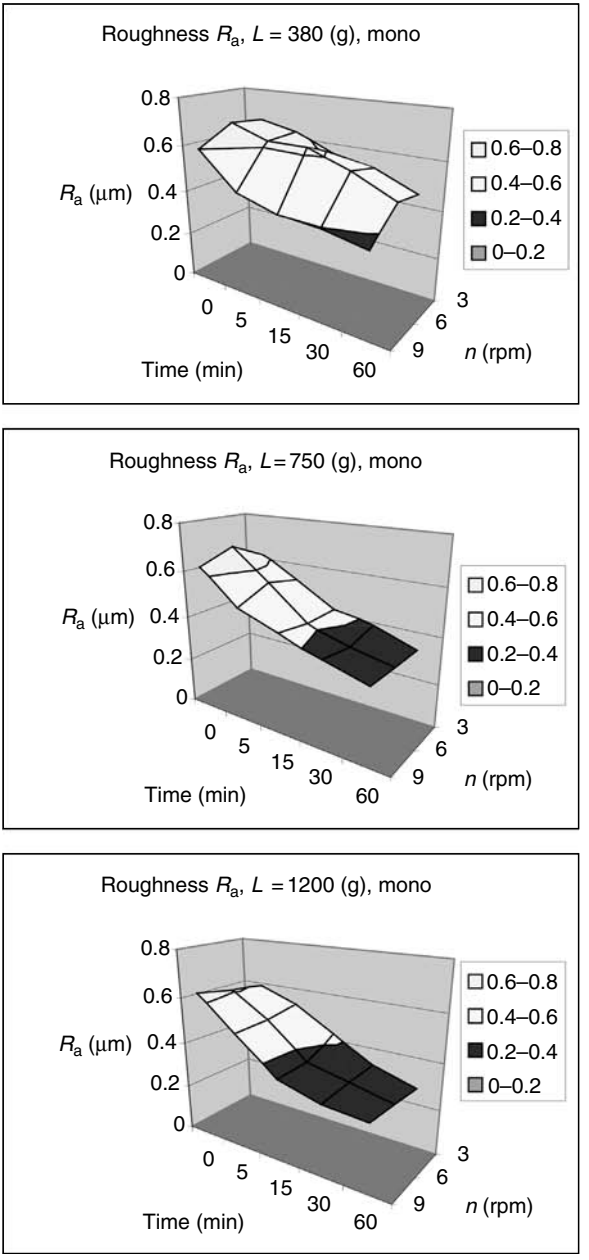


**FIGURE 4.59** Influence of time and speed on surface roughness $R_a$ for monocrystalline diamond slurry.

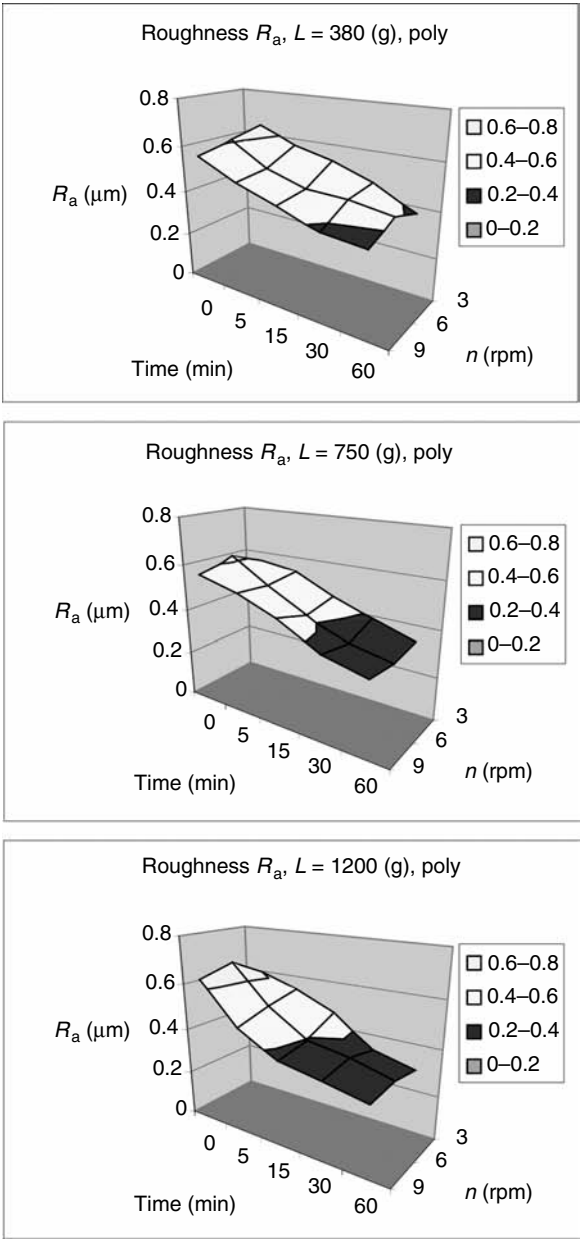


**FIGURE 4.60** Influence of time and speed on surface roughness $R_a$ for polycrystalline diamond slurry.

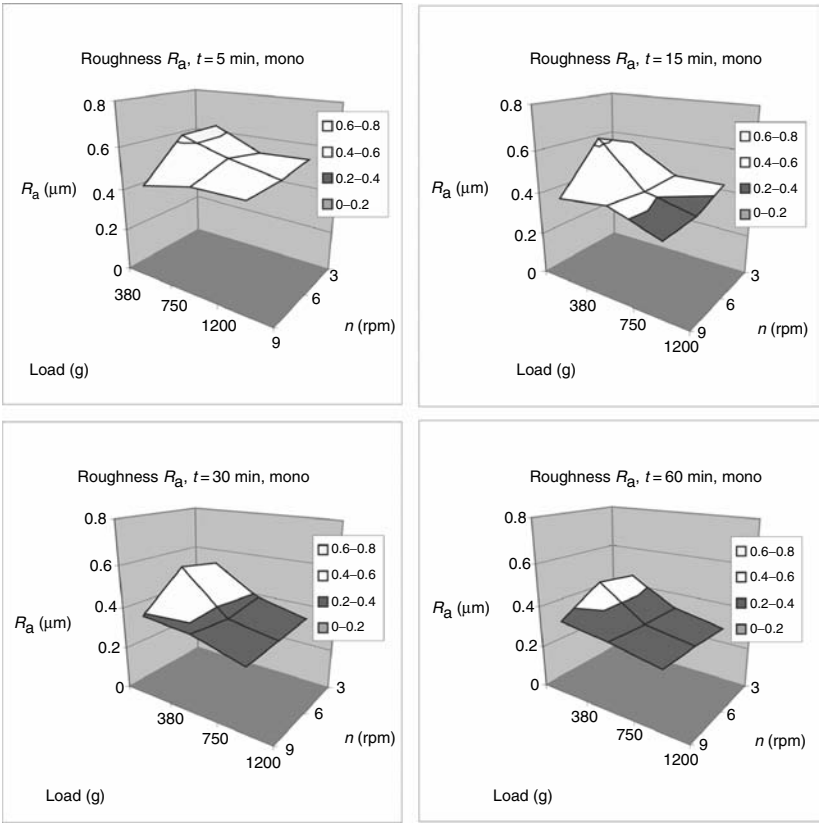


**FIGURE 4.61** Influence of load and speed on surface roughness $R_a$ for monocrystalline diamond slurry.

Figure 4.63 through Figure 4.68 illustrate MRR, which was calculated from workpiece thickness change. The above mentioned figures depict the influence of time, load, and lapping speed on material removal for both monocrystalline and polycrystalline diamond slurries. During the lapping operation, material removal is accomplished less aggressively (smaller MRRs) than when traditional machining processes are used.

MRR in the case of brittle materials is either based on brittle fracture or plastic deformation. Although the dominant tendency is for fracture of the ceramic material, it is agreed that a plastic material-removal mechanism can exist under certain conditions. The more brittle fracture, the rougher the finish. Plastic deformation mechanism generates better surface finish. MRRs decrease in time when using monocrystalline diamond as well as when using polycrystalline diamond slurry. This material-removal-descending trend is more accentuated in the first 15 min of lapping aluminum oxide

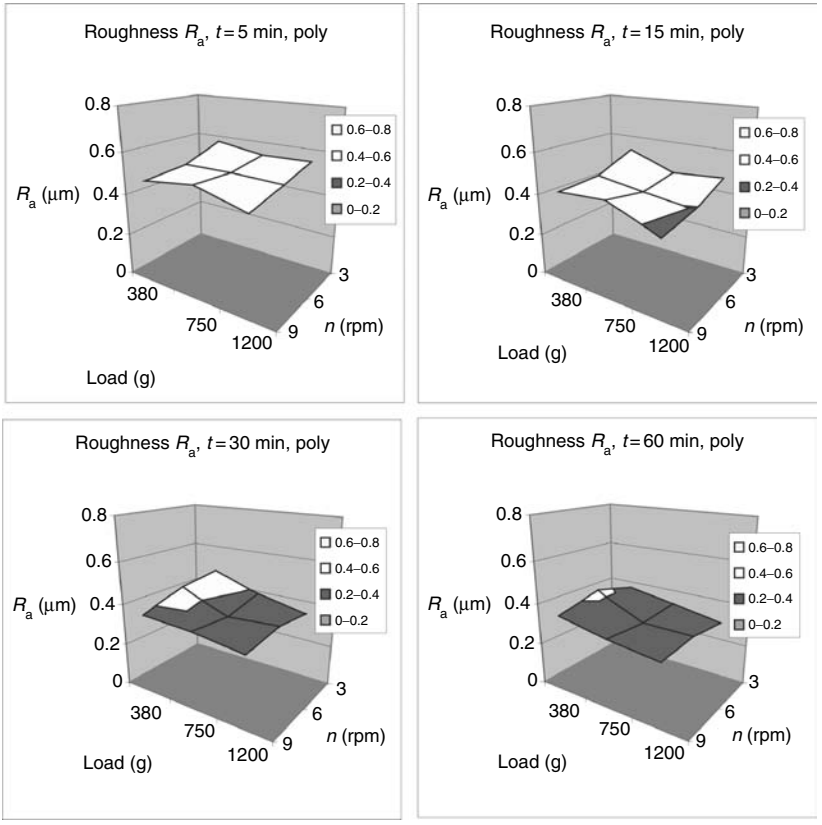


**FIGURE 4.62** Influence of load and speed on surface roughness $R_a$ for polycrystalline diamond slurry.

workpieces. This tendency is observed for higher loads and higher lapping speeds (rotations of the lapping plate). After 15 min of lapping, the removal rate tends to reach a plateau, meaning that the loads and also the speeds do not further affect much the process from this point of view.

The stock removal rate is higher with the increase in the lapping pressure and this phenomenon is more noticeable at the beginning of machining for both types of diamond used. It is considered that the mechanism of material-removal process changes from plastic deformation to brittle fracture with an increase in load. Many plastically deformed grooves were observed when lower load was used, whereas the brittle fracture became noticeable at higher loads. When time increases, the amount of material removed reduces and this could be explained by the fact that many diamond grains become blunt during machining; they lose their sharp edges and corners. Therefore, the abrading capacity of the diamond grains diminishes in time and the removal mechanism changes from brittle fracture to plastic deformation.

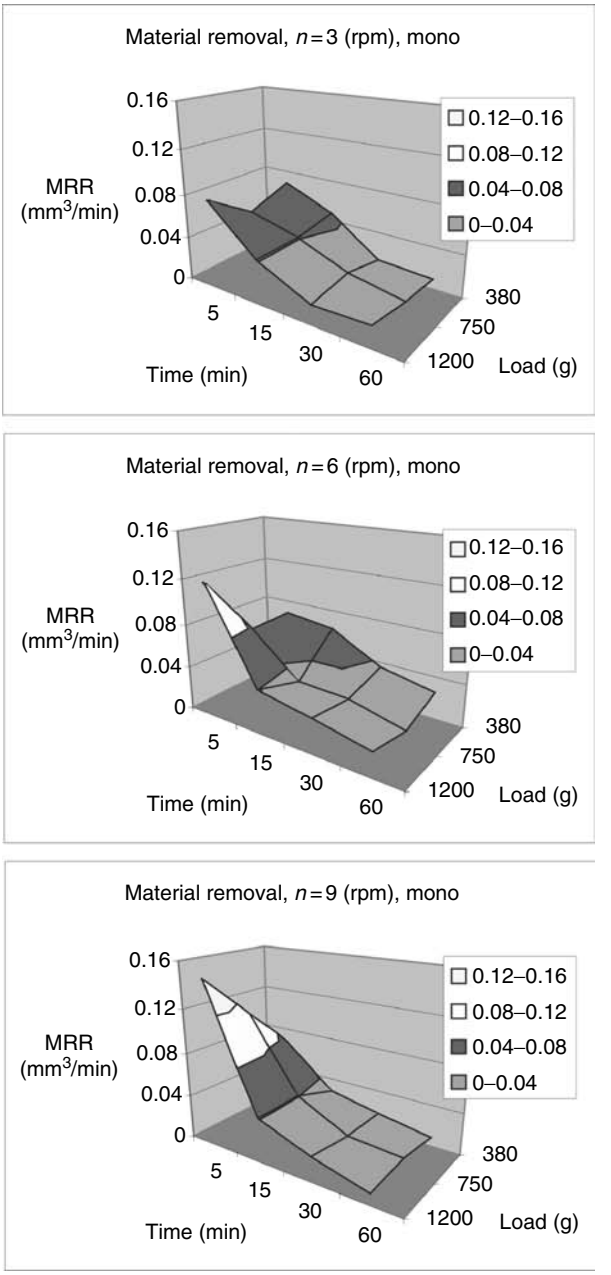


**FIGURE 4.63** Influence of time and load on material removal for monocrystalline diamond slurry.

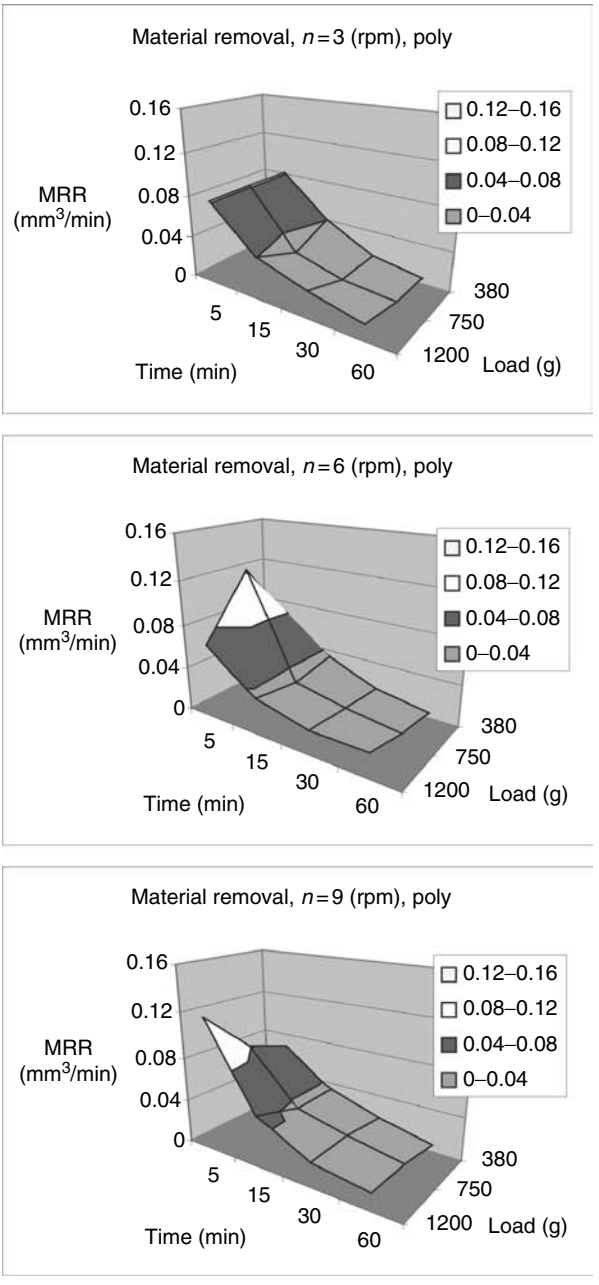


**FIGURE 4.64** Influence of time and load on material removal for polycrystalline diamond slurry.

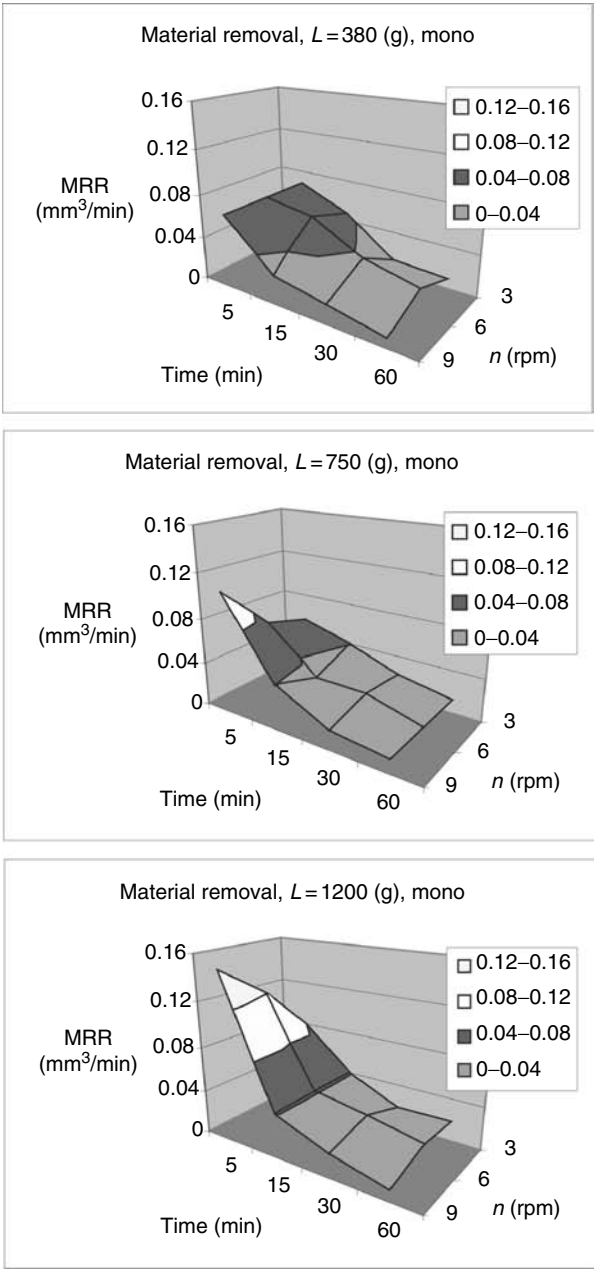


**FIGURE 4.65** Influence of time and speed on material removal for monocrystalline diamond slurry.

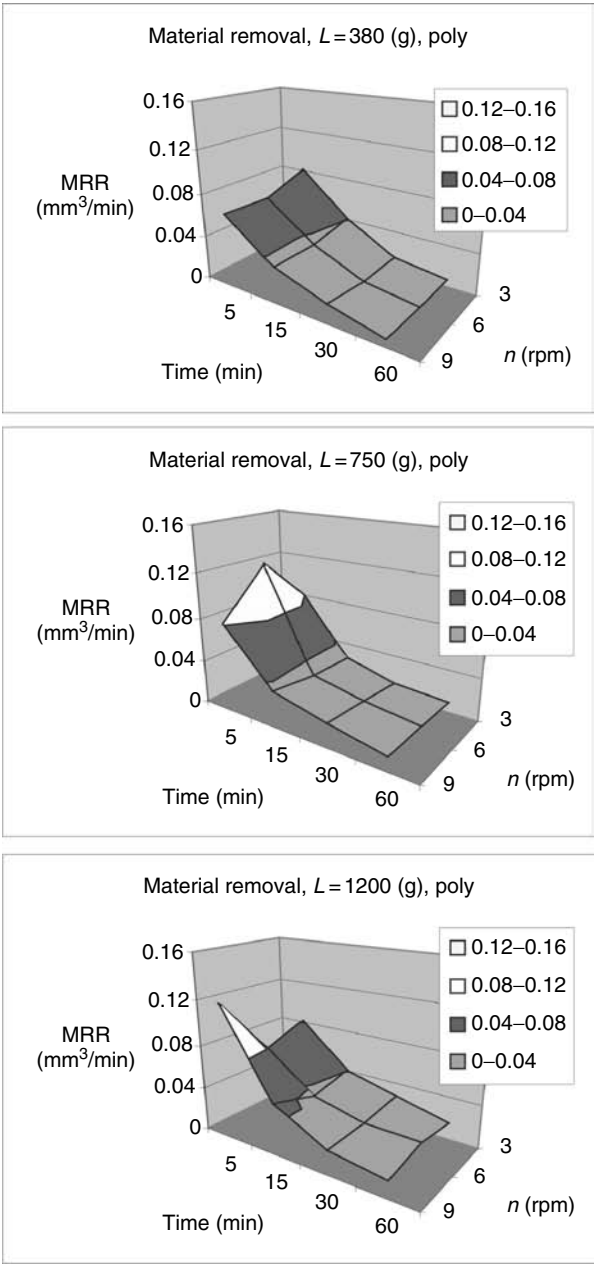


**FIGURE 4.66** Influence of time and speed on material removal for polycrystalline diamond slurry.

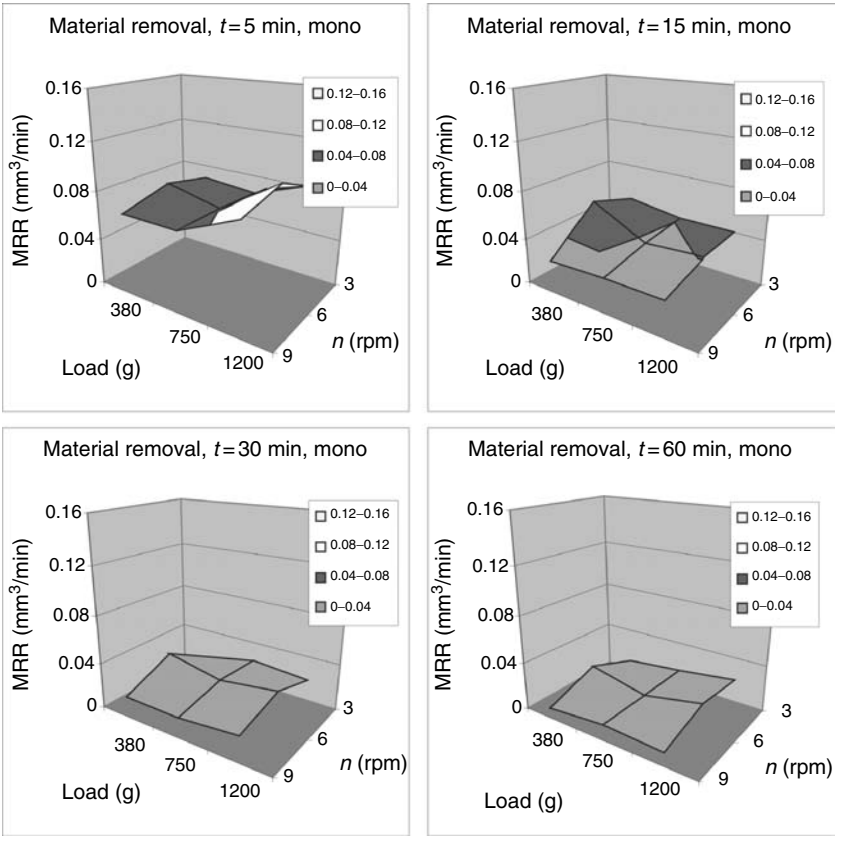


**FIGURE 4.67** Influence of load and speed on material removal for monocrystalline diamond slurry.

MRR decreases when rotation of the lapping plate increases at smaller loads. If higher weights are utilized, stock removal rate becomes higher when rotation of the lapping plate increases.

Figure 4.69a is a micrograph of the monocrystalline diamond powder. The shape of many grains is blocky with sharp edges and corners and this is different from the shape of polycrystalline diamond powder (Figure 4.69b, smoother edges without large flat surfaces).

The differences between the aspects of monocrystalline and polycrystalline diamond grains lead to different behavior while machining: it can clearly be seen from Figure 4.63 and Figure 4.64 that material removal is higher for monocrystalline diamond than for polycrystalline diamond grains. This could be due to the breakage of polycrystalline grains into much smaller particles than those resulted after the breakage of monocrystalline diamond. After

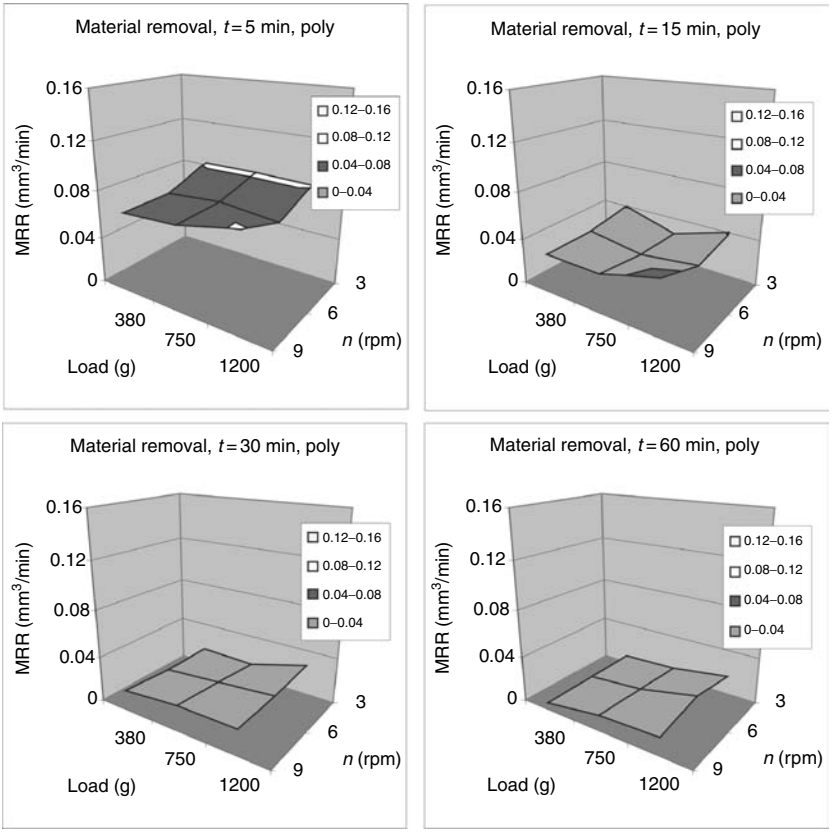


**FIGURE 4.68** Influence of load and speed on material removal for polycrystalline diamond slurry.

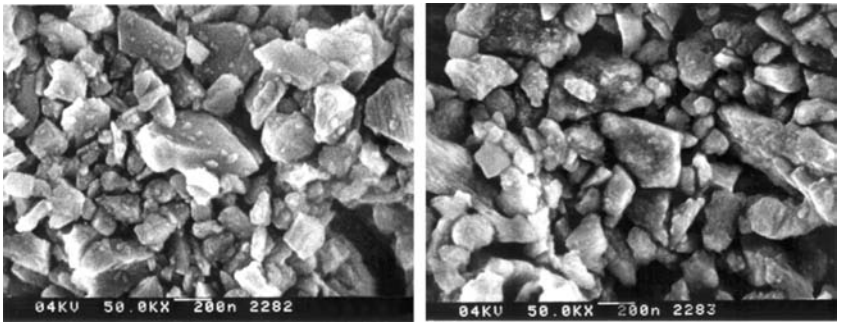


(a) (b)

**FIGURE 4.69** SEM micrograph of diamond grains: (a) monocrystalline and (b) polycrystalline. (Courtesy of Warren Diamond Powder Company.)

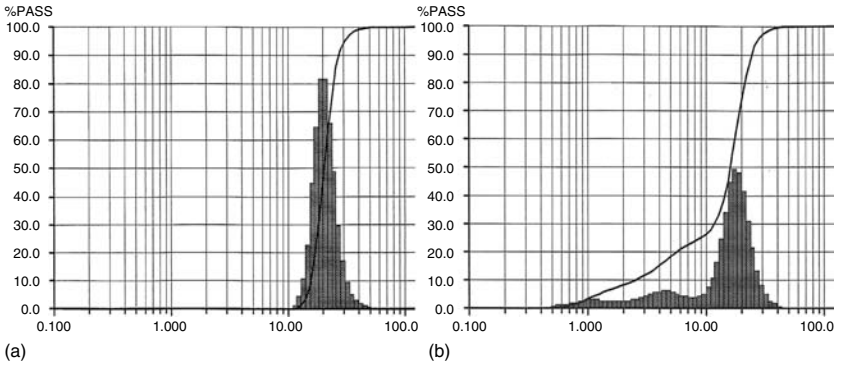


**FIGURE 4.70** Grain size distribution for 25 μm monocrystalline diamond: (a) before lapping and (b) after lapping. (Courtesy of Warren Diamond Powder Company.)

lapping, the number of larger grains is bigger for monocrystalline than for polycrystalline diamond. The different behavior of monocrystalline and polycrystalline diamond under the same load was investigated for diamond slurry of 25 μm size. The particle size distribution was measured before and after lapping under identical conditions. Figure 4.70 and Figure 4.71 prove the theoretical assumption that polycrystalline diamond is more friable than monocrystalline and breaks into smaller particles. This is beneficial for surface finishes since the abrasive grains resulting after breakage are smaller in size and have sharper corners and edges than the original grain. On the other hand, smaller grains cannot remove as much material as bigger ones. Therefore, the blocky structure of monocrystalline diamond, being responsible for its resistance to breakage, leads to higher removal rates and worse

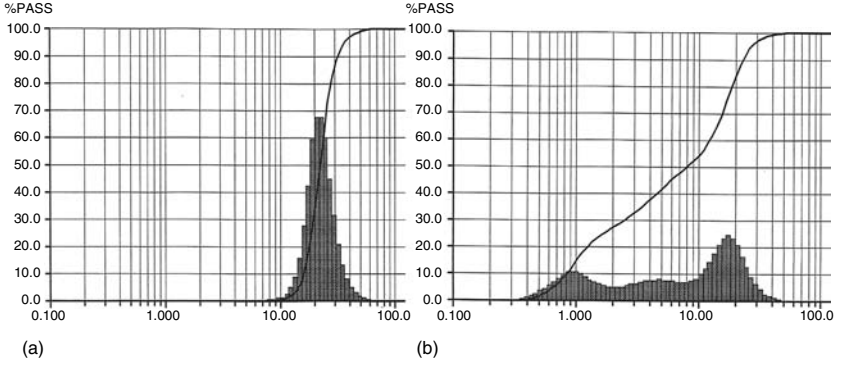


**FIGURE 4.71** Grain size distribution for 25 μm polycrystalline diamond: (a) before lapping and (b) after lapping. (Courtesy of Warren Diamond Powder Company.)

finish under high loads. This can explain why the MRR for the polycrystalline grains is lower than that for the monocrystalline diamond grains.

### 4.6.2 Test B

This set of lapping experiments was performed on workpieces made of hardened steel W-1 (62–64 HRC). The goal was to compare the behavior of mono-versus polycrystalline diamond slurry using different grain sizes and study the fracture of the diamond grains.

Table 4.12 and Table 4.13 present the experimental results for test B and Figure 4.72 through Figure 4.79 are graphical representations of the data.

**TABLE 4.12**
**Results for Monocrystalline Diamond (Test B)**

| Grain Size (μm) | Load (g) | Elapsed Time (min) | Roughness ($R_a$) (μm) | MRR ($mm^3$/min) |
|---|---|---|---|---|
| 0.75 | 91 | 5 | 0.268 | 0.1465 |
| | | 15 | 0.218 | 0.0628 |
| | | 30 | 0.189 | 0.0209 |
| | 364 | 5 | 0.233 | 0.1046 |
| | | 15 | 0.191 | 0.0523 |
| | | 30 | 0.188 | 0.2443 |
| | 1455 | 5 | 0.241 | 0.1884 |
| | | 15 | 0.187 | 0.1046 |
| | 5820 | 30 | 0.162 | 0.1256 |
| | | 5 | 0.148 | 0.7958 |
| | | 15 | 0.104 | 0.4083 |
| | | 30 | 0.104 | 0.1186 |
| | | 5 | 0.231 | 0.2093 |
| 1.5 | 91 | 15 | 0.214 | 0.0523 |
| | | 30 | 0.203 | 0.0209 |
| | 364 | 5 | 0.200 | 0.1465 |
| | | 15 | 0.159 | 0.0942 |
| | | 30 | 0.153 | 0.0837 |
| | 1455 | 5 | 0.242 | 0.1046 |
| | | 15 | 0.181 | 0.0628 |
| | | 30 | 0.150 | 0.0488 |
| | 5820 | 5 | 0.215 | 0.2094 |
| | | 15 | 0.102 | 0.2406 |
| | | 30 | 0.088 | 0.1325 |
| 3 | 91 | 5 | 0.410 | 0.0837 |
| | | 15 | 0.196 | 0.0628 |
| | | 30 | 0.0233 | 0.0348 |
| | 364 | 5 | 0.503 | 0.3141 |

**TABLE 4.12 (continued)**

| Grain Size (μm) | Load (g) | Elapsed Time (min) | Roughness ($R_a$) (μm) | MRR ($mm^3$/min) |
|---|---|---|---|---|
| | | 15 | 0.433 | 0.0732 |
| | | 30 | 0.401 | 0.0278 |
| | 1455 | 5 | 0.335 | 0.6701 |
| | | 15 | 0.183 | 0.1570 |
| | | 30 | 0.077 | 0.0418 |
| | 5820 | 5 | 0.171 | 0.5863 |
| | | 15 | 0.053 | 0.2722 |
| | | 30 | 0.069 | 0.0628 |
| 6 | 91 | 5 | 0.226 | 0.7120 |
| | | 15 | 0.103 | 0.2827 |
| | | 30 | 0.075 | 0.1465 |
| | 364 | 5 | 0.312 | 0.3979 |
| | | 15 | 0.155 | 0.1465 |
| | | 30 | 0.082 | 0.0628 |
| | 1455 | 5 | 0.233 | 0.3141 |
| | | 15 | 0.079 | 0.1570 |
| | | 30 | 0.066 | 0.2024 |
| | 5820 | 5 | 0.061 | 1.1728 |
| | | 15 | 0.052 | 0.5130 |
| | | 30 | 0.159 | 0.4956 |

**TABLE 4.13**
**Results for Polycrystalline Diamond (Test B)**

| Grain Size (μm) | Load (g) | Elapsed Time (min) | Roughness ($R_a$) (μm) | MRR ($mm^3$/min) |
|---|---|---|---|---|
| 0.75 | 91 | 5 | 0.503 | 0.2512 |
| | | 15 | 0.432 | 0.0628 |
| | | 30 | 0.378 | 0.0418 |
| | 364 | 5 | 0.418 | 0.2303 |
| | | 15 | 0.274 | 0.0314 |
| | | 30 | 0.202 | 0.0209 |
| | 1455 | 5 | 0.168 | 0.5025 |
| | | 15 | 0.090 | 0.1256 |
| | | 30 | 0.084 | 0.0837 |
| | | 5 | 0.149 | 0.0837 |
| | 5820 | 15 | 0.106 | 0.0628 |

*continued*

**TABLE 4.13 (continued)**

| Grain Size (μm) | Load (g) | Elapsed Time (min) | Roughness ($R_a$ (μm) | MRR ($mm^3$/min) |
|---|---|---|---|---|
| | | 30 | 0.098 | 1.0052 |
| 1.5 | 91 | 5 | 0.264 | 0.3141 |
| | | 15 | 0.196 | 0.0732 |
| | | 30 | 0.171 | 0.0348 |
| | 364 | 5 | 0.333 | 0.0837 |
| | | 15 | 0.310 | 0.0523 |
| | | 30 | 0.281 | 0.0278 |
| | 1455 | 5 | 0.203 | 0.2722 |
| | | 15 | 0.134 | 0.1151 |
| | | 30 | 0.154 | 0.0418 |
| | 5820 | 5 | 0.138 | 0.2512 |
| | | 15 | 0.112 | 0.1361 |
| | | 30 | 0.089 | 0.0557 |
| 3 | 91 | 5 | 0.547 | 1.2498 |
| | | 15 | 0.449 | 0.1675 |
| | | 30 | 0.328 | 0.0907 |
| | 364 | 5 | 0.540 | 0.2093 |
| | | 15 | 0.416 | 0.0314 |
| | | 30 | 0.272 | 0.0348 |
| | 1455 | 5 | 0.431 | 0.2512 |
| | | 15 | 0.437 | 0.0523 |
| | | 30 | 0.409 | 0.0348 |
| | 5820 | 5 | 0.150 | 0.3560 |
| | | 15 | 0.048 | 0.0732 |
| | | 30 | 0.088 | 0.0418 |
| 6 | 91 | 5 | 0.409 | 0.1046 |
| | | 15 | 0.348 | 0.1047 |
| | | 30 | 0.279 | 0.0627 |
| | 364 | 5 | 0.200 | 0.5654 |
| | | 15 | 0.173 | 0.1256 |
| | | 30 | 0.078 | 0.0627 |
| | 1455 | 5 | 0.162 | 0.6073 |
| | | 15 | 0.097 | 0.3141 |
| | | 30 | 0.084 | 0.1605 |
| | 5820 | 5 | 0.119 | 1.1518 |
| | | 15 | 0.086 | 0.6492 |
| | | 30 | 0.074 | 0.5863 |

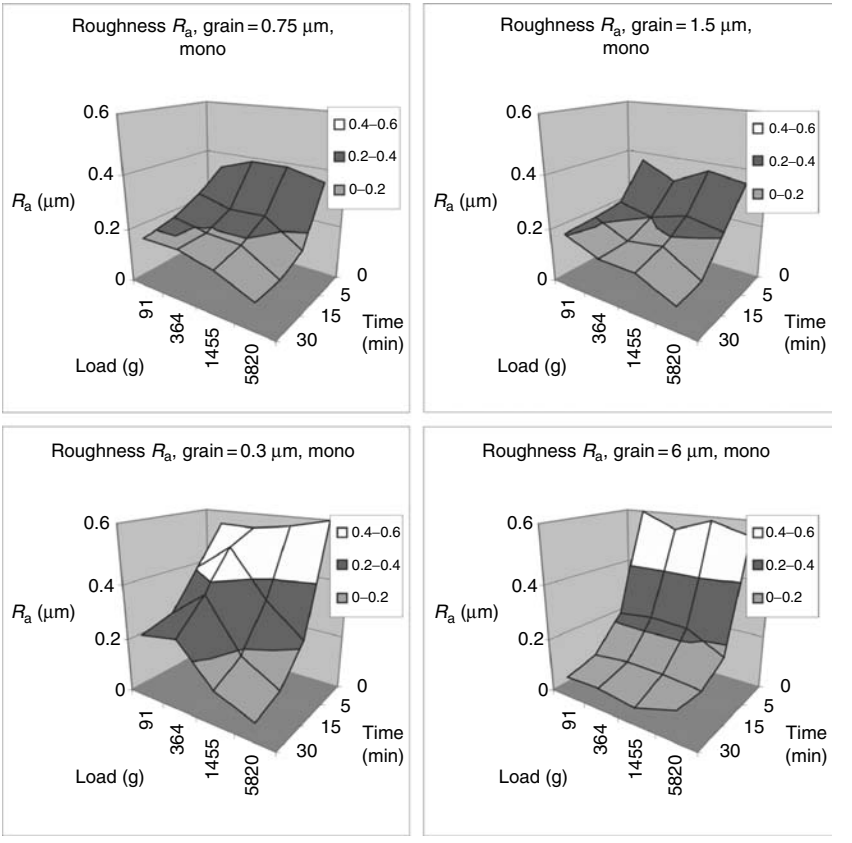


**FIGURE 4.72** Influence of load and time on surface roughness $R_a$ for monocrystalline diamond slurry.

From Figure 4.72 and Figure 4.73, it can be seen that surface roughness is more influenced by time than load for all diamond grain sizes used and for both monocrystalline and polycrystalline diamond slurries. As time increases, surface roughness is decreasing and this tendency is more accentuated at the beginning of machining. Surface finish improves significantly in the first 15 min of lapping from about 0.6 μm to values below 0.1 μm. No significant improvement in surface finish is obtained with longer lapping times: longer lapping times did not improve the surface of the workpiece. It can be concluded that lapping for 15–20 min using these grain sizes (0.75, 1.5, 3, and 6 μm) will considerably reduce the surface roughness.

Comparing the behavior of monocrystalline diamond versus polycrystalline diamond it can be concluded that, from surface roughness point of view, monocrystalline diamond generates comparable surface finish as polycrystalline diamond.

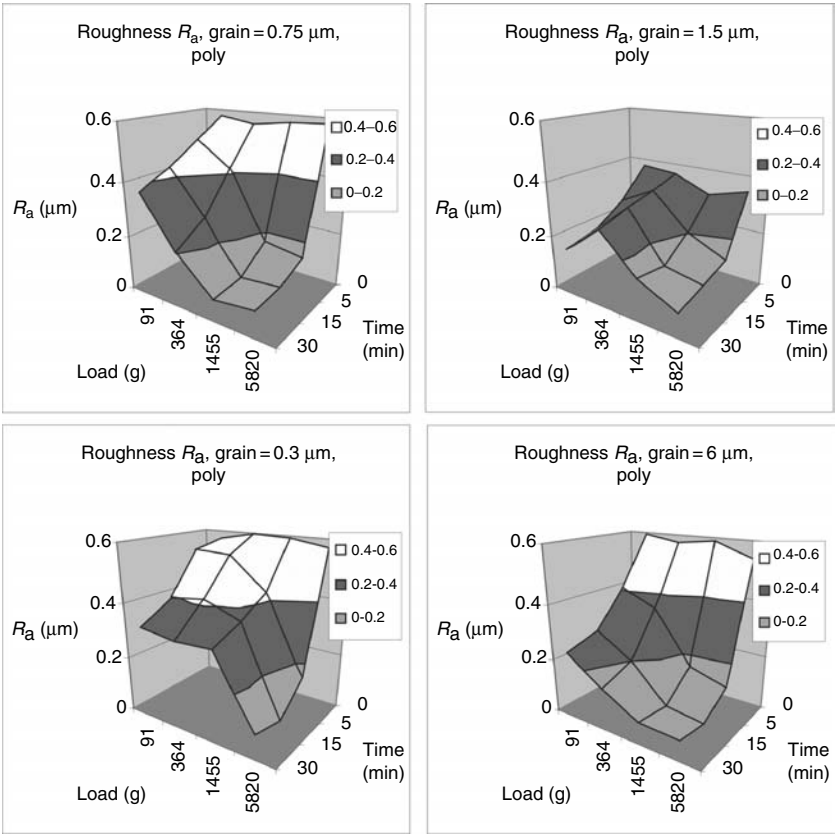


**FIGURE 4.73** Influence of load and time on surface roughness for polycrystalline diamond slurry.

This is due to different behavior of polycrystalline function of the grit size. Larger grits have a higher tendency to break under the same load than smaller ones. It seems that for the tested grit sizes, the load was not big enough to break neither monocrystalline nor polycrystalline structure. Therefore, both monocrystalline and polycrystalline structures behaved similarly from $R_a$ point of view, the surface finish being influenced only by the grit size in the sense that smaller grains generate better finish.

The load applied also influences the surface roughness. As load increases, surface finish improves for monocrystalline as well as for polycrystalline diamond.

The influence of grain size and time is depicted by Figure 4.74 and Figure 4.75. As mentioned before, surface roughness gets better in time and this process is faster at the beginning of lapping. Regarding the influence of grain

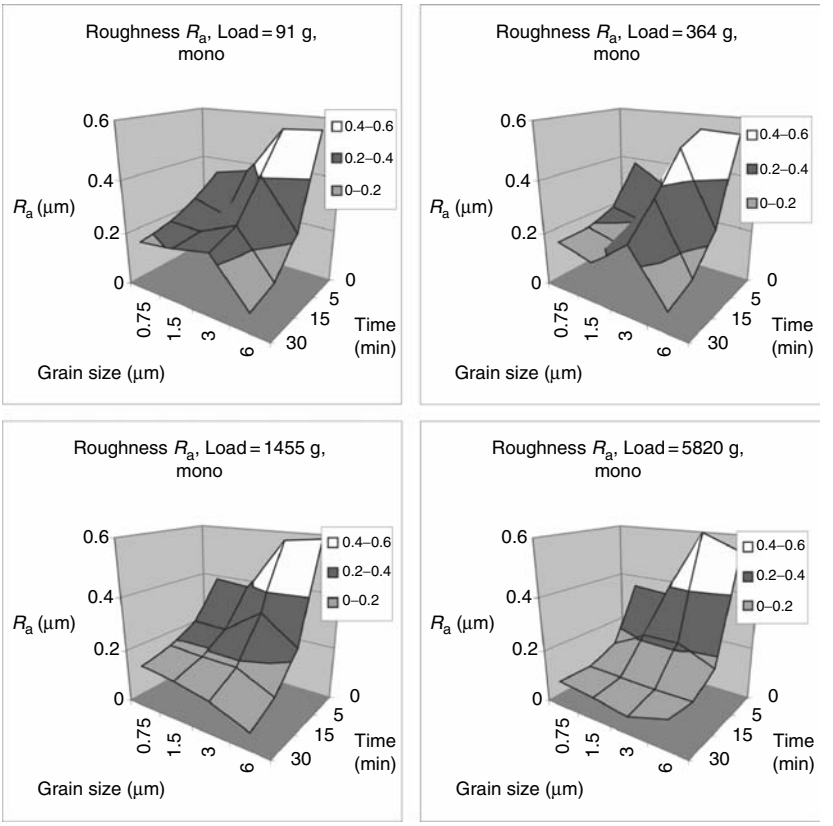


**FIGURE 4.74** Influence of grain size and time on surface roughness $R_a$ for monocrystalline diamond slurry.

sizes, they did not behave as assumed. Usually, the surface roughness improves with a decrease in abrasive size, if ideal conditions exist. In this test, better surface roughness was obtained for 0.75, 1.5, and 6 μm when monocrystalline diamond was used and surface roughness was improved for 1.5 and 6 μm when polycrystalline diamond was used.

Generally, lapping with 3 μm grain size did worsen the surface roughness especially at smaller loads, 91 and 364 g, and at the beginning of machining for monocrystalline diamond. When higher loads were applied, this tendency was not so obvious. While lapping with polycrystalline diamond slurry, the same behavior was noticed for all loads except the heaviest one, 5820 g. Material removal is graphically illustrated in Figure 4.76 through Figure 4.79. Figure 4.76 and Figure 4.77 show the influence of load and time on stock removal for monocrystalline and polycrystalline diamonds. As a general tendency, MRR decreases in time for both types of diamond. This trend is less visible for 0.75

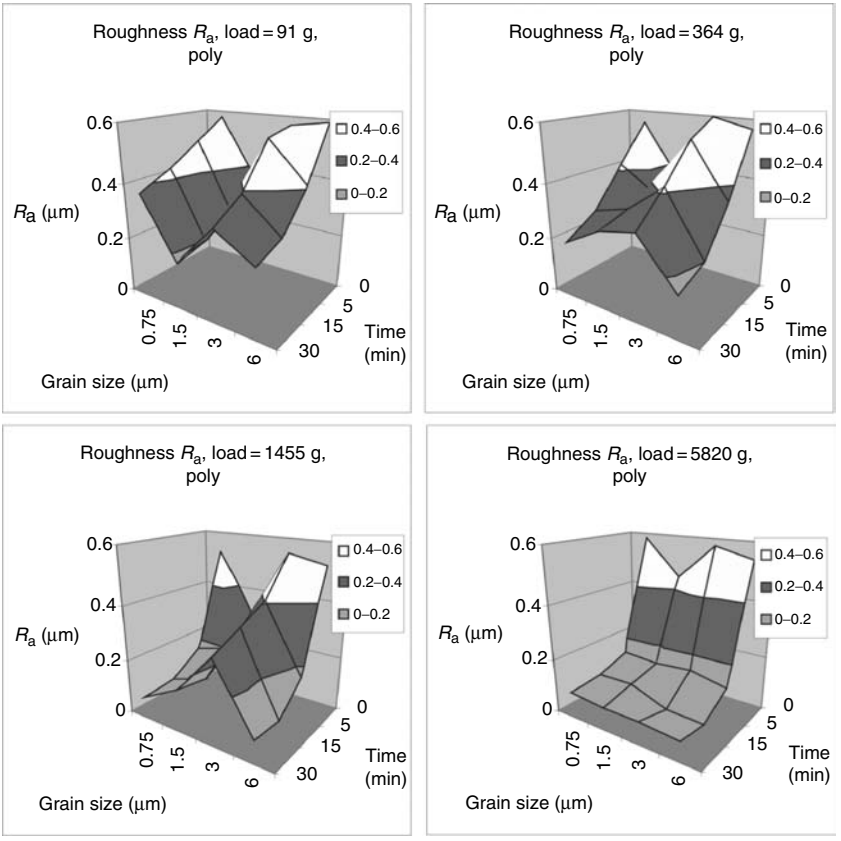


**FIGURE 4.75** Influence of grain size and time on surface roughness $R_a$ for polycrystalline diamond slurry.

μm grain size but is very observable for all the other grain sizes when monocrystalline diamond is used. The behavior of polycrystalline diamond in time is the same: MRR diminishes in time. Regarding the influence of load on MRR, it can be said that MRR increases with increasing load. With increasing load, the bed thickness (defined as the distance between the workpiece and the lapping plate) decreases. Bed thickness depends on the particle size and on the particle degradation behavior. Two effects are probably involved. Firstly, at higher loads more particles fracture during abrasion, this means that they remain sharp. Secondly, at higher loads the penetration depth of the abrasive grains increases.

Figure 4.78 and Figure 4.79 represent the influence of grain size and time on MRR. As discussed earlier, MRR decreases in time for both monocrystalline and polycrystalline diamonds and is higher for larger grain sizes.

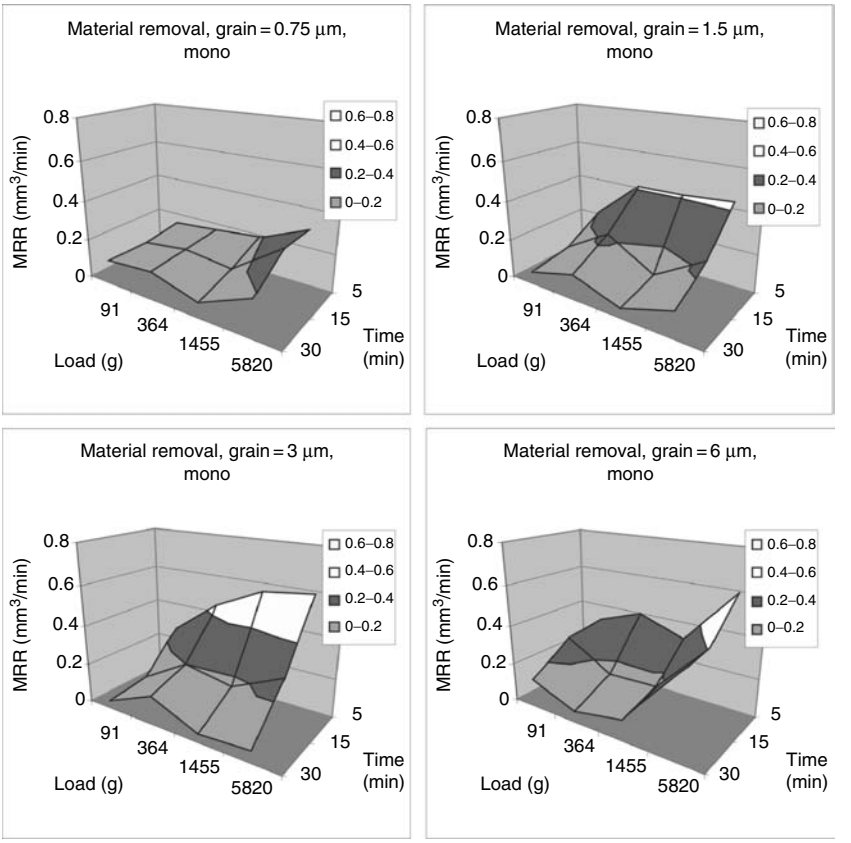


**FIGURE 4.76** Influence of load and time on material removal for monocrystalline diamond slurry.

### 4.6.3 Summary of Test A and Test B

As a general conclusion, one can say that the polycrystalline diamond is generating better surface finish than monocrystalline diamond. This is due to its greater friability resulting from the manufacturing process. This leads to the recommendation to use polycrystalline diamond for good surface finish and monocrystalline diamond for high MRR. The friability of polycrystalline diamond is directly dependent on the load applied and, therefore, load is a lapping parameter that can be used to control the behavior of the diamond grains according to the primary goal of the operation.

Both surface roughness and MRR decrease in time and this trend is more noticeable at the beginning of machining. A lapping cycle of approximately 20–30 min is long enough to obtain very good surface finish and have a high

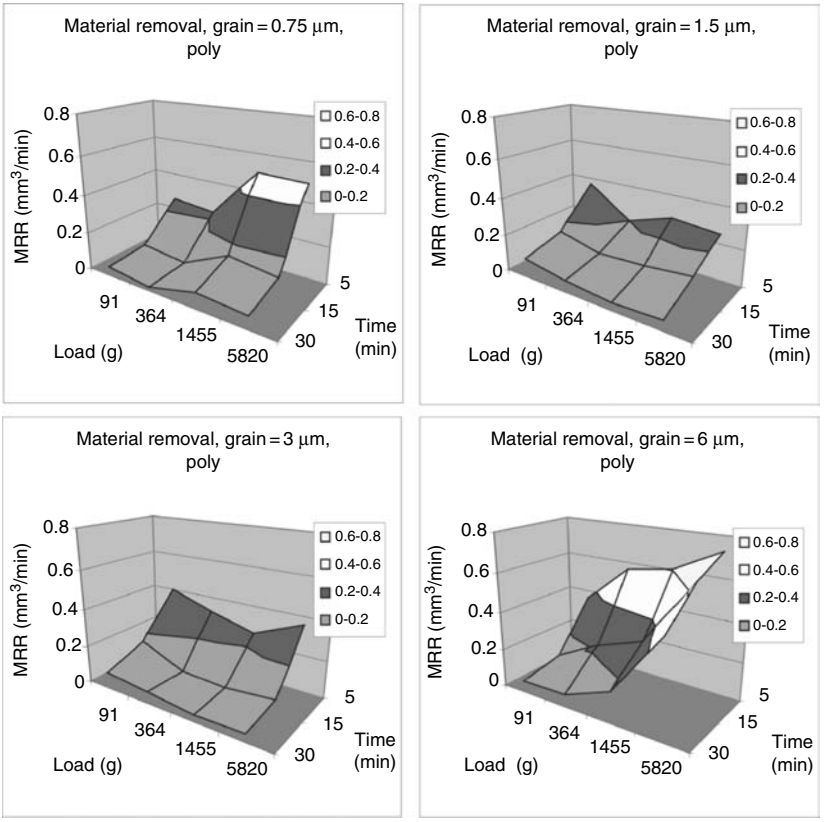


**FIGURE 4.77** Influence of load and time on material removal for polycrystalline diamond slurry.

MRR for workpieces made of aluminum oxide and hardened steel W-1. The rotation of the lapping plate (lapping speed) does not influence much the surface roughness when the range considered (3, 6, and 9 rpm) is small.

Regarding the influence of grain size on the output parameters of lapping process, it can be said that they did not behave as expected. The performance of small grain sizes is according to the theory: the smaller the grain size, the smaller the surface roughness. Bigger grain sizes showed unpredictable behavior: in the case of 6 μm grain size the surface finish noticeably improved.

### 4.6.4 Test C

Using the design of experiment (DOE) method is a typical approach to identify characteristics of any complex process by experiment. The lapping experiments are efficiently designed and performed by using the DOE concept. The DOE can be considered as a tool for screening unimportant

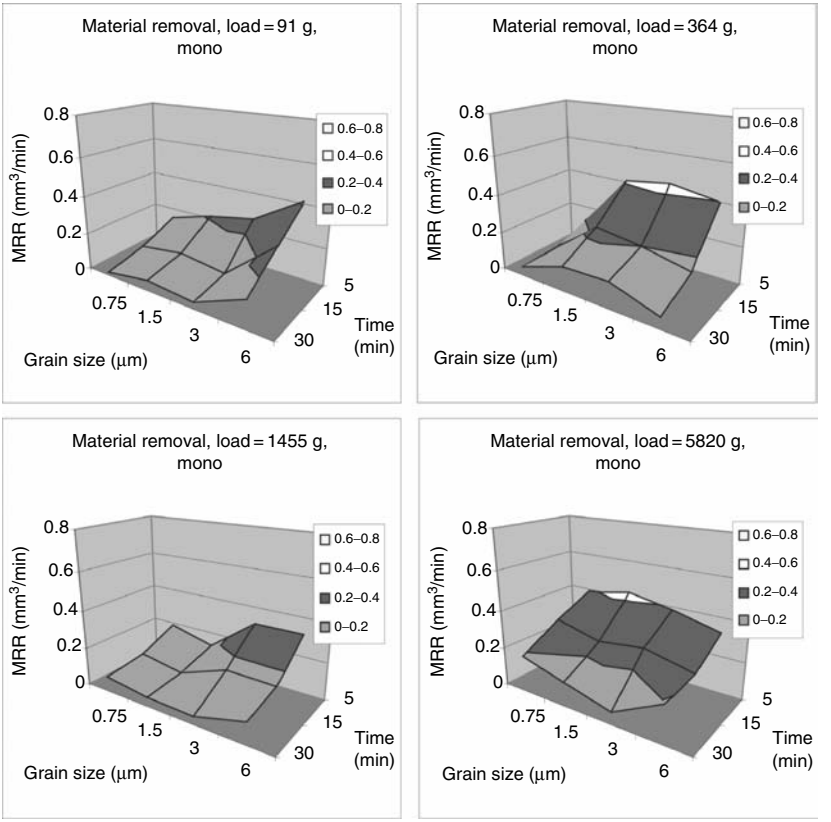


**FIGURE 4.78** Influence of grain size and time on material removal for monocrystalline diamond slurry.

variables and thus reducing time and labor. The number of experiments to be performed, if full factorial experiments are chosen, is more than 2000, which consumes a lot of time, workpiece materials, diamond slurry, etc. Therefore, fractional factorial experimental method was used in order to reduce the number of experiments to 324.

In order to find out what variables have an effect on the process performance, Yates computing method of sum of squares (ss) for ANOVA in factorial designs was used. Yates suggested a product design method that uses signal-to-noise ratio (*S*/*N* ratio). Percentage improvement of surface roughness before and after lapping is taken as one response variable whereas the percentage of change in MRR is taken as second evaluation. Here the lapping performances of both composite copper and composite iron lapping plates are individually studied and compared to each other with the help of this statistic approach.

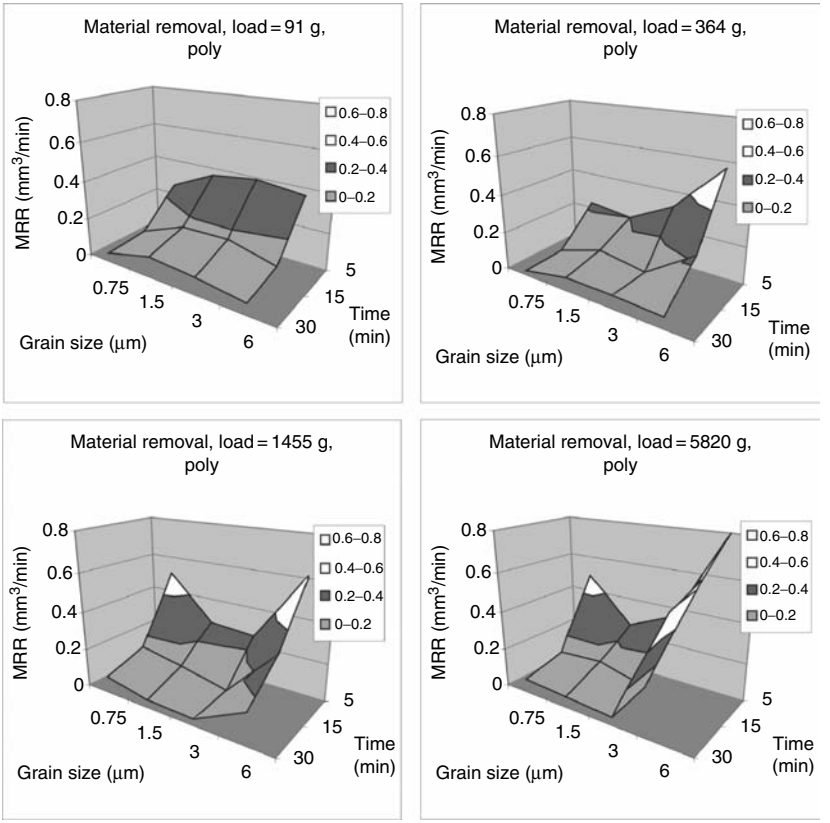


**FIGURE 4.79** Influence of grain size and time on material removal for polycrystalline diamond slurry.

The main factors that are considered important in performing experiments are workpiece material, lapping speed, and pressure applied. The other factors like the grain size, the type of carrier, and the type of lapping plate material are regarded as the blocked parameters.

### 4.6.4.1 Fractional Factorial Experiment

In Table 4.14 the input parameters, the blocked parameters, and the output parameters with their respective type, levels, and values are presented. In order to obtain a one-half fraction of the 23 design having the highest possible resolution, which is 2III 3–1 = 22, the runs were partitioned into two different blocks with the highest-order interaction $ABC$ confounded ($L = x_1 + x_2 + x_3$). $I = ABC$ as generator was employed because it will output a design having the highest resolution (III). It resulted in a 23–1 III experiment having 3 factors, 4 runs, and 3 replicates. The confounding is presented in Table 4.15.

**TABLE 4.14**
**Treatment Combination**

| Treatment Combination | *L* |
|---|---|
| (1) | 0 |
| a | 1 |
| b | 1 |
| ab | 0 |
| c | 1 |
| ac | 0 |
| bc | 0 |
| abc | 1 |

The set of aliases and their determination procedure are presented below:

$$I = ABC$$
$$A = A * I = A * ABC = A2BC = BC$$
$$B = B * I = B * ABC = AB2C = AC$$
$$C = C * I = C * ABC = ABC2 = AB$$

**TABLE 4.15**
**The Experimental Factors and Their Level**

| Parameter | Notation | Levels | Values | | | Type | Obs. |
|---|---|---|---|---|---|---|---|
| | | | Input Parameters | | | | |
| Experiments | e | 21 | | 84 | | | 4 within each block |
| Replicates | r | 3 | 1 | 2 | 3 | Qual. | |
| Piece mat. | a | 2 | W1 | | SiC | Qual. | |
| Load | b | 2 | 3 | | 5 | Quantit. | [psi] |
| Speed | c | 2 | 30 | | 60 | Quantit. | [rpm] |
| | | | Blocked Parameters | | | | |
| Slurry type | p | 2 | WB | | OB | Qual. | |
| Grain size | q | 3 | 1 | 3 | 15 | Quantit. | [microns] |
| Plate mat. | s | 2 | Iron | | Cooper | Qual. | |
| Time | t | 7 | 1 2 3 5 10 15 30 | | | Quantit. | [minutes] |
| | | | Output Parameters | | | | |
| Surface finish | $R_a$ | | | | | Quantit. | [μm] |
| Material removal rate | MRR | | | | | Quantit. | [cu.in./min] |

**TABLE 4.16**
**23–1 Design**

| Factors | | | |
|---|---|---|---|
| ***A*** | ***B*** | ***C* = *AB*** | **Treatment Combination** |
| − | − | + | c |
| + | − | − | a |
| − | + | − | b |
| + | + | + | abc |

The 23–1 design is based on 22 basic designs and the third factor $C$ given by the product of the first two factors: $C = AB$. The new design is synthesized in Table 4.16.

Within each four-run experiment, the sequence of experiments was completely randomized as presented in Table 4.17 and in Table 4.18. They were 21 one-half-fraction-23-design experiments completed for different values of blocked (fixed) parameters.

The experimental values of surface roughness $R_a$ and MRR for both copper plate and iron plate are shown in Appendix A. From the experimental values, graphs can be drawn for the different combination of speeds, pressures, and type of carrier for all grain sizes and for both lapping plates. A MATLAB program, shown in Appendix B, was written to compute the values of $R_a$ and MRR separately for all the sets and the graphs drawn were analyzed individually. The effect of lapping speed, pressure, and the type of workpiece material was studied and compared for both lapping plates. Using Yates algorithm and ANOVA, the effect of the main factors is studied on the overall lapping performance.

Table 4.19 to Table 4.30 depict the steps of ANOVA analysis for both copper and iron lapping plates and for both surface roughness $R_a$ and MRR. (Table 4.19 to 4.21 illustrates ANOVA calculations for $R_a$ when copper plate was used, Table 4.22 to 4.24 for $R_a$ iron plate, Table 4.25 to 4.27 for MRR copper plate, and Table 4.28 to 4.30 for MRR iron plate.) From the tables, the values $y_1$–$y_7$, are percentage improvements of $R_a$ and MRR, respectively, and $y(\%)$ is the averaged value of 7. *S*/*N* Ratio is Taguchi's response statistic. The use of log-type response variables in this analysis is to reduce the inequality of variance between treatments and thus satisfy the basic assumption, equal variance.

The percentage improvement of surface roughness is the main response variable and, therefore, *S*/*N* ratios are calculated for the case of "Bigger is Better" and the equations used are as follows:

$$Y_i = (\Delta R_a / R_a) \times 100$$

**TABLE 4.17**
**Randomized Sequences of Experiments for Copper Plate**

| | | | Material | W1 | SiC | W1 | SiC |
|---|---|---|---|---|---|---|---|
| | | | **Load** | **3** | | | **5** |
| Copper plate | 1 μm | WB | **Lapping Speed** | **60** | **30** | **30** | **60** |
| | | | 1 | 4 | 3 | 2 | 1 |
| | | | 2 | 2 | 1 | 4 | 3 |
| | | | 3 | 4 | 2 | 3 | 1 |
| | | | 5 | 3 | 2 | 1 | 4 |
| | | | 10 | 1 | 4 | 2 | 3 |
| | | | 15 | 3 | 4 | 1 | 2 |
| | | | 30 | 2 | 1 | 4 | 3 |
| | | | 1 | 1 | 4 | 3 | 2 |
| | | | 2 | 1 | 2 | 3 | 4 |
| | | | 3 | 1 | 3 | 2 | 4 |
| | | OB | 5 | 1 | 2 | 3 | 4 |
| | | | 10 | 1 | 3 | 2 | 4 |
| | | | 15 | 2 | 4 | 1 | 3 |
| | | | 30 | 1 | 2 | 4 | 3 |
| | | | 1 | 4 | 1 | 3 | 2 |
| | | | 2 | 2 | 3 | 1 | 4 |
| | | | 3 | 2 | 4 | 3 | 1 |
| | 3 μm | WB | 5 | 4 | 3 | 1 | 2 |
| | | | 10 | 1 | 4 | 2 | 3 |
| | | | 15 | 3 | 4 | 1 | 2 |
| | | | 30 | 2 | 1 | 4 | 3 |
| | | | 1 | 4 | 3 | 1 | 2 |
| | | | 2 | 4 | 3 | 1 | 2 |
| | | | 3 | 1 | 3 | 2 | 4 |
| | | OB | 5 | 2 | 4 | 1 | 3 |
| | | | 10 | 4 | 3 | 2 | 1 |
| | | | 15 | 4 | 3 | 1 | 2 |
| | | | 30 | 2 | 3 | 4 | 1 |
| | | | 1 | 1 | 3 | 2 | 4 |
| | | | 2 | 4 | 1 | 3 | 2 |
| | | | 3 | 3 | 2 | 1 | 4 |
| | 15 μm | WB | 5 | 4 | 2 | 3 | 1 |
| | | | 10 | 3 | 1 | 2 | 4 |
| | | | 15 | 2 | 3 | 4 | 1 |
| | | | 30 | 3 | 1 | 2 | 4 |
| | | | 1 | 3 | 1 | 4 | 2 |
| | | | 2 | 3 | 4 | 1 | 2 |
| | | | 3 | 1 | 3 | 2 | 4 |
| | | OB | 5 | 1 | 4 | 2 | 3 |
| | | | 10 | 4 | 3 | 2 | 1 |
| | | | 15 | 4 | 1 | 3 | 2 |
| | | | 30 | 4 | 2 | 1 | 3 |

**TABLE 4.18**
**Randomized Sequences of Experiments for Iron Plate**

| | | | Material | W1 | SiC | W1 | SiC |
|---|---|---|---|---|---|---|---|
| | | | Load | 3 | | 5 | |
| | | | Lapping Speed | 60 | 30 | 30 | 60 |
| Iron plate | 1 μm | WB | 1 | 1 | 2 | 4 | 3 |
| | | | 2 | 1 | 4 | 3 | 2 |
| | | | 3 | 3 | 1 | 4 | 2 |
| | | | 5 | 3 | 1 | 2 | 4 |
| | | | 10 | 1 | 4 | 3 | 2 |
| | | OB | 15 | 3 | 1 | 2 | 4 |
| | | | 30 | 3 | 2 | 1 | 4 |
| | | | 1 | 2 | 4 | 1 | 3 |
| | | | 2 | 4 | 1 | 3 | 2 |
| | | | 2 | 4 | 1 | 3 | 2 |
| | | | 3 | 3 | 2 | 4 | 1 |
| | 3 μm | WB | 5 | 1 | 4 | 2 | 3 |
| | | | 10 | 2 | 1 | 3 | 4 |
| | | | 15 | 4 | 2 | 1 | 3 |
| | | | 30 | 1 | 3 | 2 | 4 |
| | | | 1 | 3 | 4 | 2 | 1 |
| | | | 2 | 2 | 4 | 3 | 1 |
| | | | 3 | 1 | 2 | 4 | 3 |
| | | OB | 5 | 2 | 4 | 1 | 3 |
| | | | 10 | 1 | 2 | 4 | 3 |
| | | | 15 | 3 | 4 | 1 | 2 |
| | | | 30 | 4 | 1 | 3 | 2 |
| | | | 1 | 4 | 2 | 1 | 3 |
| | | | 2 | 1 | 2 | 4 | 3 |
| | | | 3 | 4 | 2 | 1 | 3 |
| | 15 μm | WB | 5 | 4 | 3 | 2 | 1 |
| | | | 10 | 1 | 4 | 2 | 3 |
| | | | 15 | 2 | 1 | 4 | 3 |
| | | | 30 | 2 | 3 | 4 | 1 |
| | | | 1 | 2 | 4 | 3 | 1 |
| | | | 2 | 2 | 1 | 4 | 3 |
| | | | 3 | 2 | 1 | 4 | 3 |
| | | OB | 5 | 4 | 3 | 2 | 1 |
| | | | 10 | 3 | 4 | 2 | 1 |
| | | | 15 | 3 | 4 | 1 | 2 |
| | | | 30 | 1 | 4 | 2 | 3 |
| | | | 1 | 2 | 3 | 1 | 4 |
| | | | 2 | 1 | 4 | 3 | 2 |
| | | | 3 | 3 | 1 | 2 | 4 |
| | | | 5 | 2 | 1 | 3 | 4 |
| | | | 10 | 3 | 1 | 2 | 4 |
| | | | 15 | 1 | 4 | 3 | 2 |
| | | | 30 | 3 | 4 | 2 | 1 |

**TABLE 4.19**
**$R_a$ – Copper Plate (Experimental Result)**

| tc | y1 | y2 | y3 | y4 | y5 | y6 | y7 | y(%) | S/N |
|---|---|---|---|---|---|---|---|---|---|
| **1** | 94.203017 | 48.047059 | 2.8985507 | 9.7014925 | 13.84297521 | 8.1534772 | 15.013055 | 27.408518 | 16.550657 |
| **a** | 29.137691 | 3.4733441 | 11.046025 | 2.7281279 | 3.094777563 | 4.0918164 | 18.418314 | 10.2843 | 12.499234 |
| **b** | 94.27485 | 58.79608 | 5.3907135 | 2.4070492 | 1.993704092 | 5.4603854 | 7.587769 | 25.130079 | 11.37614 |
| **c = ab** | 112.3054 | 47.41336 | 2.0057307 | 1.8726592 | 5.438931298 | 1.0090817 | 4.4955045 | 24.93438 | 6.4108108 |
| **c** | 112.3054 | 47.41336 | 2.0057307 | 1.8726592 | 5.438931298 | 1.0090817 | 4.4955045 | 24.93438 | 6.4108108 |
| **b = ac** | 94.27485 | 58.79608 | 5.3907135 | 2.4070492 | 1.993704092 | 5.4603854 | 7.587769 | 25.130079 | 11.37614 |
| **a = bc** | 29.137691 | 3.4733441 | 11.046025 | 2.7281279 | 3.094777563 | 4.0918164 | 18.418314 | 10.2843 | 12.499234 |
| **(1) = abc** | 94.203017 | 48.047059 | 2.8985507 | 9.7014925 | 13.84297521 | 8.1534772 | 15.013055 | 27.408518 | 16.550657 |

**TABLE 4.20**
**$R_a$ – Copper Plate (Computing Procedure of YATES' Algorithm)**

| | | Sum of Effects | | | | |
|---|---|---|---|---|---|---|
| **tc** | **Data (S/N-ratio)** | **I** | **II** | **III** | **SS** | **Mean Effect** |
| **1** | 16.550657 | 29.049892 | 46.836842 | 93.67368399 | 1096.8449 | 11.70921 |
| **a** | 12.499234 | 17.78695 | 46.836842 | 0 | 0 | 0 |
| **b** | 11.37614 | 17.78695 | −9.0167521 | 0 | 0 | 0 |
| **c = ab** | 6.4108108 | 29.049892 | 9.0167521 | −1.82781106 | 0.4176117 | −0.4569528 |
| **c** | 6.4108108 | −4.0514233 | −11.262941 | 0 | 0 | 0 |
| **b = ac** | 11.37614 | −4.9653288 | 11.262941 | 18.03350422 | 40.650909 | 4.5083761 |
| **a = bc** | 12.499234 | 4.9653288 | −0.9139055 | 22.52588223 | 63.426921 | 5.6314706 |
| **(1) = abc** | 16.550657 | 4.0514233 | −0.9139055 | 0 | 0 | 0 |

**TABLE 4.21**
**$R_a$ – Copper Plate (ANOVA Table by YATES Algorithm)**

| tc | SS | %SST | Mean Effect | Measures | df | MS | Fo | F0.05 | F0.001 | Significance |
|---|---|---|---|---|---|---|---|---|---|---|
| **1** | 1096.8449 | | 11.70921 | average | | | | | | |
| **a** | 0 | 0 | 0 | A | 1 | 0 | 0 | | | |
| **b** | 0 | 0 | 0 | B | 1 | 0 | 0 | | | |
| **c = ab** | 0.4176117 | 0.3996458 | −0.4569528 | AB = C | 1 | 0.4176117 | 5.99 | 5.99 | 35.51 | Significant |
| **c** | 0 | 0 | 0 | C | 1 | 0 | 0 | | | |
| **b = ac** | 40.650909 | 38.902088 | 4.5083761 | AC = B | 1 | 40.650909 | 584.04848 | 5.99 | 35.51 | Not |
| **a = bc** | 63.426921 | 60.698266 | 5.6314706 | BC = A | 1 | 63.426921 | 911.28089 | 5.99 | 35.51 | Not |
| **(1) = abc** | 0 | 0 | 0 | ABC | 1 | 0 | 0 | | | |
| **Error** | 0.4176117 | | | | 6 | 0.0696019 | | | | |
| **Total** | 104.49544 | 100 | | | 7 | | | | | |

**TABLE 4.22**
**$R_a$ – Iron Plate (Experimental Result)**

| tc | y1 | y2 | y3 | y4 | y5 | y6 | y7 | y(%) | S/N |
|---|---|---|---|---|---|---|---|---|---|
| **1** | 94.469716 | 41.206189 | 4.9677766 | 2.1474993 | 7.883338146 | 8.369906 | 14.665895 | 24.81576 | 13.781216 |
| **a** | 47.916667 | 2.5065648 | 1.0528893 | 1.5540708 | 2.310054096 | 4.1905712 | 5.7797449 | 9.3300802 | 6.0206345 |
| **b** | 95.602265 | 19.926874 | 12.328767 | 8.3333333 | 8.143939394 | 3.6769759 | 6.9937024 | 22.143694 | 17.20943 |
| **c = ab** | 42.355908 | 5.2431803 | 5.0492907 | 6.0268422 | 3.233629749 | 0.3132341 | 2.1733438 | 9.199347 | −1.8033439 |
| **c** | 42.355908 | 5.2431803 | 5.0492907 | 6.0268422 | 3.233629749 | 0.3132341 | 2.1733438 | 9.199347 | −1.8033439 |
| **b = ac** | 95.602265 | 19.926874 | 12.328767 | 8.3333333 | 8.143939394 | 3.6769759 | 6.9937024 | 22.143694 | 17.20943 |
| **a = bc** | 47.916667 | 2.5065648 | 1.0528893 | 1.5540708 | 2.310054096 | 4.1905712 | 5.7797449 | 9.3300802 | 6.0206345 |
| **(1) = abc** | 94.469716 | 41.206189 | 4.9677766 | 2.1474993 | 7.883338146 | 8.369906 | 14.665895 | 24.81576 | 13.781216 |

**TABLE 4.23**
**$R_a$ – Iron Plate (Computing Procedure of YATES' Algorithm)**

| | | Sum of Effects | | | | |
|---|---|---|---|---|---|---|
| **tc** | **Data (S/N-ratio)** | **I** | **II** | **III** | **SS** | **Mean Effect** |
| **1** | 13.781216 | 19.80185 | 35.207936 | 70.41587218 | 619.79938 | 8.801984 |
| **a** | 6.0206345 | 15.406086 | 35.207936 | 0 | 0 | 0 |
| **b** | 17.20943 | 15.406086 | −26.773355 | 0 | 0 | 0 |
| **c = ab** | −1.8033439 | 19.80185 | 26.773355 | −22.50438392 | 63.305912 | −5.626096 |
| **c** | −1.8033439 | −7.7605814 | −4.3957647 | 0 | 0 | 0 |
| **b = ac** | 17.20943 | −19.012773 | 4.3957647 | 53.54670967 | 358.40626 | 13.386677 |
| **a = bc** | 6.0206345 | 19.012773 | −11.252192 | 8.791529419 | 9.6613737 | 2.1978824 |
| **(1) = abc** | 13.781216 | 7.7605814 | −11.252192 | 0 | 0 | 0 |

**TABLE 4.24**
**$R_a$ – Iron Plate (ANOVA Table by YATES Algorithm)**

| tc | SS | %SST | Mean Effect | Measures | df | MS | Fo | F0.05 | F0.001 | Significance |
|---|---|---|---|---|---|---|---|---|---|---|
| **1** | 619.79938 | | 8.801984 | average | | | | | | |
| **a** | 0 | 0 | 0 | A | 1 | 0 | 0 | | | |
| **b** | 0 | 0 | 0 | B | 1 | 0 | 0 | | | |
| **c = ab** | 63.305912 | 14.675427 | −5.626096 | AB = C | 1 | 63.305912 | 39.314851 | 5.99 | 35.51 | Not |
| **c** | 0 | 0 | 0 | C | 1 | 0 | 0 | | | |
| **b = ac** | 358.40626 | 83.084896 | 13.386677 | AC = B | 1 | 358.40626 | 222.58093 | 5.99 | 35.51 | Not |
| **a = bc** | 9.6613737 | 2.2396769 | 2.1978824 | BC = A | 1 | 9.6613737 | 6 | 5.99 | 35.51 | Significant |
| **(1) = abc** | 0 | 0 | 0 | ABC | 1 | 0 | 0 | | | |
| **Error** | 9.6613737 | | | | 6 | 1.6102289 | | | | |
| **Total** | 431.37355 | | | | 7 | | | | | |

**TABLE 4.25**
**MRR – Copper Plate (Experimental Result)**

| tc | y1 | y2 | y3 | y4 | y5 | y6 | y7 | y(%) | S/N |
|---|---|---|---|---|---|---|---|---|---|
| **1** | 25.982801 | 0.4702628 | 26.288546 | 1.4791573 | 0.955414013 | 11.529628 | 11.117635 | 25.982801 | −23.98648142 |
| **a** | 18.765743 | 18.06292 | 2.7782571 | 9.5846645 | 29.72124068 | 31.075419 | 18.331374 | 18.765743 | −26.41315518 |
| **b** | 6.6889632 | 16.427718 | 8.849178 | 27.935382 | 0.364497904 | 14.47249 | 12.456371 | 6.6889632 | −23.62636854 |
| **c = ab** | 20.83947 | 13.020516 | 5.2695902 | 13.060848 | 12.53289344 | 8.6079928 | 12.221885 | 20.83947 | −22.36093097 |
| **c** | 20.83947 | 13.020516 | 5.2695902 | 13.060848 | 12.53289344 | 8.6079928 | 12.221885 | 20.83947 | −22.36093097 |
| **b = ac** | 6.6889632 | 16.427718 | 8.849178 | 27.935382 | 0.364497904 | 14.47249 | 12.456371 | 6.6889632 | −23.62636854 |
| **a = bc** | 18.765743 | 18.06292 | 2.7782571 | 9.5846645 | 29.72124068 | 31.075419 | 18.331374 | 18.765743 | −26.41315518 |
| **(1) = abc** | 25.982801 | 0.4702628 | 26.288546 | 1.4791573 | 0.955414013 | 11.529628 | 11.117635 | 25.982801 | −23.98648142 |

**TABLE 4.26**
**MRR – Copper Plate (Computing Procedure of YATES' Algorithm)**

| | | Sum of Effects | | | | |
|---|---|---|---|---|---|---|
| **tc** | **Data (S/N-ratio)** | **I** | **II** | **III** | **SS** | **Mean Effect** |
| **1** | −23.986481 | −50.399637 | −96.386936 | −192.7738722 | 4645.2207 | −24.096734 |
| **a** | −26.413155 | −45.9873 | −96.386936 | 0 | 0 | 0 |
| **b** | −23.626369 | −45.9873 | −1.1612362 | 0 | 0 | 0 |
| **c = ab** | −22.360931 | − 50.399637 | 1.1612362 | 7.384222668 | 6.8158431 | 1.8460557 |
| **c** | −22.360931 | −2.4266738 | 4.4123371 | 0 | 0 | 0 |
| **b = ac** | −23.626369 | 1.2654376 | −4.4123371 | 2.322472387 | 0.6742347 | 0.5806181 |
| **a = bc** | −26.413155 | −1.2654376 | 3.6921113 | − 8.824674188 | 9.7343593 | −2.2061685 |
| **(1) = abc** | −23.986481 | 2.4266738 | 3.6921113 | 0 | 0 | 0 |

**TABLE 4.27**
**MRR – Copper Plate (ANOVA Table by YATES Algorithm)**

| tc | SS | %SST | Mean Effect | Measures | df | MS | Fo | F0.05 | F0.001 | Significance |
|---|---|---|---|---|---|---|---|---|---|---|
| | 4645.2207 | | −24.096734 | Average | 1 | — | | | | |
| **1** | 0 | 0 | 0 | A | 1 | 0 | 0 | | | |
| **a** | 0 | 0 | 0 | B | 1 | 0 | 0 | | | |
| **b** | 6.8158431 | 39.570774 | 1.8460557 | AB = C | 1 | 1.8460557 | 16.428008 | 5.99 | 35.51 | NOT |
| **c = ab** | 0 | 0 | 0 | C | 1 | 0 | 0 | | | |
| **c** | 0.6742347 | 3.914408 | 0.5806181 | AC = B | 1 | 0.5806181 | 5.1669075 | 5.99 | 35.51 | SIG |
| **b = ac** | 9.7343593 | 56.514818 | −2.2061685 | BC = A | 1 | −2.2061685 | −19.632645 | 5.99 | 35.51 | SIG |
| **a = bc** | 0 | 0 | 0 | ABC | 1 | 0 | 0 | | | |
| **(1) = abc** | 4645.2207 | | −24.096734 | Average | 1 | — | | | | |
| **Error** | 0.6742347 | | | | **6** | **0.112372** | | | | |
| **Total** | 17.224437 | | | | **7** | | | | | |

**TABLE 4.28**
**MRR – Iron Plate (Experimental Result)**

| tc | y1 | y2 | y3 | y4 | y5 | y6 | y7 | y(%) | S/N |
|---|---|---|---|---|---|---|---|---|---|
| **1** | 15.492958 | 15.808081 | 15.812837 | 0.7695596 | 16.4898883 | 14.470787 | 13.140685 | 15.492958 | −23.08879194 |
| **a** | 42.307692 | 18.177001 | 4.2869955 | 21.904025 | 10.582535 | 15.431034 | 18.781547 | 42.307692 | −26.94402727 |
| **b** | 21.577381 | 4.9968374 | 12.07723 | 16.924125 | 0.99352839 | 15.49639 | 12.010915 | 21.577381 | −22.87787725 |
| **c = ab** | 14.146023 | 52.332001 | 31.017246 | 18.978261 | 1.82452375 | 28.013118 | 24.385195 | 14.146023 | −29.25058927 |
| **c** | 14.146023 | 52.332001 | 31.017246 | 18.978261 | 1.82452375 | 28.013118 | 24.385195 | 14.146023 | −29.25058927 |
| **b = ac** | 21.577381 | 4.9968374 | 12.07723 | 16.924125 | 0.99352839 | 15.49639 | 12.010915 | 21.577381 | −22.87787725 |
| **a = bc** | 42.307692 | 18.177001 | 4.2869955 | 21.904025 | 10.582535 | 15.431034 | 18.781547 | 42.307692 | −26.94402727 |
| **(1) = abc** | 15.492958 | 15.808081 | 15.812837 | 0.7695596 | 16.4898883 | 14.470787 | 13.140685 | 15.492958 | −23.08879194 |

**TABLE 4.29**
**MRR – Iron Plate (Computing Procedure of YATES' Algorithm)**

| | | Sum of Effects | | | | |
|---|---|---|---|---|---|---|
| **tc** | **Data (S/N-Ratio)** | **I** | **II** | **III** | **SS** | **Mean Effect** |
| **1** | −23.088792 | −50.032819 | −102.16129 | − 204.322571 | 5218.4642 | −25.540321 |
| **a** | −26.944027 | −52.128467 | −102.16129 | 0 | 0 | 0 |
| **b** | −22.877877 | −52.128467 | −10.227947 | 0 | 0 | 0 |
| **c = ab** | −29.250589 | −50.032819 | 10.227947 | −5.0349534 | 3.1688445 | −1.2587383 |
| **c** | −29.250589 | −3.8552353 | −2.0956473 | 0 | 0 | 0 |
| **b = ac** | −22.877877 | − 6.372712 | 2.0956473 | 20.4558947 | 52.305453 | 5.1139737 |
| **a = bc** | −26.944027 | 6.372712 | −2.5174767 | − 4.61312401 | 2.6601141 | −1.153281 |
| **(1) = abc** | −23.088792 | 3.8552353 | −2.5174767 | 0 | 0 | 0 |

**TABLE 4.30**
**MRR – Iron Plate (ANOVA Table by YATES Algorithm)**

| tc | SS | %SST | Mean Effect | Measures | df | MS | Fo | F0.05 | F0.001 | Significance |
|---|---|---|---|---|---|---|---|---|---|---|
| **1** | 5218.4642 | | −25.540321 | Average | | | | | | |
| **a** | 0 | 0 | 0 | A | 1 | 0 | 0 | | | |
| **b** | 0 | 0 | 0 | B | 1 | 0 | 0 | | | |
| **c = ab** | 3.1688445 | 5.4508928 | −1.2587383 | AB | 1 | −1.2587383 | 2.8391376 | 5.99 | 35.51 | SIG |
| **c** | 0 | 0 | 0 | C | 1 | 0 | 0 | | | |
| **b = ac** | 52.305453 | 89.973308 | 5.1139737 | AC = B | 1 | 5.1139737 | 11.534784 | 5.99 | 35.51 | Not |
| **a = bc** | 2.6601141 | 4.5757995 | −1.153281 | BC = A | 1 | −1.153281 | 2.6012741 | 5.99 | 35.51 | SIG |
| **(1) = abc** | 0 | 0 | 0 | 1 | 0 | 0 | | | | |
| **Error** | 2.6601141 | | | | 6 | 0.4433524 | | | | |
| **Total** | 58.134412 | 100 | | | 7 | | | | | |

where $\Delta R_a = (R_a$ before lapping$-R_a$ after lapping) and represents improvement of surface roughness.

$$y = (y_1 + y_2 + y_3 + y_4 + y_5 + y_6 + y_7)/7$$
$$s^2 = \Sigma(y_i y)^2/(n-1)$$
$$S/N = -10\log(1/n\Sigma(1/y_i^2))$$

The second table (computing procedure of Yates algorithm) shows the method of Yates algorithm used to obtain the mean effect of each variable and this is the result of Nelson's BASIC program. The first column is generated using the data ($S/N$) ratio column by the rule that the first four entries are created by adding adjacent pairwise sets of data from the response variable column, and the other four entries by subtracting adjacent pairwise sets. The second and the third columns are generated by applying the same rule, column II from column I and column III from column II. The SS and mean effects for each treatment are calculated from the following equations:

$$\text{SS} = (\text{III})/8$$

Mean effect = (III)/4, for treatments (III)/8, for overall average.
Mean effects can also be computed by subtracting the mean value of four experimental data at low level from those at high level. The table of ANOVA is constructed using SS and mean effects as shown in the tables. The error term is generated by the 5% pooling rule: the SS values of treatment combinations that are less than 5% of the total SS are pooled into error. The same procedure is applied for surface roughness and MRR.

The following set of graphs (Figure 4.80 through Figure 4.82) shows the normality of the data, the normality of the residuals, residuals versus expected values, data versus workpiece material, load and speed, and the influence of these three parameters on surface roughness. These nine graphs were drawn only for one set of experiments but they illustrate the general trend of all sets of experiments.

From the previous graphical representations of the data, it can be said that the experiment was correctly conducted. The normal probability plot of data and the normal probability plot of the residuals (Figure 4.80) show that there is a reasonably linear pattern of the data. There are two points that can be suspected as outliers but, since only the extremely located data are away from the normal, one can conclude that the extreme values of roughness parameter were measured with large errors. This might be due to workpiece material pressure speed.

Figure 4.81 illustrates that the experiment was consistent and this can be drawn as a general conclusion. Regarding the influence of the parameters on

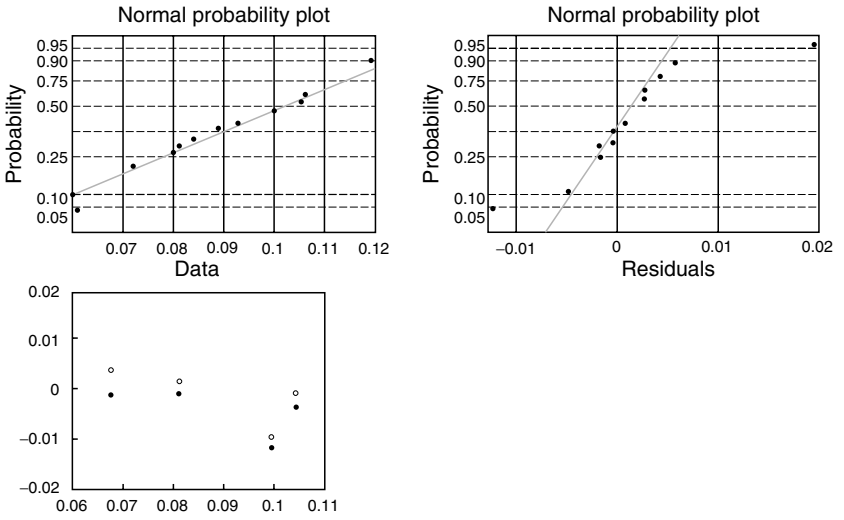


**FIGURE 4.80** Normality of the data, normality of the residuals, and residuals versus expected values.

surface roughness, taking into consideration all graphs for all sets of experiments the following conclusions can be drawn:

- From the graphs drawn for the individual sets for both types of lapping plates (copper and iron), it is observed that the data generally follow a trend line.
- Analyzing the copper plate from the surface roughness point of view, it is observed that for all grain sizes used OB (oil-based) slurry was better

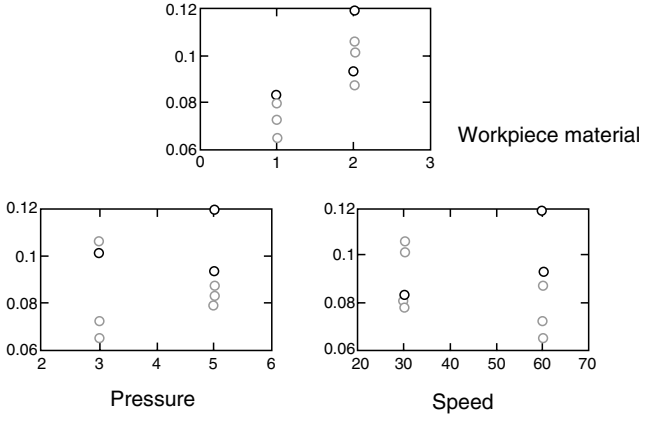


**FIGURE 4.81** Data versus workpiece material, pressure and speed.

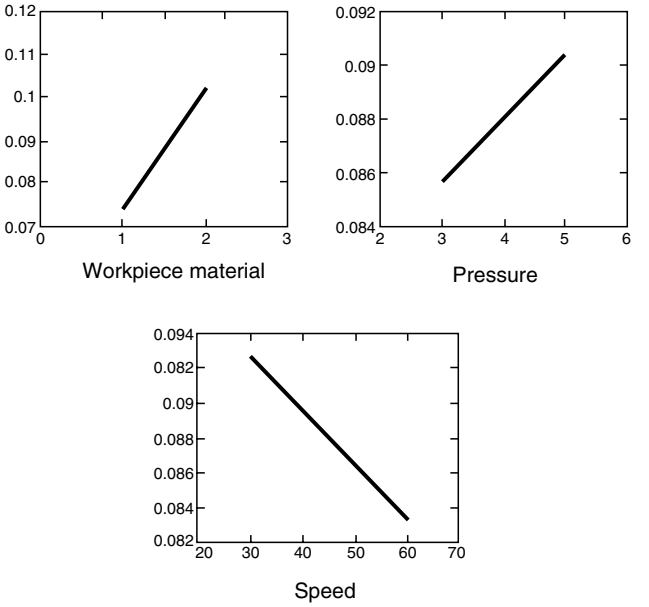


**FIGURE 4.82** Influence of workpiece material, pressure, and speed on surface roughness $R_a$.

for W-1 parts, 5 psi, and 60 rpm and WB (water-based) slurry was better for SiC parts, 3 psi, and 30 rpm.

- Investigating the iron plate from the surface roughness point of view, the general tendency is: OB slurry better for W-1 parts, 5 psi, and 60 rpm and WB slurry is better for W-1 parts, 3 psi, and 30 rpm.
- Studying the copper plate from the MRR point of view, it can be said that WB slurry is better (higher MRR) for SiC parts, 5 psi, and 60 rpm and OB is best for W-1 parts, 5 psi, and 30 rpm.
- Evaluating the iron plate from the MRR point of view, it is evident that WB slurry is good for SiC parts, 5 psi, and 60 rpm and OB slurry is best for W-1 parts, 5 psi, and 60 rpm.

From the ANOVA analysis (Table 4.19 to Table 4.30) the following general conclusions can be drawn:

– When lapping using iron lapping plate, the workpiece material is the most significant factor of the process from the surface roughness point of view. In the ranges considered, pressure and speed do not influence the lapping performance.
– When lapping with copper plate, speed is the most significant factor that influences the surface roughness. The other two factors do not contribute much in improving the surface roughness.

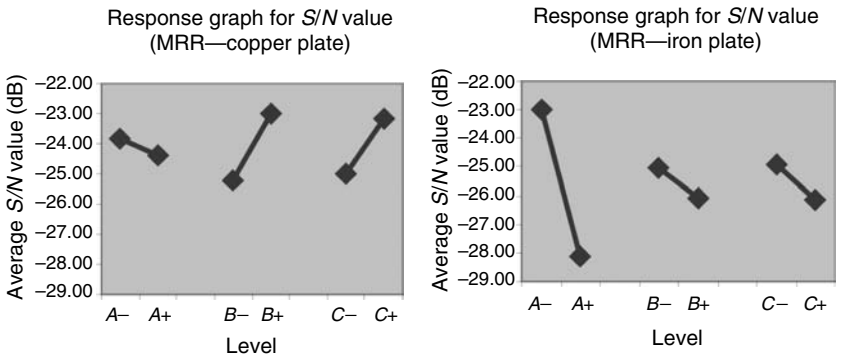


**FIGURE 4.83** Optimal combination of factors (MRR).

– From the MRR point of view, workpiece material is the most significant factor for both lapping plates used; the other two factors (pressure and speed) are not significant. In order to have good conclusions for these parameters one needs to extend their range of values.

Mean values of the *S/N* ratio for the mean effect of the three variables are shown in the following pictures. Figure 4.83 and Figure 4.84 illustrate the combination of optimal factors required to obtain a larger percentage.

Figure 4.83 shows the optimal combination of factors when a larger percentage of MRR is required:

- $A-B+C+$for copper plate meaning W-1 parts, 5 psi, and 60 rpm
- $A-B-C-$ for iron plate meaning W-1 parts, 3 psi, and 30 rpm

Figure 4.84 illustrates the optimal combination of factors for improving surface roughness: $A-B-C$ for both materials of lapping plates meaning W-1 parts, 3 psi, and 30 rpm.

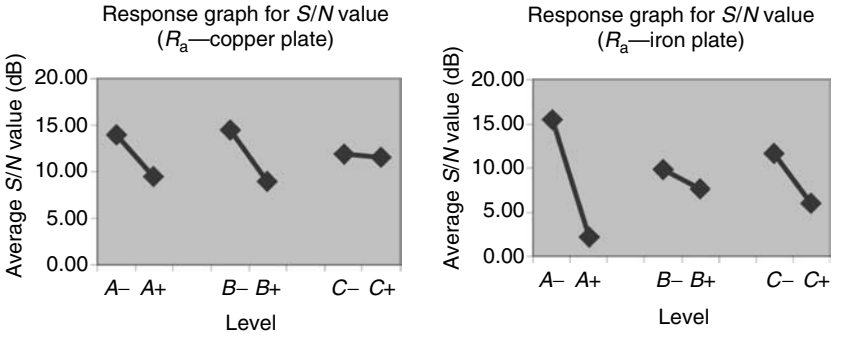


**FIGURE 4.84** Optimal combination of factors ($R_a$).

In conclusion, the material of the workpiece is the most significant factor when lapping with iron lapping plate for both surface roughness and MRR. When lapping with copper lapping plate, surface roughness is more influenced by pressure and material of the part whereas MRR is more influenced by pressure and speed. However, in order to have more conclusions on how copper lapping plate behaves, one should take into consideration expanding the range for both pressure and speed.

### 4.6.5 Modeling of Lapping Process

The typical procedure after some experiments had been carried out is to develop a model able to illustrate the phenomena that take place in the machining area and the influence of the input parameters on the output ones. Such a mathematical correlation allows conducting the process according to a desired goal, which for lapping could be a better surface finish and a lower MRR.

Finding the correlation between the lapping input parameters and the outcome of the process could reveal the proper adjustment of the process parameters that has to be done in order to achieve the best results. The model is supposed to determine the way in which each process parameter influences the process and to what degree. This kind of conclusion would help to know which of the input parameters should be slightly changed in order to achieve the maximum effect on the outcome of the process.

Basically, the mathematical modeling is helpful in optimizing the process parameters. Based on the lapping experiments (those in which diamond grain size was 0.25 μm), a model was developed. It consists of formulae showing the influence of the input lapping parameters (load, rotation of the lapping plate, and lapping time) on the output ones (surface roughness and MRR). In order to find the relationships between the input and output parameters a program, which finds the regression function that best approximates the experimental results, was used. It determines the regression function, among five types of multiple variable functions (Table 4.31), which best approximates the experimental data.

**TABLE 4.31**
**Types of Regression Functions Tried for Approximating the Experimental Data**

| | |
|---|---|
| $Y = a_0 + a_1x_1 + a_2x_2 + \ldots + a_nx_n$ | Linear dependency |
| $Y = a_0 \cdot x_1^{a1} \cdot x_2^{a2} \cdot \ \ldots \ \cdot x_n^{an}$ | Power function |
| $Y = a_0 \cdot a_1^{x1} \cdot a_2^{x2} \cdot \ \ldots \ \cdot a_n^{xn}$ | Exponential function |
| $Y = a_0 + a_1/x_1 + \ \ldots \ + a_n/x_n$ | Hyperbolic function |
| $Y = a_0 + a_1x_1 + a_2x_1^2 + \ldots + a_{2n-1}x_n + a_{2n}x_n^2$ | Second degree polynomial function |

The functions taken into consideration are the most common ones covering the basic trends that can be associated to the influence of a process parameter on the process outcome: monotone, asymptotic, or with an extreme (maximum or minimum). All of them can be made linear with a proper change of variable and therefore can be used in a linear regression analysis.

In order to run the program one needs to input the values for the process independent variables ($L$, $n$, $t$) on one hand and the values of the measured dependent variables ($R_a$, MRR) on the other. The program computes the coefficients for all five types of functions on the basis of the least-square method and selects, as the best approximation, the function that has the minimum global root-mean-squared residual errors, given by the following relationship:

$$e = \sqrt{\frac{\sum_{1}^{n} e_i^2}{N}} = \sqrt{\frac{\sum_{i=1}^{n} (y_i - y_{ci})^2}{N}} \tag{4.18}$$

where $e_i$ is called a residual and describes the error in the fit of the model at the $i$-th data point, $y_i$ the measured values of the dependent parameters ($R_a$, MRR) for the independent parameters taken into account (load, rotation of the lapping plate, lapping time), $y_{ci}$ the computed value of the function obtained through the least-square method corresponding to the same values of the independent parameters and $N$, the number of data points.

By running the program all five types of regression functions were determined (Table 4.32) for each output parameter ($R_a$ and MRR) for each type of diamond slurry (monocrystalline and polycrystalline) and the one which has the smallest global root-mean-squared residual errors was selected as being the best fit of the experimental data (highlighted rows). The differences among the values of the global root-mean-square error of the surface fitting for the two output parameters can be explained by the order of magnitude of the range in which the output parameters take values: MRR = 0.122 . . . 0.00688 mm$^3$/min and $R_a$ = 0.686 . . . 0.238 μm.

The determined regression functions that show the influence of the lapping input parameters on the output parameters (MRR and $R_a$) and can be considered as a model for the lapping process are as follows:

(a) For monocrystalline diamond slurry

$$R_a = 0.7411 - 3.4460 \cdot L + 1.3227 \cdot 10^{-7} \cdot L^2 + 3.6288 \cdot 10^{-2} \cdot n - 3.6221 \cdot 10^{-3} \cdot n^2 - 2.2882 \cdot 10^{-2} \cdot t + 4.4071 \cdot 10^{-4} \cdot \mathrm{t}\ [\mu\mathrm{m}] \tag{4.19}$$

$$\mathrm{MRR} = 0.0937 \cdot L^{0.1985} \cdot n^{0.0755} \cdot t^{-0.9962}\ [\mathrm{mm}^3/\mathrm{min}] \tag{4.20}$$

**TABLE 4.32**
**Selection of the Regression Function as Models of the Process**

| Output Parameters | Type of Regression Function | Root-Mean-Squared Residual Errors, e | |
|---|---|---|---|
| | | Monocrystalline | Polycrystalline |
| Surface Roughness | linear | $4.27 \cdot 10^{-3}$ | $2.62 \cdot 10^{-3}$ |
| | second degree polynomial | $2.11 \cdot 10^{-3}$ | $1.01 \cdot 10^{-3}$ |
| | power | $5.23 \cdot 10^{-3}$ | $3.14 \cdot 10^{-3}$ |
| | exponential | $4.06 \cdot 10^{-3}$ | $2.24 \cdot 10^{-3}$ |
| | hyperbolic | $6.49 \cdot 10^{-3}$ | $4.23 \cdot 10^{-3}$ |
| Material Removal | linear | $5.18 \cdot 10^{-4}$ | $4.31 \cdot 10^{-4}$ |
| | second degree polynomial | $2.48 \cdot 10^{-4}$ | $1.43 \cdot 10^{-4}$ |
| | power | $2.36 \cdot 10^{-4}$ | $1.27 \cdot 10^{-4}$ |
| | exponential | $4.29 \cdot 10^{-4}$ | $3.29 \cdot 10^{-4}$ |
| | hyperbolic | $2.59 \cdot 10^{-4}$ | $1.38 \cdot 10^{-4}$ |

(b) For polycrystalline diamond slurry

$$R_a = 0.7187 - 1.9849 \cdot 10^{-4} \cdot L + 9.1309 \cdot 10^{-8} - 4.4833 \cdot 10^{-4} \cdot n - 3.5245 \cdot 10^{-4} \cdot n^2 - 2.1464 \cdot 10^{-2} \cdot t + 4.0929 \cdot 10^{-4} \cdot t^2 \ [\mu m] \quad (4.21)$$

$$MRR = 3.9290 \cdot 10^{-2} \cdot L^{0.3719} \cdot n^{0.0498} \cdot t^{-1.1389} [mm^3/min] \quad (4.22)$$

where $L$ is the load (g), $n$ the rotation of the lapping plate (rpm), and $t$ the lapping time (min).

Taking into account that the determined functions are depending on multiple variables and the global root-mean-squared residual errors are the values that show the approximation level of experimental data for the entire studied ranges of variation of all independent parameters; it seems reasonable to find the intervals in which the approximation is best and which is the magnitude of the errors.

Figure 4.85 to Figure 4.88 illustrate graphically the errors in each of the experimental data point for the regression functions determined for surface roughness and material removal. The fitting error of the regression function is shown next to each data point. The values for the fitting errors were computed using the following formula:

$$\frac{y_{ci} - y_i}{y_i} 100 \ [\%] \quad (4.23)$$

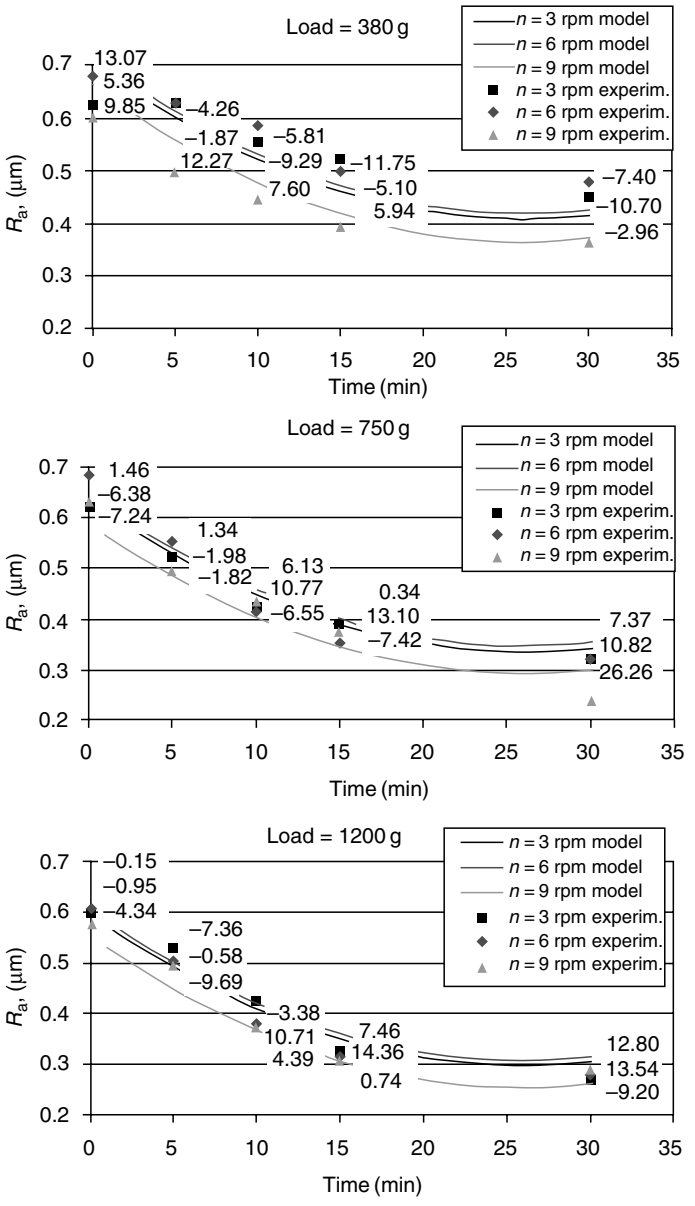


**FIGURE 4.85** Diagrams of the fit errors of the regression function for surface roughness (monocrystalline diamond slurry).

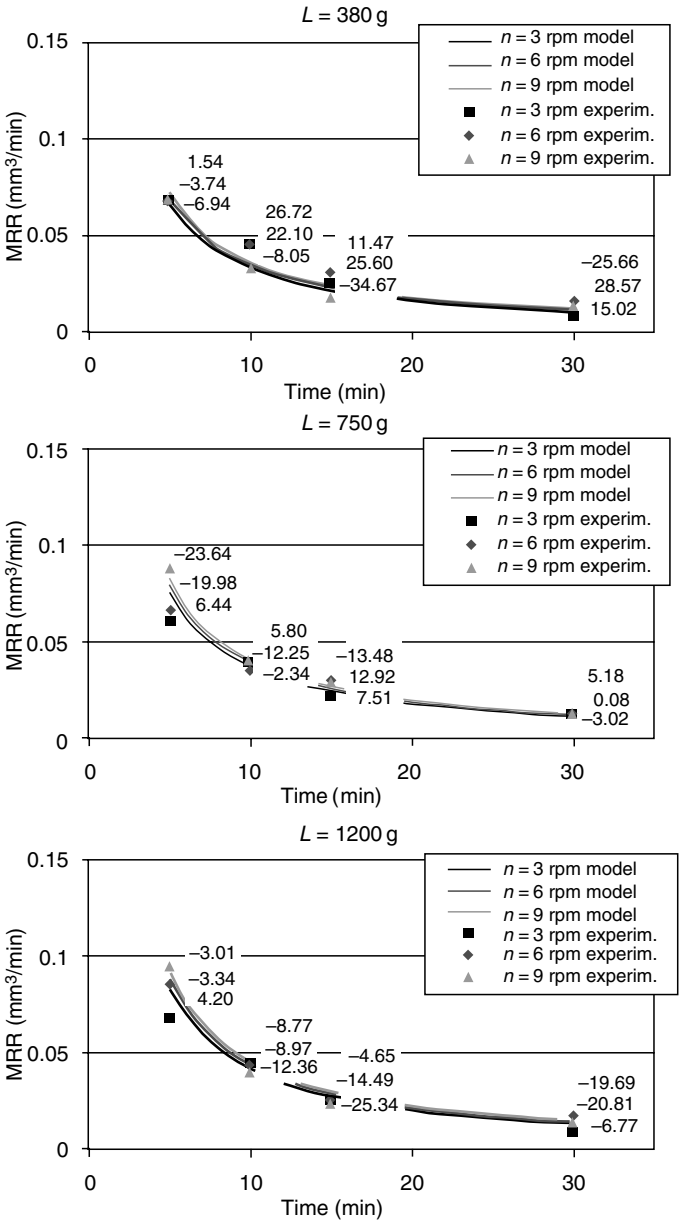


**FIGURE 4.86** Diagrams of the fit errors of the regression function for material removal rate (monocrystalline diamond slurry).

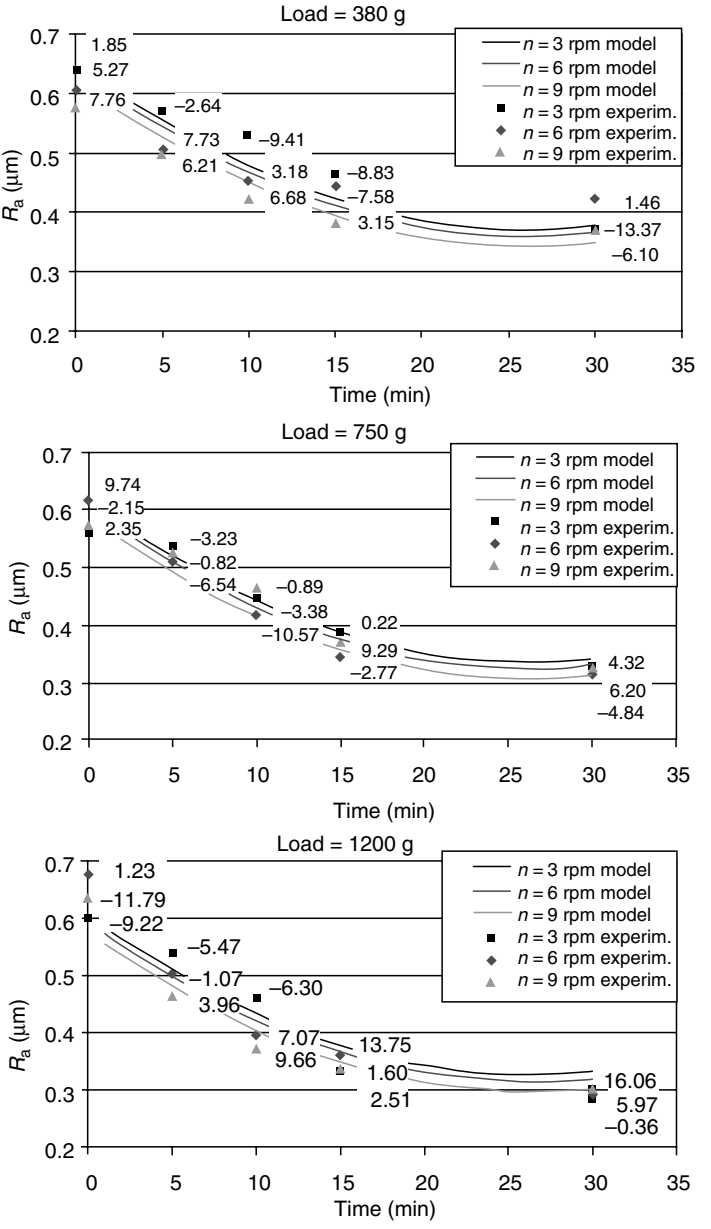


**FIGURE 4.87** Diagrams of the fit errors of the regression function for surface roughness (polycrystalline diamond slurry).

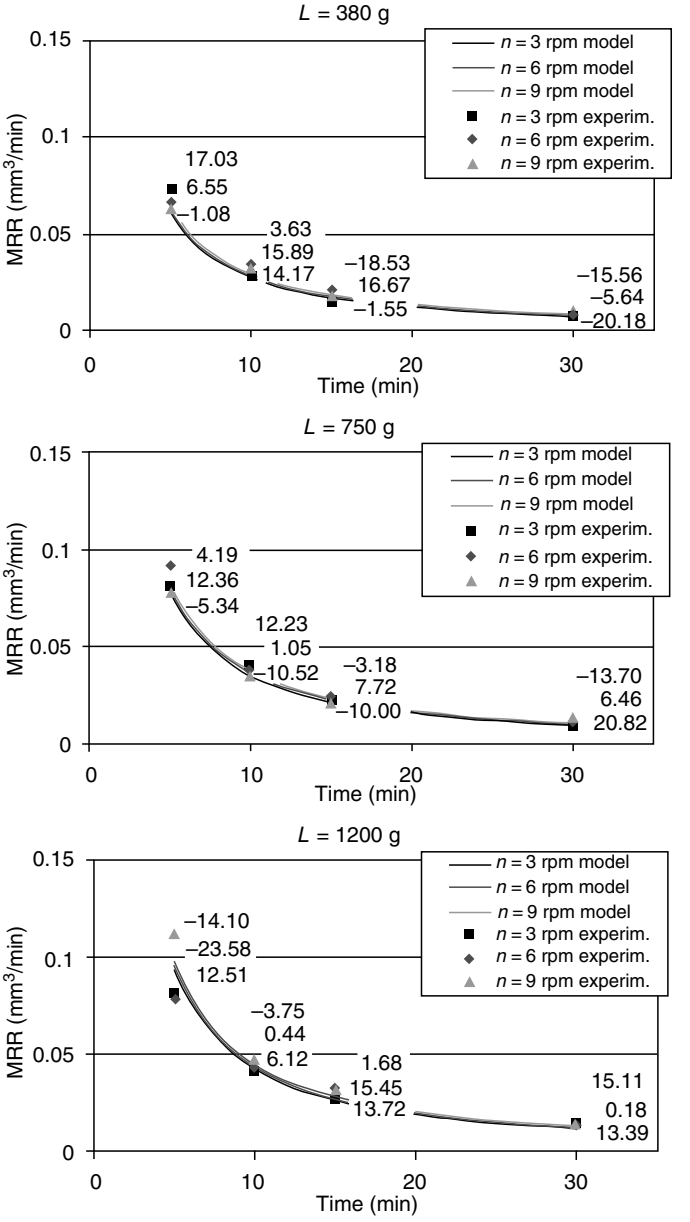


**FIGURE 4.88** Diagrams of the fit errors of the regression function for material removal rate (polycrystalline diamond slurry).

where $y_i$ are the measured values of the dependent parameters ($R_a$ and MRR) for the independent parameters taken into consideration ($L$, $n$, $t$) and $y_{ci}$ the computed value of the function obtained through the least-square method corresponding to the same values of the independent parameters. The fitting errors (Equation 4.23) were calculated as a percentage of the approximation of the regression functions (4.19, 4.20, 4.21, and 4.22) with respect to the measured values of the output parameters.

As a general conclusion after studying the mathematical model of the lapping process it can be said that the best fitting for both surface roughness and MRR was in the case of polycrystalline diamond slurry. The range of fitting errors for $R_a$ is −15.16% to 26.26% (monocrystalline diamond slurry) and −13.37% to 9.74% (polycrystalline diamond).

The range of fitting errors for MRR is −25.66% to 28.57% (monocrystalline diamond slurry) and −18.53% to 20.81% (polycrystalline diamond).

### 4.6.6 Conclusions of the Case Study

The research presented in this chapter was focused on the study of lapping parameters using monocrystalline and polycrystalline diamond slurries, parts made of ceramic materials as well as hardened steel W-1, different grain sizes for diamond slurry, and different input parameters. The experiments involved changing the values for load, lapping speed (rotation of the lapping plate), lapping time, and diamond slurry carrier in order to study their influence on lapping performance. The following output parameters were taken into consideration: surface roughness $R_a$ and MRR. To accomplish this, the lapping process was methodically studied and correspondingly a lapping set-up was built for experimental purposes.

The experiments were divided into three parts, the first two aiming to evaluate mainly the influence of diamond type on the lapping output parameters, and the third one to examine also the influence of the material of the lapping plate and the influence of the carrier on the lapping operation. The results from the first experiment (test A) were used for developing a model needed to study the degree of influence of each input parameter on the output lapping parameters that were considered.

From all the experiments done in lapping and from modeling the process, the following conclusions can be drawn:

1. Surface roughness is decreasing more rapidly at the beginning of machining for all tests carried out. An approximately 30 min lapping cycle is long enough to obtain the best surface finish.
2. Surface finish improves to some extent with time for all rotations of the lapping plate considered.
3. Surface roughness decreases faster in time when higher loads are applied for both monocrystalline and polycrystalline diamond slurries.

4. Regarding the influence of load and lapping speed on surface finish it can be concluded that roughness improves at higher speeds and lower loads when monocrystalline slurry is used and it improves at both higher speeds and loads when polycrystalline slurry is utilized.
5. Load is the parameter that plays one of the most important roles in obtaining the final surface characteristics. This was concluded from all lapping tests performed.
6. At lower load (380 g) the polycrystalline diamond produces a slightly better surface finish than the monocrystalline diamond while at higher load (1200 g), the latter behaves a little bit better from the surface roughness point of view (test A).
7. Rotation of the lapping plate, in the range considered for test A—3, 6, and 9 rpm—has no substantial influence on the surface roughness.
8. MRR decreases in time for both mono-and polycrystalline diamond slurries. This trend is more accentuated in the first 15–20 min of lapping.
9. Stock removal rate is slightly higher with the increase in the lapping pressure and this phenomenon is more noticeable at the beginning of machining for both types of diamond used.
10. MRR is higher for monocrystalline diamond slurry than for polycrystalline diamond slurry.
11. Lapping with 3 μm grain size did worsen the surface roughness especially at smaller loads, 91 and 364 g, and at the beginning of machining for monocrystalline diamond. When higher loads were applied this tendency was not so obvious (test B).
12. MRR increases with increasing load and is higher for larger diamond grain sizes.
13. When lapping using iron lapping plate, the workpiece material is the most significant factor of the process from the surface roughness point of view. In the ranges considered, pressure and speed do not influence the lapping performance (ANOVA).
14. When lapping with copper plate, speed is the most significant factor that influences the surface roughness. The other two factors do not contribute much in improving the surface roughness (ANOVA).
15. From the MRR point of view, workpiece material is the most significant factor for both lapping plates used; the other two factors (pressure and speed) are not significant. In order to have good conclusions for these parameters one needs to extend their range of values (ANOVA).
16. Optimal combination of factors when a larger percentage of MRR is required is $A-B+C+$ for copper plate (meaning W-1 parts, 5 psi, and 60 rpm) and $A-B-C-$ for iron plate (meaning W-1 parts, 3 psi, and 30 rpm).

17. Optimal combination of factors for improving surface roughness is *A–B–C–* for both materials of lapping plates meaning W-1 parts, 3 psi, and 30 rpm.
18. Mathematical correlation showing the influence of load, lapping speed, and lapping time on the lapping output parameters—surface roughness $R_a$ and MRR—was developed by regression analysis applied to the experimental data. Surface roughness is modeled by a second-order polynomial function whereas material removal is modeled by a power function.
19. For both surface roughness and material removal the best fitting was in the case of polycrystalline diamond slurry.
20. Range of fitting errors for $R_a$ is −15.16% to 26.26% (monocrystalline diamond slurry) and −13.37% to 9.74% (polycrystalline diamond).
21. Range of fitting errors for MRR is −25.66% to 28.57% (monocrystalline diamond slurry) and −18.53% to 20.81% (polycrystalline diamond).
22. Future work to be done in lapping, continuing the idea of this research work, should expand the range of values for pressure and speed and also choose more materials for workpieces in order to have more information about the influence of these parameters on lapping performances. Higher diamond grit sizes (higher than 6 μm) should be chosen with the purpose of having a better understanding of the influence of grain size on lapping surface finish.

## REFERENCES

1. Golini, D. and Jacobs, S.D. (1991). Physics of loose abrasive microgrinding. *Appl. Opt*., 30(19):2761–2777.
2. Barsoum, M. (1997). *Fundamentals of Ceramics*. McGraw-Hill, New York.
3. The Materials Information Society (2000). *Engineered Materials Handbook. Vol. 4: Ceramics and Glasses*. ASM International, The Materials Information Society.
4. Sreejith, P.S. and Ngoi, B.K.A. (2001). Material removal mechanisms in precision machining of new materials. *Int. J. Mach. Tools Manuf*., 41:1831–1843.
5. Richerson, D.W. (1992). *Modern Ceramic Engineering: Properties, Processing, and Use in Design*. Marcel Dekker, New York.
6. Lucca, D.A., Brinksmeier, E., and Goch, G. (1998). Progress in assessing surface and subsurface integrity. *Ann. CIRP*, 47(2):669–687.
7. Stachowiak, G.B. and Stachowiak, G.W. (2001). The effects of particle characteristics on three-body abrasive wear. *Wear*, 249:201–207.
8. Inamura, T. (1998). Computer simulation of microcutting. *Int. J. Jpn. Soc. Prec. Eng*., 32(4):239–245.
9. Fang, L., Zhou, Q., and Li, Q. (1998). An experimental simulation of cutting wear in three-body abrasion. *Wear*, 219:188–194.
10. Stolarski, T.A. (1999). Mechano-chemical wear of ceramics. *J. Mater. Sci*., 34:3609–3622.

11. Blau, P.J. (1997). Fifty years of research on the wear of metals. *Tribol. Int*., 30(5):321–331.
12. Grogoroudis, K. and Stephenson, D.J. (1997). Modelling low stress abrasive wear. *Wear*, 213:103–111.
13. Beckmann, G., Dierich, P., Gellrich, R., Gotzmann, J., and Pietschmann, F. (1996). Modelling of severe wear: A survey of the contributions of the Technical University of Zittau to tribology. *Tribol. Int*., 29(3):215–220.
14. Trezona, R.I., Allsopp, D.N., and Hutchings, I.M. (1999). Transitions between two-body and three-body abrasive wear: Influence of the test conditions in the microscale abrasive wear test. *Wear*, 225–229:205–214.
15. Heisel, U. and Avroutine, J. (1999). Process analysis for the evaluation of the surface formation and removal rate in lapping. *Ann. CIRP*, 48(2):229–234.
16. Verspui, M.A., With, D. de, van der Varst, P.G.T.h., Buijs, M. (1995). Bed thickness and particle size distribution in three-body abrasion. *Wear*, 188:102–1070.
17. Bifano, T.G., Dow, T.A., and Scattergood, R.O. (1991). Ductile regime grinding. A new technology for machining brittle materials. *J. Eng. Ind*., 113:184–189.
18. Williams, J.A. and Hyncica, A.M. (1992). Abrasive wear in lubricated contacts. *J. Phys. D Appl. Phys*., 25:A81–A90.
19. Ishikawa, K., Suwabe, H., Uneda, M., and Kuratam, N. (1999). Study on evaluation of ID-blade slicing characteristics utilizing elliptical vibration. *J. Soc. Grind. Eng*., 65(11):1605–1610.
20. Ishikawa, K., Suwabe, H., and Uneda, M. (1999). Study on vibration OD-blade slicing with air–mist working fluid for environment—Effect of applied vibration amplitude on slicing characteristics. *Proceedings of the American Society for Precision Engineering 1999 Annual Meeting*, 20:489–492.
21. Ishikawa, K., Suwabe, H., Kitajima, A., and Uneda, M. (2001). A basic study on slurry actions and slicing characteristics of multi-wire saw. *Proceedings of the American Society for Precision Engineering 2001 Annual Meeting*, 25:477–480.
22. Ishikawa, K., Suwabe, H., Nokura, K., Take, Y., and Uneda, M. (2002). A basic study on processing characteristics of OD-blade saw using ultrasonic vibration. *Proceedings of the American Society for Precision Engineering 2002 Annual Meeting*, 27:501–504.
23. Jin, M., Ogasawara, K., and Murakawa, M. (1998). Basic study on step vibration cutting. *Trans. NAMRI/SME,* 26:147–152.
24. Ishikawa, K., Suwabe, H., Nishide, T., and Uneda, M. (1998). A study on combined vibration drilling by ultrasonic and low-frequency vibrations for hard and brittle materials. *J. Am. Soc. Prec. Eng*., 22(4):196–205.
25. Brinksmeier, E., Preuss, W., and Schmuetz, J. (1998). Manufacture of microstructures by ultrasonic lapping. *Proceedings of the American Society for Precision Engineering 1998 Annual Meeting*, 18:169–172.
26. Ishikawa, K. (1989). *Applied Vibration Engineering*. Press of Kanazawa Institute of Technology, pp. 153–164.
27. Ishikawa, K., Suwabe, H., Ichikawa, K., and Moriya, N. (1993). High efficiency correcting process of lapping plate using correcting carrier electrodeposited diamond grains. *Proceedings of ABTEC93*, pp. 305–308.
28. Mizuno, M. and Iyama, T. (2000). Lapping of small-sized mold with ultra-sonic conveyor wave. *Adv. Abrasive Technol*., 3:359–366.

29. Ohmori, H. and Nakagawa, T. (1990). Mirror surface grinding of silicon wafers with electrolytic in-process dressing. *Ann. CIRP*, 39(1):329–332.
30. Itoh, N. and Ohmori, H. (1996). Grinding characteristics of hard and brittle materials by fine grain lapping wheels with ELID. *J. Mater. Process. Technol.*, 62:315–320.
31. Itoh, M., et al. (2002). Study on efficient grinding of sapphier using ELID method. *Progr. Machin. Technol.*, 328–333..
32. Itoh, N. and Ohmori, H. (1998). Study of precision machining with metal resin bond wheel on ELID-lap grinding. *Int. J. Electr. Machin.*, 3:13–18.
33. Itoh, N. and Ohmori, H. (1995). Grinding characteristics of metal-resin bonded wheel with ELID for hard and brittle materials. *Proceedings of the Second International Abrasive Technology Conference*, pp. 471–476.
34. Barylski, A. (1985). Contamination of graphite with abrasive during lapping of cast iron. *Stud. Mater. Gorz. Osr. Bad Ekspertyz Nauk*, Ref. T.IV. 1–2:303–306.

## BIBLIOGRAPHY

Benabdallah, H.S. and Bones, R.J. (1999). Tribological behaviour and acoustic emissions of alumina, silicon nitride and SAE52100 under dry sliding. *J. Mater. Sci.*, 34:4995–5004.

Blau, P.J. (2001). The significance and use of the friction coefficient. *Tribol. Int.*, 34:585–591.

Buijs, M. and Korpel-van Houten, K. (1993). *A Model for Lapping of Glass*. Chapman & Hall, London, pp. 3014–3020.

Buijs, M. and Korpel-van Houten, K. (1993). Three-body abrasion of brittle materials as studied by lapping. *Wear*, 166:237–245.

Chand, N. and Neogi, S. (1998). Mechanism of material removal during three-body abrasion of FRP composite. *Tribol. Lett.*, 4:81–85.

Chand, N., Naik, A., and Neogi, S. (2000). Three-body abrasion wear of short glass fibre polyester composite. *Wear*, 242:38–46.

Chandra, A., Wang, K., Huang, Y., Subhash, G., Miller, M.H., and Qu, W. (2000). Role of unloading in machining of brittle materials. *J. Manuf. Sci. Eng.*, 122:452–462.

Chang, Yu-En. (1995). Monitoring and characterization of grinding and lapping processes, PhD thesis, University of California, Berkeley, p. 174.

Chang, Y.P., Hashimura, M., and Dornfeld, D.A. (2000). An investigation of material removal mechanisms in lapping with grain size transition. *J. Manuf. Sci. Eng.*, 122:413–419.

Chauhan, R., Ahn, Y., Chandrasekar, S., and Farris, T.N. (1993). Role of indentation fracture in free abrasive machining of ceramics. *Wear*, 162–164:246–257.

Chen, C., Sakai, S., and Inasaki, I. (1991). Lapping of advanced ceramics. *Mater. Manuf. Proc.*, 6(2):211–226.

Desa, O. and Bahadur, S. (1999). Material removal and subsurface damage studies in dry and lubricated single-point scratch tests on alumina and silicon nitride. *Wear*, 225–229:1264–1275.

Dogan, C.P. and Hawk, J.A. (1995). Effect of grain boundary glass composition and devitrification on the abrasive wear of $Al_2O_3$. *Wear*, 181–183:129–137.

Dogan, C.P. and Hawk, J.A. (1999). Role of composition and microstructure in the abrasive wear of high-alumina ceramics. *Wear*, 225–229:1050–1058.

Dukino, R.D. and Swain, M.V. (1992). Comparative measurement of indentation fracture toughness with Berkovich and Vickers indenters. *J. Am. Ceram. Soc*., 75(12):3299–3304.

Dwyer-Joyce, R.S. (1999). Predicting the abrasive wear of ball bearings by lubricant debris. *Wear*, 233–235:692–701.

Fang, L., Xing, J., Liu, W., Xue, Q., Wu, G., and Zhang, X. (2001). Computer simulation of two-body abrasion processes. *Wear*, 251:1356–1360.

Gahlin, R. and Jacobson, S. (1999). The particle size effect in abrasion studied by controlled abrasive surfaces. *Wear*, 224:118–125.

Gatzen, H.H. and Maetzig, J.C. (1997). *Nanogrind. Prec. Eng*., 21:134–139.

*Grinding and Lapping Compound*. (1995). Published by United States Products Co., pp. 1–14.

Heisel, U., Avroutine, J., and Rothmund, J. (1999). Process and simulation model for lapping. *Proceedings of the First EUSPEN Conference*, Bremen, Germany, pp. 314–317.

Hilarov, V.L. (1998). Self-similar crack-generation effects in the fracture process in brittle materials. *Model. Simul. Mater. Sci. Eng*., 6:337–342.

http://warrendiamond.com

http://www.antexlap.com

http://www.engis.com

Hutchings, I.M. (1992). Ductile–brittle transitions and wear maps for the erosion and abrasion of brittle materials. *J. Phys. D Appl. Phys*., 25:A212–A221.

Indge, J.H. (1990). Lapping: More of a science, less an art form. *Ceram. Indust*., 6926–28.

Jiang, J., Sheng, F., and Ren, F. (1998). Modelling of two-body abrasive wear under multiple contact conditions. *Wear*, 217:35–45.

Khonsari, M.M. (1997). On the modeling of the multi-body interaction problems in tribology. *Wear*, 207:55–62.

Komanduri, R., Lucca, D.A., and Tani, Y. (1997). Technological advances in fine abrasive processes. *Ann. CIRP*, 46(2):545–596.

Kun, L. and Liao, T.W. (1997). Modelling of ceramic grinding processes. Part I. Number of cutting points and grinding forces per grit. *J. Mater. Process. Technol*., 65:1–10.

Lankford, J. (1981). Threshold microfracture during elastic–plastic indentation of ceramics. *J. Mater. Sci*., 16:1177–1182.

Lawn, B.R. and Evans, A.G. (1980). Elastic/plastic indentation damage in ceramics: The median/radial crack system. *J. Am. Ceram. Soc*., 63(9–10):574–581.

Lawn, B.R., Padture, N.P., Cai, H., and Guiberteau, F. (1994). Making ceramics ductile. *Science*, 263:1114–1116.

Marinescu, I.D., Tonshoff, H.K., Inasaki, I., and Pruteanu, M. (2000). *Handbook of Ceramic Grinding and Polishing*. Noyes Publications/William Andrew Publishing LLC, Norwich/New York.

Matsunaga, M. (1966). *Fundamental Studies of Lapping*, vol. 16(2). Report of the Institute of Industrial Science, University of Tokyo.

Meng, H.C. and Ludema, K.C. (1995). Wear models and predictive equations: Their form and content. *Wear*, 181–183:443–457.

Millar, J. (1987). Lapping & polishing technology. *Abrasive Eng. Soc. Mag*., 30(4):9–13.

Novak, S., Kalin, M., and Kosmac, T. (2001). Chemical aspects of wear of alumina ceramics. *Wear*, 250:318–321.

Rabinovich, V.L. and Sarin, V.K. (1996). Three dimensional modelling of indentation fracture in brittle materials. *Mater. Sci. Eng. A*, 206:208–214.

Ravikiran, A. and Jahanmir, S. (2001). Effect of contact pressure and load on wear of alumina. *Wear*, 251:980–984.

Schwartz, M. (1992). *Handbook of Structural Ceramics*. McGraw-Hill, New York.

Shibata, T., Shinohara, K., Uchiyama, T., and Otani, M. (2001). Lapping performance guide of poly-crystal diamond particles through morphological analysis. *Diamond Relat. Mater*., 10:376–382.

Somiya, S. (1984). *Advanced Technical Ceramics*. Academic Press, San Diego, CA.

Spur, G. and Engel, H. (1999). Tool engagement and surface formation in lapping of brittle materials. *Int. J. Jpn. Soc. Prec. Eng*., 33(3):191–196.

Stachowiak, G.W. (1998). Numerical characterization of wear particles morphology and angularity of particles and surfaces. *Tribol. Int*., 31(1–3):139–157.

Suresh, S. (1990). Mechanics and micromechanisms of fatigue crack growth in brittle solids. *Int. J. Fracture*, 42:41–56.

Torrance, A.A. and Buckley, T.R. (1996). A slip-line field model of abrasive wear. *Wear*, 196:35–45.

Turco, M.D. (1995). Flat lapping of zirconia-toughened alumina with diamond powder. MS thesis, University of Connecticut, p. 146.

Verspui, M.A. and de With, G. (1997). Three-body abrasion: Influence of applied load on bed thickness and particle size distribution in abrasive processes. *J. Eur. Ceram. Soc*., 17:473–477.

Verspui, M.A., de With, G., Corbijn, A., and Slikkerveer, P.J. (1999). Simulation model for the erosion of brittle materials. *Wear*, 233–235:436–443.

Walsh, R.A. (1994). *McGraw-Hill Machining and Metalworking Handbook*. McGraw-Hill, New York.

Williams, J.A. (1999). Wear modeling: Analytical, computational and mapping: A continuum mechanics approach. *Wear*, 225–229:1–17.

Zeng, R. (1998). Acoustic emission investigation of ceramic lapping process. MS thesis, Kansas State University, p. 108.

Zou, Q., Huang, P., and When, S. (1996). Abrasive wear model for lubricated sliding contacts. *Wear*, 196:72–76.

Zum Gahr, K.-H. (1998). Wear by hard particles. *Tribol. Int*., 31(10):587–596.

Zum Gahr, K.-H., Blattner, R., Hwang, D.H., and Pohlmann, K. (2001). Micro- and macro-tribological properties of SiC ceramics in sliding contact. *Wear*, 250:299–310.

## APPENDIX A
## Experimental Values for Surface Roughness and Material Removal Rate (Test C)

### Experimental Values for $R_a$ (Copper Plate)

| | | | | Time | 1 | | | 3 | | | 6 | | |
|---|---|---|---|---|---|---|---|---|---|---|---|---|---|
| Grain Size | Carrier | Workpiece | Load | rpm | 1 | 2 | 3 | 1 | 2 | 3 | 1 | 2 | 3 |
| 1 | WB | W1 | 3 | 60 | 0.26 | 0.253 | 0.254 | 0.179 | 0.075 | 0.057 | 0.116 | 0.066 | 0.05 |
| | | SiC | 3 | 30 | 0.039 | 0.032 | 0.039 | 0.036 | 0.088 | 0.035 | 0.03 | 0.039 | 0.036 |
| | | W1 | 5 | 30 | 0.063 | 0.128 | 0.295 | 0.032 | 0.035 | 0.043 | 0.048 | 0.043 | 0.048 |
| | | SiC | 5 | 60 | 0.272 | 0.332 | 0.255 | 0.043 | 0.049 | 0.045 | 0.046 | 0.043 | 0.036 |
| | OB | W1 | 3 | 60 | 0.043 | 0.038 | 0.03 | 0.025 | 0.024 | 0.025 | 0.023 | 0.021 | 0.025 |
| | | SiC | 3 | 30 | 0.031 | 0.033 | 0.061 | 0.028 | 0.027 | 0.034 | 0.029 | 0.026 | 0.029 |
| | | W1 | 5 | 30 | 0.052 | 0.042 | 0.117 | 0.022 | 0.022 | 0.023 | 0.025 | 0.025 | 0.024 |
| | | SiC | 5 | 60 | 0.032 | 0.032 | 0.044 | 0.025 | 0.026 | 0.026 | 0.024 | 0.027 | 0.027 |
| 3 | WB | W1 | 3 | 60 | 0.029 | 0.029 | 0.028 | 0.031 | 0.031 | 0.03 | 0.035 | 0.038 | 0.03 |
| | | SiC | 3 | 30 | 0.042 | 0.041 | 0.04 | 0.041 | 0.045 | 0.041 | 0.047 | 0.059 | 0.048 |
| | | W1 | 5 | 30 | 0.029 | 0.177 | 0.042 | 0.029 | 0.033 | 0.03 | 0.034 | 0.033 | 0.033 |
| | | SiC | 5 | 60 | 0.046 | 0.035 | 0.034 | 0.056 | 0.04 | 0.045 | 0.07 | 0.046 | 0.044 |
| | OB | W1 | 3 | 60 | 0.197 | 0.284 | 0.133 | 0.041 | 0.108 | 0.028 | 0.044 | 0.034 | 0.029 |
| | | SiC | 3 | 30 | 0.06 | 0.068 | 0.085 | 0.076 | 0.065 | 0.056 | 0.055 | 0.054 | 0.049 |
| | | W1 | 5 | 30 | 0.074 | 0.267 | 0.214 | 0.067 | 0.03 | 0.071 | 0.042 | 0.027 | 0.0406 |
| | | SiC | 5 | 60 | 0.079 | 0.075 | 0.055 | 0.047 | 0.057 | 0.053 | 0.056 | 0.054 | 0.055 |
| 15 | WB | W1 | 3 | 60 | 0.094 | 0.097 | 0.121 | 0.064 | 0.065 | 0.072 | 0.091 | 0.094 | 0.114 |
| | | SiC | 3 | 30 | 0.123 | 0.12 | 0.1 | 0.106 | 0.106 | 0.101 | 0.082 | 0.081 | 0.089 |
| | | W1 | 5 | 30 | 0.132 | 0.117 | 0.123 | 0.081 | 0.079 | 0.083 | 0.081 | 0.077 | 0.086 |
| | | SiC | 5 | 60 | 0.095 | 0.106 | 0.104 | 0.119 | 0.087 | 0.093 | 0.103 | 0.098 | 0.085 |
| | OB | W1 | 3 | 60 | 0.079 | 0.078 | 0.078 | 0.086 | 0.083 | 0.08 | 0.088 | 0.089 | 0.085 |
| | | SiC | 3 | 30 | 0.112 | 0.109 | 0.103 | 0.118 | 0.101 | 0.091 | 0.102 | 0.09 | 0.118 |
| | | W1 | 5 | 30 | 0.096 | 0.069 | 0.106 | 0.067 | 0.06 | 0.076 | 0.094 | 0.083 | 0.087 |
| | | SiC | 5 | 60 | 0.152 | 0.111 | 0.132 | 0.082 | 0.078 | 0.076 | 0.084 | 0.085 | 0.085 |

*continued*

## Experimental Values for $R_a$ (Copper Plate) (continued)

| | | | | Time | 11 | | | 21 | | | 36 | | |
|---|---|---|---|---|---|---|---|---|---|---|---|---|---|
| **Grain Size** | **Carrier** | **Workpiece** | **Load** | **rpm** | **1** | **2** | **3** | **1** | **2** | **3** | **1** | **2** | **3** |
| 1 | WB | W1 | 3 | 60 | 0.068 | 0.028 | 0.03 | 0.052 | 0.028 | 0.026 | 0.027 | 0.028 | 0.024 |
| | | SiC | 3 | 30 | 0.027 | 0.027 | 0.028 | 0.033 | 0.027 | 0.031 | 0.035 | 0.025 | 0.025 |
| | | W1 | 5 | 30 | 0.044 | 0.025 | 0.032 | 0.037 | 0.038 | 0.06 | 0.025 | 0.037 | 0.043 |
| | | SiC | 5 | 60 | 0.034 | 0.039 | 0.044 | 0.038 | 0.038 | 0.041 | 0.03 | 0.035 | 0.032 |
| | OB | W1 | 3 | 60 | 0.025 | 0.024 | 0.026 | 0.021 | 0.026 | 0.026 | 0.026 | 0.024 | 0.03 |
| | | SiC | 3 | 30 | 0.025 | 0.025 | 0.026 | 0.025 | 0.027 | 0.025 | 0.026 | 0.026 | 0.027 |
| | | W1 | 5 | 30 | 0.025 | 0.026 | 0.026 | 0.023 | 0.026 | 0.025 | 0.028 | 0.022 | 0.027 |
| | | SiC | 5 | 60 | 0.027 | 0.025 | 0.027 | 0.028 | 0.026 | 0.024 | 0.025 | 0.025 | 0.024 |
| 3 | WB | W1 | 3 | 60 | 0.031 | 0.028 | 0.029 | 0.031 | 0.033 | 0.029 | 0.03 | 0.029 | 0.029 |
| | | SiC | 3 | 30 | 0.044 | 0.056 | 0.043 | 0.046 | 0.063 | 0.047 | 0.049 | 0.072 | 0.058 |
| | | W1 | 5 | 30 | 0.03 | 0.032 | 0.027 | 0.029 | 0.033 | 0.032 | 0.032 | 0.03 | 0.034 |
| | | SiC | 5 | 60 | 0.065 | 0.049 | 0.051 | 0.056 | 0.052 | 0.048 | 0.077 | 0.074 | 0.05 |
| | OB | W1 | 3 | 60 | 0.035 | 0.028 | 0.028 | 0.028 | 0.025 | 0.028 | 0.027 | 0.024 | 0.028 |
| | | SiC | 3 | 30 | 0.051 | 0.053 | 0.053 | 0.055 | 0.062 | 0.069 | 0.064 | 0.084 | 0.072 |
| | | W1 | 5 | 30 | 0.031 | 0.028 | 0.031 | 0.027 | 0.027 | 0.027 | 0.027 | 0.027 | 0.024 |
| | | SiC | 5 | 60 | 0.057 | 0.063 | 0.051 | 0.056 | 0.058 | 0.048 | 0.061 | 0.073 | 0.053 |
| 15 | WB | W1 | 3 | 60 | 0.116 | 0.122 | 0.111 | 0.088 | 0.107 | 0.101 | 0.066 | 0.076 | 0.078 |
| | | SiC | 3 | 30 | 0.105 | 0.098 | 0.104 | 0.079 | 0.078 | 0.074 | 0.064 | 0.059 | 0.057 |
| | | W1 | 5 | 30 | 0.15 | 0.11 | 0.13 | 0.117 | 0.092 | 0.128 | 0.08 | 0.079 | 0.076 |
| | | SiC | 5 | 60 | 0.094 | 0.08 | 0.095 | 0.081 | 0.081 | 0.082 | 0.066 | 0.066 | 0.068 |
| | OB | W1 | 3 | 60 | 0.084 | 0.083 | 0.072 | 0.061 | 0.063 | 0.061 | 0.072 | 0.077 | 0.071 |
| | | SiC | 3 | 30 | 0.096 | 0.085 | 0.088 | 0.088 | 0.086 | 0.087 | 0.074 | 0.07 | 0.074 |
| | | W1 | 5 | 30 | 0.075 | 0.063 | 0.068 | 0.075 | 0.063 | 0.075 | 0.107 | 0.089 | 0.096 |
| | | SiC | 5 | 60 | 0.081 | 0.083 | 0.083 | 0.079 | 0.079 | 0.076 | 0.083 | 0.09 | 0.069 |

| Grain Size | Carrier | Workpiece | Load | Time rpm | 66 1 | 66 2 | 66 3 |
|---|---|---|---|---|---|---|---|
| 1 | WB | W1 | 3 | 60 | 0.026 | 0.029 | 0.024 |
| | | SiC | 3 | 30 | 0.033 | 0.025 | 0.026 |
| | | W1 | 5 | 30 | 0.024 | 0.024 | 0.024 |
| | | SiC | 5 | 60 | 0.03 | 0.03 | 0.03 |
| | OB | W1 | 3 | 60 | 0.024 | 0.024 | 0.025 |
| | | SiC | 3 | 30 | 0.026 | 0.027 | 0.027 |
| | | W1 | 5 | 30 | 0.026 | 0.025 | 0.025 |
| | | SiC | 5 | 60 | 0.023 | 0.026 | 0.023 |
| 3 | WB | W1 | 3 | 60 | 0.028 | 0.026 | 0.027 |
| | | SiC | 3 | 30 | 0.056 | 0.08 | 0.054 |
| | | W1 | 5 | 30 | 0.028 | 0.027 | 0.027 |
| | | SiC | 5 | 60 | 0.088 | 0.07 | 0.063 |
| | OB | W1 | 3 | 60 | 0.027 | 0.027 | 0.025 |
| | | SiC | 3 | 30 | 0.073 | 0.077 | 0.069 |
| | | W1 | 5 | 30 | 0.026 | 0.026 | 0.026 |
| | | SiC | 5 | 60 | 0.073 | 0.079 | 0.051 |
| 15 | WB | W1 | 3 | 60 | 0.078 | 0.086 | 0.099 |
| | | SiC | 3 | 30 | 0.1 | 0.094 | 0.094 |
| | | W1 | 5 | 30 | 0.107 | 0.114 | 0.112 |
| | | SiC | 5 | 60 | 0.081 | 0.077 | 0.08 |
| | OB | W1 | 3 | 60 | 0.088 | 0.116 | 0.102 |
| | | SiC | 3 | 30 | 0.092 | 0.096 | 0.089 |
| | | W1 | 5 | 30 | 0.114 | 0.092 | 0.103 |
| | | SiC | 5 | 60 | 0.083 | 0.066 | 0.073 |

*continued*

## Experimental Values for $R_a$ (Iron Plate)

| | | | | Time | 1 | | | 3 | | | 6 | | |
|---|---|---|---|---|---|---|---|---|---|---|---|---|---|
| Grain Size | Carrier | Workpiece | Load | rpm | 1 | 2 | 3 | 1 | 2 | 3 | 1 | 2 | 3 |
| 1 | WB | W1 | 3 | 60 | 0.209 | 0.125 | 0.197 | 0.147 | 0.095 | 0.124 | 0.111 | 0.077 | 0.113 |
| | | SiC | 3 | 30 | 0.089 | 0.092 | 0.107 | 0.083 | 0.085 | 0.103 | 0.084 | 0.097 | 0.097 |
| | | W1 | 5 | 30 | 0.147 | 0.186 | 0.139 | 0.113 | 0.111 | 0.127 | 0.062 | 0.105 | 0.08 |
| | | SiC | 5 | 60 | 0.088 | 0.089 | 0.09 | 0.084 | 0.078 | 0.096 | 0.081 | 0.076 | 0.087 |
| | OB | W1 | 3 | 60 | 0.041 | 0.056 | 0.044 | 0.029 | 0.044 | 0.028 | 0.026 | 0.033 | 0.026 |
| | | SiC | 3 | 30 | 0.049 | 0.032 | 0.042 | 0.038 | 0.033 | 0.034 | 0.031 | 0.028 | 0.034 |
| | | W1 | 5 | 30 | 0.028 | 0.047 | 0.12 | 0.027 | 0.034 | 0.049 | 0.027 | 0.028 | 0.03 |
| | | SiC | 5 | 60 | 0.041 | 0.035 | 0.0436 | 0.038 | 0.037 | 0.031 | 0.041 | 0.034 | 0.035 |
| 3 | WB | W1 | 3 | 60 | 0.134 | 0.046 | 0.051 | 0.033 | 0.033 | 0.034 | 0.044 | 0.035 | 0.03 |
| | | SiC | 3 | 30 | 0.054 | 0.048 | 0.051 | 0.055 | 0.071 | 0.064 | 0.067 | 0.072 | 0.067 |
| | | W1 | 5 | 30 | 0.045 | 0.042 | 0.044 | 0.032 | 0.033 | 0.04 | 0.039 | 0.033 | 0.033 |
| | | SiC | 5 | 60 | 0.057 | 0.044 | 0.057 | 0.098 | 0.066 | 0.058 | 0.096 | 0.062 | 0.066 |
| | OB | W1 | 3 | 60 | 0.177 | 0.237 | 0.217 | 0.047 | 0.065 | 0.032 | 0.050 | 0.033 | 0.032 |
| | | SiC | 3 | 30 | 0.051 | 0.054 | 0.086 | 0.049 | 0.059 | 0.088 | 0.056 | 0.072 | 0.088 |
| | | W1 | 5 | 30 | 0.111 | 0.091 | 0.039 | 0.045 | 0.045 | 0.033 | 0.029 | 0.031 | 0.030 |
| | | SiC | 5 | 60 | 0.055 | 0.058 | 0.057 | 0.061 | 0.07 | 0.054 | 0.074 | 0.07 | 0.055 |
| 15 | WB | W1 | 3 | 60 | 0.091 | 0.109 | 0.100 | 0.093 | 0.111 | 0.094 | 0.096 | 0.093 | 0.094 |
| | | SiC | 3 | 30 | 0.113 | 0.109 | 0.101 | 0.095 | 0.096 | 0.098 | 0.092 | 0.100 | 0.102 |
| | | W1 | 5 | 30 | 0.098 | 0.099 | 0.089 | 0.097 | 0.104 | 0.094 | 0.103 | 0.112 | 0.093 |
| | | SiC | 5 | 60 | 0.125 | 0.109 | 0.106 | 0.113 | 0.108 | 0.114 | 0.089 | 0.094 | 0.090 |
| | OB | W1 | 3 | 60 | 0.100 | 0.087 | 0.090 | 0.085 | 0.068 | 0.078 | 0.109 | 0.090 | 0.089 |
| | | SiC | 3 | 30 | 0.077 | 0.107 | 0.135 | 0.097 | 0.101 | 0.112 | 0.074 | 0.089 | 0.097 |
| | | W1 | 5 | 30 | 0.105 | 0.112 | 0.099 | 0.116 | 0.104 | 0.111 | 0.116 | 0.095 | 0.107 |
| | | SiC | 5 | 60 | 0.097 | 0.090 | 0.076 | 0.096 | 0.095 | 0.090 | 0.093 | 0.085 | 0.087 |

| | | | | Time | 11 | | | 21 | | | 36 | | |
|---|---|---|---|---|---|---|---|---|---|---|---|---|---|
| **Grain Size** | **Carrier** | **Workpiece** | **Load** | **rpm** | **1** | **2** | **3** | **1** | **2** | **3** | **1** | **2** | **3** |
| 1 | WB | W1 | 3 | 60 | 0.105 | 0.074 | 0.106 | 0.088 | 0.057 | 0.098 | 0.086 | 0.061 | 0.08 |
| | | SiC | 3 | 30 | 0.079 | 0.099 | 0.082 | 0.07 | 0.094 | 0.082 | 0.076 | 0.094 | 0.073 |
| | | W1 | 5 | 30 | 0.049 | 0.057 | 0.06 | 0.037 | 0.061 | 0.069 | 0.033 | 0.051 | 0.053 |
| | | SiC | 5 | 60 | 0.068 | 0.071 | 0.085 | 0.062 | 0.077 | 0.081 | 0.068 | 0.068 | 0.078 |
| | OB | W1 | 3 | 60 | 0.025 | 0.03 | 0.025 | 0.028 | 0.028 | 0.024 | 0.03 | 0.031 | 0.03 |
| | | SiC | 3 | 30 | 0.0316 | 0.03 | 0.034 | 0.033 | 0.031 | 0.038 | 0.035 | 0.029 | 0.033 |
| | | W1 | 5 | 30 | 0.026 | 0.027 | 0.028 | 0.03 | 0.03 | 0.024 | 0.023 | 0.026 | 0.025 |
| | | SiC | 5 | 60 | 0.041 | 0.025 | 0.034 | 0.042 | 0.027 | 0.032 | 0.043 | 0.026 | 0.029 |
| 3 | WB | W1 | 3 | 60 | 0.038 | 0.032 | 0.033 | 0.034 | 0.033 | 0.03 | 0.032 | 0.029 | 0.03 |
| | | SiC | 3 | 30 | 0.074 | 0.086 | 0.067 | 0.066 | 0.092 | 0.069 | 0.074 | 0.089 | 0.085 |
| | | W1 | 5 | 30 | 0.036 | 0.034 | 0.032 | 0.029 | 0.031 | 0.031 | 0.03 | 0.034 | 0.034 |
| | | SiC | 5 | 60 | 0.082 | 0.063 | 0.074 | 0.079 | 0.065 | 0.079 | 0.094 | 0.061 | 0.087 |
| | OB | W1 | 3 | 60 | 0.030 | 0.032 | 0.031 | 0.030 | 0.033 | 0.031 | 0.029 | 0.029 | 0.030 |
| | | SiC | 3 | 30 | 0.059 | 0.074 | 0.09 | 0.063 | 0.076 | 0.09 | 0.06 | 0.071 | 0.084 |
| | | W1 | 5 | 30 | 0.030 | 0.031 | 0.028 | 0.032 | 0.030 | 0.032 | 0.032 | 0.030 | 0.030 |
| | | SiC | 5 | 60 | 0.081 | 0.089 | 0.055 | 0.091 | 0.089 | 0.049 | 0.088 | 0.094 | 0.051 |
| 15 | WB | W1 | 3 | 60 | 0.103 | 0.106 | 0.102 | 0.116 | 0.096 | 0.111 | 0.128 | 0.109 | 0.127 |
| | | SiC | 3 | 30 | 0.094 | 0.092 | 0.090 | 0.101 | 0.097 | 0.092 | 0.075 | 0.084 | 0.084 |
| | | W1 | 5 | 30 | 0.105 | 0.097 | 0.100 | 0.092 | 0.089 | 0.085 | 0.098 | 0.105 | 0.103 |
| | | SiC | 5 | 60 | 0.080 | 0.081 | 0.077 | 0.086 | 0.083 | 0.088 | 0.088 | 0.092 | 0.084 |
| | OB | W1 | 3 | 60 | 0.109 | 0.086 | 0.087 | 0.074 | 0.065 | 0.088 | 0.114 | 0.087 | 0.090 |
| | | SiC | 3 | 30 | 0.105 | 0.092 | 0.090 | 0.079 | 0.081 | 0.082 | 0.078 | 0.078 | 0.079 |
| | | W1 | 5 | 30 | 0.093 | 0.126 | 0.097 | 0.084 | 0.098 | 0.088 | 0.100 | 0.087 | 0.113 |
| | | SiC | 5 | 60 | 0.078 | 0.076 | 0.078 | 0.086 | 0.081 | 0.080 | 0.073 | 0.075 | 0.074 |

*continued*

## Experimental Values for $R_a$ (Iron Plate) (continued)

| | | | | Time | 66 | | |
|---|---|---|---|---|---|---|---|
| Grain Size | Carrier | Workpiece | Load | rpm | 1 | 2 | 3 |
| 1 | WB | W1 | 3 | 60 | 0.079 | 0.052 | 0.068 |
| | | SiC | 3 | 30 | 0.069 | 0.09 | 0.053 |
| | | W1 | 5 | 30 | 0.037 | 0.05 | 0.049 |
| | | SiC | 5 | 60 | 0.069 | 0.075 | 0.081 |
| | OB | W1 | 3 | 60 | 0.027 | 0.025 | 0.024 |
| | | SiC | 3 | 30 | 0.035 | 0.029 | 0.034 |
| | | W1 | 5 | 30 | 0.027 | 0.029 | 0.02 |
| | | SiC | 5 | 60 | 0.032 | 0.028 | 0.023 |
| 3 | WB | W1 | 3 | 60 | 0.03 | 0.027 | 0.031 |
| | | SiC | 3 | 30 | 0.072 | 0.083 | 0.078 |
| | | W1 | 5 | 30 | 0.033 | 0.034 | 0.033 |
| | | SiC | 5 | 60 | 0.1 | 0.066 | 0.085 |
| | OB | W1 | 3 | 60 | 0.03 | 0.03 | 0.03 |
| | | SiC | 3 | 30 | 0.063 | 0.083 | 0.093 |
| | | W1 | 5 | 30 | 0.032 | 0.03 | 0.031 |
| | | SiC | 5 | 60 | 0.093 | 0.11 | 0.062 |
| 15 | WB | W1 | 3 | 60 | 0.088 | 0.085 | 0.086 |
| | | SiC | 3 | 30 | 0.066 | 0.063 | 0.064 |
| | | W1 | 5 | 30 | 0.106 | 0.089 | 0.098 |
| | | SiC | 5 | 60 | 0.095 | 0.077 | 0.069 |
| | OB | W1 | 3 | 60 | 0.097 | 0.087 | 0.089 |
| | | SiC | 3 | 30 | 0.076 | 0.077 | 0.079 |
| | | W1 | 5 | 30 | 0.075 | 0.085 | 0.076 |
| | | SiC | 5 | 60 | 0.079 | 0.081 | 0.076 |

## Experimental Values for MRR (Copper Plate)

| | | | | Time | 1 | | | 3 | | | 6 | | |
|---|---|---|---|---|---|---|---|---|---|---|---|---|---|
| Grain Size | Carrier | Workpiece | Load | rpm | 1 | 2 | 3 | 1 | 2 | 3 | 1 | 2 | 3 |
| 1 | WB | W1 | 3 | 60 | 0.0968 | 0.0645 | 0.0645 | 0.0645 | 0.1452 | 0.0323 | 0.0323 | 0.0108 | 0.0108 |
| | | SiC | 3 | 30 | 0.0323 | 0.0323 | 0.0645 | 0.1290 | 0.0161 | 0.1129 | 0.0215 | 0.0108 | 0.0430 |
| | | W1 | 5 | 30 | 0.0766 | 0.0766 | 0.2043 | 0.0511 | 0.0766 | 0.2490 | 0.0596 | 0.0724 | 0.0809 |
| | | SiC | 5 | 60 | 0.2299 | 0.2682 | 0.1149 | 0.1213 | 0.1341 | 0.1596 | 0.0128 | 0.0383 | 0.1149 |
| | OB | W1 | 3 | 60 | 0.2258 | 0.0645 | 0.2258 | 0.0161 | 0.0806 | 1.5161 | 0.0860 | 0.0538 | 0.0430 |
| | | SiC | 3 | 30 | 0.0645 | 0.0968 | 0.0323 | 0.0323 | 0.1613 | 0.1290 | 0.0430 | 0.1290 | 0.1398 |
| | | W1 | 5 | 30 | 0.5109 | 0.4087 | 0.5236 | 0.4151 | 0.4278 | 0.4534 | 0.0979 | 0.3023 | 0.0468 |
| | | SiC | 5 | 60 | 0.2937 | 0.3065 | 0.2682 | 0.2874 | 0.2746 | 0.3129 | 0.0468 | 0.1958 | 0.0639 |
| 3 | WB | W1 | 3 | 60 | 0.1290 | 0.0645 | 0.0323 | 0.2742 | 0.0968 | 0.3710 | 0.2581 | 0.0538 | 0.1935 |
| | | SiC | 3 | 30 | 0.0323 | 0.2903 | 0.5484 | 0.7581 | 0.4355 | 0.4355 | 0.1505 | 0.4086 | 0.8172 |
| | | W1 | 5 | 30 | 0.8812 | 0.7791 | 1.1239 | 0.2043 | 0.4853 | 0.1852 | 0.1618 | 0.2639 | 0.3321 |
| | | SiC | 5 | 60 | 0.3321 | 0.2171 | 0.3959 | 0.5492 | 0.4662 | 0.4342 | 0.1958 | 0.1277 | 0.1745 |
| | OB | W1 | 3 | 60 | 0.0323 | 0.1935 | 0.1935 | 0.0323 | 0.1129 | 0.0806 | 0.0430 | 0.0538 | 0.1075 |
| | | SiC | 3 | 30 | 0.1290 | 0.1613 | 0.3871 | 0.0645 | 0.0968 | 0.2903 | 0.0538 | 0.0753 | 0.2258 |
| | | W1 | 5 | 30 | 0.1660 | 0.1022 | 0.3704 | 0.1341 | 0.0830 | 0.1533 | 0.0085 | 0.1362 | 0.0426 |
| | | SiC | 5 | 60 | 0.8174 | 0.1916 | 0.2427 | 0.1213 | 0.4087 | 0.1980 | 0.1022 | 0.1703 | 0.0681 |
| 15 | WB | W1 | 3 | 60 | 0.7742 | 2.2581 | 2.7742 | 1.5000 | 2.7419 | 1.5645 | 1.0645 | 1.6129 | 2.2796 |
| | | SiC | 3 | 30 | 2.4516 | 3.0323 | 1.9355 | 4.8387 | 5.1290 | 3.4516 | 6.4624 | 2.7097 | 2.4516 |
| | | W1 | 5 | 30 | 0.7280 | 1.0089 | 0.8301 | 0.6258 | 0.2682 | 0.3640 | 0.7748 | 1.0132 | 0.8685 |
| | | SiC | 5 | 60 | 0.6003 | 0.5492 | 0.7407 | 0.5683 | 0.4087 | 0.4981 | 0.3959 | 0.3917 | 0.4470 |
| | OB | W1 | 3 | 60 | 2.0323 | 1.5806 | 2.0000 | 2.1613 | 2.2258 | 2.1935 | 2.6022 | 1.6452 | 2.3118 |
| | | SiC | 3 | 30 | 2.7419 | 5.3226 | 4.5484 | 2.6613 | 3.8226 | 3.9032 | 5.0323 | 5.9032 | 5.2366 |
| | | W1 | 5 | 30 | 0.9451 | 0.7152 | 0.9451 | 0.9515 | 1.3857 | 1.1814 | 1.0260 | 1.3495 | 1.0941 |
| | | SiC | 5 | 60 | 0.8557 | 0.7535 | 0.4598 | 0.8429 | 0.8493 | 0.4917 | 1.1877 | 1.2984 | 0.9238 |

*continued*

## Experimental Values for MRR (Copper Plate) (continued)

| | | | | Time | 11 | | | 21 | | | 36 | | |
|---|---|---|---|---|---|---|---|---|---|---|---|---|---|
| Grain Size | Carrier | Workpiece | Load | rpm | 1 | 2 | 3 | 1 | 2 | 3 | 1 | 2 | 3 |
| 1 | WB | W1 | 3 | 60 | 0.0065 | 0.0129 | 0.0065 | 0.0032 | 0.0484 | 0.0032 | 0.0022 | 0.0086 | 0.0065 |
| | | SiC | 3 | 30 | 0.0065 | 0.0065 | 0.0065 | 0.0129 | 0.0032 | 0.0355 | 0.0108 | 0.0108 | 0.0065 |
| | | W1 | 5 | 30 | 0.0077 | 0.0026 | 0.0102 | 0.0140 | 0.0077 | 0.0102 | 0.0051 | 0.0485 | 0.0077 |
| | | SiC | 5 | 60 | 0.0026 | 0.0128 | 0.0230 | 0.0140 | 0.0089 | 0.0051 | 0.0298 | 0.0307 | 0.0026 |
| | OB | W1 | 3 | 60 | 0.0710 | 0.0452 | 0.0323 | 0.0935 | 0.0710 | 0.0097 | 0.0258 | 0.0280 | 0.0710 |
| | | SiC | 3 | 30 | 0.0516 | 0.1032 | 0.1226 | 0.0613 | 0.0097 | 0.1871 | 0.0430 | 0.0065 | 0.0516 |
| | | W1 | 5 | 30 | 0.0153 | 0.1967 | 0.0179 | 0.2120 | 0.0983 | 0.0332 | 0.1771 | 0.0528 | 0.0153 |
| | | SiC | 5 | 60 | 0.2886 | 0.2605 | 0.1788 | 0.1137 | 0.2235 | 0.1073 | 0.0605 | 0.1652 | 0.2886 |
| 3 | WB | W1 | 3 | 60 | 0.1161 | 0.0194 | 0.0903 | 0.0710 | 0.0161 | 0.0581 | 0.0753 | 0.0043 | 0.1161 |
| | | SiC | 3 | 30 | 0.0710 | 0.2774 | 0.2516 | 0.0129 | 0.0903 | 0.1129 | 0.0215 | 0.0387 | 0.0710 |
| | | W1 | 5 | 30 | 0.1201 | 0.2375 | 0.2835 | 0.0983 | 0.2899 | 0.2605 | 0.0451 | 0.1107 | 0.1201 |
| | | SiC | 5 | 60 | 0.2120 | 0.1967 | 0.2043 | 0.2375 | 0.0128 | 0.0345 | 0.1737 | 0.1456 | 0.2120 |
| | OB | W1 | 3 | 60 | 0.0129 | 0.0516 | 0.0452 | 0.0065 | 0.0032 | 0.0032 | 0.0043 | 0.0215 | 0.0129 |
| | | SiC | 3 | 30 | 0.0645 | 0.0323 | 0.2258 | 0.0226 | 0.0161 | 0.1258 | 0.0151 | 0.0043 | 0.0645 |
| | | W1 | 5 | 30 | 0.0460 | 0.0996 | 0.0894 | 0.0089 | 0.0332 | 0.0307 | 0.0545 | 0.0477 | 0.0460 |
| | | SiC | 5 | 60 | 0.1098 | 0.2120 | 0.1201 | 0.0358 | 0.1673 | 0.0153 | 0.0587 | 0.1047 | 0.1098 |
| 15 | WB | W1 | 3 | 60 | 1.3097 | 2.8065 | 1.8258 | 1.5032 | 2.0613 | 1.4903 | 0.4495 | 0.6624 | 1.3097 |
| | | SiC | 3 | 30 | 6.2323 | 3.9935 | 4.0323 | 5.3355 | 3.8387 | 3.3355 | 5.6022 | 3.9634 | 6.2323 |
| | | W1 | 5 | 30 | 0.4291 | 0.4240 | 0.4163 | 0.4036 | 0.5964 | 0.5785 | 0.4598 | 0.5279 | 0.4291 |
| | | SiC | 5 | 60 | 0.3934 | 0.4036 | 0.5645 | 0.4074 | 0.4215 | 0.4610 | 0.4785 | 0.4496 | 0.3934 |
| | OB | W1 | 3 | 60 | 1.7548 | 1.8903 | 2.0194 | 1.4419 | 1.9452 | 2.1258 | 2.4710 | 1.7806 | 1.7548 |
| | | SiC | 3 | 30 | 6.0452 | 5.3613 | 4.6065 | 4.2774 | 5.4839 | 4.4161 | 2.9355 | 3.7677 | 6.0452 |
| | | W1 | 5 | 30 | 1.1954 | 1.1571 | 0.9502 | 1.2171 | 0.7957 | 0.9259 | 1.1077 | 1.2916 | 1.1954 |
| | | SiC | 5 | 60 | 1.3487 | 1.1826 | 0.7688 | 1.0077 | 0.6858 | 0.7126 | 0.9655 | 0.7007 | 1.3487 |

| | | | | Time | 66 | | |
|---|---|---|---|---|---|---|---|
| **Grain Size** | **Carrier** | **Workpiece** | **Load** | **rpm** | **1** | **2** | **3** |
| 1 | WB | W1 | 3 | 60 | 0.0022 | 0.0043 | 0.0097 |
| | | SiC | 3 | 30 | 0.0387 | 0.0065 | 0.0065 |
| | | W1 | 5 | 30 | 0.0264 | 0.0370 | 0.0460 |
| | | SiC | 5 | 60 | 0.0417 | 0.0209 | 0.0192 |
| | OB | W1 | 3 | 60 | 0.0108 | 0.0032 | 0.0204 |
| | | SiC | 3 | 30 | 0.0387 | 0.0043 | 0.0022 |
| | | W1 | 5 | 30 | 0.0051 | 0.0451 | 0.0426 |
| | | SiC | 5 | 60 | 0.0307 | 0.0958 | 0.1162 |
| 3 | WB | W1 | 3 | 60 | 0.0366 | 0.0796 | 0.0075 |
| | | SiC | 3 | 30 | 0.1183 | 0.0043 | 0.0290 |
| | | W1 | 5 | 30 | 0.0971 | 0.0605 | 0.0851 |
| | | SiC | 5 | 60 | 0.0894 | 0.1188 | 0.1430 |
| | OB | W1 | 3 | 60 | 0.0086 | 0.0022 | 0.0140 |
| | | SiC | 3 | 30 | 0.0430 | 0.0075 | 0.0086 |
| | | W1 | 5 | 30 | 0.0664 | 0.0426 | 0.0345 |
| | | SiC | 5 | 60 | 0.0962 | 0.0285 | 0.0289 |
| 15 | WB | W1 | 3 | 60 | 0.5462 | 1.2710 | 1.8215 |
| | | SiC | 3 | 30 | 2.6731 | 4.8495 | 4.3032 |
| | | W1 | 5 | 30 | 0.5126 | 0.5015 | 0.6020 |
| | | SiC | 5 | 60 | 0.5100 | 0.4274 | 0.3814 |
| | OB | W1 | 3 | 60 | 1.5613 | 1.9280 | 1.9269 |
| | | SiC | 3 | 30 | 4.6151 | 3.1022 | 3.5710 |
| | | W1 | 5 | 30 | 0.9246 | 0.9170 | 1.0209 |
| | | SiC | 5 | 60 | 0.5577 | 0.7833 | 0.5909 |

*continued*

## Experimental Values for MRR (Iron Plate)

| | | | | Time | 1 | | | 3 | | | 6 | | |
|---|---|---|---|---|---|---|---|---|---|---|---|---|---|
| Grain Size | Carrier | Workpiece | Load | rpm | 1 | 2 | 3 | 1 | 2 | 3 | 1 | 2 | 3 |
| 1 | WB | W1 | 3 | 60 | 0.2581 | 0.0968 | 0.1613 | 0.0645 | 0.0484 | 0.1613 | 0.0538 | 0.0215 | 0.1075 |
| | | SiC | 3 | 30 | 0.2581 | 0.5161 | 0.5806 | 0.1452 | 0.2097 | 0.0645 | 0.0323 | 0.1183 | 0.0215 |
| | | W1 | 5 | 30 | 0.0894 | 0.1916 | 0.0639 | 0.0447 | 0.0639 | 0.0383 | 0.0128 | 0.0170 | 0.0213 |
| | | SiC | 5 | 60 | 0.1788 | 0.1277 | 0.0766 | 0.0511 | 0.0830 | 0.0128 | 0.0639 | 0.0128 | 0.0213 |
| | OB | W1 | 3 | 60 | 0.0323 | 0.0968 | 0.0323 | 0.0323 | 0.0484 | 0.0323 | 0.0215 | 0.0538 | 0.0108 |
| | | SiC | 3 | 30 | 0.0323 | 0.1935 | 0.2581 | 0.0161 | 0.0968 | 0.0968 | 0.0108 | 0.0753 | 0.0538 |
| | | W1 | 5 | 30 | 0.3576 | 0.4215 | 0.4598 | 0.1277 | 0.0958 | 0.0894 | 0.0766 | 0.0766 | 0.1149 |
| | | SiC | 5 | 60 | 0.3704 | 0.2554 | 0.2299 | 0.2107 | 0.1852 | 0.1086 | 0.1235 | 0.1064 | 0.1107 |
| 3 | WB | W1 | 3 | 60 | 0.1935 | 0.0323 | 0.1935 | 0.2903 | 0.0968 | 0.1774 | 0.2043 | 0.0645 | 0.0753 |
| | | SiC | 3 | 30 | 0.0323 | 0.8065 | 0.2903 | 0.1452 | 0.7258 | 0.6452 | 0.0323 | 0.4301 | 0.2688 |
| | | W1 | 5 | 30 | 0.3065 | 0.5109 | 0.5236 | 0.1980 | 0.4342 | 0.4406 | 0.0809 | 0.2852 | 0.3065 |
| | | SiC | 5 | 60 | 0.5875 | 0.6258 | 0.3193 | 0.1916 | 0.3959 | 0.1596 | 0.2214 | 0.2639 | 0.2341 |
| | OB | W1 | 3 | 60 | 0.0323 | 0.0645 | 0.0323 | 0.0484 | 0.0645 | 0.0161 | 0.0753 | 0.0323 | 0.0430 |
| | | SiC | 3 | 30 | 0.0323 | 0.0323 | 0.0645 | 0.0484 | 0.0645 | 0.1613 | 0.0538 | 0.0215 | 0.2043 |
| | | W1 | 5 | 30 | 0.2554 | 0.3065 | 0.0128 | 0.2363 | 0.1213 | 0.2810 | 0.0553 | 0.1277 | 0.1575 |
| | | SiC | 5 | 60 | 0.3065 | 0.5747 | 0.5364 | 0.1533 | 0.2554 | 0.1149 | 0.1107 | 0.1149 | 0.1235 |
| 15 | WB | W1 | 3 | 60 | 0.5161 | 1.1613 | 1.1613 | 0.1290 | 0.0484 | 3.0806 | 2.4086 | 1.4086 | 1.9355 |
| | | SiC | 3 | 30 | 2.0000 | 1.5806 | 2.8710 | 7.8065 | 3.4516 | 0.0484 | 4.1505 | 16.1398 | 6.4624 |
| | | W1 | 5 | 30 | 1.2261 | 0.6386 | 0.6641 | 1.0026 | 0.6450 | 0.6960 | 0.8472 | 0.7195 | 0.6386 |
| | | SiC | 5 | 60 | 0.6130 | 0.5109 | 0.7918 | 0.5428 | 0.5811 | 0.6833 | 0.5577 | 0.7195 | 0.7620 |
| | OB | W1 | 3 | 60 | 0.9032 | 0.8065 | 1.3548 | 1.2097 | 1.4839 | 3.1129 | 1.0215 | 1.3011 | 3.1505 |
| | | SiC | 3 | 30 | 1.3226 | 7.8065 | 6.0645 | 1.8226 | 6.8387 | 5.8548 | 2.8710 | 5.0538 | 7.0215 |
| | | W1 | 5 | 30 | 1.6731 | 1.1111 | 1.1622 | 1.7241 | 1.1047 | 1.0856 | 1.2644 | 1.1281 | 1.1665 |
| | | SiC | 5 | 60 | 0.7535 | 0.7407 | 0.9834 | 0.9834 | 0.8301 | 1.1877 | 1.0089 | 0.8259 | 1.0132 |

| | | | | Time | 11 | | | 21 | | | 36 | | |
|---|---|---|---|---|---|---|---|---|---|---|---|---|---|
| **Grain Size** | **Carrier** | **Workpiece** | **Load** | **rpm** | **1** | **2** | **3** | **1** | **2** | **3** | **1** | **2** | **3** |
| 1 | WB | W1 | 3 | 60 | 0.0452 | 0.0194 | 0.0839 | 0.0129 | 0.0032 | 0.0161 | 0.0194 | 0.0022 | 0.0559 |
| | | SiC | 3 | 30 | 0.0645 | 0.0774 | 0.0065 | 0.0323 | 0.0065 | 0.0032 | 0.0108 | 0.0194 | 0.0022 |
| | | W1 | 5 | 30 | 0.0051 | 0.0128 | 0.0179 | 0.0051 | 0.0013 | 0.0038 | 0.0034 | 0.0026 | 0.0017 |
| | | SiC | 5 | 60 | 0.0230 | 0.0128 | 0.0128 | 0.0102 | 0.0038 | 0.0051 | 0.0085 | 0.0077 | 0.0068 |
| | OB | W1 | 3 | 60 | 0.0129 | 0.0387 | 0.0065 | 0.0065 | 0.0419 | 0.0032 | 0.0043 | 0.0538 | 0.0043 |
| | | SiC | 3 | 30 | 0.0129 | 0.0710 | 0.0452 | 0.0065 | 0.0452 | 0.0323 | 0.0043 | 0.0258 | 0.0237 |
| | | W1 | 5 | 30 | 0.0690 | 0.0383 | 0.1022 | 0.0383 | 0.0524 | 0.0549 | 0.0034 | 0.0043 | 0.0077 |
| | | SiC | 5 | 60 | 0.0894 | 0.0664 | 0.0817 | 0.0140 | 0.0153 | 0.0741 | 0.0119 | 0.0187 | 0.0332 |
| 3 | WB | W1 | 3 | 60 | 0.0968 | 0.0323 | 0.0581 | 0.0871 | 0.0194 | 0.0290 | 0.0602 | 0.0194 | 0.0108 |
| | | SiC | 3 | 30 | 0.0258 | 0.3355 | 0.2000 | 0.0032 | 0.2290 | 0.1677 | 0.0043 | 0.1871 | 0.0796 |
| | | W1 | 5 | 30 | 0.0945 | 0.2631 | 0.2452 | 0.1124 | 0.1073 | 0.1086 | 0.0255 | 0.0528 | 0.0494 |
| | | SiC | 5 | 60 | 0.1967 | 0.1890 | 0.1149 | 0.1315 | 0.1111 | 0.1226 | 0.1175 | 0.0851 | 0.1013 |
| | OB | W1 | 3 | 60 | 0.0452 | 0.0258 | 0.0065 | 0.0419 | 0.0194 | 0.0097 | 0.0495 | 0.0323 | 0.0129 |
| | | SiC | 3 | 30 | 0.0774 | 0.0452 | 0.1290 | 0.0161 | 0.0194 | 0.1387 | 0.0258 | 0.0194 | 0.0688 |
| | | W1 | 5 | 30 | 0.0971 | 0.1124 | 0.0971 | 0.0766 | 0.0881 | 0.0907 | 0.0775 | 0.1005 | 0.0843 |
| | | SiC | 5 | 60 | 0.1022 | 0.0690 | 0.0690 | 0.0817 | 0.0651 | 0.0856 | 0.0519 | 0.0494 | 0.0468 |
| 15 | WB | W1 | 3 | 60 | 1.3161 | 2.3097 | 1.8452 | 1.2677 | 1.7000 | 1.4968 | 1.4903 | 1.2344 | 2.1290 |
| | | SiC | 3 | 30 | 4.3871 | 6.2129 | 5.8839 | 4.7032 | 2.7613 | 5.7000 | 4.0495 | 4.6194 | 4.1376 |
| | | W1 | 5 | 30 | 0.5441 | 0.4777 | 0.5057 | 0.7433 | 0.6194 | 0.7612 | 0.6488 | 0.6122 | 0.6249 |
| | | SiC | 5 | 60 | 0.5441 | 0.4674 | 0.5185 | 0.4853 | 0.5594 | 0.5121 | 0.4538 | 0.5432 | 0.6275 |
| | OB | W1 | 3 | 60 | 0.9548 | 1.9548 | 3.6516 | 1.3710 | 1.1387 | 2.5000 | 0.8817 | 1.2882 | 1.3828 |
| | | SiC | 3 | 30 | 2.2452 | 4.5419 | 5.3161 | 2.8742 | 3.4839 | 3.8226 | 3.4839 | 4.0301 | 2.8151 |
| | | W1 | 5 | 30 | 1.3640 | 0.8276 | 1.1009 | 1.3525 | 0.7446 | 1.0600 | 1.2295 | 0.8216 | 0.6777 |
| | | SiC | 5 | 60 | 1.0064 | 1.1060 | 0.9527 | 0.8404 | 0.7178 | 0.8352 | 0.7833 | 0.8685 | 0.9017 |

*continued*

## Experimental Values for MRR (Iron Plate) (continued)

| | | | | Time | 66 | | |
|---|---|---|---|---|---|---|---|
| Grain Size | Carrier | Workpiece | Load | rpm | 1 | 2 | 3 |
| 1 | WB | W1 | 3 | 60 | 0.0118 | 0.0011 | 0.0204 |
| | | SiC | 3 | 30 | 0.0108 | 0.0118 | 0.0043 |
| | | W1 | 5 | 30 | 0.0009 | 0.0013 | 0.0013 |
| | | SiC | 5 | 60 | 0.0072 | 0.0030 | 0.0017 |
| | OB | W1 | 3 | 60 | 0.0022 | 0.0366 | 0.0032 |
| | | SiC | 3 | 30 | 0.0032 | 0.0667 | 0.0419 |
| | | W1 | 5 | 30 | 0.0319 | 0.0268 | 0.0307 |
| | | SiC | 5 | 60 | 0.0051 | 0.0038 | 0.0085 |
| 3 | WB | W1 | 3 | 60 | 0.0237 | 0.0086 | 0.0237 |
| | | SiC | 3 | 30 | 0.0011 | 0.0505 | 0.0624 |
| | | W1 | 5 | 30 | 0.0272 | 0.0498 | 0.0451 |
| | | SiC | 5 | 60 | 0.0438 | 0.0379 | 0.0443 |
| | OB | W1 | 3 | 60 | 0.0387 | 0.0118 | 0.0011 |
| | | SiC | 3 | 30 | 0.0247 | 0.0129 | 0.0656 |
| | | W1 | 5 | 30 | 0.1111 | 0.1328 | 0.0809 |
| | | SiC | 5 | 60 | 0.0243 | 0.0213 | 0.0209 |
| 15 | WB | W1 | 3 | 60 | 1.0118 | 0.7097 | 0.8720 |
| | | SiC | 3 | 30 | 1.9151 | 2.5194 | 2.6419 |
| | | W1 | 5 | 30 | 0.5837 | 0.6530 | 0.6484 |
| | | SiC | 5 | 60 | 0.5330 | 0.5189 | 0.6177 |
| | OB | W1 | 3 | 60 | 1.1548 | 1.3172 | 2.1355 |
| | | SiC | 3 | 30 | 3.1151 | 3.1957 | 3.2505 |
| | | W1 | 5 | 30 | 0.8689 | 0.4449 | 0.5615 |
| | | SiC | 5 | 60 | 0.7599 | 0.6041 | 0.7305 |

## APPENDIX B
## The MATLAB Source Code That Was Designed to Model the Problem

```
clear;
'*************************************************
% Load the ROUGH_DATA matrix with the respective
experimental values
ROUGH_DATA = [
0.111  0.077  0.113;
0.084  0.097  0.097;
0.062  0.105  0.08
0.081  0.076  0.087
];
% DO NOT EDIT UNDER THIS LINE
%%%%%%%%%%%%%%%%%%%%%%%%%%%%%%%%%%%%%%%%%%%%%%%%
MAT = [1 2]; %MAT1 is W1, while MAT2 is SiC
LOAD = [3 5];
SPEED = [30 60];
A = [
    -1  -1   1;
     1  -1  -1;
    -1   1  -1;
     1   1   1;
];
DATA = sum(ROUGH_DATA, 2);
CONTRAST = A'*DATA./size(ROUGH_DATA, 2)
ESTIMATES = CONTRAST./2
REGR_COEFF = ESTIMATES./2;
SUM_OF_SQUARES = (CONTRAST.^2)./4
SSModel = sum(SUM_OF_SQUARES)
SST = sum(sum(ROUGH_DATA.^2, 1), 2)-
sum(sum(ROUGH_DATA, 1), 2)^2/(size(ROUGH_DATA, 1)*
  size(ROUGH_DATA, 2))
SSE = SST-sum(sum(SUM_OF_SQUARES, 1), 2)
R_Squared_in_percents = SSModel*100/SST
PERCENT_CONTRIB = (SUM_OF_SQUARES./SST)*100
PERCENT_CONTRIB_ERR = SSE*100/SST
DOF = 1;
MEAN_SQUARES = SUM_OF_SQUARES./DOF
MSE = SSE/7
FO = MEAN_SQUARES./MSE
COEFF_REGR = ESTIMATES./2
INTERCEPT = sum(sum(ROUGH_DATA, 1),2)/
  (size(ROUGH_DATA, 1)*size(ROUGH_DATA, 2))
```

```
PREDICTED_VALUE = INTERCEPT+A*COEFF_REGR
I3 = [1 1 1];
PREDICTED_VALUE1 = PREDICTED_VALUE*I3;
ERR = ROUGH_DATA-PREDICTED_VALUE1

for i = 1:4;
    for j = 1:3;
       RESIDUALS(1, j+3*(i-1)) = ERR(i, j);
    end;
end;

k = 0;
for i = 1:2:3;
    for j = 1:3;
        k = k+1;
       MAT_DATA(1, k) = ROUGH_DATA(i, j);
    end;
end;

k = 0;
for i = 2:2:4;
    for j = 1:3;
        k = k+1;
       MAT_DATA(2, k) = ROUGH_DATA(i, j);
    end;
end;

MAT_DATA
MAT_MEAN = mean(MAT_dATA, 2)

k = 0;
for i = 1:2;
    for j = 1:3;
        k = k+1;
       LOAD_DATA(1, k) = ROUGH_DATA(i, j);
    end;
end;

k = 0;
for i = 3:4;
    for j = 1:3;
        k = k+1;
        LOAD_DATA(2, k) = ROUGH_DATA(i, j);
    end;
end;

LOAD_DATA
```

```
LOAD_MEAN=mean(LOAD_DATA, 2)

k=0;
for i=2:3;
    for j=1:3;
        k=k+1;
        SPEED_DATA(1, k)=ROUGH_DATA(i, j);
    end;
end;

k=0;
for i=1:3:4;
    for j=1:3;
        k=k+1;
        SPEED_DATA(2, k)=ROUGH_DATA (i, j);
    end;
end;

SPEED_DATA
SPEED_MEAN=mean(SPEED_DATA, 2)

k=0;
for i=1:4;
    for j=1:3;
        k=k+1;
        ALT_DATA(1, k)=ROUGH_DATA(i, j);
    end;
end;

ALT_DATA
```

# 5 Lapping and Lapping Machines

*Toshiro K. Doi and Daizo Ichikawa*

## CONTENTS

5.1 Introduction ..... 265
5.2 Processing Principles of the Lapping and Its Characteristics ..... 266
5.2.1 Lapping Factors ..... 267
5.2.1.1 Motion Type ..... 267
5.2.1.2 Lap (Lapping Plate) ..... 268
5.2.1.3 Abrasives and Reagent in the Lapping Slurry ..... 268
5.2.1.4 Mechanical Lapping Conditions ..... 268
5.2.2 Processing Accuracy in the Lapping ..... 269
5.2.2.1 Conditioning Ring ..... 269
5.2.2.2 Cooling of Lapping Plate and Cooling Device ..... 270
5.2.2.3 Grooves in the Lapping Plate ..... 271
5.3 Lapping Machine ..... 272
5.3.1 Oscar-Type Lens Lapping Machine ..... 272
5.3.2 Conditioning Ring Type Lapping Machine ..... 273
5.3.3 Both-Sides Simultaneous Lapping Machine ..... 274
5.4 Both-Sides Simultaneous Lapping Machine Equipped with a New Micromotion Mechanism ..... 275
5.5 Conclusions ..... 278
References ..... 279

## 5.1 INTRODUCTION

Lapping is generally applied to the rough processing before the finishing process, or to the intermediate processing, depending on the types of workpieces and the intended purposes. Lapping, which is one of the polishing processes aimed to obtain better accuracy of the shape, employs loose abrasive processing methods. Lapping slurry is supplied onto the rotating hard tool (lapping plate), against which workpieces are pressed down, and the relative movements among the workpieces, abrasives, and rotating plate are performed. Lapped surfaces appear to be a frosted glass. Lapping is a typical processing method integrated before the polishing process in the fabrication process of glass lens, prisms, quartzes, and silicon wafers for LSI.

This chapter deals with the processing principles of the lapping and lapping machines.

## 5.2 PROCESSING PRINCIPLES OF THE LAPPING AND ITS CHARACTERISTICS

Relative motion to slide the plate and workpieces against each other while dispersing slurry consisted of abrasives and water solution over the lapping plate is common in both lapping and polishing. The main difference in lapping and polishing is that lapping is based on the crushing actions produced by the rolling of the abrasives dispersed over the hard plate (cast iron, glass, etc.) generating cracks and scratches on the workpieces, while polishing is based on the microscratch actions of the abrasives embedded in the soft pad (polisher). Besides scratching actions, polishing goes through the other complicated processes including the material flow and the chemical reactions between materials and abrasives or processing reagents. Meanwhile, mechanical actions are the main processing mechanism in the lapping process.

Basically, lapping is a transcribing process of the lapping plate surface to the workpieces. In microscopic view, the abrasives roll in-between the lapping plate and the workpieces that are held by the plate surface, and crush the workpiece surfaces generating scratches on the surfaces. The abrasives are also held by the facing workpieces, and simultaneously scratch the plate surface as a reciprocal behavior. The ratio of the stock of removal (processed amount) between the workpieces and the lapping plate varies depending on the types and conditions of the workpieces, abrasives, lapping reagent, and lapping plate. A processing mechanism of the lapping is indicated in Figure 5.1. As lapping progresses, cutting chips are generated from the workpieces, and the lapping plate is abraded while the abrasives are being crushed.

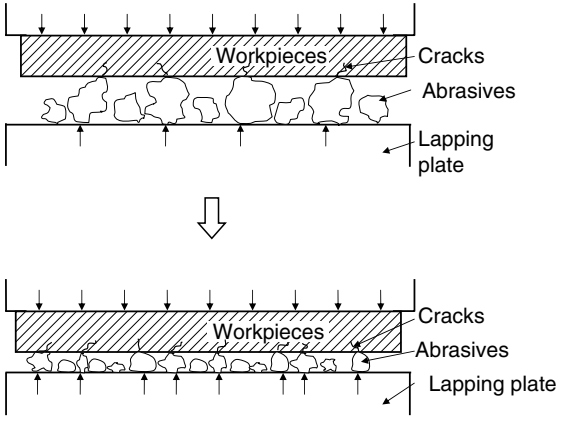


**FIGURE 5.1** Processing mechanism in lapping.

**TABLE 5.1**
**Main Factors of Lapping**

| | | Lapping |
|---|---|---|
| Motion type | Processing type | Single-side processing, both-sides processing, conditioning ring |
| | Processing motion | Rotation, reciprocating, forced drive, driven |
| Tool | Material | Hard material (cast iron, glass, etc.) |
| | Shape | Flat, spherical, aspherical, groove (crosscut, spiral, hexagonal) |
| Abrasives | Type | Hardness, shape, metal oxide, carbide, diamond |
| | Particle size | 1–30 μm |
| Reagent | Water-based, oil-based, additive (surfactant, alkali, etc.) | |
| Relative speed | 5–40 (m/min) | |
| Processing pressure | 30–300 ($gf/cm^2$) | |
| Processing time | (Control over stock of removal and processing accuracy) | |

As shown in Table 5.1, lapping factors consist of the type of the relative motion between the lapping plate and workpieces, type of the lapping plate and abrasives, type of the lapping reagents to which abrasives are dispersed, and mechanical conditions such as processing pressure and relative speed.

## 5.2.1 Lapping Factors

### 5.2.1.1 Motion Type

The ideal movement in the single-side lapping is that when a workpiece slides over the lapping plate, the trajectory of the relative movements at any point of the workpiece should be smooth forming a continuous curving line, and the length of the trajectory from each point should be the same. Motion type in the lapping machine is a fundamental factor to secure processing accuracy, and there are the following two types: (1) lens processing (lapping/polishing) method, which allows the workpieces to make reciprocating motions while rotating on its own axis on the revolving lapping plate surface, and (2) ring method, which places workpieces inside the rotating ring (or condition ring) set properly between the center and periphery of the lapping plate. By altering the position and amplitude of the reciprocal movement, and the number of rotation of the workpieces, these two methods allow a change of the density of the trajectories, and a control over the amount of the lapping plate abrasion. They can also condition the shape of the lapping plate surface.

Besides the single-side lapping, there is a both-sides lapping, which simultaneously laps both sides of the workpieces housed in the carriers

(wafer holder) that are placed symmetrically on the lapping plate and held in-between the upper and lower lapping plates, allowing the workpieces to have the same trajectories. As lapping pressure works preferentially on thicker workpieces, it has the beneficial effect of minimizing the thickness variations and parallelism errors of the workpieces.

#### 5.2.1.2 Lap (Lapping Plate)

Lapping principle rests on the transcription of the lapping plate surface to the workpiece, which explains why its surface accuracy and material are so critical. Normally, the lapping plate is made of cast iron, consists of the hard cementite and relatively soft ferrite. This is very beneficial to the lapping because unevenness of the abrasive size (particle distribution of the abrasives) can be eased by the ferrite, whereas cementite can promote the cutting actions of the abrasives further. In general, the lapping plate surface is grooved with the exception of the lapping plate designed for small workpieces. The most popular shapes of grooves are crosscut, followed by the concentric circle and spiral. These grooves are very effective not only in artificially creating the functions similar to that of the cast iron mentioned above, but also in holding and supplying lapping slurries and discharging cutting chips as well as in deconcentrating the pressure distributions.

#### 5.2.1.3 Abrasives and Reagent in the Lapping Slurry

In general, alumina ($Al_2O_3$) or silicon carbide (SiC) of diameter 1–50 μm is used for the lapping abrasives, as both are very hard with an efficient cutting action. Alumina abrasives are round-shaped with high toughness, which makes them hard to be crushed, whereas silicon carbide abrasives are easily crushed due to its sharp cutting edge. Depending on the mechanical characteristics of the workpieces, either of these abrasives is chosen.

Usually, the average size of the abrasives is proportional to the processing efficiency and surface roughness of the workpiece. Typically, the size of the abrasives is sequentially reduced to half during the lapping process. This condition is very rational to ensure perfect removal of the projected surface topographies and work-damaged layers generated in the previous processes so that predetermined shape of the workpieces can be obtained.

On the other, reagents in the lapping slurry work to lubricate and evenly disperse abrasives, allowing rolling of the abrasives and discharge (transferring function) of cutting chips. Although water (or purified water) is usually used, oil or oil-based water solution is used when mechanical removal actions of the abrasives need to be subdued, and the coefficient of friction should be controlled.

#### 5.2.1.4 Mechanical Lapping Conditions

Processing characteristics in lapping involve removal rate, lapping friction, surface roughness, and processed-damaged layers, which are affected by the

material of the lapping plates, the abrasives and lapping reagents, and the relative speed (rotation number, drive distance).

Typically, the following equation (called Preston's formula) is applied:

$$\text{(Stock of removal)} = \alpha \times \text{(processing pressure)} \times \text{(relative speed)} \times \text{(processing time)}$$

The parameter $\alpha$ depends on the processing conditions such as size, type, and density of the abrasives.

Horizontal lapping friction during lapping is related to the mechanical properties of the workpiece. Generally, the harder the workpieces are, the friction tends to be higher, and when processing pressure increases, the processing friction also tends to increase. Increase of the processing friction along with the increase of processing pressure occurs due to subsequent increment of the number of acting abrasives, and increasing cutting depth of the abrasives. However, when the processing pressure exceeds over a certain level, processing friction becomes steady as the removal action of the workpiece reaches the limit for crushing.

When the size of the abrasives becomes large, the roughness of the lapped surface becomes large, leaving deeper cracks on the layers. Abrasives with crushing function have a tendency to leave a number of microscratches on the surface of workpieces, while abrasives with high elasticity tend to produce long scratches.

### 5.2.2 Processing Accuracy in the Lapping

The most influential and deciding factor to the processing accuracy of the workpieces is the flatness of the lapping plate. With the increase of the lapping time, surface precision of the lapping plate deteriorates, requires reconditioning. Reconditioning is normally done by removing the lapping plate from the machine, whose surface is then ground or lapped, or by placing a conditioning ring on the lapping plate to recondition the plate. As the former method significantly lowers the working efficiency in removing and remounting the lapping plate, the latter is preferred.

Temperature change caused by the friction heat generated during the lapping and environmental temperatures also affects the shape accuracy of the lapping plate. Therefore, it is desirable to maintain the working room at a constant temperature. As the friction heat from the long run lapping in particular deforms the lapping plate and degrades its flatness, it is essential to cool the plate down during the lapping in order to keep the plate to a certain temperature.

#### 5.2.2.1 Conditioning Ring

Conditioning ring with parallelism and flatness is usually made of the same material as the lapping plate, and is doughnut-shaped or with an eccentric

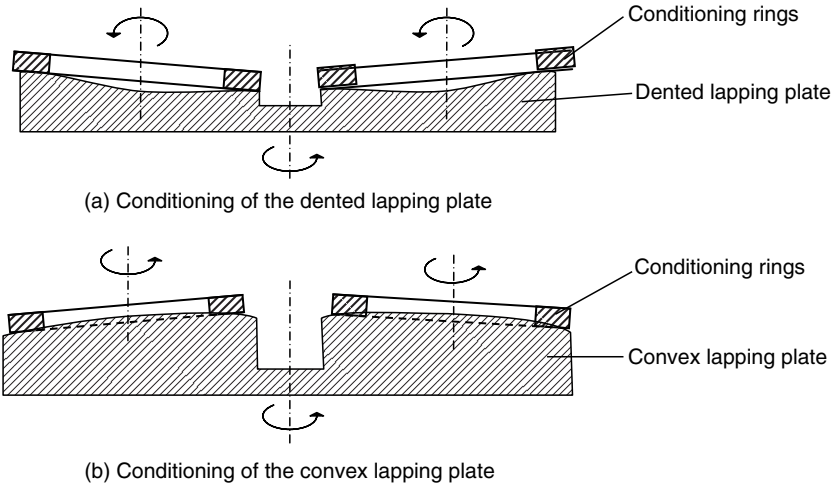
Conditioning rings
Dented lapping plate
(a) Conditioning of the dented lapping plate
Conditioning rings
Convex lapping plate
(b) Conditioning of the convex lapping plate

**FIGURE 5.2** Conditioning methods of the lapping plate with a conditioning ring.

hole. By rotating the conditioning ring both on its axis and across the lapping plate, the lapping plate is lapped until it recovers the specified accuracy.

In order to recondition the plate that is dented as in the Figure 5.2a, conditioning rings are placed slightly toward the edge of the plate and run while lapping slurry is being supplied onto the plate. Depending on the level of the dent, the rotary and revolutionary ratio is changed, or the conditioning rings are rotated in the opposite direction of the lapping plate. When the lapping plate has become convex as indicated in Figure 5.2b, the conditioning rings should be placed slightly toward the center, and then the lapping plate and the conditioning rings are set to rotate in the same direction. The difference in the relative speeds between the center and edge of the lapping plate allows the plate to gain its original flatness. The rotation ratio between the lapping plate and the conditioning ring should be changed according to the level of the conditioning needed.

#### 5.2.2.2 Cooling of Lapping Plate and Cooling Device

Cooling of the lapping plate prevents its shape accuracy from deterioration to be caused by the heat deformation of the lapping plate during the lapping. It also prevents the wax that adheres workpieces from softening.

To keep the temperature of the lapping plate constant, temperature is usually controlled by water-cooling, chiller, which regulates the temperature of the cooling water. Typically, the chiller, an external cooling device, and a heater are combined to control the temperature of the lapping plate within a given tolerance. Figure 5.3 shows an example of the cooling system, incorporated into a both-sides simultaneous lapping machine. Cooling water,

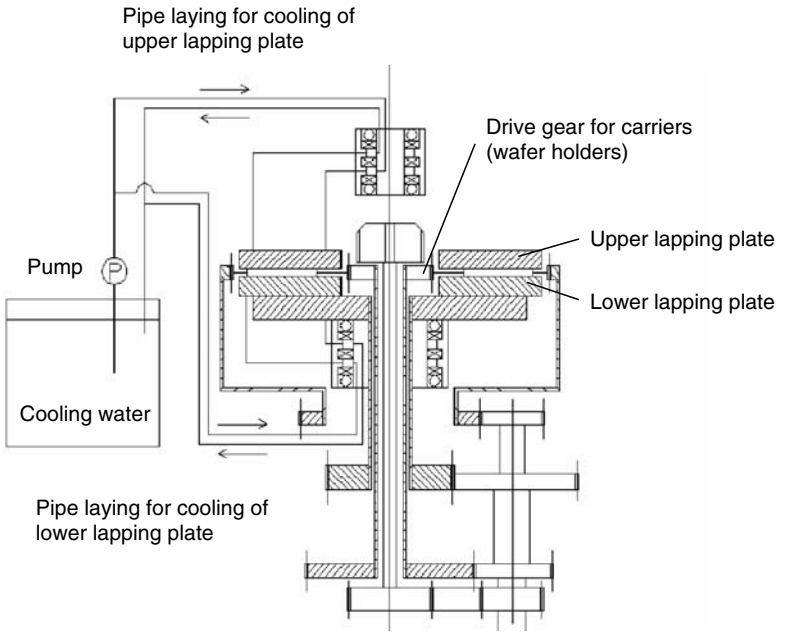


**FIGURE 5.3** Cooling system of the lapping plate (simultaneous both-sides lapping machine).

regulated to a constant temperature, flows through the channels formed on the lapping plates to keep temperatures constant.

#### 5.2.2.3 Grooves in the Lapping Plate

Generally, surfaces of the lapping plates are grooved about 1 mm width in the form of grate or diamond. The grooves serve to hold slurries, remove cutting chips, and evenly supply slurries to the workpieces. More importantly, grooves uniformize the distribution of the pressure beneath the workpiece, which works to improve the flatness accuracy of the workpiece as indicated in Figure 5.4. When even distribution load is applied to the workpieces placed on the nongrooved lapping plate, the stress distribution beneath the workpieces becomes the biggest in the periphery of the workpieces, although it is not as notable as in the elastic body that is pressed against the rigid body as often argued in the elasticity theory.

When the lapping plate is grooved, the pressure is distributed between the neighboring grooves. Such pressure distribution is interrupted by the grooves, making the pressure distribution beneath the workpieces small and uniform. As both workpieces and lapping plates work relatively, workpieces can be lapped to a uniform and high accuracy flatness. The grooves formed in the lapping plate are essential to secure the lapping accuracy. Due to its ability to

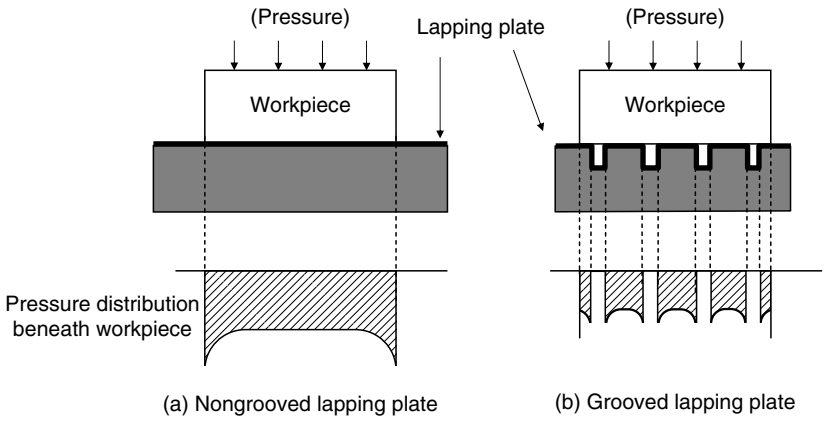


**FIGURE 5.4** Effect of grooves in the lapping plate.

hold and supply abrasives, the groove's contribution to the improvement of lapping efficiency is very significant. The grooves also serve to discharge cutting chips, contributing to improve the quality of the workpiece surfaces.

## 5.3 LAPPING MACHINE

Various types of lapping machines have been commercially developed. Lapping by means of sliding workpieces over the rotating lapping plate as mentioned above is important especially in light of not only from producing cutting chips but also from the high-precision lapping, transcribing the flat surface of the lapping plate to the workpieces. In the lapping, abrasives not only remove the projecting surfaces of the workpieces but also abrade the lapping plate at the same time, which requires the surface of the lapping plate to be always kept accurately flat. In the regular lapping machines, relative movements of the lapping plate and workpieces are induced from respective rotations and reciprocal movements.

### 5.3.1 Oscar-Type Lens Lapping Machine

From a long time ago, lens lapping machines are used in the fabrication process of the optical parts. The structure of the machine is comparatively simple and it is not a very high-precision machine. However, the versatility of the machine is high as employed for the lapping of several different shapes, including flat, spherical, and aspherical surfaces. In the lapping, reciprocal movements of the workpieces (or lapping plate) are induced in such a way that the workpieces to which load is applied through a pivot are pressed against a rotating, disk-type lapping plate made of cast iron (or workpieces). As the workpieces are held only by the pivot, they follow the rotation of the

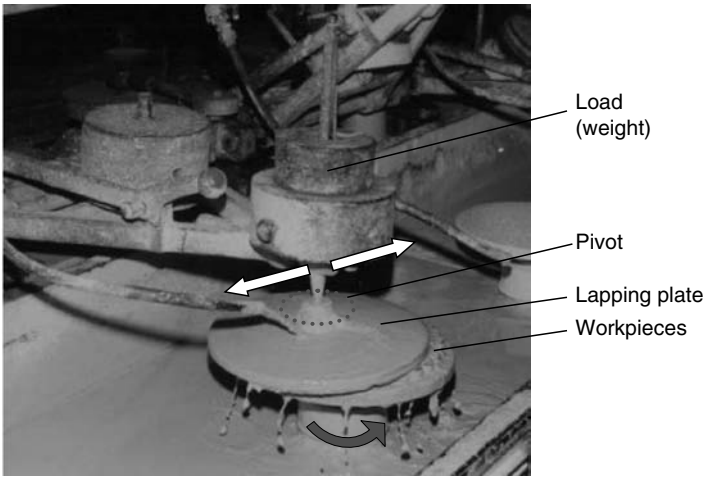


**FIGURE 5.5** Oscar-type lens lapping machine.

lapping plate, contributing to the uniformization of the kinetic trajectories. In this Oscar-type machine, it is critical that the amplitude of the reciprocal movements and the rotation number of the lapping plate are set adequately according to the size of workpieces and lapping plate. Figure 5.5 shows an external view of a typical lens lapping machine.

### 5.3.2 Conditioning Ring Type Lapping Machine

The conditioning ring type lapping machine features comparatively easy operation among various single-side lapping machines, and is mainly applied to lap workpieces to a flat. Lapping is performed through simple rotations of both the doughnut-shaped ring, mounted on the rotating lapping plate, and workpieces placed inside the ring. Using the conditioning ring, this lapping method features in situ conditioning of the abraded lapping plate caused by the workpieces and abrasives. Such effect of conditioning during lapping is also applied to the pitch polishing that abrades the tool significantly. Pitch polishing is used for the lapping of optical parts such as lens and prisms from long ago.

This conditioning ring type machine is usually used for flat lapping. However, in view of its lapping principle that is the transcription of the planar surface of the lapping plate, the machine can be also employed for the fabrication of high-precision long focal point reflecting mirrors, if a lapping plate is made to a given shape of convex or concave.

The lapping machine with the kinetic mechanism of this processing method can realize high-precision processing as the relative speed becomes constant at any point of the contacting areas between the lapping plate and the

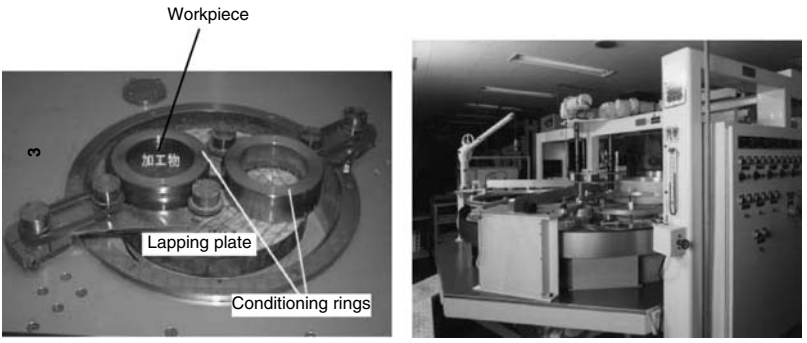


(a) Compact conditioning ring type machine

(b) Large conditioning ring type machine (Lapping plate: 2.5 m in diameter, maximum workpieces: 600 mm)

**FIGURE 5.6** Exterior views of conditioning ring type lapping machines (compact and large-sized machines).

workpieces or conditioning ring when rotation number of the lapping plate coincides with that of the workpieces or conditioning ring. In other words, it is extremely important to have control of the rotation numbers of each workpiece, conditioning ring, and lapping plate. When the size of the lapping plate in this machine is made infinitely large, the method corresponds to the belt lapping method.

Figure 5.6 shows exterior views of the compact and large conditioning ring type lapping machines. The large-sized machine is currently used for the ultraprecision lapping of the large reflecting mirrors, mounted in the laser fusion system. This machine is able to process (lapping and polishing) workpieces of a maximum of 600 mm size, as it has a lapping plate of 2.5 m in diameter.

### 5.3.3 Both-Sides Simultaneous Lapping Machine

When a number of substrate-shaped workpieces need to be lapped, a both-sides lapping machine is used that simultaneously laps both sides of the workpieces. More than two workpieces are set in-between the two facing lapping plates mounted one above the other, and relative movements are given to the lapping plates and workpieces. Generally, the lapping plates are doughnut-shaped with a hole in the center. There are two-motion type and four-motion type machines. Two-motion type machine makes the carrier that holds workpieces rotate on its own axis across the lapping plates that are kept still (without rotation). Four-motion type machine additionally provides forward and reversible rotations to each lapping plate (rotate top and bottom plates in the opposite direction).

Figure 5.7 is a photograph and processing diagram of a four-way motion type, both-sides simultaneous lapping machine. Both two-way and four-way machines can easily secure processing accuracy of flatness, parallelism, and thickness.

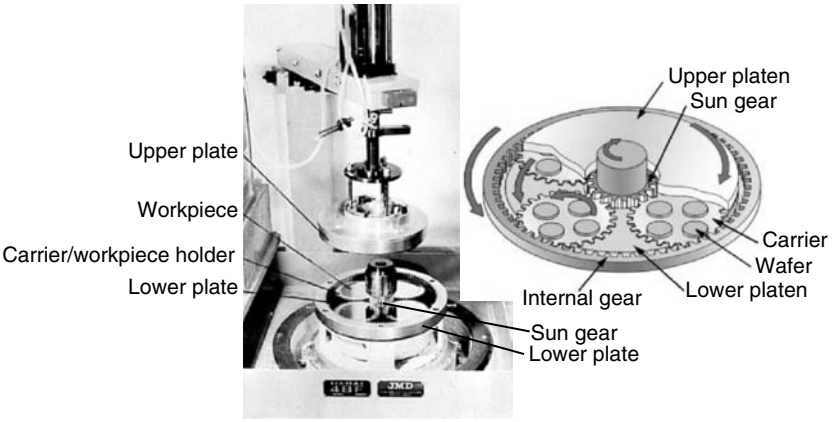


**FIGURE 5.7** Photography and schematic figure of a four-way motion type, both-sides simultaneous lapping machine.

However, the two-way motion machine is subjected to a risk of abrasion in the motion transferring gears due to rotations and orbital motions induced to the carrier. Conditioning of the lapping plates during operation in the both-sides lapping machine is not as easy as in the single-side lapping machine, requiring more careful attention to the plate conditioning. Usually, the lapping process is suspended at certain intervals of lapping time, and the lapping plates are conditioned with the rings specially designed for conditioning during a specified length of time. In order to minimize the variations in the parallelism or thickness of the workpieces, the workpieces are placed on the lapping plate in such a way that the thickness across the plate is well balanced, which serves to minimize the tilt of the upper lapping plate as small as possible, and is indispensable for the ultra-precision fabrication of block gage. Both-sides simultaneous lapping machine is employed in the fabrication process of wafers including silicon wafers, magnetic disk substrates, mask glass substrates, and quartz crystals.

## 5.4 BOTH-SIDES SIMULTANEOUS LAPPING MACHINE EQUIPPED WITH A NEW MICROMOTION MECHANISM [1–3]

Professor Doi et al. propose integration of a new kinetic mechanism into the lapping machines. In 1991 the author proposed micromotion kinetic mechanism (sometimes called "orbital motion") that allows workpieces to make same small circle orbital motions at any point of the wafers without revolving the lapping plates, and relative speeds to become uniform at any point in the range of $v$ in tens of m/min.

In recognition of the extreme importance of securing a uniform pressurization mechanism and uniform relative speeds across a wafer, this kinetic mechanism was originally devised for the introduction into the planarization CMP machines aiming at the global planarization of ultra-LSI device wafers. The basic concept is common to both lapping and polishing where the stock of removal $M$ is given by Preston's law

$$M = \alpha p \nu t$$

where $\alpha$ is a parameter to be established by the processing conditions, $p$ is the processing pressure, $\nu$ is the relative speed, and $t$ is the processing time.

Basically, wafer surfaces can be processed uniformly if processing pressure $p$ and relative speed $\nu$ are exactly controlled within the processing conditions that meet the above equation.

With regard to the relative speed $\nu$, the micromotion mechanism allows the processing plate to draw the same circle motions at any point of the wafer, which makes relative speeds uniform. Consequently, high-precision surfaces can be obtained in theory. Figure 5.8 is a diagram of the single-side processing principles incorporating a micromotion mechanism (orbital motions).

An explanation is provided on a both-sides simultaneous polishing machine equipped with a micromotion (orbital) kinetic mechanism, an advanced

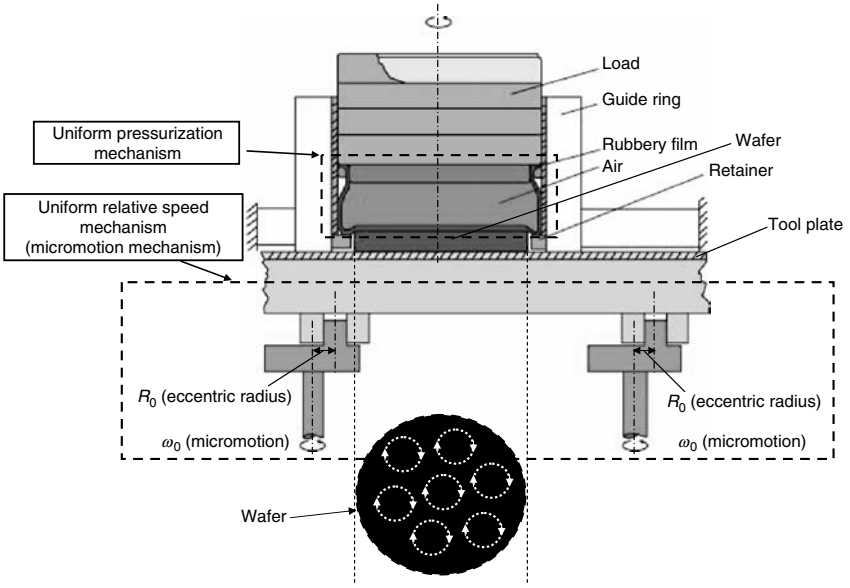


**FIGURE 5.8** Diagram of the single-side processing principles incorporating a micromotion mechanism (orbital motions).

machine of the conventional single-side polishing machine. Theoretical studies in relation to the flatness of the wafer surfaces polished with this new machine were conducted while focusing attention on the average speed distributions along the wafer. Subsequently, the study has confirmed that, with the uniform relative speeds obtained with the micromotion kinetic mechanism, it is possible to polish wafer surfaces uniformly with this new machine.

In developing the above polishing machine, it was our challenge to solve the following problems present in the conventional both-sides simultaneous polishing machines that are currently being used on a commercial basis. The conventional machine adopts the following mechanism (as shown in Figure 5.7):

- Generation of foreign substances from the toothing areas between the carrier and the center (sun) gear or internal gear
- Load to the carrier is too big to be able to increase the processing pressure
- Hard to automatize the machine due to fixed wafer placing location

Taking into account that the uniformization of relative speed $v$ is a key point to secure processing precision, a new micromotion (eccentric small circle) kinetic mechanism without using gears was introduced in the both-sides simultaneous polishing machines. Figure 5.9 is a diagram of the machine,

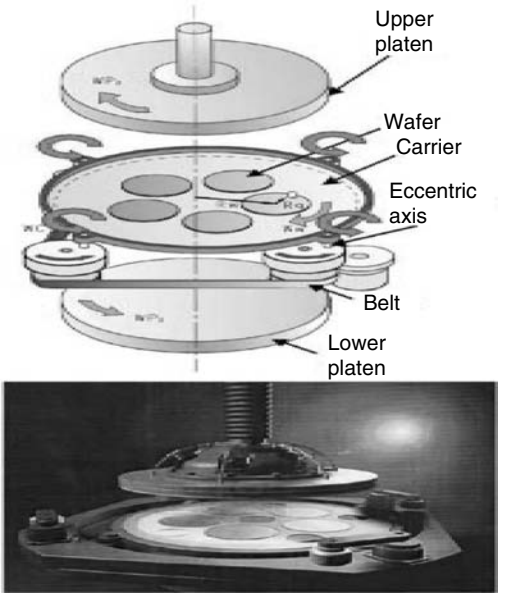


**FIGURE 5.9** Schematic figure/principles of the micromotion introduced by the both-sides simultaneous lapping/polishing machine.

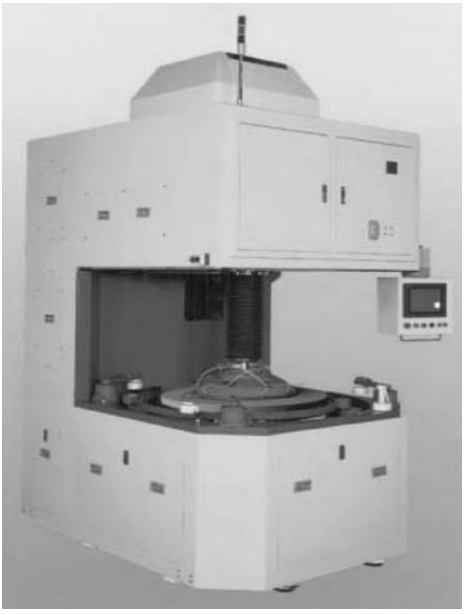

**FIGURE 5.10** The external view of the polishing machine with the micromotion (LPD-300 manufactured by Fujikoshi Machineries, Inc.).

showing the principles of the micromotion introduced by the both-sides simultaneous polishing machine. The external view of the machine (LPD-300 manufactured by Fujikoshi Machineries, Inc.) is shown in Figure 5.10. The machine can accommodate as many as 12 and 5 pieces of 8 and 12 in. wafers, respectively per batch. In comparison with the conventional ones, the footprint is reduced by 30%.

This concept of the micromotion in the polishing machine can be applied to the simultaneous lapping machines, either single side or both sides. However, high pressure cannot be applied when both sides of thin wafers are simultaneously lapped. Instead, relative speed $v$ should be increased for high-efficiency lapping. In this case, the machine should be designed taking into consideration whether or not the wafers rotate on its axis. Needless to say that it is a prerequisite to strictly control the ratio between the rotation numbers of the micromotion mechanism and the revolution numbers of the lapping plate. The possibility of developing new both-sides simultaneous lapping machines incorporating the micromotion mechanism is currently being studied.

## 5.5 CONCLUSIONS

In light of progressing lapping technology as one of the loose abrasive lapping methods, lapping principles and lapping factors are discussed in this chapter

introducing the progress of the machines from conventional ones to the latest development referring to the possibility of integrating the micromotion mechanism already adopted into the both-sides simultaneous polishing machine to the lapping machines.

## REFERENCES

1. T. Doy, H. Jeong, T. Nakagawa, H. Ohmori, and T. Kasai: Global planarization technique/CMP by high precision polishing and its characteristics. *Proceedings of ISSM'95* (1995), 214–217.
2. H. Jeong, H. Ohmori, T. Doy, and T. Nakagawa: Integrated planarization technique with consistency in abrasive machining for advanced semiconductor chip fabrication, *Proceedings of Annals of the CIRP* (1996), 311–314.
3. T.K. Doy, K. Ichikawa, H. Miyairi, T. Kasai, H. Ohmori, S. Kanda, and A. Kajikura: Development of a both sides simuiltaneous polishing system for 300 mm silicon wafers, aiming at the production of nanotopography-free surfaces, Proceedings the 3rd Internation Symposium. On Advanced Science & Technology Silicon Materials (2000). 248–257.

# 6 Polishing Technology

*Toshiro K. Doi*

## CONTENTS

6.1 Polishing Principles ..... 282
*Toshiro K. Doi*
6.2 Processing Accuracy and Damaged Layer ..... 283
*Toshio Kasai*
6.3 Polishing Machines ..... 286
*Toshio Kasai*
6.3.1 Single-Side Polishing ..... 286
6.3.1.1 Metallurgical Polishing Machine and Rough Lapping Machine ..... 287
6.3.1.2 Glass-Lens-Polishing Machine ..... 288
6.3.1.3 Conditioning Ring-Type Polishing Machine and Ring-Tool Polishing Machine ..... 289
6.3.1.4 Nonspherical Surface Polishing Machine ..... 290
6.3.2 Double-Sided Polishing ..... 291
*Toshio Kasai*
6.4 Mechanochemical Polishing and Chemical Mechanical Polishing ..... 292
*Toshiro K. Doi*
6.4.1 Mechanochemical Polishing ..... 293
6.4.2 Chemical Mechanical Polishing ..... 296
6.4.2.1 Progress of MCP–CMP ..... 296
6.4.2.2 Requirements for Polishing ..... 297
6.4.2.3 Basic Mechanism of CMP for Silicon Crystal ..... 298
6.4.2.4 Examples of Polishing Characteristics ..... 301
6.5 Noncontact Polishing ..... 305
*Toshio Kasai*
6.6 Magnetoabrasive Finishing ..... 307
*Hitomi Yamaguchi*
6.6.1 Introduction ..... 307
6.6.2 Outline of Magnetoabrasive Finishing ..... 307
6.6.3 Advantages of Magnetoabrasive Finishing ..... 308
6.6.4 Internal Finishing of Nonferromagnetic Bent Tubes ..... 309
6.6.5 Edge and Surface Finishing of Access Arms of Magnetic Disk Units ..... 310
6.7 Polishing Process Applying Electrophoretic Deposition ..... 312
*Junichi Ikeno*

6.7.1 Introduction ..... 312
6.7.2 Electrophoretic Deposition ..... 312
6.7.3 Development of EPD Pellets ..... 312
6.7.4 Experimental Results ..... 315
6.7.5 Conclusion ..... 317
6.8 Electroabrasive Mirror Polishing Process ..... 317
*Junichi Ikeno*
6.8.1 Introduction ..... 317
6.8.2 Description ..... 318
6.8.3 Manual Polishing and Its Automation ..... 319
6.8.4 Experimental Results ..... 319
6.8.5 Conclusion ..... 322
6.9 P-MAC Polishing ..... 324
*Toshio Kasai*
6.9.1 Analysis on the Mechanism of Various Polishing Methods ..... 324
6.9.2 P-MAC Polishing for Small Pieces of GaAs Single Crystals ..... 327
6.9.2.1 Processing Efficiency ..... 327
6.9.2.2 Accuracy ..... 328
6.9.2.3 Surface Roughness ..... 328
6.9.3 P-MAC Polishing Machine Manufacturing and GaAs Wafer Polishing ..... 329
6.10 Colloidal Silica Polishing ..... 330
*Toshiro K. Doi*
References ..... 338

Lapping or polishing is one of the technologies that advanced along with the history of humankind. Recently, with increasing demands for functional enhancement, ultralapping or polishing has been recognized as a critical technology for the functional materials of the precision machinery components, optical components, and electronic components. For instance, in line with the rapid progress in miniaturization and high integration in electronic components, the dimensional accuracy of the components is shifting from on the order of micrometers ($10^{-6}$ m) to nanometers ($10^{-9}$ m).

Ultraprecision polishing is a technology that accurately produces geometrically dimensional shapes in the nanometer order. These functional materials or components should be produced to a completely smooth mirror surface to work as functional materials. This chapter deals with the ultraprecision polishing technology to produce a complete smooth surface, or damage-free surface without any affected layer or strain, which are the basic requirements for the functional materials. Also mentioned in this chapter are the applications of the polishing technology to the fabrication of such components.

## 6.1 POLISHING PRINCIPLES

*TOSHIRO K. DOI*

Polishing is carried out without letting fine abrasive particles generate brittle fractures on the work surfaces, while removing these materials little by

little only by means of plastic deformation, to finally produce a smooth mirror surface.

For such polishing, fine abrasives of below 1 μm and pads of pitch, wax, synthetic resin, or artificial leather are used to realize smooth mirror finishing. Fine abrasive particles are retained on the pad surface resiliently and plastically, and the work surfaces are scratched microscopically. Polishing actions are by far smaller if compared with lapping, contributing to the successful applications to the brittle materials.

As assumed in the past, the generation of fine plastic-cutting chips by the scratching behaviors of abrasives can be the influencing mechanism, which, however, given that the mechanical actions are extremely small, seems irrational unless other actions are taken into account. For instance, the rough surfaces are planarized as the works are frictionized by the abrasives or pad-inducing surface flow, or the work surface material is chemically dissolved in the reagent. It is also presumed that direct chemical actions between the work and abrasives promote further the mechanical actions mentioned before, and possibly vice versa.

On the other hand, influences of the mechanical actions of the abrasives (ultra-microcutting actions) that correspond to the cutting blade, and of the frictional actions of the pads can be considered as the factors that produce affected layers during polishing. Through experience, the mechanical actions induced by dust or impurities in the room atmosphere or in the slurry are known to result in the affected layers. Previous studies indicate that the affected layers reached as deep as 3 μm in the pitch polishing of crystalline quartz. However, polishing technology has progressed, aiming to minimize the affected layers, which have almost reached the depth below the level of detection, although such depth depends on the works and polishing conditions. A study of the affected layer proves that in the ultimate sense, polishing advances by mechanical actions and chemical actions. Mechanical actions involve removal and frictional actions, whereas chemical actions involve dissolving and generating actions of reaction product layer (membrane). Combining these actions, various characteristic polishing conditions can be established or innovative polishing methods for the ultraprecision polishing will be discovered.

Figure 6.1 shows the relationship between the polishing mechanisms and polishing methods based on the above-mentioned concepts.

## 6.2 PROCESSING ACCURACY AND DAMAGED LAYER

*TOSHIO KASAI*

In lapping and polishing of manufacturing devices, the geometrical accuracy and quality are always required on worked surfaces, as shown in Figure 6.2. In this kind of machining, while a workpiece and a tool are rubbed against each other under pressure and the minute chips are generated by abrasive grains in slurry, a work surface is finished to smooth the surface and the shape accuracy

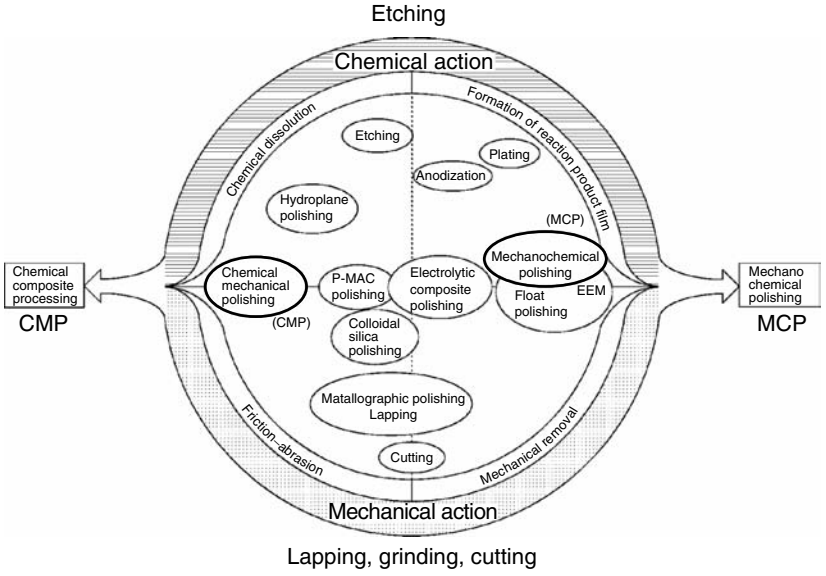


**FIGURE 6.1** Polishing mechanisms and polishing method.

of a plane or spherical surface of the tool is transferred to the work surfaces. Therefore, such process is defined as shape transfer machining with pressure method. Lapping and polishing are different from cutting and grinding that

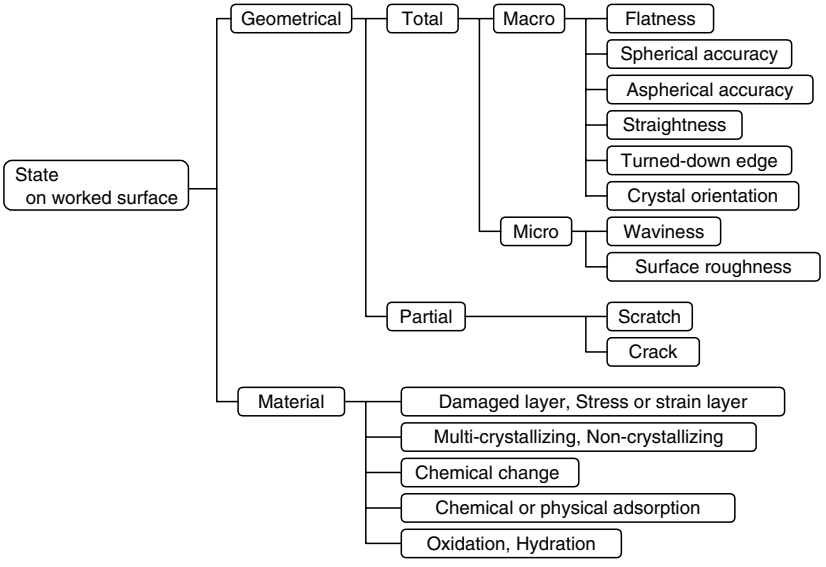


**FIGURE 6.2** Accuracy and quality required in device fabrications.

utilize the shape transfer machining with tool motion method in which the geometrical accuracy is determined by the motion accuracy of a workpiece and a tool under a fixed depth of cut.

When a high degree of flatness or spherical accuracy and the minimization of a turned-down edge generated around the outer work surface is required in lapping and polishing, the tool surface accuracy counts, because the shape of the tool surface such as a lap or a polishing pad is intrinsically transferred to the work surface. In this case, the shape accuracy of the tool surface can be copied from the reference surface by contact and sliding; however, it is common practice to adopt the conditions to maintain tool shape accuracy by making good control of the tool wear during the process. A turned-down edge around the outer work surface is generated as a result of the mechanical action concentrated on the edge of the workpiece during this process. Since such trouble is caused by elastic deformation of a polishing pad, a smooth polishing pad with minimal elastic deformation should be used [1,2].

Furthermore, in order to achieve high accuracy in parallelism, angle, crystal orientation, and thickness, lapping or polishing condition is applied to the correction of these errors under which the stock removal is proportional to the relative speed between the workpiece and the tool, pressure, and time. For instance, in correcting the error, lapping or polishing is carried out only for a given time under uniform or eccentric pressure and fixed tool speed [3–5]. In addition, the preparation of measuring methods and instruments to obtain a high accuracy is required because the results of measurement are reflected in correcting lapping or polishing. Therefore, it is recommended that a processing machine, measuring instrument, and evaluation equipment should be placed in close proximity at a manufacturing site.

The principle of the chip generation should be well examined in order to obtain a mirrorlike surface of high quality. The abrasive grains in slurry primarily work toward mechanically chipping off from the work surface, and the traces of chip generation are detected as the ups and downs of surface roughness. When using the slurry including bigger or harder particles than primary abrasive grains and the polishing pad dirtying with such particles, the rough surface having unexpectedly deep scratches may be given. Especially, it should be carefully noted that these defects tend to increase in proportion to the lapping or polishing time, because most of lapping or polishing machines employ a periodic motion.

There will be no problem if all energy spent for the stock removal is consumed through chip generation; however, the energy partially remaining on the worked surface generates a damaged layer as the residual strain and stress. Deep cracks can remain on the worked surface due to the unwanted dust.

Therefore, in polishing for a high-quality mirror surface, it is important to utilize minute abrasive grains and to prevent dust from contaminating. The quality of polished surface is determined by the level of the following factors: removing large particles and dust in slurry, washing workpieces and a lapping

or polishing jig, taking dust-proof measures in the lapping or polishing environment, separating lapping and polishing rooms, and worker's awareness about maintaining clean conditions.

A soft tool is employed to reduce mechanical action by abrasive grains and dust. This has proven to be highly effective in polishing. However, new problems such as the significant tool wear and the generation of the turned-down edge around the workpiece might possibly occur, presenting difficulties in achieving the required accuracy.

In order to enhance machining accuracy and efficiency, chemicals for dissolving work materials can be added to the slurry. If the surface layer caused by the mechanical action of abrasive grains can be dissolved, the stock removal amount will increase and the damaged layer will be removed. However, in such condition as generating scratches, it is essential to dissolve the surface layer excessively in order to avoid the difficulty of obtaining the expected smooth surface.

Concerning the damaged layer on mirror-polished surface, the adopting base of polishing conditions is diverse when taking account of the kind, component, and perfection of work material and the device performances. Silicon wafers are made up of an almost-perfect single crystal ingot. Chemical mechanical polishing (CMP, or mechanochemical polishing, MCP) is applied to supply perfect crystal surface on wafers making no disturbance in the atomic and molecular arrangement, because the subsequent device process includes crystal-epitaxial growth on the wafer. Colloidal silica and a soft-foamed polyurethane pad are used here.

## 6.3 POLISHING MACHINES

*TOSHIO KASAI*

### 6.3.1 Single-Side Polishing

Lapping and polishing machines have a relative motion mechanism, rubbing a workpiece and a polishing pad together to carry out the process. The predecessors of polishing used a relative motion by their hands, and required a significant amount of time to achieve the desired result. However, the uniformity of the relative motion was essential for obtaining shape accuracy in a plane surface and a spherical surface, and the inefficient work by human hands naturally led to the development of lapping and polishing machines.

Current styles of polishing machines use motor drives. Generally, the machine is designed to affect the complete surface of all workpieces and tools evenly by means of a relative motion obtained in conjunction with the rotary and reciprocating motions. A lens-polishing machine, which has been improved as a result of various modifications, is an example of a production machine that can be used to obtain a plane surface, a spherical surface, and a nonspherical surface. In addition, another type of polishing machine equipped

with an innovative relative polishing motion has been proposed. The introduction of high-technology elements, attending the additional measurement, control, advanced computer technology, and highly clean environment, has improved the quality of works and sophistication of the polishing machines. Further details of the fundamental motion for single-side polishing are described later.

#### 6.3.1.1 Metallurgical Polishing Machine and Rough Lapping Machine

Metallurgical polishing machines and rough lapping machines employ the simplest structure for revolving a tool plate. Polishing progresses as the worker's hand presses the workpiece against the revolving tool plate under dispersing slurry, therefore, this case is defined as semihand polishing or semihand lapping.

Metallurgical polishing machines are used to obtain a mirror-finished surface that is essential for microscopic examination in metallography. For this polishing method, workpieces are placed on a felt-polishing pad adhered to the rotating tool plate by a worker's hand. Since the felt is made of animal fibers, which wear off easily, concave traces are easily made along the same circumference of the rotating plate as shown in Figure 6.3. Workpieces usually become a convex-finished surface by copying the concave surface of the tool plate. A reasonable condition for maintaining the original flatness by making a success of even wears on the felt-polishing pad is necessary, so that the flatness of the workpiece can be obtained. Reciprocating motion is effectively applied to rub the workpiece repeatedly across the radius or the diameter of the rotating polishing pad. For small work materials, dummy materials are placed around them for the purpose of making the work surface appear larger on sight.

In a rough lapping machine, the work operation is performed by a reciprocating motion in the direction of the radius or across the diameter of the rotating cast-iron lap as shown in Figure 6.4. Since the size of the abrasive grain in lapping slurry may be larger than 10 μm, the cast-iron, despite its

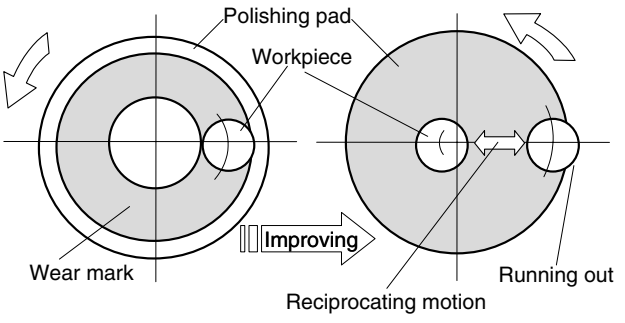


**FIGURE 6.3** Motion of workpiece in metallurgical polishing.

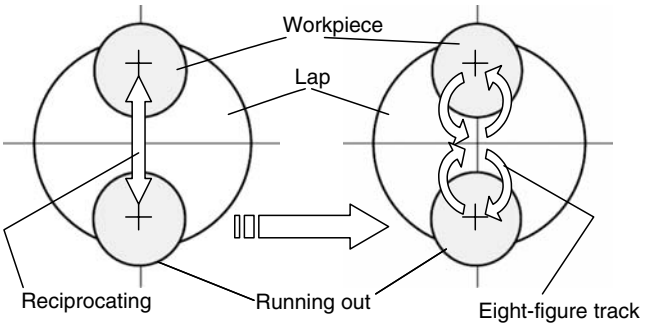


**FIGURE 6.4** Motion of work in rough lapping machine.

hardness, wears away as lapping progresses. By ensuring an even wear of the lap surface, the original accuracy of the plane or spherical surface of the lap can be maintained.

Figure 6.3 and Figure 6.4 show two or three types of motions found in metallurgical polishing and rough lapping machines. The reciprocating motion requires that the workpiece should run out to the edge of the tool in order to generate even wear of the tool surface. In addition, it is desirable to give a steady rotation to the workpieces by hands, though worker's skill may be required. When the reciprocating motion is attempted by a straight-line, it tends to be an elliptic motion and the skilled hands can describe an eight-figure locus passing through the center of the tool, due to the rotation of the tool.

#### 6.3.1.2 Glass-Lens-Polishing Machine

A lens-polishing machine is used as a substitute to a hand operation in the polishing methods described above. This machine, used for lapping and polishing plane surfaces, spherical surfaces, and nonspherical surfaces, utilizes a circular-shaped workpiece and tool called an "upper plate" and a "lower plate," respectively.

Regarding the fundamental motion in a lens-polishing machine, the upper plate is placed facing the lower plate, which is rotated by a motor whereas the center of the upper plate is pressed from its backside by the pivot axis. In this condition, the upper plate rotates in, following with the revolution of the lower plate by the turning torque generated by the polishing resistance between both the plates. Polishing is carried out with the reciprocating motion of the upper plate, which draws an arc locus on the lower plate by the crank mechanism.

Figure 6.5 shows the reciprocating motions in a common lens-polishing machine and others. The rotation of the upper plate may fluctuate not only due to the effect from the reciprocating motion and the rotation of the lower plate but also due to the positional relationship and change of the contact

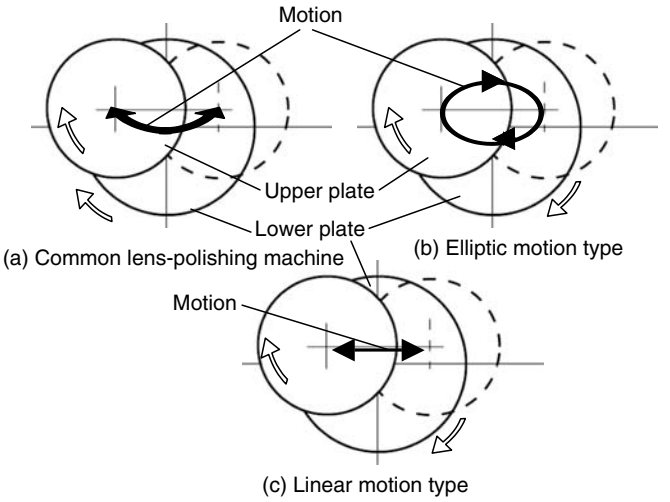


**FIGURE 6.5** Motion between upper plate and lower plate of lens-polishing machine.

condition between the upper plate and the lower plate. There is a delicate relationship between the machining motion and accuracy in polishing, therefore, the worker's experience and skills are required to properly adjust the machine's operation.

#### 6.3.1.3 Conditioning Ring-Type Polishing Machine and Ring-Tool Polishing Machine

These machines are mostly applied to plane polishing whereas some of them are employed for manufacturing the long focal reflecting mirrors by using a concave or convex surface tool. As shown in Figure 6.6, a conditional

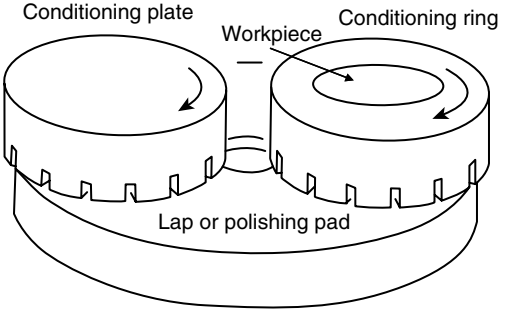


**FIGURE 6.6** Conditioning ring/plate-polishing machine.

ring-type polishing machine has a simple structure in which the workpiece, conditioning ring, and plate face the polishing pad as ring tool at the eccentric position. Rotation of workpiece and polishing pad can give the relative motion. In polishing workpiece whose diameter is smaller than the width of the ring tool, the tool wears off as forming concave curve on the ring tool width whereas the worn and deteriorated tool surface is repaired by using the conditional ring and plate. In other words, utilization of the conditional ring and plate can make the work diameter larger and encourage the even wear of the tool, so that the flatness can be maintained on workpiece and tool [6].

When the speed between the tool, workpiece, and conditioning ring is adjusted in the same ratio, a constant relative speed is maintained on both sides contacting each other. The stock removal and the wear of the tool are proportional to the lapping speed, pressure, and time, therefore, the pressure and time should be monitored to achieve high-precision polishing.

There is a case in which new motions are added to the rotation of the workpiece, conditioning ring, and plate. In order to control an even wear of the tool, the conditions giving reciprocating motions of straight, arc, and circular locus on the tool radius or diameter to them are proposed. When the radius of a ring tool is infinite, the process such as the belt polishing is applicable. The belt polishing proceeds by having the belt tool run against the workpiece or by pressing the abrasive tape on a workpiece moving at a high speed.

#### 6.3.1.4 Nonspherical Surface Polishing Machine

In polishing an on-axis aspherical surface, a spherical surface is initially obtained by a lens-polishing machine and then the desired aspherical surface is achieved by adjusting the tool diameter and the amplitude of the reciprocating. However, aspherical devices may vary in form. For polishing an off-axis aspherical surface, the semimirror surface obtained previously by numerically controlled (NC) grinding is taken to perfect mirror finishing and accuracy correcting. In this case, a unique polishing method and conditions are applied. As Figure 6.7 shows, the correcting polishing for aspheric accuracy progresses by using a circular or boat-shaped small tool designated for the relative motion with a subtle rocking motion in a circular or an elliptical figure locus and scanning the tools by means of residence time control [7,8]. This residence time control is based on an error difference between the design value and the measured value of work surface, and a computer control is introduced. Another polishing method is applied under the condition that a ball- or a roll-shaped small tool is set under the closed contact on a workpiece, and polishing is accomplished under noncontact conditions by tool rotation, as elastic emission machining (EEM) [9].

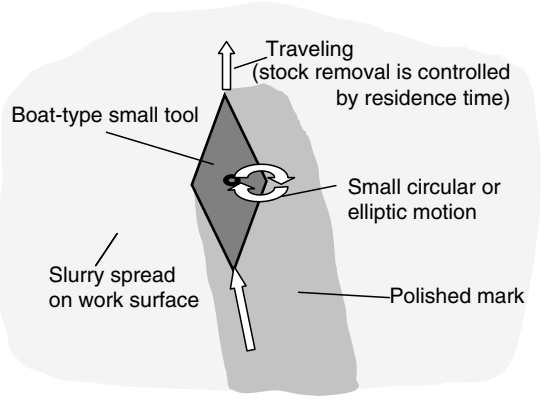


**FIGURE 6.7** Computer-controlled aspheric polishing by using small tool method.

### 6.3.2 Double-Sided Polishing

***Toshio Kasai***

Double-sided polishing machines are extensively used in manufacturing silicon wafers, magnetic disk substrates, glass mask substrates, and quartz oscillator substrates.

In the single-sided lapping and polishing of these substrates, there is a limitation in obtaining parallelism on workpieces. In addition, since each surface of workpieces is not lapped or polished simultaneously, the difference of damaged layers and stress between both sides causes the bend as both-side stress of workpiece balances each other. It results in a waste of time in not only parallel lapping or polishing, but also work setting and measuring as the related works. In these cases, the adoption of double-sided polishing has been a reasonable approach to the fabrication of substrates.

A double-sided polishing machine adopts a motion that is similar to a ring-tool-type machine for single-side polishing. As shown in Figure 6.8, the workpieces set in gear-type carriers are placed on the lower tool plate and then loaded with the upper tool plate. As upper and lower tool plates are of larger diameter than workpieces, a lot of workpieces can be lapped or polished simultaneously and finished to the parallel successfully. Usage of five carriers for workpieces is commonly effective for double-sided polishing, as they are evenly distributed on the tool surface.

It was desirable for double-sided lapping or polishing that the relative motion between workpieces, upper and lower plates was unified, and two-motion-type machine system was proposed, which had the fixed upper and lower plates and the rotation and revolution mechanisms for carriers. On the other hand, there is a four-motion-type double-sided polishing or lapping machine, which adds the opposite rotation to both upper and lower plates.

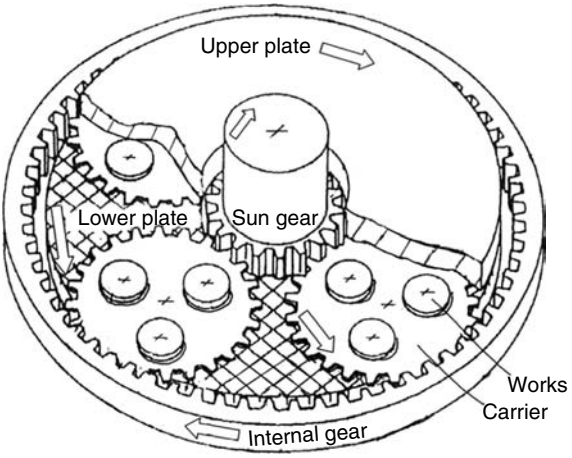


**FIGURE 6.8** Double-sided polishing machine.

A three-motion-type double-sided polishing or lapping machine with the fixed tool plate has also been proposed. In polishing or lapping for adjusting thickness of very thin quartz substrates, the machine system operating on workpieces is held by the carriers between the upper and lower plates oscillating eccentrically by a width of about 10 mm. And the vertical-type double-sided lapping or polishing machines are proposed as unique machines whereby lapping or polishing proceeds holding a 14 in. diameter metal-disk substrate vertically and pressing both their sides with the tool plates [10].

The vertical-type double-sided lapping or polishing machines have been utilized for lapping the substrates as workpieces, and are also applied to polishing as well. The gear-type carriers holding the workpieces are used; the carriers are thinner than the workpieces. The scratch generated by dust, which is carried to the polishing pad surface by the gear carriers, has been pointed out as a potential problem. Recently, a new-type machine for double-sided polishing of silicon wafers has been proposed, which is shown in Figure 6.9. The carrier holding workpieces is of larger diameter than the oppositely rotating upper and lower tool plates, supported by their out positions and a small circular rocking motion between them as a characteristic of this machine system [11].

## 6.4 MECHANOCHEMICAL POLISHING AND CHEMICAL MECHANICAL POLISHING

*TOSHIRO K. DOI*

Mechanochemistry is a series of physical and chemical phenomena that are in action when mechanical energies applied to the work when processes by

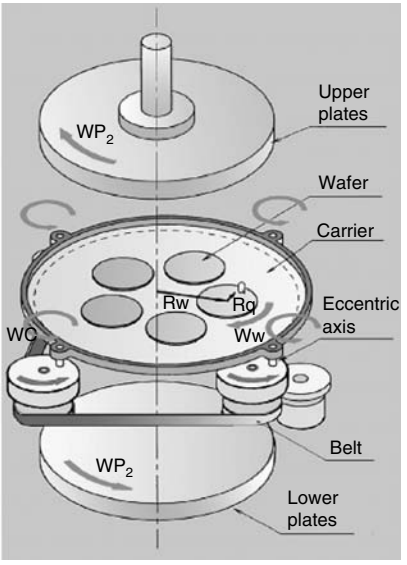


**FIGURE 6.9** Schematic figure of the micromotion polishing.

compression, shearing, rolling and bend are carried out, and the physical and chemical properties of the materials (thermal decomposition reaction, phase transformation, etc.) or the chemical reactions to the surrounding materials (solid-phase reaction, hydration reaction, oxidization and reduction reactions) are promoted [12]. They are the phenomena known for a long time in the fields of grinding (trituration), friction, and wear of powder materials. Especially as far as the ultrafine particles are concerned, the chemical interactions in the contact interface have significantly more possibilities of becoming a governing factor over the material alteration than the physical properties of the material.

In this section, polishing related to the mechanochemistry is reviewed.

### 6.4.1 Mechanochemical Polishing

MCP is characterized by the use of powders as abrasives, which are mechanically softer than the works and could react chemically with the works. In general, this method is based on the solid-state reactions, which implies that polishing in dry conditions is more effective than the polishing with water. Figure 6.10 shows a contact status of the work with soft abrasives. Different from conventional mechanical polishing with hard abrasives, soft abrasives result in significantly less generation of scratches and damaged layers by the abrasive push in or scratching actions as it is the soft abrasives, not works, that transform the shapes at the contact point [13].

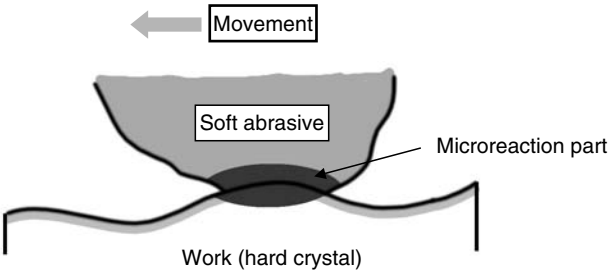


**FIGURE 6.10** Contact status of the work with soft abrasives in mechanochemical polishing. (From Yasunaga, N., et al., *Proc. ICPE*, 32, 32, 1974.)

Basic polishing mechanism is explained here by taking sapphire polishing ($\alpha$-$Al_2O_3$) as an example. Powders (hardness below 50% of $\alpha$-$Al_2O_3$) like $SiO_2$ and iron oxide ($\alpha$-$Fe_2O_3$, $Fe_3O_4$) that could generate solid-state reactions with $Al_2O_3$ are supplied in dry conditions or together with some adequate solution (reagent) under similar kinetic behavior to the lapping or polishing method [14]. Solid-phase reactions are generated from both the supplied powders (abrasives) and sapphire at the contact point within a momentary contact time. Polishing progresses when such reacted areas are removed on the order of angstroms or nanometers by frictional force.

When abrasives of $SiO_2$, $Fe_2O_3$, or MgO are selected, solid-phase reactions with $Al_2O_3$ occur, producing mullite, various solid solutions, and Mg–Al spinel, respectively. When polishing is performed with the particles that produce such solid-state reactions in dry conditions or with proper solution (reagent), high-temperature and high-pressure ambient is generated by the frictional energy at the contact area between the work and polishing abrasives, generating solid-phase reactions within the contact time, which accompany counterdiffusions between them. Polishing advances as such reacted spots are further removed microscopically by frictional forces.

Figure 6.11 shows polishing rates of sapphire using various polishing abrasives [15]. The hardness of sapphire is about 9 on the Mohs scale. When hard abrasives SiC are used, very efficient polishing is observed. Meanwhile, it was not possible to achieve efficient polishing with abrasives with Mohs hardness below 9 for polishings dependent on mechanical actions. However, when the abrasives such as $SiO_2$ and $Fe_2O_3$ that undergo mechanochemical reactions with sapphire are used, high polishing efficiency in particular was attained without showing dependency on the hardness.

This polishing method features no use of soft polishers (pads) as excess energy applied to the work surface via abrasives can be absorbed by the distortion breakdown of the polishing abrasives. As a consequence, in the MCP, pads of mild steel, fused quartz, or ceramics can be used, contributing to maintaining flatness whereas in the conventional polishing with soft pads,

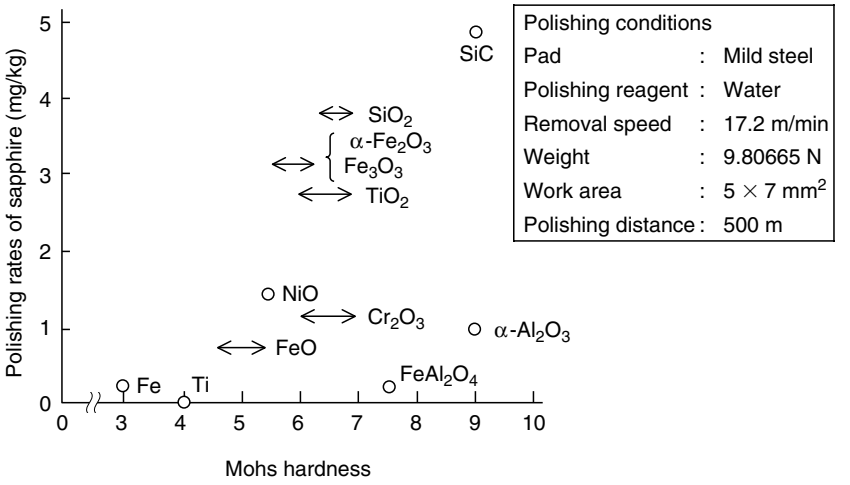


**FIGURE 6.11** Polishing rates of sapphire using various abrasives.

the flatness deteriorates as the stock of removal increases. MCP is extremely effective in keeping flatness.

Figure 6.12 is an example of the polishing efficiencies of MCP with sapphire as a work. $SiO_2$ and $\alpha$-$Fe_2O_3$ abrasives with mechanochemical effects on sapphire indicate high polishing efficiency especially in the dry process, irrespective of the size of the abrasives, proving that MCP provides better efficiency than mechanical polishing with diamond abrasives (paste) [15].

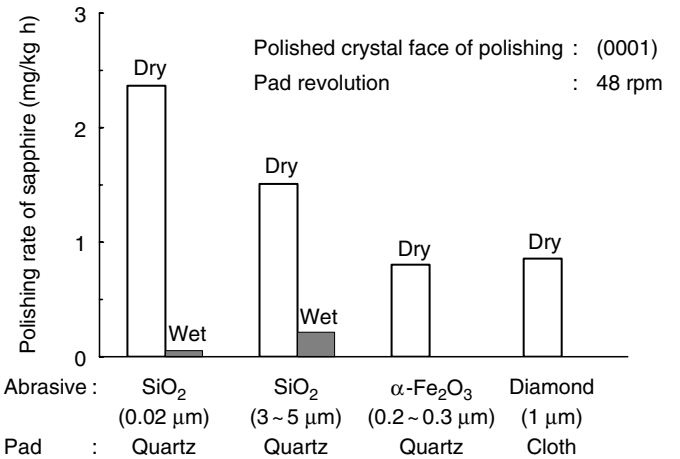
Polished crystal face of polishing : (0001)
Pad revolution : 48 rpm
Polishing rate of sapphire (mg/kg h)
Dry
Wet
Abrasive : SiO2 (0.02 μm) SiO2 (3 ~ 5 μm) α-Fe2O3 (0.2 ~ 0.3 μm) Diamond (1 μm)
Pad : Quartz Quartz Quartz Cloth

**FIGURE 6.12** Polishing efficiencies in mechanochemical polishing of sapphire by various abrasives. (From Yasunaga, N., et al., *Proc. ICPE*, 32, 32, 1974.)

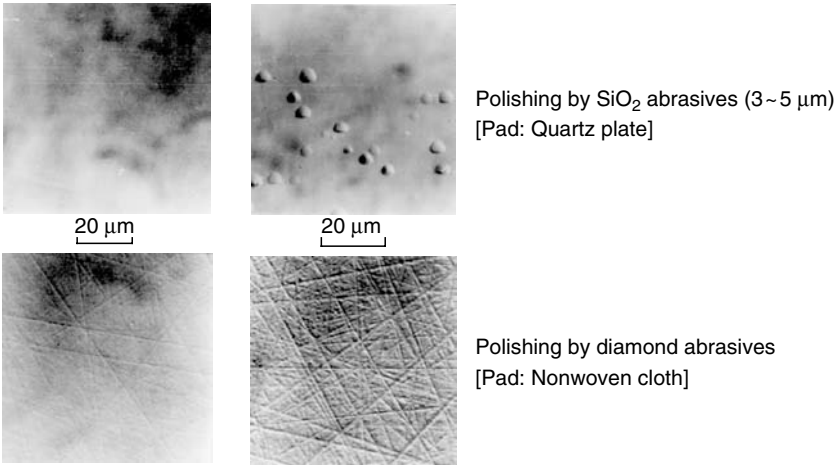


**FIGURE 6.13** Process surface by mechanochemical polishing (upper) and mechanical polishing (lower).

Processed surfaces by MCP and mechanical polishing with diamond abrasives are shown in Figure 6.13a together with differential interference microscopic photographs of the above surfaces slightly etched by phosphoric acid in Figure 6.13b [15].

The surface processed by the MCP shows absolutely no scratches. Even after etching, etch pits only were observed on the surface that corresponds to the dislocation density inherent in the bulk. MCP has been proved to produce excellent surfaces without generation of damaged layers.

The dimensions of mechanochemical reaction layers produced between the abrasives and work can determine the stock of removal in this polishing method. The formation of reaction layers at the contact point is dependent on the temperatures and pressures, reaching as high as 5 nm in a momentaneous period of $10^{-3}$ to $10^{-4}$ s. The miniaturization and uniformity of such reaction layers are the determining factors of the final polishing accuracy of the MCP method.

## 6.4.2 Chemical Mechanical Polishing

### 6.4.2.1 Progress of MCP–CMP

The polishing principle of the CMP or MCP in the ultraprecision polishing is in brief a processing method that promotes polishing by inducing or activating solid-phase reaction (dry process) or solid–liquid phase reaction (wet process)

by the mechanical energy produced by the abrasives. Wet process is normally applied to the ultraprecision polishing of semiconductor materials.

CMP is a polishing mechanism with mechanical removal and chemical dissolution, and MCP is a mechanism to remove reaction products by mechanical work involving friction and abrasion induced by the chemical work. Technically CMP and MCP should be distinguished however, but they are treated the same here as wet-type MCP.

Regh and Silvey [16] are believed to be the first to conduct CMP–MCP of a single crystal silicon semiconductors in the 1960s based on the displacement reaction of Cu ion

$$2Cu^2 + Si \rightarrow Cu + Si^{4+}/Si^{4+} + 6F^- \rightarrow SiF^{2-}$$

using mixed solutions of $NH_4F$ and $Cu(NO_3)$.

Later Mendel [17] of IBM proposed MCP of a single crystal silicon applying chemical reactions

$$Si + 4NaOH \rightarrow Na_4SiO_4 + 2H_2$$

of alkaline solutions such as NaOH, which has become a basis for today's polishing process of silicon wafers. Today, alkaline colloidal silica is widely used in the polishing of silicon wafers.

#### 6.4.2.2 Requirements for Polishing

Quality wafers are absolutely necessary in the finishing process for the device formation. Figure 6.14 shows basic requirements for the wafers to be polished, relationship between slurries (consisting of the abrasives or particles dispersed in polishing solution) and pads with regard to such requirements, and their influencing factors. The following are the items used to determine the quality of the processed surfaces:

- Flatness or TTV, LTV
- Scratch or microscratch
- Dimple or peel
- Microroughness or ripple, haze
- Residual strain or oxidation-induced stacking fault (OSF)

These defects differ in the frequency of occurrence, depending not only on the rigidity of the polishing machine and kinetic mode, but also on adhesion, materials, and accuracy of a wafer-holding jig, pressurization and cooling methods, including pad, slurry, and mechanical polishing conditions.

For CMP in the finishing process of silicon wafers, severe conditions such as roughness of 1 to 2 nm Ry and free from OSF [18], microscratch, haze, and

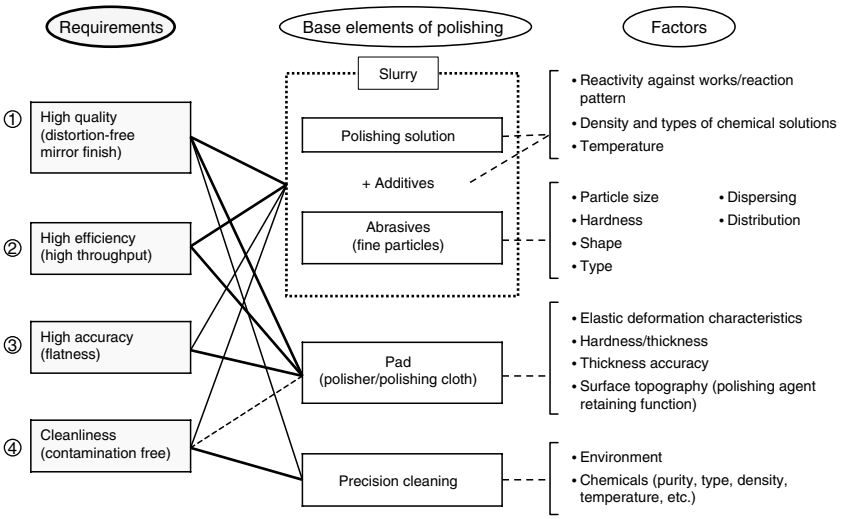


**FIGURE 6.14** Basic requirements for the wafers to be polished, the relationships between slurries and pads, and influencing factor.

impurity are essential, which requires CMP to be performed in several steps. Currently first and second polishings, and even third and fourth polishings are performed each time with appropriate combinations of slurries and pads (Table 6.1).

### 6.4.2.3 Basic Mechanism of CMP for Silicon Crystal

As the effect of chemical actions of CMP on polishing rate is extremely large, polishing rate $V$ (excluding the polishing rate based on the mechanical actions

**TABLE 6.1**
**Example of Si Wafer Polishing Conditions for ULSI Fabrications**

| | Processing Conditions | |
|---|---|---|
| **Process** | **Stock of Removal (μm)** | **Target** |
| First polishing | 10 to 15 | High efficiency<br>Smooth mirror surface (20 ~ 40 Å Ry) |
| Second polishing | 0.5 to 1 | OSF-free[a]<br>Improvement of surface roughness (10 ~ 20 Å Ry) |
| Third and fourth polishing | 0.1 to 0.3 | Haze-free<br>Contamination free |

[a]OSF is the oxidation-induced stacking fault.

$V_M$ from the total polishing rate) can be calculated using Arrhenius' rate equation:

$$V = V_0 \exp\{-E_0/R(T + \Delta T)\}$$
$$= V_0 \exp\{-(E_0 - E^*)/RT\}$$

where $V_0$ is a parameter determined by the polishing conditions, $R$ is a gas constant, $T$ is a temperature (K) of processing reaction system, $\Delta T$ is a temperature rise (K, $0 < \Delta T/T < 1$), and $E_0$ is an activation energy (kcal/mol) of intrinsic reaction system of slurry and work (Si) [19,20].

$E^*$ is an apparently decreased amount of activation energy $E_0$ by the strain energy stored on the surface by the mechanical actions induced by the abrasives (particles), or by the heat energy induced by the frictional heat [20]. Figure 6.15 shows an Arrhenius plot of the polishing rates in relation to the varying pad temperatures [21]. As the abrasive concentration and polishing pressure increased, apparent activation energy decreased, which supports the above equation.

The correlation between the heat value $Q$ obtained from the friction resistance measured during processing and the heat energy $E$ (kcal/h) obtained on the basis of $E^*$ was investigated, from which a relation of $E = \alpha Q - \beta$ (parameter $\alpha$ is a conversion efficiency that becomes a processing energy $E$, contributing to the polishing) was derived [21]. It is further clarified that friction mode is not caused by simple scratch actions but attributable to adhesion. In fact, it has been confirmed that the slurry consisted of colloidal silica, to which fine silicon particles similar to a Si wafer appropriate to

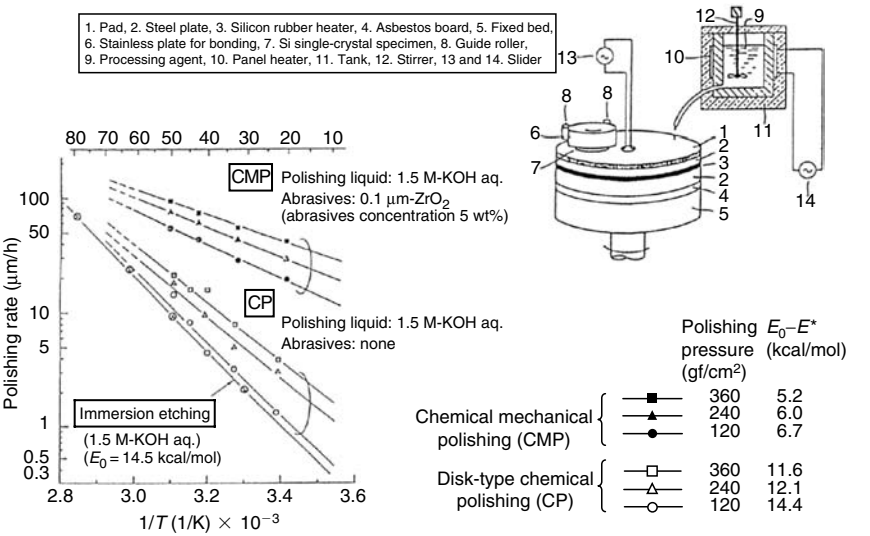


**FIGURE 6.15** Dependency of processing rates on temperature (Arrhenius plot).

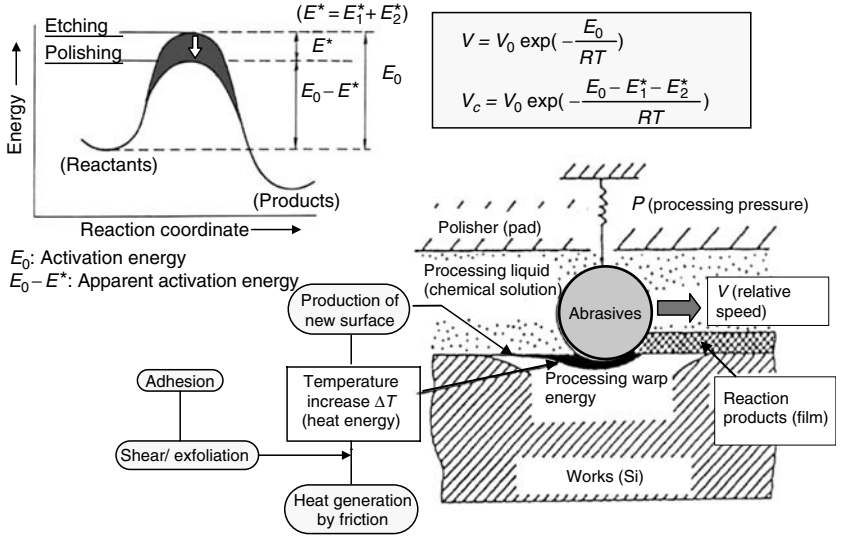


**FIGURE 6.16** Model of processing promotions factors in Si crystal CMP.

induce adhesions are added, which increases the polishing rate. Activation factors of the velocity (polishing rate) component of the chemical actions $V$ are shown in Figure 6.16 with a diagram of the abrasive behaviors during Si wafer CMP [10]. Figure 6.17 shows a chart of macroscopic-processing mechanism in Si CMP.

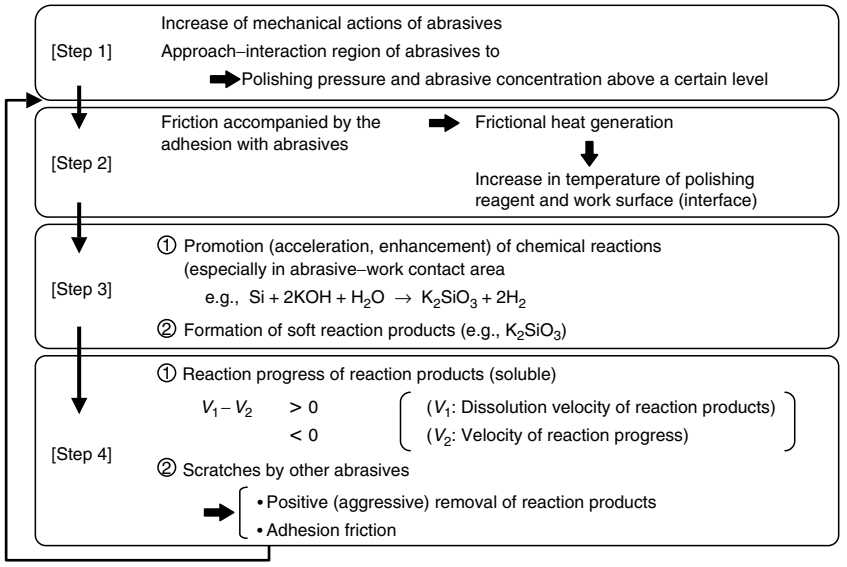
[Step 1]
Increase of mechanical actions of abrasives
Approach–interaction region of abrasives to
Polishing pressure and abrasive concentration above a certain level
[Step 2]
Friction accompanied by the adhesion with abrasives
Frictional heat generation
Increase in temperature of polishing reagent and work surface (interface)
[Step 3]
① Promotion (acceleration, enhancement) of chemical reactions (especially in abrasive–work contact area
e.g., $Si + 2KOH + H_2O \rightarrow K_2SiO_3 + 2H_2$
② Formation of soft reaction products (e.g., $K_2SiO_3$)
[Step 4]
① Reaction progress of reaction products (soluble)
$V_1 - V_2 > 0$
$< 0$
($V_1$: Dissolution velocity of reaction products)
($V_2$: Velocity of reaction progress)
② Scratches by other abrasives
• Positive (aggressive) removal of reaction products
• Adhesion friction

**FIGURE 6.17** Macroscopic-processing mechanism of Si-CMP.

Meanwhile, Fussetter and coworkers carried out microscopic study on the mechanism of Si CMP with following findings:

- When $OH^-$ ion contacts a silicon pole surface, silicon atomic bond is segmentized, promoting Si–OH bond.
- Silicon atom newly appeared on the surface combines with $H^+$ (proton), forming Si–H.
- Meantime, $OH^-$ ion that is left behind contacts with silicon atom.

During this process, $OH^-$ ion is supplied onto the Si wafer surface where the effect of water is important. Such $OH^-$ ions are retained in abundance in the surfaces of $SiO_2$ particles dispersed in the slurry, which contribute to the dissociation of Si–Si bond (Figure 6.18). Behaviors of such actions largely differ depending on pH values of the slurry and contact conditions with the pad.

In any event, both chemical actions and membranous reaction products formed on the surface are essential for the finishing process of silicon wafers since the projected areas of the pad to which abrasives are adhered remove such membrane, serving to restrain direct mechanical actions on Si wafer, and successfully leading to the realization of high-quality processed surfaces.

### 6.4.2.4 Examples of Polishing Characteristics

For the improvement of mechanochemical effects to subsequently increase polishing efficiency, the following two methods can be considered as

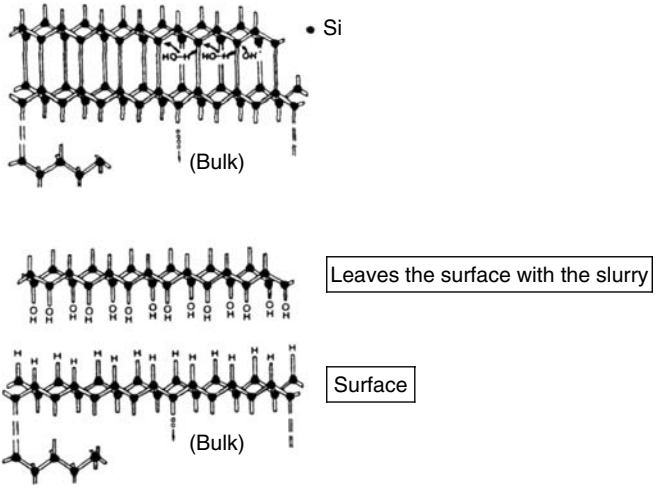


**FIGURE 6.18** Removal mechanism in chemical mechanical polishing (CMP) of silicon crystal. (From H. Fussetter et al., Proc. MRS Symp., 386, 1996, 1997.)

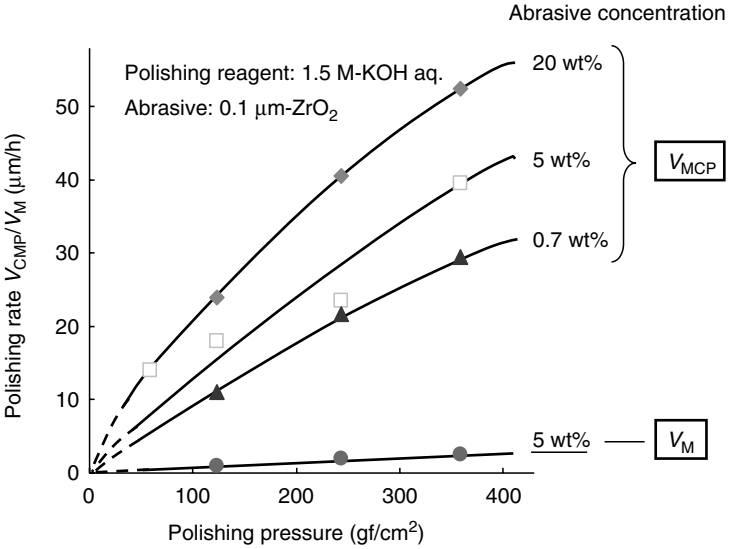


**FIGURE 6.19** Relationship between polishing pressure and polishing rate (workpiece: Si crystal).

effective: (1) to intensify mechanical energy to be applied or (2) to increase the degree of chemical activities of the slurry around the crystals.

Both polishing rates $V_M$ in CMP and in mechanical polishing increase as polishing pressure increases. Increase of the chemical effect in $V_{CMP}$, or mechanochemical effect, is enhanced by the mechanical actions induced and promoted by the increased polishing pressure (Figure 6.19). By thickening slurry concentration, $V_{CMP}$ and $V_M$ also increase as polishing pressure increases. This is explained by the increase of the amount of the abrasives working on the silicon wafer surfaces due to thickened slurry concentration.

Increase of relative speed between pad and wafer (number of pad revolutions) that increases the frequency of the abrasives acting on the crystal surfaces also serves to increase mechanical actions with a subsequent increase of $V_{CMP}$. Types of abrasives (including hardness and particle size) that work on the crystal surfaces are also the contributing factors. Figure 6.20 is a comparison of $V_{CMP}$ obtained using different types of abrasives [21]. Depending on the types of abrasives, $V_{CMP}$ and chemical action ratio $\gamma$ varied. Even among the same $SiO_2$ abrasives, differences in $V_{CMP}$ were observed depending on the production method and specific surface area. These are attributable to the magnitude of the mechanical actions in accordance with the differences in the surface conditions of the abrasives, and to the stability of abrasives in chemical solutions.

In the meantime, following are considered the methods that directly increase the degree of chemical activities of polishing reagent around crystals:

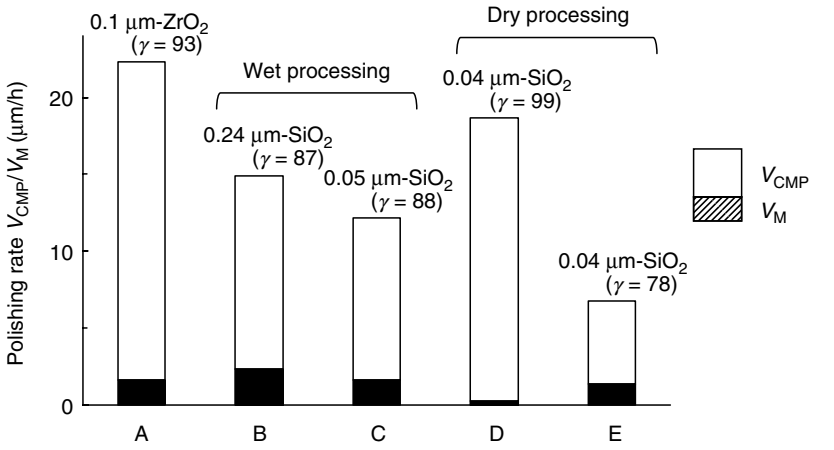


**FIGURE 6.20** Polishing rates $V_{CMP}$, $V_M$ in chemical mechanical polishing and mechanical polishing by various abrasives (workpiece: Si substrate).

1. To use chemical solutions of high chemical activities for polishing reagent
2. To apply other energies to polishing reagent such as heat energy and light energy

Figure 6.21 shows dependency of the etching rate $V_E$ of a simple immersion type and the CMP rate $V_{CMP}$ on the concentration level of polishing reagent (KOH solution). As the concentration level of KOH solution

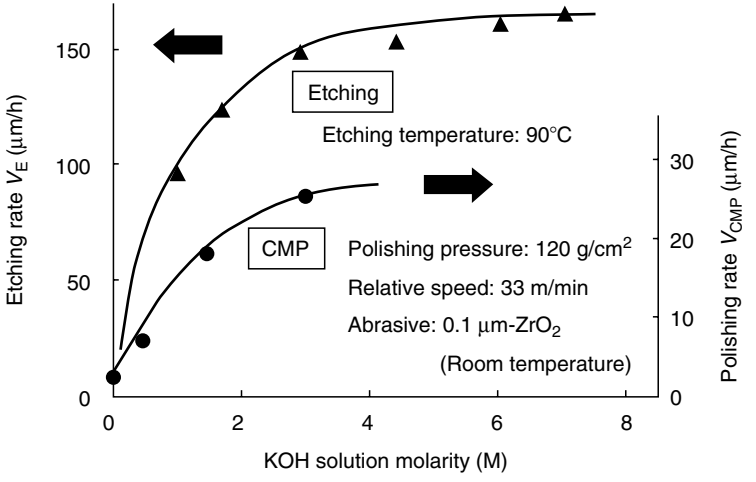


**FIGURE 6.21** KOH solution molarity effect on etching rate and polishing rate in chemical mechanical polishing.

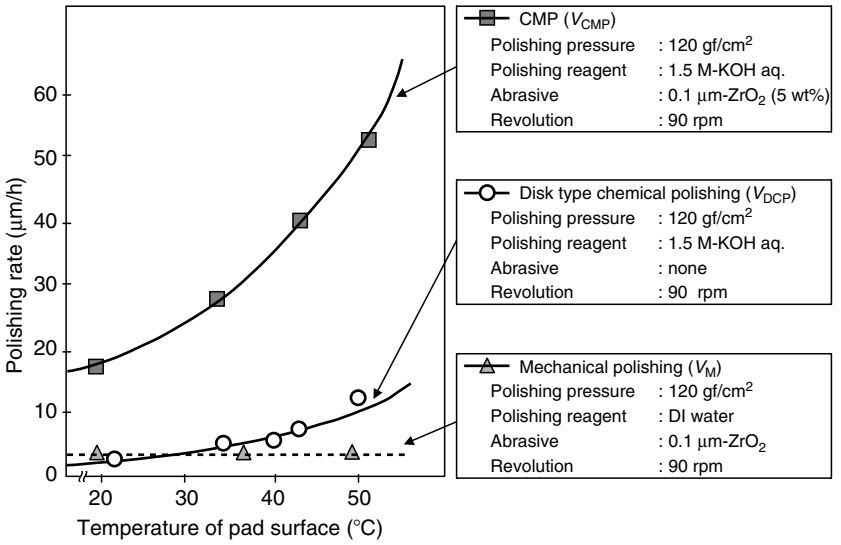


**FIGURE 6.22** Relationship between polishing pressure and polishing rate (workpiece: Si crystal).

increased, $V_E$ and $V_{CMP}$ increased, which were observed to be closer to saturation at around 3 M. Figure 6.22 shows a relationship between the pad temperature and $V_{CMP}$ [20]. These polishing characteristics were obtained using a thermomechanical polishing machine. $V_{CMP}$ increased exponentially with the increase of the pad surface temperature, and reached the level three times more than that of the room temperature at 50°C. Disk-type chemical polishing rate $V_{DCP}$ with the polishing reagent (KOH solution) without abrasives also increased with the increase in the pad surface temperature, which, however, is no more than the 20th part of $V_{CMP}$ at the room temperature. Normal chemical polishing rate $V_M$ without chemical solutions is of course not dependent on temperature. Under the same temperature conditions, CMP rate $V_{CMP}$ is found to be the largest as follows:

$$V_{CMP} > V_M + V_{DCP}$$

Mechanochemical reactions contributed to such an increase of polishing rate.

These imply that polishing rate is influenced significantly by the chemical actions induced by polishing reagent and by the combined and superposed effects of chemical actions induced by abrasives. As already mentioned in the study on a processing mechanism shown in Figure 6.16, the effect of heat generated from shearing and peeling of the agglutinations produced between the crystal and abrasives is presumably large. Agglutinations tend to occur when two materials of similar mechanical natures or of the same kind slide each other.

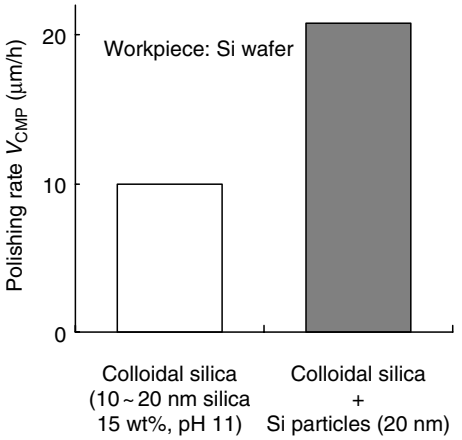


**FIGURE 6.23** A comparison of the polishing rate $V_{CMP}$ of Si wafer (effect of Si particles).

Figure 6.23 is a comparison of the polishing rates $V_{CMP}$ of Si wafers with two different slurries: (1) containing colloidal silica ($SiO_2$ fine particles of 100 to 200 Å dispersed in alkaline solution of pH 9 to 11) that has been used conventionally as finishing slurry of Si wafers and (2) containing fine Si abrasives (particles) added to the above slurry (1), since such Si particles of the same nature as Si wafer are thought to become most easily agglutinated with Si wafer [22]. When fine Si particles were added, polishing rate improved more than twice the other, and defect-free surface was obtained. The polished Si wafer was found OSF-free, which confirms that damage-free, high-quality surface is effectively produced.

## 6.5 NONCONTACT POLISHING

*TOSHIO KASAI*

There is a distinctive polishing method whereby polishing advances with slurry layer under a noncontact condition between the workpiece and the tool, in a number of polishing methods. Float polishing [23] and EEM [24] belong to this method. These differ considerably from a close contact condition in polishing glass lenses and mirrorlike metal dies.

In float polishing for high accuracy and high quality, as shown in Figure 6.24, a machine system having an ultraprecision hydrostatic-type rotary bearing and a highly accurate air slide is used to provide for a flat and mirror tin tool plate as a soft metal tool. A tin ring-type tool plate as polishing pad is mirror-cut by using a diamond-cutting tool on polishing machine. Tin tool plate mirror-cut appears to be perfectly flat when rotating and coming to a standstill. A suitable amount of slurry is supplied and stored in a circular-shaped frame along the

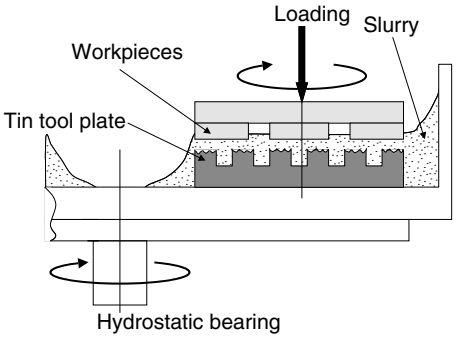


**FIGURE 6.24** Schematic model of float polishing.

outer edge of the tin tool plate. Polishing advances by pressing the workpieces against the tool surface, which is always covered with slurry, and the flatness on workpieces is copied from the tin tool surface. The most important point in starting this polishing is that the workpieces that have been finished to rather convex and mirror surface with the previous polishing should be used.

Floating condition is attained with the hydroplaning phenomenon under a suitable tool rotation and slurry supplying. The cavitation generated in the slurry layer can make the abrasive grains undulate with the fluid [25]; the work surfaces are attacked by the activated abrasives, and the high-quality and ultraprecision polishing advances. However, when applying such polishing to the rough work surfaces commonly lapped, the workpiece does not float enough with the hydroplaning effect. As a result, the mirror-cut tin tool plate will change into a muddy surface by the friction with the work and the float polishing will not be able to stand up.

EEM enables a workpiece and a tool to come to noncontact condition by utilizing another principle. Either a rubbery ball or a roller as a rotating tool is employed there. The tool is supported by the spring and contacts the work surface when not rotating. The slurry layer or flow is formed between tool and work surface as soon as the tool rotation starts, as shown in Figure 6.25.

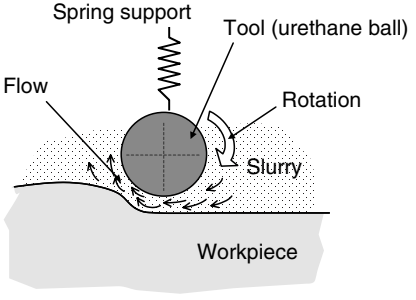


**FIGURE 6.25** Schematic model of elastic emission machining (EEM).

Abrasive grains having the large gravity in slurry flow attack the work surface under very shallow angle with the centrifugal force of tool rotation, and stock removing is carried out. A part on the work surface can be polished by tool scanning under computer control; EEM is one of the shape-collecting polishings and can be applied for fabricating the aspherical surface.

## 6.6 MAGNETOABRASIVE FINISHING

*HITOMI YAMAGUCHI*

### 6.6.1 Introduction

Some combinations of different phenomena may have unexpected yet rather beneficial effects. For instance, the combination of a magnetic field with the mechanical action of a magnetic tool against a workpiece gives rise to the magnetic-field-assisted finishing process, which shows potential for overcoming problems associated with more conventional finishing processes. This idea was initially presented in the former Soviet Union in 1938 [26]. Since then, research on the process has been undertaken in Bulgaria, German Democratic Republic (now Germany), and the United States. The first patent known to us was granted in the United States in 1958, and full-scale research on magnetic-field-assisted finishing started to appear in the 1960s [26,27]. Research groups in Japan have developed the process since 1981 and succeeded in putting the process to practical use [28].

In the 1990s, the process applicability started to be recognized by the public as the processing mechanism and the advantages of the process became better understood. Magnetoabrasive finishing is one of the magnetic-field-assisted finishing processes and has recently attracted considerable attention in practical use. The following section outlines magnetoabrasive finishing and its advantages and introduces representative examples of the process application.

### 6.6.2 Outline of Magnetoabrasive Finishing

Figure 6.26 shows an example of the magnetoabrasive finishing, specifically, cylindrical magnetoabrasive finishing [29]. The magnetic-abrasive particles introduced between the poles are linked to each other by magnetic force. The magnetic force acting on the magnetic abrasive is a function of the volume and susceptibility of the magnetic abrasive, and the magnetic field, specifically the magnetic field intensity and the gradients, at the finishing area [29]. This magnetic force is transferred to the target surface as the finishing force. The rotation and vibration of the workpiece cause relative motion between the magnetic abrasive and the target surfaces, achieving finishing action.

Aluminum oxide composite magnetic abrasive is commercially available magnetic abrasive and is generally used for this finishing process. It contains aluminum oxide sintered with iron in an inert gas atmosphere with high temperature and pressure [29], or as a product of a Thermit reaction in

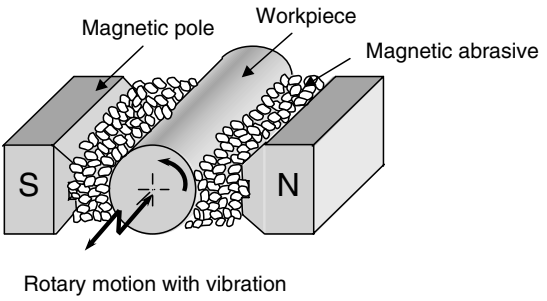


**FIGURE 6.26** Schematic of cylindrical magnetic abrasive finishing. (After Shinmura, T., et al., *Bull. Jpn. Soc. Prec. Eng.*, 19(1), 54, 1985.)

aluminum and iron oxide in an inert gas atmosphere [30]. Since the variety of the composite magnetic abrasive is limited in the market due to the complicated manufacturing process, the replacement of the composite magnetic abrasive by a mixture of ferrous media and conventional abrasive slurry has been considered [30–34]. The ferrous media consists of any shape of ferrous material, e.g., powders, balls, pins, and flakes. The processes using composite magnetic abrasive or mixtures of ferrous particles and slurry are generally called "magnetic-abrasive finishing" or "magnetoabrasive finishing."

### 6.6.3 Advantages of Magnetoabrasive Finishing [35]

Figure 6.27 shows a schematic of the motion of ferrous particles, including magnetic abrasive, in a magnetic field. In a magnetic field, particles link together along the lines of magnetic flux, suspended by magnetic force. Because the magnetic flux flows unimpeded through the workpiece material, it is possible to influence the motion of a ferrous particle, even if the particle is not directly in contact with the magnetic pole, by controlling the magnetic

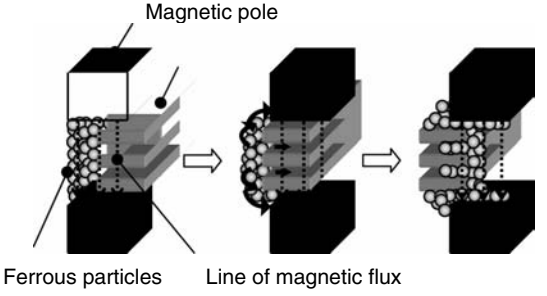


**FIGURE 6.27** Schematic of motion of ferrous particles in magnetic field. (After Japan Society for Precision Engineering, *Seimitsukakojituyobinran*, Nikkan Kogyo Shinbun Ltd., Tokyo, 559, 2000, [in Japanese].)

field from outside. The ferrous particle chains connected by magnetic force take advantage of the flexibility of the magnetic particle chain configuration. This unique behavior of the magnetic particles enables the finishing operation to be applied not only to easily accessible surfaces but also to areas that are hard to reach by means of conventional mechanical techniques. This is a distinct advantage of magnetoabrasive finishing and an example of the beneficial effects resulting from the merger of two different phenomena.

The process applications in practical use found in the open literature include the following:

1. *Internal finishing*: Complex-shaped tubes, integrated straight and bent sections [36]
2. *Edge and surface finishing*: Access arms (carriages) of magnetic disk units [37] and razor blades [38]

The following section introduces the representative examples of the process applications such as the internal finishing of nonferromagnetic bent tubes and the edge and surface finishing of access arms for magnetic disks.

### 6.6.4 Internal Finishing of Nonferromagnetic Bent Tubes [36]

The piping systems used in critical applications, such as aerospace components and semiconductor plants, require especially smoothly finished inner surfaces to prevent the contamination of gas and liquid. Since the piping systems generally corrode at the joints, it is desirable to provide piping systems consisting of complex-shaped tubes, which incorporate straight and bent sections, to minimize the number of joints. This considerably increases the difficulty of internal finishing of the tubes by conventional techniques. The magnetoabrasive finishing process is effectively used for internal finishing of the complicated piping systems.

Figure 6.28 shows a schematic of the internal magnetic-abrasive finishing process using a pole rotation system for nonferromagnetic bent tubes. The

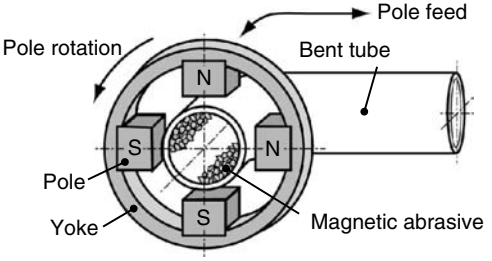


**FIGURE 6.28** Schematic of internal magnetic abrasive finishing process for nonferromagnetic bent tube. (From Yamaguchi, H., Shinmura, T., and Kobayashi, A., *JSME Int. J.*, 44(1), 275, 2001.)

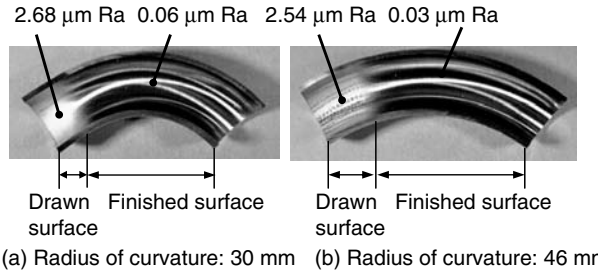


**FIGURE 6.29** Photographs of inner surface of SUS304 90° elbow. (From Yamaguchi, H., Shinmura, T., and Kobayashi, A., *JSME Int. J.*, 44(1), 275, 2001.)

poles, consisting of small permanent magnets, generate the magnetic field needed for attracting magnetic abrasive to the finishing area and for generating the magnetic force needed for finishing.

When the poles rotate around the tube, the magnetic abrasive, driven by magnetic force, rotates along the inner surface of the tube together with the poles. Material is removed from the surface as a result of the finishing force consisting of the magnetic and centrifugal forces experienced by the rotating magnetic abrasive. Manipulating the rotating poles along the tube axis causes the abrasive to trace the inner surface of the tube following the poles' motion, finishing the entire inner surface of the tube.

Figure 6.29 shows an example of finished surface of SUS304 stainless steel elbow by using this method. This illustrates the feasibility of the process to achieve nearly uniform internal finishing of bent tubes in a single iteration.

### 6.6.5 Edge and Surface Finishing of Access Arms of Magnetic Disk Units [37]

Access arms for magnetic disk units require rigorously controlled accuracy of dimension and surface profile. Edge finishing of the access arm is one of the key technologies used to improve storage capacity and to reduce the size of the magnetic disk unit. The edge finishing to eliminate burrs left by previous cutting processes has been typically performed by hand; this increases not only the production cost but also the variations in quality. The magnetic-field-assisted finishing process was proposed to replace the manual work of the access arm. This makes use of the flexibility of the magnetic tool chains suspended by magnetic force.

Figure 6.30 shows a two-dimensional schematic of the processing principle. Opposed magnetic poles generate a continuous magnetic field between

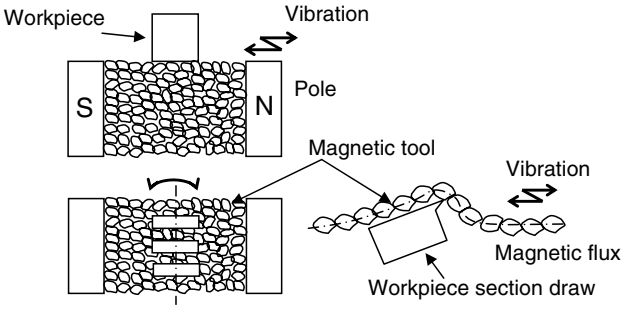


**FIGURE 6.30** Schematic of processing principle. (After Shimbo, Y., in *Applied Electromagnetics and Mechanics*, Takagi, T. and Uesaka, M., Eds., *Japan Society of Applied Electromagnetics and Mechanics*, Tokyo, 131, 2001.)

them. The magnetic tools, which are ferrous pins with sharp edges, are introduced into the magnetic field link together by magnetic force along the lines of magnetic flux. When the nonferrous workpiece is inserted into the magnetic tools, the magnetic tool chains conform around the workpiece and press on the surfaces of the workpiece by magnetic force. The vibration of the magnetic tools in the direction normal to the flow of magnetic flux forces the reconfiguration of the magnetic tool chains around the workpiece repeatedly. This results in relative motion against the edge of the workpiece, achieving both edge and surface finishing of the workpiece.

Figure 6.31 shows micrographs of the tips of the access arm before and after finishing by the use of this method obtained by scanning electron microscopy (SEM) [35]. The expansion of the diameter of the caulking hole is controlled within 1 to 2 μm, and the change in the pitch is no more than 5 μm with negligible disturbance of the surface flatness. This demonstrates the process feasibility for the fine finishing of precision components.

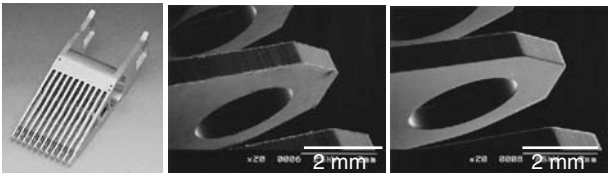


(a) Access arm (b) Before finishing (c) After finishing

**FIGURE 6.31** SEM micrographs of edge of access arm before and after finishing. (After Japan Society for Precision Engineering, *Seimitsukakojituyobinran*, Nikkan Kogyo Shinbun Ltd., Tokyo, 559, 2000, [in Japanese].)

## 6.7 POLISHING PROCESS APPLYING ELECTROPHORETIC DEPOSITION

*JUNICHI IKENO*

### 6.7.1 Introduction

Grinding is a highly efficient finishing process for both hard and brittle materials, but it is difficult to obtain a smooth surface of less than 10 nm Ry and to prevent the occurrence of scratch marks by grinding. If a smooth surface can be achieved by grinding, the production process will be simplified through the elimination of polishing process. The main goal of nanometer grinding is to keep the grain depth of cut less than 100 nm [39].

For precious grinding operation, a grain-sized self-sharpening process is necessary. It is necessary to fabricate a grinding wheel bonded with the ultrafine abrasives uniformly, because highly homogenous bonding strength of a grinding wheel causes the grain-sized self-sharpening process. As a result, the grinding wheel can prevent from weakening the grinding ability. A grinding wheel with ultrafine abrasives and highly homogenous bonding strength is able to perform a smooth surface of less than 10 nm Ry for both hard and brittle materials. A fine grinding wheel with highly homogenous bonding strength is fabricated by using the electrophoretic deposition of ultrafine abrasives. The ultrafine abrasive pellets consist of colloidal silica and polyvinyl alcohol (PVA) bonding agent, which are used for the nanometer grinding of silicon [40].

### 6.7.2 Electrophoretic Deposition

For nanometer grinding, ultrafine grinding wheels with highly homogenous bonding strength is developed by applying the electrophoretic deposition (EPD). When the ultrafine silica abrasives are mixed in an alkaline solution, they become negatively charged. If an electric field is applied, the charged abrasive particles move to the anode and adhere to it, which is called as electrophoretic deposition (EPD). Applying electrophoretic deposition, the EPD pellets are produced, which are highly homogenous with suitable bonding strength compared to the xerogel pellets. The EPD pellets provide a smooth surface roughness without any grinding marks.

### 6.7.3 Development of EPD Pellets

Usually, the diameter of colloidal silica ranges from 10 to 20 nm. The ultrafine silica abrasives are negatively charged in an alkaline solution ($pH > 2$) and they are dispersed homogenously in the solution due to the repulsive force acting between the particles. When an electromagnetic field is applied, the abrasives move to an anode and deposit there, which is called as electrophoretic deposition (EPD). This phenomenon is effective for the fabrication of ultrafine abrasive pellets called EPD pellets. When the silica

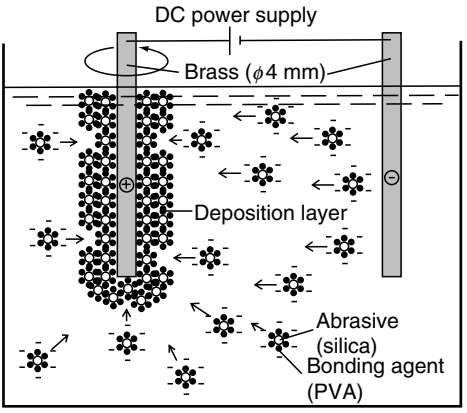


**FIGURE 6.32** Fabrication of ultrafine abrasive pellet.

particles deposit to an anode and become dry, the deposition layer cracks. In order to use the EPD pellets as grinding wheels, it is necessary to include a bonding agent in the pellets. To envelope each silica abrasive homogenously and to move it to anode by the EPD action, PVA is used as a bonding agent, which is one of the nonionized polymers. PVA bonding agent can resist to pressure, tensile force, wear, and shock, which are all essential mechanical properties as a bonding agent for the grinding wheel. The PVA bonding agent adheres to the silica particles and becomes negatively charged. When an electric field is applied to the system, the silica particles covered by the PVA agents move to the rotating anode to produce a uniform layer. The basic principle of production process of EPD pellets by applying EPD phenomenon is shown in Figure 6.32. Figure 6.33 shows that the growth rate of the deposition layer on the anode is 7.5 to 10.5 mm/s in the radial direction

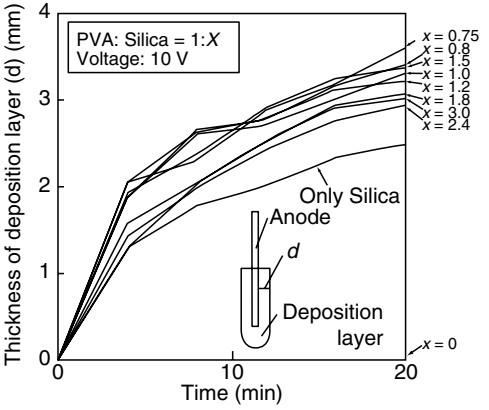


**FIGURE 6.33** Growth rate of the deposition layer.

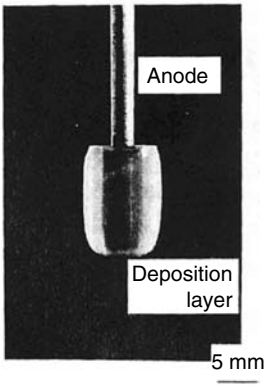


**FIGURE 6.34** Deposition layer produced by the electrophoretic deposition.

when the applied voltage is 10 V and the mixture ratio of silica (concentration 30.0 wt%) and PVA (concentration 4.8 wt%) varies from 0.6 to 3.0. The growth rate of the deposition layer increased with the increase of the concentration of PVA and applied voltage. The deposition layer produced by the EPD is shown in Figure 6.34. By slicing, the abrasive stick EPD pellets are produced. Figure 6.35 shows some dried EPD pellets. It is observed that the deposition layer is too soft when the mixture ratio is less than 0.6; moreover, cracking takes place on the layer during drying when the mixture ratio is more than 1.5. The optimal mixture ratio is found as 0.8. Xerogel is a bonding agent and desiccated mixture of the abrasives. It is used to compare the performance of EPD pellets. The variation in the ratios of weight and thickness are examined during drying process of EPD pellets. It is found that when the mixture ratio is 0.8, the variation ratio of weight is 33.3% and the

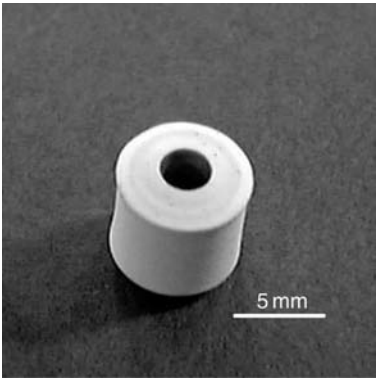


**FIGURE 6.35** EPD abrasive pellets.

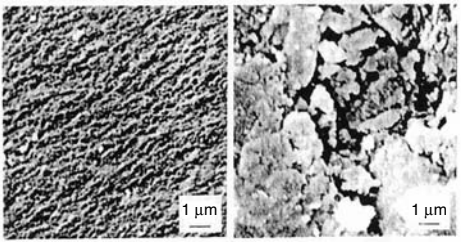


**FIGURE 6.36** Microscopic view of EPD pellet and xerogel.

thickness is 67.9%. The bulk density increased moderately when the EPD pellets or xerogel pellets contained a large amount of PVA. PVA contains more water than silica, thus a pellet with a large amount of PVA shrinks markedly during drying process and as a result, bulk density increases. The variation ratio of bulk density for xerogel pellets is more than 100% at all mixture ratios, whereas the variation ratio of bulk density for EPD pellets is more than 100% at the mixture ratio of 0.8. This means that xerogel pellets contain more PVA than the EPD pellets. The microscopic view of EPD pellets and xerogel pellets are shown in Figure 6.36.

### 6.7.4 Experimental Results

Some experiments have been carried out to show the effectiveness of the proposed method. Figure 6.37 shows the experimental setup for nanometer grinding by EPD pellets. The experimental result shows that the bonding strength increases with the increase of the concentration of PVA. The hardness test of EPD pellets and xerogel pellets shows that the hardness of EPD pellets is half of the xerogel pellets, but the size of pores in EPD pellets is very smaller than the xerogel pellets. From this point, we confirmed that EPD

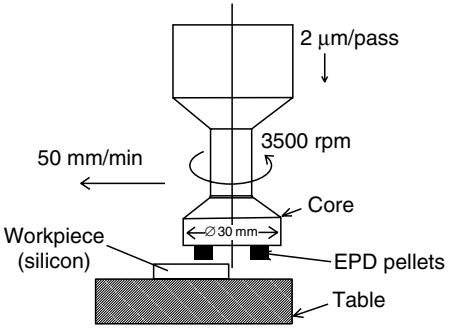


**FIGURE 6.37** Experimental setup for the nanometer grinding by EPD pellets.

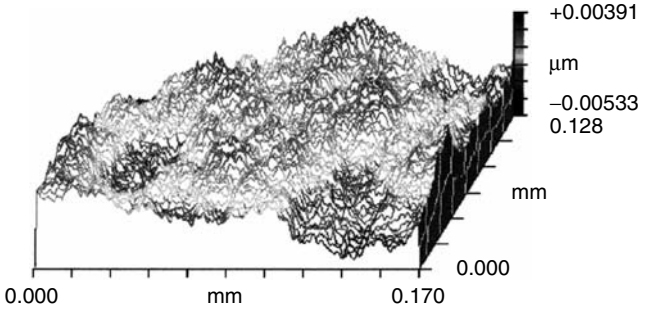


**FIGURE 6.38** Surface roughness of EPD-grounded silicon wafer.

pellets are highly homogenous than the xerogel pellets. The grinding experiment has been carried out using EPD pellets and xerogel pellets at a conventional machining center. The workpiece is a silicon wafer, which has a diameter of 8 in. The grinding surface of silicon wafer using EPD pellets is smoother than that of xerogel pellets. Figure 6.38 shows the surface profile of silicon wafer after grinding with EPD pellets. Finished surface of silicon wafer after grinding with EPD pellets is shown in Figure 6.39. The experimental results show that the surface roughness by EPD pellets is less than

**FIGURE 6.39** EPD-grounded 8 in. diameter silicon wafer.

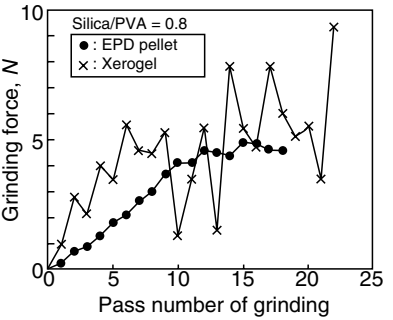


**FIGURE 6.40** Relationship between grinding force and pass number of grinding.

10 nm Ry and there are no grinding marks, but the surface roughness by xerogel pellets is more than 0.1 μm and grinding marks are observed on the surface. The experimental result for grinding force is shown in Figure 6.40. For EPD pellets, the force increased with the number of traverses and becomes constant after 15 traverses. On the other hand for xerogel pellets, the grinding force is unstable.

### 6.7.5 Conclusion

Highly homogenous EPD pellets have been fabricated applying EPD in order to accomplish nanometer grinding of both hard and brittle materials. The physical properties and the grinding abilities of EPD pellets are examined experimentally. EPD pellets have higher density and higher bonding strength compared to the xerogel pellets. EPD pellets are highly homogenous and the pores in the pellets are smaller than xerogel pellets. A super smooth surface of silicon wafer with surface roughness less than 10 nm Ry compared to silicon wafer without any grinding marks is possible by the grinding process using EPD pellets. The low bonding strength of the EPD pellets enables a high removal rate and prevents the loading of swarf.

## 6.8 ELECTROABRASIVE MIRROR POLISHING PROCESS

*JUNICHI IKENO*

### 6.8.1 Introduction

Conventional polishing process has low efficiency with higher accuracy and higher surface roughness, which is applicable for both conductive and nonconductive materials. But the polishing process by the electrical effect has higher efficiency with lower accuracy and lower surface roughness, which is applicable for conductive material only. To improve the accuracy and surface roughness of conductive materials, electro-compounding polishing method was proposed [41].

But the uncommon, big-size, and low-accuracy machine is not suitable for mirror polishing in practical use. To obtain a smooth surface of less than 20 nm Ry for various shapes and size of workpiece is a challenging task. For precious and flexible grinding operations, it is necessary to control the polishing modes for finishing levels of flatness and surface roughness. Electroabrasive mirror polishing can be applied to most of the conductive materials and has a remarkable feature of high efficiency and quality of finishing. Section 6.8.5 reviews the contributions of electroabrasive mirror polishing process [41,42]. By this process, using free abrasives, a turned metal surface can be mirror polished with an accuracy of the surface roughness between 1 nm Ra and 10 nm Ry.

This process is very flexible and useful for various shapes and sizes of metal surfaces for the requirements of finishing levels of flatness and surface roughness, depending on the polishing modes of free abrasives or fixed ones by using tools made of soft materials according to roughness of metal surface.

### 6.8.2 Description

Electroabrasive mirror polishing process is for improving surface roughness of metals effectively at a low current density in $NaNO_3$ solution with a rotating electrode tool covered with a nonwoven nylon fabric sheet for rough polishing or a polyurethane pad for mirror polishing. A passive oxide film formed on the metal surface by the electrolytic process of $NaNO_3$ solution, which is used to improve the surface roughness efficiently on the principle of selective removal of microscopic raised parts. The basic principle of electroabrasive mirror polishing process is shown in Figure 6.41. Electrolysis occurs at the elevated area where abrasives rub off the film to increase the removal rate and it does not occur at sunken area where the removal rate is nearly zero.

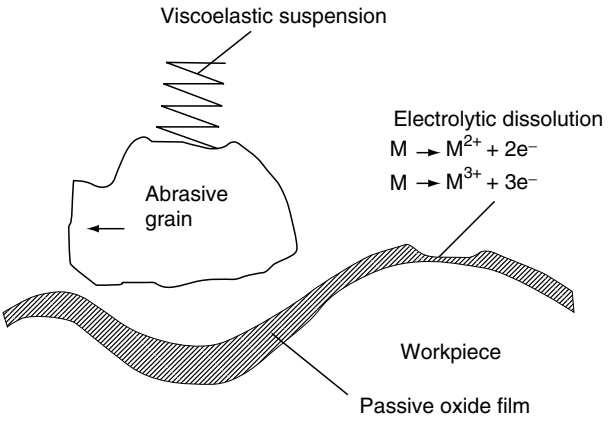


**FIGURE 6.41** Basic principle of the electroabrasive polishing process.

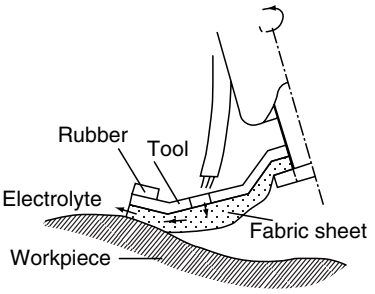


**FIGURE 6.42** Electroabrasive hand polisher.

### 6.8.3 Manual Polishing and Its Automation

Manual polishers are developed for the application on metals, both for flat and curved surface as shown in Figure 6.42. In this process, the electrolyte is fed to the metal surface by the centrifugal effect of rotating tool. For practical applications, these manual polishers are utilized for the automation process with a XY table, which is operated by a controller as shown in Figure 6.43. Constant load method has been considered for the automation process. A through-feed type mirror polishing apparatus with 40 tool electrodes is developed for mass production. In this process, a plate up to 1.5 m in width can be continuously fed with the maximum feed rate of 350 mm/min for mirror polishing.

### 6.8.4 Experimental Results

To show the effectiveness of the proposed method, experiments have been carried out. The polishing process is applied to the internal surface polishing of a small pipe. A precision electroabrasive polishing process is developed using Oscar-type polishing machine to obtain a highly smooth surface.

Figure 6.44 shows the fabrication process of a tool electrode for internal surface polishing of a small pipe. Winding urethane or nonfabric nylon tape around a core-wire electrode and to fix them at both the ends by glue forms the tool electrode. A schematic view of polishing method for internal surface of a small pipe is shown in Figure 6.45. Electroabrasive polishing is applied for the polishing process of the inner surface of SUS316L pipes of about 4 mm in diameter and 35 mm in length. By increasing the tool diameter of 1 mm larger than the pipe diameter provides a working pressure of 10 kPa. The tool electrode rotates at 23 rpm and reciprocates at 7 Hz with an amplitude of 8 mm in order to obtain an abrasive grain crossing angle sufficiently to avoid circular scratches. During initial, intermediate, and final stages of polishing process, the tool electrode is covered with #500, #3000 nylon fabric sheets, and urethane sheet, respectively. The process time is 4 min at a current density of 0.2 to 0.3 $A/cm^2$. The surface roughness obtained by this process

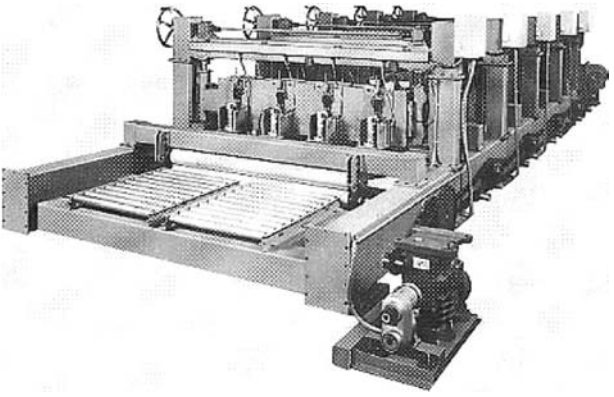

**FIGURE 6.43** Automated mirror polishing machine.

is one-tenth or less than the conventional electropolishing process. Figure 6.46 shows the surface roughness during the initial and intermediate stages, respectively, and the surface roughness of final polishing stage is shown in Figure 6.47. The experimental result shows that the surface roughness of a small pipe is improved from 3 to 0.05 μm Ry. Figure 6.48 shows a photograph of the internal surface of a small pipe after electroabrasive polishing process. The experimental results show that the removal rate increases rapidly with the increase of applied current density.

Figure 6.49 shows a schematic view of electroabrasive polishing method with an Oscar-type polisher. In this experiment, stainless steel, aluminum and its alloys, titanium, and tungsten are used as work materials to obtain surface

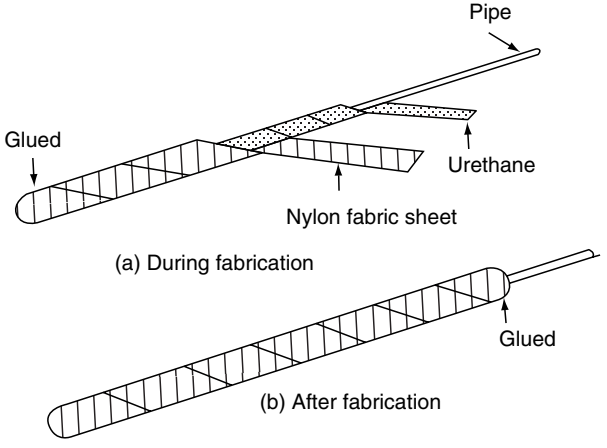


**FIGURE 6.44** Fabrication of tool electrode for internal surface polishing of a small pipe.

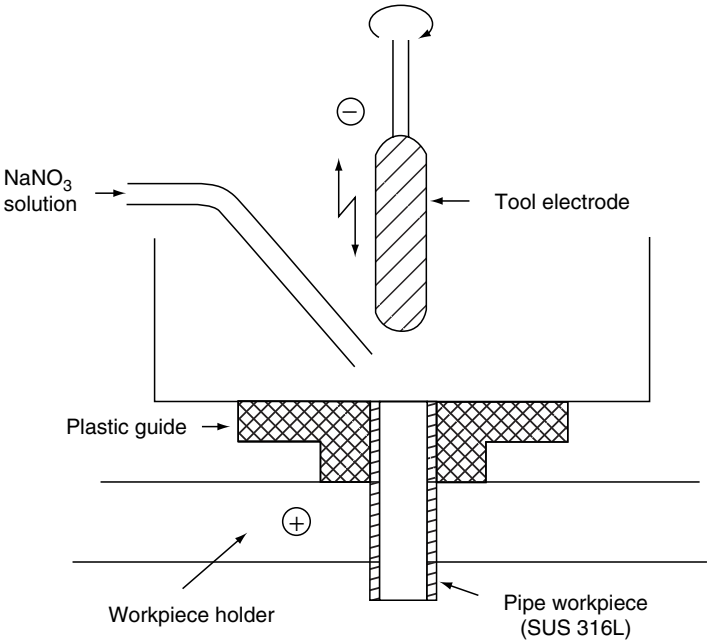


**FIGURE 6.45** Electroabrasive internal surface polishing method for a small pipe.

roughness of 1 nm Ra and 10 nm Ry and also flatness of 1 μm in 100 mm length. Figure 6.50 shows the effect of pH of abrasives and applied voltage on the polishing rate. This experimental result shows that when the applied voltage increases, the polishing rate is also increased. Moreover, if the pH of silica abrasives increases the polishing rate also increases, but when the pH of colloidal silica increases the polishing rate decreases. Figure 6.51 shows the effect of pH of abrasives and applied voltage on

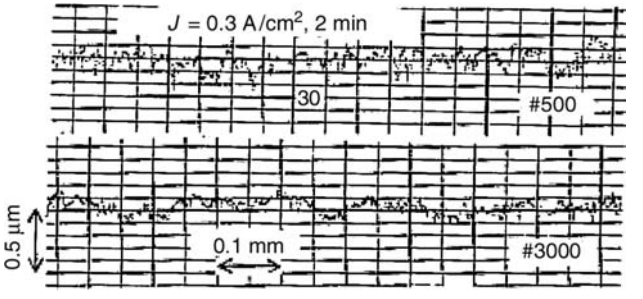


**FIGURE 6.46** Internal surface profile of a small pipe at initial (#500) and intermediate (#3000) stage.

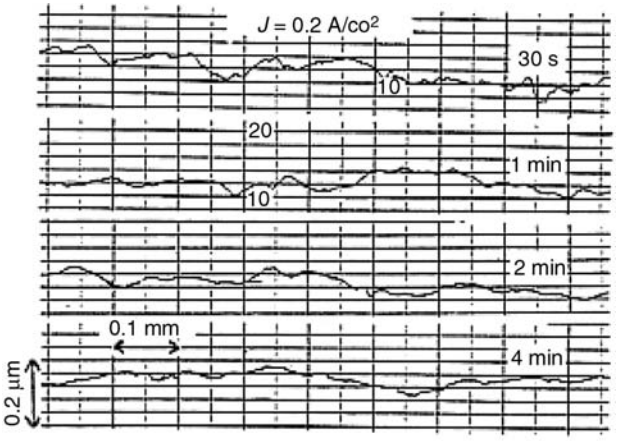


**FIGURE 6.47** Internal surface profile of a small pipe at final stage.

the surface roughness. This experimental result shows that when the applied voltage increases up to 10 V, the surface roughness decreases markedly for silica abrasives. Moreover, if the pH of silica abrasives increases the surface roughness decreases markedly, but there is a little effect of pH of colloidal silica on the surface roughness.

### 6.8.5 Conclusion

This section reviews the contributions of electroabrasive mirror polishing process. Electroabrasive mirror polishing process is very effective for

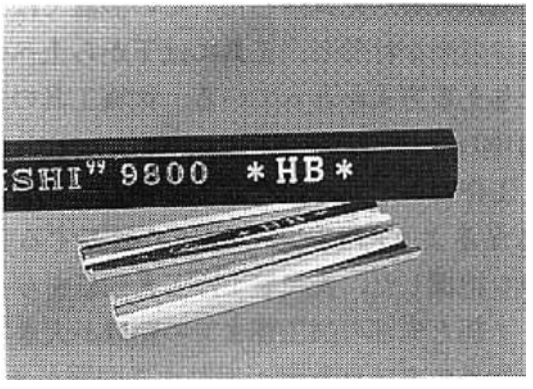


**FIGURE 6.48** Photograph of internal surface of a small pipe.

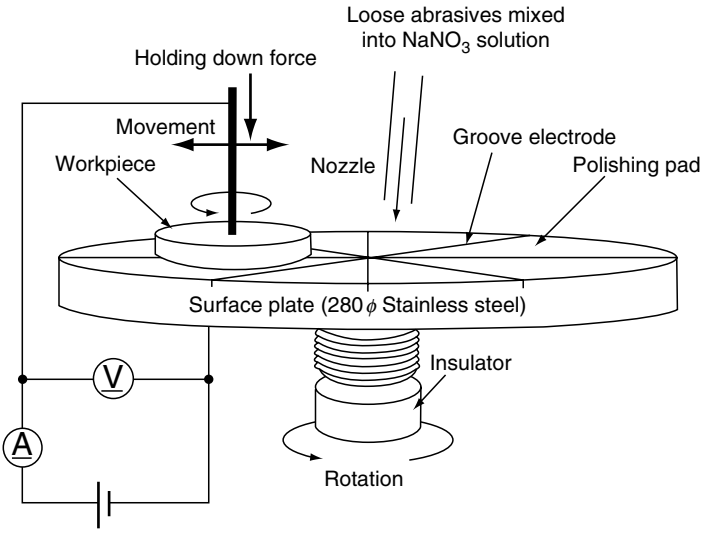


**FIGURE 6.49** Oscar-type electroabrasive polishing machine.

conductive materials on counts of efficiency, accuracy, and surface roughness. For polishing nonconductive materials, this method is not useful. Electroabrasive mirror polishing process is for improving metal surface roughness effectively at a low current density in $NaNO_3$ solution with rotating tool electrodes covered with a nonwoven nylon fabric sheet for rough polishing or a polyurethane pad for mirror polishing. An electroabrasive polishing process for the internal surface polishing of a small pipe has been described for practical use. A precision electroabrasive polishing process is also

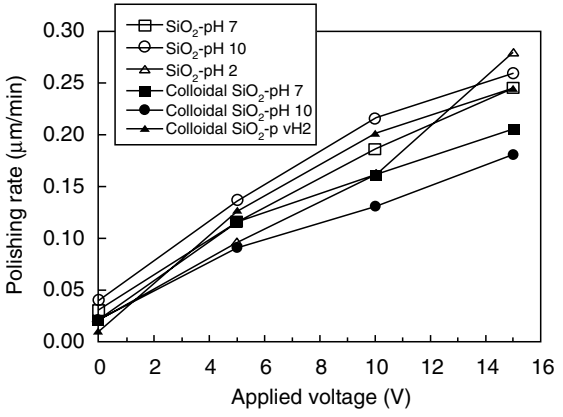


**FIGURE 6.50** Effect of pH and abrasive type on polishing rate.

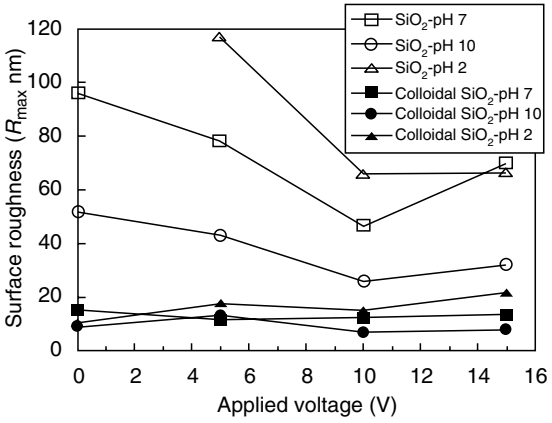


**FIGURE 6.51** Effect of pH and abrasive type on surface roughness.

explained for conductive materials using Oscar-type polishing machine to obtain a highly smooth surface.

## 6.9 P-MAC POLISHING

*TOSHIO KASAI*

Progressive mechanical and chemical (P-MAC) polishing [43] is a disk-type chemical polishing method, which abrades a workpiece against a polishing pad and carried out by chemically dissolving the work surface [43]. Although various kinds of polishing methods for mirrorlike surface have been proposed, P-MAC polishing has been introduced as a new polishing method under the analysis of work material removing mechanism to achieve a mirror surface. P-MAC, whose letter P stands for "progressive," is characterized by changing the polishing mechanism and conditions proceeding positively during the process [44].

### 6.9.1 Analysis on the Mechanism of Various Polishing Methods

The stock removal mechanism in polishing is simply summarized in Figure 6.52. Stock removal is caused in combination with (1) a mechanical action, including (1a) mechanically removing (cutting, scratching) and (1b) friction, and (2) a chemical action, including (2a) dissolving and (2b) a film formation [45]. For example, in CMP (MCP) of a silicon wafer, a soft hydration film is formed on the wafer surface, which is removed by slurry and polishing pad, and a high-quality finishing is achieved. For polishing glass, the same mechanical and chemical actions are combined [46,47]. Most of the polishing methods are defined in the upper half of the complex ring of the stock

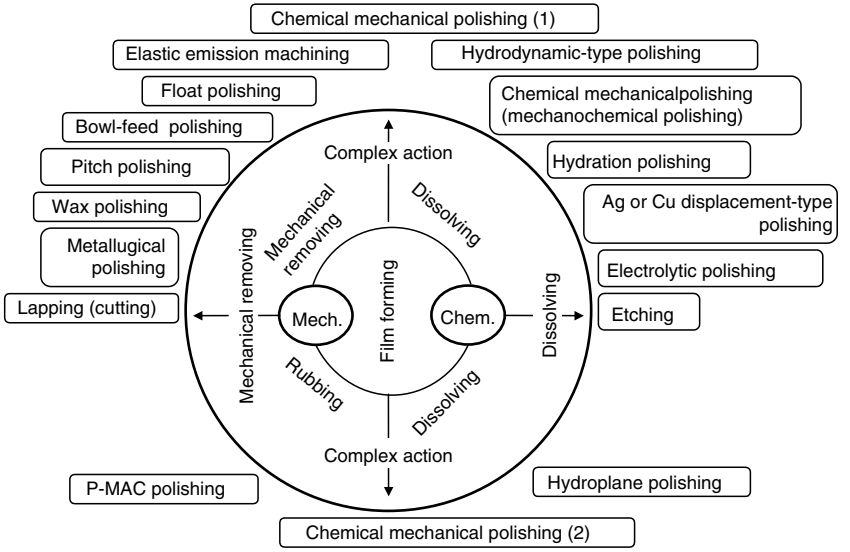


**FIGURE 6.52** Classification of polishing methods based on stock removal mechanism.

removal mechanism; P-MAC polishing is situated in the lower half, thereby, differentiating itself from regular machining methods.

Table 6.2 shows the relationship between a workpiece and a polishing pad during the process. There are three conditions: (1) closed contact condition, which is similar to pitch polishing. A polishing pad has check-patterned grooves to charge or discharge slurry easily, where the work and the polishing pad are abraded under a closed contact condition. (2) Semicontact condition, which is applied to CMP (MCP) of a silicon wafer. As the polishing pad has no groove and the workpiece has a large diameter, a semicontact condition between a noncontact condition based on a hydroplane phenomenon and a closed contact condition is controlled by the polishing pressure, as an intermingled condition. (3) Noncontact condition, which is similar to EEM and float polishing. The workpiece and the polishing pad become noncontact due to floating effect caused by a hydroplane phenomenon. Every polishing method utilizes one of the above conditions, and it seems that the same condition is used during polishing.

The changes of stock removing mechanism in P-MAC polishing are: (1) the atomic arrangements of rough surface caused in the previous process are affected by the mechanical friction with the polishing pad; chemical dissolving of affected part progresses and brings a smooth surface. (2) When an appropriate smooth surface is obtained, polishing proceeds with dissolving of working fluid film under the condition of no mechanical friction. As a result, the damage-free surface with a high accuracy is achieved.

**TABLE 6.2**
**Classification of Polishing Conditions Based on Relationship between Workpiece and Polishing**

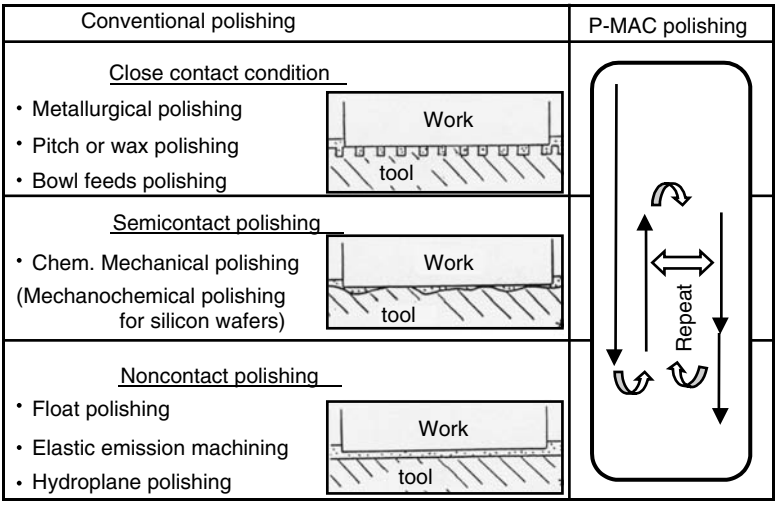


In usual polishing, the stock removal is proportional to the relative speed between the workpiece and the polishing pad, pressure, and time, however, polishing by chemical dissolving is achieved under different conditions. As no abrasive grain is used, it is important to choose appropriate chemicals taking account into the processing efficiency and surface quality. The additive concentration and temperature of the working fluid directly affects the processing efficiency. The speed, pressure, and time may cause a rise in temperature in the polishing atmosphere and the damage of atomic arrangements, which influence the chemical dissolving. Furthermore, the pressure will lessen the thickness of working fluid layer, and the speed may exchange smoothly between fresh and tired working fluid and decrease the layer thickness due to the dispersion.

In P-MAC polishing of compound semiconductor wafer belonging to the III–V and II–VI groups, a Br-methanol solution used in mirror etching is adopted as a working fluid. Since bromide of work materials is dissolved into methanol without generating hydrogen gas, there is no concern that bubbles will be trapped in thin layer between the workpiece and polishing pad. The relatively thick layer of working fluid is formed under low speed or pressure, and the stock removal as a processing efficiency is obtained by using a suitable Br concentration. Although various methods to adjust the gap between workpiece and polishing pad can be considered, the difference of the stock removal amount in polishing different kinds of work materials is available.

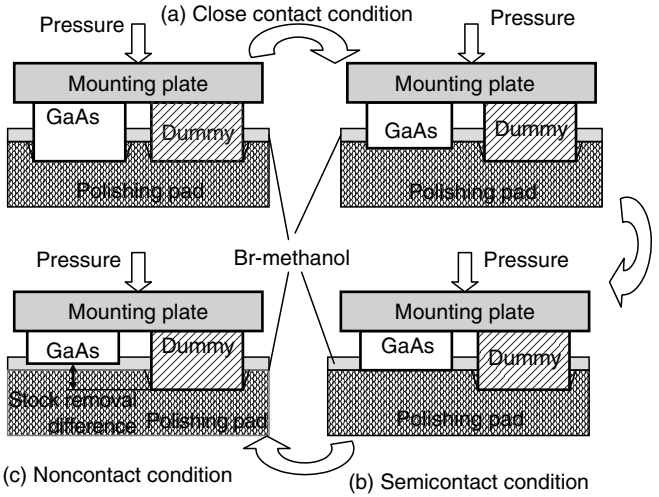


**FIGURE 6.53** Growth model of stock removal difference between GaAs crystal and dummy material.

Figure 6.53 shows a growth model of the difference of stock removal amount in Br-methanol solution use, where a GaAs single-crystal work is waxed on a plate at the same height with dummy material. As only GaAs single crystals are polished with Br-methanol solution, the gap and polishing condition between the workpiece and the polishing pad change step by step. They are in the close contact condition at the early stage of polishing, then followed by the semicontact condition, and finally the noncontact condition.

### 6.9.2 P-MAC Polishing for Small Pieces of GaAs Single Crystals

A workpiece of GaAs single crystals of 5 mm × 6 mm × 0.5 mm surrounded by a sapphire of dummy material were waxed on a polishing jig of 60 mm diameter. Utilizing a conditioning ring-type polishing machine with a polishing pad of 30 mm × 180 mm inside and outside diameter, the polishing progressed by setting the workpiece in a conditioning ring of 60 mm × 90 mm inside and outside diameter. The polishing speed was fixed at 20 m/min.

Br-methanol solution, with an extremely strong smell, was made up by adding Br of 0.25% to 2.0% in a methanol solution including 20% ethylene glycol. A soft-foamed polyurethane sheet was used for silicon wafers and a foamed fluorocarbon sheet was used as a polishing pad.

#### 6.9.2.1 Processing Efficiency

The stock removal in P-MAC polishing is determined by changing the Br concentration in the solution. Figure 6.54 shows the relationship between the

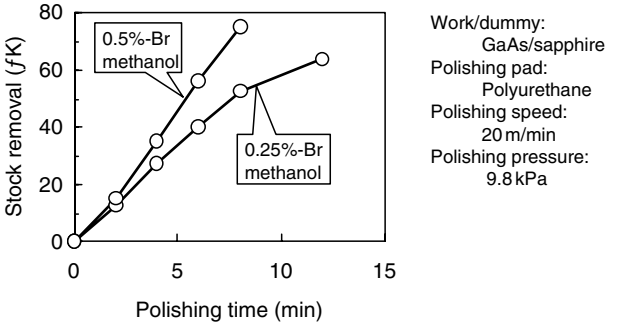


**FIGURE 6.54** Relationship between stock removal, Br concentration, and time in P-MAC polishing of GaAs crystal.

polishing time and the stock removal amount using two kinds of solutions with different Br concentrations. In both cases, there is no difference of quality in the surface roughness or the mirror-finished level.

When a large stock removal amount is attempted in usual polishing, a large-size grain and the high relative speed and pressure between the work material and the polishing pad are applied. High rigidity and high-rotation speed are required for current silicon wafer polishing machines. However, for P-MAC polishing, the rigidity is not as important, but it must be corrosion-proof. It is supposed to belong to a new polishing method.

#### 6.9.2.2 Accuracy

The effective improvement of turned-down edge in this polishing is shown in Figure 6.55. As polishing advances, a difference in height between workpiece of GaAs single crystal and the dummy material reaches until 40 μm. The turned-down edge at the start is obviously improved.

#### 6.9.2.3 Surface Roughness

The biggest problem faced in P-MAC polishing was how the surface roughness should be improved. A silicon wafer is ordinarily finished to 1–2 nm Rz in surface roughness. Regarding GaAs wafers, at least the same level of the high quality on the finished surface will be required.

In P-MAC polishing by using the soft-foamed polyurethane sheet for silicon wafers, the surface roughness on polished GaAs, InP, ZnSe, and CdTe workpieces remained at 20 nm Rz, respectively. It is presumed that the mechanical friction of the surface irregularity on polishing pad forms rough surface on the crystal workpieces by joining the chemical solution together under the semicontact condition. When using a smooth soft-foamed polyurethane pad that is hot pressed, the surface roughness was improved to

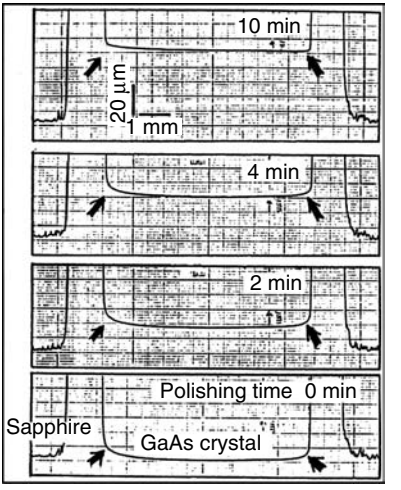


**FIGURE 6.55** Improvement of turned-down edge in P-MAC polishing.

8 nm Rz under P-MAC polishing condition, which shows that the proper selection of the polishing pad is important.

When a fluorocarbon-foamed sheet that was far softer and smoother than soft-foamed polyurethane was used, the surface roughness reaching 0.2 nm Rz could be achieved. This implies that the compound semiconductor GaAs wafers can be polished to the negligible surface roughness as well as silicon wafers by CMP. In addition, this type of polishing pad has the advantage of having not only the chemical resistance against Br-methanol solution, but also high durability.

### 6.9.3 P-MAC Polishing Machine Manufacturing and GaAs Wafer Polishing

For P-MAC polishing GaAs wafers: (1) a fully automatic P-MAC polishing machine was prepared. The entire process could progress automatically as taking a GaAs wafer out from the cassette, polishing, washing, drying, and then putting it back to the cassette. (2) Concerning changes of the closed contact condition, the semicontact condition, and the noncontact condition between a wafer and a polishing pad, the repeating system for the free and fixed condition between wafer and dummy was adopted. (3) A vacuum system was used in fixing the wafer on the machine. (4) Methanol was used to clean the wafer after polishing [48].

In order to obtain a mirrorlike surface smoothly from rough surface, it was necessary to employ a process where the closed contact conditions and the semicontact conditions repeat several times. It should be repeated frequently because a minute surface roughness was achieved quickly by using short-time intervals, for example, 30 s rather than intervals of 1 or 2 min.

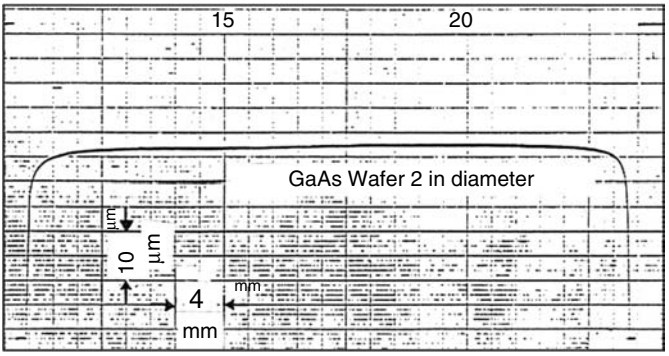


**FIGURE 6.56** Straightness on P-MAC polished 2 in. diameter GaAs wafer.

Figure 6.56 shows the straightness of a polished wafer. Excluding the outer 3 mm, a flatness of 1–2 μm is achieved on the whole area of the wafer.

The concept and verification of P-MAC polishing was described. In P-MAC polishing, the stock removal of compound semiconductor material such as GaAs wafers was achieved by chemical-dissolving effect of working fluid with no abrasive. This polishing condition can remove the ups and downs of surface roughness and attain a damage-free and mirrorlike surface by properly utilizing the mechanical friction and the chemical reaction.

## 6.10 COLLOIDAL SILICA POLISHING

*TOSHIRO K. DOI*

Colloidal silica used in this process is prepared by dispersing $SiO_2$ particles (abrasives) of 100 to 200 Å in the alkaline solution of pH 10. Normally, the slurries prepared by simply dispersing fine abrasives to 15 to 20 wt% are difficult to apply during polishing. However, in a colloidal state, as much as 50 wt% of silica particles can be present in the slurry, which is expected to increase the amount of particles that work on polishing, leading to the realization of high polishing efficiency. Moreover, dispersed ultrafine $SiO_2$ particles are found to be highly uniformly spherical, which are not observed in the existing abrasives (Figure 6.57).

The effect of chemical actions of $SiO_2$ particles on sapphire in the wet polishing is self-explanatory as shown in Figure 6.58. In wet polishing with fine $SiO_2$ particles of size 160 Å, the polishing rate is about one-twentieth of dry polishing, which is attributable to the fact that, due to presence of water, the temperature of the working particles does not rise as much as it does in dry polishing, and the surface activities drastically drop by the absorption of water in $SiO_2$ particles. If ultrafine $SiO_2$ particles are used in dry polishing, its polishing rate reaches 4 times that of $SiO_2$ particles of 1 μm, i.e., 60 times larger in size, exhibiting behaviors opposite to other mechanical polishings.

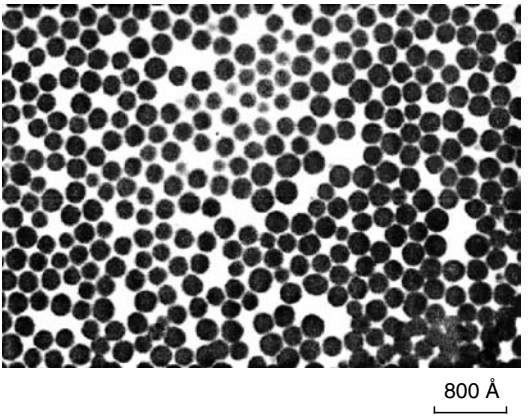


**FIGURE 6.57** An example of colloidal silica (TEM) (Nalco 2350).

Chemical actions induced by $SiO_2$ particles are the main promoting factors of polishing in dry polishing whereas in wet polishing, as the temperature in the contact point does not reach the counterdiffusion temperature region where solid-state reaction occurs, almost no chemical actions occur there practically [49]. In other words, it is presumed that the polishing of sapphire single crystals with colloidal silica progresses mainly by means of mechanical removal actions thereof.

Figure 6.59 shows a surface topography (roughness) of the sapphire surface polished with colloidal silica, which produced the surface to a roughness

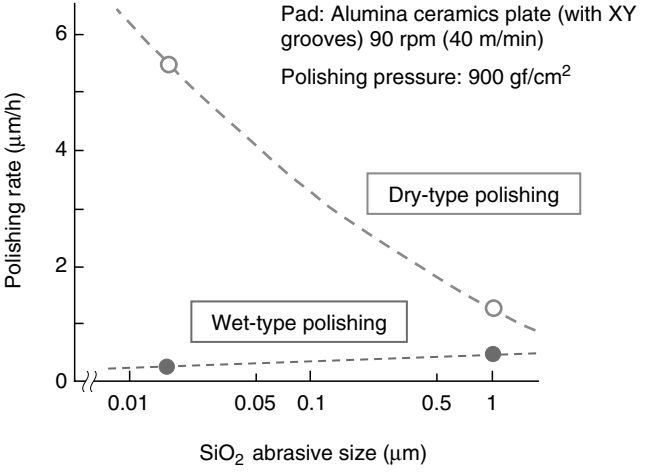


**FIGURE 6.58** Relationship between particle size and polishing rate of $SiO_2$ in dry-type and wet-type polishing.

**FIGURE 6.59** Surface roughness of sapphire single crystal polished by colloidal silica slurry.

of 10 Å $R_{max}$. Polishing should have been performed presumably in the atomic or molecular unit removal order. Furthermore, silicon thin film (3000 Å) was epitaxially grown on the processed surface of the sapphire single crystal, and observed with an electron microscope, which shows no defect caused by the polishing but exhibits excellent crystalline film as can be seen from the comparative photographs shown in Figure 6.60. As just described, the polishing of sapphire single crystals with the colloidal silica containing ultrafine particles is anticipated to be an extremely effective measure to produce damage-free, smooth, mirror surfaces.

Figure 6.61 shows polishing characteristics of colloidal silica on single crystals such as sapphire, GGG ($Gd_3Ga_3O_{12}$), $LiTaO_3$, and silicon that are the component materials for electronic and optical communications. Polishing rates are proportional to the polishing pressures, and polishing is possible on any of such materials. However, polishing pressure necessary to obtain a constant speed varies depending on the crystals, which is easily considered dependent on the mechanical properties of the workpieces as the polishing mechanism is based on the mechanical removing actions induced by colloidal silica [50].

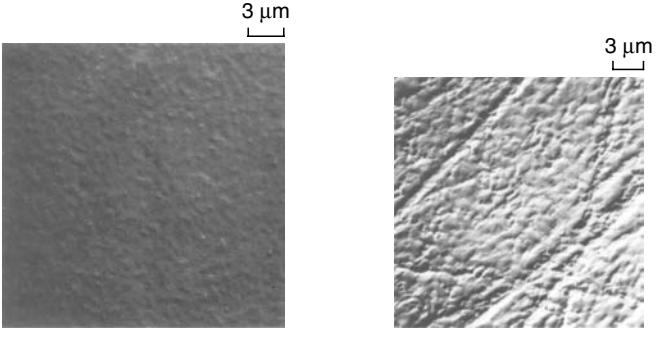


(a) Epitaxial film on surface polished by colloidal silica

(b) Epitaxial film on surface polished by fine diamond abrasives

**FIGURE 6.60** Example of electron microscopic photographs of epitaxially grown Si thin films on sapphire single crystal treated in various ways (Si thin film: about 3000 Å, substrate: sapphire single crystal (1102).

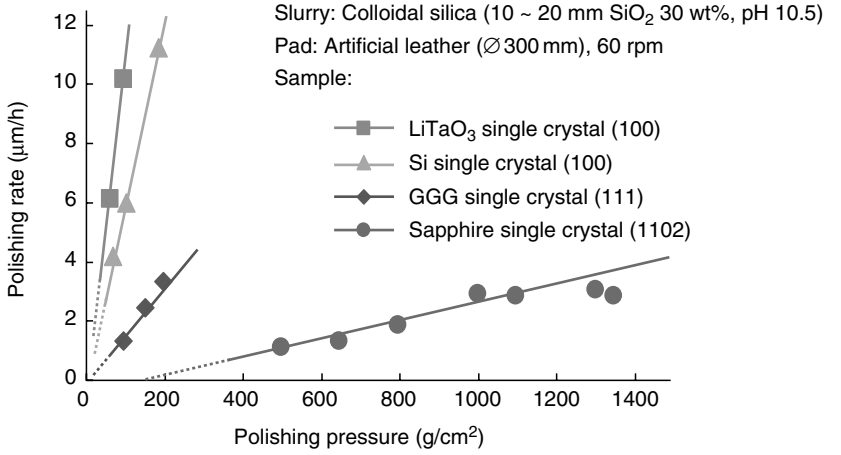


**FIGURE 6.61** Relationship between polishing pressure and polishing rate of various crystals using colloidal silica.

Figure 6.62 shows relationships between Vickers hardness $H_v$ (kgf/mm$^2$) of each crystal and required polishing pressures, taking polishing rates $V$ (μm/h) as a parameter. From the chart, their relationship is derived as $P = 10^{-4} \exp(K_1 \times K_v)$, where $K_1$ is the constant to be determined by polishing conditions. Meanwhile, $K_1$ obtained at each $V = 1$, 3, and 5 μm/h can be calculated as $K_1 = 2 \times 10^{-4}\, V + 1.4 \times 10^{-3}$.

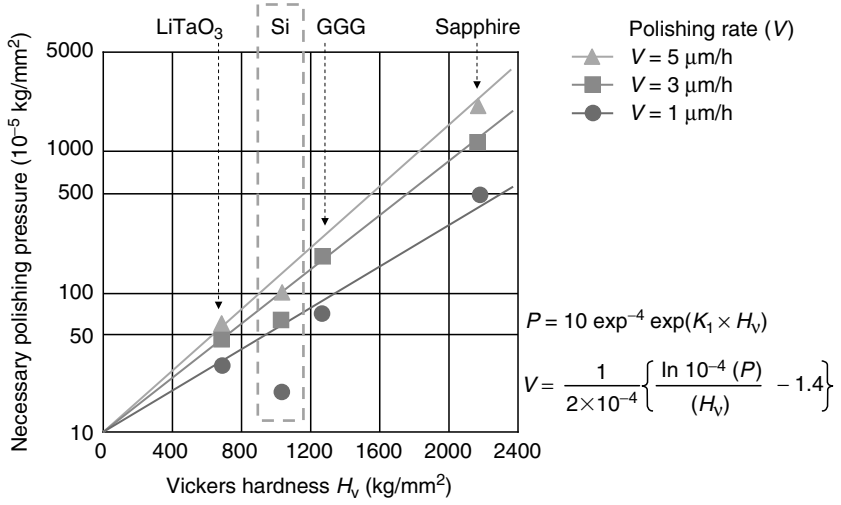


**FIGURE 6.62** Relationship between necessary processing pressure and Vickers hardness of various kinds of crystals.

From both equations above, $V$ is expressed as

$$V = 5 \times 10^{-3}\{(1/H_v) \ln 10^4 P - 1.4 \times 10^{-3}\} \quad (6.1)$$

In other words, polishing rate $V$ is proportional to the reciprocal number of the hardness $H_v$ of the crystals, and is similar to the relationship between the stock of wear in frictional abrasion and hardness [51].

This polishing method can realize a damage-free mirror surface using ultrafine $SiO_2$ particles dispersed in colloidal silica and a soft elastic polisher (artificial leather). From this viewpoint, it is hard to think that polishing is enhanced by the scratching actions of the particles just retained in the polisher as the conventional pitch polishing. This is anticipated from the fact that even though ultrafine $TiO_2$ (with diameter of 150 Å) particles, similar to the hardness and size of $SiO_2$ fine particles, are dispersed in alkaline solution of pH 10, they do not become colloidal slurry, and besides, have almost no effect on the sapphire polishing.

As shown in Figure 6.63, let us assume that the colloidal silica is dispersed on an elastic artificial leather (pad) having excellent slurry-retaining functions, and the work is pressing the pad at high pressure. Although the crystals remain in close contact with the elastic polisher, very thin film-like colloidal silica remains in existence as in the boundary lubrication due to the pad structure shown in Figure 6.63a. When shearing stress is applied to this

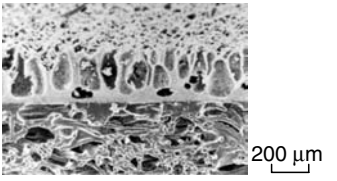


(a) Structure of artificial leather pad (SEM photograph)

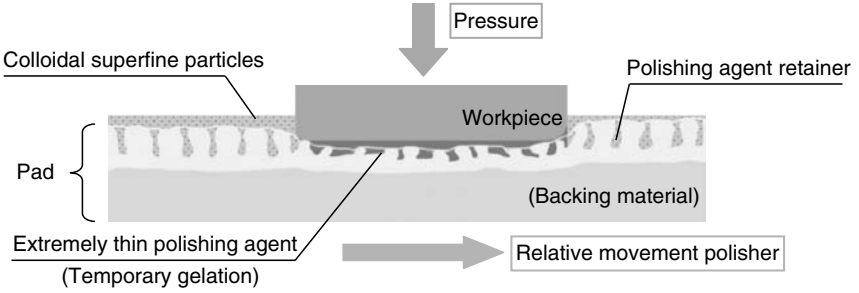


(b) Constitutional diagram of the colloidal silica polishing

**FIGURE 6.63** Artificial leather pad (SEM photograph) and schematic diagram of colloidal silica polishing.

film-like colloidal silica under high pressure or friction heat, it is assumed that reversible gelatinization phenomenon appears temporarily. For this reason, ultrafine $SiO_2$ particles appear to be fixed firmly to the liquid, and thanks to its mechanical microremoval actions, damage-free, mirror surfaces are created. Figure 6.63b is a schematic diagram showing a polishing state by this polishing method.

In accordance with the above examination, polishing rate can be adjusted by changing gelatinization speed. Figure 6.64 shows polishing characteristics of sapphire single crystals with colloidal silica, to which electrolytic sodium sulfate ($Na_2SO_4$) and ethylene glycol ($HOCH_2CH_2OH$) are added as an accelerator of gelatinization and as an inhibitor thereof, respectively. Polishing rate increased as the addition of $Na_2SO_4$ increased whereas it decreased when $HOCH_2CH_2OH$ was added. From this data, the effect of each compound is clear [50].

According to the above, the polishing actions induced by the colloidal silica are dependent largely on the mechanical microremoval effect that accompanies friction and abrasion since ultrafine $SiO_2$ particles are firmly retained in the polisher by means of the temporal gelatinization phenomenon occurring beneath the processed surface. Such friction and abrasion are regarded as an adhesive abrasion since $SiO_2$ particles are apt to adhere firmly to the crystals (high-temperature reaction test) [49]. It is presumed that damage-free, mirror surfaces are produced by the shearing and peeling of the adhered portions of atomic order that is of minimum size, which does not generate strains around.

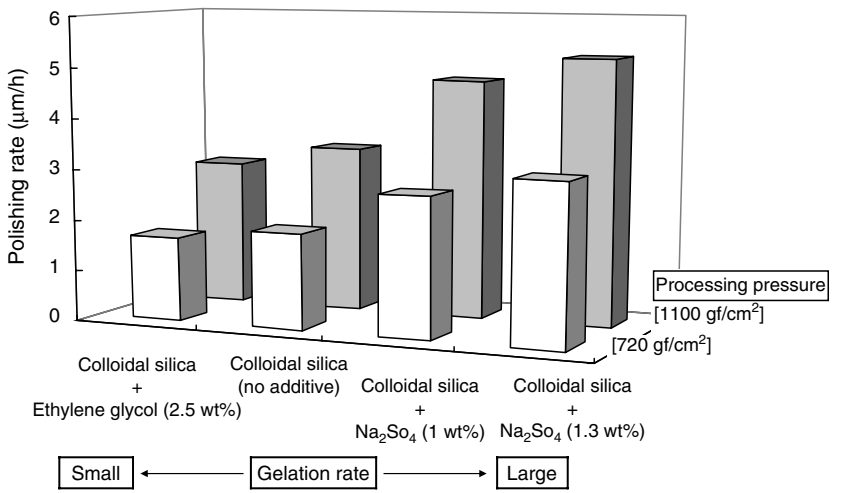


**FIGURE 6.64** Comparative polishing rates of sapphire single crystals at different gelation rates of colloidal silica.

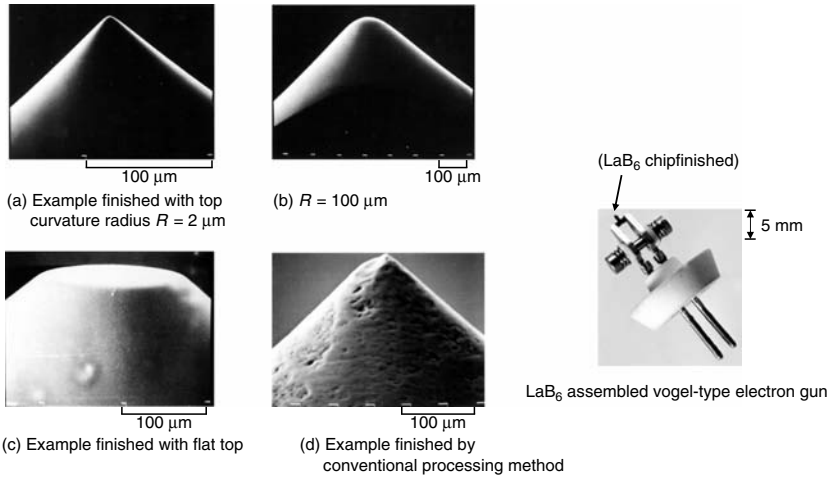
100 μm
(a) Example finished with top curvature radius R = 2 μm
100 μm
(b) R = 100 μm
(LaB6 chipfinished)
5 mm
LaB6 assembled vogel-type electron gun
100 μm
(c) Example finished with flat top
100 μm
(d) Example finished by conventional processing method

**FIGURE 6.65** Example of processed strain-free mirrorlike surface by the colloidal silica polishing technique and conventional processing technique on the top and lateral sides of $LaB_6$ single-crystal chips for use in an electron gun (SEM photograph).

This polishing method can apply to almost all crystals to produce damage-free, mirror surfaces as shown in Figure 6.61. As a special application, photographs of the processed tips of $LaB_6$ single crystals ($0.75 \times 0.6 \times 2.2$ mm chip) for electron gun are shown in Figure 6.65, for which polishing reagent, composed of ultrafine particles of below 500 Å dispersed (colloidal) in pure water, and a hard special polisher (pad) was employed [52]. Although $LaB_6$ single crystals are chemically stable and mechanically very hard (microhardness of 2770 $kg/mm^2$), an extremely smooth mirror surface was produced.

In conclusion, I would like to discuss the surface qualities obtained by this polishing method, providing some comparative evaluations with the conventional processing. Figure 6.66 shows photographs of the film surfaces that are epitaxially grown on the surfaces of $LiTaO_3$ by the present polishing method and conventional pitch polishing. The photograph in Figure 6.66a reveals that defect-free, epitaxial films are grown on the surface processed by the present polishing method whereas the photograph in Figure 6.66b shows epitaxial films with a number of defects grown on the surfaces processed by the conventional processing methods [53].

Pursuant to the above, slurries in which ultrafine particles are dispersed in a colloidal state enable the polishing of those single crystals with different hardnesses, delivering excellent mirror surfaces of around 10 Å $R_{max}$ without any residual strains.

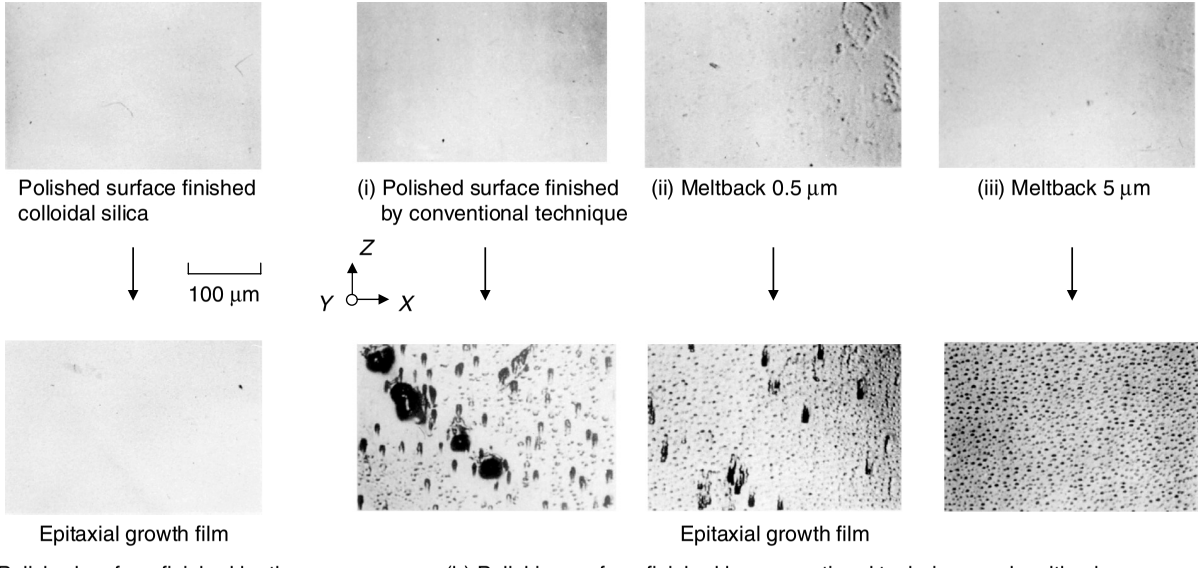
Polished surface finished colloidal silica
(i) Polished surface finished by conventional technique
(ii) Meltback 0.5 μm
(iii) Meltback 5 μm
100 μm
Z
Y
X
Epitaxial growth film
Epitaxial growth film
(a) Polished surface finished by the present processing technique and epitaxial film grown thereon
(b) Polishing surface finished by conventional technique and meltback surface at each depth, and epitaxial surface grown at each surface

**FIGURE 6.66** Photograph of surface and epitaxial growth film of $LiTaO_3$ single crystal polished by the present processing technique and the conventional processing technique.

## REFERENCES


1. Otte, G., An improved method for the production of optically flat surfaces, *J. Sci. Instrum.*, 42, 911 (1965).
2. Lerstner, A., Progress report on Teflon polishing for precision optical flats, *Appl. Opt.*, 11(4), 960 (1972).
3. Twyman, F., *Prism and Lens Making*, 2nd ed., Hilger & Watts Ltd., London, 1952, p. 373.
4. Rumsay, J., The effect of eccentric loading of optical flat during grinding or polishing, *J. Sci. Instrum.*, 32(9), 338 (1955).
5. Kasai, T., *Study on precision machining of flat planes,* Electric Communication *Laboratories* Report No. 13634, NTT Public Corporation (in Japanese) (1979).
6. Kasai, T., *Lapping and polishing*, *Ultraprecision Machining Technology*, Kumagaya Memorial Committee Meeting, Japan Society of Grinding Engineers, 1984, p. 451 (in Japanese).
7. Bajuk, D.J., Computer controlled generation of rotationally symmetric aspheric surfaces, *Opt. Eng.*, 15(5), 401 (1976).
8. Becker, K. and Beckstette, K., M400 and P400—A pair of machines for computer controlled fine correction of optical surfaces, *Proceeding of the International Congress for Ultraprecision Technology in Aachen/PRG*, 1998, pp. 212–223.
9. Mori, Y., Yamauchi, K., and Endou, K., Elastic emission machining, *Prec. Eng.*, 9(3), 123 (1986).
10. Kasai, T., *Study on precision machining of flat planes*, Electric Communication Laboratories Report No. 13634, NTT Public Corporation, 1979, p. 175 (in Japanese).
11. Doy, K.T. et al., Development of a both sides simultaneous polishing system for 300 mm silicon wafers, aiming at the production of nanotopography-free surfaces, *Proceedings of the Third International Symposium on Advanced Science and Technology of Silicon Materials*, 2000, pp. 248–257.
12. Kubo, T., *Introduction to Mechanochemistry* (in Japanese), Tokyo Kagaku Dojin Co., Tokyo, 1971, p. 5.
13. Yasunaga, N. et al., Mechanochemical polishing of single crystals with soft powders, *Proc. ICPE*, 32, 32–37 (1974).
14. Duwell, E.J. and Butzke, H.C., Effect of interface composition on the wear rate of sapphire, *ASLE Trans.*, 7, 101 (1964).
15. Yasunaga, N. et al., Sapphire abrasion in friction between quartz and the sapphire, *J. JSPE*, 44(8), 939 (1978) (in Japanese).
16. Regh, J. and Silvey, G., *Electro Chem. Soc.*, Fall Meeting, 266, 119 (1966).
17. Mendel, E., Polishing of silicon, *SCP Solid State Technol.*, 10(8), 27 (1967).
18. Karaki, T., Wet-type mechanochemical polishing of Si wafers, *Tool Eng.*, 24, 38 (1984) (in Japanese).
19. Karaki, T. and Kasai, T., Mechano-chemical polishing characteristics of GGG single crystal using acid solution, *J. JSPE*, 44(3), 333 (1978).
20. Karaki, T. et al., Facilitation mechanism of polishing rate in mechano-chemical polishing of Si single crystals, *J. JSPE*, 46(3), 331 (1980) (in Japanese).
21. Karaki, T. and Watanabe, J., Effect of frictional heat on removal rate in mechano-chemical polishing of crystals used in electronics, *ASME Wear Mater.*, 227 (1983).

22. Doy, T.K., Optical and electro-optical engineering contact, *SPIE*, 27(8), 482 (1989) (in Japanese).
23. Namba, Y., Mechanism of Float Polishing, Technical Digest at Topical Meeting on Science of Polishing, *OSA* (1984, 4) Tub-A2.
24. Mori, Y., Yamauchi, K., and Endo, K., Elastic emission machining, *Prec. Eng.*, 9(3), 123 (1987).
25. Sato, Y., Knight, J.D., and Somerday, B., Observation and prediction of cavities in a lubricant between non-parallel disks in relative rotation, *Tribol. Trans.*, 35(1), 170 (1992).
26. Baron, Y.M., *Technology of Abrasive Machining in a Magnetic Field*, Masinostrojenije, St. Petersburg, 1975 (in Russian).
27. Ruben, H.J., *Advances in Surface Treatments*, vol. 5., Niku-Kari, A. (Ed.), Pergamon Press, New York, 1987, p. 239.
28. Shinmura, T. and Yamaguchi, H., Magnetic-field-assisted machining process and its industrial applications, *J. Magnetics Soc. Jpn.*, 23(9), 1946 (1999) (in Japanese).
29. Shinmura, T., et al., Study on magnetic-abrasive process—Process principle and finishing possibility, *Bull. Jpn. Soc. Prec. Eng.*, 19(1), 54(1985).
30. Kureha Chemistry Industry Co. Ltd, Composite whetstone particle for magnetic abrasion and production thereof, *Japan Patents* 61-250084, A, 1986.
31. Anzai, M., Sudo, T., Otaki, H., and Nakagawa, T., Experiment of magnetic assisted finishing using slurry abrasive, *J. Jpn. Soc. Abrasive Technol.*, 37(1), 51 (1993) (in Japanese).
32. Fox, M., Shinmura, T., and Komanduri, R., Magnetic abrasive finishing of rollers, *Ann. CIRP*, 43(1), 181 (1994).
33. Shinmura, T., Yamaguchi, H., and Watanabe, M., Study of a new internal finishing process by the application of magnetic abrasive machining—Development of an abrasive slurry circulating system and its effects on the finishing characteristics, *J. Jpn. Soc. Prec. Eng.*, 67(4), 575 (2001) (in Japanese).
34. Geeng-Wei, C., Biing-Hwa, Y., and Rong-Tzong, H., Study on cylindrical magnetic abrasive finishing using unbonded magnetic abrasives, *Int. J. Mach. Tool Manuf.*, 42, 575 (2002).
35. Japan Society for Precision Engineering, *Seimitsukakojituyobinran*, Nikkan Kogyo Shinbun Ltd., Tokyo, 2000, p. 559 (in Japanese).
36. Yamaguchi, H., Shinmura, T., and Kobayashi, A., Development of an internal magnetic abrasive finishing process for nonferromagnetic complex shaped tubes, *JSME Int. J.*, 44(1), 275 (2001).
37. Shimbo, Y., Development of a new process for deburring and edge finishing of complex shapes industrial precision parts by the application of magnetic field-assisted machining, in *Applied Electromagnetics and Mechanics*, Takagi, T. and Uesaka, M. (Eds.), *Jpn. Soc. Appl. Electromagn. Mech.,* Tokyo, 2001, p. 131.
38. Anzai, M., Nakagawa, T., Yoshioka, N., and Banno, S., Development of magnetic abrasive finishing system for electric razor blades, *Proceedings of the Japan Society of Precision Engineering Fall Annual Meeting*, 1999, p. 221 (in Japanese).
39. Ohmori, H. and Nakagawa, T., Mirror surface grinding of silicon wafers with electrolytic in-process dressing, *Ann. CIRP*, 39(1), 329 (1990).
40. Ikeno, J., Tani, Y., and Sato, H., Development of highly homogeneous pellets applying electrophoretic deposition of ultrafine abrasives for nanometer grinding, *Ann. CIRP*, 43(1), 319 (1994).

41. Kimoto, Y., Electro compounding polishing of stainless steel, *J. Electro Machining Soc*., 12(23), 1 (1978) (in Japanese).
42. Seimiya, S., Electro-abrasive mirror polishing and its application, *J. JFWA*, 3(4), 163 (1996) (in Japanese).
43. Iiyama, S., Ida, I., Yamaguchi, M., and Sugane, K., Chemical polishing of GaAs Single crystals, *Rev. Elec. Commun. Lab*., 18(3–4), 235 (1970).
44. Kasai, T. and Kobayashi, A., Progressive Mechanical and Chemical Polishing, Technical Digest at Topical Meeting on Science of Polishing, *OSA* (1984, 4) TuB-A2.
45. Kasai, T., Horio, K., Doy, K.T., and Kobayashi, A., Improvement of conventional polishing conditions for obtaining super smooth surfaces of glass and metal works, *Ann. CIRP*, 39(1), 321 (1990).
46. Izumitani, T. and Adachi, S., Polishing Mechanism of Fused Silica Glass, Topical Meeting on the Science of Polishing, Technical Digest, *OSA* (1984) TuB-Al-1-3.
47. Brown,N.J., Some speculations on the mechanisms of abrasive grinding and polishing, *Prec. Eng*., 9(3), 129 (1987).
48. Kasai, T., Matsumoto, F., and Kobayasi, A., Newly developed fully automatic polishing machines for obtainable super-smooth surfaces of compound semiconductor wafers, *Ann. CIRP*, 37(1), 537 (1988).
49. Karaki, T. et al., Strain-free polishing of sapphire single crystal colloidal silica, *J. JSPE*, 47(12), 1458 (1981) (in Japanese).
50. T.K. Doy, Colloidal silica polishing based on micromechanical removal action and its applications, *Sensor&Mater*., 3, 153 (1981).
51. T. Kasai and T.K. Doy. Tribology from a viewpoint of ultraprecision polishing technology, *J. Tribology*, 375, 539 (1992).
52. T.K. Doy et al., New precision contouring process of LaB6 crystals used for electron guns, *J. Ceram. Soc. Jpn*., 107(6), 502 (1999).
53. S. Kondo, K. Sugii, S. Miyazawa and S.Uehara, LPE growth of Li(Nb,Ta)$O_3$ solid-solution thin film waveguide on $LiTaO_3$ substrate. *J. Cryst. Growth*, 46(3), 314 (1979).

# 7 Chemical Mechanical Polishing and Its Applications in ULSI Process

*Toshiro K. Doi*

## CONTENTS

7.1 Orientations and Role of CMP in Semiconductor Process ..... 343
*Toshiro K. Doi*
7.1.1 Relation of Planarization CMP with ULSI Device Process ..... 343
7.1.2 Ultraprecision Polishing and CMP in the Fabrication Process of ULSI Devices ..... 344
7.1.2.1 Outline of ULSI Device Fabrication Process ..... 345
7.1.2.2 Ultraprecision Polishing and CMP of Bare Silicon Wafers ..... 346
7.1.3 Planarization CMP and Its Roles ..... 349
7.1.3.1 Reasons for Planarization ..... 349
7.1.3.2 Background for Introducing Planarization CMP and Its Application Process ..... 350
7.2 Basic Concept of Planarization CMP ..... 354
*Toshiro K. Doi*
7.2.1 Basics of CMP—Progress of Ultraprecision Polishing and Its Applications ..... 356
7.2.2 Requirements and Points to Be Noted for Planarization CMP ..... 357
7.2.3 Basic Design Concept of CMP System ..... 359
7.2.4 Works to Be Polished by CMP and Defects Caused by Polishing ..... 359
7.3 Basic Technology of Planarization CMP ..... 363
7.3.1 CMP Machine System ..... 363
*Toshiro K. Doi*
7.3.1.1 Polishing Station ..... 365
7.3.1.2 Cleaning Station ..... 369

7.3.2 Slurries for CMP ..... 370
*Masaharu Kinoshita*
7.3.2.1 Basis of CMP Slurries ..... 370
7.3.2.2 ILD CMP Slurry ..... 371
7.3.2.3 STI CMP Slurry ..... 373
7.3.2.4 W-CMP Slurry ..... 381
7.3.2.5 Cu CMP Slurry ..... 386
7.3.3 Pads for Planarization CMP ..... 396
*Masanobu Hanazono and Masaharu Kinoshita*
7.3.3.1 Basic Properties of the CMP Polishing Pad ..... 396
7.3.3.2 Pad Conditioning and Polishing Performance ..... 404
7.3.3.3 Improvement for New Pads ..... 411
7.3.4 Modeling and Simulation of CMP Processes ..... 414
*Masaharu Kinoshita*
7.3.4.1 Purpose of Modeling ..... 414
7.3.4.2 Modeling of Planarization Process ..... 415
7.3.4.3 Modeling of the Polishing Pad and Planarization ..... 424
7.3.4.4 Modeling of Slurry Behavior ..... 431
7.4 The Study Case of Device Wafer ..... 436
*Keisuke Suzuki*
7.4.1 Introduction of CMP Technology ..... 437
7.4.2 History of CMP Technology ..... 439
7.4.3 Device Integration and CMP ..... 443
7.4.3.1 Device Fabrication ..... 443
7.4.3.2 Problems in Integration ..... 444
7.4.4 Present State of the CMP Development ..... 449
7.4.4.1 STI–CMP ..... 449
7.4.4.2 Tungsten CMP ..... 452
7.4.4.3 Cu and Low-*k* CMP ..... 452
7.4.5 Development of Endpoint Detection Method ..... 458
7.4.6 Future Prospects ..... 459
7.5 Thin Film Magnetic Recording Heads ..... 460
*Masanobu Hanazono*
7.5.1 Structure and Read and Write Mechanism of Thin Film Magnetic Head ..... 460
7.5.2 CMP Process for Thin Film Magnetic Heads ..... 463
7.5.2.1 Smoothing of Alumina Basecoat Film Surface ..... 463
7.5.2.2 Bottom Shield CMP ..... 464
7.5.2.3 Bottom Pole and Top Shield CMP ..... 465
7.5.2.4 Cu Damascene Process ..... 466
7.5.2.5 Overcoat CMP ..... 467
7.6 CMP of Compound Semiconductor Wafers ..... 468
*Toshiro K. Doi*
7.6.1 Polishing Characteristics of GaAs Crystal Wafers ..... 469
7.6.2 Polishing Characteristics of CdTe Crystal Wafers ..... 471
References ..... 473

Taking a general view of the development of ultralarge-scale integration (ULSI) devices, the background that requires chemical mechanical polishing (CMP) as a processing method of multilevel interconnections and planarization is clarified. Requirements for CMP, system construction method, and key element technologies are discussed here while reviewing the latest trends of ULSI devices and the needs of planarization CMP with its process. Moreover, case examples of the actual planarization CMP of device wafers are introduced here, referring also to the application cases to other fields.

## 7.1 ORIENTATIONS AND ROLE OF CMP IN SEMICONDUCTOR PROCESS

*TOSHIRO K. DOI*

### 7.1.1 Relation of Planarization CMP with ULSI Device Process

Semiconductor Manufacturing Technology Institute (SEMATECH) in the United States has completed a road map on the technical trends of DRAM up to the year 2016, coming out with a scenario toward the realization of 64G-bit DRAM, which announced that we had run into the era of ULSI of G-bit class. As a consequence, silicon wafers have been becoming large from $\phi 8''$ to $\phi 12''$.

Table 7.1 is a summary of technical trends of memories (DRAM) and logics. The large-scale integration (LSI) technology, in which DRAM technology played a leading role as a technology driver, has resulted in rapid progress toward the wide-ranging technologies. Today, G-class DRAM with a minimum line width of 0.13 μm is mass produced, which has driven the development of devices with further small line width of 0.1 μm or below as a next generation device.

**TABLE 7.1**
**Roadmap of Semiconductor Technology (2001 ITRS)**

| Year of Production | 2001 | 2003 | 2005 | 2007 | 2010 | 2016 |
|---|---|---|---|---|---|---|
| DRAM 1/2 pitch (nm) | 130 | 100 | 80 | 65 | 45 | 22 |
| Overlay accuracy (nm) | 46 | 35 | 28 | 23 | 18 | 9 |
| Gate length (nm) | 90 | 65 | 45 | 35 | 25 | 13 |
| Number of metal levels | 7 | 8 | 8 ~ 9 | 9 | 9 ~ 10 | 11 |
| CD control (nm) | 8 | 5.5 | 3.9 | 3.1 | 2.2 | 11 |
| Tox (equivalent) (nm) | 1.3 ~ 1.6 | 1.1 ~ 1.6 | 0.8 ~ 1.3 | 0.6 ~ 1.1 | 0.5 ~ 0.8 | 0.4 ~ 0.5 |
| Junction depth (nm) | 48 ~ 95 | 33 ~ 66 | 27 ~ 47 | 18 ~ 37 | 13 ~ 26 | 7 ~ 13 |
| Metal cladding (nm) | 16 | 12 | 9 | 7 | 5 | 2.5 |
| Intermetal dielectric $k$ | 3.0 ~ 3.6 | 3.0 ~ 3.6 | 2.6 ~ 3.1 | 2.3 ~ 2.7 | 2.1 | 1.8 |

Also the size of gate electrode in the logic devices has reduced to 0.14 μm, prompting the miniaturization of devices. In other words, miniaturization has been pursued, aiming at the realization of high integration and high efficiency devices. The backbone technology that supported this topmost priority of miniaturization is a multilevel interconnection technique, and it is the planarization CMP, a theme of this chapter that made the multilevel interconnection possible.

The cross sections of ULSI devices have drastically changed by the introduction of planarization CMP, derived from the ultraprecision polishing, a proven technique as a finishing process of bare silicon wafers. Its impact on the multilevel interconnections is large.

As interconnections are patterned on a planarized interlayer film, patterning over the gaps is unnecessary, though it is still a problem in lithography, allowing the patterning made more minute. Planarization CMP applies not only to the planarization of interlevel dielectric layers but also to the planarization of metal plug and STI that is indispensable to make future devices highly efficient and minute [1].

Furthermore, without planarization CMP technology, materialization of damascene interconnections proposed by IBM, USA, as an embedded wiring method would not have been possible [2]. Cu interconnections that is a long cherished dream was also realized by CMP technology using damascene or dual damascene wiring method.

As mentioned above, planarization CMP, a derived technology from the ultraprecision polishing technique, has completely changed the multilevel interconnection process technique for ULSI devices, and even prompted the introduction of Cu materials into the process that is ideal wiring metal but considered hard to apply. If we think of future potential application fields, planarization CMP is extremely important [1].

### 7.1.2 Ultraprecision Polishing and CMP in the Fabrication Process of ULSI Devices

Figure 7.1 shows a flow chart of ULSI device fabrication process from the growth of silicon crystals, wafer fabrication, and device fabrication processes to the completion of device fabrication. In the semiconductor fabrication process, wafers are produced through the formation of silicon single crystals, periphery grinding, notch formation, slicing, beveling, lapping (or grinding), etching, ultraprecision polishing (mirror polishing), and ultraprecision cleaning in this order, using only precision processing technique. This process is referred to as the wafer fabrication process. Subsequently, it enters into the device fabrication process, which is divided into two processes as (1) a wafer process (referred to as preprocess) where wafers generally undergo the device fabrication process and (2) an assembly and test process (referred to as postprocess) where chip fabrication and assembly are undertaken.

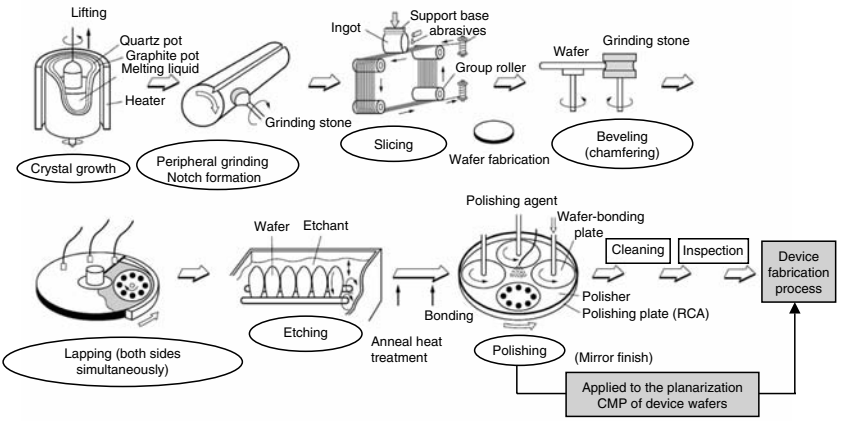


**FIGURE 7.1** Fabrication process of bare silicon wafers.

### 7.1.2.1 Outline of ULSI Device Fabrication Process

As shown in Figure 7.2, layout of the pattern relative to the circuit design and circuit configuration is designed in the device fabrications so as to accomplish the desired functions. After layout design of the pattern, masks equivalent to the photographic negatives are fabricated. Various fine patterns formed on a mask are exposed on the bare silicon wafers that have undergone the fine polishing and precision cleaning. Using such masks, formations of isolation structure, p- and n-well regions by ion implantation and gate oxide films or

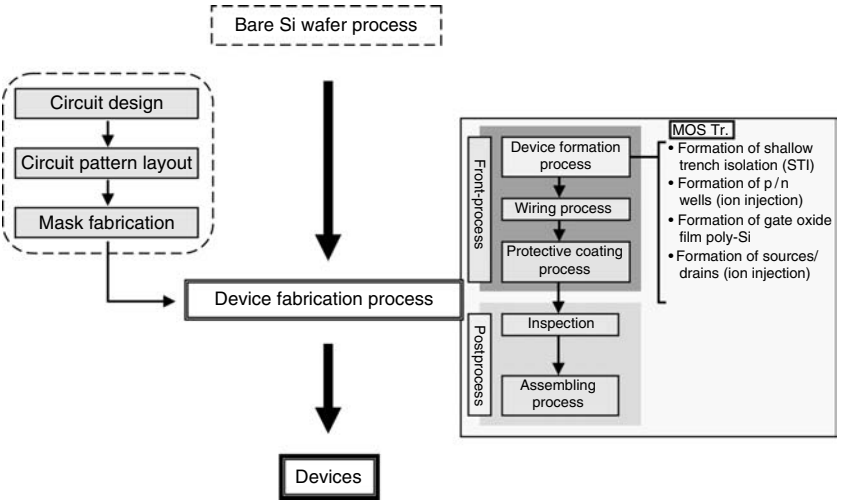


**FIGURE 7.2** Devices fabrication processes flow.

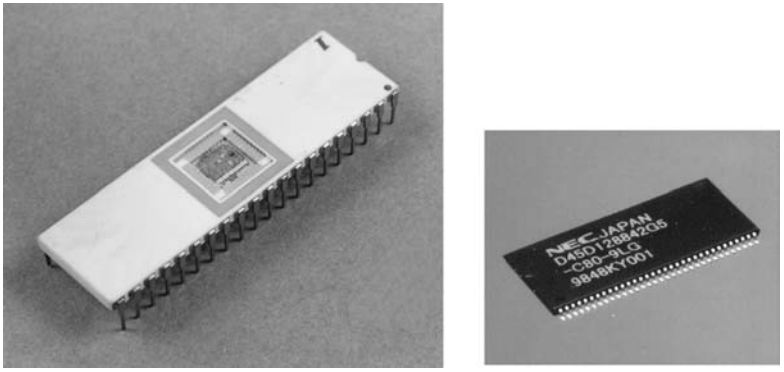


**FIGURE 7.3** Examples of typical finished packages, dual in-line package (DIP) and flat package.

polysilicon films among others are performed. MOS transistors are produced using such techniques.

Recently, the minimum design rule of the patterns to be exposed has shrunk below 0.2 μm. In this process, multilevel interconnections are formed by connecting various transistors alternately to secure device performances. Multilevel interconnections are made in such a way that each of the interlevel dielectric layer, hole aperture to connect upper and bottom layers of the interconnection, and interconnection layer are formed repeatedly one after another. To carry out the multilevel interconnections, it is necessary to microscopically planarize irregular surfaces induced each time so that various kinds of layers are formed repeatedly. CMP is the essential technology for this planarization Process. Upon completion of the multilevel interconnection process, a protective film is coated over the surface. This preprocess where wafers are processed is referred to as the wafer process. The wafers, after the wafer process, consecutively enter into the postprocess for the chip assembly and test, or assembly and test process. The most typical finished packages, dual in-line package (DIP), and flat package are shown in Figure 7.3.

The process to produce ULSI is explained in the above section. In the next section, we will discuss on the ultraprecision polishing and CMP of bare silicon wafers, which is a basis for the planarization CMP.

### 7.1.2.2 Ultraprecision Polishing and CMP of Bare Silicon Wafers

There are two polishing methods for silicon wafers (both-sides simultaneous polishing like lapping and single-sided polishing). In the single-sided polishing, there are several wafer-holding methods such as vacuum chucking method, wax adhering method, and water chucking by the surface tension between the backing film and template without any adhesives like wax.

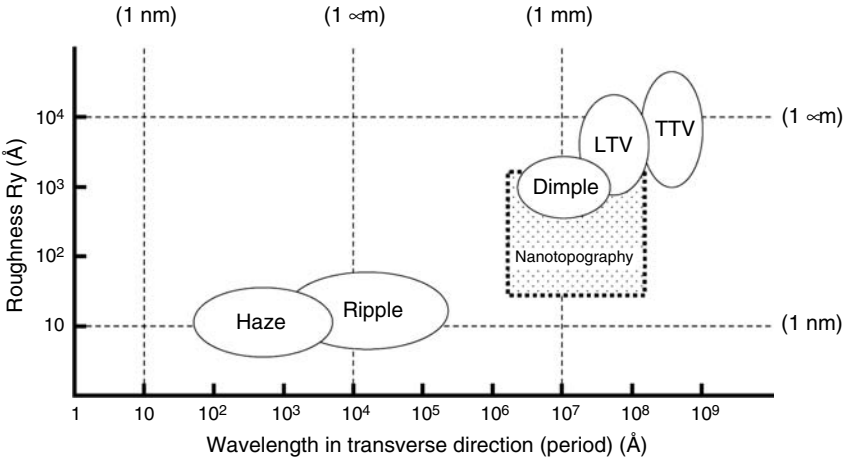


**FIGURE 7.4** Relation between transverse wavelength of the phenomenon appeared on the processed silicon wafer and its roughness.

Currently the single-sided polishing is more popular with a high-precision wafer-bonding method to the ceramics plate using a bonding agent. The backing film or template method is also applied to total thickness variation (TTV) and local thickness variation (LTV) that take no count of the precision. In connection with the planarization CMP of STI, the minimization of nanotopography of silicon wafers (Figure 7.4) has recently become an important issue, for which the both-sides simultaneous polishing is attracting attention as it can result in wafers with a high precision [3]. In light of the impurity-free residue, it is believed that the both-sides simultaneous polishing method is widely applied to the finishing process of $\phi$300 mm wafers.

In this polishing process, silicon wafer surfaces are required to be 1–2 nm Ry in roughness, oxidation-induced stacking fault (OSF free), microscratch free, and haze free. These surfaces should have high-precision finishing as the time polishing is complete. Therefore, polishing process is generally performed in several steps. The first step is aimed at efficiently producing planar, mirror surface. The second step is aimed at producing OSF-free surface and improving surface roughness. The third step or fourth step is aimed at the production of haze-free and contamination-free surfaces [4]. Table 7.2 indicates examples of polishing aims and polishing conditions for each step.

On completion of polishing, the wafers undergo a precision cleaning, to which RCA cleaning (cleaning on the basis of SC-1 cleaning—$NH_4H(1)+H_2O_2+H_2O(5)$, diluted HF (DHF) cleaning, and SC-2 cleaning—$HCl(1)+H_2O_2(1)+H_2O(5)$ [5]) is commonly applied to clean the silicon wafers contaminated during polishing process and to thoroughly remove residuals like particles (Table 7.3).

**TABLE 7.2**
**An Example of Si Wafer Polishing Conditions for ULSI Fabrications**

| | Processing Conditions | | | | |
|---|---|---|---|---|---|
| **Process** | **Slurry (Polishing Reagent and Abrasives)** | **Pad (Polisher/ Polishing Pad)** | **Polishing Pressure** | **Stock of Removal** | **Target** |
| First polishing | $SiO_2$ type abrasives (or $ZrO_2$): particle size 500 ~ 700 Å<br>Polishing reagent: alkaline solution (pH 10–11) | Polyurethane impregnated Polyester nonwoven cloth (hard type) | $3 \sim 8\,N/cm^2$ | 10 ~ 15 μm | High efficiency<br>Smooth mirror surface (20 ~ 40 Ry) |
| Second polishing | $SiO_2$ type abrasives: Particle size 500 ~ 700 Å or 100 ~ 200<br>Polishing reagent: alkaline solution (pH 10–11) | Foamed polyurethane (artificial leather) or Polyester nonwoven cloth (soft type) | $1 \sim 3\,N/cm^2$ | ~1 μm | OSF-free[a]<br>Improvement of surface roughness (10 ~ 20 Ry) |
| Third ~ Fourth polishing | $SiO_2$ type abrasives: particle size 100 ~ 200<br>Polishing reagent: ammonia or amine type (pH 8–10) | Foamed polyurethane (artificial leather) (soft type) | $1\,N/cm^2$ or less | 0.1 ~ 0.3 m | Haze-free<br>Contamination free |

[a]OSF: Oxidation-induced stacking fault.

**TABLE 7.3**
**Standard Cleaning Procedure for Si Wafers**

| Procedure | Temperature (°C) | Effect | |
|---|---|---|---|
| Sulfuric acid + hydrogen peroxide (1:0.25/1:1) | 120 ~ 150 | Metal, organic substances | SPM ("Piranha clean") |
| (DIW rinse) | RT | | |
| Dilute HF | RT | Native silicon dioxide etching | |
| (DIW rinse) | RT | | |
| Ammonium hydroxide + hydrogen peroxide + DIW (1:1:4 ~ 1:1:5) | 80 ~ 90 | Particles, organic substances | (SC-1 or APM) |
| (DIW rinse) | RT | | |
| Hydrochloric acid + hydrogen peroxide + DIW (1:1:4 ~ 1:1:5) | 80 ~ 90 | Metal | (SC-2 or HPM) |
| (DIW rinse) | RT | | RCA Cleaning |
| Dilute HF | RT | Hydrogen dead-end | |
| (DIW rinse) | RT | | |

After undergoing the above polishing and cleaning processes, the wafers are transferred to the device fabrication process. The above-mentioned ultra-precision polishing technology for silicon wafers is going to be applied to the planarization CMP of the device wafers as described later.

### 7.1.3 Planarization CMP and Its Roles

#### 7.1.3.1 Reasons for Planarization

For the purpose of delivering ULSI toward high integration and high performance, it is extremely effective to make interconnections multilevel. If multilevel interconnections are desired to be achieved when trying to accomplish device miniaturization, the existing process has its limit. Because the gaps tend to become larger in conformity to the surface topography of the lower layer, the step coverage in the film formation process becomes worse as the number of interconnection layers increases. Therefore, improvement of such step coverage is essential to produce multilevel interconnections by planarizing it in an appropriate process.

In the meantime, when the device fabrication process advances, the irregularities get further amplified reaching to the extent that the resolution and depth of focus (DOF) in the photolithography are hard to be compatible, making it difficult to simultaneously focus on both surface concaves and convexes. The resolution can be improved using either short-wavelength light or optical system that is larger than the numerical aperture (NA). However, when $\lambda$ is made small,

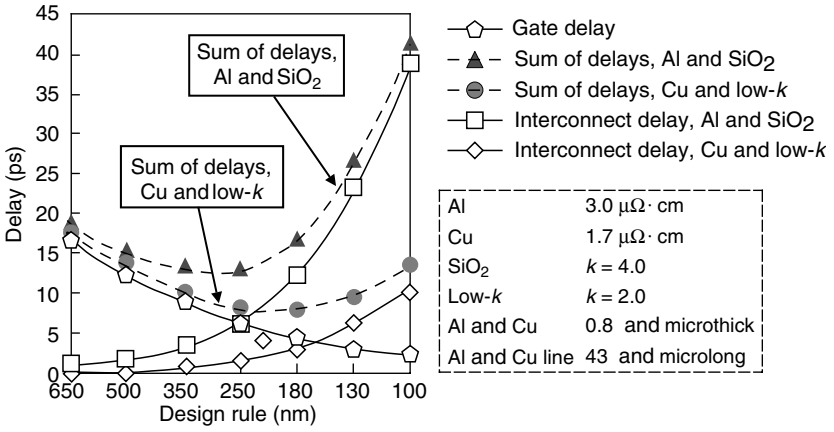


**FIGURE 7.5** Transistor and interconnect delay.

and NA is made large, the DOF becomes shallow, making the exposure difficult for nonflat surface. For the miniaturization of interconnections in ULSI fabrication process, it cannot progress to the next process unless surfaces of interlevel dielectric layers are flatter than the DOF.

Figure 7.5 shows an example of the relations between the design rule and the number of interconnection layers and minimum interconnection width in the logic ULSI [6]. As the wavelength is increasingly becoming short, the focus margin becomes small during exposure. As a consequence, it is essential to produce surfaces whose gaps are below the DOF.

As mentioned above, in an appropriate step of the process, planarization is required to remove surface irregularities of the device wafer, which is, in brief, aimed to form multilevel interconnections to cope effectively with the wiring delay and to deal with the DOF in the lithography [1]. This is the reason for performing CMP as a planarization process of wafer surface in the device fabrication process.

#### 7.1.3.2 Background for Introducing Planarization CMP and Its Application Process

Existing planarization techniques can be divided into four methods including etch-back method, film formation method, fluidization method, and selective growth method as indicated in Table 7.4.

These planarization methods have their limits to processing efficiency depending on the film types such as metal or dielectric layer. Besides, a fatal problem pointed out is that the area that these methods can planarize is extremely limited to somewhere between several μm and 10 μm (or at most 100 μm).

The surface topographies of planarized wafers are classified into three types as summarized in Figure 7.6 as against the cross sections not planarized.

**TABLE 7.4**
**Conventional Planarization Techniques and Features**

| Type | Techniques | Features |
|---|---|---|
| Etch-back method | Sputter<br>RIE<br>Plasma etching | • Easy process<br>• Hard to control etching |
| Deposition method | Bias sputter<br>Bias ECR<br>Plasma CVD<br>RF plasma CVD | • Planarization in concurrence with film deposition<br>• High possibility of damage<br>• Excess dusts |
| Fluidization method | Re-flow<br>SOG (spin-on-glass)<br>(FB sputter) | • Easy to handle<br>• Sparse and instable film<br>• Migration acceleration |
| Selective growth | Selective CVD<br>(plug method)<br>Selective epitaxial growth | • Embedding only where necessary (hole) is possible<br>• Low controllability over selective growth<br>• Instable |

It is ideal to preferentially planarize projected areas only on a rough surface to produce a smooth flat surface, regardless of the substrate conditions. This is termed global planarization. For the improvement of yield and reliability, it is indispensable to achieve global planarization across an entire wafer surface.

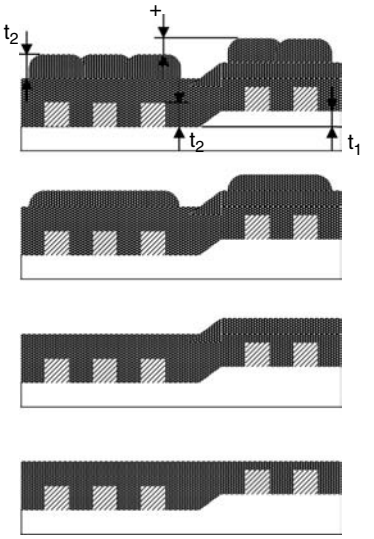


**FIGURE 7.6** Planarization mode of a device wafer.

This planarization polishing or CMP is an applied technology of the ultraprecision polishing that has achieved successful results as a mirror-finish processing in the polishing process of bare silicon wafers. Planarization polishing or CMP mechanically produces a large surface to a flat surface. Such a simple concept leads to the user-friendly comprehensibility. Besides, the possibility of planarizing large-sized area like a wafer, needless to say chip size area, is practical. Polishing in the wafer processing, especially mechanochemical polishing or CMP, has supported cutting edge optomechatronics industry, including semiconductor industry over the years, delivering excellent results. Therefore, it is a natural development that such a technology and the know-how have been diverted and applied to the planarization polishing or CMP. However, it is not like that the planarization of device wafers can be realized by simply diverting existing polishing techniques as it is. There are still many problems remaining. The technology referred to as polishing or CMP dates back to the second half of the year 1960 when IBM unveiled the development of a concept of the current mechanochemical polishing or CMP for Si using NaOH solutions.

Dielectric isolation (DI) wafer for LSI to withstand high pressure was a typical product manufactured in the early stage of the polishing technology introduced into the device fabrication process [7]. A study on DI wafers (Figure 7.7) for the LSI for digital subscriber circuits has been carried out since the first half of 1980 when mechanochemical polishing or CMP was introduced in its fabrication process [8].

Figure 7.8 is an exterior view of a fully automatic cassette-to-cassette polishing machine developed at that time, which seems to be the world's first fully automatic polishing machine [9].

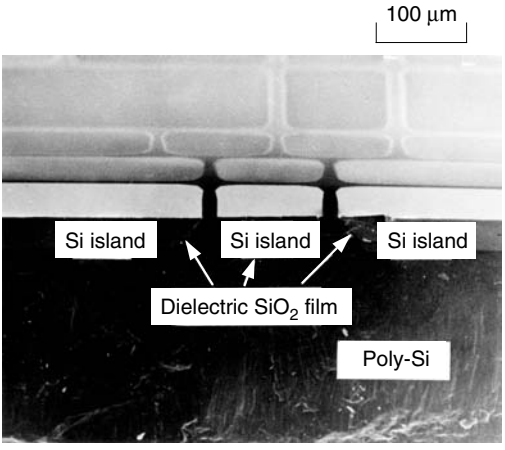


**FIGURE 7.7** DI (dielectric isolation) wafers for digital subscriber circuits made by introducing CMP technique. (From NTT in 1983.)

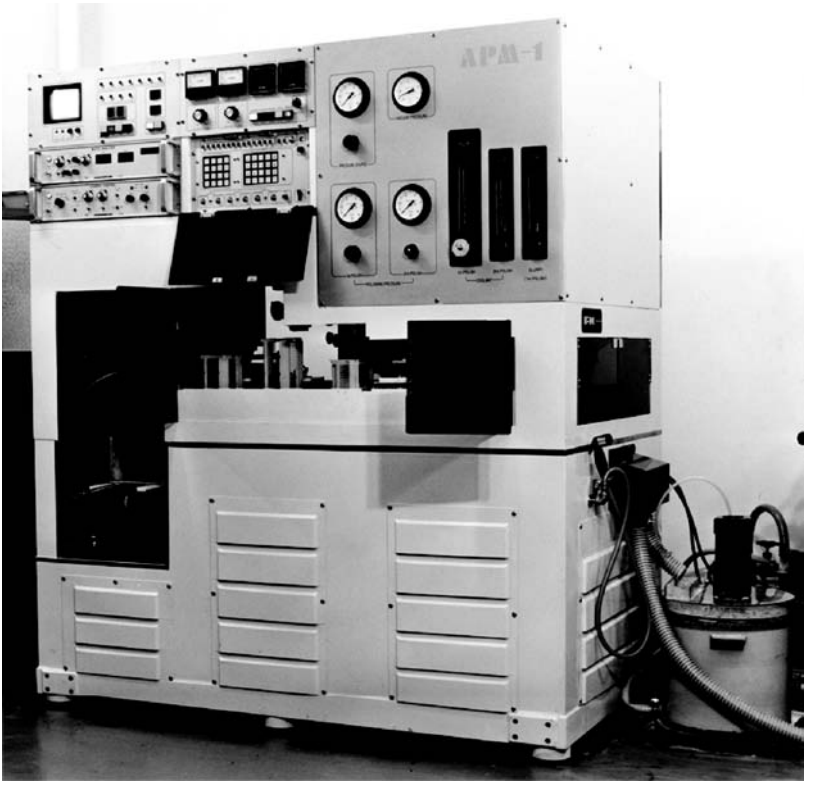


**FIGURE 7.8** A fully automatic cassette-to-casette polishing machine for DI wafer process. (From NTT & Fujikoshi Machinery Corp. in 1985.)

Such being the case, the bare silicon wafer CMP has progressed toward planarization polishing or CMP for LSI devices. However, the process applicable is supposed to vary depending on the LSI types. As is the case with the planarization by etch-back method, CMP is basically applied to the device, isolation, and interconnection processes on $SiO_2$ film (oxide film) as interlevel dielectric layers, metal film (W, Al, Cu, etc.) as interconnection materials, and polycrystalline silicon (poly-Si) and single crystal silicon as capacitor materials.

Figure 7.9 shows a sectional diagram of a device and the processes to which planarization CMP is applied. From the bottom, they are STI CMP, interlevel dielectric (ILD) layer CMP, W-plug damascene CMP, and wiring metals (Al, Cu) damascene CMP. When the plug and ILD are formed simultaneously, it is termed a dual damascene CMP.

Figure 7.10 indicates Cu wiring process by the dual damascene method. Basic requirements for the wafer planarization in the device fabrication process and its related processing factors and conditions are shown in Table 7.5.

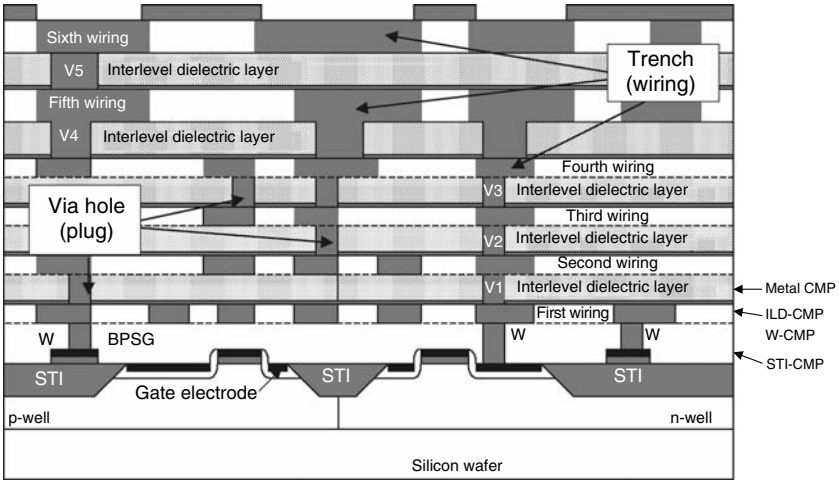


**FIGURE 7.9** Sectional diagram of a device and the processes to which planarization CMP is applied.

## 7.2 BASIC CONCEPT OF PLANARIZATION CMP

*TOSHIRO K. DOI*

This section deals with the polishing mechanism of planarization CMP while discussing how ultraprecision polishing technology has been applied to a planarization CMP so that we can understand the basics of planarization

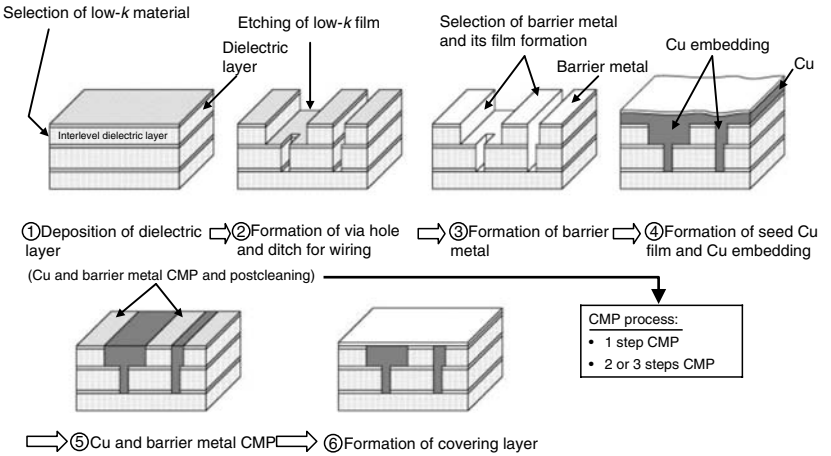
Selection of low-k material
Etching of low-k film
Dielectric layer
Selection of barrier metal and its film formation
Cu embedding
Barrier metal
Cu
Interlevel dielectric layer
①Deposition of dielectric layer
②Formation of via hole and ditch for wiring
③Formation of barrier metal
④Formation of seed Cu film and Cu embedding
(Cu and barrier metal CMP and postcleaning)
CMP process:
• 1 step CMP
• 2 or 3 steps CMP
⑤Cu and barrier metal CMP
⑥Formation of covering layer

**FIGURE 7.10** Cu wiring formation process by Cu-dual damascene and subsequent works in each process.

**TABLE 7.5**
**Basic Requirements for Planarization CMP**

| Requirements | Description | Relative Factors |
|---|---|---|
| Planarity | Preferential removal of projecting features only within the specified processing margin (normally 0.5 ~ 1 μm) to achieve desired smoothness and flatness | Pad types (hardness, surface profile), relative speed, polishing pressure, slurry type and stability, pattern dimensions and density, dummy pattern |
| Uniformity | Planarization across the entire surface of large-sized wafer (ϕ12″) | Uniform pressurization, pad uniformity (thickness accuracy, groove pattern, etc.) and hardness, uniform flow and supply of slurry retainer-ring adjustment, dressing |
| Clarification of polishing end point | Detection of polishing end point (specified stock of removal) to finishing polishing | *Polishing time control*: pad and slurry stability, timing of dressing, stopper, etc.<br>*In-situ monitoring*: improvement of motor current and optical film thickness measurement toward higher precision and better reproducibility |
| High-quality processed surface | Damage-free processed surface (scratches, breakage, etc.) | Slurry agglomeration and particle distribution, filtering, impurities inside pad, falling off particles from dresser, |
| High cleanliness processed surface | Removal of contaminated particles and metals by post-CMP cleaning | Wet conditions maintained and postcleaning, chemical cleaning (low concentration solution, same sign zeta potential liquid), physical cleaning (scrub, mega-sonic, ice-scrub, super high-pressure jet, etc.), wafer spin dry |
| High throughput and low cost | Polishing conditions and equipment for realization of low processing cost and high throughput | Consumable cut-down, dressing-free, higher efficiency-oriented postcleaning, efficient pad replacement, wafer transportation, slurry recycle and circulation, planarity securement |

CMP. Through the requirements for planarization CMP and points to be noted, basic design concept of CMP system was worked out including workpieces to be polished by CMP and polishing factors.

### 7.2.1 Basics of CMP—Progress of Ultraprecision Polishing and Its Applications

A variety of polishing methods have been proposed so far. Earlier, the optical polishing as a mirror-finish method was especially popular for glasses that were considered difficult to be processed by the cutting or grinding method. Subsequently, clarification of the polishing mechanism of optical glasses as a finishing method of semiconductor silicon wafers has progressed, leading to the wide recognition of the importance of the mirror polishing to be upgraded and ultraprecise, which encouraged the emersion of several ultraprecision polishing methods. Such polishing methods are the originals of the present global planarization CMP.

Recently, characteristic polishing methods have been proposed using various abrasives and polishing reagents. Without denying the interpretation of the traditional processing mechanisms, but recognizing the existence of various mechanical actions and chemical actions induced by the combined polishing materials such as the work materials to be polished, slurries, and pads, a chemical and mechanical compound polishing was worked out, taking advantage of such characteristics. The typical examples thereof are the CMP and mechanochemical polishing (MCP). As a matter of convenience, both are handled here as the same, and referred to as CMP.

In this section, mirror finishing or smooth surface polishing is discussed. As shown in Figure 7.11 (1) the projected areas of the residual surface features formed in the previous process are preferentially removed or (2) both projected and recessed areas on the wafer surface are removed, however, placing emphasis on the removal of the projected areas. The former is the optical polishing that is not affected too much by the presence of damaged layers, whereas the latter is the mechanochemical polishing of bare silicon wafers that require complete removal of the damaged layers. In this case, as the stock of removal (polishing margin) is as big as 10 to 15 μm, it can finally realize smooth planarization even with a soft pad, whereas, in the planarization CMP of the device wafers, the polishing margin is no more than 0.5 to 1 μm, and moreover, complete planarization is essential by removing projected areas only. Such planarization CMP of device wafers corresponds to the case of optical polishing. In case that only projected areas are to be preferentially removed, it is advantageous to have membranous reaction products formed as shown in Figure 7.12 to facilitate sequential removal of its projected areas while controlling the polishing not to process the recessed areas or protect them. This becomes effective in preventing dishing and erosion, which are discussed later.

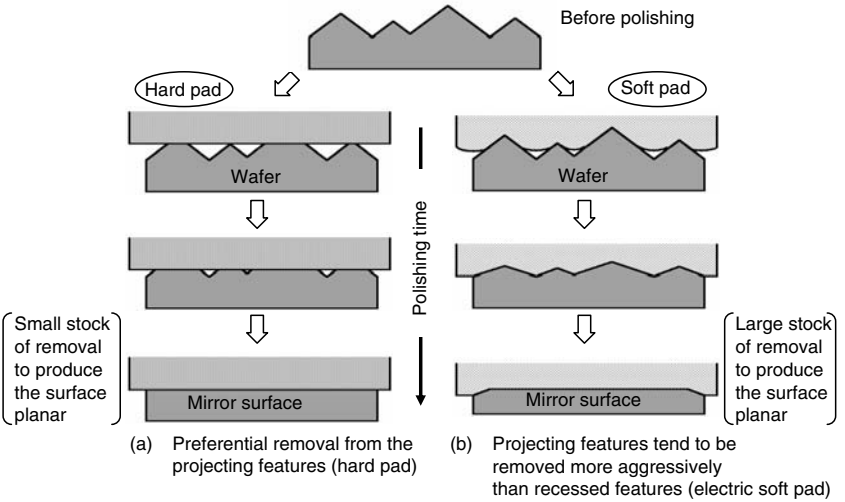
Before polishing
Hard pad
Soft pad
Wafer
Wafer
Polishing time
Small stock of removal to produce the surface planar
Large stock of removal to produce the surface planar
Mirror surface
Mirror surface
(a) Preferential removal from the projecting features (hard pad)
(b) Projecting features tend to be removed more aggressively than recessed features (electric soft pad)

**FIGURE 7.11** A model of smoothening and planarization of rough surfaces by polishing. (Original drawing by Kasai.)

### 7.2.2 Requirements and Points to Be Noted for Planarization CMP

The main requirements and points to be noted are as follows:

- To process minute topographic features to a smooth and planar surface: Fine projected areas of a high-density pattern should be preferentially removed. The stock of removal (polishing margin) is roughly 0.5 to 1 μm depending on the type of devices and works to be processed. Within such narrow range, all gaps across a wafer should be removed uniformly

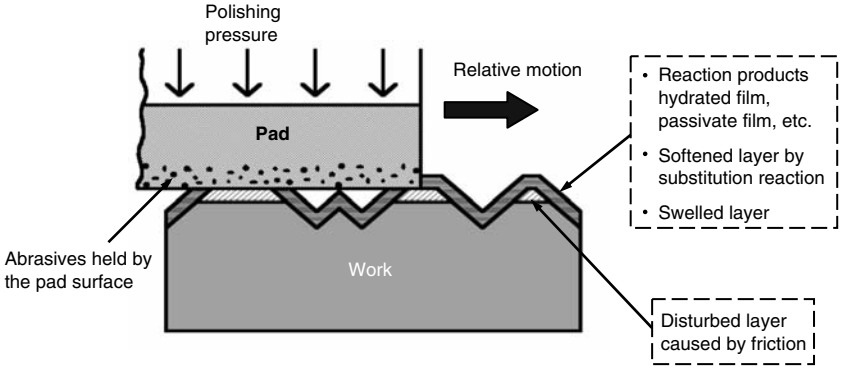


**FIGURE 7.12** Diagram of planarization by the formation and removal of film type reaction products. (Original drawing by Kasai.)

without polishing the recessed areas of the pattern. For which, a surface reference polishing method should be worked out, taking into consideration that the reference of the polishing surface is the surface where devices are formed. The surfaces to be polished should be infinitely made damage-free, as the presence of any cracks and distortions on the surfaces can cause functional problems.

- To make the surface to be processed washable and contamination free:
  In the polishing with slurry, slurries and pads generally become a source of contamination. Especially, metal ion has a fatal effect on the electric properties of the devices. It is fundamental to select polishing materials and conditions that do not cause or leave such contaminations. It is also necessary to establish polishing conditions that allow the cleaning in conformity to the postprecision cleaning method, for which the cleaning conditions, which are that the zeta potential sign of the particles in slurry coincides with that of the cleaning liquid, should be applied, taking into consideration the residuals of the ingredients contained in the slurries.
- To make the polishing endpoint detection:
  The reference surface for CMP is the surface of the device wafer. Topographic features of the wafer are removed little by little preferentially from the projected areas across the wafer. Polishing should stop when a desired amount (~1 μm) is removed, when the fluctuations of the remaining film thickness should be, for instance, within ±5%. As it is obvious, fixing the polishing end point is a must here.

  Under the present situations, although in-situ measuring technique has advanced, polishing end point is still generally controlled by the processing time of the stock of removal fixed previously depending on the device types. This requires establishment of repeatable polishing conditions and techniques through the optimization of pads and slurries including pad conditioning. However, it is a primary goal to establish high resolution, in-situ measurement method.
- To have high throughput:
  In the device fabrication process, CMP process should not become a rate-determining step. To obtain a productivity that matches the throughput of the stepper or more, it is necessary to secure high polishing efficiency and low-cost oriented process.
- To accommodate large-sized wafers:
  Recently, $\phi 12''$ ($\phi 300$ mm) wafers have won popularity over $\phi 8''$ wafers, and are being introduced in CMP process, which has driven us to work to establish the polishing methods and conditions for high-precision CMP of large-sized wafers of $\phi 12''$ or more when manufacturing CMP machines.
- To consider the planarization technology as a comprehensive technology:
  As the problems pertinent to the planarization technology are extended over various fields, planarization technology cannot be realized without

comprehensive technology through close collaborations of not only processing engineers but also researchers and engineers from other fields such as measurement, cleaning, and device fabrication fields. From this viewpoint, the Planarization CMP Technical Committee (Chairman: T.K. Doy) of Japan Society of Precision Engineering is encouraging close exchanges with people from all fields, particularly from device-related fields to share information and insight for the comprehensive goal [10].

The basic requirements for planarization CMP with some related factors are shown in Table 7.6.

### 7.2.3 Basic Design Concept of CMP System

As a finish process of bare silicon wafers, polishing has been dealing with increasingly severe conditions, fighting to improve quality and accuracy of wafers. To introduce the polishing to the device fabrication process, realization of high precision, high efficiency, and cleanliness is indispensable together with automatization of full peripheral equipments.

CMP system design is summarized in the following three basic points:

- The polishing system should be equipped with a cleaning unit, a mini-environment unit, and handling systems of the loading and unloading stations of wafer cassettes and of wafer transfer apparatus, whereas systems of slurry supply and disposal of waste solutions should be in compliance with fab environment.
- In terms of automatization, the system should be equipped with a monitoring unit of CMP process such as polishing pressure distribution, polishing end point, pH of slurries, pad loading and temperature, and with an adaptive control unit thereof.
- As a part of a semiconductor fabrication line, CMP system should be centrally controlled.

Table 7.6 is a summary of the basic design concept for building a CMP machine, and the points to develop CMP machines.

### 7.2.4 Works to Be Polished by CMP and Defects Caused by Polishing

Depending on the types of LSI devices, work materials to be polished by CMP vary such as $SiO_2$ for interlevel dielectric layer or embedded dielectric layer, metals (Cu, Al, W) for wiring or connection (plug) of each wiring layer, barrier metals (Ta, TaN, TiN, WN) to prevent metal diffusion, and $Si_3N_4$ for the polysilicon-made stopper or dielectric layer [1]. Moreover, a defect-free, high-quality polishing is of utmost importance when producing planar and

## TABLE 7.6
## Point of CMP Machine System Development

| Items | | | | | | |
|---|---|---|---|---|---|---|
| | Main Units—Functions | | | | Consumables | |
| | Main Polishing Station | | Wafer Cleaning Station | Wafer Transportation Station | | |
| Targets | Head Platen | Conditioning | | | Slurry | Pad |
| Uniformity across a wafer and wafer-to-wafer<br>Planarization<br>Rate stability, high throughput<br>Cleaning<br>Low-cost | Rigidity (polishing-resistant, polishing pressure-resistant), wafer retaining pressurization method, backing material (wafer-chucking characteristics, warp-correction characteristics, uniform pressurization performance, vacuum-chucking performance), shape and size of retainer, uniformity of trail density (no. of rotation, oscillation, vibration, amplitude), avoidance of resonance point, long stability of various movements | Same as in the left. Uniform motion mechanism of tools (grinding stone), uniformity of trail density (uniform processing of pad surface) | High efficiency slurry removal, full removal of metal contamination and particles (below 109 $cm^{-2}$), single wafer cleaning and its stability, cleaning process (brush scrub, mega-sonic, cleaning fluid, temperature, time, etc.) | Wafer loading or unloading station, cassette-to-cassette, wafer reversing mechanism, high speed transfer, dust generation prevention | Particle size distribution, dispersibility, pH value, additive, stability, types and shapes of abrasives, temperature control | Elastic deformation characteristics, tracking ability, surface texture, shape, pressure distribution (across a wafer: uniformization, local area: projected areas only high pressure), control of hydroplane phenomenon, temperature control |

| | | | | | |
|---|---|---|---|---|---|
| Remarks | • Endpoint detection monitoring technique (low dust generation design, airflow control, etc.)<br>• High accuracy, high rigidity, light weight design<br>• Low thermal expansion material design | • Chemical proof measures | • System control technique | • Central supply · control system<br>• Wastewater treatment technique<br>• Low cost and recycling<br>• Aggressive slurry | • Low cost<br>• Long stability<br>• Slurry-less pad |

**TABLE 7.7**
**Aims of Polishing (CMP) and Its Factor**

| Requirements | Base Elements of Polishing | Factors |
|---|---|---|
| High quality (distortion-free mirror finish) | Slurry Polishing solution + (additires) | • Reactivity against works/ reaction pattern<br>• Density and types of chemicals solution<br>• Temperature |
| High efficiency (high throughput) | Abrasives (fine particles) | • Particle size<br>• Hardness<br>• Shape<br>• Type<br>• Dispersing<br>• Distribution |
| High accuracy (flatness) | Pad (polisher/ polishing cloth) | • Elastic deformation characteristics<br>• Hardness and thickness<br>• Thickness accuracy<br>• Surface topography (polishing agent retaining function) |
| Cleanliness (contamination free) | Precision cleaning | • Environment<br>• Chemicals (purity, type, density, temperature, etc.) |

irregularity-free or gap-free surfaces within a given polishing margin. It goes without saying that high polishing efficiency (throughput) is indispensable to satisfy the production basis.

Table 7.7 schematically shows macrorequirements in the fabrication process of LSI devices and the relationship between slurries (composed of particles and its dispersing reagent) and pads, with the influencing factors thereof. Due to a large number of contributing factors, all-round investigations become necessary to feed them back to the CMP system and polishing conditions.

When a patterned device wafer is polished, generation of various polishing defects is anticipated. Figure 7.13 is an example of polishing defects induced during metal CMP, such as thinning, recess and erosion, dishing, microscratch, and keyhole. As indicated in the figure, the causes of the generation of such defects are mostly related to either of the excess polishing, or slurry and pad. As a consequence, it goes without saying that polishing

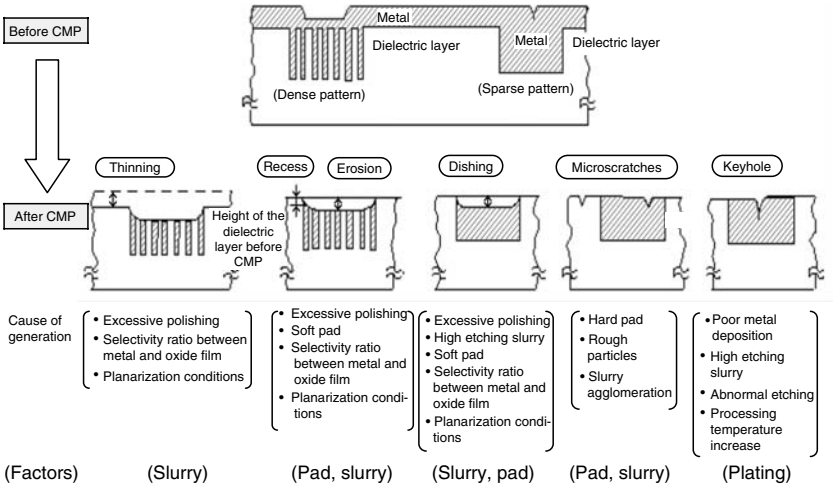


**FIGURE 7.13** Typical processing defects and phenomena caused during metal CMP, and its causes.

planarity and uniformity should be secured by optimizing polishing conditions and achieving defect-free polished surfaces.

## 7.3 BASIC TECHNOLOGY OF PLANARIZATION CMP

### 7.3.1 CMP Machine System

***Toshiro K. Doi***

As mentioned in the previous section, there are several requirements for CMP for the planarization of wafers in the device fabrication process. Main requirements are as follows:

1. Planarization of the patterns with various forms of microscopic features to a uniform and smooth surface across a wafer
2. Post-CMP cleaning of the processed surfaces
3. Clear polishing end point
4. High throughput with stable polishing and cleaning characteristics
5. Small footprint and lightweight system

Roughly, the above requirements 1, 3, and 4 belong to the group of polishing, and requirements 2 and 4 to the cleaning. Point 5 is concerned with the design of the whole machine system. For points 3 and 4, it is fundamental to stabilize polishing characteristics while building CMP machine system taking transportation system and in-situ measurement into account.

CMP machine system is built with the polishing station, cleaning station, and transportation system with a control system mounted on each of them. CMP machine system is basically the same as the polishing machine of bare silicon wafers. However, as extremely high accuracy is required for CMP machine system, a variety of improvements and features have been fully worked out to the component parts of each system and unit. As CMP is one of the semiconductor device fabrication processes, it is essential for the CMP machine system to have a wide range of advanced equipments and functions incorporated, including fully automatic cassette-to-cassette, clean room matching, link with the systems like polishing and cleaning systems, in situ measurement (endpoint detection), and communication facility with host computer.

Figure 7.14 is a schematic representation of CMP machine system, indicating linkages between each element and control factors. The core parts of this CMP machine system are the CMP station and post-CMP cleaning station with respective transportation and control systems where element techniques for the various types of the instruments and tools are important. Due to the relations between the planarization accuracy and throughput, the platens with their driving mechanisms, slurry with its supply and control mechanisms, pad with its conditioning unit, and wafer retainer with its uniform pressurization

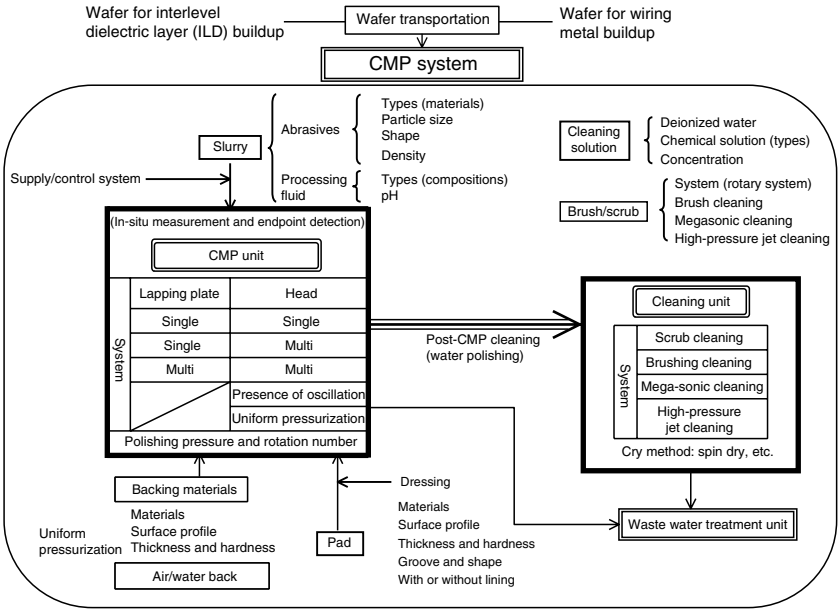


**FIGURE 7.14** CMP system configuration and unit control factors in the planarization process of ULSI device wafers.

mechanism are recognized as key points in this polishing station. On the other, the basic function of the cleaning station is to remove particles and metal impurities through the rough cleaning by deionized water polishing, followed by the finish cleaning and drying.

#### 7.3.1.1 Polishing Station

Figure 7.15 shows the basic structure diagram of the polishing unit in the platen rotary-type CMP machine system, equipped with (1) a polishing head with its driving mechanism, which rotates the platen and applies pressures onto the wafers while retaining wafers, and across from it, (2) polishing platen with its driving mechanism to which polishing pad is adhered, others such as (3) polishing pad with its conditioning (dressing) mechanism, (4) wafer and chuck surface cleaning unit, and (5) slurry supply mechanism are also main component parts comprising the polishing station.

##### *7.3.1.1.1 Polishing Head*

In the planarization CMP of the device wafers, flatness precision of the processed surface should be within 10 nm whereas the margin allowed for the polishing is only 1 μm and not more. Consequently, how to retain wafers precisely and how to apply uniform pressure to them become extremely important. It is no exaggeration to say that the polishing head that retains

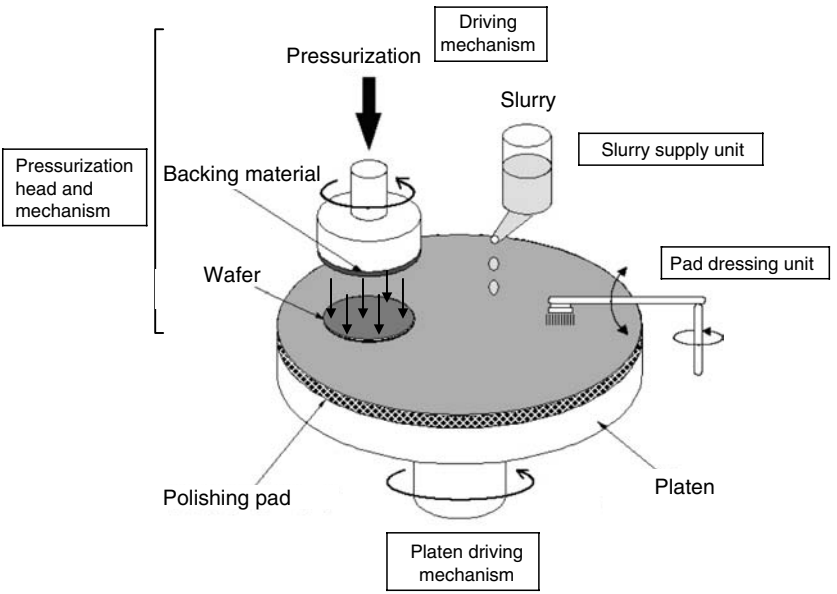


**FIGURE 7.15** General construction of polishing mechanism.

and pressurizes wafers is exactly a core part of the polishing station. Such a head is structurally constituted of three parts, including (1) a part that uniformly pressurizes the reverse sides of the wafers, (2) a ring to prevent wafers from coming off (retainer-ring), and (3) a wafer retaining chuck for wafer transportation.

In the polishing head, the above-mentioned point 1 is considered most important as it directly determines uniformity over the wafers. It is common today that a pressurization control mechanism is incorporated into the retainer-ring (point 2) to prevent wafers from falling off during polishing and to minimize wafer dull-edge so as to improve the accuracy of the wafers. As to the chuck (point 3), the wafers are chucked and retained inside the retainer of the heads and placed on the pad surface. The chucking is released immediately before the polishing. On completion of the polishing and water polishing, the wafers are rechucked for transportation to the next station where the wafers are released. Such chucking functions, although not directly involved in the polishing precision, are important as such chucking ensures accurate wafer retaining and positioning. In Figure 7.16 a typical uniform pressurization method is illustrated [1].

#### *7.3.1.1.2 Pad Platen*

The platen to which a pad is adhered revolves almost in conformity with the revolution of the head (several tens of revolutions/min). Surface precision of the platen is critical as is the case with that of bare silicon wafer polishing, which requires necessary control over the temperature increase of the pad surface during polishing.

| Datum plane | System | | | Wafer retainer | Accuracy | Remarks (figures below) |
|---|---|---|---|---|---|---|
| Wafer surface | (A) Elastic material interposed pressurization system (backing film, insert materials, etc.) | | | yes | O | ① |
| | (B) Fluid pressurization method | Indirect | Air back | yes | ◎ (O) | ② |
| | | | Water back | yes | ◎ (O) | |
| | | Direct | Air back | yes | ◎ | ③ |
| | | | Water back | yes | ◎ | |
| | (C) (A) and (B) combination method | | | yes | O (◎) | – |
| Wafer reverse side | (D) Vacuum chucking, plate bonding | | | | × (Δ) | – |

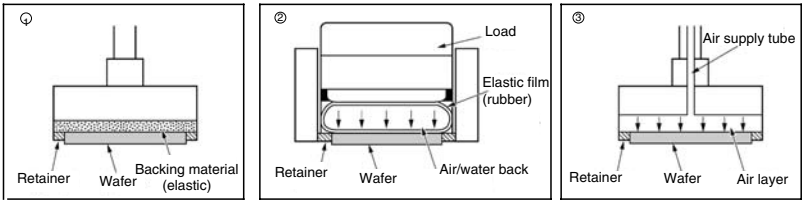


**FIGURE 7.16** Uniform wafer pressurization method.

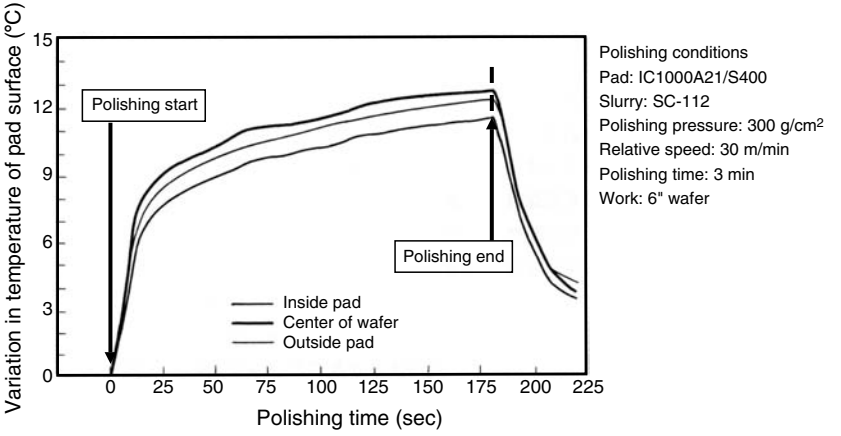


**FIGURE 7.17** Variation in temperature of pad surface during CMP (without cooling of platen).

The polishing time of the device wafers in CMP is less than one-tenth of that of bare silicon wafers, contributing to a smaller temperature increase of the pad surface than the other. However, as you will see from Figure 7.17 that shows the temperature fluctuations of the pad surfaces during CMP; the characteristics of the device wafer CMP are vulnerable to the instability as the polishing completes abruptly when the temperature is still rising. Consequently, temperature control by water cooling over the rotary platen is indispensable for the CMP machine.

Meanwhile, very high load is applied to the platen during polishing. For instance, when a $\phi 8''$ wafer is processed at a pressure of 500 g/cm$^2$, about 160 kg is applied to the area ($\phi 8''$) of the platen where the wafer is. Consequently, a large bearing whose size is equivalent to four-fifths of the diameter of the rotary platen is adopted to increase rigidity of the rotary platen and prevent deformation thereof, aiming to secure accuracy (uniformity in particular) of the polished wafers.

#### *7.3.1.1.3 Pad Conditioning (Dressing)*

It is of utmost importance to maintain processing ability of the pads, or to obtain constant and stable polishing characteristics, which is still more required particularly when a processing end point is determined by the polishing time. As polishing advances, pad surfaces become loaded (clogged), which inevitably deteriorates polishing characteristics, requiring conditioning of the pad from time to time so as to make the pad surfaces to the initial conditions.

Currently popular conditioning method consists of the removal of the pad surface layer where loading (clogging) occurred with diamond wheels. Such conditioning is performed in situ or every certain number of wafers processed.

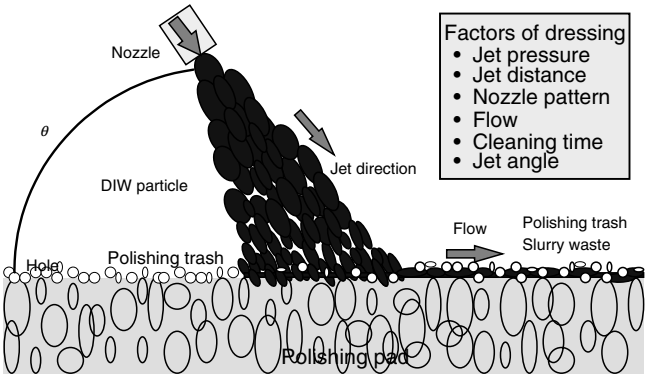


**FIGURE 7.18** Pad dressing model by super high-pressure microjet.

Figure 7.18 shows a pad conditioning introduced by Asahi Sunac Corp., which successfully brings back the original state of the pad surfaces by jet spraying the pad surface with ultrahigh-pressure water of several tens to hundreds MPa converted from ultrapure water to remove the loaded layers and reaction products adhered to the fine pores of the pad surfaces without grinding down the pad surface (Figure 7.19). This conditioning method is found most suitable for nonwoven cloth like Suba or artificial leather (suede-like Politex) used for Si-CMP than for IC1000 pads [11].

#### *7.3.1.1.4 Slurry Supply Mechanism*

Unless slurry is supplied properly, the particles in the slurry tend to become agglomerated, and induce processing damages to the wafer like micro-scratches. Slurries should be supplied adequately and should be free from drying or sedimentation.

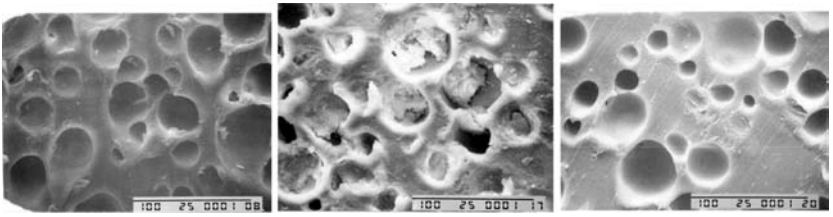

(a) A new polishing pad (b) After polishing (c) After HPMJ dressing

• Polishing conditions

| | |
|---|---|
| Polishing objects | Oxygen films on silicon wafer |
| Slurry | Silica type slurry |
| Polishing pad | Bubble urethane type |
| Polishing time | 1200 s |

• Dressing conditions

| | |
|---|---|
| Jet pressure | 12 MPa |
| Jet distance | 100 mm |
| Jet flow | 1.1 L/min |
| Jet time | 30 s (pad piece) |

× 500

**FIGURE 7.19** SEM images of the bubble urethane type polishing pad surface.

Either vacuum system or pump system is equipped with the central supply system in the mass production line. Both systems supply slurries to the polishing station while circulating them through the slurry pipe.

#### 7.3.1.2 Cleaning Station

Processed wafers are transferred to the wafer cleaning station where the particles and impurities adhered to the wafers during polishing process are washed off. The particles and impurities are generated by the slurry or pads. As it is presumed that the number of particles just after CMP reaches from thousand to tens of thousands per $cm^2$, and impurities to $10^{14}$ per $cm^2$, it is common to transfer the wafers to the cleaning station only after such particles and impurities are roughly removed by water polishing on completion of CMP [12].
Currently popular cleaning process flow is as follows:

Brush cleaning (Figure 7.20) ⟶ Ultrasonic cleaning ⟶ Spin drying

Diluted chemical solutions are also used in combination with the above cleaning processes, depending on the types of slurries and works used in CMP. For brush cleaning, roll-type or disk-type polyvinyl alcohol (PVA) materials are often used, which is adequately soft for the purpose. When zeta potentials of the particles in CMP slurries and PVA are taken into account, the brush cleaning fluid can be deionized water, alkaline solution (i.e., ammoniac water), or acid solution (i.e., dilute hydrofluoric acid). In other words, in accordance with the relationship between pH value and zeta potentials shown in Figure 7.21, a brush cleaning fluid of the same sign between PVA and slurry particles should be selected for use [1].

For the ultrasonic cleaning, a megasonic cleaning is introduced that irradiates ultrahigh sonic wave of megahertz class frequency to the processed wafers in solution. By using megahertz class frequency, cavitation threshold values ascend when removal effect of the fine particles increases and generation of damages decreases. As a summary here, the cleaning fluid should be chosen on the basis of zeta potentials as mentioned above.

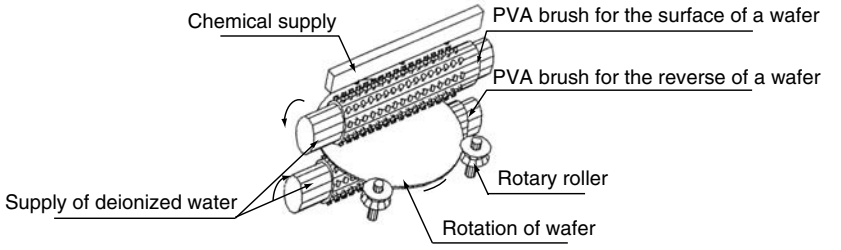
Chemical supply
PVA brush for the surface of a wafer
PVA brush for the reverse of a wafer
Rotary roller
Supply of deionized water
Rotation of wafer

**FIGURE 7.20** An example of brush scrubbing method for cleaning after CMP of wafer.

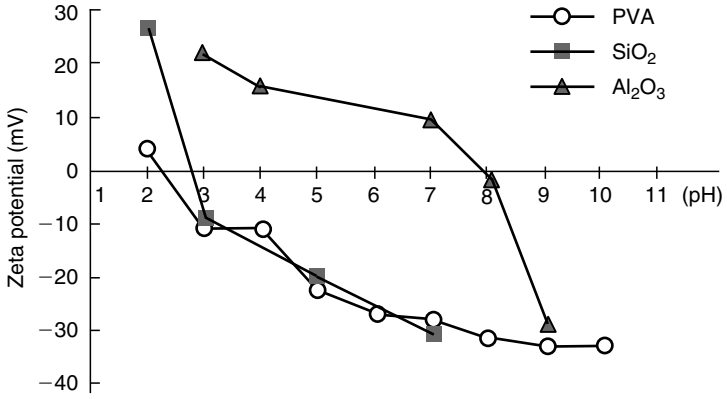


**FIGURE 7.21** Dependency on pH value of zeta potential in various slurry and PVA. (From de Larios, J.M., *Chemical-Mechanical Planarization of Semiconductor Materials*, M.R. Oliver (Ed.), Springer, New York, 262, 2003.)

## 7.3.2 Slurries for CMP

***Masaharu Kinoshita***

### 7.3.2.1 Basis of CMP Slurries

CMP slurries are composed of three major elements such as abrasive particle, distilled water, and additive agents. The abrasive particle's function is to remove material along with assisting in the reduction of friction between a polishing pad and wafer. This function results in the improvement of lubrication property of slurry. Distilled water is a transportation media of abrasive particles as well as the lubricant and cooling agent between polishing pad and wafer. The lubrication is closely connected with the tribological mechanism during CMP process [13]. Figure 7.22 shows how the abrasive concentration

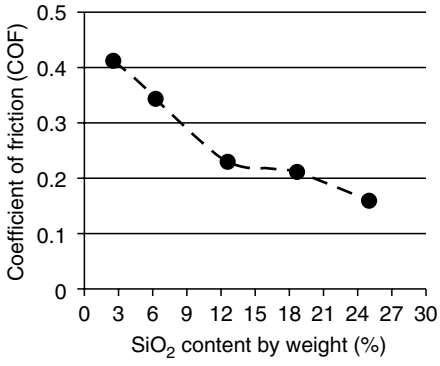


**FIGURE 7.22** Effect of abrasive concentration on COF.

affects the coefficient of friction (COF). Results clearly indicate that abrasive particles contribute dramatically to the lubricity of the system such that at low abrasive contents, the wafer and pad are more intimately in contact with one another, thus leading to higher values of COF. At high abrasive concentrations, the particles allow significant rolling between the wafer and pad surfaces, thus reducing the COF. Additive agents can control the slurry properties such as physical, chemical, and electrical [14,15]. The formulation of additive agents still remains know-how (key intellectual property) for the slurry suppliers. Additive agents include acids, bases, corrosion inhibitors, and surfactants. Acids and bases react differently to generate various surface active and inactive layers by chemical reaction and also to resolve surface materials. The inhibitor controls or suppresses the reaction rate of the CMP process. Particle dispersion in the slurry also controls the particle adhesion on the wafer surface and can be facilitated by a surfactant, which adjusts the zeta potential of the particle.

High-performing slurries are designed by combining these three elements along with the performance requirements of the specific CMP polishing step. Slurry development should also satisfy requirements of polished wafer quality and CMP process productivity. Major concerns for quality performances include reducing defectivity on the polished surface, minimizing dishing, thinning and erosion on patterned wafer, and stabilizing the removal rate. The increase of removal rate is a factor to be considered for productivity improvement of the various CMP processing steps. Additionally, environment friendly slurries are also desired for disposal and ease of post-CMP cleaning issues.

The issues for slurry designing are summarized as follows:

- Slurry components and their performance
- Abrasive materials, their manufacturing processes, size, profile, and properties
- Dispersion, coagulation, and sedimentation characteristics of abrasive particles
- Additive agents and their functions
- Selectivity for different materials when polishing
- Characterization of slurry
- Filtering of abrasive particles
- Slurry waste treatment and recycling

#### 7.3.2.2 ILD CMP Slurry

CMP for interlayer dielectrics (ILD) requires very low defectivity performance. Moreover, the recent move to low-$k$ dielectrics, which will replace conventional TEOS ILD film, is providing new challenges to the industry and suppliers and necessitating new product development to meet its unique properties. These low-$k$ dielectrics are materials with inferior mechanical abrasive resistance to TEOS.

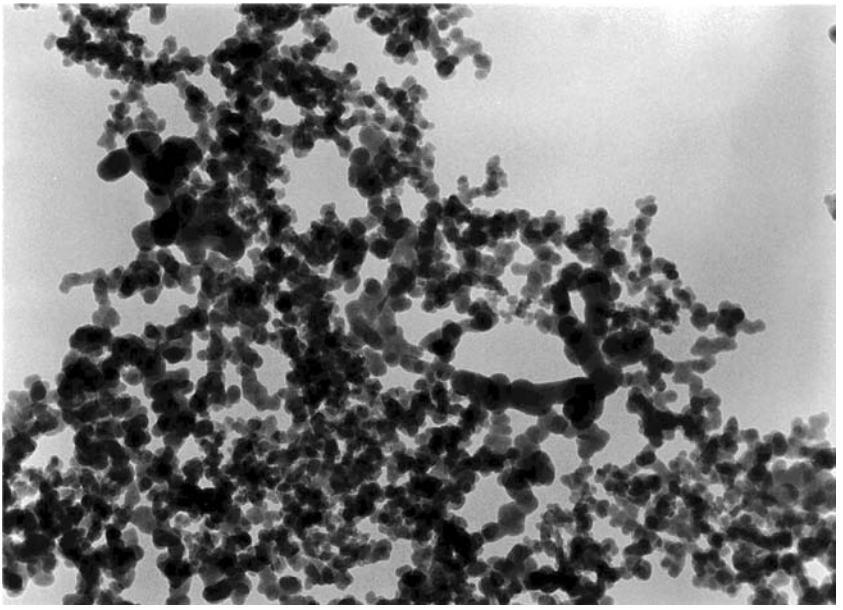

**FIGURE 7.23** TEM image of fumed silica in ILD1300 slurry. (Rohm and Haas Electronic Materials CMP Inc., formerly Rodel.)

Fumed silica and colloidal silica are the two major abrasives used for ILD slurry. Figures 7.23 and Figure 7.24 show TEM images of fumed and colloidal silica, respectively. Fumed silica particles are synthesized from $SiCl_4$ in a hydrogen–oxygen flame, by which metal contamination-free particles can be obtained. As synthesized fumed silica particles have a very broad size distribution as shown in Figure 7.25, filtering larger particles is required to make ILD slurry. Dispersing fumed silica particles in water and then chemically stabilizing the material produce ILD slurry. There exist several different kinds of methods for filtering larger particles. High-pressure homogenizing is a method in which particles collide together and then break into smaller particles by using a jet mill as illustrated in Figure 7.26. Particle collision can be done either in a dry solid state or in a wet solution state with water. Another method is centrifugal separation. Centrifugal separation is a method for separating particles with mass difference by centrifugal force as shown in Figure 7.27. High dispersion can also be obtained by kneading highly concentrated particles under high shear force with equipment shown in Figure 7.28. Additional filtering effects may be necessary by using fiber filtering and decantation.

Larger particle components in the slurry may cause scratches on the polished wafer. Scratches with brittle fractures, which are sometimes called chatter marks, are killer defects. Empirically, a correlation exists between scratch counts and a number of particles larger than 0.1 μm in slurry. The

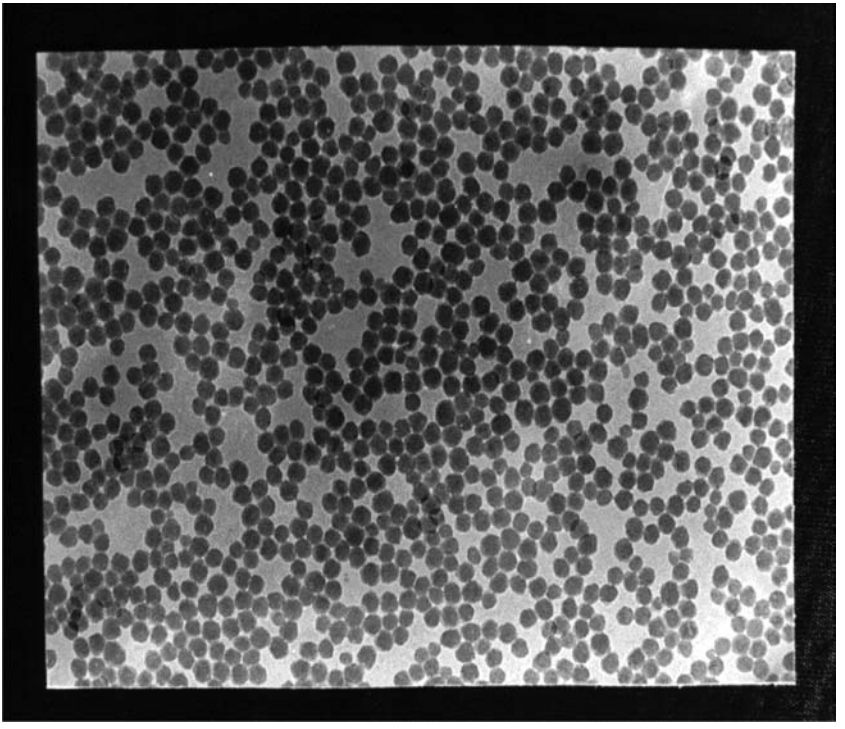

**FIGURE 7.24** TEM image of colloidal silica particles (50–70 nm). (Klebosol™-Clariant).

chatter mark scratch counts are significantly reduced, shown in Figure 7.29, when the large particles are decreased to less than 1/100 in the original slurry. Either filtering or decantation, as shown in Figure 7.30, can also significantly reduce other small defects.

The typical ILD CMP performance is shown in Figure 7.31. The removal rate is more or less 2000 Å/min with nonuniformity performance of less than 5%. Figure 7.32 shows the planarization efficiency performance of the ILD CMP process.

#### 7.3.2.3 STI CMP Slurry

Shallow trench isolation (STI) is a process to isolate one active transistor device region from another. A layer of silicon nitride protects the active regions on the silicon. The oxide that is deposited to fill the trench also deposits on top of the active regions, and hence requires to be planarized. Figure 7.33 illustrates an STI process and Figure 7.34 shows a scanning electron microscope (SEM) image of the active region island structure before

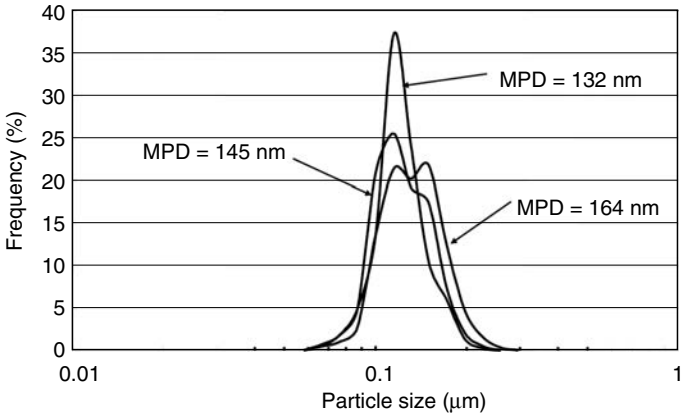


**FIGURE 7.25** Fumed silica particle distribution.

oxide filling. Presently, two approaches are used for this planarization as depicted in Figure 7.35: one involves a combination of reverse etch-back process followed by CMP and the other, a one-step or direct CMP process. The latter approach is much preferred as it eliminates one lithography step and causes considerable reduction in process cost of ownership (COO). This approach is incorporated into device designs at the 0.18 μm node or less as the benefits of the change become necessary and justifiable [16–18].

The main technological breakthrough to direct CMP process for STI planarization comes from a consumable set that delivers a high rate on the oxide, a high selectivity to nitride, and good planarization efficiency. Conventional oxide polishing slurries based on fumed silica have very little selectivity toward silicon nitride. Conversely, ceria powder has a high polish rate for silicon oxide, traditionally used in glass polishing, but has relatively

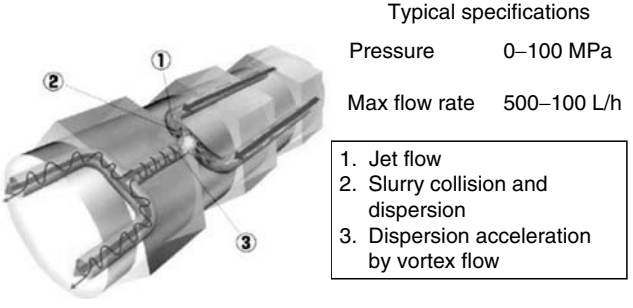


**FIGURE 7.26** High-pressure homogenizer. Genus Py(py50-10abt-r). (Courtesy of Hakusui Tech Co., Ltd.)

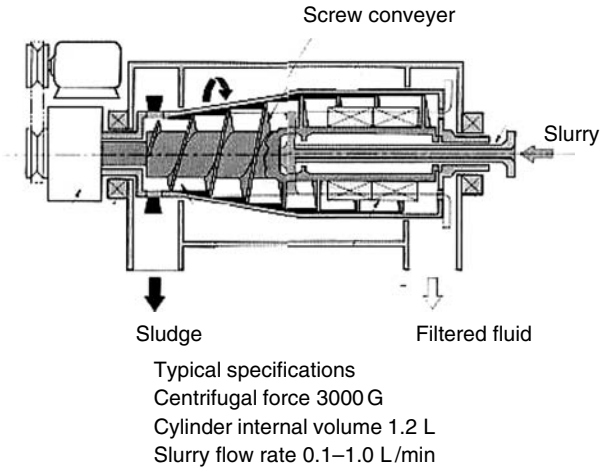


**FIGURE 7.27** Centrifugal separation, decanter centrifuges (DS-10v). (Courtesy of Mitsubishi Kakoki Co., Ltd.)

low polish rate for silicon nitride. Therefore, cerium oxide slurries have become the best fit for STI CMP polishing as they can achieve the planarity as well as low oxide dishing and nitride erosion.

Figure 7.36 shows a typical distribution of ceria particles, indicating a narrow particle size distribution without big particles [19]. The relative planarity performance capability between a variety of STI CMP slurries is shown in Figure 7.37. These are standard silica slurries, run with a stacked IC1010 pad or a harder solo IC1020 pad, two silica HSSs, and a ceria HSS. HSS stands for high selectivity slurry. The IC1010 and IC1020 are porous urethane pads made by Rodel Inc. The WID stands for within die planarization efficiency. The result shows that the ceria high selectivity slurry differentiates the performance with relatively lower range for both trench depth

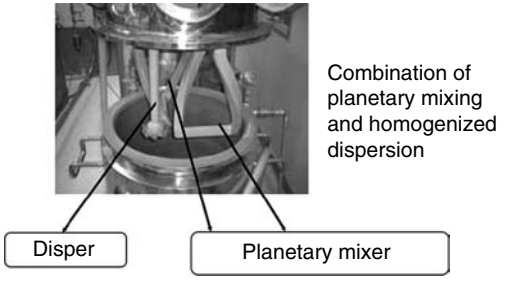


**FIGURE 7.28** High shear stress dispersion, hivis disper mix(hm-3d-50). (Courtesy of Tokushu Kika Kogyo Co., Ltd.)

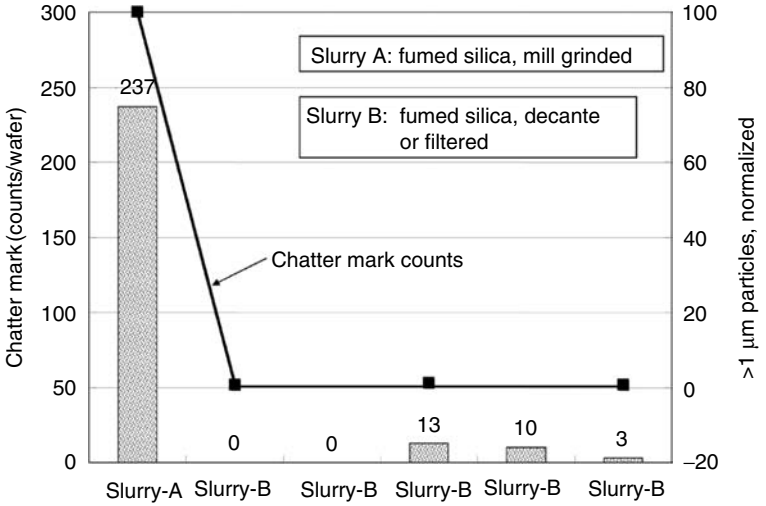


**FIGURE 7.29** Chatter mark and large particles in slurries.

variation and nitride thickness variation [20]. A typical performance of ceria slurry is summarized in Table 7.8. The oxide to nitride polish rate selectivity is 200:1. The dishing is also lower compared to silica slurry as shown in Figure 7.38 [17].

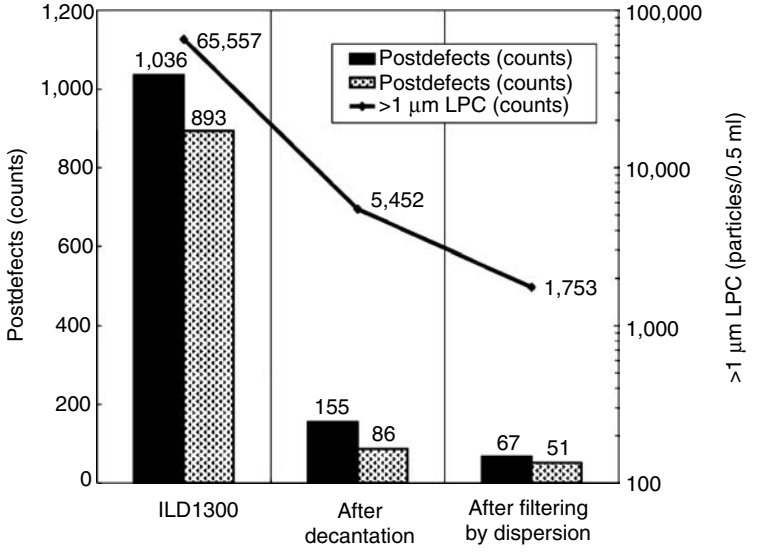


**FIGURE 7.30** Defect reduction by decreasing larger particles in ILD slurry.

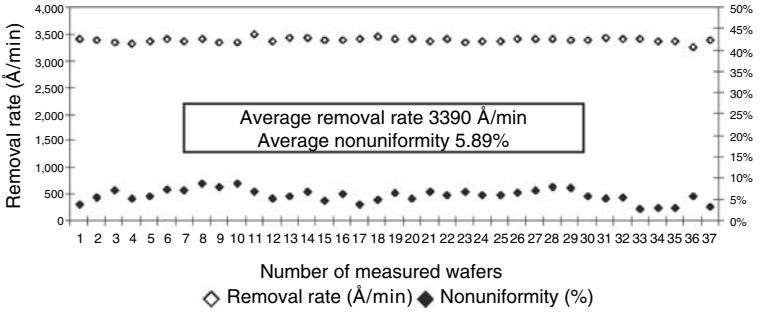


**FIGURE 7.31** Removal rate and nonuniformity for fumed silica ILD slurry baseline, ILD1300 slurry with IC1400/K groove pad.

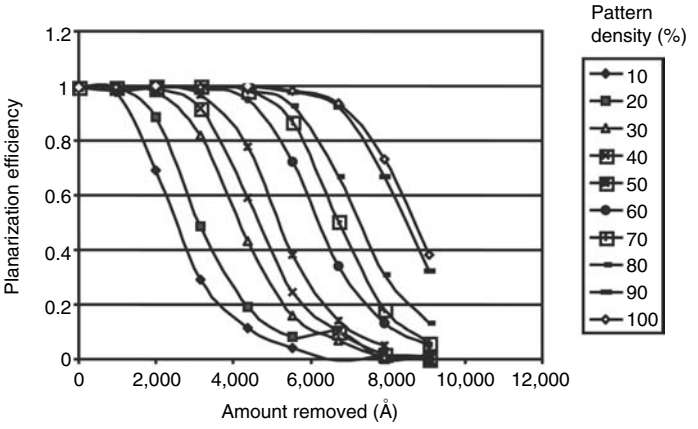


**FIGURE 7.32** Planarization efficiency for fumed silica ILD slurry. (From Lawing, S., Polishing rate, pad surface, morphology and pad conditioning in oxide chemical mechanical polishing, I1-Fifth International Symposium on Chemical Mechanical Polishing (CMP), ECS 201st Meeting, Philadelphia, 2002.)

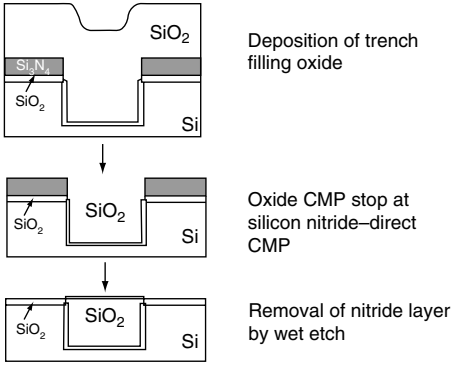


**FIGURE 7.33** CMP for shallow trench isolation.

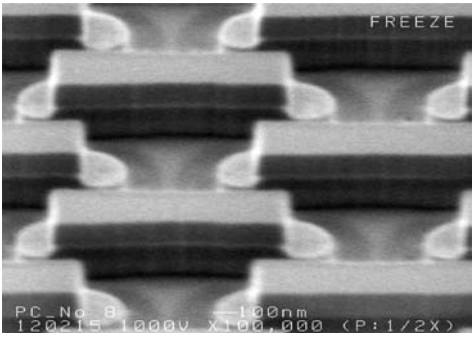


**FIGURE 7.34** SEM image of active region islands for shallow trench isolation.

The high selectivity slurry consists of two parts: a ceria-based abrasive and a planarity selective additive. To achieve both the high selectivity and planarity, the effect of the additives is very important. Topography reduction is first done by removing the up feature, whereas the down feature remains unpolished. Ceria particles are coated by the additive chemical and become inert to the chemical reaction on the down feature surface. On the up feature surface, mechanical force acts on the ceria particles and abrades the oxide surface. Then the polishing mechanism with ceria slurry is understood as shown in Figure 7.39. Under lower down force, the polish rate remains low, but when down force increases, the polish rate goes up. The result is given in Figure 7.40, which indicates non-Prestonian-type polishing mechanism, that is, the polish rate is not proportional to polish pressure and relative velocity. Differentiating the zeta potential between the nitride and oxide surfaces can

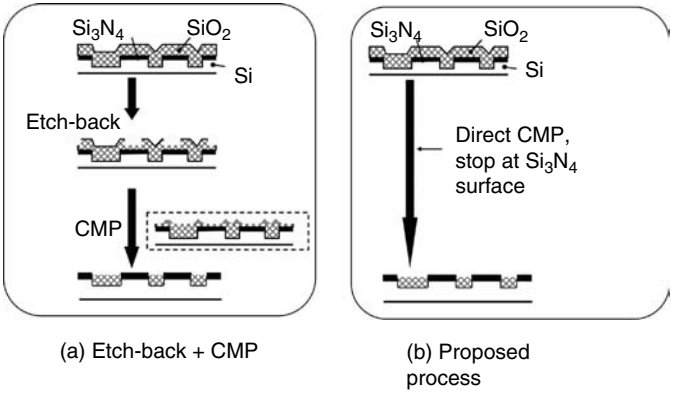


**FIGURE 7.35** (a) Alternative STI processes using CMP and (b) direct STI.

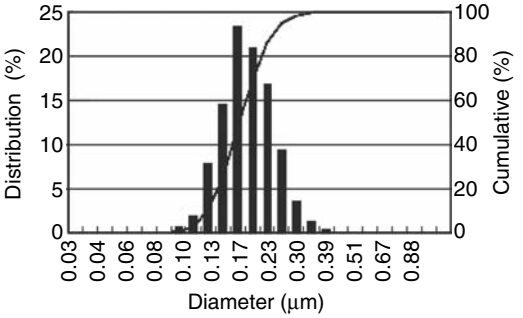


**FIGURE 7.36** Caria particle distribution. (From Leduc, P., Aiming for perfect planarization, CMP-MIC, 2002.)

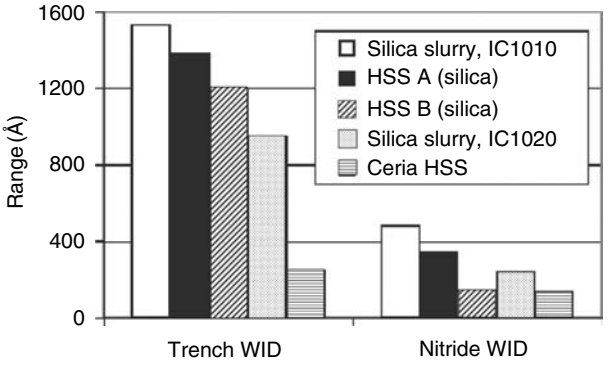


**FIGURE 7.37** Relative performance of various slurries in direct STI.

**TABLE 7.8**
**Typical Performance of Ceria Slurry**

| Item | Ceria Slurry | Silica Slurry |
|---|---|---|
| Planarization remained gap (Å) | ~500 | 2000 |
| Selectivity ($SiO_2$/SiN) | ~200 | 3 |
| SiN polished thickness (after CMP) (Å) | 23 | 250 |
| Dishing at 500 μm (Å) | 200 | 800 |
| Defect (count/cm$^2$) | 0.02–0.05 | 0.1–0.3 |
| STI process | Direct polish | Reverse mask |
| Particle content as used (%) | 1–2 | 12 |

*Source*: From Hanazono, M., et al., Why $CeO_2$ is promising for STI? *CAMP*, Clarkson University, 2001.

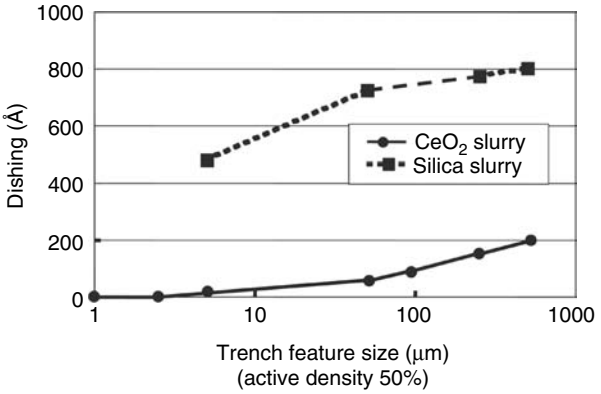


**FIGURE 7.38** Dishing of the trench for STI CMP.

generate selectivity. As illustrated in Figure 7.41, the additive can be easily adsorbed on the nitride surface, because of the nearly zero zeta potential, and protect the surface from removal. However, the oxide surface stays at a higher zeta potential, which reduces the additive adsorption and thus results in higher oxide removal. The effect of the additive to oxide and nitride selectivity is given in Figure 7.42. As shown in Figure 7.42, increasing the additive drives down the removal rate, but this reduction does stabilize at a point.

The abrasive and additive were mixed and delivered to the CMP tool. Accurate mixing and dispensing, short residence time, and accurate flow control are required for ceria slurry delivery because ceria is a high-density material that easily falls out of suspension. Defectivity is also severely controlled in STI. Even though initial microscratch levels remain fairly low,

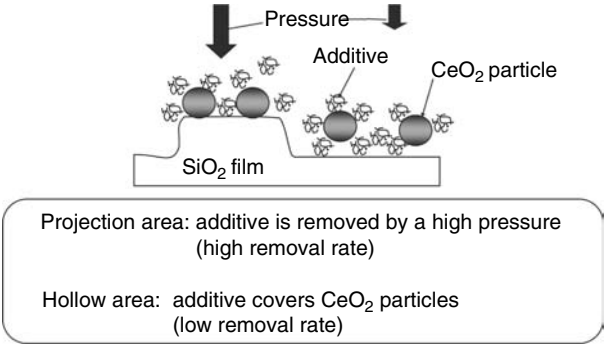


**FIGURE 7.39** Polishing model for high selective ceria slurry.

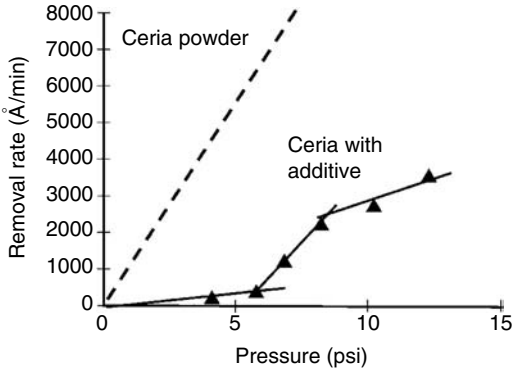


**FIGURE 7.40** Non-Prestonian behavior of ceria slurry.

they tend to increase rapidly as oxide is cleared from the nitride as shown in Figure 7.43 [20]. Considering the complex interaction between abrasive particles, additive chemistries and the wafer surface as the nitride is exposed, the late stages of removal and clearing play a critical role in final defect performance.

### 7.3.2.4 W-CMP Slurry

Tungsten (W) material is used for interconnection plugs and vias. As tungsten is a very hard material, the surface is at first oxidized and then the oxide layer is removed in CMP, which is illustrated in Figure 7.44. W-CMP slurry consists of abrasive slurry and an oxidizer. Conventional abrasives are silica and alumina. Oxidizers are selected from acid groups such as potassium iodate, ferric nitrate, and hydrogen peroxide. A performance comparison by using different W-CMP slurries is summarized in Table 7.9 [21]. The first-

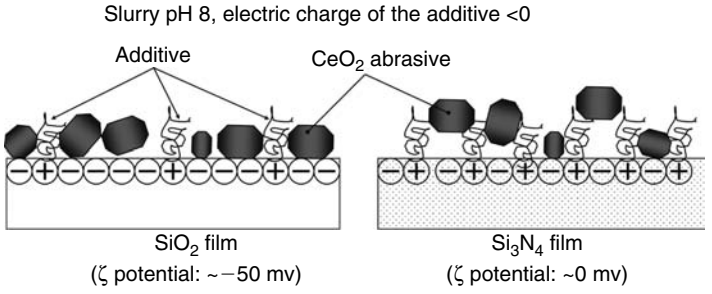


**FIGURE 7.41** Selective adsorption of the additive in ceria slurry.

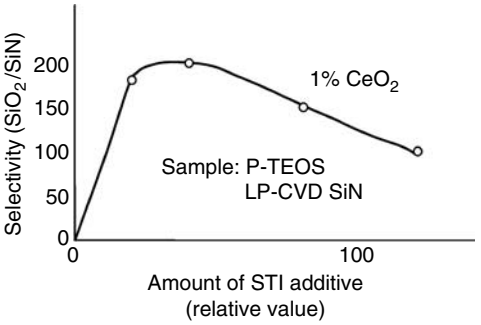


**FIGURE 7.42** Effect of additive to selectivity oxide vs. nitride.

generation slurry has good oxide selectivity and low oxide erosion performance, but has a disadvantage for metal contamination, pad staining, and is prone to settling after mix. However, in Table 7.9, this slurry shows large erosion results, which might be caused by a softer polishing pad. The second-generation slurry has a high pH value and less static etching characteristic, but poor selectivity and pad staining result. The third-generation slurry has a high throughput, good selectivity, and ease of handling, but has a high static etching.

W polish rate increases with the lower pH value. At this point the strong oxidizer gives higher W polish selectivity to oxide. The high selectivity will help ensure stopping on the oxide layer, however the erosion occurs. Oxide erosion occurs when there is selective removal of the oxide in areas where

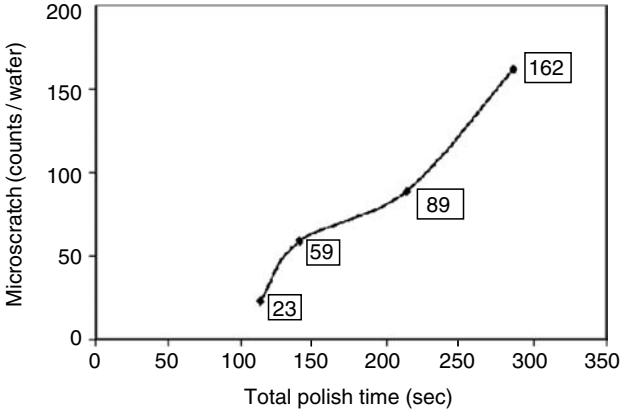


**FIGURE 7.43** Progressive increase of microscratch during unoptimized STI CMP process with ceria slurry.

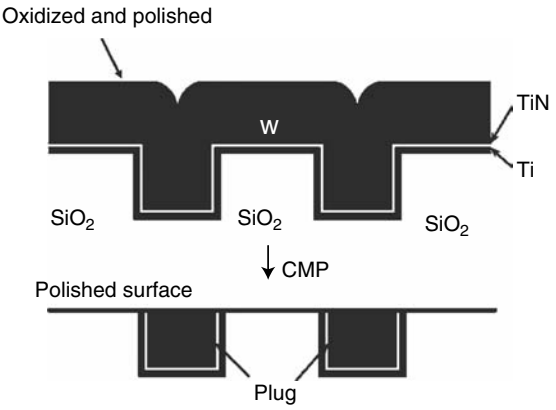


**FIGURE 7.44** Tungsten CMP.

there are patterns as depicted in Figure 7.45. This selective erosion of the oxide negatively impacts the integration of the next metal level as it introduces nonplanarity at the via or contact level. Nonplanarity at the contact level is also of great concern because it limits the resolution of subsequent lithography steps necessary in forming the next metal level. Oxide erosion also depends on the solid concentration of abrasive particles and oxidizer concentration in the slurry. Figure 7.46 and Figure 7.47 provide a description of these effects. Reducing the solid content of the slurry significantly reduces

**TABLE 7.9**
**W-CMP Performance Comparison by Different Slurries**

| | First Generation Slurry | Second Generation Slurry | Third Generation Slurry |
|---|---|---|---|
| Abrasive particle | Alumina | Alumina | Silica |
| Particle size (nm) | 100 | 230 | 200 |
| Oxidizer | $Fe(NO_3)_3$ | $KIO_3$ | $H_2O_2$ |
| pH | 1.6 | 4.3 | 2.3 |
| Polishing pad | Suba 500(P)/Suba | IC1000(P)/Suba | IC1000(P)/Suba |
| Polish rate (nm/min) | 400 | 310 | 350 |
| Selectivity (W:TEOS) | 35:1 | 22:1 | 100:1 |
| Dishing (nm) (plug 0.4 × space 5.0 μm) | 45 | 15 | 15 |
| Oxide erosion (nm) (plug 0.4 × space 0.4 μm) | 300 | 80 | 120 |
| Surface roughness RMS (nm) MAX | 1.079<br>7.593 | 1.151<br>12.391 | 0.192<br>1.65 |

*Source*: From Namiki, K., *Ebara Eng. Rev.*, 183, 63, 1994.

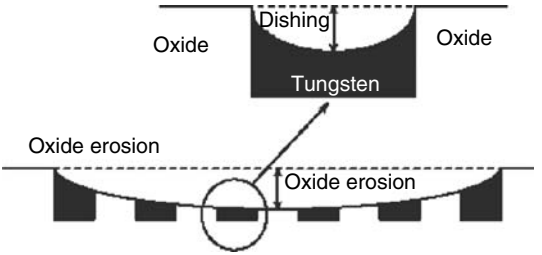


**FIGURE 7.45** Tungsten plug dishing and oxide erosion.

the oxide erosion, and reducing the peroxide concentration of the slurry slightly reduces the amount of oxide erosion, more significantly for the line patterns than the plug patterns [22]. Oxide erosion is a result of the combination of the slurry and pad selection. Figure 7.48 shows a comparison between oxide erosion results obtained with a peroxide-based slurry compared with a ferric-based slurry. A hard pad (Rodel IC1000) was used for the peroxide-based slurry and a soft pad (Rodel politex) for the ferric-based slurry. The hard pad with peroxide-based slurry result showed significantly less oxide erosion than the soft pad with ferric-based slurry result. The difference in pad hardness, rather than slurry type, may also be the reason for the difference in oxide erosion [22,23].

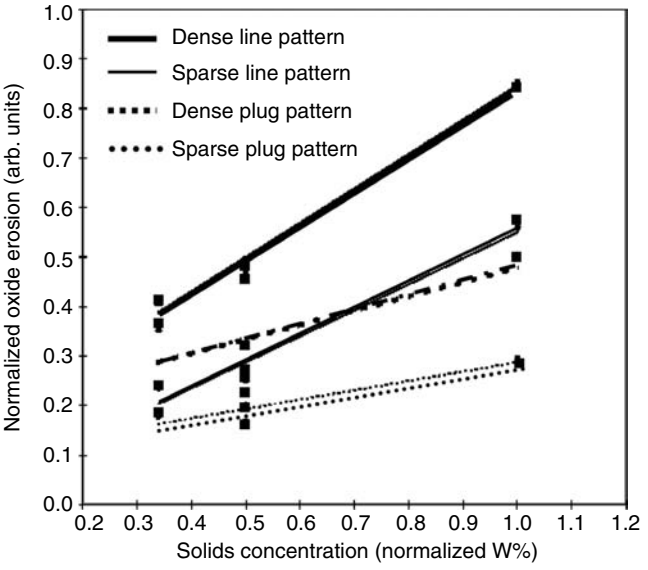


**FIGURE 7.46** Effect of solid content to oxide erosion. (From Lum, P., Oxide erosion characterization of a tungsten CMP process, CMP-MIC, 207, 1999.)

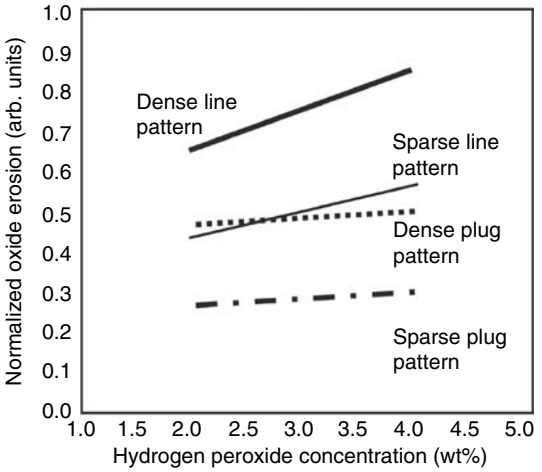


**FIGURE 7.47** Effect of oxidizer concentration to oxide erosion. (From Lum, P., Oxide erosion characterization of a tungsten CMP process, CMP-MIC, 207, 1999.)

For further reduction of W defectivity and improved dishing and erosion results, a new type of W slurry has been developed. This is called the fourth-generation slurry, which is based on periodic acid as an oxidizer with fine alumina or silica particles. The particle distributions in slurries are quite

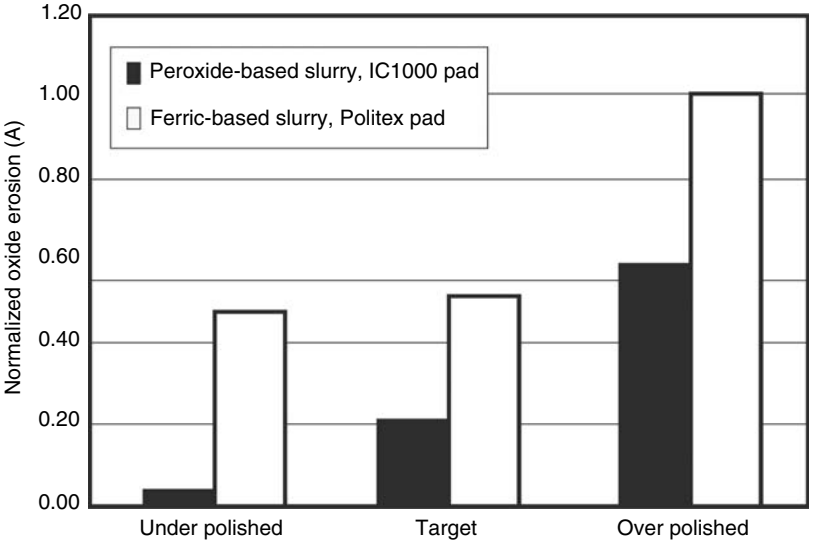


**FIGURE 7.48** Oxide erosion with a combination of slurry and pad. (From Lum, P., Oxide erosion characterization of a tungsten CMP process, CMP-MIC, 207, 1999.)

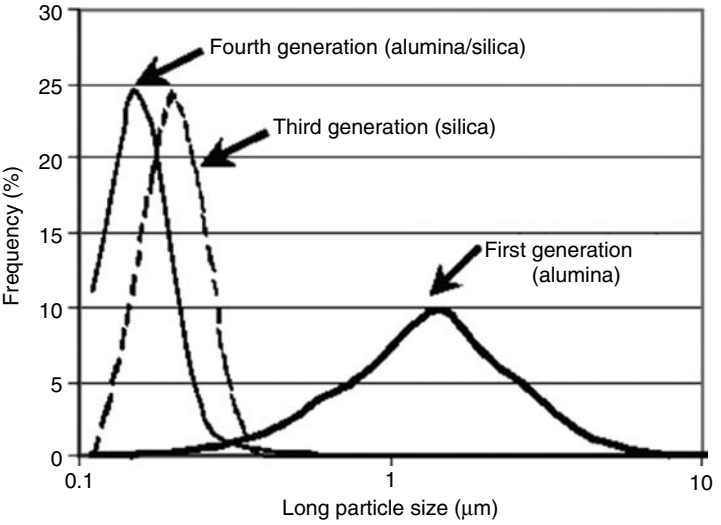


**FIGURE 7.49** Abrasive particle size distribution for each generation of W slurry. (From Peterson, M., et al., Fourth Generation W Damascene Slurry, CMP Technology for ULSI Interconnect, SEMICON West 2000, Q-1.)

different from generation to generation. The fourth-generation slurry has a smaller particle distribution than the first- and second-generation slurries as shown in Figure 7.49 [24]. Periodic acid ($H_5IO_6$) is a stronger acid and oxidant than $KIO_3$. Tungsten dissolves freely in periodic acid solutions. The dissolution rates follow the order: $W \gg WO_2 > WO_3$. During dissolution, periodate is reduced to iodate and iodide. Dissolution rates in periodic acid are higher than that in potassium iodate solutions. Figure 7.50 shows Tafel plots for W dissolution in a slurry under different pH values [25]. The CMP baseline for periodic-acid-based slurry is shown in Figure 7.51. As can be seen, good removal rate stability and nonuniformity are obtained.

Because of the large particle size, the first-generation slurries are followed by an oxide buff to remove several hundred angstroms of damaged oxide. This buff also helps to improve overall planarity. The smaller abrasive particle distribution may help to reduce the defect counts at W-CMP. Figure 7.52 shows an example of excellent defectivity results with a single-step process using the periodic-acid-based slurry.

### 7.3.2.5 Cu CMP Slurry

#### *7.3.2.5.1 Two-Step Process and Selectivity*

Copper (Cu) is now a promising material for multilayer interconnection. The process using copper is aggravated by the fact that copper does not adhere to oxides, unlike aluminum. The approach to this problem is to deposit a barrier

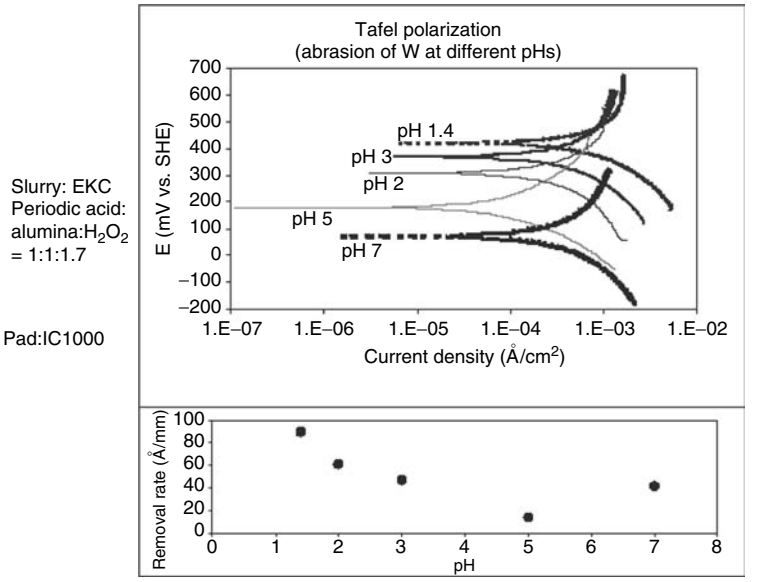


**FIGURE 7.50** Dissolution of W film in a slurry at 6 psi. (From Gaghavan, S., et al., Periodate as an oxidant for tungsten CMP, NSF I/UCRC Center for Microcontamination Control at Arizona and Rensselaer, CMPUG, October 2001.)

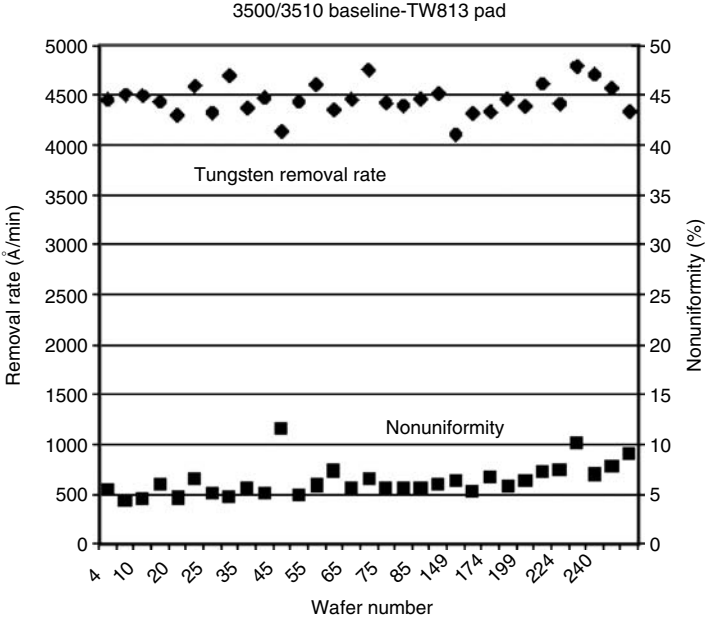


**FIGURE 7.51** Periodic acid-based W CMP slurry baseline. (From Peterson, M., et al., Fourth Generation W Damascene Slurry, CMP Technology for ULSI Interconnect, SEMICON West 2000, Q-1.)

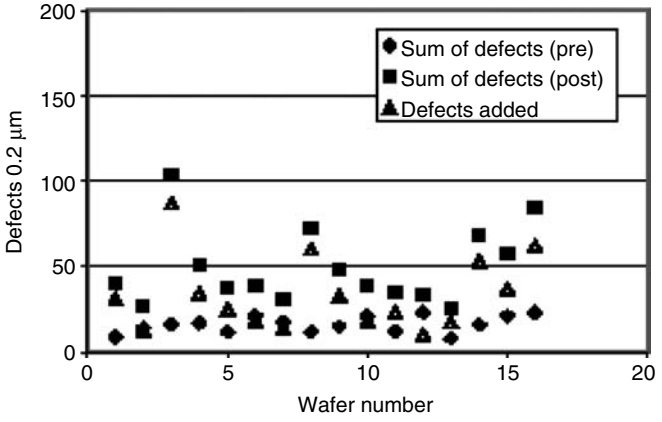


**FIGURE 7.52** Defectivity after W CMP using periodic-acid-based slurry. (From Gaghavan, S., et al., Periodate as an oxidant for tungsten CMP, NSF I/UCRC Center for Microcontamination Control at Arizona and Rensselaer, CMPUG, October 2001.)

layer, which adheres to both copper and oxide, between the two materials. Tantalum (Ta) and tantalum nitride (TaN) have been found to provide good adhesion to both copper and oxide. However, the removal rate for copper, oxide, Ta, and TaN are not the same during CMP and the trait is referred to as selectivity. Ta is a very hard material, and is much slower to remove than copper and oxide. Within Cu-CMP there are challenges for removing more than three different materials in the processes, eliminating metal residues, accomplishing low dishing, low erosion, and low metal and oxide losses. For accomplishing these requirements, Cu-CMP is done in two steps by using two types of slurries. In the first step the bulk copper is removed and in the second step barrier material or residual copper, barrier metal, and portion of the dielectric film are removed. In the case of a selective slurry process, all the copper is removed with first step polishing slurry, and barrier is removed with the second step polishing slurry. In the nonselective slurry process, bulk copper is removed with first step polishing slurry and residual copper, barrier, and some portion of the dielectric layer are removed with second step polishing slurry. Figure 7.53 shows a cross-sectional view of the Cu damascene interconnection planarized by CMP.

#### *7.3.2.5.2 Pourbaix Diagrams for Cu–$H_2O$ System*

Cu-CMP slurry formation is based on Pourbaix diagrams. Figure 7.54 shows a diagram for the Cu–$H_2O$ system [26]. Cu is stable in reduction potential domain, which is in minus potential region, where the Cu surface is polished mechanically. In an acidic solution, where the oxidation–reduction potential (ORP) is more than 0.16 V, copper dissolves as $Cu^{2+}$ ions. This is an etching process. On the other hand, in a basic solution with pH value of more than 7.5,

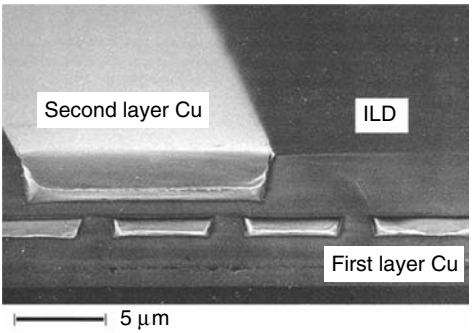


**FIGURE 7.53** Cross-sectional view of Cu damascene interconnection.

the copper surface is coated by $Cu_2O$ film, which protects Cu dissolution, and again becomes stable. When the ORP goes higher, the CuO phase becomes another stable state. In these cases, removing the oxide film layer mechanically polishes the copper surface. In Cu–$NH_3$–$H_2O$ solution, dissolved $NH_3$ forms a complex with the copper ion and copper solubility is increased between pH 7 and 9. Thus, the copper polishing is also possible in a basic solution, but the polishing mechanism is based on an etching process. The disadvantage of using high static etch rate slurry is the high Cu removal rate in the recessed area. To prevent such a copper dissolution, reagents can be added to the slurry to form a passivating surface film that protects the copper from dissolution.

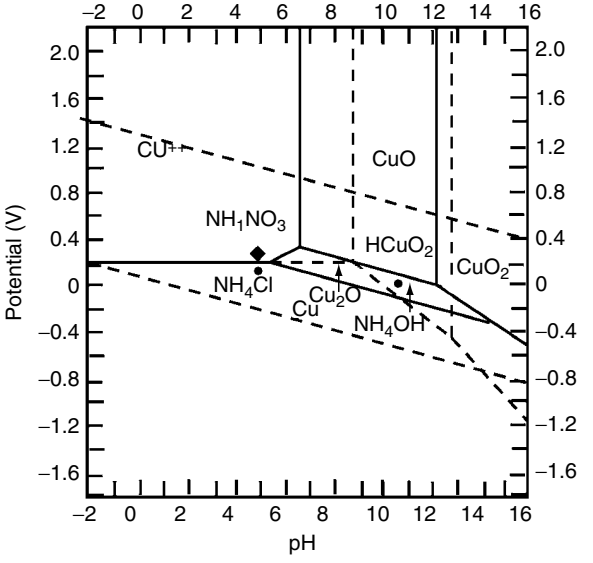


**FIGURE 7.54** Pourbaix diagram for Cu–$H_2O$ system.

Benzotriazole (BTA) is known to inhibit corrosion of copper in aqueous solution by forming Cu–BTA monolayer.

#### *7.3.2.5.3 Organic Acid–Based Slurry*

Conventionally ferricyanide and nitric acid have been used as oxidizers in Cu slurries. To meet the constant demand for lower dishing and corrosion results, organic acids have replaced conventional chemicals as an effective additive in slurries. The basis of Cu-CMP using organic acid is that the Cu hydrate reacts with organic acid and forms a Cu chelate complex. Glycine is an amino acetic acid, which has the simplest structure among the amino acid group and is also one of the additives used for Cu-CMP slurry [27]. It reacts with Cu hydrate and forms Cu–glycine complex, which is soluble in aqueous solution. To accelerate the Cu hydrate formation, hydrogen peroxide ($H_2O_2$) is added in slurry. Hydrogen peroxide oxidizes copper surface as well as contributes to form a protective layer from etching. Although dipping into the glycine solution does not dissolve copper, the dissolution rate increases by adding a small amount of hydrogen peroxide. However, the excess amount of hydrogen peroxide addition tends to inhibit dissolution as shown in Figure 7.55 and finally stops dissolution, which indicates that the copper surface is passivated. Polish rate for glycine-based slurry shows a similar tendency to etching rate, but the mechanical abrasion of passivated film layer continues even after the etching stops. Then the up feature continues to be polished, leaving the recess area unetched. Thus planarization can be realized.

Quinaldic acid is another organic acid additive used for Cu-CMP slurry. Being different from glycine, quinaldic acid makes a Cu–quinaldic acid chelate complex formed with hydrated copper, which is intrinsically insoluble in aqueous media. Figure 7.56 shows polarization curves for Cu–$H_2O$ system. When the Cu film is immersed in the hydrogen peroxide solution, copper

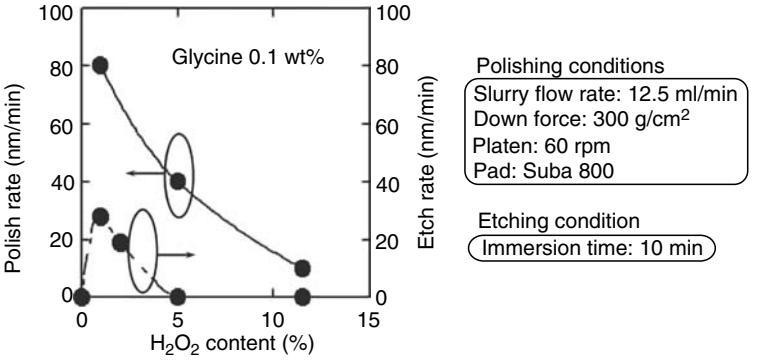


**FIGURE 7.55** Polish and etch rate dependency on hydrogen peroxide concentration in glycine-based slurry.

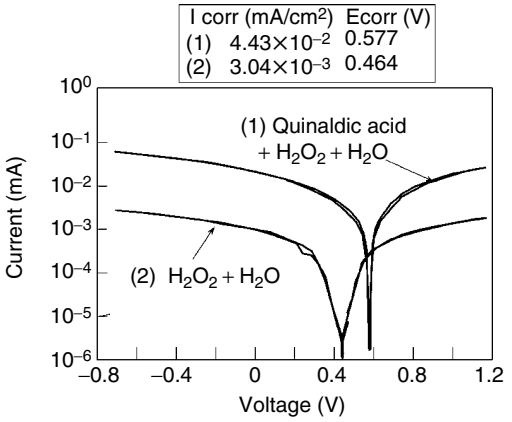


**FIGURE 7.56** Polarization curves for Cu–$H_2O$ system.

oxide is formed on the surface. The addition of quinaldic acid increases the polarization voltage and corrosion current. In Pourbaix diagram for Cu–$H_2O$, the polarization voltage corresponds to a region where copper oxide is absent. The chemical analysis proved that organic compounds with Cu are formed on the surface. The polishing mechanism for Cu-CMP using quinaldic acid–based slurry is illustrated in Figure 7.57. The Cu–quinaldic acid complex is formed on Cu surface by reaction with Cu hydrate and quinaldic acid. The mechanical abrasions by a polishing pad, and particles in the slurry, foster to remove the complex and reveal a new Cu surface, whereas the complex formed on the recessed surface remains nonabraded as well as unetched

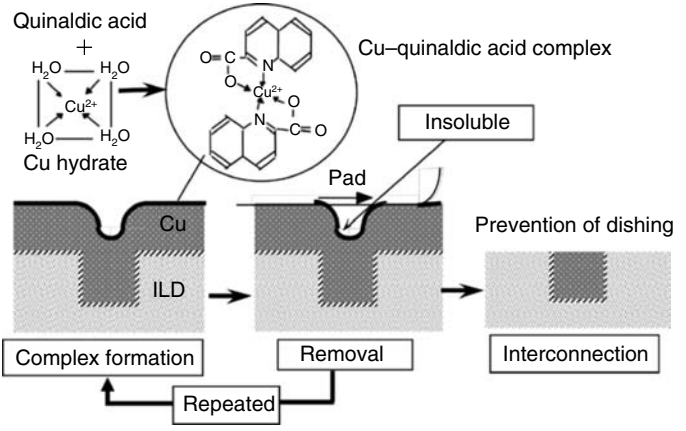


**FIGURE 7.57** Polishing mechanism of Cu-CMP by using organic acid–based slurry.

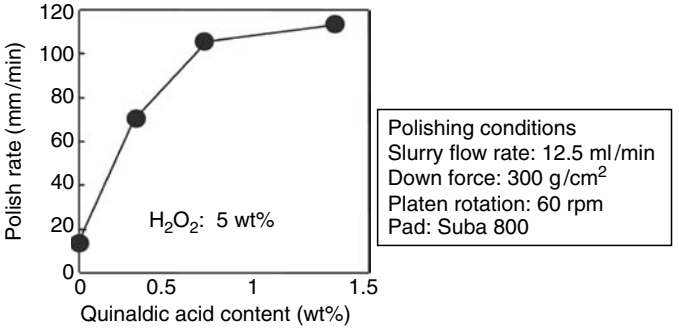


**FIGURE 7.58** Effect of Quinaldic acid content on Cu polish rate.

because of insolubility. This process is repeated until the surface topography is planarized. Cu polish rate increases accordingly with quinaldic acid content, and saturates at more than 1 wt% as shown in Figure 7.58. The hydrogen peroxide content also affects the polishing rate as shown in Figure 7.59 [28].

#### *7.3.2.5.4 Role of Abrasive Particles*

There are many options for abrasive particles in Cu-CMP slurries. Alumina abrasive particles increase removal rate up to twice as much as colloidal silica; however, defectivity tends to be worse. There are different phases of alumina particles depending on baking conditions. Figure 7.60 shows different phases of alumina particles dependent on their hydration ratio. The α-alumina is the hardest alumina with no water content and gives the highest polish rate, but results in high scratching. Figure 7.61 shows that the lower the

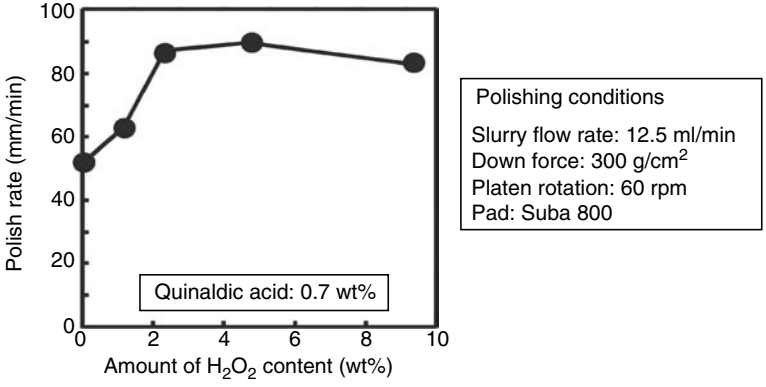


**FIGURE 7.59** Effect of $H_2O_2$ content on Cu polish rate.

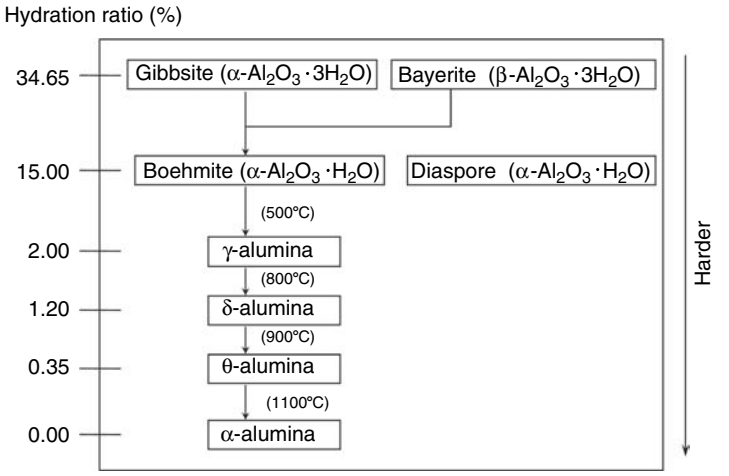


**FIGURE 7.60** Different phases of alumina particles.

hydration ratio, the higher the polish rate. The θ-alumina slurry demonstrates a very high polishing rate in the quinaldic acid–based slurry. Besides, some water content in alumina facilitates to reduce scratching. The colloidal silica does not contribute much for increasing polish rate in Cu-CMP slurry, but facilitates a lubrication between wafer and pad, which affords to reduce defectivity and copper residue. Zeta potential of abrasive particles is also an important factor to facilitate selectivity as shown in Figure 7.62. With addition of anion surfactant, alumina particle exerts a repulsive force on Cu

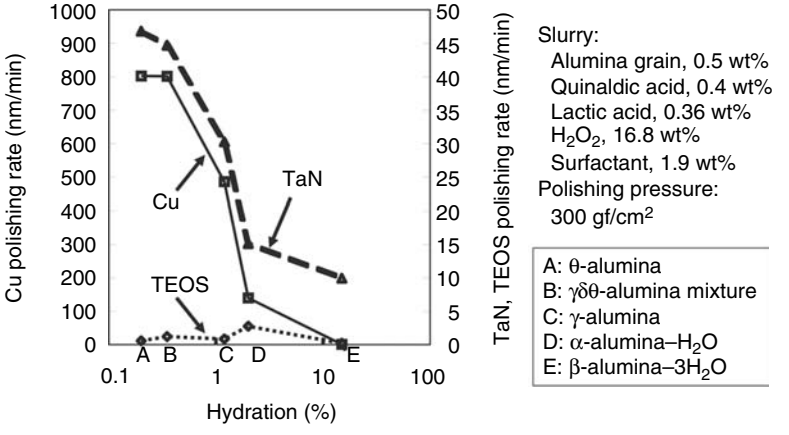


**FIGURE 7.61** Polishing rate dependency on hydration of alumina grain.

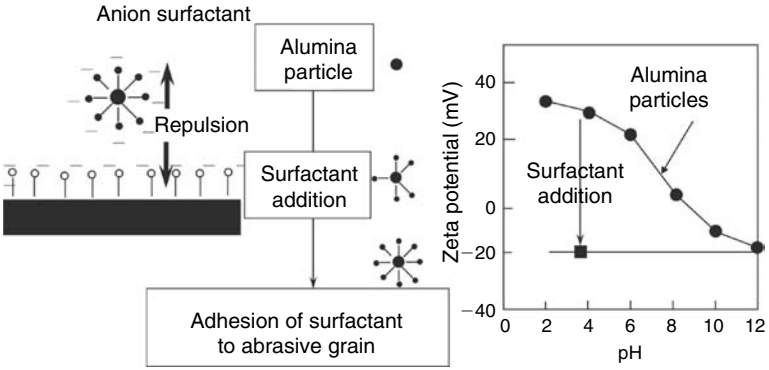


**FIGURE 7.62** Zeta potential control of alumina abrasive particle.

surface. It assists for a recessed part not to be polished, whereas an up feature part is polished.

#### *7.3.2.5.5 Slurry for Cu and Low-k CMP*

Copper and low-*k* materials are currently being implemented in metal interconnects as a means to reduce the RC delay for 0.90 nm or less logic device. In general, the hardness of low-*k* materials are much lower than that of ordinary oxide-based film such as TEOS and borophosphosilicate glass (BPSG). Table 7.10 shows a typical removal rate for Cu, barrier metal, oxide, and low-*k* dielectric material [29]. The low-*k* dielectrics have a wide range of materials varying from diamondlike carbon-doped oxide (CDO) CVD film to porous organic spin on film. Figure 7.63 shows the topography generated after first step polishing for both oxide and Black Diamond (CDO of AMAT). Planarization performance seems similar for both materials.

**TABLE 7.10**
**Example of Removal Rate Difference between Selective and Nonselective Slurries for Cu-CMP**

| | First Step Slurry | | Second Step Slurry | |
|---|---|---|---|---|
| **Film** | **Nonselective** | **Selective** | **Nonselective** | **Selective** |
| Copper | 8277 | 2105 | 624 | 227 |
| TaN | 235 | 22 | 510 | 606 |
| Black Diamond™ | | | 780 | 26 |
| BLOK | | | 350 | 50 |

*Source*: From Wijekoon, K., et al., Chemical mechanical polishing of copper-CVD low *k* films: A comparison of selective and nonselective processes, *VMIC*, November 2001.

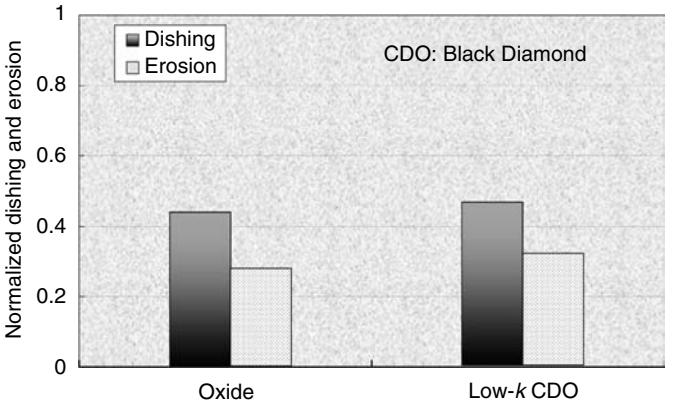


**FIGURE 7.63** Topography after first step CMP for oxide and low-*k* material. (From Wijekoon, K., et al., Chemical mechanical polishing of copper-CVD low *k* films: A comparison of selective and nonselective processes, *VMIC*, November 2001.)

However, the selective slurry process results in relatively lower topography than the nonselective slurry process as indicated in Figure 7.64. Even after the completion of CMP processes, the selective slurry process gives a better topography. The solid content in the nonselective slurry also affects topography. Figure 7.65 shows that the lower solid content results in higher erosion

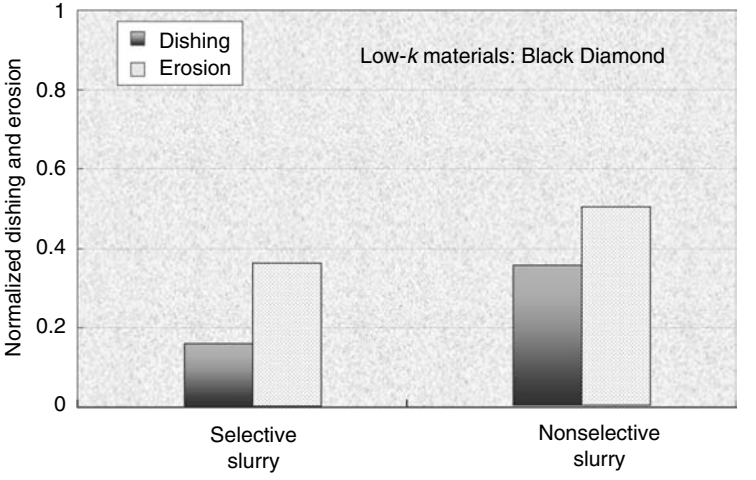


**FIGURE 7.64** Topography performance depending on slurry selectivity after first step CMP for Cu/low-*k*. (From Wijekoon, K., et al., Chemical mechanical polishing of copper-CVD low *k* films: A comparison of selective and nonselective processes, *VMIC*, November 2001.)

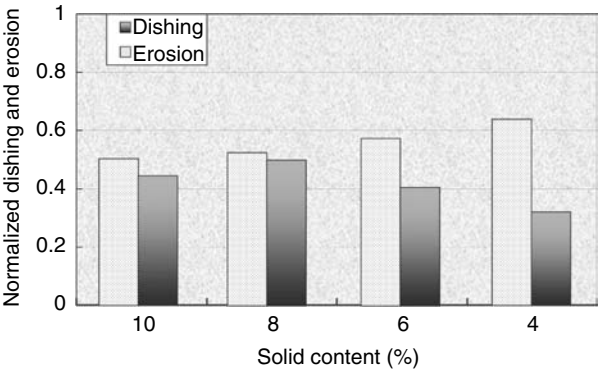


**FIGURE 7.65** Effect of solid content in nonselective slurry on topography. (From Wijekoon, K., et al., Chemical mechanical polishing of copper-CVD low *k* films: A comparison of selective and nonselective processes, *VMIC*, November 2001.)

and lower dishing. However, for lower solid content slurries, it may be necessary to polish for a longer time to clear the copper residue [29].

#### *7.3.2.5.6 Abrasive-Free Slurry*

Abrasive-free Cu-CMP is reported to afford much lower dishing and erosion results [30,31]. On the other hand, the lack of abrasive particles creates a large challenge to eliminate metal residues, low dishing, low erosion, low metal, and oxide losses. When tuning the polishing conditions for abrasive-free slurry, chemistries alone cannot solve the Cu residue issue, keeping dishing low. Friction control assists to stabilize polishing and to eliminate Cu residue. The polishing rate is assumed to be proportional to the friction between the substrate and the pad. By keeping friction constant, pressure is allowed to drift down when the barrier layer is exposed, and to drift back when Cu is cleared, as shown in Figure 7.66. A copper sheet resistance comparison between abrasive-free Cu-CMP and common Cu polishing slurry is shown in Figure 7.67. Abrasive-free data are shown in almost vertical lines, which suggests that abrasive-free Cu-CMP slurry provides better electrical performance [32].

## 7.3.3 Pads for Planarization CMP

***Masanobu Hanazono and Masaharu Kinoshita***

### 7.3.3.1 Basic Properties of the CMP Polishing Pad

#### *7.3.3.1.1 Pad Properties and Polishing Performance*

The polishing pad used for CMP processing is made of polyurethane material. The polyurethane pad had been commonly used in glass polishing for many years. Additionally, polymer-impregnated felts and poromeric pad have been the standard pad for silicon wafer polishing. The IC1000 (Trademark of

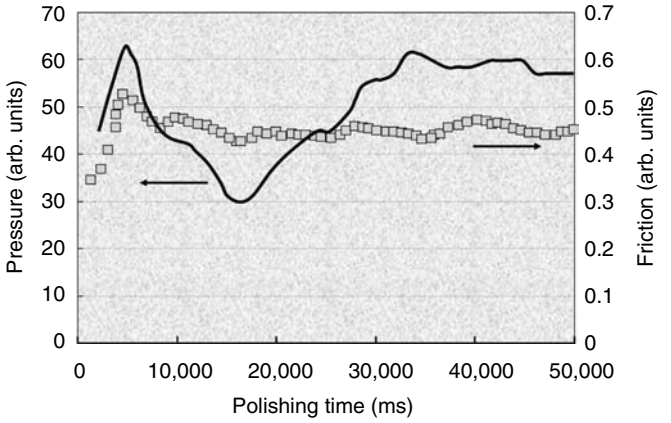


**FIGURE 7.66** Pressure and friction behavior under friction control polishing. (From Ki, S., et al., A low cost and residue-free abrasive-free copper CMP process with low dishing, erosion and oxide loss, IITC 2001/IEEE.)

Rohm and Haas Electronic Materials CMP Inc., formerly Rodel Inc.) pad, which is now a de facto standard for CMP polishing pad, was developed for ILD CMP under the basis of urethane technology for polishing. The cross-sectional structure of IC1000 pad is shown in Figure 7.68. It is composed of urethane matrix and randomly distributed micropores. The pores are spherical in nature and range in diameters from 30 to 50 μm. The fraction of the pore is

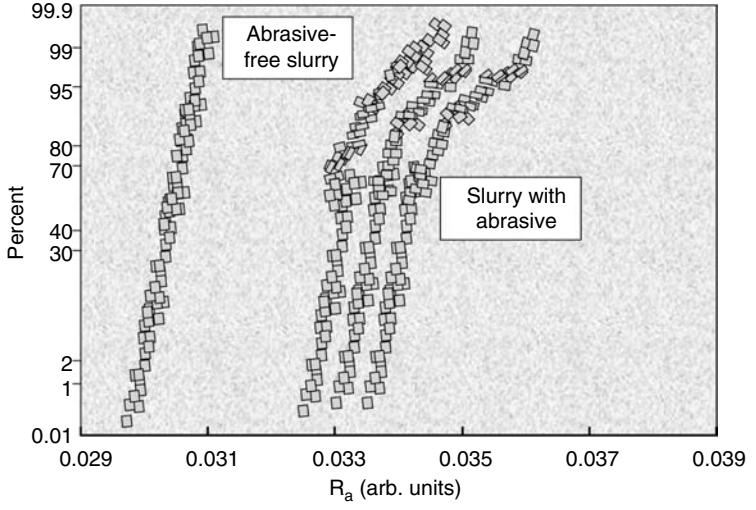


**FIGURE 7.67** Copper sheet resistance comparison between abrasive-free and slurry processes. (From Ki, S., et al., A low cost and residue-free abrasive-free copper CMP process with low dishing, erosion and oxide loss, IITC 2001/IEEE.)

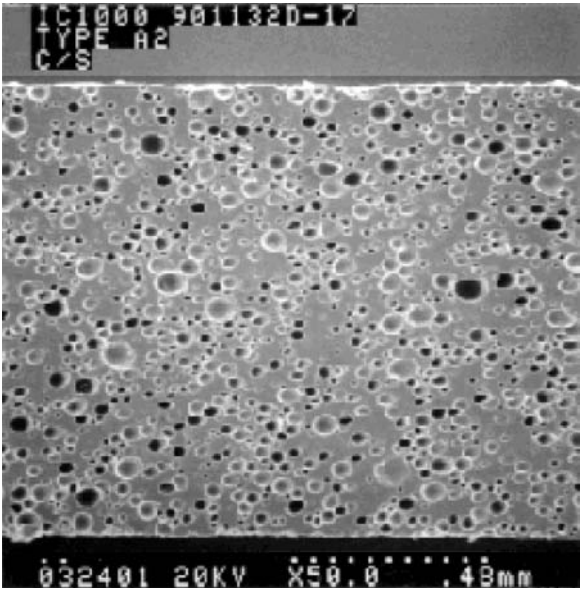


**FIGURE 7.68** Cross-sectional view of IC1000™ pad.

about 35% of the pad total volume, but can be changed by manufacturing conditions. The higher the porosity, the lower the pad density. Table 7.11 shows the typical specifications of the IC1000 pad. The pore radial size and distribution are also controlled to obtain a specific pad hardness and elastic modulus. Hardness is measured by using the Shore D hardness test. Figure 7.69 shows the effect of density on pad hardness. Typical density of the IC1000 pad is in the range between 0.63 and 0.85 g/cm$^3$ and the corresponding hardness ranges from 52 to 62.

The pad properties are closely related with polishing performance in CMP and the relationship is complex. The polishing performance should be viewed from three levels of scale. They include wafer scale, die scale, and feature

**TABLE 7.11**
**IC1000 Pad Physical Properties**

| | Type | | | |
|---|---|---|---|---|
| | **51/A1** | **52/A2** | **53/A3** | **54/A4** |
| Density (g/cm$^3$) | 0.63–0.80 | 0.74–0.85 | 0.70–0.85 | 0.63–0.80 |
| Hardness (Shore D) | 52–62 | | | |
| Compressibility (%) | 0.5–6.0 | | | |

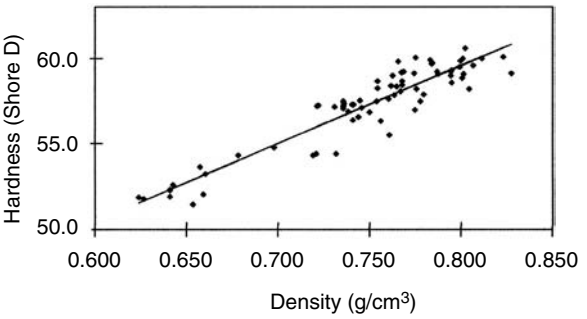


**FIGURE 7.69** Relationship between hardness and density for IC1000 urethane pad. (From Jams, D., Control of polishing pad physical properties and their relationship to polishing performance, Fifth International CAMP Symposium, Clarkson University, August 2000.)

scale as listed in Table 7.12. The pad properties are also strongly interdependent. The correlation of pad properties with polishing performance is summarized in Table 7.13. Removal rate is dependent on the pad density, texture, and hydrophilicity. It has also been found that porous pads achieve a higher removal rate against nonporous pad as shown in Figure 7.70. Nonuniformity depends on pad density, stiffness, texture, roughness, and pad compressibility. Pad life depends on pad tensile properties, stiffness, texture, and abrasion resistance. Pad density and hardness also affect defectivity. Planarization is affected by pad stiffness, compressibility, and roughness. Metal interconnect dishing and oxide loss are affected by pad density, hardness, roughness, and compressibility [33,34].

#### *7.3.3.1.2 Elastic and Viscoelastic Properties of Polishing Pad*

The pad modulus of elasticity and compressibility have been found to influence planarization performance. Figure 7.71 shows the stress distribution on

**TABLE 7.12**
**Polishing Performance**

| Wafer Scale | Die Scale | Feature Scale |
|---|---|---|
| Removal rate | Planarization | Conductor dishing |
| Nonuniformity | Defectivity | Oxide loss |
| Edge effects | | Selectivity |
| Macroscratches | | Defectivity |
| Pad life | | Roughness |

*Source*: From Jams, D., Pad properties during polishing and their effects on polishing performance. CAMPS Sixth International CMP Symposium, Clarkson University, August 2001.

**TABLE 7.13**
**Relationship between Pad Properties and Polishing Performance**

| Pad Properties | Polishing Scale | | | Condition Ability |
|---|---|---|---|---|
| | Wafer | Die | Feature | |
| Density (porosity) | Removal rate<br>Nonuniformity | Defectivity | Conductor dishing<br>Oxide loss | Yes |
| Hardness | Macroscratch | Defectivity | Defectivity<br>Roughness<br>Conductor dishing<br>Oxide loss | Yes |
| Tensile properties | Pad life | | | Yes |
| Abrasion resistance | Pad life | | | Yes |
| Stiffness | Edge effects<br>Nonuniformity | Planarization | | |
| Modulus | | | | Yes |
| Thickness | Pad life | | | |
| Top pad compressibility | | Planarization | Conductor dishing<br>Oxide loss | |
| Base pad compressibility | Edge effects<br>Nonuniformity | Planarization | | |
| Pad texture (grooves) | Pad life<br>Removal rate<br>Edge effects<br>Nonuniformity | | | |
| Pad roughness | Removal rate<br>Nonuniformity | Planarization | Conductor dishing<br>Oxide loss | Yes |
| Hydrophilicity | Removal rate | | | Yes |

*Source*: From Jams, D., Control of polishing pad physical properties and their relationship to polishing performance. CAMP Fifth International CMP Symposium, Clarkson University, August 2000.

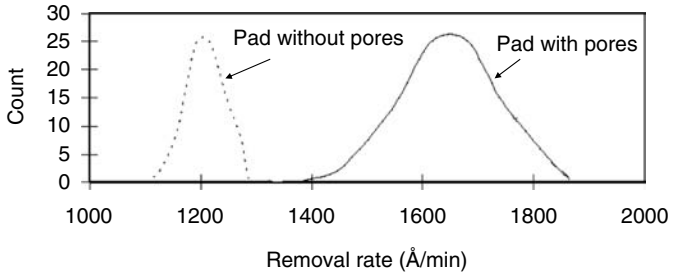


**FIGURE 7.70** Effect of porosity to removal rate. (From Jams, D., Control of polishing pad physical properties and their relationship to polishing performance, CAMP Fifth International CMP Symposium, Clarkson University, August 2000.)

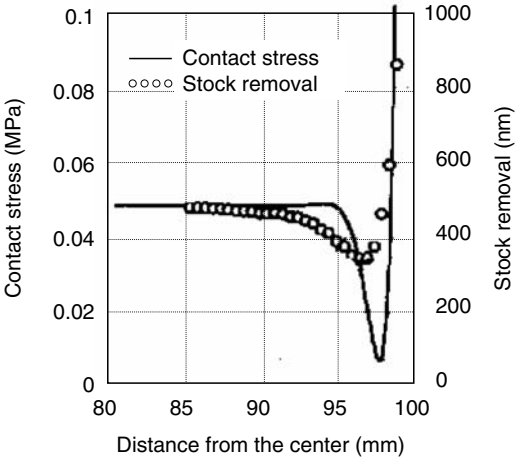


**FIGURE 7.71** Stress distribution at the edge of wafer. (From Nishioka, T., Influence of stress distribution for CMP [in Japanese], Tribology Conference, 1997.)

the wafer surface under the vertical down force through the pad [35]. The contact stress goes up significantly at the wafer edge after once decreasing. This causes a nonuniform removal rate distribution at the wafer edge. A typical property of the urethane pad density on elastic modulus is shown in Figure 7.72. With increasing density, the elastic modulus also increases. As polishing is a dynamic process often at elevated temperatures, the dynamic mechanical analysis is very important. A cyclic strain is applied to the pad sample and the resulting stress measured. In dynamic mechanical analysis, the viscoelasticity takes an important role. Figure 7.73 shows typical experimental data for the elastic modulus and tan delta, depending on the different curing conditions of the pad. The measured modulus shows the linear characteristic for the typical polishing temperature range. However, the pad loses its elastic property at higher temperature. Polishing performance of the pad deteriorates significantly at temperature higher than 60°C. Urethane pad properties are not the same when the pad is in dry as in wet. Table 7.14 shows the % change in pad properties in an oxide CMP slurry. ILD1300 is ammonium-based slurry, whereas ILD1200 and SS25 are potassium-based slurries. Pad properties will also change according to slurry chemicals used in the CMP process step [33,34].

#### *7.3.3.1.3 Composite Pad Structure*

In CMP, both the global and local planarizations of the wafer should be achieved at the same time. To planarize the patterned wafer with a stock removal less than 1 μm, polishing with higher rate of step height reduction is

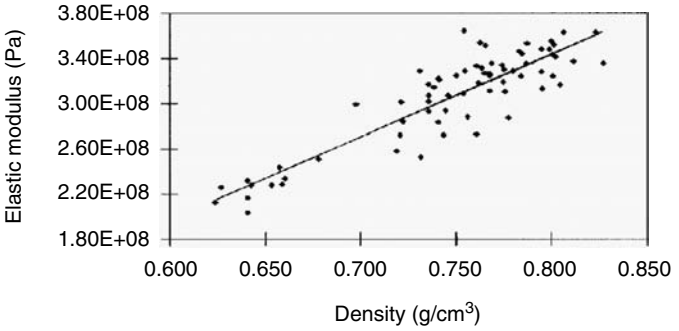


**FIGURE 7.72** Elastic modulus dependency on density.

required. This means that the higher topography pattern should be selectively removed at first to obtain a smooth and planer surface in a short period of time, and then the total wafer topography will be reduced to zero. When the surface topography is not uniform, the pad will be subjected to the wafer surface warp and irregularity. The composite pad structure was designed to accomplish the requirement. Figure 7.74 shows the cross-sectional structures of two types of the composite pads IC1000 stacked on a Suba 400 base pad and a closed cell foam base. The latter pad is named IC1400. The top pad has

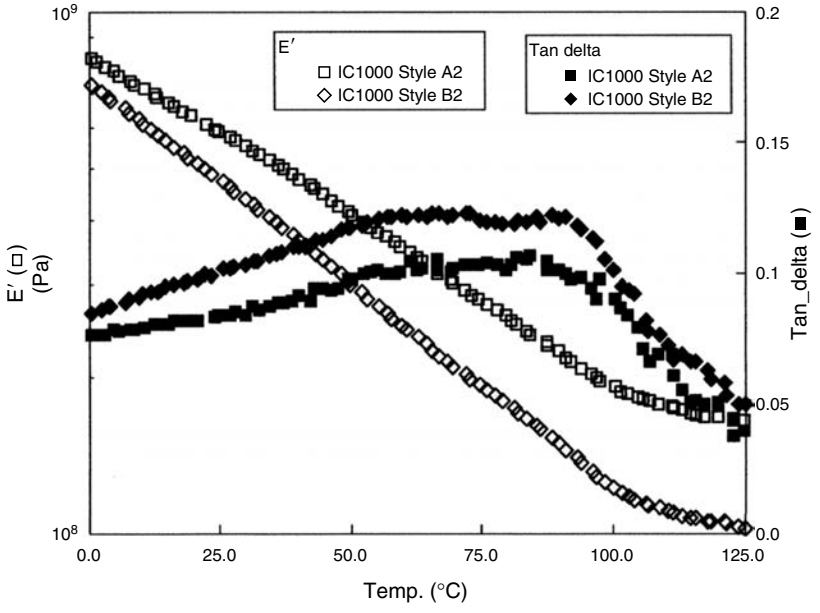


**FIGURE 7.73** Viscoelastic properties of urethane pads.

**TABLE 7.14**
**Pad Property Change at Immersion in Slurry**

| | % Change in Property | | |
|---|---|---|---|
| **Property** | **ILD1300** | **ILD1200** | **SS25** |
| Hardness (Shore D) | −10.2 | −8.8 | −9.1 |
| Proportional limit (psi) | −46.8 | −32.9 | −18.6 |
| Elongation to break (%) | 35.0 | 16.5 | 7.5 |
| $E'$ (Pa) at 40°C, 10 rad/sec | −44.1 | −15.5 | −18.7 |

*Notes*:
IC1000 Style 5
100 hours immersion at ambient temperature
ILD1300: ammonia-based slurry (Rodel)
ILD1200: potassium-based slurry (Rodel)
SS25: potassium-based slurry (Cabot)
*Source*: From Jams, D., Pad properties during polishing and their effects on polishing. Performance, CAMP Sixth International CAMP Symposium, Clarkson University, August 2001.

a higher hardness property compared to the base pad. Good die-scale planarity can be obtained by using a solo IC1000 pad, but the wafer scale planarity tends to deteriorate. The softer base pad helps to improve the wafer scale planarity, keeping die-scale planarity unchanged [36].

Pad stiffness depends on many parameters such as moduli and thickness of the stacked pad, polishing layer groove design, and base pad compressibility. The planarization efficiency or the planarization quotient, which is defined as shown in Figure 7.75, can be improved by optimizing the stiffness

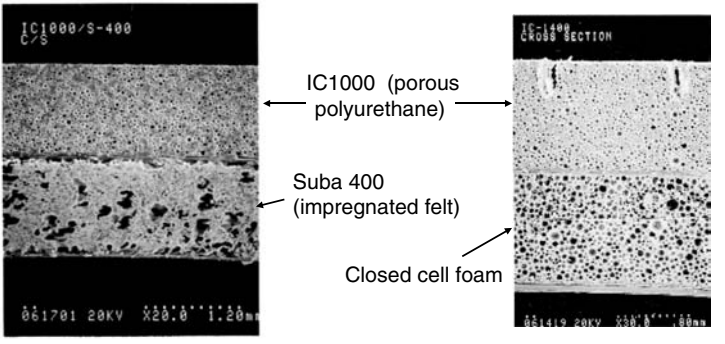


(a) IC1000/Suba 400 (b) IC1400

**FIGURE 7.74** Cross-sectional view of the composite pads.

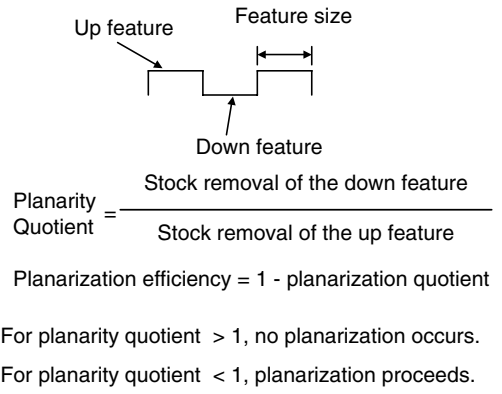
Up feature
Feature size
Down feature
Planarity Quotient = Stock removal of the down feature / Stock removal of the up feature
Planarization efficiency = 1 - planarization quotient
For planarity quotient > 1, no planarization occurs.
For planarity quotient < 1, planarization proceeds.

**FIGURE 7.75** Definition of planarization efficiency or planarization quotient.

design. Pad stiffness is defined as constant × modulus × thickness. It has been found that pattern density effects during oxide CMP are largely determined by the modulus properties of the composite polishing pad. Figure 7.76 shows the pad elastic modulus of composite pads. The modulus of the stacked pad is inferior to the solo pad. Planarity in feature scale can be improved by stacked pad stiffness as shown in Figure 7.77. Pad stiffness is a more complex property for a stacked pad [33].

#### *7.3.3.1.4 Pad Surface Asperity and Grooves*

The pore is useful for holding slurry during polishing. In addition, grooves and perforations are made to the pad to enhance the polishing performance. The reasons for grooves and perforations are as follows: prevent wafer hydroplaning, ensure uniform slurry distribution, act as channels to remove polishing debris, control overall and localized pad stiffness, and to prevent wafer from sticking on the pad when unloading. Figure 7.78 shows the example of groove and perforation patterns. Groove and perforation design performance has been found to be dependent on the CMP tool that also affects the CMP performance. AMAT Mirra tool prefers circular groove patterns, however, Ebara EPO tool prefers perforation and *XY* straight-line grooves. Pad users spend a great deal of time optimizing groove and perforation design by changing the groove dimension and combining groove with perforation to improve the removal rate and uniformity.

### 7.3.3.2 Pad Conditioning and Polishing Performance

#### *7.3.3.2.1 Conditioner*

Standard polyurethane CMP pads need to be conditioned before start of use. Traditionally, conditioners are diamond abrasive disks, by which a thin layer of pad material is abraded. Figure 7.79 shows close-up views of a variety of

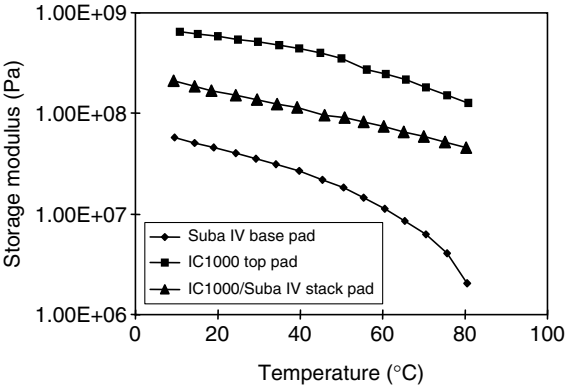


(a) IC1000/SUBA IV pad

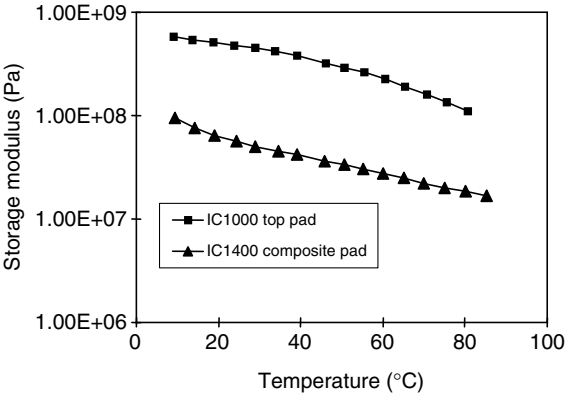


(b) IC1400 pad

**FIGURE 7.76** Composite pads DMA modulus vs. temperature.

diamond conditioners. Embedded diamond grains are dispersed either randomly or regularly, which reflect a different design concept and manufacturing method of conditioner. In the nickel plating, the diamond is held in place by electroplated Ni. However, the diamond retention and chemical resistance tend to be poor. The conventional brazing is a high-temperature process under which the diamond grains are incorporated in a metal matrix. In sintering, the diamonds are incorporated in a metal matrix with pressure and temperature. Retention and chemical resistance is similar to brazing. The favorable diamond conditioner architecture can be described by such parameters as a diamond spacing, protrusion height, chemical bonding with blazed matrix, and coating on the diamond grid, which is illustrated in Figure 7.80. The protrusion height should be uniform to obtain a uniform pad conditioning.

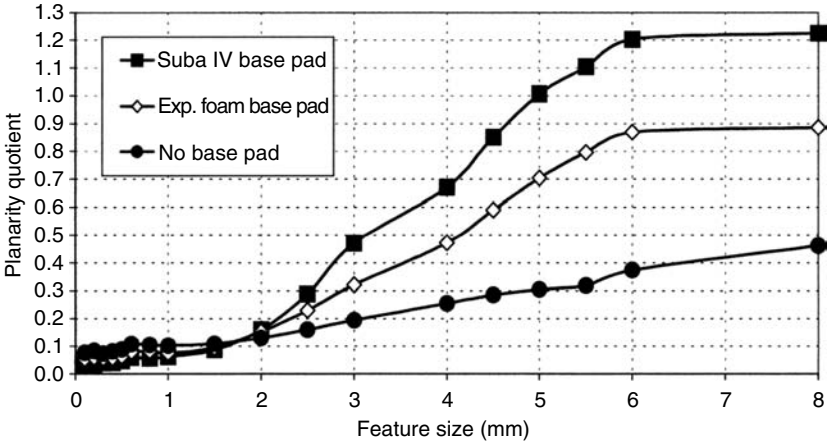


**FIGURE 7.77** Planarity improvement by using composite pads.

A robust brazed matrix and an overcoated film on the diamond grain are the key features for preventing diamond pullout, reducing risk of defectivity, and increasing conditioner lifetime. For metal CMP application, enhanced resistance to acid slurry is also required.

*7.3.3.2.2 Conditioning Process*

The pad is generally broken-in by polishing at least 25 blanket wafers. Conditioning determines the surface asperity of the pad. To maintain the

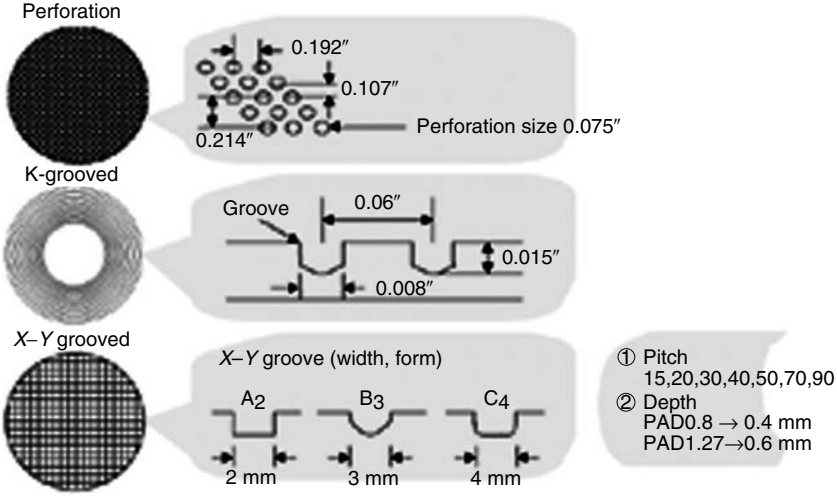


**FIGURE 7.78** Grooves and perforation designs for IC1000 pad.

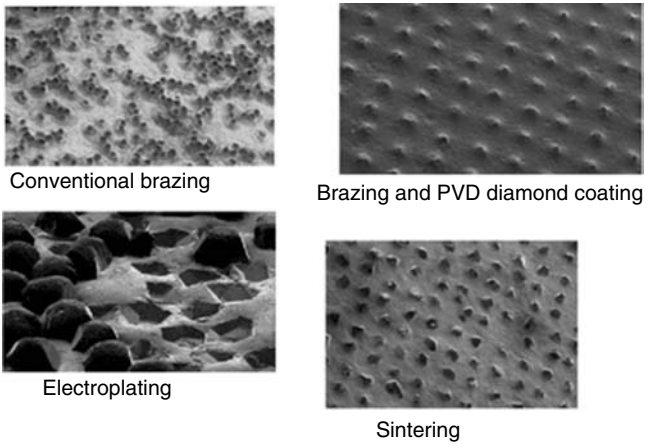


**FIGURE 7.79** Close-up views of different type of conditioners. (Courtesy of Kinik.)

surface asperity, pad conditioning is done after each CMP operation. Pad conditioning helps maintain removal rate stability and thereby enhances the longevity of the pad. Without conditioning, polish removal rate tends to drop steadily. Pad conditioning is done either in situ or ex situ. In-situ conditioning is the process where the pad is conditioned during the polishing cycle. Ex-situ conditioning occurs when the pad is conditioned between the wafers' polishing cycle. As CMP itself has an effect of smoothing the pad surface, a more consistent removal rate can be maintained with the in-situ conditioning.

The cross section of IC1000 pad surface such as depicted in Figure 7.81 shows pores as well as asperities generated by conditioning. Figure 7.82 shows the pad surface profile after conditioning. There is a less planar area on the top and there also appears to be deeper conditioner grooves in the pad surface. Figure 7.83 shows the pad surface profile taken after CMP. The roughness of the surface between the pore openings is relatively flat, whereas

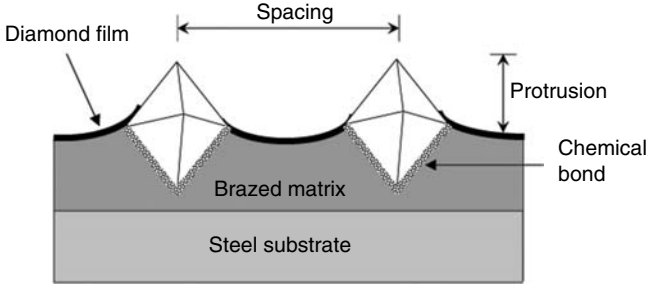


**FIGURE 7.80** Pad conditioner architecture of Kinik diagrid conditioner.

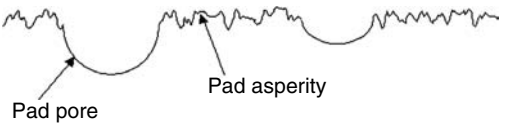


**FIGURE 7.81** Diagram of cross section of IC1000 pad surface. (From Oliver, M.R., et al., CMP pad surface roughness and CMP removal rate, ECS Fall Conference, Phoenix, Arizona, October 2000.)

the pores are larger and deeper. There is a clear relationship between the decrease of polish removal rate and the reduction of asperity height as shown in Figure 7.84 and Figure 7.85. The removal rate falls off in the absence of conditioning and also as the average asperity height decreases [37].

By using analytical techniques, subtle variations in the pad surface morphology can be quantified. Vertical scanning interferometry images show the difference between conditioning-dominated and wafer-dominated pad surfaces as shown in Figure 7.86. A probability distribution represented as a function of pad height for conditioning and wafer dominated is provided. The effect of pad–conditioner contact is to restore and maintain a random distribution of surface asperities through the removal or modification of the damaged layer induced by pad–wafer contact [38].

#### *7.3.3.2.3 Pad Surface Profile and Planarization Uniformity*

The user can modify the pad profile and the relative polishing pressure thus affecting polish uniformity across the wafer. By changing the conditioner

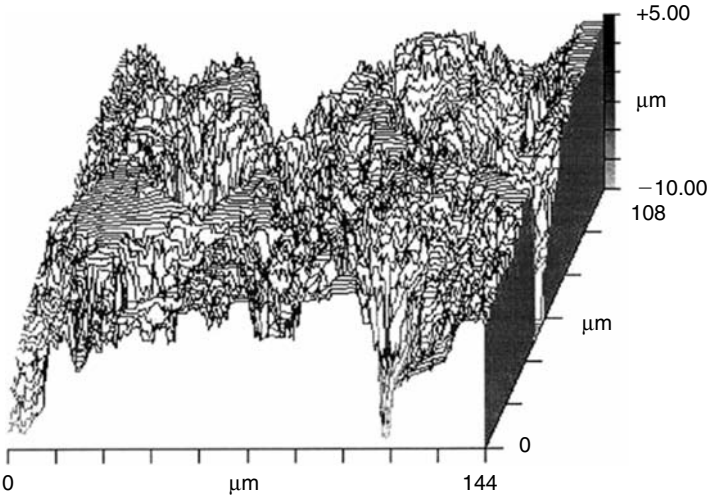


**FIGURE 7.82** IC1000 pad surface profile after conditioning. (Zygo New View 5030.) (From Oliver, M.R., et al., CMP pad surface roughness and CMP removal rate, ECS Fall Conference, Phoenix, Arizona, October 2000.)

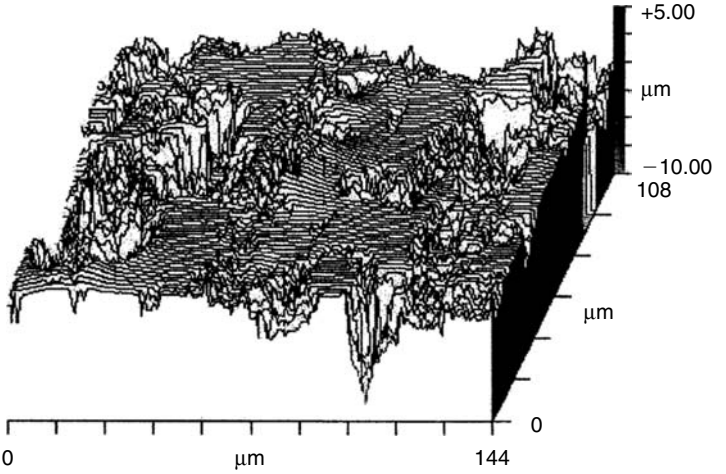


**FIGURE 7.83** IC1000 pad profile after polishing. (Zygo New View 5030.) (From Oliver, M.R., et al., CMP pad surface roughness and CMP removal rate, ECS Fall Conference, Phoenix, Arizona, October 2000.)

sweep length, the postconditioning pad profiles vary from constant erosion profile across the pad to a bell-shaped profile as shown in Figure 7.87. The amount of pad erosion is proportional to the time the conditioner spends at a given point. It indicates that the pad erosion is proportional to linear velocity of the conditioner and is inversely proportional to the area conditioned. The pad profile also affects the removal rate uniformity of the wafer and the stability over extended conditioning time.

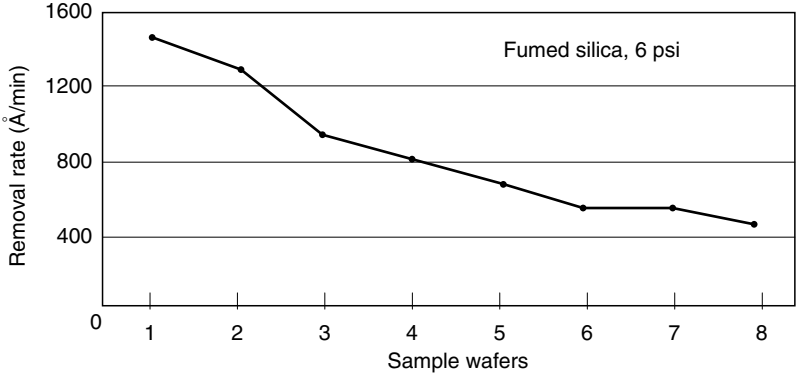


**FIGURE 7.84** Average polish removal rate over 1 min intervals in the absence of conditioning. (From Oliver, M.R., et al., CMP pad surface roughness and CMP removal rate, ECS Fall Conference, Phoenix, Arizona, October 2000.)

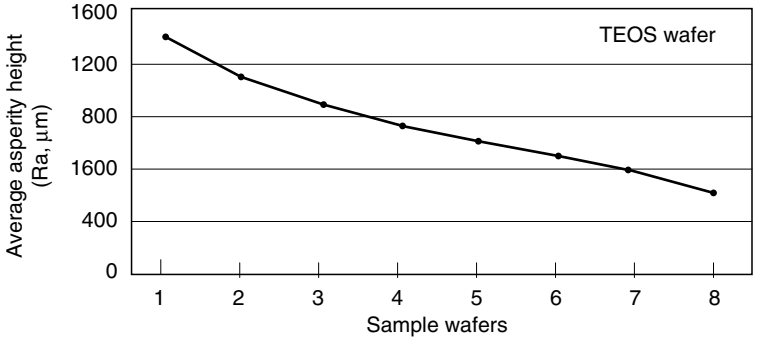


**FIGURE 7.85** Average asperity height after polishing over 1 min intervals in the absence of conditioning. (From Oliver, M.R., et al., CMP pad surface roughness and CMP removal rate, ECS Fall Conference, Phoenix, Arizona, October 2000.)

With the slightly sloped pad profile, the oxide removal rate remains constant over the accumulated conditioning time and the nonuniformity of removal rate over the wafer is small. With the concaved pad profile, removal rate profile on the wafer is edge fast, and with the Bell profile is edge slow [39].

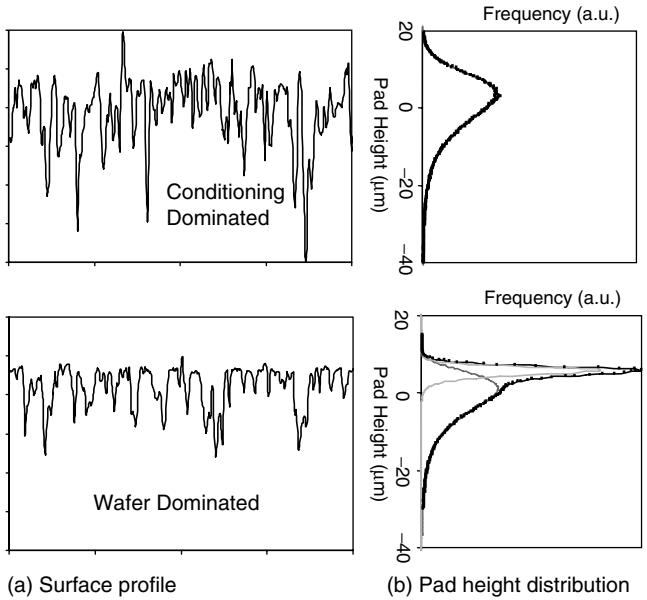


**FIGURE 7.86** Pad surface morphology. (From Lawing, A.S., Polishing rate, pad surface, morphology and pad conditioning in oxide chemical mechanical polishing, I1-Fifth International Symposium on Chemical Mechanical Polishing (CMP), ECS 201st Meeting, Philadelphia, 2002.)

(*continued*)

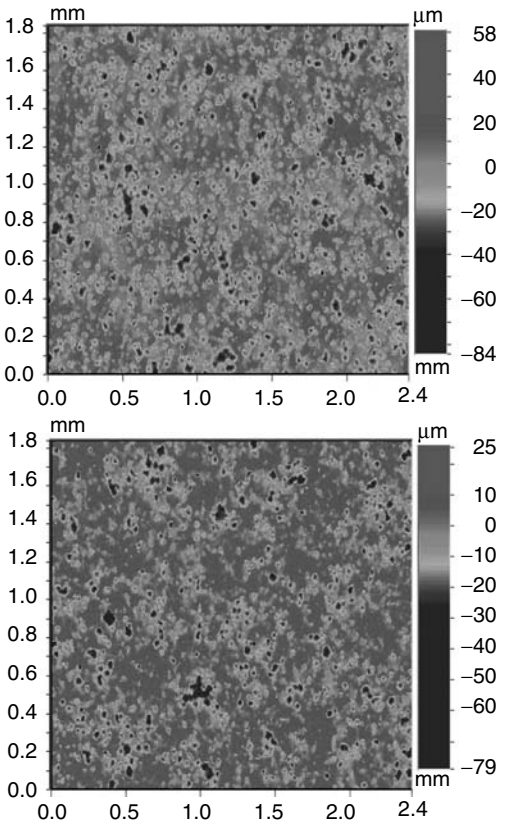


(c) Scanning interferometry image

**FIGURE 7.86 (continued)**

### 7.3.3.3 Improvement for New Pads

#### *7.3.3.3.1 Nonporous Pad*

Porous urethane pad shows a good CMP process performance. However, a variation of pad properties and process performance remains to be resolved as a result of the pore size variation and nonuniformity of pore distribution. Nonporous pad has benefits for more consistent physical properties, removal rate, planarity improvement, longer pad life, and lower defectivity, if the surface asperity is well controlled. OXP4000, a nonporous pad that was developed by Rohm and Haas Electronic Materials CMP, Inc. has an ability to control pad surface topography through conditioning. However, pad conditioning becomes more critical for obtaining a stable CMP performance. Nonporous pads also need to be grooved for proper slurry circulation and residue removal. Pad conditioning on the OXP4000 pad changes surface

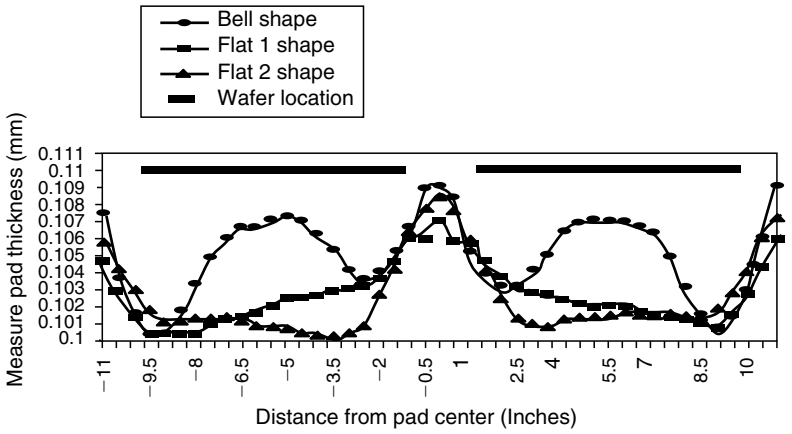


**FIGURE 7.87** Postpolish pad profile. (From Freeman, P., et al., Characterization of pad conditioning profiles in oxide chemical–mechanical polishing, CMP-MIC Conference, 57, 1996.)

roughness significantly [38]. Figure 7.88 shows the height distribution of the pad asperity. OXP4000 pad surface has a very narrow and sharp asperity height distribution, which indicates that the pad surface topography can be controlled more uniformly than IC1000. Three profiles correspond to the different conditioning modes of abrasion depth. In oxide CMP, the wafer planarizes

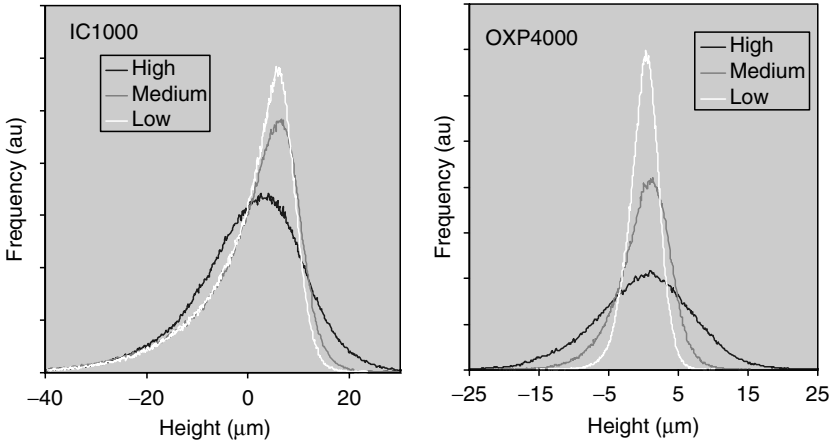


**FIGURE 7.88** Pad surface height distribution for porous and nonporous pads. (From Lawing, A.S., Polishing rate, pad surface, morphology and pad conditioning in oxide chemical mechanical polishing, I1-Fifth International Symposium on Chemical Mechanical Polishing (CMP), ECS 201st Meeting, Philadelphia, 2002.)

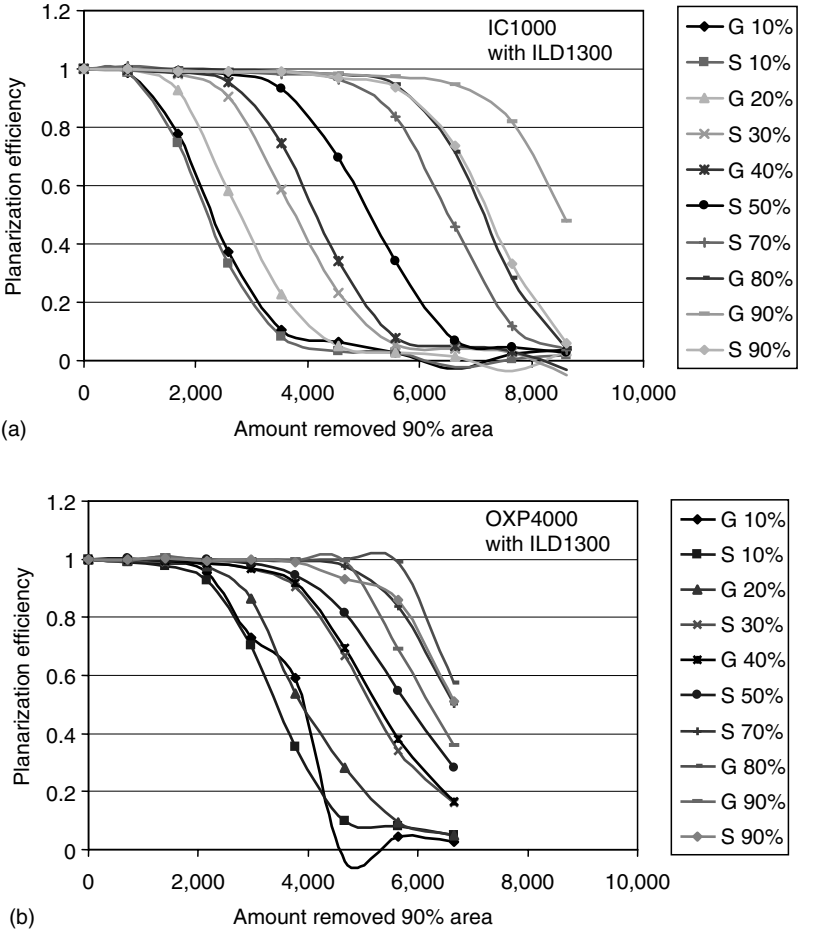


**FIGURE 7.89** Planarization efficiency of oxide CMP with different pads (a) IC1000 porous pad with ILD1300 slurry and (b) OXP4000 nonporous pad with ILD1300 slurry. (From Lawing, A.S., Polishing rate, pad surface, morphology and pad conditioning in oxide chemical mechanical polishing, I1-Fifth International Symposium on Chemical Mechanical Polishing [CMP], ECS 201st Meeting, Philadelphia, 2002.)

faster with OXP4000 than with IC1000 as shown in Figure 7.89. This facilitates the reduction of dishing and erosion for STI CMP application [39].

#### *7.3.3.3.2 Fixed Abrasive Pad*

A fixed abrasive pad is another challenge for CMP. Fixed abrasive pads have an enhanced mechanical removal property that results in a high selectivity for STI CMP. 3M developed the fixed abrasive technology for CMP. 3M's Slurry

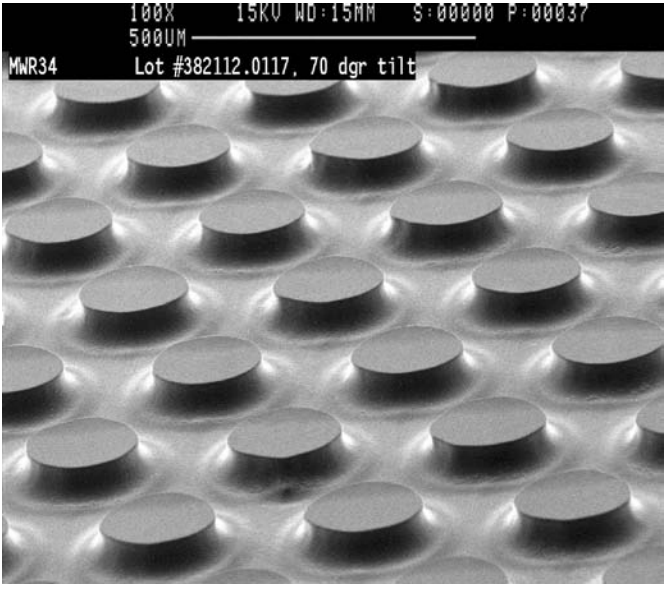


**FIGURE 7.90** Fixed abrasive pad. (Courtesy of 3M.)

Free (trademark) consists of precisely formed, structured abrasive features bonded to a polyester film backing. The micro-replicated poststructures are typically 200 μm in diameter and 40 μm high, spaced to a 10% bearing area. Each post contains submicron (average particle size is less than 0.5 μm) ceria particles evenly dispersed and captured within a toughened composite binder. The fixed abrasive materials are typically configured in a roll form for use on web-type CMP polisher. Subpad used with the 3M slurry-free fixed abrasive material typically consists of a rigid polycarbonate layer bonded to a more resilient foam or urethane-impregnated felt layer. Figure 7.90 shows a fixed abrasive pad [40]. The topographical selectivity is 200:1 and oxide to nitride selectivity is 1.2:1. Typical STI CMP performance is shown in Figure 7.91.

## 7.3.4 Modeling and Simulation of CMP Processes

*Masaharu Kinoshita*

### 7.3.4.1 Purpose of Modeling

Understanding the polishing mechanism of the CMP process greatly contributes to the topography prediction after planarization, the optimization of cost of consumables, the process optimization, and the improvement of wafer quality. CMP process modeling is broadly classified into three categories [41–52]:

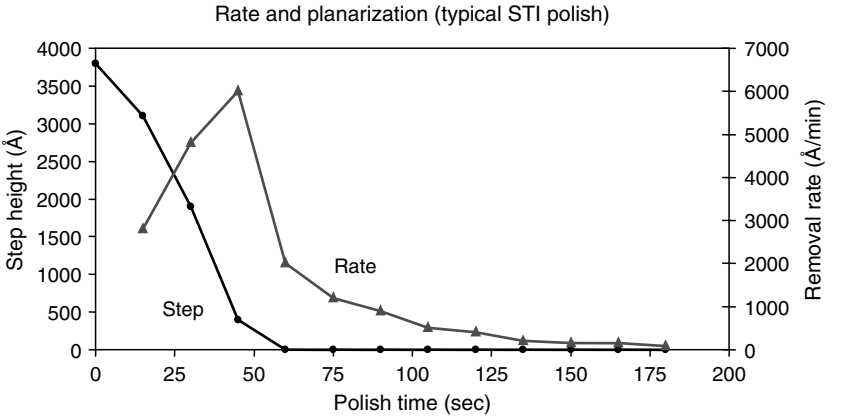


**FIGURE 7.91** Planarization by fixed abrasive pad (3M M3100). (From Gagliardi, J.J., et al., Total planarization of the MIT 961 Mask Set wafers coated with HDP oxide, CMP-MIC Conference, March 2000.)

1. Modeling of planarization process regarding to the surface topography and pattern density
2. Modeling of the effect of polishing pad physical properties on planarization
3. Modeling of the effect of slurry behaviors on planarization

The methodology for simulation is based on two types of models such as phenomenological and analytical. In the former, empirical equations for step height reduction are derived using experimental results for planarization of up and down feature patterns. The latter models are based on Preston's equation, in which polish removal rate is proportional to the product of the polishing pressure and relative speed to wafer; therefore, the distribution of polishing pressure is obtained from the elastic theory of the polishing pad and the fluid dynamics of the slurry. Both models consider that the CMP process involves the issue of mechanical force applied to the wafer surface.

### 7.3.4.2 Modeling of Planarization Process

#### *7.3.4.2.1 Hard Model*

It is known empirically that the up feature planarizes easier than down feature and lower density pattern also planarizes faster than dense pattern. Figure 7.92 shows the up and down features in pattern profile. In ILD CMP, empirical observation indicates that the planarization rate increases depending on feature size, such as the following:

Small up feature > large up feature > small down feature > large down feature

As a blanket wafer provides an ultimate surface of large up feature pattern, the polish rate of a blanket wafer is taken as a reference. Introducing an index $D_0$ to indicate pattern dependency, defined as $D_0 =$ (polish rate of

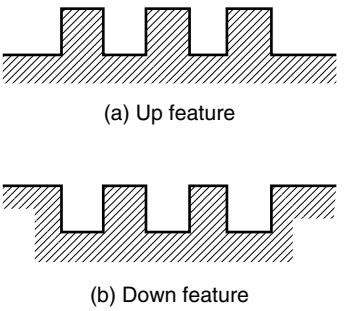


**FIGURE 7.92** Patterned wafer features (a) up feature and (b) down feature.

down feature)/(polish rate of a blanket wafer), planarization process can be described as follows: when $D_0$ is small, polishing of down feature patterns does not proceed, but selective polishing of up feature patterns advances. When $D_0$ approaches 1, planarization is completed and down feature patterns are polished similar to up feature patterns. Thus, according to CMP, ratio of up and down feature pattern areas varies. Experiments show that the polishing rate of down feature decreases linearly when $D_0 > 0.3$, and it logarithmically decreases when $D_0 < 0.3$ [42]. Figure 7.93 shows a step height reduction curve for $D_0 < 0.3$, which is expressed by an experimental equation as

$$S/S_0 = \exp[-(1 - D_0)Ut/S_0] \tag{7.1}$$

where $D$ is the polishing rate for down feature, $U$ is the polishing rate for up feature (constant), $S$ is the step height in the pattern, and $S_0$ is the initial step height related to $D_0$ [42].

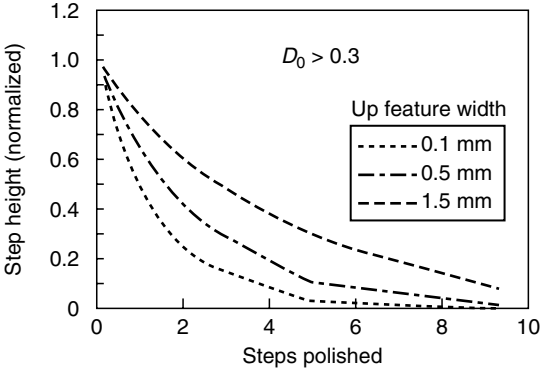


**FIGURE 7.93** Simulation of step height reduction rate for down feature pattern (normalized by initial step height as 0.6 μm). (From Burke, P.A., Semi-empirical modeling of $SiO_2$ chemical–mechanical polishing planarization. *Proceedings of the VMIC Conference*, pp. 379–389, 1991.)

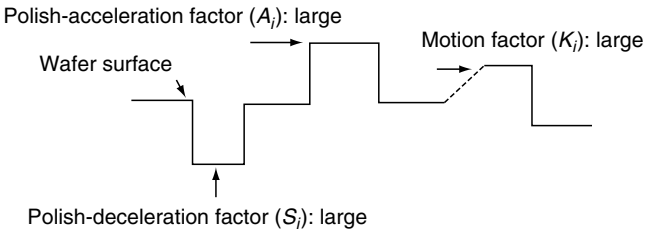


**FIGURE 7.94** Profiling factors for a variety of pattern features. (From Warnock, J., *J. Electrochem. Soc.*, 138(8), 2398, 1991.)

#### *7.3.4.2.2 Soft Model*

Assuming that a polishing pad is soft, the hard model can be extended to soft model by introducing the feature-dependent polish rate factors. By setting the polish-acceleration factor at up feature ($A_i$), the polish-deceleration factor at down feature ($S_i$), and the motion factor at slope ($K_i$) as shown in Figure 7.94, polish rate $R_i$ at each point on wafer is expressed as follows [43]:

$$R_i = K_i A_i S_i \geq 1 \tag{7.2}$$

Equation 7.2 indicates that $R_i$ increases with increasing $A_i$ at up feature, whereas $R_i$ decreases with increasing $S_i$ at down feature. The value of $K_i$ increases as the slope increases. Therefore, $R_i = K_i A_i / S_i = 1$ holds at a planar surface. Assuming that the polish rate is proportional to the polishing pressure, $A_i$ and $S_i$ have a reciprocal relationship at each point, and the following equation holds for $n$ points on the wafer:

$$\sum A_i / S_i = n \tag{7.3}$$

Meanwhile, if we designate $z_i$ as the height in the vertical direction at point $i$, the pad properties can be expressed using a logarithmic function as

$$S_i = \exp(\Delta z_i / z_o) \tag{7.4}$$

$$\Delta z_i = \sum z_i W_i \tag{7.5}$$

$$W_i = 1/\cosh(r_i / r_o) \tag{7.6}$$

where $W_i$ is a weighting function with respect to the scale in the horizontal direction, along which deformation of the pad is generated. As the polishing rate increases at large slopes, $K_i$ is obtained as follows, designating the slope angle to be $\alpha_i$:

$$K_i = 1 + K_0 \tan \alpha_i \tag{7.7}$$

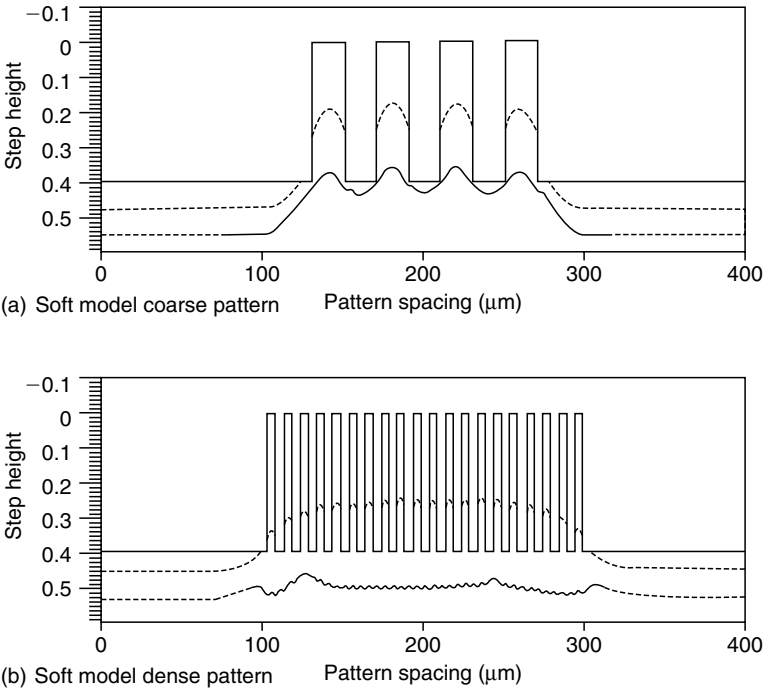


**FIGURE 7.95** Simulated topography by using soft model (SILVACO). (From Stine, B., Ouma, D., Divecha, R., Boning, D., Chung, J., Hetherington, D.L., Ali, I., Shinn, G., Clark, J., Nakagawa, O.S., and Oh, S.-Y., A closed-form analytic model for ILD thickness variation in CMP processes, *Proceedings of the CMP-MIC*, Santa Clara, pp. 1–8, 1997.)

Substituting Equation 7.3 through Equation 7.7 into Equation 7.2, numerical simulation for a soft model is possible.

Hard and soft models are phenomenological simulation methods, which are commercially available as simulation software ATHENA (Silvaco). Figure 7.95 shows examples of simulations.

#### *7.3.4.2.3 Model Using Pattern Density*

The contacting area between polishing pad and wafer varies during polishing because of the wafer topography change. For modeling a planarization process on wafer scale, pattern dependency on topography can be quantitatively expressed by using the interaction distance, *id,* and the planarization length [44]. Pattern density $\rho$ is defined as a rectangular area (density window) enclosed by interaction distances: $\rho =$ (area of the up features)/(area of the density window). In a region where two neighboring sections with different

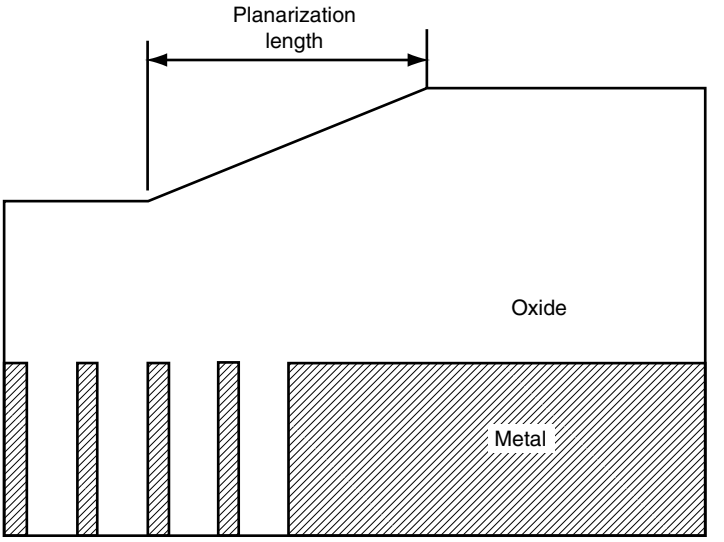


**FIGURE 7.96** Definition of planarization. (From Stine, B., Ouma, D., Divecha, R., Boning, D., Chung, J., Hetherington, D.L., Ali, I., Shihn, G., Clark, J., Nakagawa, O.S., and Oh, S.-Y., A closed-form analytic model for ILD thickness variation in CMP processes, *Proceedings of the CMP-MIC*, Santa Clara, pp. 1–8, 1997.)

pattern densities are present, the section with the smaller pattern density is polished faster; therefore, a slope is produced at the boundary of these sections due to height difference. The length of this slope is designated as the planarization length (Figure 7.96). For example, a density mask in which 25 pattern structures with different line and space ($L/S$) patterns are arranged at 2 mm square intervals as shown in Figure 7.97. The pattern density differs at each of the 25 pattern structures, because $L/S$ values are different. Meanwhile, the pattern density in the density window differs between the case in which the interaction distance, *id*, on the mask is set at 1 mm and the case in which the *id* is set at 10 mm. Because there is a correlation between pattern density and interaction distance, it is important to decide a value of the interaction distance in actual simulations. On the basis of experimentally obtained results of the relationship between the change in the film thickness of ILD films and pattern density, interaction distances of 3.2–3.5 mm are considered to be appropriate.

Using the above definition of pattern density, Preston's equation (Equation 7.8) can be rewritten as an equation in which surface topography is considered:

$$R = kPv \tag{7.8}$$

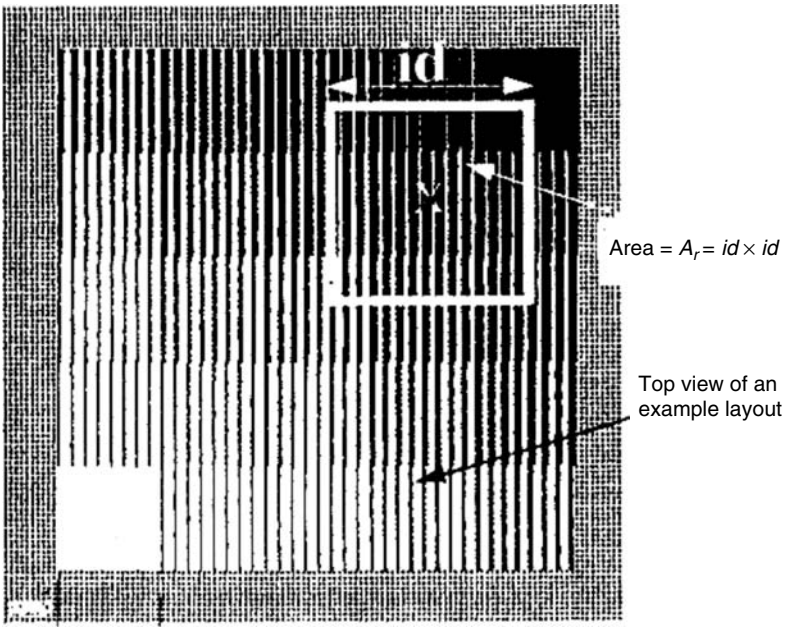


**FIGURE 7.97** Interaction distance and patterned mask. (From Stine, B., Ouma, D., Divecha, R., Boning, D., Chung, J., Hetherington, D.L., Ali, I., Shinn, G., Clark, J., Nakagawa, O.S., and Oh, S.-Y., A closed-form analytic model for ILD thickness variation in CMP processes, *Proceedings of the CMP-MIC*, Santa Clara, pp. 1–8, 1997.)

where $R$ is the polishing rate, $P$ is the polishing pressure, $v$ is the wafer relative velocity, and $k$ is the Preston coefficient. In this form of Preston's equation, substituting the polishing rate $R$ with the removal rate of ILD film $dz/dt$, and denoting the contact area between wafer and polishing pad in the density window as $A$ and the polishing force as $F$, Equation 7.8 can be rewritten as

$$dz/dt = kFv/(id)^2 \cdot \rho(x,y,z) \tag{7.9}$$

in which

$$P = F/A, \quad A = \rho(x,y,z)(id)^2 K = kFv/(id)^2 \tag{7.10}$$

then

$$dz/dt = K/\rho(x,y,z) \tag{7.11}$$

In this equation, $(id)^2$ is the area of the density window and $\rho(x,y,z)$ is the pattern density. The pattern density is a function of position $(x,y)$ inside

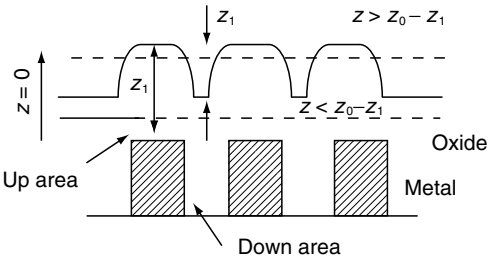


**FIGURE 7.98** Illustrated model of ILD. (From Stine, B., Ouma, D., Divecha, R., Boning, D., Chung, J., Hetherington, D.L., Ali, I., Shinn, G., Clark, J., Nakagawa, O.S., and Oh, S.-Y., A closed-form analytic model for ILD thickness variation in CMP processes, *Proceedings of the CMP-MIC*, Santa Clara, pp. 1–8, 1997.)

the wafer, as well as a function of the film thickness ($z$) (Figure 7.98). Therefore, by solving Equation 7.11 for each density window, it is possible to determine the pattern dependency in the wafer. In this equation, $K$ is the removal rate of a blanket wafer (flat-film wafer with a pattern density of 100%).

The surface topography of oxide films is determined by factors such as deposition conditions, line, and space of IC pattern. We assume the following conditions concerning the pattern density and polishing rate:

- $\rho(x,y,z) = \rho_0(x,y)$ $z > z_0 - z_1$ up to the removal of step height
  $1$ $z < z_0 - z_1$ after the removal of step height

In this equation, $z_0$ is the initial thickness of oxide film, $z_1$ is the initial step height.

- Polishing rate of down feature $\ll$ polishing rate of up feature

As a result of this assumption, the step height reduction process, i.e., planarization, is expressed by the following two equations. When only the up features are removed, i.e., $Kt < \rho_0(x,y)z_1$

$$z = z_0 - [Kt/\rho_0(x,y)] \tag{7.12}$$

After the up features are removed, i.e., $Kt > \rho_0(x,y)z_1$

$$z = z_0 - z_1 - Kt + \rho_0(x,y)z_1 \tag{7.13}$$

When initial step height is removed, the entire surface is in contact with polishing pad. At this point, the pattern density is increased by an amount associated with the down features, and therefore the polishing pressure is decreased, resulting in a decrease in the polishing rate.

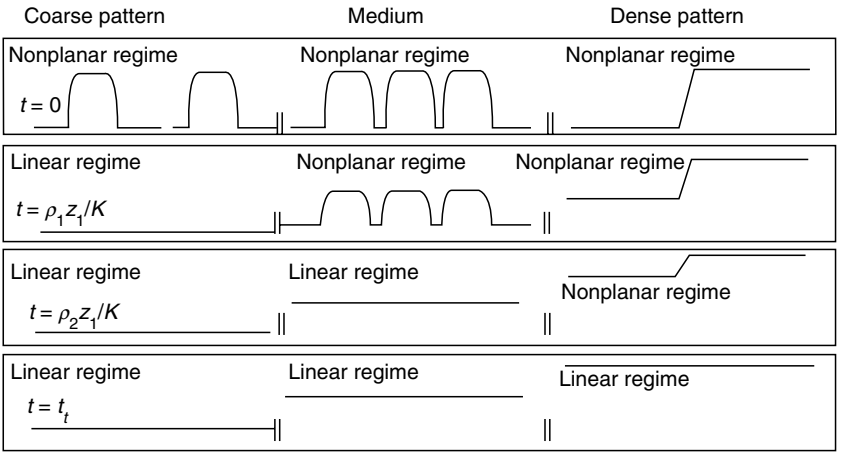


**FIGURE 7.99** Simulation of polish time dependent topography on pattern density for ILD. (From Stine, B., Ouma, D., Divecha, R., Boning, D., Chung, J., Hetherington, D.L., Ali, I., Shinn, G., Clark, J., Nakagawa, O.S., and Oh, S.-Y., A closed-form analytic model for ILD thickness variation in CMP processes, *Proceedings of the CMP-MIC*, Santa Clara, pp. 1–8, 1997.)

Using this model, the final state of planarization in which sparse, intermediate, and dense pattern densities are present in a mixed state can be well explained. Namely, as shown in Figure 7.99, initial step height with sparse patterns is removed at an earlier stage and local planarization advances; when in regions with dense patterns, initial step height reduction advances gradually and progress of planarization is slow. Regions with intermediate-density patterns are in between these two cases. As a result, a slope is produced at the boundary of the three patterns by the height differences.

Figure 7.100 and Figure 7.101 show examples of simulation results. These figures demonstrate well that the residual thickness of the ILD film differs depending on the pattern density. However, with this model, simulation results do not agree well with experimental results when pattern densities are 15% or lower.

#### *7.3.4.2.4 Model of Local Topography in Cu-CMP*

In Cu-CMP, modeling of local planarization including dishing and erosion is required. The difference in the polishing rate between Cu, barrier metal, and oxide film, as well as the selectivity should be considered. Cu-CMP process in which a damascene structure interconnection is formed consists of three-step polishing.

In the first step, Cu overburden layer is polished and Cu surface topography is rapidly planarized.

In the second step, residual Cu and the barrier metal layer are removed. During this process, the polishing rate selectivity of Cu or barrier metal

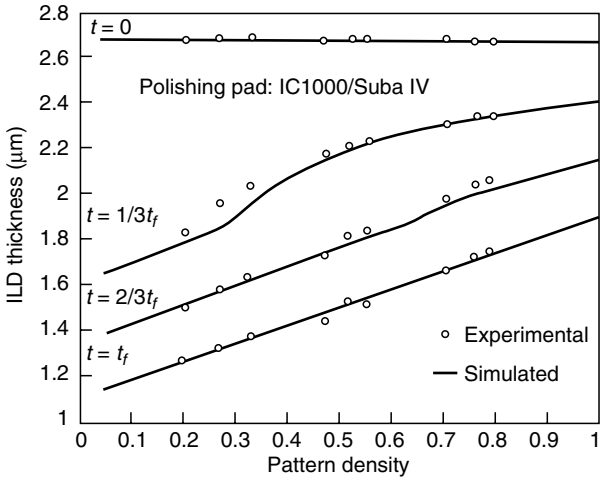


**FIGURE 7.100** Simulation of pattern density vs. ILD thickness (μm).

is made close to 1, so that dishing in the Cu interconnection line should be kept minimal.

In the third step, the overpolishing can afford a topography correction, so that uniformity in the entire wafer surface is achieved. As the interlayer oxide film is removed during this process, thinning and erosion should be suppressed as much as possible.

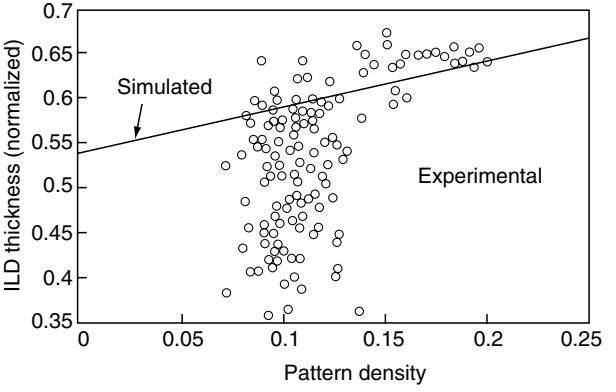


**FIGURE 7.101** Simulation of pattern density versus ILD thickness (normalized). (From Stine, B., Ouma, D., Divecha, R., Boning, D., Chung, J., Hetherington, D.L., Ali, I., Shinn, G., Clark, J., Nakagawa, O.S., and Oh, S.-Y., A closed-form analytic model for ILD thickness variation in CMP processes, *Proceedings of the CMP-MIC*, Santa Clara, pp. 1–8, 1997.)

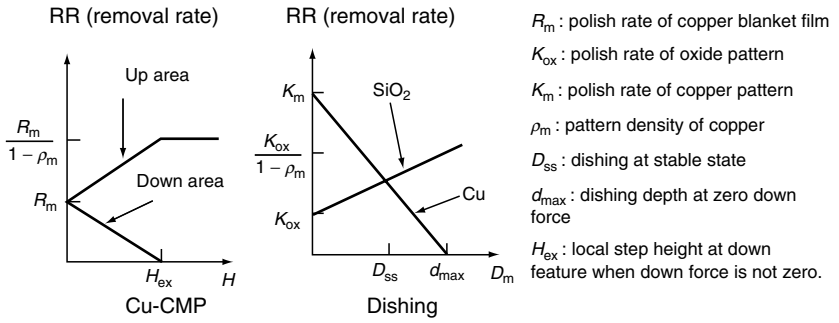


**FIGURE 7.102** Diagram of polish rate for Cu-CMP. (From Tugbawa, T. and et al., A mathematical model of pattern dependencies in copper CMP processes, *Electrochem. Soc* Honolulu Meeting, 1999.)

Diagrams showing the polishing rate at each step of Cu-CMP are depicted in Figure 7.102 [45]. A mathematical model of the dishing of Cu and erosion of oxide film is obtained using these diagrams, as

$$D_m = d_0 \cdot \exp[(t_c - t)/\tau_3] + D_{ss}\{1 - \exp[(t_c - t)/\tau_3]\} \tag{7.14}$$

$$E_{ox} = K_{ox}[1 + D_{ss}\rho_m/d_{max}(1 - \rho_m)](t - t_c) + [K_{ox}(D_{ss} - d_0)\rho_m/d_{max}(1 - \rho_m)/\tau_3]\,[\exp(t_c - t)/\tau_3 - 1] \tag{7.15}$$

In this equation, $t_c$ is the time required to reach the barrier metal and remove it, $\tau_3$ is the time constant, $d_0$ is the depth of dishing at the final period of the second step, and $\rho_m$ is the pattern density of Cu. Figure 7.103 shows simulation results of dishing and erosion.

To model the chemical etching processes observed in Cu-CMP polishing, we should not treat the Preston coefficient as a constant, but should rather divide the coefficient into one in which chemical reactions are incorporated based on findings regarding activation energy and chemical reaction theory.

### 7.3.4.3 Modeling of the Polishing Pad and Planarization

The basic characteristic of material removal in CMP assumes to follow the Preston's equation (Equation 7.8), where all physical factors in CMP are included in the Preston coefficient $k$. If we assume that Preston's equation holds at any point on a wafer, all we need to know is $k$, $P$, and $v$ at each point. During steady CMP process in which $k$ and $v$ are assumed to be constant, simulation of planarization process can be done by obtaining the distribution of the contact pressure between the polishing pad and wafer and also by assuming these values at each point. Either the finite element method (FEM) or boundary element method (BEM) is used for the simulation.

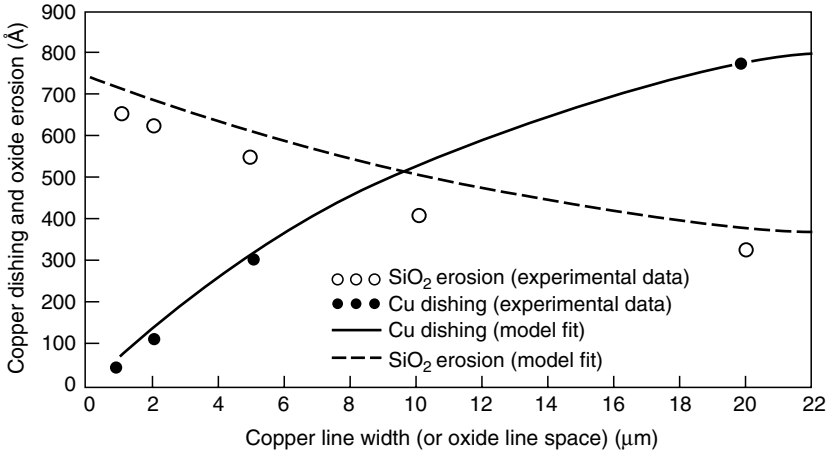


**FIGURE 7.103** Simulation results of dishing and erosion for Cu-CMP.

#### *7.3.4.3.1 Distribution of Contact Pressure between Polishing Pad and Wafer*

Assuming that a polishing pad is a perfect elastic body and that a wafer is in contact with the polishing pad by down force, the stress distribution on the wafer surface can be analyzed by a plain strain model [53]. The contact pressure rapidly increases at the wafer edge. Designating the Poisson ratio and the shear coefficient of a polishing pad as $v$ and $\mu$, respectively, when the pressure distribution (as shown in Figure 7.104) is uniform with respect to $\mu$ of the polishing pad, the pressure distribution also shows a complex behavior with respect to $v$. When $v$ exceeds a certain value, the pressure distribution at the center of the wafer becomes higher than that at the edge. In addition, designating the thickness of the polishing pad as $h$ and wafer radius as $r_0$, the pressure at the center of the wafer becomes high when the normalized value of $H\ (=h/r_0)$ is less than 1 ($H<1$). Therefore, to achieve uniform planarization, it is necessary to use a polishing pad with small $n$ and large $H$.

#### *7.3.4.3.2 Deformation of Pad, and Dishing and Erosion*

##### *7.3.4.3.2.1 Bending Deformation*

Bending deformation of a polishing pad is obtained from the equation of deflection for beams subjected to a uniform load:

$$y = wL^3/384EI = 5wL^4/32Et^3 \tag{7.16}$$

In this equation, $w$ is the load per unit length of the trench width, $L$ is the trench width, $E$ is Young's modulus of the pad, and $I$ is the polar moment of inertia of an area which is obtained as $t^3L/12$ where $t$ is the pad thickness.

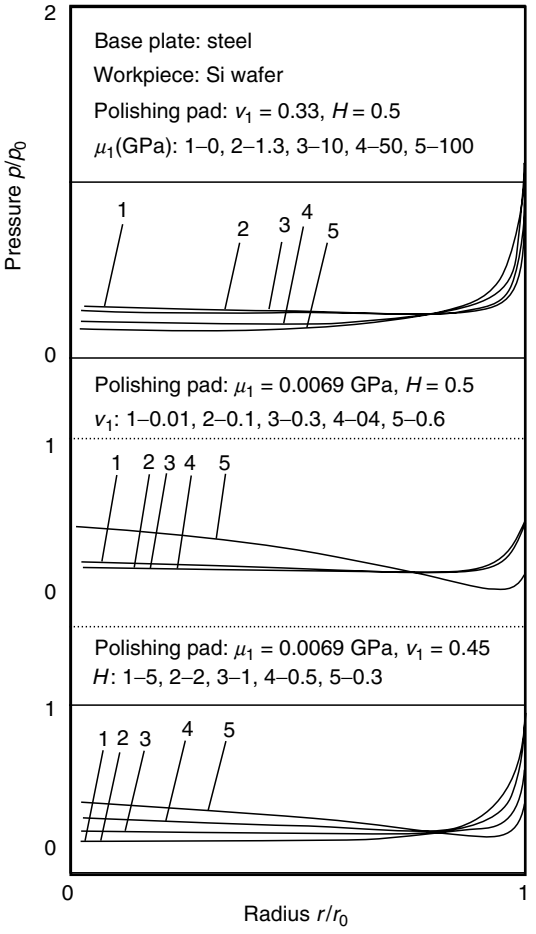


**FIGURE 7.104** Contact pressure of distribution on pad. (From Yang, L., *Solid State Technol.,* 111, 2000.)

Dishing can result from pad bending deformation during polishing; however, actual amounts of dishing are much smaller than this value [46]. Therefore, the simulation can be done by considering a compression of the effective surface thickness ($t' < t$), instead of using the pad total thickness, and a dishing is evaluated. For evaluating erosion, the reduced Young's modulus ($E' < E$) is used by considering the surface roughness. Accordingly, in actual simulations, $t'$ and $E'$ are determined by combining experimental results. These values do not express true material properties, but provide their equivalent values. To perform analytical simulations, deformation behavior of polishing pads should be considered using other methods, and the thickness

and the value of Young's modulus of the section that truly contributes to the deformation should be determined.

*7.3.4.3.2.2 Conformity of Polishing Pad to Surface Topography*

Conformity of the polishing pad to the pattern profile is another important factor to determine the planarization process. With regard to the trench pattern dimension to pad elasticity, the following three cases can be considered:

1. $w \leq w_0$: trench width is sufficiently narrow and the polishing pad does not deform. The step height reduction rate is expressed as the polishing rate at up feature.
2. $w_0 < w \leq w_m$: the polishing pad shows a sufficient compression characteristic as well as partial conformity. Namely, contact occurs in accordance with the trench profile, depending on its size.
3. $w_m \leq w$: the polishing pad shows a sufficient compression characteristic and conformity; both up and down features are identically polished and step height is not reduced.

By setting parameters for Cu trenches as shown in Figure 7.105, equations of planarization are derived for the above three cases [47]. The basic equation of step height reduction rate is obtained from the difference in the polishing rate between up and down features in Preston's equation, which is expressed as

$$dh_s/dt = R_1 - R_h = k_{cu}E(H_1 + \Delta H)v/H - K_{cu}EH_h v/H \tag{7.17}$$

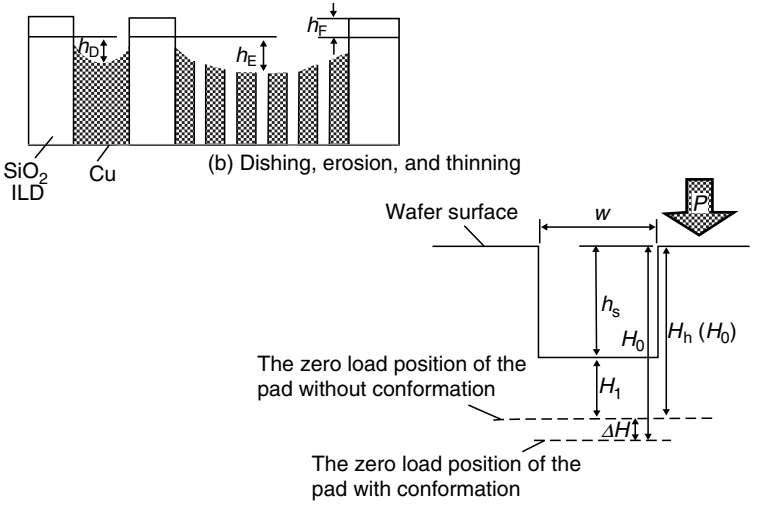


**FIGURE 7.105** Modeling parameters for Cu-CMP. (From Yang, L., *Solid State Technol.*, 111, 2000.)

where $R_l$ and $R_h$ are the polishing rates at down and up features, respectively,$k_{Cu}$ is the Preston coefficient of Cu, $E$ is Young's modulus, $H$ is the pad thickness, $H_l$ is the compression depth at concave feature of the pad, and $H_h$ is the compression depth at convex feature of the pad. $\Delta H$ is the increment of the compression depth of the pad when conformity of the polishing pad is taken into consideration; this value varies depending on the size of the pattern width. Therefore, we assume that the following relationship:

$$dH_0'/H_0 = \xi dw/w \tag{7.18}$$

holds. In this equation, $\xi$ is the material property constant, which represents conformity of the polishing pad. For $w_1 < w \leq w_m$, the following equation is derived from Equation 7.18 as a planarization model of Cu:

$$h_s = h_{so}\exp(-k_c v/H)t + (PH/E)[\xi \ln(w/w_o) - 1]\,[1 - \exp(k_{cu}Ev/H)t] \tag{7.19}$$

where $h_{so}$ is the initial height difference.

Model equations for dishing and erosion are derived based on the above-described concept using the difference in the polishing rate. Cu dishing can be described using the polishing rate difference between barrier metal and Cu as

$$dh_D/dt = R_{BM} - R_{cu} = k_{BM}E(H_{BM}/H)v - k_{cu}E(H_{cu}/H)v \tag{7.20}$$

Designating the selectivity of polishing rate between Cu and barrier metal as $S$, we obtain

$$S = R_{cu}/R_{BM} = k_{cu}/k_{BM} \tag{7.21}$$

A dishing model in which conformity of the polishing pad is taken into consideration is obtained as

$$h_D = [(S-1)/S](PH/E)\xi \ln(w/w_o)[1 - \exp(-k_{cu}Ev/H)t] \tag{7.22}$$

When overpolishing is performed, the erosion of the oxide film is obtained using differences in the polishing rate between dense pattern and no pattern regions. Designating $\eta$ as pattern density, the erosion is given as

$$h_e = \eta\rho(PH/E)\xi \ln(w/w_o)\{1 - \exp[-k_{ox}Evt/H(1-\eta\rho)]\} \tag{7.23}$$

where $w$ is the width of the trench array where erosion occurs. Figure 7.106 and Figure 7.107 show simulation results. Table 7.15 lists the process parameters used for the simulation.

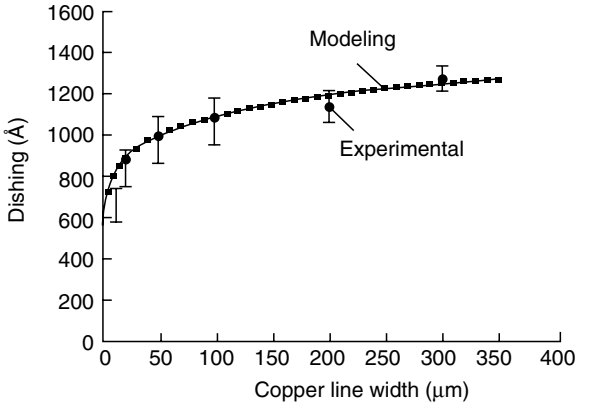


**FIGURE 7.106** Dishing simulation of copper line width. (From Yang, L., *Solid State Technol.*, 111, 2000.)

*7.3.4.3.2.3 Simulation Using a Solo Pad and a Stacked Pad*

If the polishing pad is a perfectly elastic body and is subject to down force ($P$), the polishing pad displacement ($w$) parallel to thickness can be obtained from the theory of an elastic body as

$$w = Pf(r) \tag{7.24}$$

The term $f(r)$ is a function with respect to the distance $r$ from the point force. In the case of solo pad, $f(r)$ is obtained as a Boussinesq solution, designating

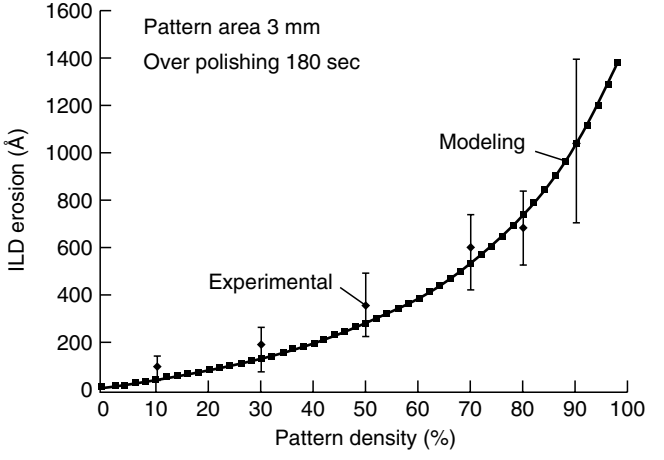


**FIGURE 7.107** ILD erosion simulation.

**TABLE 7.15**
**Process Parameter Values for CMP Process Modeling**

| Parameter | Value |
|---|---|
| Copper Preston coeffiicient ($K_{cu}$) | $4.65 \times 10^{-13}$ (step 1/slurry 1) $Pa^{-1}$ |
| | $1.94 \times 10^{-13}$ (step 2/slurry 2) $Pa^{-1}$ |
| Oxide Preston coefficient | $1.94 \times 10^{-14}$ (step 2/slurry 2) $Pa^{-1}$ |
| Polish pressure ($P$) | $3.45 \times 10^{4}$ (step 1/slurry 1) Pa |
| | $1.03 \times 10^{4}$ (step 2/slurry 2) Pa |
| Linear velocity ($V$) | 0.146 (step 2/slurry 2) m/sec |
| | 0.831 (step 2/slurry 2) m/sec |
| Pad thickness ($H$) | $1.27 \times 10^{-13}$ m |
| Pad Young's modulus ($E$) | $1 \times 10^{8}$ Pa |
| Pad conformity ($\xi$) | 0.11 |
| Effective minimum linewidth ($W_o$) | 0.01 μm |
| Polish rate selectivity ($S$) | 12 (Cu/Ta) (step 2/slurry 2) |
| | 10 ($Cu/Sio_2$) (step 2/slurry 2) |
| Copper film thickness ($I$) | 10,000 Å |

Young's modulus and Poisson ratio of the polishing pad as $E$ and $\nu$, respectively; $f(r)$ is expressed as

$$f(r) = (1 - v^2)/\pi Er \tag{7.25}$$

In the case of stacked pad, $f(r)$ can be obtained as a sum of $f_1$ and $f_2$; $f_1$ can be described as a Boussinesq solution and $f_2$ can be described as a Herz solution. Namely, the following equation is obtained:

$$f(r) = f_1(r) + f_2(r) \tag{7.26}$$

where

$$f_1(r) = (1 - v^2)/\pi Er \tag{7.27}$$

$$f_2(r) = -(1^2/2\pi D)kei(r/1) \tag{7.28}$$

$$D = E_1/t_1^3/12(1 - v^2) \tag{7.29}$$

$$1 = \sqrt[4]{(Dt_2/E_2)} \tag{7.30}$$

The term $kei$ is a Bessel function, $E_1$ and $E_2$ are Young's modulus at the top and bottom layers of the polishing pad, and $t_1$ and $t_2$ are their corresponding thicknesses.

With respect to up and down features and contact conditions of a polishing pad, a reference plane and reference pressure with respect to the load

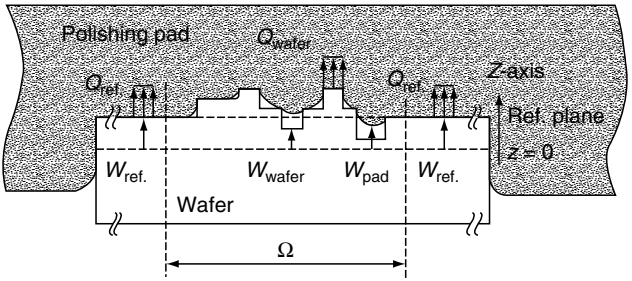


**FIGURE 7.108** Model for CMP simulation. (From Yoshida, T. Three-dimensional chemical-mechanical polishing process model by BEM. *The Electro. Soc.*, Honolulu Meeting, 1999.)

applied to the plane are set, as shown in Figure 7.108. The reference plane is taken on a flat-film section, which includes the convex and concave patterns, and the reference pressure is selected so that the pressure at this reference plane becomes zero. Boundary conditions of boundary elements are determined as displacements relative to the reference plane as well as pressure differences relative to the reference pressure, and the final polishing pressure, $Q_{i,wafer}$, is determined. The polishing rate is obtained by substituting this final polishing pressure into Preston's equation, and a three-dimensional pattern simulation is performed for the CMP using a solo polishing pad. As shown in Figure 7.109, differences in the step height reduction rates for patterns from 0.2 to 4 mm are shown [48,49].

### 7.3.4.4 Modeling of Slurry Behavior

The relationship between polishing rate and relative speed of wafer in CMP resembles the Stribeck curve, which is well known in the theory of fluid bearing [50]. With the Stribeck curve, as the Hersey number ( = viscosity × velocity/pressure) increases, the state changes from boundary lubrication to mixture lubrication and then to fluid-dynamic lubrication (Figure 7.110).

#### *7.3.4.4.1 Pressure from the Fluid and Polishing Rate*

When the slurry is assumed to be a Newtonian fluid with constant viscosity, the fluid flow between a polishing pad and a wafer can be described by the three-dimensional Navier–Stokes equations as

$$\mathbf{u} \cdot \nabla \mathbf{u} = -(1/\rho) \cdot \nabla p + \mu/\rho \cdot \nabla^2 \mathbf{u} \tag{7.31}$$

$$\mathbf{u} = 0 \tag{7.32}$$

where $\rho$ is the fluid density, $\mu$ is the dynamic viscosity, $p$ is the pressure, and $\mathbf{u}$ is the velocity vector at an arbitrary position in the fluid. Here the

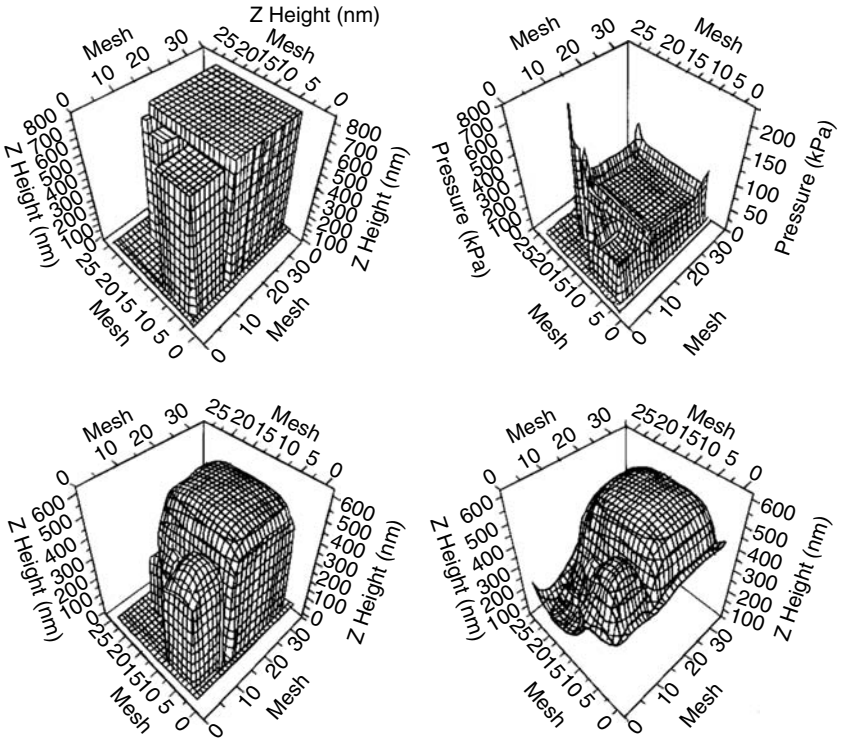


**FIGURE 7.109** Three dimensionality of oxide pattern. (From Yoshida, T. Three-dimensional chemical mechanical-polishing process model by BEM. *The Electrochemical Society*, Honolulu Meeting, 1999.)

two-dimensional pattern shape and boundary conditions shown in Figure 7.111 are considered. The surface stress $\sigma$ is related to the flow field by

$$\sigma_{ij} = -p\delta_{ij} + \mu(\partial_{ui}/\partial_{xi} + \partial_{uj}/\partial_{xj}) \tag{7.33}$$

where $\sigma_{ij}$ is Kronecker's delta, $\sigma_{11}$ and $\sigma_{22}$ are the vertical stresses in the $x_1$ and $x_2$ directions, respectively, and $\sigma_{12} = \sigma_{21}$ represent shear stress in the $x_1$ and $x_2$ directions, respectively. Assuming that removal is continuously performed with an infinitesimal unit, the removal speed in the direction perpendicular to the surface is expressed as a function of vertical pressure $\sigma$ and shear stress $\tau$ applied to the wafer.

$$R_n = f[\tau(t), \sigma(t)] \tag{7.34}$$

By integrating the above equation with respect to time and using the finite element method, a pattern shape at arbitrary time can be obtained.

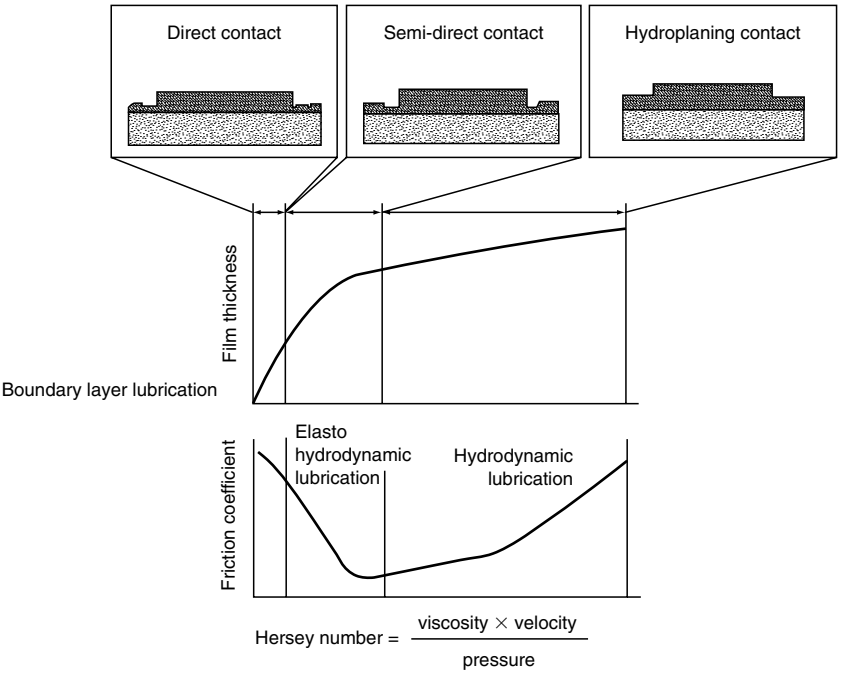


**FIGURE 7.110** Stribeck curve.

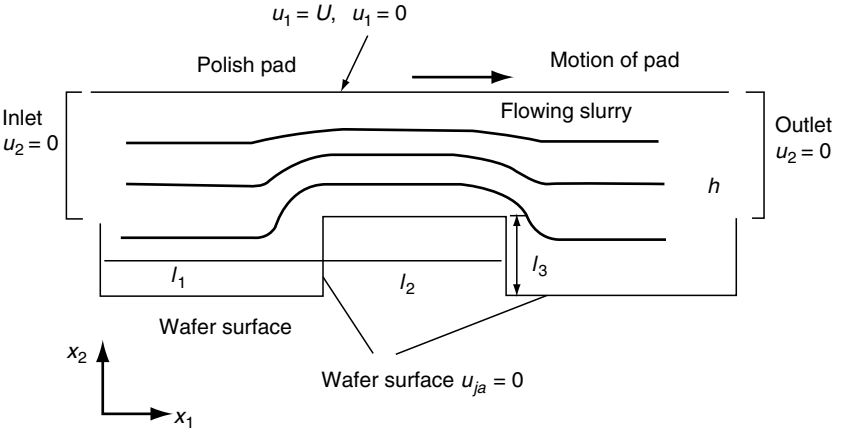


**FIGURE 7.111** Boundary conditions for hydrodynamic analysis. (From Runnels, S.R. and Eyman L.M., *J. Electrochem. Soc.*, 141(6), 1698, 1994.)

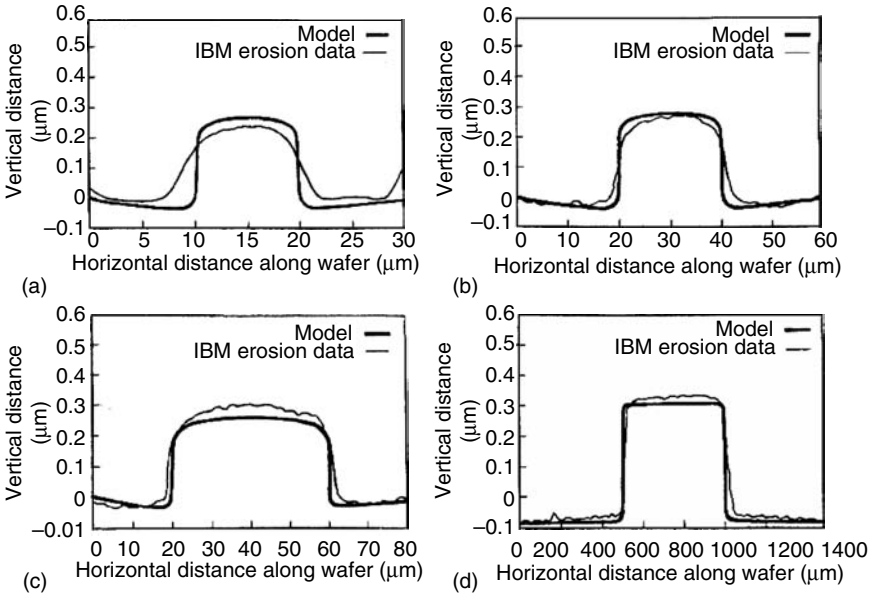


**FIGURE 7.112** Removal, based on slurry flow shear force. (From Runnels, S.R. and Eyman L.M., *J. Electrochem. Soc.*, 141(6), 1698, 1994.)

As a model of the function $f$, Runnels [51,52] used the following Tayler series expansion equation:

$$R_n = \mathbf{a}\sigma(\tau + \mathbf{b}\tau^2) \tag{7.35}$$

where **a** is the effect of a material property, i.e., mechanical removal reaction due to flow, and **b** is the effect of a chemical property, i.e., a constant that represents the etching reaction. Assuming that the vertical stress due to the fluid is almost constant over the pattern-shape surface, simulation is performed by replacing this vertical stress with the stress applied to the wafer. Figure 7.112 shows the comparison between results of this model and experimental data. The effectiveness of the model is confirmed for the pattern shape of size 10 μm or larger. Figure 7.113 shows the planarization rate when the thickness of the slurry fluid layer is used as a parameter. Planarization rate increases as the fluid-layer thickness decreases. Here, fluid with a Reynolds number of 0.1 or less is assumed.

#### *7.3.4.4.2 Behavior of Abrasive Particles in Slurry*

To understand the mechanical aspects of CMP, it is essential to obtain the behavior of abrasive particles in slurry. Luo [54] produced a model for the problem of solid contact among a polishing pad, abrasive particles, and wafer. In his model, surface roughness of the polishing pad is replaced by a periodic

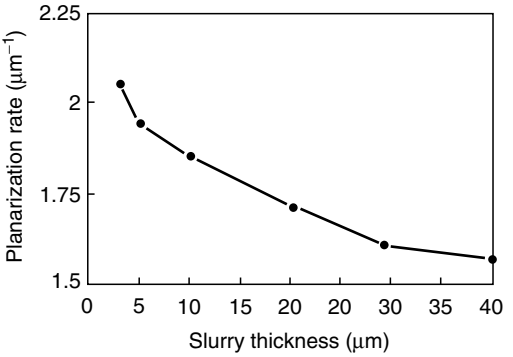


**FIGURE 7.113** Planarization rate dependent on slurry of thickness (simulated by Equation 7.36).

function, the average number of reacting abrasive particles is obtained using the material-removal volume due to single-grain abrasive grains, and particle-size distribution is taken into consideration.

Philipossian [55] obtained the relationship between abrasive particle size and the Stokes number in slurry. The Stokes number is obtained using the particle density in the slurry $\rho_p$, average coagulation diameter of grains $D$, relative speed between pad and wafer $u$, viscosity of slurry $m$, and fluid length (cross-sectional area or diameter of groove) of the groove of the polishing pad $L$ as

$$S_t = \rho_p D_2 u/\mu L \tag{7.36}$$

where a fluid with a Reynolds number of 0.1 or less is assumed. Figure 7.114 shows Stokes numbers of various types of slurry. In the case of abrasive grains with a grain size of 2–3 μm or less, $S_t < 0.1$ holds, indicating that the abrasive grains move in accordance with the flow of the fluid.

#### *7.3.4.4.3 Slurry Flow between Wafer and Pad*

Polishing removal rate and uniformity depend on the slurry flow between wafer and pad. Slurry starvation under the wafer causes aheat generation and a deterioration of uniformity. G. Muldowney made a detailed numerical modeling of the slurry flow between wafer and polishing pad. In order to describe the pad surface asperity and slurry flow channel he defined three factors such as flow height, characteristic length and void fraction among asperity heights and modeled the heat and mass transport of slurry. The transient slurry mixing dynamics has shown the infusion of fresh slurry and the slurry backflow induced by the wafer rotation. The pad conditioning affects a lot pad texture and fine texture gives a favorable slurry flow compared to coarse texture as shown in Figure 7.115 [56–58].

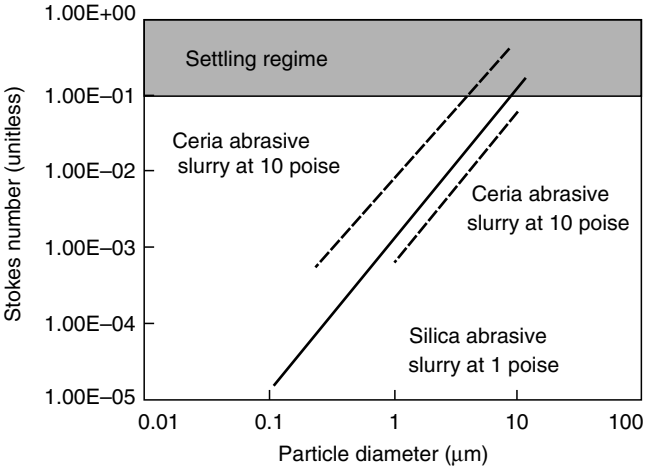


**FIGURE 7.114** Stokes number and abrasive particle size (pad groove 500 μm wide, 300 μm dap, slurry flow rate 0.44/msec). (From Philipossion, A., Selected process consumable technology requirements for advanced CMP process, the CMP Technical Meeting, San Francisco, 2000.)

## 7.4 THE STUDY CASE OF DEVICE WAFER

*KEISUKE SUZUKI*

The first application of CMP to the fabrication of semiconductor devices was the planarization of steps present in interconnects. As the CMP has planarizing properties that cannot be achieved by conventional methods, it has been

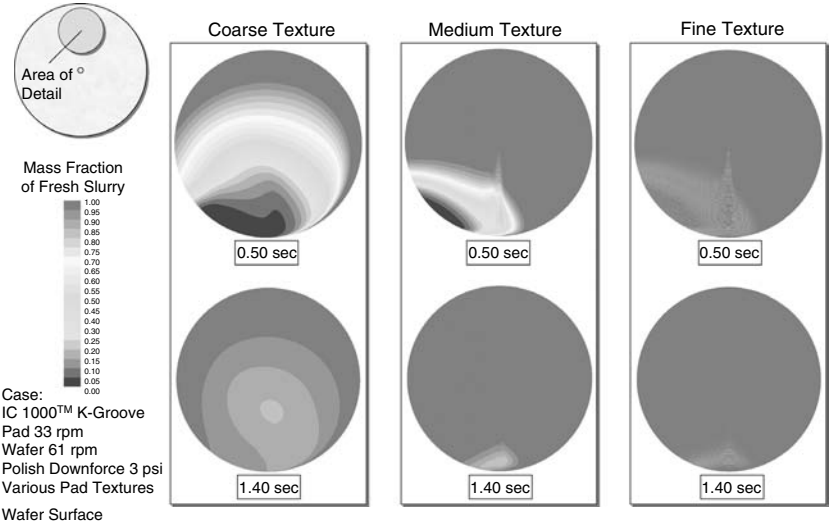


**FIGURE 7.115** Effect of pad texture on transient slurry mixing.

diffused as the innovative method of planarization rapidly. Concurrent with the shrinkage of transistors and interconnects to realize higher frequency and large storage of the devices, new materials such as Cu and low-$k$ materials have been adopted. At the same time, other than the relaxation of steps, CMP has been applied to these new materials with improvements of polishing systems and abrasive materials (slurry and pads). This section introduces the transition of CMP technology for the fabrications of semiconductor devices, and describes its future perspectives.

### 7.4.1 Introduction of CMP Technology

CMP technology was introduced by IBM and Intel in the late 1980s as a technique for planarizing ILD films. Before that, the prevailing methods for planarizing ILD films had been spin-on-glass (SOG) coating method [59] and the reflow of BPSG [60] as shown in Figure 7.116. However, as high-level flatness has been required as the feature size of integrated circuit shrinking down to sub-0.35 μm, these methods have fallen into disuse. Consequently, the newly introduced technique is CMP. The conventional methods were limited to an irregularity of 100 nm even in a fine pattern of 10 μm or below, which was easy to planarize. Also, the use of

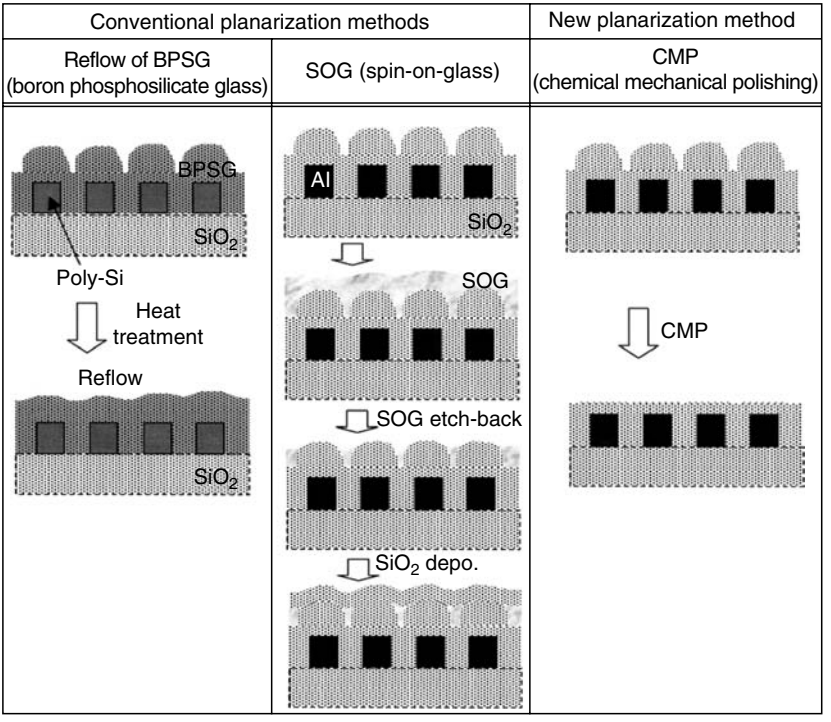


**FIGURE 7.116** The methods for planarizing ILD films.

CMP enables planarization to 20 nm or below even over a wide area of approximately 2 mm, and a high planarity can be secured.

Figure 7.117 shows the cross sections of chips with and without CMP processing [61]. When CMP processing is performed, wirings are arranged in

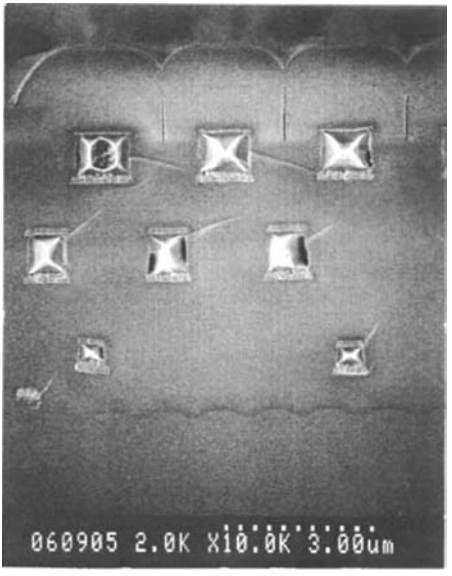


(a) With CMP

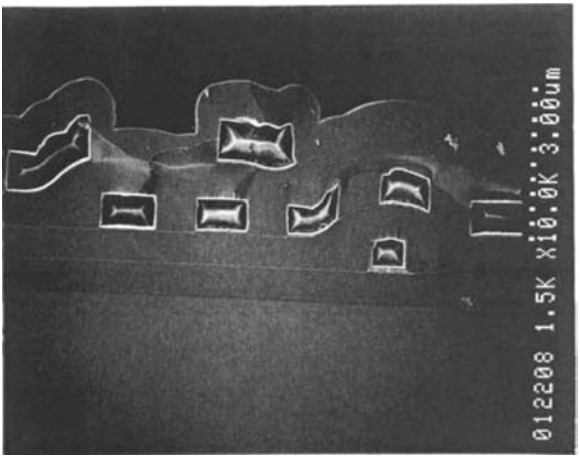


(b) Without CMP

**FIGURE 7.117** The cross-sectional SEM photographs of chips (a) with and (b) without CMP. (From Keüchi Kimura, Doctoral thesis of Osaka University, 31, 2002.)

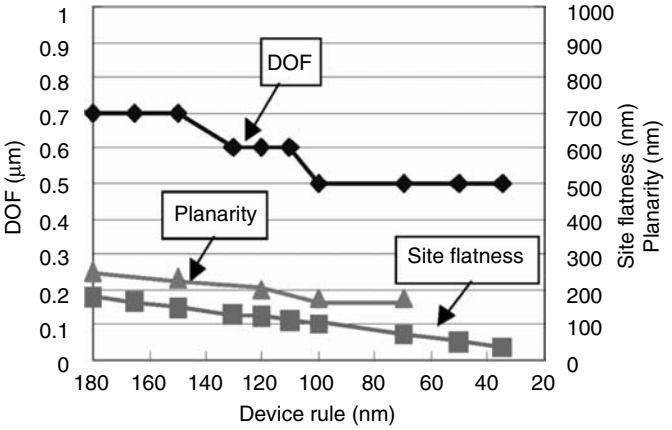


**FIGURE 7.118** The DOF, and the allowance of planarity and site flatness in each generation. (From International Technology Roadmap for Semiconductor, 1998.)

an orderly fashion. When no CMP processing is performed, a number of steps exist in interconnects. If the steps on wirings are larger than the DOF of lithography, defocusing occurs. Therefore, the steps on the devices must be smaller than the DOF in lithography [62]. Figure 7.118 shows the DOF, step relaxing properties, and the allowance of planarity and site flatness in each generation [63]. The DOF and the NA in lithography are determined by the wavelength of the light source. This relationship is, as Equation 7.37 shows, that the shorter the wavelength of the light source used in lithography, the smaller is the DOF. On the other hand, the reduction of the light source wavelength improves the resolution, from the relationship of Equation 7.38. This resolution determines the minimum dimension of transistors and interconnects patterns. Therefore, to realize the miniaturized patterns of the devices, there are no ways other than eventually making the steps present in the devices equal to or smaller than the DOF.

$$R = K_1(\lambda/\mathrm{NA}) \tag{7.37}$$

$$\mathrm{DOF} = K_2(\lambda/\mathrm{NA}^2) \tag{7.38}$$

where $R$ is the resolution, DOF the depth of focus, NA the numerical aperture of the lens, and $K_1$ and $K_2$ are process constants ($K_1$: 0.6–0.7, $K_2$: $\pm 0.5$).

### 7.4.2 History of CMP Technology

Presently, the applications of CMP technology are not only for the planarization of interlayer films but also for the STI, the formation of W contacts and Cu interconnects [64–66]. This is because the structures of devices

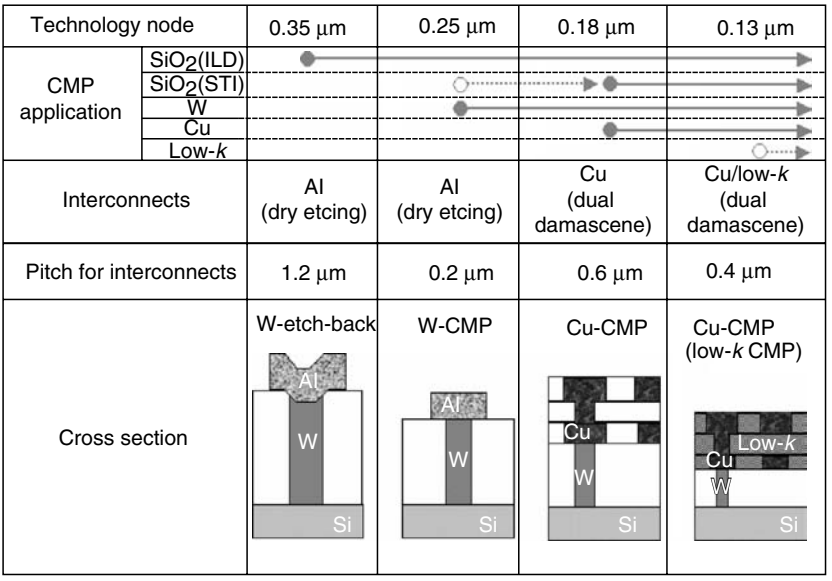


**FIGURE 7.119** The application examples of the CMP technology in each generation of devices.

were significantly altered with the size reduction of transistors and interconnects, as well as because the new materials were introduced. Figure 7.119 summarizes the application examples of the CMP technology in each generation of devices.

In the 0.35 μm generation, CMP was chiefly used for the planarization of the ILD films (e.g., plasma $SiO_2$ films). In the 0.25 μm generation, W-CMP was adopted for the contact portion that connects the electrode and wiring of a device. Before the introduction of W-CMP, W-etch-back was prevailing. In this method, as Figure 7.120 shows, the poor controllability of end point causes recess around 100 nm. As the recess causes the first-layer interconnect to be open, the etch-back method has its limits.

STI-CMP was introduced in the 0.25 μm generation. The role of STI is as an electrical insulation between transistors. The background of the adoption of the STI method was the necessity of sufficient dimensional accuracy due to smaller size for the field and active areas. Specifically, in conventional LOCOS methods, as the insulating film is grown by thermal oxidation, as Figure 7.121 shows, a bird's beak is produced around the LOCOS portion. The production of the bird's beak lowers the dimensional accuracy on the active area. Therefore, the STI method utilizing silicon etching, which has high processing accuracy, was chiefly used.

In the 0.18 μm generation, Cu-CMP was introduced. In this generation, wiring materials shifted from Al to Cu. At the same time, as Figure 7.122

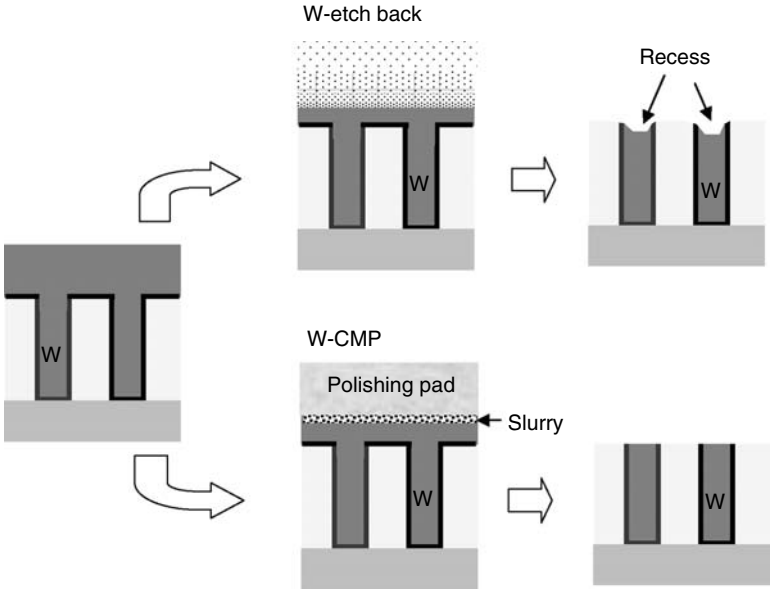


**FIGURE 7.120** The contact processes using (a) W-etch-back and (b) W-CMP.

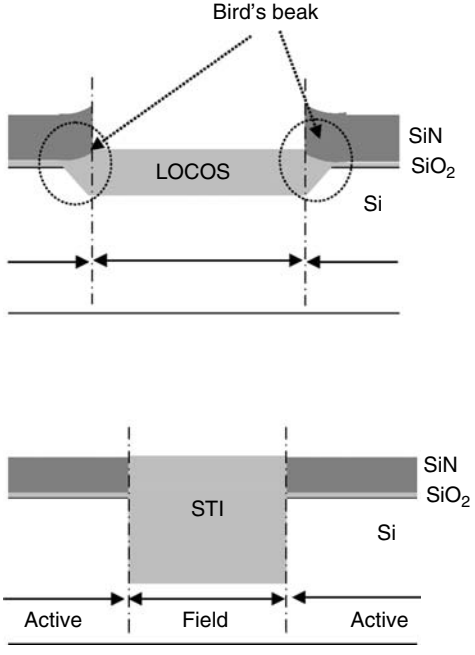


**FIGURE 7.121** Comparison LOCOS method with STI method. In the case of LOCOS method, the bird's beak lowers the dimensional accuracy on the active area.

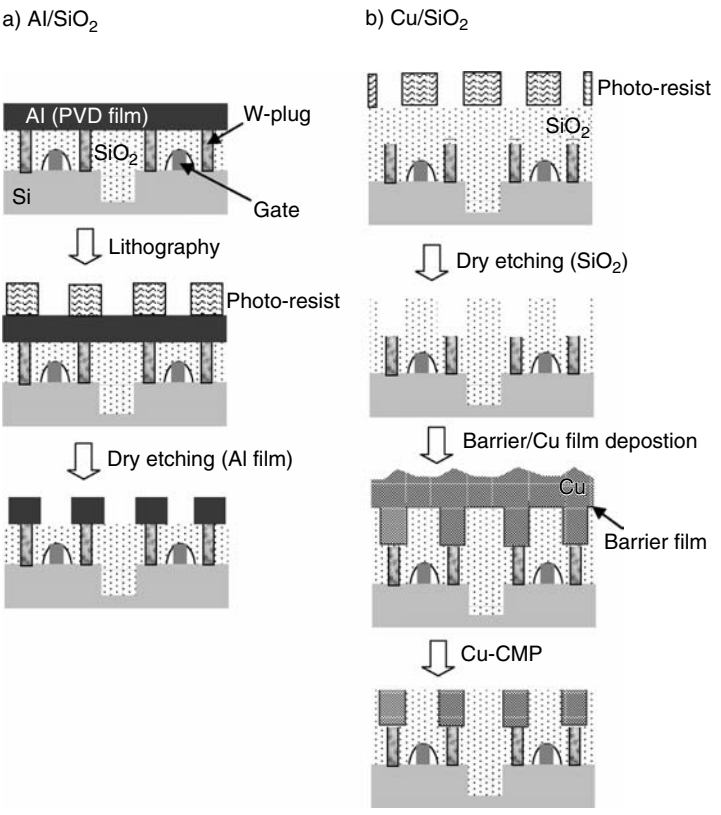


**FIGURE 7.122** Process flows of $Al/SiO_2$ and $Cu/SiO_2$ interconnects. The fabrication method of Cu interconnect is called as the damascene method. (IBM named the damascene method. The term damascene has the meaning of incrustation.) The damascene method is generally divided into the single damascene method for forming a single layer, such as the first layer, and the dual damascene method for simultaneously forming via contacts and wirings (two layers), such as the second layer and the upper layers.

shows, the formation of interconnects was changed from conventional methods as Al and $SiO_2$ interconnect to damascene method, because there is no etching gas for Cu film, patterning is impossible unlike Al. As the resistivity of Cu is lower than that of Al, the resistance of the Cu wirings becomes lower. If the resistance of wirings is low, the delay time of signal transmission propagated in a device decreases. In general, wiring delay is represented by $\tau = RC$ ($\tau$ is the delay time of the interconnect, $R$ the wiring resistance, and $C$ the capacitance between wirings) [67]. From this relationship, an increase in wiring resistance and capacitance between the wirings delays the transmission of signals. In other words, wiring resistance is

increased due to the decreasing dimensions of the wiring structure, which results in higher delay time of the interconnect. On the other hand, the same thing can be applied to the capacitance between wirings. If the capacitance between wirings lowers, delay time of the interconnect decreases. Therefore, a material having a low dielectric constant, called low-$k$ material, is used to lower the capacitance between wirings. (An oxide film conventionally used has a dielectric constant, $k$, of 4.4.) If this is used in a sub-0.13 μm device and beyond, the effect of the capacitance between wirings is significant. Therefore, in this generation, low-$k$ materials of $k \approx 2.8$, such as a SiOC film and an organic film, are used on this generation [68,69].

### 7.4.3 Device Integration and CMP

#### 7.4.3.1 Device Fabrication

Since the IC device shrinks down to 0.13 μm generation and beyond, high-end ULSI device using Cu wiring and low-$k$ (ILD) has developed. A cross section of Cu multilayered interconnects are shown in Figure 7.123 [70]. In the cross section of the chip, seven layers of Cu wirings are formed on a transistor. When such a device is fabricated, CMP is applied to a wide range from STI to the interconnect process.

Figure 7.124 shows a process flow when a device is fabricated. For STI process, initially, an oxide film and a SiN film were patterned by dry-etch process. Si is selectively etched off to form a trench in the Si substrate. After the trench has been formed, an oxide film (HDP-$SiO_2$) is deposited, and STI-CMP processing is performed until the SiN film is exposed. This SiN film is called the stopper film. It plays a role to protect active areas as it cannot be polished by the CMP for the oxide film. Thereafter, ion implantation is performed for adjusting the operating voltage ($V_{th}$) of the transistor. Then, through the formation of a gate electrode, and after the formation of an extension by ion implantation, the electrode is formed using S/D implantations. The transistor is fabricated through these processes.

Next, the interconnect process is described. After an oxide film (PMD film) is formed, the step reflecting the height of the gate electrode is planarized using PMD-CMP. Thereafter, a contact hole is opened, and a W film is deposited by W-CVD. Then a W plug (contact) is formed by W-CMP. In the formation of a first-layer Cu and low-$k$ interconnect, a stop film (SiC, etc.), a low-$k$ film, and a stopper film (SiC, etc.) are formed in this order. The thickness of the low-$k$ film is usually 300 to 600 nm. Then, after forming a trench, a barrier film (TaN) is formed to prevent the diffusion of Cu into the low-$k$ film. A Cu seed film (of a thickness of approximately 100 nm), which becomes an electrode for plating, is deposited by PVD. Then Cu plating (several micrometers) and Cu-CMP processing are performed to form the first-layer interconnect (single damascene method). In the formation of the second-layer interconnect and the following interconnects, after

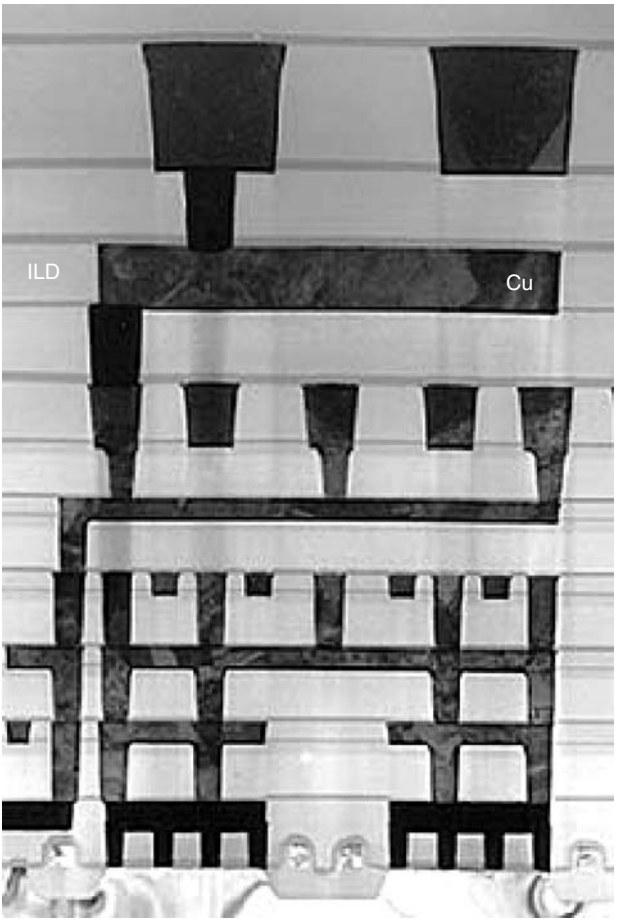


**FIGURE 7.123** Cross-sectional TEM photograph of Cu multilayer interconnect. (From Ohashi, N., et al., *Proceeding of IITC*, 140, 2001.)

opening the VIA, trenches for wiring are formed. Then in the same manner as the first layer, a barrier film, a Cu seed film, and a Cu-plated film are deposited, and VIA contacts and wirings are simultaneously formed by Cu-CMP (dual damascene method).

### 7.4.3.2 Problems in Integration

In the entire CMP process, it is ideal for integration to realize a flat surface without steps after polishing. In reality, however, the problem of the formation of dishing and erosion, as shown in Figure 7.125, arises. Such dishing and erosion cause steps in the device. Figure 7.126 summarizes the problems of CMP for each process.

| | Figure | Process |
|---|---|---|
| STI | | $SiO_2$ deposition |
| | 1 | SiN deposition |
| | | SiN/Si dry etching |
| | 2 | HDP-$SiO_2$ deposition |
| | 3 | STI-CMP |
| | | SiN/$SiO_2$ remove |
| Vth | | Vth implantation |
| Gate | | Poly-Si deposition |
| | | Poly-Si lithography |
| | | Poly-Si dry etching |
| Extension | | Implantation 1 |
| | | $SiO_2$ deposition |
| | 4 | Dry etching (aeolotropy) |
| S/D | | Implantation 2 |
| PWD | 5 | HDP-$SiO_2$ deposition |
| | 6 | PMD-CMP |
| Contact | | Contact lithography |
| | | Contact etching |
| | | Ti/TiN deposition |
| | 7 | W deposition |
| | 8 | W-CMP |
| 1M (single damascene) | | $SiO_2$(SiC) deposition |
| | | Low-*k* deposition |
| | 9 | $SiO_2$(SiC) deposition |
| | | Trench lithography |
| | | Trench etching |
| | | Barrier deposition |
| | | Cu PVD |
| | 10 | Cu electroplated |
| | 11 | Cu-CMP |
| 2M (dual damascene) | | $SiO_2$(SiC) deposition |
| | | Low-*k* deposition |
| | | $SiO_2$(SiC) deposition |
| | | Low-*k* deposition |
| | 12 | $SiO_2$(SiC) deposition |
| | | VIA lithography |
| | | VIA etching |
| | | Trench lithography |
| | | Trench etching |
| | | Barrier deposition |
| | | Cu PVD |
| | 13 | Cu electroplated |
| | 14 | Cu-CMP |
| 3M | | |
| 4M | | |
| 5M | | |
| 6M | | |

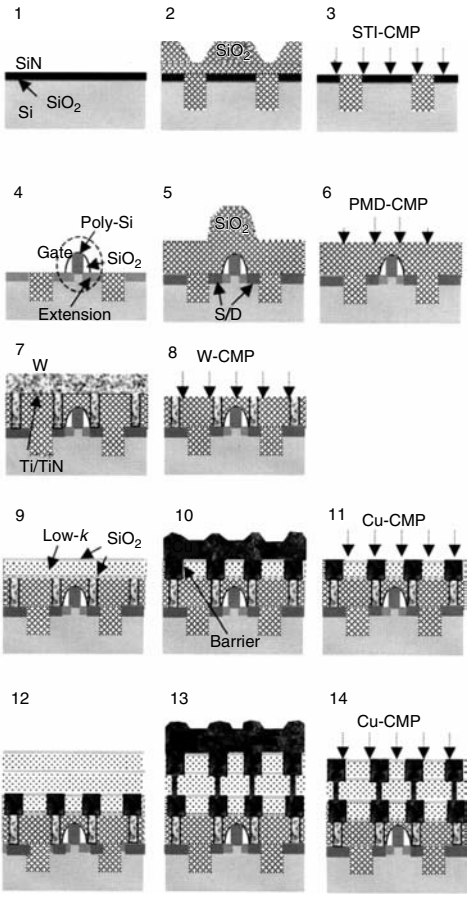


**FIGURE 7.124** Fabrication sequence of the high-end ULSI devices.

In the STI-CMP process, the residual oxide film on the SiN film and the abrasion of the SiN film raise problems. If an oxide film is present on the SiN film, as Figure 7.127 shows, the SiN covered with the oxide film will remain after SiN removal using phosphoric acid in the next process. In this case, the transistor itself cannot be fabricated, causing a fatal defect. Such a residue of the oxide film is produced, as Figure 7.128 shows, unless the steps present before polishing have been removed. In the other case, the occurrence of erosion causes the abrasion of SiN (the stopper film). As the active area is ground by CMP, this defect causes the defective operations of the transistor.

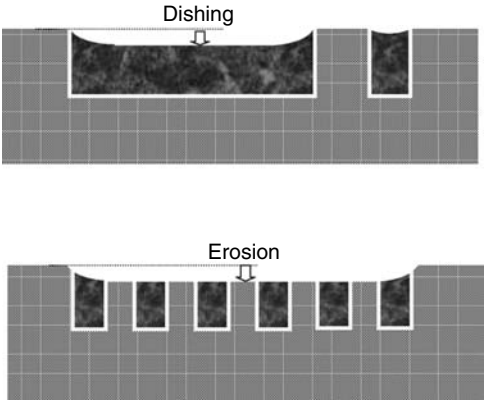


**FIGURE 7.125** Illustrations of dishing and erosion. Dishing means the film loss of the center portion in a wide trench. On the other hand, the entire reduction of the film in the portion of dense narrow trenches is called erosion.

Therefore, in STI-CMP, the reduction of the SiN film must be prevented through the selection of appropriate slurry.

The problem with the PMD-CMP is the removal of steps from a wide pattern area such as on the capacitors. Particularly if a fallen portion is left between capacitor portions after CMP, the residue of W is caused after the following W-CMP process. The present countermeasures include methods for improving step relaxation by avoiding such a pattern layout in design and by raising the hardness of pads.

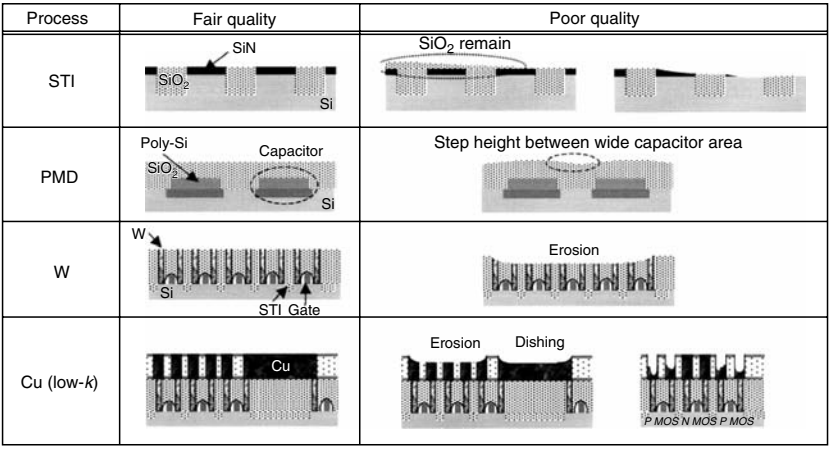


**FIGURE 7.126** Problems of the CMP for each process.

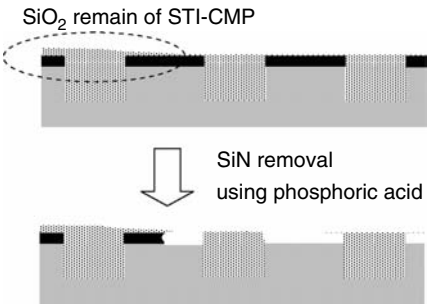


**FIGURE 7.127** SiN film remain on active area after SiN removal using phosphoric acid.

The problem with the W-CMP is the erosion produced in dense contact patterned area. (The present ability is the erosion of 20–50 nm.) The steps produced here cause residual Cu films in the boundaries of layers, as Figure 7.129 shows.

Cu-CMP has several problems such as dishing, erosion, voids, scratches, corrosion, and delamination. Dishing and erosion produced in Cu-CMP cause

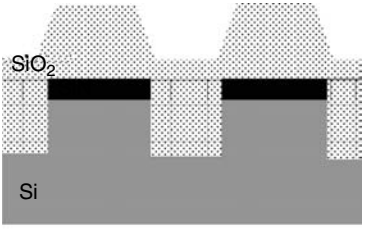


a) Before CMP

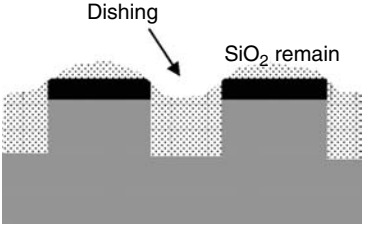


b) After CMP

**FIGURE 7.128** A mechanism of producing the dishing and the $SiO_2$ film remain on SiN (a) before CMP and (b) after CMP. (If STI-CMP has poor performance for step height reduction, these serious problems arise.)

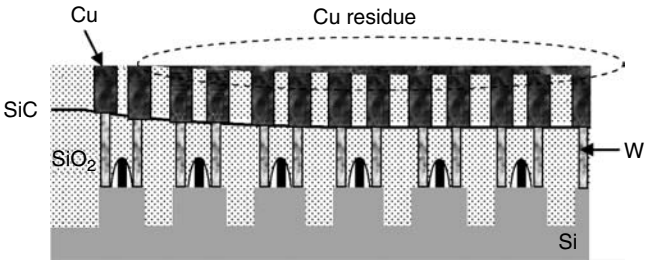


**FIGURE 7.129** Residual Cu film in the first layer caused by erosion of W-CMP process.

increase in wiring resistance and the occurrence of steps. Particularly in the Cu–low-*k* process, the occurrence of erosion will wear the cap film, as Figure 7.130 shows. At this time, water and chemical components in the slurry cause the dielectric constant of the low-*k* film to increase, as Figure 7.131 shows. The incorporation of voids in plating has been pointed out as another problem of the Cu film. These voids grow with annealing, and appear as pits after CMP. Although scratches and the oxidation of the Cu surface have been confirmed, these are caused by coarse particles in the slurry or water droplets remaining after cleaning. Corrosion occurs during cleaning after Cu-CMP by the photochemical effect. The potential generated in a transistor (P–N junction) accelerates the corrosion of the surface of the Cu film, as Figure 7.132 shows [71,72]. Therefore, the postcleaning of Cu-CMP is usually performed in a dark place. The problem of the delamination of the Cu film becomes marked with a low-*k* film of $k = 2.2$. This low-*k* film is highly brittle, and

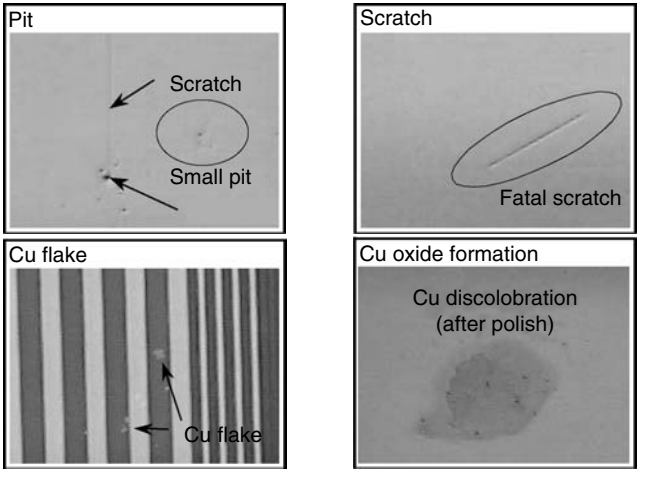


**FIGURE 7.130** Typical defects of Cu-CMP.

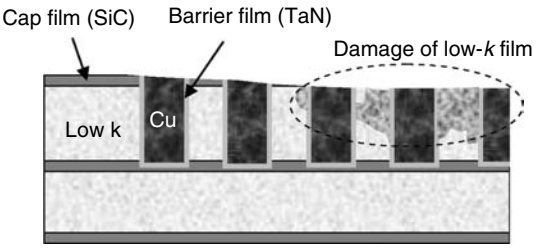


**FIGURE 7.131** Damage of low-*k* film by wearing the cap film.

delamination occurs by friction during polishing (refer to Figure 7.133) [73]. To solve this problem, the use of a low processing pressure has been proposed to lower the COF during polishing.

### 7.4.4 Present State of the CMP Development

As interconnect design rule continues to shrink, the requirement level to the CMP technology has increasingly been elevated. Under these situations, the developments of the CMP technologies that inhibit dishing and erosion, and utilize ultra-low-*k* materials are demanded. Here, the present state of development in each elemental process will be introduced.

#### 7.4.4.1 STI–CMP

One of the subjects to be developed in STI–CMP is the reduction of the thickness of the stopper film (SiN film). If the reduction of the thickness of the stopper film is realized, the aspect ratio of a trench can be minimized (refer to Figure 7.134). The advantage of minimizing the aspect ratio is to inhibit the occurrence of voids when a HDP oxide film is filled in the trench. This problem becomes more critical with the advance of the shrinkage of

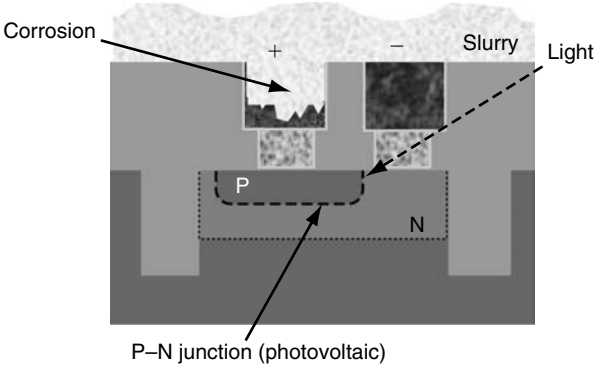


**FIGURE 7.132** The corrosion of the photochemical effect.

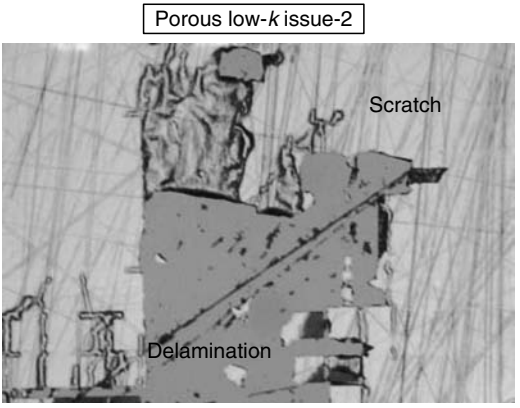


**FIGURE 7.133** Delamination of Cu film. (From Nobuo Hayasaka, Selete Symposium, May 28, 2002.)

semiconductor devices. Therefore, in future, the problem of minimizing the thickness of the SiN film must be solved. However, the thickness of the SiN film is determined estimating decrease in the thickness of the SiN film, and dishing that occurs in the trench. Figure 7.135 shows cross-sectional SEM images before and after the STI-CMP process [74]. Although steps are present before STI, they are planarized after CMP, and are polished to the stopper film (SiN film) in these pictures. Ideally, the stopper film should not have been polished, and dishing should have been nearly zero. If this state could be accomplished, the thickness of the SiN film would be infinitely thinned. However, in reality, the SiN film is polished and dishing occurs. With the present ability of CMP, the thickness of the stopper film will be around 100 nm. To reduce the film thickness, several kinds of slurries that have a high selected ratio of the SiN film and the oxide film and good step-relaxation properties have been developed.

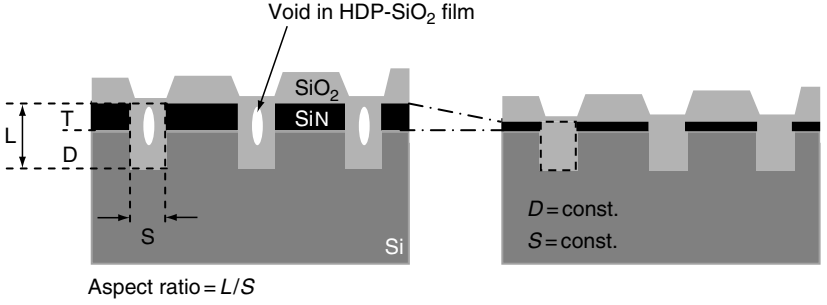


**FIGURE 7.134** The aspect ratio of the trenches for STI. The aspect ratio of a trench can be minimized by the reduction of the thickness of the stopper film.

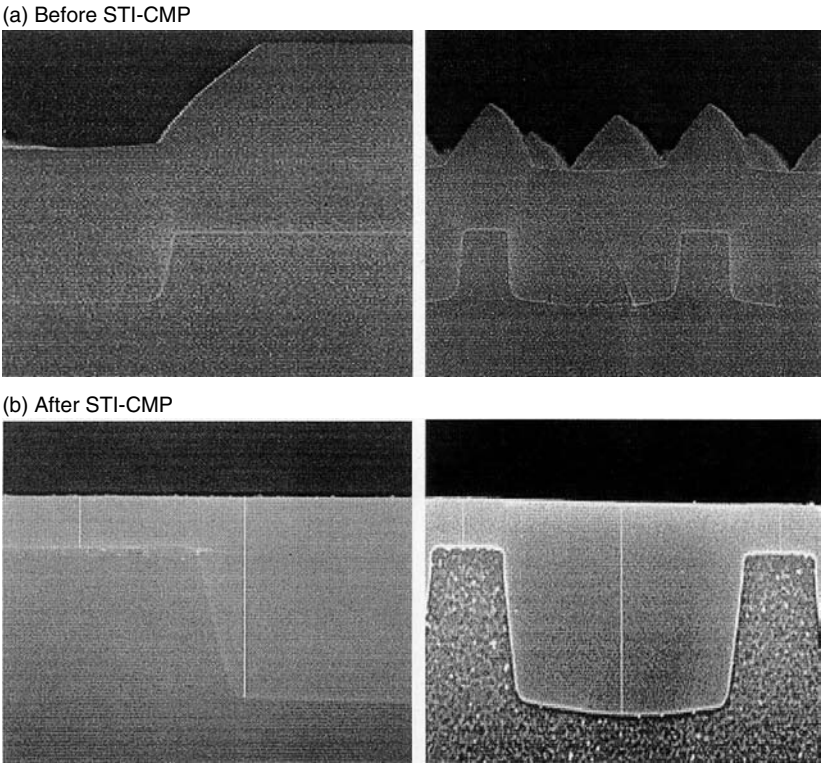


**FIGURE 7.135** Cross-sectional SEM images before and after the STI-CMP process. (From Andreas Romer et al., *Proceeding of CMP-MIC*, 2000.)

Next, the state of the development of slurry will be described. The slurries developed in STI are broadly classified into silica-based slurry and ceria-based slurry. As ceria-based slurry can polish oxide films at a high polishing rate, it has attracted attention from its early stages as the slurry for the CMP of oxide films. However, it has several problems to be solved, such as high manufacturing costs, purity, and the occurrence of scratches. Therefore, in recent years, some manufacturers have made efforts to improve slurry, including the minimization of scratches, by the improvement of additives contained in the slurry, and by cost reduction. Furthermore, as this slurry has good step-relaxation properties and a high selected ratio of the SiN film, it has been prevailing as the slurry for STI-CMP. On the other hand, in the case of silica-based slurry, few scratches occur. As these slurries have a low selective ratio to the stopper film (SiN film), it has a disadvantageous factor for the reduction of the thickness of the SiN film. For these reasons, the number of manufacturers who use silica-based slurry for STI-CMP is decreasing.

Lastly, the examples of the evaluation of STI-CMP will be described. Figure 7.136 shows the change in the thickness of an SiN film, an oxide film

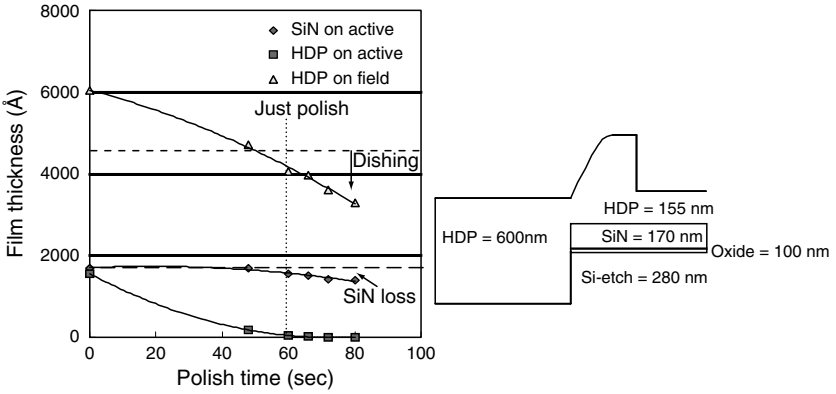


**FIGURE 7.136** The change in the thickness of an SiN film, an oxide film on the field, and an oxide film on the active portion when polished by a silica-based slurry.

on the field, and an oxide film on the active portion when polished by a silica-based slurry. Here, the polishing rate on the active portion is initially a little higher than that on the field. At this time, sufficient flatness must be secured until the oxide film on the SiN film is removed. Furthermore, after just polishing, the progress of polishing is inhibited by the SiN film. However, since here, dishing occurred because the oxide film on the field has been polished. The value of dishing produced here must minimize to a value lower than the thickness of SiN film.

### 7.4.4.2 Tungsten CMP

The development of tungsten CMP leads to the prevention of erosion in the contact areas and the application to the damascene gate-forming process [75,76]. The erosion in the contact areas has become a serious problem with the miniaturization of devices. The reason for this is that erosion leads to Cu residue on first layer after Cu-CMP in the next process.

On the other hand, W-CMP is applied to the damascene gate process. In the damascene gate process, after a trench of a gate shape, as Figure 7.137 shows, a W film is formed, and a gate electrode is formed using W-CMP. The occurrence of dishing at this time caused the defective operation of the transistor. For this, in W-CMP, the development of new polishing methods and slurries has been expedited to cope with dishing and erosion.

### 7.4.4.3 Cu and Low-*k* CMP

In Cu-CMP, the development of slurries and pads, other than processing apparatuses, is important. In fact, even if the same apparatus is used under the same conditions, the polishing properties are dramatically changed if different slurries or different pads are used.

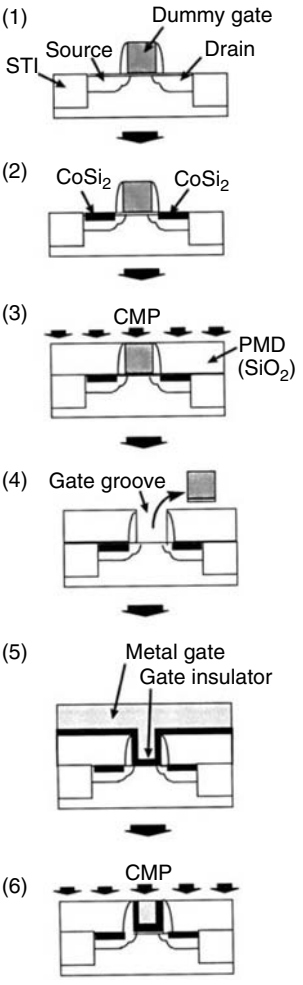


**FIGURE 7.137** Process flow of the damascene gate transistor. (From Matsuda, S., et al., Proceeding of 2001 Symposium on VLSI Technology Digest of Technical Papers, Kyoto, 64, 2001.)

At present, two-step polishing is prevailing in Cu-CMP process. Different slurries are used in the first step and the second step [77]. (The Cu film is polished in the first step, and the barrier film is polished in the second step. Refer to Figure 7.138.) This is because the hardness and reactivity of the Cu film and the barrier film are absolutely different. Therefore, the performance required here differs in every polishing step. Here, the state of the development of Cu-CMP for each polishing step will be described.

In the first step, a Cu film of a thickness between 0.5 and 2 μm is simultaneously polished. As a large amount of Cu film must be removed,

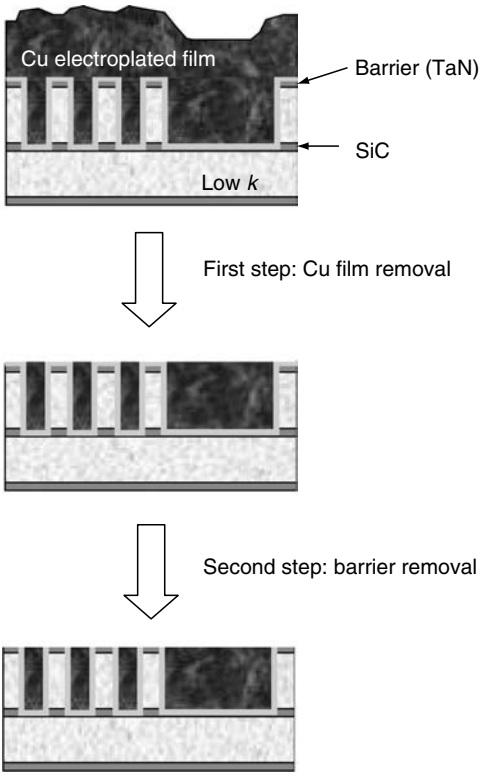


**FIGURE 7.138** The two intrinsic steps in Cu-CMP. (Over polish occurs at first step and second step, due to nonuniform removal rate within wafer.)

a high polishing rate and good distribution are required, and at the same time, dishing and erosion must be prevented. To prevent erosion, the selectivity between the Cu film and the barrier film is important. If the selectivity is high, even when the polished quantity is excessive, as Figure 7.139 shows, erosion can be prevented. The selectivity differs depending on the kind of the slurry. Therefore, the selection of the slurry is important for the development of Cu-CMP. Particularly in recent years, a polishing fluid composed of a solution containing no abrasive grains, and abrasive-free polishing (AFP), which polishes with a conventional urethane foam pad, has been developed [78,79]. A high selectivity has thereby been accomplished. On the other hand, dishing occurs in the initial step of the plating film (over plating) and in the excessive polishing process. Generally in the first step of polishing, the steps after forming films must be relaxed. If the step-relaxation ability is high, the effect of the steps formed in the initial stage of plating can be minimized. Therefore, to prevent dishing, the step-relaxation ability must be secured, for example, by optimizing the hardness of the pad. Also to minimize the dishing under

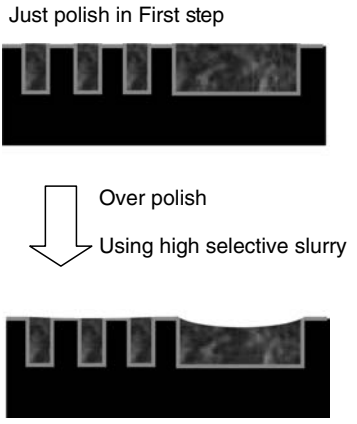


**FIGURE 7.139** The dishing and the erosion after over polish treatment of first step using high selective slurry.

overpolishing process, the time of overpolishing must be shortened. For this purpose, a good within a wafer (WIW) uniformity is required, because poor uniformity leads to long overpolishing, resulting in large dishing. To secure good WIW uniformity, the pressurizing mechanism of the processing head itself has been improved, and the type or the shape of the groove of the pad has been optimized as Figure 7.140 shows. The improvement of the processing head has been tried by providing a pressurizing mechanism to the retainer portion, as Figure 7.141 shows, and by adopting a zone control mechanism.

In the second step, the selectivity is critical. The selectivity also differs depending on slurries. The slurries presently used in the second step are broadly

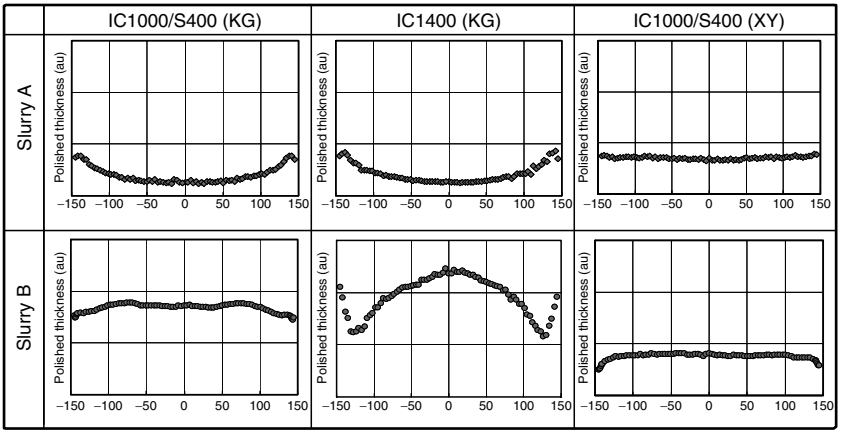


**FIGURE 7.140** Polishing profiles of several kinds of the pads using slurry A and B.

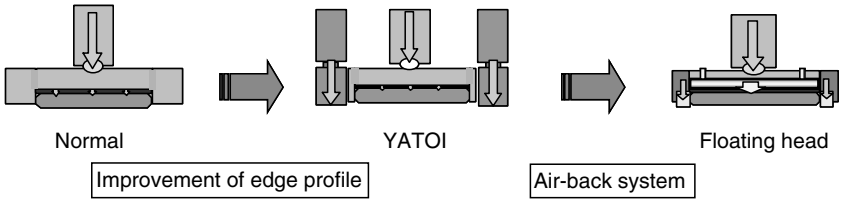


**FIGURE 7.141** Evolution of polishing head (EBARA).

classified into high selective slurry and low selective slurry. Figure 7.142 summarizes polishing stages using high selective slurry and low selective slurry. As high selective slurry polishes only the barrier film, the wear of the

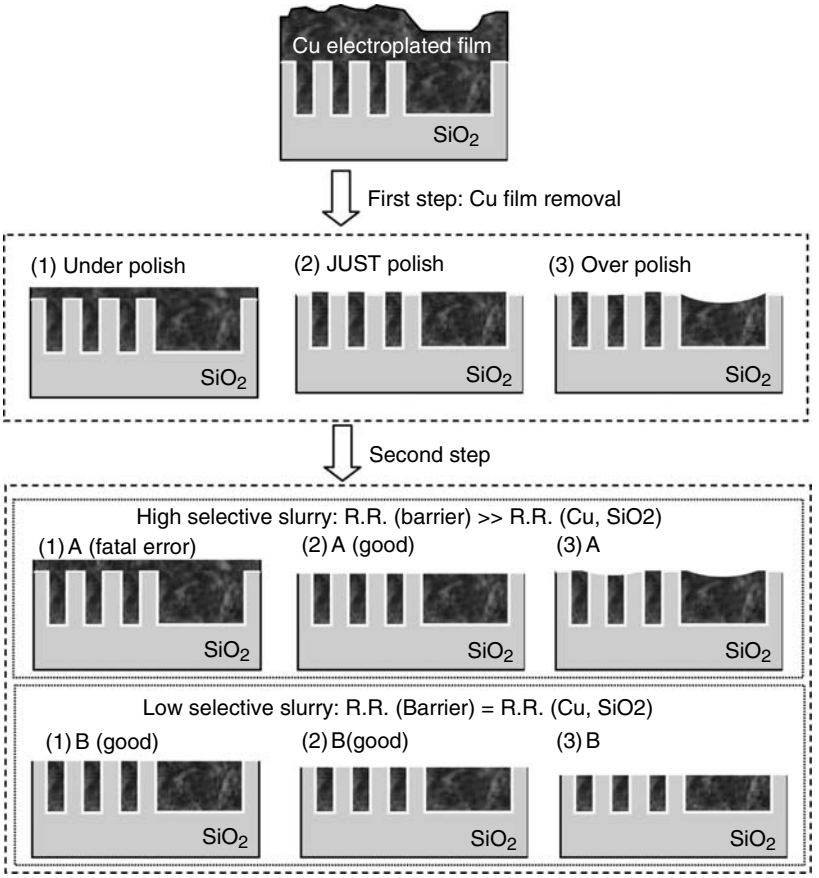


**FIGURE 7.142** Polishing stages using high selective slurry and low selective slurry of second step polish. In the case of low selective slurry, it cannot be applied to the ultra-low-*k* film, as this slurry polished all the films simultaneously.

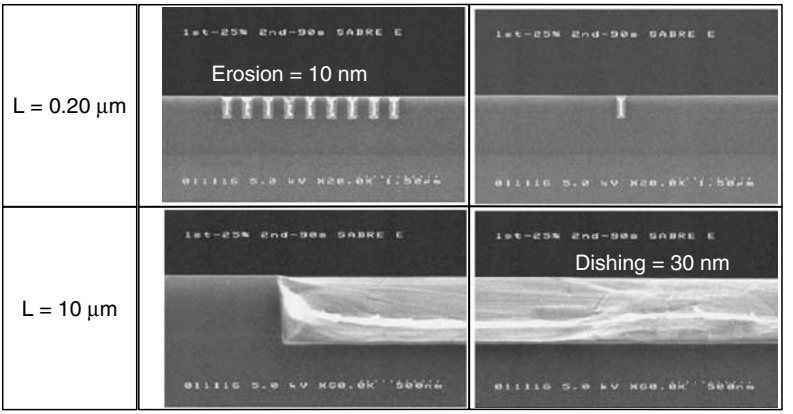


**FIGURE 7.143** Cross-sectional profiles after polishing. (Second-step polishing was treated using high selective slurry.)

oxide film or the low-$k$ capping film is extremely small. Therefore, when a low-$k$ film is applied, the damage of the low-$k$ film itself can be minimized. However, as the Cu film is polished a little, if residual Cu film remains after the first polishing, the second step slurry cannot remove it. On the other hand, as the low selective slurry polishes the Cu film simultaneously with the barrier film and the oxide film, the residual Cu film after the first step can be removed easily. However, because this slurry polished all the films simultaneously, it cannot be applied to the low-$k$ film.

Next, the application examples of the test element group (TEG) wafer will be introduced. Figure 7.143 shows the cross-sectional profiles after polishing (second step polishing). In these wafers, in the 10 μm line, 30 nm dishing occurs; and in 0.2 μm/0.2 μm, 10 nm erosion occurs. These CMP processes are evaluated to the low-$k$ film of the level of $k = 2.8$. A wiring-shaped TEG was fabricated, and the wiring resistance within a wafer was measured using the four-terminal method. The results are shown in Figure 7.144. In this figure, every rule showed an even value for the wafer. Although the resistance is partly increased at 0.16 μm, this is because the OPC was not corrected sufficiently. Furthermore, for a low-$k$ film (porous film) of the $k = 2.2$ level, research and development is conducted at a number of research institutions [80]. Here, as the strength of the low-$k$ film itself is low, the delamination of the film occurs. Therefore, the improvement of abrasive grains, the reduction of friction force (including the development of new slurry) and the development of electrolytic polishing, as well as the optimization of polishing conditions, must be carried out from the new point of view.

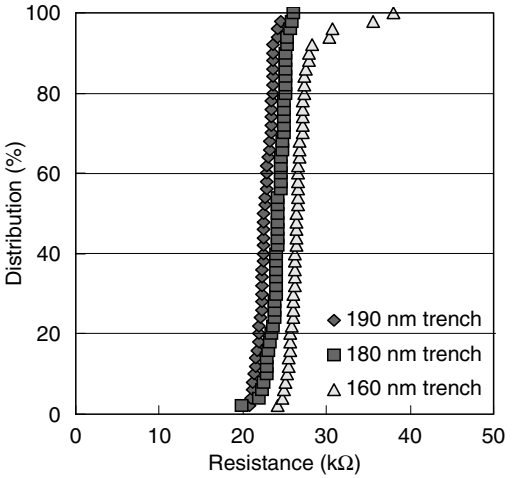


**FIGURE 7.144** Cu wiring resistance within a wafer.

### 7.4.5 Development of Endpoint Detection Method

The method for endpoint detection (EPD) is an important technology for the process control of CMP. The methods for monitoring the endpoint differ depending on the subjective processes and patterns, and in application to CMP, they often depend on the know-how of process engineers.

Presently prevailing EPD technologies are broadly classified into three methods, as shown in Figure 7.145. The first method is the torque current end point detection. The principle of this method is to monitor the friction force generated between the surface to be polished and the pad during polishing. Actually, this is the method to detect a torque current generated when a platen is rotated at a constant speed, and this method is used in W-CMP and

| Endpoint detection | Torque current | Eddy current | Optical |
|---|---|---|---|
| Schematic | 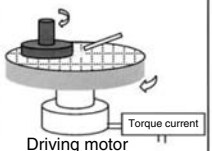  | 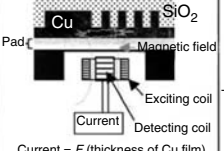  | 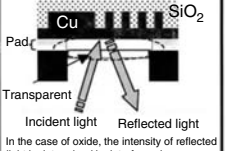 Cu SiO2 Pad Transparent Incident light Reflected light In the case of oxide, the intensity of reflected light is determined by interface phenomenon |
| Application | W-CMP STI-CMP | Cu-CMP (W-CMP) | Cu-CMP STI-CMP (W-CMP) |

**FIGURE 7.145** Typical endpoint detecting methods of the CMP.

STI-CMP. The second method is the endpoint detection by eddy current, which uses sensors buried under the pad. Two spiral coils are buried under the pad, one of which is made to generate magnetic force, and the metal film on the wafer is made to generate an eddy current. This eddy current generates a new magnetic field, and this magnetic force is sensed by another coil. As this magnetic force is proportional to the thickness of the metal film (such as Cu), the film thickness can be measured. The third method is the optical endpoint detection, in which laser or light beams are directly radiated onto the surface to be polished (wafer surface), and the change in the reflectance is observed. As a specific example, although Cu has a high reflectance, it decreases when a barrier or an insulating film appears as removed Cu film by the CMP process. This difference in reflectance directly reflects information from the surface to be polished, and the endpoint can be detected at a high accuracy. However, with increase in the number of layers of interconnects, as the reflected components from the underlying layers affect the measurement concurrent, the detecting accuracy may be lowered. In this case, the above-described torque detecting method or eddy current method may be used in combination.

The prevailing endpoint detecting methods were described above. Actually, the detection of the endpoint cannot be said to be a completed technology, as the optimal detecting method changes depending on the quality of the film and the pattern of the devices. Therefore, it is in the present situation that the know-how acquired by CMP engineers is freely used to optimize the endpoint detecting methods for each process.

### 7.4.6 Future Prospects

The challenge of the CMP technology is the introduction to low-*k* films. When the dielectric constant is lowered, the strength of the film itself is weakened. Therefore, in CMP, the development of the so-called "soft polishing," which prevents the damage of the film itself, will be required in the future. Here the introduction of low-pressure polishing, and the development of a polishing system, slurry, and pads making erosion and dishing approach limitlessly to zero will be required.

The CMP technology still promotes the miniaturization of semiconductor devices. This is because the improvement of the polishing technology by polishing apparatuses, slurries, and pads achieved high processing accuracy that endures miniaturization. However, for CMP to be more diffused in the future, the reduction of the costs and the improvement of yield are required. For this purpose, problems such as the reduction of costs for slurries and pads, the cleaning method after CMP, and the production of dust in clean rooms must be solved in the future. The further improvement of CMP technology is expected for the development of mass-production technology in the 65 nm generation and beyond.

## 7.5 THIN FILM MAGNETIC RECORDING HEADS

*MASANOBU HANAZONO*

### 7.5.1 Structure and Read and Write Mechanism of Thin Film Magnetic Head

Thin film giant magnetoresistive (GMR) read and inductive write magnetic heads are now widely used as the key devices to support the increasing demand of area density for the hard disk drive (HDD) systems. Figure 7.146 shows the progression of increasing area density in magnetic recording HDD systems over the past 30 y [81]. From Figure 7.146 we can realize that since the last 10 y, area density of HDD systems has sustained an annual increase as high as 100%. These increases in area density have been supported by the improvements of

- Thin film heads (TFH) with an air bearing surface, called sliders
- Rotating disk coated with a thin film medium
- Spindle motor to drive the disk
- Electromagnetic voice-coil rotary actuator to move the slider across the surface

Figure 7.147 illustrates an overview of a HDD system.

TFH was developed through thin film processing technologies, similar to that used in the fabrication of ULSI semiconductor devices [82]. TFH fabrication processing activities are conducted in a clean room facility with

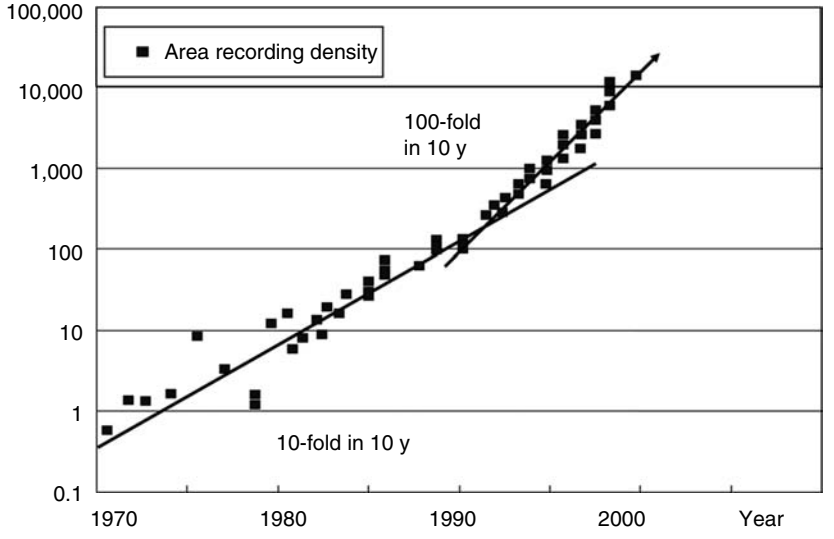


**FIGURE 7.146** Trend of area density for hard disk drive systems.

**FIGURE 7.147** Overview of HDD system. (Courtesy of Hitachi Ltd.)

capabilities for electroplating, fine line photolithography, reactive etching, ion milling, chemical mechanical polishing (CMP), thin film metal and insulator depositions, and wet etching. The read and write heads are fabricated on ceramic substrates (wafers). After wafer processing, the substrate is sliced to individual bars using a diamond wheel. They are then finished using an advanced lapping process with individual head close-loop control. Finally, the bars are diced into individual heads (called sliders) using a diamond wheel. These processes are schematically shown in Figure 7.148.

Figure 7.149 shows a plain view of the TFH. Figure 7.150 shows a schematic structure of the multilayered TFH and the roles of each layer. From this figure we can see the read and write TFH consisting of an electromagnetic coil writer head and a GMR reader head. In an inductive writer, the electromagnetic coil induces the magnetic flux in the loops (poles) and then the induced magnetic field between two pole tips (write gap) writes information on the disk. In a GMR reader, the magnetic field from the disk changes the resistance of the GMR sensor and this resistance change indicates the transition information. The GMR sensor gets the data back by seeing the vertical magnetic field transition from the disk. The distance between the two shields is referred as the read gap. This determines the linear density of recording.

Figure 7.151 shows a cross-sectional view of a TFH at the air-bearing surface of the slider. A typical GMR sensor stack has a total thickness of 420 Å. This stack consists of multilayers, antiferromagnetic exchange layer (Ni–Mn), magnetically pinned layer (Co–Fe), conductor (Cu), diffusion barrier (Co–Fe), magnetically free layer (Ni–Fe), and tantalum for oxidation protection [83]. Figure 7.152 shows the precisions of these multilayers,

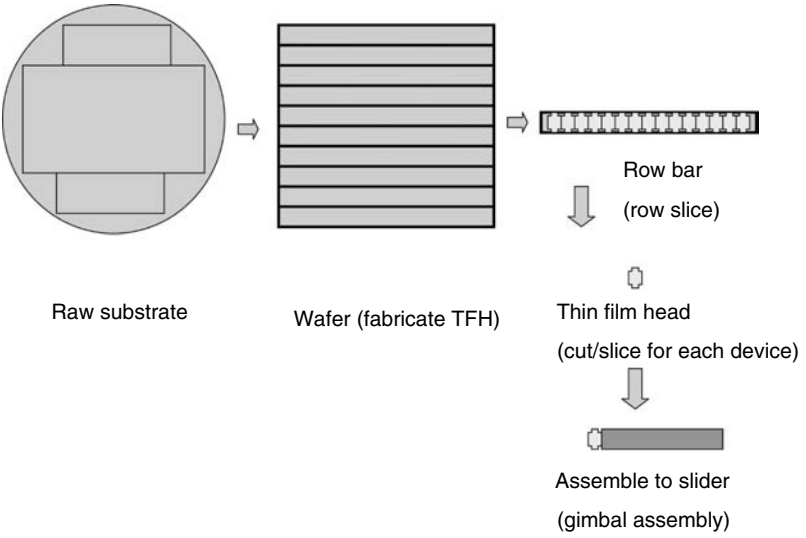


**FIGURE 7.148** Thin film head assemble process.

including typical thickness of each layer. From this figure, we can realize that the TFH structure consists of more than 15 materials. Each layer is defined by photolithography and additive processing. The simplified TFH fabrication process flows are summarized in Table 7.16. From this table we can realize that the fabrication of TFH includes five CMP process steps.

To keep doubling the area recording density annually, the critical dimensions (read and write feature size) in TFHs must decrease. This is obtained by actively shrinking the device dimensions and developing the new magnetic materials. The critical dimensions in the read and write heads have become

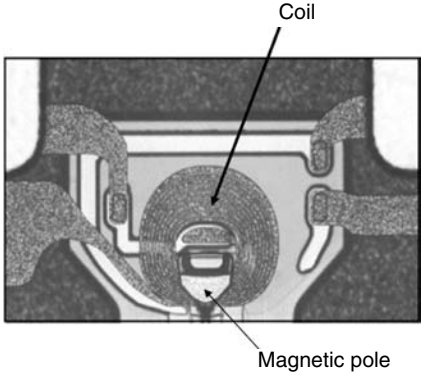


**FIGURE 7.149** Plane view of thin film head. (Courtesy of Hitachi Ltd.)

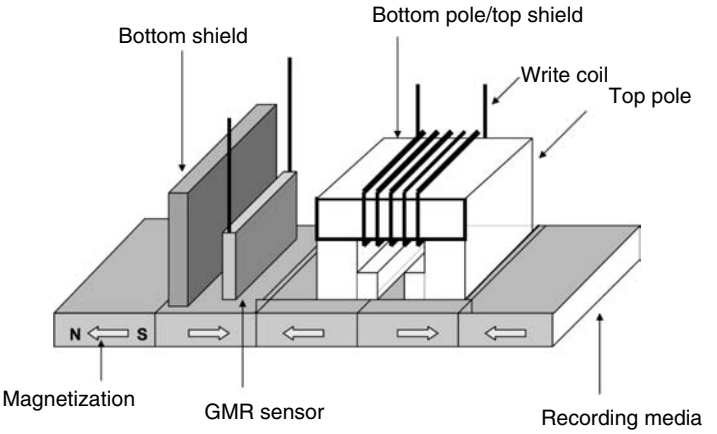


**FIGURE 7.150** Thin film head schematic.

smaller than those in the semiconductors [84]. To realize these requirements, the application of CMP is an essential process for the planarization of many layers [85–87].

In Table 7.16 and Figure 7.153, potential steps for application of CMP treatments are shown. From these, we can identify five portions requiring CMP treatment. Each CMP process is discussed in the following section.

## 7.5.2 CMP Process for Thin Film Magnetic Heads

### 7.5.2.1 Smoothing of Alumina Basecoat Film Surface

AlTiC (64% $Al_2O_3$, 36% TiC) is a typical advanced ceramic material used for the TFH-fabricating wafer substrate. The surface of this ceramic material is not smooth enough for photolithography of less than 1 μm definition devices. Followed by the sputter deposition of the thick (3 μm) $Al_2O_3$ film, the CMP treatment of the $Al_2O_3$ film surface is performed to obtain the ultraflat surface

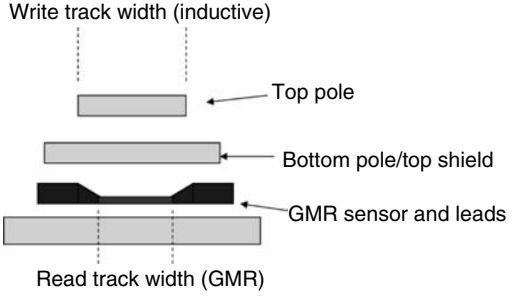


**FIGURE 7.151** Cross-sectional view of a thin film head at the air bearing surface.

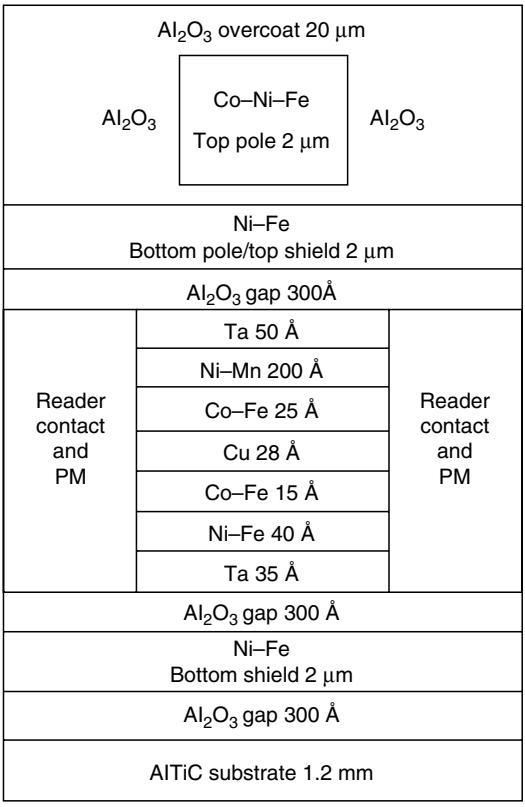


**FIGURE 7.152** Precision of multilayers for TFH from bottom to top at the air-bearing surface.

required for photolithography processing. This process also provides electrical isolation from the substrate. This step is shown in Figure 7.154. Because the bottom shield is plated on the basecoat, as is illustrated in Figure 7.153, reduced surface defects and roughness in the basecoat result in excellent magnetic properties for the bottom shield. For $Al_2O_3$ CMP slurry, an alkaline solution was selected for high removal rate of $Al_2O_3$ and low removal rate of Ni–Fe. This slurry was also applied for $Al_2O_3$ film CMP in the following CMP.

### 7.5.2.2 Bottom Shield CMP

The process flow of the bottom shield is illustrated in Figure 7.155. In this figure, steps 1 through 6 are called the frame plating method. This process was specially developed for the fabrication of the TFH to obtain high-resolution patterns, even if more than micrometer order of thickness multilayers were

**TABLE 7.16**
**TFH Fabrication Process Flow and Requirements for CMP**

| Step Number | Purpose | Material | Thickness (Typical) | CMP Applied Step | Effects of CMP |
|---|---|---|---|---|---|
| 1 | Substrate | AlTiC | 1.2 mm | | |
| 2 | Basecoat | $Al_2O_3$ | 2 μm | CMP | Substrate roughness repair |
| 3 | Bottom shield | Ni-Fe | 2 μm | CMP | High selectivity $Al_2O_3$/Ni–Fe to reduce step height and stabilization of GMR sensor |
| 4 | Read gap 1 | $Al_2O_3$ | 30 nm | | |
| 5 | GMR sensor | Co–Fe | 45 nm | | |
| 6 | Read gap 2 | $Al_2O_3$ | 30 nm | | |
| 7 | Bottom pole/ top shield | Ni–Fe | 3 μm | CMP | Step height reduction for narrow track width write head |
| 8 | Write gap | $Al_2O_3$ | ~0.2 μm | | |
| 9 | Inductive coil | Cu | 2 μm | CMP | High selectivity Cu/organic insulator to fabricate write coil |
| 10 | Upper pole | Ni–Fe | 3 μm | | |
| 11 | Over-coat | $Al_2O_3$ | 20 μm | CMP | High selectivity $Al_2O_3$/Cu to fabricate outer lead Cu pad |

laminated. The sputter-deposited $Al_2O_3$ film was CMP treated to obtain global planarization through the whole substrate. This CMP process was performed by two steps. Step 1 is $Al_2O_3$ CMP to quickly remove the isolation. Step 2 is metal CMP to polish Ni–Fe surface. The CMP process smoothes the Ni–Fe surface and reduces Ni–Fe protrusion. For Ni–Fe CMP slurry, an acid base solution was selected to ensure a high selectivity of Ni–Fe/$Al_2O_3$.

### 7.5.2.3 Bottom Pole and Top Shield CMP

This process is similar to the bottom shield process as illustrated in Figure 7.156. To obtain superior properties of TFH, the application of Co–Ni–Fe materials have garnered recent attention in the marketplace. This material is much more chemically active compared to the conventional Ni–Fe material. To obtain satisfactory results, modification of CMP slurry or adjustment (for example pH) of CMP process conditions might be required.

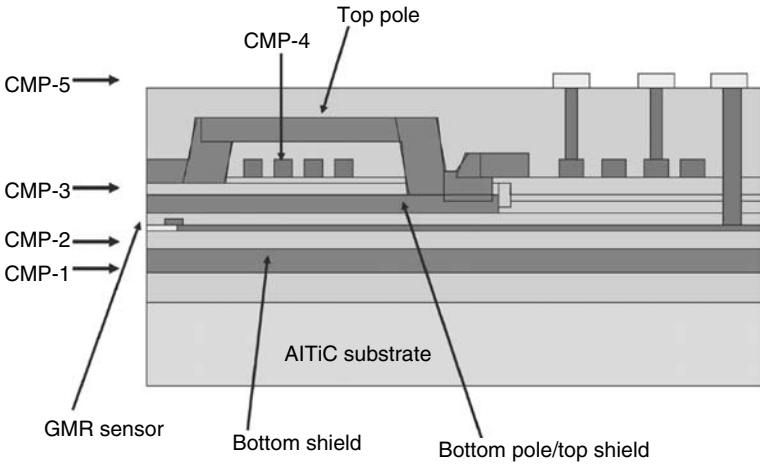


**FIGURE 7.153** Cross-section schematic of thin film head.

### 7.5.2.4 Cu Damascene Process

To fabricate a high signal speed semiconductor, application of Cu damascene process has been enthusiastically adopted. Recently, abrasive-free Cu-CMP slurries have been developed. This new slurry is well understood to reduce dishing and erosion for fine and large feature pattern. Application of this Cu slurry for the fabrication of write Cu coil of TFH, as is shown in Figure 7.157, revealed reduction of dishing and erosion less than half compared with conventional particle-containing slurries. On the basis of this data, application of abrasive-free Cu slurries for TFH is now under development. To narrow the coil pitch photo process extendable, additional CMP treatment of $Al_2O_3$ film will also be revealed.

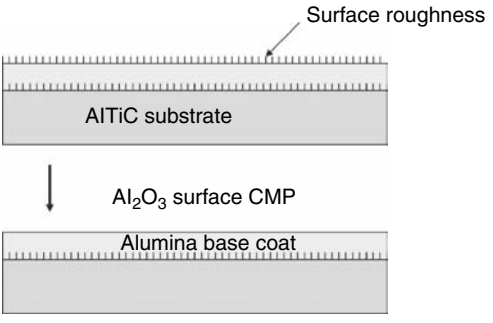


**FIGURE 7.154** $Al_2O_3$ base coat surface CMP.

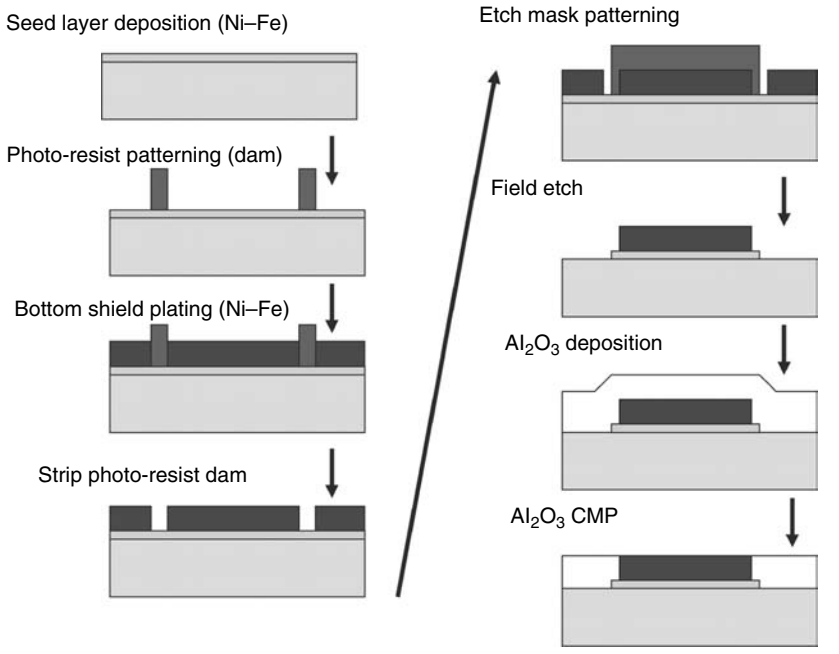


**FIGURE 7.155** Bottom shield CMP.

### 7.5.2.5 Overcoat CMP

After $Al_2O_3$ overcoat deposition, a CMP process step is performed for two purposes. One is to open up Cu studs for the connection with outer circuits. The other is to bring the overcoat thickness into specification. After this CMP

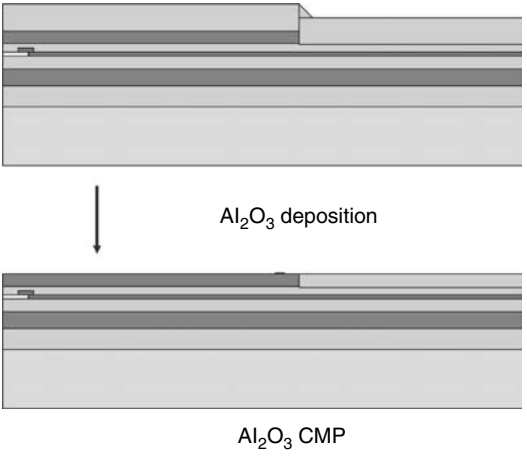


**FIGURE 7.156** Bottom pole and top shield CMP.

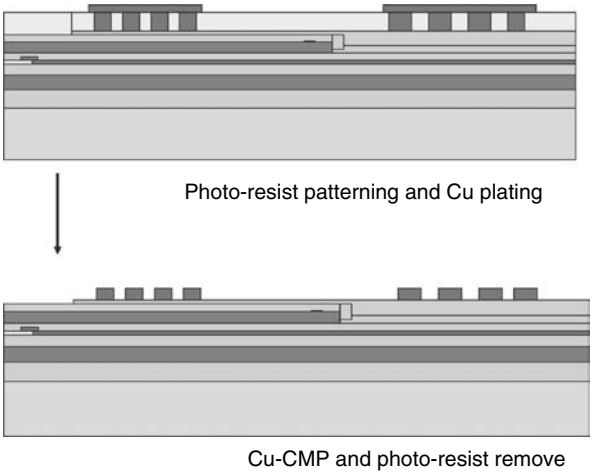


**FIGURE 7.157** Patterning of Cu conductor by CMP.

treatment, gold plating is done to ease the bonding process. Schematics of this process are shown in Figure 7.158.

## 7.6 CMP OF COMPOUND SEMICONDUCTOR WAFERS

*TOSHIRO K. DOI*

Conventionally, mixed solution of bromine (Br) and methanol or liquid solution of sodium hypochlorite (NaClO) has been used for the polishing of compound semiconductor wafers such as GaAs, InP, and CdTe [88]. As these

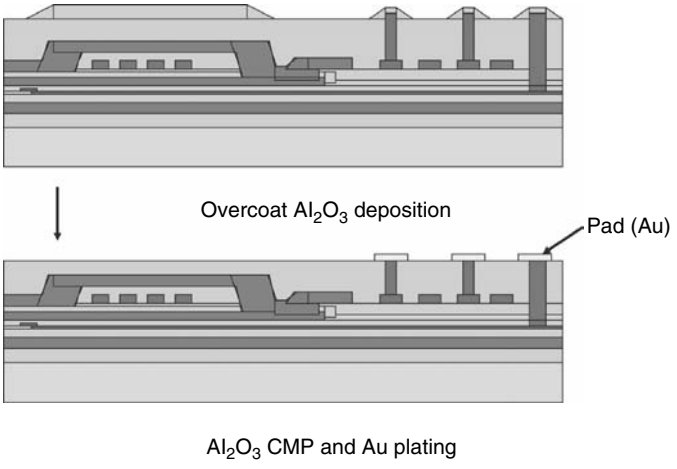


**FIGURE 7.158** $Al_2O_3$ overcoat CMP.

solutions have a short life as polishing reagents and are hazardous chemicals with acute oxidization and strong odor, a specially designed polishing machine with special working environment and facilities is required, which, however, poses a large problem to the polishing work.

In the following text, CMP characteristics of compound semiconductors observed using new high-quality slurry, which is practically harmless, developed on the basis of the polishing mechanism of CMP or MCP are mentioned.

### 7.6.1 Polishing Characteristics of GaAs Crystal Wafers

Nontoxic sodium bromite ($NaBrO_2$) that is used as a starch-off agent in textile processing or as a slime control agent of industrial water is inexpensive, and features mild oxidization as it does not generate hazardous gas [89].

When disk-type chemical polishing is done using only sodium bromite, a membrane (stains) that is a reaction product tends to remain on the processed surface causing the rough surface. By adding nonionic solution (DN agent) that has an interface osmotic function to the bromic acid natrium solution, such membrane can be expanded facilitating easy removal of the same, which leads to a successful production of a smooth flat surface. Reaction products are positively removed if fine particles are mixed in such solution, resulting in a high efficiency polishing. Figure 7.159 shows relations of surface roughness

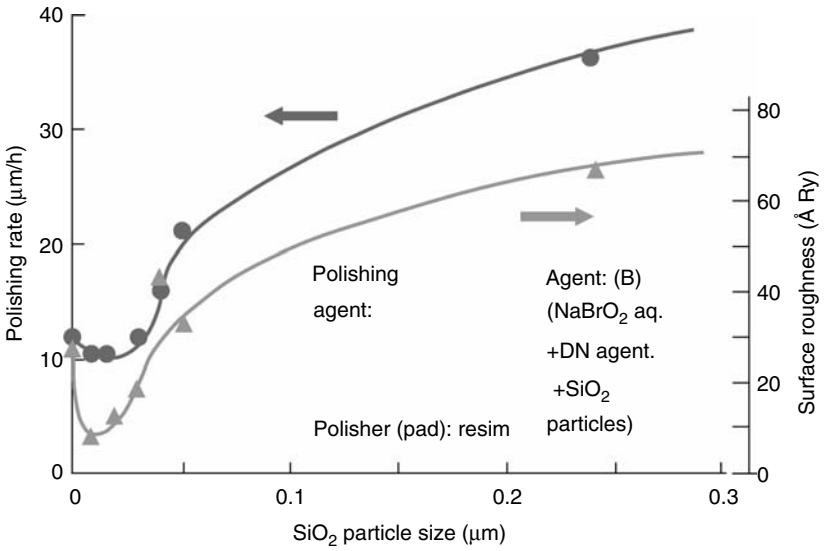


**FIGURE 7.159** Relation between $SiO_2$ particle size and polishing rate and surface roughness (specimen: GaAs).

of GaAs crystals with CMP rate using $NaBrO_2$ solution (containing 0.6% NaOH) to which DN agent and $SiO_2$ fine particles are added [90]. As the size of $SiO_2$ particles becomes large, polishing speed increases. This mixed-type slurry produces the surface of GaAs crystal to a smooth surface with a roughness below 10 Å Ry.

On the basis of these polishing characteristics, processing mechanisms [90] are summarized as follows:

1. Both Ga and As are oxidized by $NaBrO_2$ solution, and produce gallium oxide ($Ga_2O_3$) and arsenic pentoxide ($As_2O_5$), respectively, as reaction products

$$2GaAs + 4NaBrO_2 + 4NaBr \rightarrow Ga_2O_3 + As_2O_5 + 8NaBr \tag{7.37}$$

2. Generated $As_2O_5$ immediately turns into natrium arsenate ($Na_3As_2O_5$) by NaOH

$$As_2O_5 + 6NaOH \rightarrow 2Na_3As_2O_4 + 3H_2O \tag{7.38}$$

3. Meanwhile, $Ga_2O_3$ turns into gallium hydroxide $Ga(OH)_3$ by alkali hydroxide

$$Ga_2O_3 + 6OH^- \rightarrow 2Ga(OH)_3 + 3O_2^- \tag{7.39}$$

   This $Ga(OH)_3$ easily dissolves in natrium hydroxide.
4. The above chemical reactions are further promoted by the mechanical actions of the added particles and the friction heat of the processed surface while the above three reactions and the surface-active penetration function driven by DN agent are acting.

From the above polishing mechanism of GaAs, it is basically understood that even the slurry consisting of the oxidant, to which small amount of alkali hydroxide is added, is effective for the polishing of GaAs crystals. Of course, it is also essential to produce high-quality surface by adding DN agent having interface penetration function to the above slurry that facilitates the removal of reaction products (stains and membranes).

Figure 7.160 shows polishing characteristics obtained by polishing with simple slurry consisting of $H_2O_2$ to which a small amount of NaOH and DN agent is added [90]. The polishing rate becomes the maximum at pH 10, when similar surface quality to that of $NaBrO_2$ solution is obtained. However, although $SiO_2$ fine particles are added, the increase in the polishing rate was not so notable as with $NaBrO_2$ because presumably reaction products were not formed on the surface as firmly as they were with $NaBrO_2$.

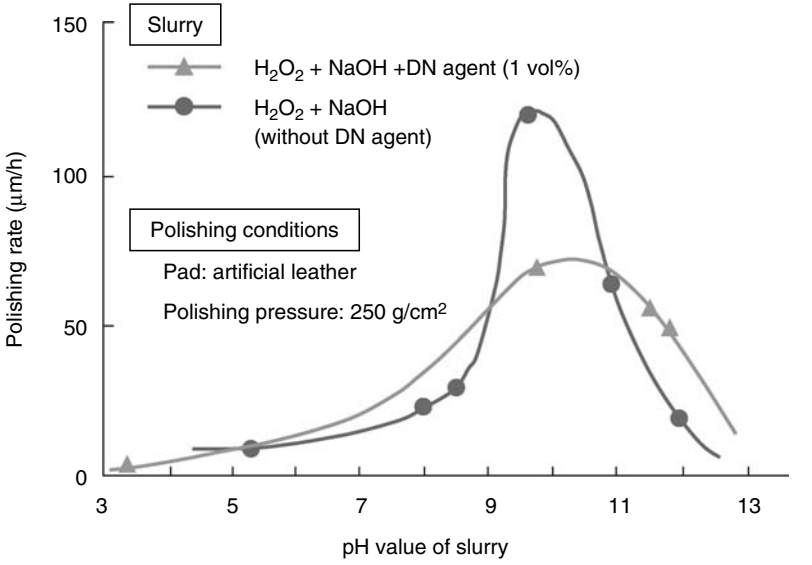


**FIGURE 7.160** An example of polishing characteristics of GaAs by using another slurry containing $H_2O_2$ (oxidizing agent), NaOH (alkali), and DN agent (nonionic solvent).

### 7.6.2 Polishing Characteristics of CdTe Crystal Wafers

As opposed to the above-mentioned GaAs crystal that is a compound semiconductor of III–V group, CdTe crystal is a compound semiconductor of II–VI group and is drawing attention as substrates especially for infrared and radiation detectors, light emitting diode, and solar battery. As is the case with GaAs crystal, CdTe is very soft due to its prominent cleavages with a Mohs hardness of 2.8 as against 4.5 of GaAs.

On the basis of the polishing mechanism of GaAs crystals, a guiding principle for the selection of slurries for CdTe crystals is studied, which indicates that polishing reagents that can oxidize CdTe surface should be selected. Assuming it is the basic mechanism that the oxides such as $CdTeO_3$ generated by the slurry are removed with a pad or fine particles, we focus here on the oxidizing breach that is harmless and used also at home.

Figure 7.161 shows polishing rates of CdTe crystals versus slurries with oxidizing bleache as a main solution [91]. From the microscopic observation of the processed surface, the slurries to which DN agent is added, as used in the chemical compound polishing of GaAs wafers, produced the surfaces more uniform than others without DN agent. However, the effect of DN agent was not so remarkable as that of GaAs crystals. The roughness of the processed surfaces is below 20 Å Ry, which means that compared with the surfaces processed with the conventional slurries, better surfaces are efficiently obtained.

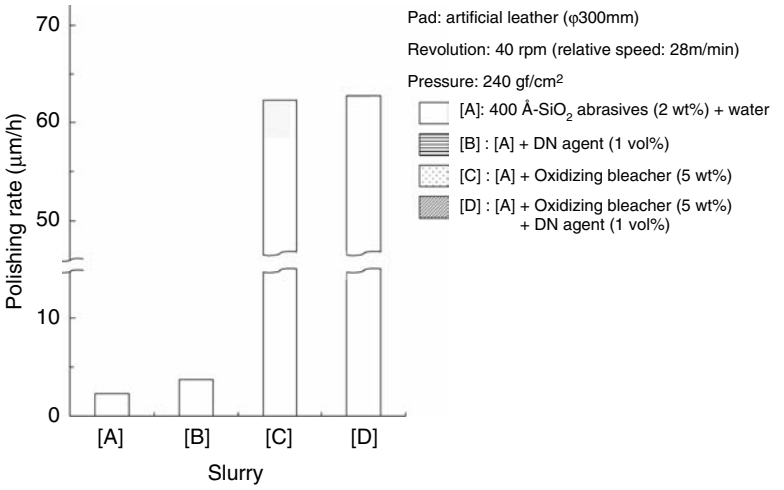


**FIGURE 7.161** Polishing rate by various slurries (workpiece: CdTe).

From the polishing experiments and results of chemical analyses conducted so far, processing mechanism in the chemical compound polishing of CdTe single crystals [91] is explained as follows (Figure 7.162).

Firstly, CdTe surfaces should be made apt to oxidization using DN agent, and then CdTe wafer surfaces should be oxidized with oxidizing bleach. Subsequently, some reaction products are produced on the surfaces. Such oxide film or reaction products are removed by the mechanical actions of the abrasives and pad. High-quality surfaces are created by repeating the above process sequentially.

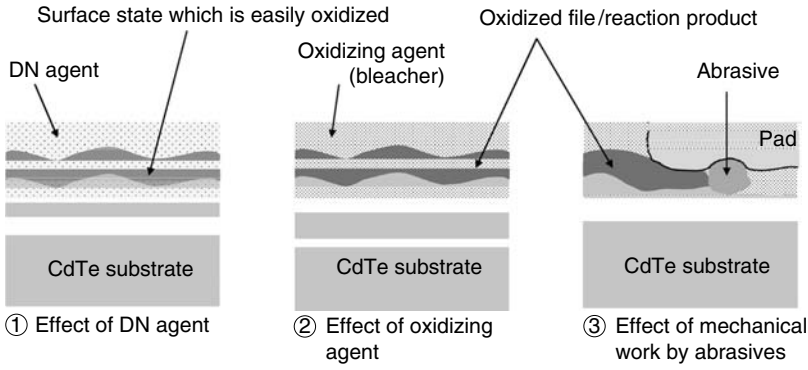


**FIGURE 7.162** Process mechanism for chemical compound polishing of a CdTe single-crystal substrate consisting of oxidizing agent (bleacher), DN agent, and fine $SiO_2$ abrasives.

Polishing mechanism of chemical compound slurries has been discussed above, taking GaAs and CdTe crystals as examples. The mechanism is found to be basically similar to the mechanism of the mechanical chemical compound polishing of Si crystals.

The following are the summary of the basic mechanical chemical compound polishing of semiconductor crystals in a sequential order:

1. Abrasive concentrations and polishing pressures including others to be within the given conditions (tools and abrasives, etc. to work on the work surface)
2. Chemical reactions with polishing reagent (polishing reagent should react chemically with crystals)
3. Generation of soft reaction products (should be in a state of easy removal)
4. Removal of reaction products (aggressive removal by fine particles)

In the case of compound semiconductors (particularly GaAs), addition of solutions like DN that has interface penetration functions is effective in the third stage. In the fourth stage, besides removal of reaction products by the fine particles (or pad), chemical actions generated in the second stage are promoted by the exposure of new surface and friction heat.

## REFERENCES

1. T.K. Doy. *Details of Semiconductor CMP Technology* (in Japanese), Kogyo-chosakai Publishing co., Ltd., Tokyo, Japan, 2001.
2. C.W. Kaanta, et al. *Proceedings of the VLSI Multilevel Interconnects Conference*, 144, 1991.
3. T.K. Doy, et al. *Proceedings of the Third International Symposium on Advanced Science and Technology of Silicon Materials*, 2000.
4. T. Karaki. Wet-type mechanochemical polishing of Si wafers. *Tool Engineer*, 24 (1984) 38–45 (in Japanese).
5. W. Kern, et al. Cleaning solutions based on hydrogen peroxide for use in silicon semiconductor technology. *RCA Review*, 31 (1970) 187–206.
6. M. Bohr. *International Electron Devices Meeting Technical Digest*, IEEE, New York, 1995, p. 241.
7. T. Sakurai and K. Kato. A new complementary dielectric isolation process for high-voltage devices. *IEEE Trans. Elect. Dev.*, 28(10) (1981) 1199.
8. F. Ohira, T. Karaki, and J. Watanabe. Abrasive machining system for dielectric isolated substrates, *ECS 165th Spring Meeting*, 1984, pp. 178–179.
9. T. Karaki, et al. New automatic polishing machine for silicon wafers (in Japanese), *JSPE Spring Meeting*, 1984, pp. 753–754.
10. The Planarization CMP Technical Committee, *JSPE Planarization, CMP and Its Applications*, vol. 5 (2002).

11. Y. Seike, S. Kawashima, K. Miyachi, and T.K. Doy. A development of super high-pressure microjet system for pad dressing and post-CMP cleaning in CMP process. *Proc. VMIC*, (2002) 411–414.
12. T. Doi and M. Kinoshita (Ed.). A Library of CMP planarization technology and application, *Global Net Corp*., Tokyo, 2006, p. 4 (in Japanese).
13. A. Philipossian, et al. Role of slurry flow rate and solids content on critical tribological and fluid dynamics attributes of ILD CMP, *Annual Spring Convention*, *Japan Society of Precision Engineering*, March 2002.
14. S. Hamamoto, et al. Influence of surfactants on polishing performances of CMP slurry, *Report of Cooperative Research Center*, Saitama University, No. 2, 2001.
15. M.L. Free, et al. Using surfactants in iron-based CMP slurries to minimize residual particles. *Micro*, May (1998) 29.
16. T. Detzel, et al. Comparison of the performance of slurries for shallow trench isolation processing, *CMP-MIC*, 1997, p. 202.
17. M. Hanazono, et al. Why $CeO_2$ is promising for STI? *CAMP* 2001, Clarkson University.
18. K. Devriendt. Shallow trench isolation, the process and its integration issues, *Semi Education*, *Advances in CMP Technology Course*, Semicon Europe, 2001.
19. P. Leduc, et al. Aiming for perfect planarization, *CMP-MIC*, 2002.
20. B.A. Bonner, et al. Improved direct polish STI CMP process with high selectivity slurry, reduced microscratching and increased productivity, *CMP-MIC*, March 2002.
21. K. Namiki, et al. Tungsten CMP process. *Ebara Engineering Review*, 183 (1994) 63.
22. R. Lum, et al. Oxide erosion characterization of a tungsten CMP process, *CMP-MIC*, 1999, p. 207.
23. K. Wijekoon, et al. Tungsten CMP process developed. *Solid State Technology*, April 1998.
24. M. Peterson, et al. Fourth Generation W Damascene Slurry, *CMP Technology for ULSI Interconnect*, SEMICON West 2000, Q-1.
25. S. Gaghavan, et al. Periodate as an oxidant for tungsten CMP, NSF I/UCRC Center for Microcontamination Control at Arizona and Rensselaer, *CMPUG*, October 2001.
26. J.M. Steigerwald, et al. *Chemical Mechanical Planarization of Microelectronic Materials*, John Wiley & Sons, New York, 1997.
27. H. Hirabayashi, et al. Chemical mechanical polishing of copper using a slurry composed of glycine and hydrogen peroxide, *CMP-MIC Conference*, 1996, 100.
28. H. Hirabayashi, et al. Development of slurry for Cu-CMP using quinaldic acid, *1998 Autumn JSAP Annual meeting, and 2000 Autumn JSAP Annual meeting*, Japan Society of Applied Physics (in Japanese).
29. K. Wijekoon, et al. Chemical mechanical polishing of Copper-CVD low *k* films: A comparison of selective and non-selective processes, *VMIC*, November 2001.
30. S. Kondo, N. Sakuma, Y. Homma, Y. Goto, N. Ohashi, H. Yamaguchi, and N. Owada. Abrasive-free polishing for copper damascene interconnection. *J. Electrochem. Soc*., 147 (2000) 3907.
31. J. Amanokura, et al. Development of new abrasive free copper CMP solutions based on electrochemical and film analysis method, *MRS*, 2002.
32. S. Ki, et al. A low cost and residue-free abrasive-free copper CMP process with low dishing, erosion and oxide loss, *IITC* 2001/IEEE.

33. D. Jams. Pad properties during polishing and their effects on polishing performance, *CAMP Sixth International CMP Symposium*, Clarkson University, August 2001.
34. D. James. Control of polishing pad physical properties and their relationship to polishing performance, *CAMP Fifth International CMP Symposium*, Clarkson University, August 2000.
35. T. Nishioka. Influence of stress distribution for CMP (in Japanese), *Tribology Conference*, 1997.
36. D.L. Hetherington, et al. Optimizing dielectric CMP planarization processes, *Proceedings of CMP-MIC 2000 Conference*, March (2000) 339.
37. M.R. Oliver, et al. CMP pad surface roughness and CMP removal rate, *ECS Fall Conference*, Phoenix, Arizona, October 23, 2000.
38. A.S. Lawing. Polishing rate, pad surface, morphology and pad conditioning in oxide chemical mechanical polishing, I1-Fifth International Symposium on Chemical Mechanical Polishing (CMP), *ECS 201st Meeting*, Philadelphia, 2002.
39. P. Freeman, et al. Characterization of pad conditioning profiles in oxide chemical–mechanical polishing, *CMP-MIC Conference*, 1996, 57.
40. J.J. Gagliardi, et al. Total planarization of the MIT 961 MaskSet wafers coated with HDP oxide, *CMP-MIC Conference*, March 2000.
41. G. Nantz and L.E. Camilletti. Modeling of chemical–mechanical polishing: A review. *IEEE Trans. Semicond. Manuf.*, 8(4) (1995) 382–389.
42. P.A. Burke. Semi-empirical modeling of $SiO_2$ chemical–mechanical polishing planarization. *Proceedings of the VMIC Conference*, 1991, pp. 379–384.
43. J. Warnock. A two-dimensional process model for chemimechanical polish planarization. *J. Electrochem. Soc.*, 138(8) (1991) 2398–2402.
44. B. Stine, D. Ouma, R. Divecha, D. Boning, J. Chung, D.L. Hetherington, I. Ali, G. Shinn, J. Clark, O.S. Nakagawa, and S.-Y. Oh. A closed-form analytic model for ILD thickness variation in CMP processes. *Proceedings of the CMP-MIC*, Santa Clara, February 1997, pp. 1–8.
45. T. Tugbawa, T. Park, D. Boning, T. Pan, P. Li, S. Hymes, T. Brown, and L. Camilletti. A mathematical model of pattern dependencies in copper CMP processes (invited paper). *Third International Symposium on Chemical Mechanical Polishing in IC Device Manufacturing, 196th Electrochemical Meeting*, Honolulu, HI, October 1999.
46. J.M. Staigerwald, R. Zirpoli, S.P. Murarka, D. Price, and R.J. Gutmann. Pattern geometry effects in the chemical–mechanical polishing of inlaid copper structures. *J. Electrochem. Soc.*, 141(10) (1994) 2842–2848.
47. L. Yang. Modeling CMP for copper dual damascene interconnects. *Solid State Technol.*, June (2000) 111–121.
48. T. Yoshida. Three-dimensional chemical–mechanical polishing process model by BEM. Electrochemical Society *Proceedings of the Third International Symposium on Chemical Mechanical Planarization in IC Device Manufacturing*, Honolulu, HI, October 1999.
49. T. Yoshida. A model of stacked polishing pad for 3-D CMP simulation. The Electrochemical Society, *Proceedings of the Third International Symposium on chemical Mechanical Planarigation in IC Device Manufacturing*, Honolulu Meeting, Abs#1288, October, 1999.
50. D. Dornfeld. Mechanical aspects of CMP. *VMIC*, June 2000.

51. S.R. Runnels and L.M. Eyman. Tribology analysis of chemical–mechanical polishing. *J. Electrochem. Soc*., 141(6) (1994) 1698–1701.
52. S.R. Runnels. Feature-scale fluid based erosion modeling for chemical–mechanical polishing. *J. Electrochem. Soc*., 141(7) (1994) 1900–1904.
53. G.O. Cai, Y.S. Lu, R. Cai, and H.W. Zheng. Analysis on lapping and polishing pressure distribution. *Ann. CIRP*, 47(1) (1998) 235–238.
54. J. Luo. Investigation of material removal mechanism in chemical mechanical polishing (CMP): Theory and modeling. *1999 LMA Research Report*, University of California, Berkeley.
55. A. Philipossian. Selected process consumable technology requirements for advanced CMP process, *The CMP Technical Meeting 2000 in San Francisco*, Part 1, sponsored by CMP Special Committee, The Japan Society of Precision Engineering, July 2000.
56. G. Muldowney. Characterization of CMP pad surfaces using a porous media flow approach, *Proceedings of AIChE Annual Meeting*, 2003.
57. G. Muldowney. Slurry mixin dynamics in CMP polishing pads of various groove arrays. *Proceedings of CAMP 9th International Symposium on CMP*, Lake Placid, August 2004.
58. G. Muldowney. The Effect of pad growth and texturing on CMP process performance, The *1st PacRim-CMP International Conference*, Tokyo Denki University, Tokyo, December 2004.
59. W. Kern, R.K Smeltzer. *Solid state technology*. June (1985) 171–179.
60. J.D. Romero, M. Khan, H. Fatemi, and *J. Turlo, J. Mater. Ref*., 69 (1991) 1996.
61. Keiichi Kimura. *Doctoral thesis of Osaka University* (2002) 31.
62. A. Offner. *Photographic Sci. and Eng*. 23 (1979) 374.
63. International Technology Roadmap for Semiconductor (1998).
64. N. Oda, et al. *Proceeding of 2002 Symposium on VLST Technology Digest of Technical Papers*, Kyoto, 2002.
65. A.K. Stamper, et al. *Proceeding of ADMETA 2002*, 60–61, 2002.
66. M. Matsuura, et al. *Proceeding of ADMETA 2002*, 62–63, 2002.
67. International Technology Roadmap for Semiconductor (2002)
68. G. Passemard, et al. *Proceeding of Advance Metallization Conference*, 357, 1999.
69. H.W. Thompson, et al. *Proceeding of IITC*, 59, 1999
70. N. Ohashi, et al. *Proceeding of IITC*, 140, 2001.
71. Y. Homma, et al. *J. Electrochem. Soc*., 147, (2000) 1193.
72. Y. Yamaguchi et al. *Proceeding of IITC*, 264, 2000.
73. Nobuo Hayasaka, Selete Symposium 2002 May 28, 2002.
74. Andreas Romer, et al. *Proceeding of CMP-MIC 2000*, 2000.
75. S. Matsuda, et al. *Proceeding of 2001 Symposium on VLSI Technology Digest of Technical Papers*, Kyoto, 64, 2001.
76. K. Matsuo, et al. *Proceeding of International CMP Symposium 2000*, 23, 2000.
77. S. Kordic, A. Inard, and P. Motte. *Proceeding of CMP-MIC 2001* 341–348, 2004.
78. Youhei Yamada, et al. *Proceeding of ADMETA 2002*, 112, 2002.
79. N. Ohashi, et al. *Proceeding of IITC 2001*, 140–142, 2001.
80. S.M. Jang, et al. *Proceeding of 2002 Symposium on VLSI Technology Digest Technical Paper*, 2002.
81. M. Oshiki, et al. Next-generation data storage technology. *Fujitsu*, 52(4) (2001) 353–360.

82. F. Liu, et al. Magnetic recording at a high data rate of 1 Gb/s. *IEEE Trans. Magn.*, 37 (2001) 613–618.
83. S.W. Yuan, et al. Advanced write heads for high density and high data rate recording. *IEEE Trans. Magn.*, 38 (2002) 1873–1878.
84. N. Robertson, et al. High performance write head using 45/55 Ni–Fe. *IEEE Trans. Magn.*, 33 (1997) 2818–2820.
85. E. Lee, et al. Chemical mechanical planarization of thin film read/write heads. *VMIC*, March (2000) 433–440.
86. M. Jiang, et al. Application of chemical mechanical polishing in thin film magnetic head wafer fabrication. *Short Course on CMP Planarization for ULSI Multilevel Interconnection*, February 26, 2002.
87. S. J. Tracy, et al. Planarization of $Al_2O_3$ and encapsulated Ni–Fe for GMR head manufacturing using a single layer unfilled cast elastomer polishing pad, *Semicon Taiwan*, September 2001.
88. T. Ookawa, et al. Fundamental study on mirror polishing for GaAs wafers (in Japanese). *J. JSAT*, 47(2) (2003) 88–92.
89. H. Nakata and T.K. Doy. *JSPE Spring Meeting* (1988) 91 (in Japanese).
90. T.K. Doy, T. Kageyama, T. Kasai, and T. Nakagawa. A new processing technique of GaAs single crystals and its mechanism. *Int. J. Jpn. Soc. Prec. Eng.*, 30(1) (1996) 16–22.
91. T.K. Doy, T. Kasai, and T. Nakagawa. A new processing technique of CdTe single crystals used for opto-electronics advances in science and technology, *Adv. Mat. Opt. Electro-Opt. Commun. Technol.*, (1995) 541–548.

# Index

## A


Abbott curves, 63, 65
Abrasion mechanism, 1
  two-body and three-body, 118–120
Abrasive(s), 177–178
  aluminum oxide ($Al_2O_3$), 97, 104, 130, 132, 268, 294, 307, 392
  artificial, 103
  belt grinding, 12
  boron carbide, 130
  calcined alumina, 130, 132
  charged plate, 103
  coarse, 97
  corundum, 104, 132
  with crushing function, 269
  cubic boron nitride, 3, 104, 131
  diamond, 3, 97, 103–104, 183, 295–296
  $Fe_2O_3$, 294
  fused alumina, 104
  garnet, 104
  hardness of, 3
  importance of, 3
  MgO, 294
  microcutting embedded, 2
  as microscopic cutting tool, 125
  motional pattern of, 116
  natural, 103
  norbide, 104
  pad, 2
  particles, 1
  process, 1
  role in lapping, 272
  rolling, 2, 103
  rolling and sliding action of, 117
  silicon carbide (SiC), 104, 130, 132, 268
  $SiO_2$, 294
  sliding, 2, 103
  slurry, 105
  unfused alumina, 102, 105, 132
  zeta potential of, 393
Abrasive-free polishing (AFP) technique, 454
Abrasive processes
  finishing, 93
  high-precision, 93
Abrasive wears, 135–136
ACCUPRO AR-10 hardness tester, 177, 179
Active grain concentration, 68
Additive agents, 371
Agglutinations, 304
$Al_2O_3$ film, 463–464
AlTiC, 463
Altzschner, 1
Aluminum oxide, 174, *see* Abrasive(s)
AMAT Mirra tool, 404
Ammoniac water, 369
Analytical models, 57
Angular velocities, calculation of, 38
ANOVA analysis, 216–217, 227, 231, 233
  of surface roughness
    for copper plate, 219–221, 225
    for iron plate, 222–224
Arrhenius plot, of polishing rates, 299
Arrhenius' rate equation, 299
ATHENA software, 418
Atomic force microscopy (AFM), 163
Attritions wear, 4
Auto stirrer, 109
Axial cracks, 18–19
Axial–lateral crack system, 60–61
Axial–radial–lateral crack system, 19


## B


Basalt, 9
Beilby, theory of, 16
Beilby layers, 16
Belt polishing, 290

Benzotriazole (BTA), 390
Bessel function, 430
Black Diamond, 394
Blanchard rotary surface grinding machine, 181
Blasting, 12
Blocky grainings, 21
Borazon TM CBN, 104
Borophosphosilicate glass (BPSG), 394
Both-sides simultaneous lapping machine, *see* Lapping, machine
Boundary conditions
  of boundary elements, 431
  for hydrodynamic analysis, 433
Boundary element method (BEM), 424
Boussinesq solution, 429–430
Boussinesquian state of stress, 18, 20, 63
Boussinesquian state of tension, 60
Brittle crack formation, 20
Brittle material, 1
Br-methanol solution, 326–327, 329
Bromine (Br), 468

## C

Carbide ceramics, 128
Carbon-doped oxide (CDO), 394–395
Carrier, 108
Cast-iron lap, 287
CdTe crystal, 471
Cemented carbide alloy, 168; *see also* ELID-lap grinding, experimental results
Centrifugal separation method, 372
Ceramic finishing process, 2
Ceramic materials
  nonoxide ceramics, 128
  oxide ceramics, 128
  silicate ceramics, 128
Ceramic seal industry, 1
Ceria
  powder, 374, 378
  slurry, 379
Charging technique, 2
Chatter marks, 372
Chemical mechanical polishing; *see also* Thin film magnetic recording heads
  aims of, 362
  basic mechanism of, for silicon crystal, 298–301
  basic requirements for planarization, 355
  classification
    based on relationship between work piece and polishing, 326
    based on stock removal mechanism, 325
  cleaning station, 369–370
  close contact condition in, 305
  of compound semiconductor wafers
    polishing characterstics of CdTe crystal wafers, 471–473
    polishing characterstics of GaAs crystal wafers, 469–471
  examples of, 301–305
  interlevel dielectric (ILD) layer of, 353
  machine system, technology of, 363–369
    configuration and unit control factors of, 364
  modeling and simulaton of
    modeling of planarization process, 415–424
    modeling of polishing pad and planarization, 424–431
    modeling of slurry behavior, 431–436
    purpose of modeling, 414–415
  in noncontact condition, 325, 327
  overcoat, 467–468
  pads for, planarization of
    basic properties of, *see* Chemical mechanical polishing pads, basic properties of
    conditioning and polishing of, *see* Chemical mechanical polishing pads, conditioning and polishing performance
  polishing unit, 365–369

polishing works and its defects, 359–363
process modeling parameters of, 430
progress of MCP-CMP, 296–297
relationship between polishing pressure and polishing rate, 302, 304
removal mechanism in, 301
requirements for, 297–298
in semi conductor process, *see* chemical mechanical polishing, in semi conductor process
in semi contact condition, 325, 327
for shallow trench isolation, 377
of Si, 300
slurries for
basis of CMP slurries, 370–371
Cu-CMP slurries, *see* Cu-CMP slurries
ILD CMP slurries, 371–373
STI CMP slurries, 373–381
W CMP slurries, 381–386
system design concept of, 359
system machine development, 360–361
tribological mechanism during, 370–371
Chemical mechanical polishing, in semi conductor process
basic concept of
basics of CMP ultra precision polishing, 356–357
design concept of, 359
requirements and points to be noted for, 357–359
works to be published by, 359–363
planarization of, 349–354
with ULSI device process, 343–344
and ultra precision polishing, 344–349
Chemical mechanical polishing pads
basic properties of
composite pad structure, 401–404
elastic and viscoelastic properties of, 399–401
pad properties and polishing performance, 396–399
pad surface asperity and grooves, 404
relationship between pad properties and pad performance, 400
conditioning and polishing performance
conditioner, 404–406
conditioning process, 406–408
pad surface profile and planarization uniformity, 408–411
types of
fixed abrasive pad, 413–414
nonporous pad, 411–413
Chip generation, principle of, 285
Chucking functions, 366
Circular axial cracks, 18
Class path lengths, 52–54
CMP–MCP, of single crystal silicon semiconductors, 297
Coefficient of friction (COF), 75, 371
Cole-Parmer peristaltic pump, 178–180
Colloidal silica, 286, 330
polishing characteristics
on $Gd_3Ga_3O_{12}$, 333
on $LiTaO_3$, 333
on sapphire, 333
on silicon, 333
Colloidal silica polishing, 330–337
constitutional diagram of, 334
Computer numerical control (CNC) machining, 108
Conditional ring/plate-polishing machine, *see* Polishing machines
Conditional rings, 289–290
Conditioning rings, 98, 107, 116, 182, 187, 269–270, 274
diamond plated, 108
solid ceramic, 107
stainless-steel-backed ceramic, 107
type lapping machine, *see* Lapping, machine
Conical crack, 18
Conventional pitch polishing, 334
Copper damascene process, 466
Copper dishing, 428

Copper film
  delamination of, 448, 450
  seed, 443–444, 459
Copper hydrate formation, 390
Copper plate, randomized experiment sequences, 257
Corundum, *see* Abrasive(s)
Cost of ownership (COO), 374
Crack formation, 18
Crack system, 17
Critical particle size, 140
Cubic boron nitride, *see* Abrasive(s)
Cu-CMP polishing process, 424, 453–454
Cu-CMP slurries
  abrasive free, 396
  and low-k CMP, 394–396
  organic acid-based, 390–392
  pourbaix diagrams for Cu-$H_2O$ system, 388–390
  removal rate difference between selective and nonselective, 394
  resistance comparison of abrasive free and residue free, 397
  role of abrasive particles in, 392–394
  topography performance depending on selectivity of, 395
  two-step process and selectivity of, 386–388
Cu–glycine complex, 390
Cu–$NH_3$–$H_2O$ solution, 389
Cu–quinaldic acid complex, 391
Cutting edge radius, 58
Cutting edge wear, 33
CVD-SiC, 162, 165
Cycle angle, 43–44
Cycle time, 42
Cycloids, 35
Cylindrical lapping, *see* Lapping, method

## D

Damascene gate-forming process, 452
Damascene method, 442–443
Depth of focus (DOF), 349–350, 439
Design of experiment (DOE) method, 212
Device fabrications
  accuracy and quality required in, 284
  processes flow in, 345
Device wafer, case study of
  Cu and low-K CMP, 452–458
  device integration and CMP, 443–444
  STI-CMP, 449–452
  Tungsten CMP, 452
Diamond grainings, 21
Dielectric isolation (DI) wafers, 352
Dilute hydrofluoric acid, 369
DIN 8580, 29
DIN 8589, 12
  part 15, 12–15
Dip lapping, 15
Dislocation cracks, 23
DN agent, 469–472
Double-sided lapping, *see* Lapping, methods
Double-sided polishing machines, *see* Polishing machines
Double-wheel lapping machines, 11, 14
DRAM technology, 343
Dual in-line package (DIP), 346
Ductile material, 1
Ductile regime machining, 138
Duomat ZL 500, 47

## E

Ebara EPO tool, 404, 456
Elastic emission machining (EEM), 290, 305–306, 325
Elasticity module, 21
Elastic–plastic contact case, 18
Electrical discharge machining (EDM), 108
Electroabrasive mirror polishing process, 317–318
  description of, 318
  experimental results, 319–322
  manual polishing, 319
Electro-compounding polishing method, 317

Electrolysis, 318
Electrolytic dressing, 168
Electrolytic sodium sulfate ($Na_2SO_4$), 335
Electrophoretic deposition (EPD), 312
  development of pellets, 312–315
  experimental results, 315–317
ELID-lap grinding
  characteristics of
    effects of grain size on surface roughness and removal mechanism, 163–164
    efficient mirror surface finish by, 165–166
  desk top system
    background, 166
    concept of, 167–168
  experimental methods, 163, 168
  experimental results
    grinding characteristics of cemented carbide alloy, 168–170
    grinding characteristics of nitrided steel, 170–172
    grinding characteristics of sapphire, 172–173
  experimental systems, 162, 168
  principle of, 160–161
ELID ultraprecision grinding, 166
Elliptic motion, 288
Endpoint detection (EPD), 364
  method, 458–459
    development of, 456–459
Engagement pressure quotient, 34
Epicycloids, 48, 54
Erosion pits, 141
Ethylene glycol ($HOCH_2CH_2OH$), 335

## F

Face lapping machine, 10
Ferric nitrate, 381
Film thickness ratio, 140
Fine grinding, 1
Finite element method (FEM), 424
Floating conditions, 306
Float polishing, 305
Fluorocarbon-foamed sheet, 329
FR-4, *see* Lamitex
Fractional factorial experiment, 214–215
Fracture theory, 118
Free abrasive cutting, 12
Fused alumina, *see* Abrasive(s)

## G

Garnet, *see* Abrasive(s)
Gaussian distribution function, 61
Gaussian normal distribution, 58
Gemstones, 9
Geometrical parameters, of relative movement, 37–39
Germanium, 9
Giant magnetoresistive (GMR) read, 460–461
Glass-Lens polishing machine, *see* Polishing machines
GR-10, *see* Lamitex
Grain agglomerates, 77
Grain aperture angle, 60–61
Grain breakage, 21, 33
Grain engagement mechanism, 16, 20–21, 23–24, 61
  frequency of, 67, 69–70
  scratching, 20
Grain movements, 19
Grain size, for standardized control conditions, 21
  Stotko parameters, 21–22
Grain size distribution, 22
Grain splintering, 21, 33
Granite, 9
Grinding operation, 1, 312
  by linear cutting, 12
Grooving deformation, of material, 17

## H

Half-penny-cracks, 18, 64, 69
Half-penny-lateral-crack system, 20
Hall–Petch relation, 16
Hard disk drive (HDD) systems, 460
Hazardous waste, 9
HDP-$SiO_2$ film, 443
Hersey number, 431

Hertzian conical cracks, 18, 59
Hertzian equations, 58
Hertzian load, 58
Hertzian stress field, 18
Herz solution, 430
Hexoloy-sintered alpha silicon carbide, 174
  properties of, 176
High-precision carbide tools, 13
High-pressure homogenizing technique, 372
High-temperature reaction test, 335
Hommel Tester LV 15, 179
Hommel tester T1000 E roughness meter, 184–185
Honing, 1, 12
Horizontal lapping friction, 269
HR-120 precision scale, 179
Hydration films, 324
Hydraulic pistons, 13
Hydrogen gas, 326
Hydrogen peroxide, 381, 390
Hydroplaning effect, 306
Hydrostatic stress, 18
Hypocycloid path curves, 54
Hypocycloids, 47

## I

IBM, 344
IC1000 pad, 396–397, 403
  cross-sectional view of, 398
  grooves and perforation designs for, 406
  physical properties of, 398
  surface profile after conditioning, 408
  surface profile after polishing, 409
IC1010 pad, 375
IC1020 pad, 375
IC1400 pad, 405
  diagram cross section of, 408
IC1000/SUBA IV pad, 405
ILD erosion simulation, 429
ILD films, 420, 422, 437
  methods for planarizing, 437
Incipient cracks, 18
Inductive write magnetic heads, 460
In-situ measuring technique, 358
Internal cylindrical peripheral lapping, 13–14
Iron plate, randomized experiment sequences of, 258
Isotropic properties, 9

## J

Johannsson, Swede C.E., 10–11

## K

Kernel roughness depth, 65
Kinematical concept, 10
Kinematical parameters
  cycle angle and part-cycle angle, 43
  cycle time and part-cycle time, 42
  pitch circle radius, 42
  of relative movement, 37–39
Kinik diagrid conditioner, 407
KOH solution, 303–304
Kronecker's delta, 432
K35 SPD, 178
K35 SYN, 178

## L

$LaB_6$ single crystals, 336
Lamitex, 108
Lapmaster lapping machine, 98, 178–179
Lapping, 1–3, 265
  abrasives used in, 32
  of brittle materials, 123
    ceramic materials, 127
    introduction, 125
  of ceramics, 20
  characteristics of, 9
  controlled, 114
  definition of, 12
  of ductile materials, 72, 93
    introduction, 93–97
    mechanism of the process, 115–120
    physics of the process, 97–114

factors in, 267
fluids, 134
fundamentals of, 7
general consideration, 9
historical developments, 9–11
machine, 2, 9
both-side simultaneous, 274–275
both-side simultaneous equipped with micro-motion mechanism, 275–278
conditioning ring type, 273–274
measuring procedures, 184–188
oscar type lens type, 272–273
medium of, 32
methods, 109
cylindrical lapping, 113
double-side lapping, 111
lapping with bonded abrasives, 114
single-side lapping, 109
of monocrystal materials, 20, 63
oil, 77
and out of flatness condition, 110–111
plane-parallel, 24
and polishing processes, mechanics of, 1
and polishing slurries, 4
pressure, 12, 16, 21, 59, 76–77, 99, 151, 161, 196, 243, 268
principle of, 9–10
processes, *see also* Nontraditional lapping processes
advantages of, 114
characteristics of, 94–95, 98–99
classification of, 12
for desired finishing, 95–97
formation of removal system, 27
fundamentals of, 129
abrasive, 129
lapping fluid, 129
lapping plate, 129
indentation models, 118
fracture theory, 118
shear theory, 118
mechanisms of, 15, 266
modeling of, 235–242
parameters of removal system, 26
principles of, *see* Lapping, processing principles of
process models and simulation, 57
process parameters, 27
as removal system, *see* Lapping, as removal system
stock of removal, 269
subsurface damage, 25
subsurface-related work result, 27
subsurface stress, 25
surface formation, 25
working gap, 29
work parameters, 115
process model, 75
process parameters of, 27
and reconditioning, 269
and removal of microhardness, 22–23
in residual-stress-poor machining, 22
setup for, 178–184
subsurface damage, 15
symbols and abbreviations of, 81–85
tools, 29
wheels, 31
description of workpiece geometry by geometric function, 50
movements of workpieces relative to, 36
path length distribution, 50
profile and grain wear during machining, 49
Lapping, as removal system
formation of, 27–28
parameters of, 26–27
removal system, 24–25
of subsurface damage, 25
of subsurface-related work result, 27
of subsurface stress, 25
in surface formation, 25
and working gap, 29
Lapping, processing principles of
lapping factors
abrasives and reagent in lapping, 268
lap (lapping plate), 267–268
mechanical conditions, 268–269
motion type, 267
processing accuracy in

conditioning ring, 269–270
cooling of lapping plate and cooling device, 270–271
grooves lapping plate, 271–272
Lapping grains, cutting effect of, 17
Lapping-in technique, 15
Lapping performance, 22
Lap plate, 99, 268
ceramic plate, 101
cooling of, 270–271
copper plate, 100–101
grooves in, 271–272
iron lap plate, 100
tin or lead plate, 101
tin plate, 101
Large-scale integration (LSI) technology, 343
Laser cutting, 108
Lateral cracks, 18–19, 66, 118, 138
Leonardo da Vinci, 10
Lexan, 109
Limit processing pressure, 147
Linde powders, 96
$LiTaO_3$ film, 337
Local thickness variations (LTV), 347
LOCOS methods, 440
vs STI method, 441
LSI devices, 359, 362
Lubrication, 133
Luo model, of solid contacts, 434–435

## M

Machine settings, 34
engagement pressure, 34
process kinematics, 34–35
Machine tool technology, 1
Macrofracture, 4
Macrokinematics, 36
Magneto abrasive finishing
advantages of, 308–309
finishing operations in, 309
edge and surface finishing, of access arms of magnetic disk units, 310–312
internal finishing of non-ferro magnetice bent tubes, 309–310
outline of, 307–308
Manganese steel, 22
Manual polishing, 319
Marble, 9
Masterflex Tygon silicon tubing, 178, 180
Material displacement process, 138
Material removal and grain engagement mechanisms
of brittle-hard materials, 17
of ductile materials, 16
in specified lapping abrasive, 21
for subsurface damage, 22
Material-removal process, 138, 140
Material-removal rate (MRR), 127, 132, 195, 210
for copper plate, 226–227
for iron plate, 228–230
MATLAB program, 216
MCP, *see* Mechanochemical polishing
Mechanochemical polishing, 293–296
Mechanochemistry, 292
Metallurgical polishing machines, *see* Polishing machines
Metal–resin bonding system, 162
Microcrack networks, 23
Microcrack systems, 18
Microcutting abrasives, 2
Microfracture, 4
Microkinematics, 37
Micromachining processes, 1
Micromotion kinetic mechanism, 275–278
Mirror-finish method, 356
Mitutoyomicrometer, 186
Model lapping tests, 16, 24
Modulated cycloidal movements, 35
Mohs 9, 104
Mohs scale, 294
of hardness, 131
Monocrystalline diamond, 201
test results, 189, 204–205
MOS transistors, 346
Movement patterns, description of
determination of path pattern of workpiece point, 46
kinematical parameters, 42
possible path movements, 44

progression of path velocity, 48
rotational speed ratio, definition of, 41
M2 tool steel, 3
Multilevel interconnections, 346

## N

Nanometer grinding, 312
$NaNO_3$ solution, 318, 323
NaOH solutions, 352
Navier–Stokes equations, 431
Nelson's BASIC program, 231
Neolithic time, 1
Newtonian fluid, 431
Nitrided steel, *see* ELID-lap grinding, experimental results
Nitriding method, 171
Ni–Zn–ferrite, 23
Noncontact polishing, 305–307
Nonmetallic elemental solids, 127
Nonoxide ceramics, 128
Non-Prestonian-type polishing mechanism, 378
Nonspherical surface polishing machine, *see* Polishing machines
Nontoxic sodium bromite ($NaBrO_2$), 469–470
Nontraditional lapping processes
low frequency vibration, 143–146
and experimental technique, 146–147
low-frequency vibration lapping plate correcting techniques, using rectangular correcting carrier
correcting of lapping plate, 152
correcting process by rectangular correcting carrier, 156–158
experimental apparatus and method, 155–156
friction distance characteristics of rectangular correcting carrier, 153–155
processing characteristics and mechanism, 147–151
processing surface roughness, 151–152
ultrasonic vibration vs low frequency vibration, 142
using ultrasonic vibration
application to lapping, 158–159
principle of ultrasonic exciter, 158
vibration, 142–143
Numerical aperture (NA), 349–350
Numerical models, 57

## O

One-sided and two-sided machining, cutting conditions in, 54
Orbital motions, *see* Micromotion kinetic mechanism
Oscar-type lens lapping machine, *see* Lapping, machine
Oscar-type polishing machine, 319–320, 324
Oxidation–reduction potential (ORP), 388
Oxide ceramics, 128
Oxide erosion, 382–384
Oxide patterns, three dimensionality of, 432
Oxidizers, 381
OXP4000 pad, 411–413

## P

Pad conditioning, 367–368, 435; *see also* Chemical mechanical polishing pads, conditioning and polishing performance
Pad dressing model, 368
Pad surface morphology, 410
Pairwise lapping, 15
Parallel gauge blocks, 10
Part-cycle angle, 43
Part-cycle time, 42
Parts carriers, 108
Path curves and movements, calculation of, 36–37, 39
path acceleration and scalar acceleration, 41
path curvature, 41
path curve, 40

path velocity, 40
progression of, 48–49
Path length distribution, 51–54
Path pattern, of workpiece point, 46–48
Path-related workpiece height reduction, 56
Pattern density, 418, 422–423
Phenolic, 109
Phosphoric acid etching, 296
Photolithography, 349
Pin disk system, 146
Pitch circle radius, 42–43, 45
Pitch polishing, 273, 283
Planarization CMP Technical Committee, 359
Planarization process, modeling of
in Cu-CMP, 422–424
hard model, 415–417
of rough surfaces, 357
soft model, 417–418
using pattern density, 418–422
Planarization quotient, 403–404
Planarized wafers, surface topography of, 351
Plane-parallel lapping, 13
Planetary kinematics, 56
fundamentals of, 35
cycle and part cycle, 37
definition, 35
macrokinematics, 36
microkinematics, 37
path curve, 36
path movement, 37
Planetary movement patterns, 49
Plastic deformation, 9, 139
ratio, 23
Plastic zone, 18, 20, 60, 118, 138
P-MAC polishing, 324
machine manufacturing and GaAs wafer polishing, 329–330
for small pieces of GaAs single crystals, 327–329
vs. other polishing methods, 324–327
Poisson number, of workpiece, 60
Poisson ratio, 58
Poisson ratio distribution, 425, 430
Polish-deceleration factor, 417
Polishing machines, 286
double side polishing, 291–292
single side polishing
conditioning ring type polishing machine, 289–290
glass-lens polishing machine, 288–289
metallurgical polishing machine, 287–288
non-spherical surface polishing machine, 290–291
ring-tool polishing machine, 289–290
rough lapping machine, 287–288
Polishing margin, 357
Polishing pads, 2, 108
and planarization, modeling of
bending deformation of pad, 425–427
confirmity of pad to surface topography, 427–428
distribution of contact pressure between polishing pad and wafer, 425
simulation using solo pad and stacked pad, 429–431
Polishing principles, 282–283
Polishing process
of colloidal silica, 330
with electro abrasive mirror, 317–322
with electrophoretic deposition, 312–317
with P-MAC
GaAs wafer polishing with, 329–330
manufacturing of P-MAC machines, 329–330
polishing of small pieces of GaAs single crystals, 327–329
vs. other polishing methods, 324–327
Politex, 368
Polycrystalline diamond, 201, 203
test results, 190, 205–206
Polyurethane pad, 396, 404
Polyvinyl alcohol (PVA), 312–313, 369
Potassium iodate, 381
Pourbaix diagram, for Cu–$H_2O$, 388–391

Pressurization control mechanism, 366
Preston coefficient, 420, 424
Preston's equation, 415, 419–420, 427, 431
Preston's formula, 269
Preston's law, 276
Process grain size distribution, 33
Processing accuracy and damaged layer, 283–286
Process kinematics, 34–35
Process models and simulation, 57
  according to Buijs and Korpel-van Houten, 61–62
  according to Chauhan et al, 59–61
  according to Engel, 63–72
  according to Evans, 72–73
  according to Heisel, 73–81
  according to Imanaka, 58–59
  summarizing assessment of process models, 62
Profile lapping, 14
ProfileView 3.44 software, 179
Pseudostatic indentation model, of ductile lapping, 72
Punch and die tooling, 108
PVC, 108

## Q

Quasistatistical process, 20
Quinaldic acid, 390

## R

Radial cracks, 18–19
Radial scratches, 20
Randomized experiment sequences
  of copper plate, 257
  of iron plate, 258
RCA cleaning process, 347
Read or write heads, 1
Reciprocating motion, 287–288
Reconditioning process, 269
Rectangular correcting carrier, 152–158
Residence time control, 290
Reynolds number, in slurry, 435
Rodel IC1000, 384
Rodel politex, 384
Rolling abrasive, 2
Rolling grain movement, 20
Rolling resistance coefficient, 74, 79
Roll lapping, 14
Rotational–indentation model, 19
Rotational speed ratio, 41, 45–46, 48
Rough lapping machines, *see* Polishing machines
Roughness average parameter, 185
Rubber pads, 108

## S

Sandstone-grinding wheel, 1
Sapphires, 294; *see also* ELID-lap grinding, experimental results
Scanning electron microscopy (SEM), 16, 23, 163, 311, 373
Schist-shaped grains, 17
Semiconductor manufacturing, 1
Semiconductor Manufacturing Technology Institute (SEMATECH), 343
Semiconductor technology, 343
Shallow trench isolation process, 373
Shape-transferring counterparts, 12
Shear theory, 118
Shore D hardness test, 398
Si-CMP, macroscopic processing of, 301
Silicate ceramics, 128
Silicon, 9, 17, 23
Silicon carbide, *see* Abrasive(s)
Single-plate vertical lapping machine, 11
Single-side polishing machine, *see* Polishing machines
Single-wheel lapping machine, 10
SiOC film, 443
$SiO_2$ film, 353
$SiO_2$ particles, chemical actions of, 330–331
SIRD, 24
Si wafers
  fabrication process of, 345
  polishing conditions of, for ULSI fabrications, 298, 348

polishing methods, 346–347
precision cleaning of, 347–348
requirements in polishing process of, 347
standard cleaning procedure of, 349
SKD11 steel, 159
SKD61 steel, 171
Sliding abrasive, 2
Slurries, 31; *see also* Chemical mechanical polishing, slurries for
$Al_2O_3$ CMP, 464
behavior of abrasive particles in, 434–435
ceria, 379
non-Prestonian behavior of, 381
polishing model for high selective, 380
conventional oxide polishing, 374
diamond, 130, 179, 187
first-generation, 386
fourth generation, 385–386
ILD1200, 401
issues for designing of, 371
monocrystalline diamond, 236
Ni–Fe CMP, 465
pad properties in, 403
polishing mechanism of chemical compound, 473
polishing stages using high and low selective, 456
polycrystalline diamond, 126, 186, 209, 237
Reynolds number, 435
SS25, 401
starvation, 435
Stokes number in, 435
third generation, 382
topography reduction in, 378
tungsten, 381–386
water-based monocrystalline, 186
water soluble, 105–106
Slurry supply mechanism, 368–369
Soda-lime glass, 18
Sodium hypochlorite (NaClO), 468
Soft-foamed polyurethane sheet, 328
Sol gel technology, 3
Solid-phase reaction, 294, 296
Sphere geometry, 61
Spin-on-glass (SOG) coating method, 437
Spring steel, 108
(S4889)STD–MA formulation, 178
Stable grinding performance, 172
Stable ring crack, 18
Stähli Läpp-Technik Company, 47
Statistical principles, use of, 61
STI-CMP processing, 443, 445, 449–452, 459
Stokes average diameter, 59
Stokes number, in slurry, 435
Stribeck curve, 431, 433
(S1313–T4)STD–MA formulation, 178
Suba 400 base pad, 402
Superabrasive particles, 1
Superfinishing, 1
Surface lapping, 12
Surface modification process, 138
Surface precision, of platen, 366
Surface smoothing operation, *see* Polishing process
SUS316L pipes, 319
SUS304 stainless steel elbow, 310

## T

Taguchi's response statistic, 216
Tantalum nitride (TaN), 388
Tantalum (Ta), 388
TEOS ILD film, 371
Test element group (TEG) wafers, 457
Theory of Beilby, 16
Thermit reaction, 307
Thin film magnetic recording heads; *see also* Chemical mechanical polishing
CMP process for
bottom pole and top shield CMP, 465–466
bottom shield CMP, 464–465
Cu dama scence process, 466–467
overcoat CMP, 467–468

smoothing of Alumina basecoat at film surface, 463–464
fabrication process and requirements for CMP, 465
structure and mechanisms of, 460–463
Thread lapping, 14
Time-related workpiece height reduction, 55–56
Tool motion method, 285
Tool specifications
of lapping abrasives, 32–33
of lapping medium, 32
of lapping process, 29–31
of lapping wheels, 31
in process grain size distribution, 33–34
of slurry, 31–32
tool components and characteristics in plane-parallel lapping, 30
Total thickness variations (TTV), 347
Transmission electron microscopy (TEM), 23
Tungsten (W) slurry, 381–386

## U

ULSI device fabrication process, 460
outline of, 345–346
ultraprecision polishing and CMP of bare silicon wafers, 346–349
Ultralarge-scale integration (ULSI) devices, 343
Ultra-LSI device wafers, 276
Ultraprecision polishing, 282–283, 296
Ultrasonic-assisted lapping, 15
Ultrasonic exciter, 158
Ultrasonic frequency, 15
Ultrasonic vibration, *see* Nontraditional lapping processes
Uneven wear, 110
Urethane pad, 401–402
porous, 411

## V

Vacuum chucking method, 346
Valve pins, 13
Vapor lapping, 15
Vickers hardness, 333
Vickers indentation tests, 19
Vinyl, 109

## W

Warren Diamond Powder Company, 178
Water chucking method, by surface tension, 346
Waviness, 184
Wax adhering method, 346
Wear debris formation, 137
Wear mode, 4
Wet process, 297
Wheel blunting, 4
Wheel breakdown, 4
Within a wafer (WIW) uniformity, in polishing, 455
Working gap, 29, 33, 61, 64, 73, 76, 81, 137
height of, 66
volume, 67
Workpiece geometry, 50–51
Workpiece materials, 174–177

## X

Xerogel, 314–317

## Y

Yates algorithm, 231
Young's modulus, 17, 58, 138
of pad, 425–427, 430

## Z

Zinc, 109

**Manufacturing and Industrial Engineering**

Lapping and polishing are currently the most precise surface finishing processes for mechanical and electronic components. Unfortunately, most improvements in either methods or understanding of the physical processes involved are closely guarded as proprietary information. The Handbook of Lapping and Polishing is the first source in English to bring to the light of day the physical fundamentals and advanced technologies at the leading edge of modern lapping and polishing practice.

Collecting decisive work contributed by industrial and academic experts from the USA, Germany, and Japan, this authoritative resource presents the latest lapping and polishing technologies along with case studies that illustrate their value. After a brief introduction, the book explains the fundamental concepts and major types of lapping and polishing processes. The discussion then turns to lapping of ductile and brittle materials followed by an in-depth look at lapping machines and equipment. Rounding out the presentation, the final chapters discuss polishing technologies and equipment as well as the latest on chemical–mechanical polishing (CMP) and its applications in the semiconductor industry.

*Guiding the selection of the best process and hardware, this book…*

- Provides authoritative and reliable information on the latest developments in lapping and polishing theory and technology
- Examines lapping process mechanisms, subsurface damage, material removal, tool specification, modeling, and simulation
- Presents an extensive case study on lapping of brittle materials and another on CMP for semiconductors
- Outlines the major hardware used for lapping and polishing processes, emphasizing accuracy and intended application

Offering an integrated approach to both theory and practical applications under a single cover, the Handbook of Lapping and Polishing supplies a definitive survey of the most advanced surface finishing technologies available.

DK4113
ISBN 1-57444-670-3
90000
9 781574 446708

CRC Press
Taylor & Francis Group
an informa business
www.taylorandfrancisgroup.com

6000 Broken Sound Parkway, NW
Suite 300, Boca Raton, FL 33487
270 Madison Avenue
New York, NY 10016
2 Park Square, Milton Park
Abingdon, Oxon OX14 4RN, UK